Defense Nuclear Agency
Alexandria, VA 22310-3398

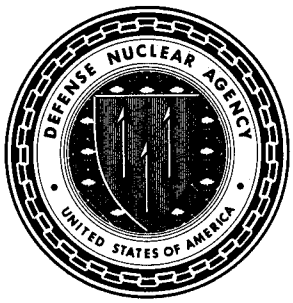

DNA-TR-94-117

Dust Sweep-Up Experiments

Richard G. Batt
Alden A. Peabody II
TRW Inc.
Space & Electronics Group
One Space Park
Redondo Beach, CA 90278–1078

November 1995

Technical Report

CONTRACT No. DNA 001-92-C-0108

DISCLAIMER NOTICE

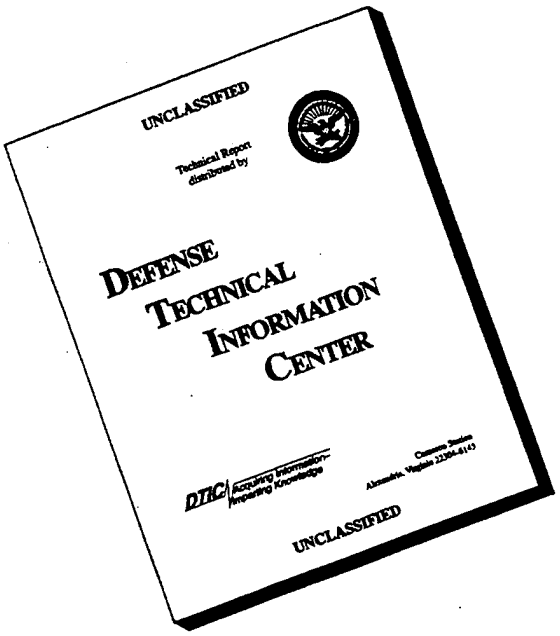

THIS DOCUMENT IS BEST QUALITY AVAILABLE. THE COPY FURNISHED TO DTIC CONTAINED A SIGNIFICANT NUMBER OF PAGES WHICH DO NOT REPRODUCE LEGIBLY.

DISTRIBUTION LIST UPDATE

This mailer is provided to enable DNA to maintain current distribution lists for reports. (We would appreciate your providing the requested information.)

NOTE:
Please return the mailing label from the document so that any additions, changes, corrections or deletions can be made easily. For distribution cancellation or more information call DNA/IMAS (703) 325-1036.

☐ Add the individual listed to your distribution list.

☐ Delete the cited organization/individual.

☐ Change of address.

NAME: _____

ORGANIZATION: _____

OLD ADDRESS	CURRENT ADDRESS
_____	_____
_____	_____
_____	_____

TELEPHONE NUMBER: ( ) _____

DNA PUBLICATION NUMBER/TITLE	CHANGES/DELETIONS/ADDITIONS, etc.) *(Attach Sheet if more Space is Required)*
_____	_____
_____	_____
_____	_____

DNA OR OTHER GOVERNMENT CONTRACT NUMBER: _____

CERTIFICATION OF NEED-TO-KNOW BY GOVERNMENT SPONSOR (if other than DNA):

SPONSORING ORGANIZATION: _____

CONTRACTING OFFICER OR REPRESENTATIVE: _____

SIGNATURE: _____

CUT HERE AND RETURN

REPORT DOCUMENTATION PAGE

Form Approved OMB No. 0704-0188

1. AGENCY USE ONLY *(Leave blank)*	2. REPORT DATE	3. REPORT TYPE AND DATES COVERED
	951101	Technical 920623-940723

4. TITLE AND SUBTITLE
Dust Sweep-Up Experiments

5. FUNDING NUMBERS
C - DNA 001-92-C-0108
PE - 62715H
PR - AC
TA - BD
WU - DH321690

6. AUTHOR(S)
Richard G. Batt and Alden A. Peabody, II

7. PERFORMING ORGANIZATION NAME(S) AND ADDRESS(ES)
TRW Inc.
Space & Electronics Group
One Space Park
Redondo Beach, CA 90278-1078

8. PERFORMING ORGANIZATION REPORT NUMBER

9. SPONSORING/MONITORING AGENCY NAME(S) AND ADDRESS(ES)
Defense Nuclear Agency
6801 Telegraph Road
Alexandria, VA 22310-3398
SPWE/Byers

10. SPONSORING/MONITORING AGENCY REPORT NUMBER
DNA-TR-94-117

11. SUPPLEMENTARY NOTES
This work was sponsored by the Defense Nuclear Agency under RDT&E RMC Code B4662D AC BD 00010 4400A 25904D.

12a. DISTRIBUTION/AVAILABILITY STATEMENT
Approved for public release; distribution is unlimited.

12b. DISTRIBUTION CODE

13. ABSTRACT *(Maximum 200 words)*

The current documentation reports results obtained from a recent technical study which included: diagnostics support for a series of agent expulsion experiments at the Waterways Experiment Station (WES), further analysis of wind tunnel measured results from the Dust Sweep Up investigation completed just prior to the present program and dust scouring experiments for soils simulating such real surface "textures" as ridges, clods, stubble, gravel and moisture content.

Some typical findings from the Real Surface experimental study include: 1. Real surface "textures" consistently caused reduction in lofting rates relative to flat erodible soil beds. (For the range of surface conditions tested no enhancement was observed.) A parameter, the Soil Erodibility Factor (SEF) which varies from 1

14. SUBJECT TERMS			15. NUMBER OF PAGES
Dust Sweep-Up	Threshold Velocities	Boundary Layer	276
Soil Erosion	Expulsion Jets	Dust Lofting	16. PRICE CODE
Real Surface Sweep-Up	Chem/Bio Plume Dispersion	Airblast Jets	

17. SECURITY CLASSIFICATION OF REPORT	18. SECURITY CLASSIFICATION OF THIS PAGE	19. SECURITY CLASSIFICATION OF ABSTRACT	20. LIMITATION OF ABSTRACT
UNCLASSIFIED	UNCLASSIFIED	UNCLASSIFIED	SAR

CLASSIFIED BY:

N/A since Unclassified.

DECLASSIFY ON:
N/A since Unclassified.

13. ABSTRACT (Continued).

to 0 depending on the real surface condition of interest, showed promise at providing an approximate method for treating dust lofting for realistic soils. For example, soil loss data for non-erodible ridge experiments collapsed favorably when scaled with ridge elevation as normalized by ridge spacing. Soil loss was shown to reduce to 10% of flat erodible soil values when the normalized elevation was 10% or greater; 2. Unique threshold velocities for large particles (gravel, rock, etc.) as measured herein were substantially higher ($\simeq$ x 3) at movement onset than established results based on extrapolating low-speed/small-particle results. Dust mass lofting to altitude will therefore be moderately larger when predicted based on historical velocity criteria as compared to current results. Favorable correlation for established/current measurements with a drag to weight ratio of ($\simeq$) 3 was demonstrated; and 3. For soils "moist-to-the-touch" negligible dust lofting was experienced even up to wind tunnel speeds as high as 375 ft/sec. Moisture content for these "moist" soils was of the order of 5% to 25% at test time. When sufficient cure time was provided and soils dried out to surface moisture levels of 1-2%, thin frangible crusts were formed on the surface. Dust lofting did occur for these "crust" soils but at substantially higher values of shear velocity than nominal for dry loose soil beds. Since such a minimal amount of moisture effectively eliminates lofting, it may be appropriate to treat the soil moisture issue on the basis of an either/or approximation, namely, the soil surface is either moist or dry corresponding to an SEF of 0 or 1, respectively.

ERRATA

for

DNA-TR-94-117

UNCLASSIFIED

Dust Sweep-Up Experiments

This report was published without the Disclaimer Notice on the inside of the Front Cover. The Disclaimer Notice should read:

Review of this material does not imply Department of Defense endorsement of factual accuracy or opinion.

Please insert the Disclaimer Notice, using the adhesive-backed paper provided, on the inside front cover.

"Review of this material does not imply Department of Defense indorsement of factual accuracy or Opinion."

PREFACE

The work reviewed in this report was sponsored by the Defense Nuclear Agency under the "Dust Sweep-Up Experiments" program (DSUE program; DNA001-92-C-0108). The authors wish to especially thank Dr. Charles R. Gallaway and Lt. Col. Mark E. Byers, the contract technical monitors at the start and conclusion of the DSUE program, respectively, for their direction, support and encouragement. Special thanks are also due to Dr. Allen Kuhl (LLNL), Mr. Tom Mazzola (RDA), Mr. Dick Denison (CRT), and Dr. Phillip Hookham (CRT) for their many valuable discussions and technical recommendations. Mr. Paul Graham of the Waterways Experiment Station (WES) must be singled out for a special note of appreciation for his outstanding direction and cooperation in supporting TRW on their diagnostics task on WES Event 23.

The authors also wish to acknowledge their indebtedness to Professor Toshi Kubota, DSUE program consultant, and Mr. Mike Petach (TRW) for their many important and creative technical contributions.

CONVERSION TABLE

Conversion factors for U.S. Customary to metric (SI) units of measurement.

MULTIPLY → / ← TO GET	BY → / ← BY	TO GET / DIVIDE
angstrom	1.000 000 X E -10	meters (m)
atmosphere (normal)	1.013 25 X E +2	kilo pascal (kPa)
bar	1.000 000 X E +2	kilo pascal (kPa)
barn	1.000 000 X E -28	meter^2 (m^2)
British thermal unit (thermochemical)	1.054 350 X E +3	joule (J)
calorie (thermochemical)	4.184 000	joule (J)
cal (thermochemical/cm^2)	4.184 000 X E -2	mega joule/m^2 (MJ/m^2)
curie	3.700 000 X E +1	*giga becquerel (GBq)
degree (angle)	1.745 329 X E -2	radian (rad)
degree Fahrenheit	$t_k = (t^\circ f + 459.67)/1.8$	degree kelvin (K)
electron volt	1.602 19 X E -19	joule (J)
erg	1.000 000 X E -7	joule (J)
erg/second	1.000 000 X E -7	watt (W)
foot	3.048 000 X E -1	meter (m)
foot-pound-force	1.355 818	joule (J)
gallon (U.S. liquid)	3.785 412 X E -3	meter^3 (m^3)
inch	2.540 000 X E -2	meter (m)
jerk	1.000 000 X E +9	joule (J)
joule/kilogram (J/kg) radiation dose absorbed	1.000 000	Gray (Gy)
kilotons	4.183	terajoules
kip (1000 lbf)	4.448 222 X E +3	newton (N)
kip/inch^2 (ksi)	6.894 757 X E +3	kilo pascal (kPa)
ktap	1.000 000 X E +2	newton-second/m^2 (N-s/m^2)
micron	1.000 000 X E -6	meter (m)
mil	2.540 000 X E -5	meter (m)
mile (international)	1.609 344 X E +3	meter (m)
ounce	2.834 952 X E -2	kilogram (kg)
pound-force (lbs avoirdupois)	4.448 222	newton (N)
pound-force inch	1.129 848 X E -1	newton-meter (N·m)
pound-force/inch	1.751 268 X E +2	newton/meter (N/m)
pound-force/foot^2	4.788 026 X E -2	kilo pascal (kPa)
pound-force/inch^2 (psi)	6.894 757	kilo pascal (kPa)
pound-mass (lbm avoirdupois)	4.535 924 X E -1	kilogram (kg)
pound-mass-foot^2 (moment of inertia)	4.214 011 X E -2	kilogram-meter^2 (kg·m^2)
pound-mass/foot^3	1.601 846 X E +1	kilogram/meter^3 (kg/m^3)
rad (radiation dose absorbed)	1.000 000 X E -2	**Gray (Gy)
roentgen	2.579 760 X E -4	coulomb/kilogram (C/kg)
shake	1.000 000 X E -8	second (s)
slug	1.459 390 X E +1	kilogram (kg)
torr (mm Hg, 0° C)	1.333 22 X E -1	kilo pascal (kPa)

*The becquerel (Bq) is the SI unit of radioactivity; 1 Bq = 1 event/s.
**The Gray (GY) is the SI unit of absorbed radiation.

TABLE OF CONTENTS

Section		Page
	PREFACE	iii
	CONVERSION TABLE	iv
	FIGURES	vi
1	INTRODUCTION	1
2	COLLATERAL EFFECTS DIAGNOSTICS SUPPORT	5
	2.1 EXPERIMENTAL TECHNIQUE	5
	2.2 RESULTS AND DISCUSSION	10
	2.2.1 WES 1 Snob/Greg Data	10
	2.2.2 WES 3 Snob/Greg Data	15
	2.2.3 WES 5 Snob/Greg Data	17
3	FURTHER REVIEW OF DSU EXPERIMENTAL RESULTS	58
	3.1 CLEAN FLOW VELOCITY SCALING	58
	3.2 SHEAR VELOCITY SCALING OF WSMR/OTTAWA SAND VELOCITY DATA	59
	3.3 DUSTY BOUNDARY LAYER CORRELATIONS	60
	3.4 CORRELATION OF DSU SCOURING RATE MEASUREMENTS	61
4	REAL SURFACE (RS) DUST LOFTING EXPERIMENTS	92
	4.1 RIDGES/CLODS/STUBBLE	94
	4.2 RANDOM ROUGHNESS RESULTS (GRAVEL SEEDED WSMR)	99
	4.3 DISCRETE ROUGHNESS (LEADING EDGE DISTURBANCES)	103
	4.4 THRESHOLD VELOCITIES FOR LARGE PARTICLES (GRAVEL SOIL BEDS)	104
	4.5 THRESHOLD VELOCITIES FOR MOIST WSMR SOIL BEDS	108
5	CONCLUSIONS	154
6	REFERENCES	163
Appendix		
	PRE/POST TEST PHOTOGRAPHS OF DUST BED SURFACES FOR REAL SURFACE EXPERIMENTS	A-1

FIGURES

Figure		Page
2-1	View of WES expulsion experiments test facility with front steel door removed.....	23
2-2	Configuration layout for WES test facility indicating location details for temperature and pressure measurements inside the test chamber.....	24
2-3	Tracer material layout for WES 1 event.....	25
2-4	Tracer material layout for WES 3 event.....	26
2-5	Tracer material layout for WES 5 event.....	27
2-6	Tracer material layout for WES 7 event.....	28
2-7	Snob/Greg probe configuration and yoke mounting holder.....	29
2-8	Configuration drawing of Snob/Greg yoke (Dimension: Inches).....	30
2-9	Configuration drawing of Snob/Greg probe installation on WES 1.....	31
2-10	Pre test photograph of Snob/Greg probe installation for WES 1 event.....	32
2-11	Close-up view of Snob/Greg probe installation prior to WES 1 event.....	33
2-12	Pre test photograph of Snob/Greg rake installation at vent door opening for WES 5 event.....	34
2-13	WES 1 Snob/Greg raw data time histories (1 ms per sample; 11.6" elevation; radial location: ± 0.625").....	35
2-14	WES 1 Snob/Greg thermally corrected data (1 ms per sample).....	36
2-15	WES 1 Snob/Greg thermally corrected data (sample rate: 16μs, t < 0.26 sec; 1 ms, t > 0.26 sec).....	37

2-16 Pre test photograph of particle collector assembly for vent discharge flow on WES 1 event..... 38

2-17 WES 1 dust momentum flux time history..... 39

2-18 WES 1 flow field time histories for vent pipe airblast jet (γ = 1.4; 1 ms per sample)..... 40

2-19 WES 1 vent pipe temperature (TIPI)..... 41

2-20 Velocity for WES 1 vent pipe flow at Snob/Greg probe location..... 42

2-21 Post test photograph of tracer material layout for WES 1 event..... 43

2-22 WES 3 Snob/Greg thermally corrected pressure data (0.35 ms per sample; 10 point average)..... 44

2-23 WES 3 flow field time histories for vent pipe airblast jet..... 45

2-24 Estimates of temperature and velocity for WES 3 vent pipe flow at Snob/Greg probe location..... 46

2-25 WES 5/Yoke 1 Snob/Greg pressure measurements at door vent opening (Thermally corrected; 3" elevation)..... 47

2-26 WES 5/Yoke 1 flow field time histories for the vent door exit opening..... 48

2-27 WES 5/Yoke 1 dust parameter time histories for the vent door exit opening..... 49

2-28 WES 5/Yoke 2 Snob/.Greg pressure measurements at door vent opening (Thermally corrected; 7.5" elevation)..... 50

2-29 WES 5/Yoke 2 flow field time histories for vent door opening..... 51

2-30 Thermocouple temperature data from WES 5/Yoke 2 T/C and comparison with room chamber temperature measurements (T11)..... 52

2-31 WES 5/Yoke 3 Snob/Greg pressure measurements at door vent opening (Thermally corrected; 12.5" elevation)..... 53

2-32	WES 5/Yoke 3 flow field time histories for vent door opening.....	54
2-33	WES 5/Yoke 4 Snob/Greg pressure measurements at vent pipe exhaust (Thermally corrected; 11.6" elevation).....	55
2-34	WES 5/Yoke 4 flow field time histories for vent pipe exhaust.....	56
2-35	Estimate for temperature and velocity for WES 5 vent pipe flow at Snob/Greg probe location.....	57
3-1	Velocity profiles for clean "Astroturf" boundary layers (21' 4" location).....	65
3-2	Velocity profile summary for clean Astroturf boundary layers (21' 4" location)...	66
3-3	Velocity defect profile summary for clean Astroturf boundary layers (21' 4" location).....	67
3-4	Log height velocity profiles for WSMR DSU experiments.....	68
3-5	Log height velocity profiles for Ottawa sand DSU experiments.....	69
3-6	DSU shear velocity summary.....	70
3-7	Velocity scaling summary for DSU experiments.....	71
3-8	Power law velocity scaling summary for DSU experiments (Surface elevation).....	72
3-9	Semilog velocity scaling summary for DSU experiments (Surface elevation).....	73
3-10	Lin-lin velocity scaling summary for DSU experiments (Surface elevation).....	74
3-11	Velocity defect scaling summary for DSU experiments (Surface elevation).....	75
3-12	Power law velocity scaling summary for DSU experiments (Profile focus elevation).....	76
3-13	Semilog velocity scaling summary for DSU experiments (Profile focus elevation).....	77

3-14	Velocity profile scaling for Hartenbaum Ottawa sand experiments (17 foot bed length; profile focus elevation).....	78
3-15	Loading factor profiles for WSMR DSU experiments.....	79
3-16	Loading factor profiles for Ottawa sand DSU experiments.....	80
3-17	Power law scaling of normalized loading factor profiles for DSU experiments (Surface elevation).....	81
3-18	Semilog scaling of normalized loading factor profiles for DSU experiments (Surface elevation).....	82
3-19	Power law scaling of normalized loading factor profile for DSU experiments (Profile focus elevation).....	83
3-20	Semilog scaling of normalized loading factor profiles for DSU experiments (Profile focus elevation.....	84
3-21	Scouring rate summaries for DSU experiments.....	85
3-22	Mach number scaling of scouring rate data for DSU experiments.....	86
3-23	Soil loss summary.....	87
3-24	Particle size scaling of scouring rate data for DSU experiments.....	88
3-25	Shear velocity scaling of scouring rate data for DSU experiments.....	89
3-26	Schmidt number scaling for DSU experiments (Normalized loading factor).....	90
3-27	Schmidt number scaling for DSU experiments (Loading factor).....	91
4-1	DSU Wind Tunnel test section (north side view looking upstream towards facility contraction section).....	113
4-2	X-Ray dust density diagnostics schematic.....	114
4-3	Post test photographs of Gravel Seeded WSMR dust bed: FS74, 367 FPS.....	115

4-4	Pre test photographs of ridge dust bed.....	116
4-5	Side view photographs at 9' test station of ridge dust bed: RS33, 124 FPS, 2" elevation.....	117
4-6	Post test photographs of ridge dust bed: RS32, 116 FPS, 1" elevation.....	118
4-7	Dependence of normalized soil loss on ridge elevation (Ridge separation: one foot).....	119
4-8	Real surface veloctiy profiles at 21' 4" station for ridge soil beds.....	120
4-9	Dependence of normalized soil loss on ridge separation.....	121
4-10	Pre test photographs of clod dust bed looking upstream.....	122
4-11	Pre test photographs looking downstream of stubble dust bed.....	123
4-12	Soil loss versus non-erodible real surface elevation (Axial separation: one foot).....	124
4-13	Real surface velocity profiles at 21' 4" station.....	125
4-14	Downstream view photographs of Gravel Seeded WSMR dust bed: RS70, 130 FPS.....	126
4-15	Downstream view photographs of Gravel Seeded WSMR dust bed: RS73, 227 FPS.....	127
4-16	Downstream view photographs of Gravel Seeded WSMR dust bed: RS74, 367 FPS.....	128
4-17	Downstream view photographs of Gravel Seeded WSMR dust bed at diagnostics station: RS74, 367 FPS.....	129
4-18	Summary of gravel impacts on Bagnold collector and probe strut.....	130
4-19	Soil loss for Gravel Seeded WSMR dust beds.....	131

4-20 Dependence of soil loss on flow exposure time for Gravel Seeded WSMR dust beds..... 132

4-21 Integrated soil loss as a function of flow exposure time for Gravel Seeded WSMR dust beds..... 133

4-22 Typical photographs of P Gravel "dust" bed, RS102 - 107: Pre test..... 134

4-23 Typical photographs of P Gravel "dust" bed, RS102 - 107: Post test..... 135

4-24 Typical photographs of Coarse Gravel "dust" bed, RS93 - 97: Pre test..... 136

4-25 Typical photographs of Coarse Gravel "dust" bed, RS93 - 97: Post test..... 137

4-26 Flow field time histories at 21' 4" station for "P" gravel lofting onset experiments: RS104..... 138

4-27 Flow field time histories at 21' 4" station for "P" gravel lofting onset experiments: RS105..... 139

4-28 Flow field time histories at 21' 4" station for "P" gravel lofting onset experiments: RS107..... 140

4-29 Flow field time histories at 21' 4" station for "Coarse" gravel lofting onset experiments: RS93..... 141

4-30 Flow field time histories at 21' 4" section location for "Coarse" gravel lofting onset experiments: RS96..... 142

4-31 Flow field time histories at 21' 4" station for "Coarse" gravel lofting onset experiments: RS97..... 143

4-32 Typical log height velocity profiles for gravel lofting onset experiments..... 144

4-33 Shear velocity summary..... 145

4-34 Combined shear velocity summary..... 146

4-35 Particle velocity scaling..... 147

4-36	Threshold velocity experiments (RS120, 5%/1% soil moisture, 48 hour cure).....	148
4-37	Threshold velocity experiments (RS125, 5%/2% soil moisture, 24 hour cure).....	149
4-38	Threshold velocity experiments (RS124, 5%/5% soil moisture, 1 hour cure).....	150
4-39	Threshold velocity experiments for moist WSMR soil bed (RS119, 10%/8% soil moisture, 24 hour cure).....	151
4-40	Threshold velocity experiments for moist WSMR soil bed (RS117, 15%/12% soil moisture, 24 hour cure).....	152
4-41	Threshold velocity experiments for moist WSMR soil bed (RS115, 25%/18% soil moisture, 24 hour cure).....	153
A-1	Photographs of Bagnold slot collector and Snob/Greg probe rake - 21' 4" test section location.....	A-2
A-2	Photographs at 9' test section location of ridge dust bed: RS32, 116 fps, 1" elevation.....	A-3
A-3	Overhead photographs at 9' test section location of ridge dust bed: RS38, 227 fps, 1" elevation.....	A-4
A-4	Post test side view photograph at 9' test section location of ridge dust bed: RS38, 227 fps, 1" elevation.....	A-5
A-5	Post test photographs of ridge dust bed: 230 fps, 2" elevation.....	A-6
A-6	Side view photographs at 9' test section location of ridge dust bed: RS39, 367 fps, 1" elevation.....	A-7
A-7	Photographs of ridge dust bed: RS128, 124 fps, 1" elevation; 2' separation.....	A-8
A-8	Photographs of ridge dust bed at 9' station: RS128, 124 fps, 1" elevation, 2' separation.....	A-9
A-9	Post test photograph looking downstream of ridge dust bed: RS129, 240 fps, 1" elevation, 2' separation.....	A-10

A-10 Post test photographs of ridge dust bed at 9' station: RS129, 240 fps, 1" elevation, 2' separation..... A-11

A-11 Photographs of ridge dust bed at 9' station: RS130, 372 fps, 1" elevation, 2' separation..... A-12

A-12 Pre test photograph looking upstream of ridge dust bed: RS126, 116 fps, 2" elevation, 2' separation..... A-13

A-13 Post test photographs of ridge dust bed: RS126, 116 fps, 2" elevation, 2' separation..... A-14

A-14 Post test photographs of ridge dust bed at 9' station: RS126, 116 fps, 2" elevation, 2' separation..... A-15

A-15 Photographs of ridge dust bed looking downstream: RS127, 238 fps, 2" elevation, 2' separation..... A-16

A-16 Photographs of ridge dust bed at 9' station: RS127, 238 fps, 2" elevation, 2' separation..... A-17

A-17 Post test photographs of ridge dust bed: RS131, 376 fps, 2" elevation, 2' separation.. A-18

A-18 Photographs of ridge dust bed at 9' station: RS131, 376 fps, 2" elevation, 2' separation..... A-19

A-19 Post test photographs of clod dust bed: RS46, 120 fps, 1" elevation..... A-20

A-20 Post test photographs of cloud dust bed: RS49, 127 fps, 2" elevation..... A-21

A-21 Post test photographs of clod dust bed: RS49, 127 fps, 2" elevation..... A-22

A-22 Post test photograph of clod dust bed: RS49, 127 fps, 2" elevation - Leading edge view looking downstream, 6' test section location..... A-23

A-23 Post test photographs of clod dust bed: RS47, 234 fps, 1" elevation..... A-24

A-24	Post test photograph of clod dust bed: RS50, 222 fps, 2" elevation - Upstream view..	A-25
A-25	Pre test close up photograph at 9' station of clod dust bed: RS50, 222 fps, 2" elevation.....	A-26
A-26	Post test photographs at 9' station of clod dust bed: RS50, 222 fps, 2" elevation...	A-27
A-27	Post test photographs of clod dust bed: RS48, 361 fps, 1" elevation.....	A-28
A-28	Photographs looking upstream of stubble dust bed: RS58, 121 fps, 1" elevation.....	A-29
A-29	Photographs of stubble dust bed: RS56, 121 fps, 2" elevation.....	A-30
A-30	Photographs of stubble dust bed leading edge - 6' test section location: RS59, 230 fps, 1" elevation.....	A-31
A-31	Photographs of stubble dust bed: RS57, 231 fps, 2" elevation.....	A-32
A-32	Side view photographs at 9' test section location of stubble dust bed: RS57, 231 fps, 2" elevation.....	A-33
A-33	Post test photographs of stubble dust bed: RS60, 335 fps, 1" elevation.....	A-34
A-34	Overhead view photographs at 9' test section location of stubble dust bed: RS60, 335 fps, 1" elevation.....	A-35
A-35	Post test photographs of stubble dust bed: RS61, 356 fps, 2" elevation.....	A-36
A-36	Upstream view photographs of Gravel Seeded WSMR dust bed: RS70, 130 fps.....	A-37
A-37	Downstream view photographs of Gravel Seeded WSMR dust bed at diagnostics station: RS70, 130 fps.....	A-38
A-38	Overhead view photographs of Gravel Seeded WSMR dust bed at 9' location: RS70, 130 fps.....	A-39
A-39	Post test photograph of Gravel Seeded WSMR dust bed: RS70, 130 fps - Overhead view at 9' location looking upstream.....	A-40

A-40 Overhead close up view photographs of Gravel Seeded WSMR dust bed at 9' location: RS70, 130 fps..... A-41

A-41 Overhead close up view photographs of Gravel Seeded WSMR dust bed at 15' location: RS70, 130 fps..... A-42

A-42 Post test photograph of Gravel Seeded WSMR dust bed: RS70, 130 fps - Side view at 9' location..... A-43

A-43 Post test photographs of Gravel Seeded WSMR dust bed: RS71, 122 fps..... A-44

A-44 Post test photographs of Gravel Seeded WSMR dust bed: RS71, 122 fps..... A-45

A-45 Post test photographs of Gravel Seeded WSMR dust bed: RS71, 122 fps..... A-46

A-46 Post test photographs of Gravel Seeded WSMR dust bed: RS72, 134 fps..... A-47

A-47 Post test photographs of Gravel Seeded WSMR dust bed: RS72, 134 fps..... A-48

A-48 Post test photographs of Gravel Seeded WSMR dust bed: RS72, 134 fps..... A-49

A-49 Upstream view photographs of Gravel Seeded WSMR dust bed: RS73, 227 fps..... A-50

A-50 Downstream view photographs of Gravel Seeded WSMR dust bed at diagnostics station: RS73, 227 fps..... A-51

A-51 Overhead photographs of Gravel Seeded WSMR dust bed at 9' location: RS73, 227 fps.. A-52

A-52 Post test overhead view photograph of Gravel Seeded WSMR dust bed looking upstream at 9' location: RS73, 227 fps..... A-53

A-53 Overhead close up view photographs of Gravel Seeded WSMR dust bed at 9' location: RS73, 227 fps..... A-54

A-54 Overhead close up view photographs of Gravel Seeded WSMR dust bed at 15' location: RS73, 227 fps..... A-55

A-55	Upstream view photographs of Gravel Seeded WSMR dust bed: RS74, 367 fps.....	A-56
A-56	Post test upstream view of Gravel Seeded WSMR dust bed: RS74, 367 fps.....	A-57
A-57	Overhead view photographs of Gravel Seeded WSMR dust bed at 9' location: RS74, 367 fps.....	A-58
A-58	Post test overhead view photograph of Gravel Seeded WSMR dust bed looking upstream at 9' location: RS74, 367 fps.....	A-59
A-59	Overhead close up view photographs of Gravel Seeded WSMR dust bed at 9' location: RS74, 367 fps.....	A-60
A-60	Overhead close up view photographs of Gravel Seeded WSMR dust bed at 15' location: RS74, 367 fps.....	A-61
A-61	Post test photographs of Snob/Greg probe rake and Bagnold collector: RS74, 367 fps.....	A-62
A-62	Post test photographs of Snob/Greg probe nose tips: RS74, 367 fps.....	A-63
A-63	Post test photograph of Snob/Greg probe rake and Bagnold collector: RS74, 367 fps.....	A-64
A-64	Pre test photographs of WSMR dust bed with leading edge disturbance - 1.5" ridge: RS62, 124 fps.....	A-65
A-65	Post test photographs of WSMR dust bed with leading edge disturbance - 1" ridge: RS64, 124 fps.....	A-66
A-66	Post test photographs of WSMR dust bed with leading edge disturbance - 1.5" ridge: RS62, 124 fps.....	A-67
A-67	Post test photographs of WSMR dust bed with leading edge disturbance - 1.5" ridge: RS63, 229 fps.....	A-68
A-68	Pre test photographs of WSMR dust bed with leading edge disturbance - Single row clods: RS55, 122 fps, 2" RS elevation....	A-69

A-69 Post test photographs of WSMR dust bed with leading edge disturbance - Single row clods: RS55, 122 fps, 2" RS elevation.... A-70

A-70 Pre test photographs of WSMR dust bed with leading edge disturbance - Single row clods: RS68, 129 fps, 7" RS elevation.... A-71

A-71 Post test photographs of WSMR dust bed with leading edge disturbance - Single row clods: RS68, 129 fps, 7" RS elevation.... A-72

A-72 Post test photographs of WSMR dust bed with leading edge disturbance - Single row clods: RS69, 234 fps, 7" RS elevation.... A-73

A-73 Pre test photographs of WSMR dust bed with leading edge disturbance - Double row clods: RS52, 235 fps, 1" RS elevation.... A-74

A-74 Post test photographs of WSMR dust bed with leading edge disturbance - Double row clods: RS51, 127 fps, 1" RS elevation.... A-75

A-75 Post test photographs of WSMR dust bed with leading edge disturbance - Double row clods: RS51, 127 fps, 1" RS elevation.... A-76

A-76 Post test photographs of WSMR dust bed with leading edge disturbance - Double row clods: RS52, 235 fps, 1" RS elevation.... A-77

A-77 Pre test photographs of WSMR dust bed with leading edge disturbance - Double row clods: RS53, 122 fps, 2" RS elevation.... A-78

A-78 Post test photographs of WSMR dust bed with leading edge disturbance - Double row clods: RS53, 122 fps, 2" RS elevation.... A-79

A-79 Post test photographs of WSMR dust bed with leading edge disturbance - Double row clods: RS54, 232 fps, 2" RS elevation.... A-80

A-80 Pre test photographs of WSMR dust bed with leading edge disturbance - Vortex generator array: RS76, 234 fps, 1" RS elevation..... A-81

A-81 Post test photographs of WSMR dust bed with leading edge disturbance - Vortex generator array: RS75, 122 fps, 1" RS elevation..... A-82

A-82 Post test photographs of WSMR dust bed with leading edge disturbance - Vortex generator array: RS76, 234 fps, 1" RS elevation..... A-83

A-83 Post test photographs of WSMR dust bed with leading edge disturbance - Vortex generator array: RS76, 234 fps, 1" RS elevation..... A-84

A-84 Post test photographs of WSMR dust bed with leading edge disturbance - Vortex generator array: RS77, 364 fps, 1" RS elevation..... A-85

A-85 Post test photographs of WSMR dust bed with leading edge disturbance - Vortex generator array: RS77, 364 fps, 1" RS elevation..... A-86

A-86 Pre test photographs of WSMR dust bed with leading edge disturbance - Vortex generator array: RS80, 367 fps, 2" RS elevation..... A-87

A-87 Post test photographs of WSMR dust bed with leading edge disturbance - Vortex generator array: RS78, 120 fps, 2" RS elevation..... A-88

A-88 Post test photographs of WSMR dust bed with leading edge disturbance - Vortex generator array: RS79, 232 fps, 2" RS elevation..... A-89

A-89 Post test photographs of WSMR dust bed with leading edge disturbance - Vortex generator array: RS80, 367 fps, 2" RS elevation..... A-90

SECTION 1
INTRODUCTION

Since the early 1980's, the Defense Nuclear Agency has been investigating the phenomenology of dust lofting due to airblast dust entrainment and high speed boundary layer flows. Both field tests (Pre Direct Course, 1982; Direct Course, 1983; Mini Scale, 1984; Minor Scale, 1985; Misty Picture, 1987 and Miser's Gold, 1989) and laboratory scale experiments (e.g., Batt et al, 1986, 1990, 1992, and 1993) have been performed, all in support of refining/upgrading dust sweep-up models and hydrocode predictions of Nuclear Event (NE)/High Explosive (HE) dust cloud behavior. Companion analytical studies (e.g. Rosenblatt, et al, 1985; Denison and Baum, 1986; Pierce, 1989; Barthel, 1990; Bacon et al 1991; Kuhl et al, 1993) have been conducted simultaneously with the experimental effort and close interaction between the two technical approaches has been maintained (e.g. Gaj and Small, 1989; Kuhl et al, 1990; Schneider et al, 1993; Hookham et al, 1994). The current documentation reports results obtained from a recent technical study which included diagnostics support for a series of agent expulsion experiments at the Waterways Experiment Station (WES), further analysis of wind tunnel measured results from the Dust Sweep Up investigation completed just prior to the present program (Batt et al, 1993) and dust scouring experiments for soils simulating such real surface "textures" as ridges, clods, stubble, gravel and moisture content.

The dispersion of the discharge plume from hardened chemical/biological (CB) storage bunkers due to conventional bomb strike damage represents a threat to friendly forces and non-combatants. DNA, in addressing this issue under its Collateral Effects Environment program, chartered WES to conduct a series of experiments during CY 92 and 93 to investigate expulsion of agent simulants from scale model structures due to internal detonations (Graham, 1993 and 1994). The experimental study was performed using a 1/6th scale steel facility and the effects of vent

opening, simulant layout and detonation size/location were investigated. Both internal and external diagnostics were fielded in support of the investigation with TRW providing instrumentation (Snob/Greg probes) to measure discharge plume characteristics on three of the WES test events.

Over the years, a number of approaches have been considered by NE hydrocode developers for treating dust sweep-up. Such approaches include not only direct numerical simulation techniques, e.g. Kuhl (1990), but various analytical methods for modeling the airblast induced dusty boundary layer. In general these latter models are based on a "dusty law of the wall" formulation (e.g., Denison, 1986) using ether mixing length (Rosenblatt, et al, 1985) or K-ε (Pierce, 1989; Barthel, 1990) turbulence models. In some cases, closure of the governing hydrocode calculations for the ground's boundary condition has been accommodated by use of a power law dependence of scouring rate on edge mass flux (Gaj and Small, 1989). This closure issue is an important concern of the modelers since an approach is required which is both realistic and yet compatible with the flow's governing equations and calculation format (mesh configuration, etc.).

Recently, modelers have been in favor of characterizing boundary layer performance in terms of local shear velocities (Gaj and Small, 1989; Denison, 1990; Pierce, 1989; Traci and Su, 1988) and a threshold friction velocity for "particle suspension" (e.g., Gaj and Small, 1989). Evidence of the wide variation in sweep-up formulation is illustrated by the diversity in magnitude and trends for the calculated scouring rates. A demonstration of scouring rate sensitivity to threshold velocity is available in the excellent and comprehensive review by Gaj and Small (1989) which documents results of calculations of sweep-up performance for a wide range of surface texture/soil condition.

Measured dust sweep-up results from the DSU wind tunnel experiments by Batt, et al (1963) have extended the "monosized" Ottawa sand data of Hartenbaum (1971), for one axial distance, to multiple soil bed lengths and to desert soil conditions (WSMR dust). The DSU velocity and dust density profile data and redundant measurements of dust scouring rates have already provided some use in validating/upgrading several of the noted sweep-up models (e.g. Hookham et al, 1994). It was known at the time of the Batt, et al (1993) results, however, that additional analysis of the assembled data base was appropriate in order to fully interpret the combined set of measurements. For that reason, Task Two under the DSUE program was scoped out to perform such an extended review effort, with the present write-up summarizing those scaling results not reported on previously.

The existing DSU dust lofting results (Batt et al, 1993) correspond to measurements for flat erodible soil beds. Similar data for realistic soils under high speed flow conditions are limited in extent and/or unavailable. The lack of detailed results for real surface dust lofting causes code calculations to be performed in many cases with unproven assumptions regarding the sweep-up process. Without applicable data with which to anchor the respective models, wide disparity and trends in final results is commonplace. The real surface dust scouring data to be reported on herein were obtained in the DSU program wind tunnel and thus extend the DSU measurements to realistic soils, i.e. real surface soils with ridges, clods, stubble, "gravel", moisture, etc.

In Section 2, which follows, Snob/Greg data from the WES expulsion experiments are presented. Section 3 discusses findings from the extended review and analysis of the DSU measurements and results from the current real surface experiments on dust lofting are provided in Section 4. Conclusions from the study are summarized in Section 5 and report references are listed in

Section 6. The report's Appendix documents selected pre/post test photographs of soil beds for many of the real surface experiments.

SECTION 2

COLLATERAL EFFECTS DIAGNOSTICS SUPPORT

The current documentation reviews and summarizes results from TRW's diagnostics support on three of WES' expulsion tests (WES 1, 3 and 5) using Snob/Greg probes.

2.1 EXPERIMENTAL TECHNIQUE.

All WES expulsion experiments (Graham, 1993 and 1994) were performed in a steel test facility scaled to 1/6th the size of a nominally configured storage bunker tested on the Dice Throw detonation event (White Sands Missile Range, 1979). A photograph of the WES expulsion structure is provided in Figure 2-1 with the steel front door removed. Overall dimensions for the facility (20"H x 68" L x 52"W) are given in Figure 2-2 which also indicates location and type of WES measurement diagnostics. The facility's vent pipe (2 1/2" diameter, 17" long), which is representative of a bomb penetration hole, is shown in Figure 2-1 centered on the roof of the upper left chamber. This chamber was used for the TRW/WES experiments with the internal detonations being generated by either 0.95 lb (WES 1) or 0.19 lb (WES 3 and 5) of C4 explosive charges. Each charge was positioned along the room centerline at one half (WES 1) or one-quarter (WES 3 and 5) of the distance from the back wall. Simulant material, either spheriglass beads (WES 1, 3 and 5) or fine tracer material (WES 1) was installed on the test chamber floor in either plastic containers (WES 3) or exposed layers/piles (WES 1 and 5). The glass beads corresponded to an untapped bulk density of 88 lb/ft^3 and a mass mean particle size of 66 microns. The bulk density for the tracer material, dry color pigments or a biological agent simulant known as Bassillus Thruingiensis (BT) powder, ranged from 29 to 45 lb/ft^3. Figures 2-3 through 2-6 show configuration layouts for the simulant materials and overall test details are provided in the Test Matrix of Table 2-1.

Events 1 and 3 were conducted with discharge gases/simulant being expelled only through the ceiling vent pipe. To approximate the effects of external door venting, WES 5 was also configured with an open front door sized by shifting the structure's front door plate to create an opening 7"W x 20"H. More complete descriptions of test conditions and test setup details are provided in Graham (1993, 1994).

A photograph of a Snob/Greg probe yoke as used on WES Events 1, 3 and 5 is given in Figure 2-7a. Each yoke for Events 3 and 5 was also equipped with a Medtherm thermocouple (TCFW 202) mounted on the yoke centerline and aligned with the leading edges of the Snob/Greg probes. All T/C's (Chromel/Alumel) were of the butt-welded type and each was equipped with a bleed hole diffuser radiation shield. For ceiling vent yokes (WES 1, 3 and 5) the Snob/Greg probe pairs were mounted 11.6" above the vent exit plane with the Snob/Greg probes straddling the vent centerline ($\pm$0.625").

Configuration drawings for the Snob and Greg probes are given in Figures 2-7b and 2-7c, respectively. The design of the dual probe yoke holder is provided in Figure 2-8. All exterior surfaces of probes and holders were thermally and abrasively protected for the WES experiments with a coating of Devcon's flexane rubber adhesive. For the vent plume measurements the holder was installed in a cruciform mounting structure configured to provide 3D positioning adjustment. To minimize flow interference effects all flow-facing edges of support members were machined to knife edge sharpness. A schematic drawing of the vent mounting assembly is provided in Figure 2-9 and pretest photographs of the assembly as installed are given in Figures 2-10 and 2-11.

On Events 1 and 3 Snob/Greg measurements were performed only at the 11.6" ceiling vent location whereas for WES 5, Snob/Greg data were obtained at both the ceiling vent station (Yoke 4) as well as at three external door locations (Figure 2-12). The "door" yokes

were horizontally oriented at elevations of 3" (Yoke 1), 7.5" (Yoke 2) and 12.5" (Yoke 3) above the chamber floor. Leading edges of each Snob/Greg probe pair were co-located 4" away from the door exit plane with each probe positioned ± .0625" on either side of the opening centerline.

Except for Yoke 2 of WES 5, whose T/C probe tip size was 0.005"D ($t_{response} \simeq$ 25 ms), all T/C's correspond to probe tips of 0.010"D (100 ms). Although all probes survived, a result made possible by intentional use of "sturdy" T/C probes rather than fine wire thermal diagnostics, signal return difficulties and time response limitations were experienced. As a result only data from the Yoke 2 measurements on WES 5 will be presented herein.

The Snob probe (gas only pressure) has been designed as a "tri" sensor probe (Figure 2-7b) wherein three separate transducers are installed in the probe body to measure total, static and differential (dynamic) pressure of the local flow (Batt, et al, 1993). The operating principal behind the vented cavity configuration of the Tri Sensor Snob is based on the results of Dussard and Shapiro (1958) who demonstrated that measurements of air total pressure under particulate flow conditions are possible with a vented cavity approach. Their innovative design concept permitted particle flow-through while causing air stagnation due to the area constriction at the discharge nozzle. Their results pointed out that the cavity length-to-diameter ratio should be ≥ 5 and that the total pressure sensing tap must be located "close" to the probe's leading edge to ensure negligible enhancement of measured total pressure due to air/dust interaction effects. For this reason conventional total pressure probes cannot be used in dusty flows because measured pressures include both air stagnation pressure and dust momentum flux contributions. Typically, dusty flow pressure measurements show that air-only total pressures (Snob) are lower than corresponding Greg pressures (gas-plus-dust "total" pressure). Reduced velocity data using conventional total pressure diagnostics would then "measure" velocities on the high

side with data users being unable to assess the extent or onset time of dust loading phenomena.

A measure of the flow's gas-plus-dust total "pressure" is provided by the Greg gauge whose front-face force plate is coupled directly to the transducer's sensing element (Figure 2-4c). The Greg gauge as well as the Tri Sensor Snob are manufactured by Kulite, Inc. and have been extensively tested at high loadings in shock tubes, wind tunnels and under field test conditions. The gauges have proven to be reliable in terms of survival performance and calibration/baseline stability. To accommodate mild thermal sensitivity effects, all transducers are temperature compensated in terms of both linearity coefficient and baseline offset. Also all Snob and Greg probes have not only been oven and pressure chamber calibrated but have received end-to-end integration/validation testing in TRW's 17" Shock Tube at shock overpressures consistent with WES flow conditions.

The basic performance theory behind Snob/Greg measurements in dusty flows can be summarized in an approximate manner by reviewing the dusty gas stagnation pressure relationships for incompressible flow:

$$P_S = p + 1/2\rho_a u_a^2 + C_s \rho_d u_a^2 \qquad (Snob) \qquad (2.1)$$

$$P_G = p + 1/2\,\rho_a u_a^2 + C_G\,\rho_d u_d^2 \qquad (Greg) \qquad (2.2)$$

Here, p, ρ and u refer to the local static pressure, density and velocity with subscripts a, d, S and G referring to air, dust, Snob, and Greg, respectively. C_S and C_G represent dust registry coefficients which for "ideal/perfect" gauges, wherein particles can be assumed to be sufficiently "large" as to be uninfluenced by probe geometrics, are 0 and 1, respectively. In principle the "perfect" Snob responds only to gas phase pressures whereas the Greg probe measures both the gas stagnation pressure and the full

effects of local dust momentum flux. For the ideal case, the dust momentum flux thus becomes:

$$\rho_d u_d^2 = P_G - P_S \tag{2.3}$$

and under conditions of equilibrium dusty flow (i.e., $u_d = u_a$ the dust loading factor k $(= \rho_d / \rho_a)$ is given by:

$$k = \frac{P_G - P_S}{2(P_S - p)} \tag{2.4}$$

Corresponding relationships for Mach number (M) and dynamic pressure (q) are given by:

$$M = \{[p / P_S)^{(\gamma-1)/\gamma} - 1](\frac{2}{\gamma - 1})\}^{0.5} \tag{2.5}$$

where p = local static pressure (also measured by the Tri Sensor Snob)

γ = specific heat ratio ($\simeq$ 1.2 - 1.4)

$$q = \frac{\gamma}{2} pM^2 \tag{2.6}$$

Finally, combining the above results with assumed and/or measured temperature data (T), both velocity (u) and dust density (ρ) can be deduced as follows:

$$u = Ma \tag{2.7}$$

$$a = [\gamma \overline{R} T]^{0.5} \tag{2.8}$$

where a = speed of sound

$\overline{R}$ = gas constant

$$\rho_d = k\,(P / \bar{R}T) \qquad (2.9)$$

For all events, Snob/Greg data were recorded both by TRW using a Kontron portable computer (386/20) and by WES with a 12 bit digitizer recorder. Raw and processed results have been retained on storage discs and can be further reduced to assist additional analyses and/or to evaluate finer time resolution features if warranted.

2.2 RESULTS AND DISCUSSION.

2.2.1 WES 1 Snob/Greg Data.

All eight output signals (4 transducer and 4 "thermal" channels) for the WES 1 event (10 December 1992; 0.95 lbs C4 explosive charge) were recorded on two RC electronics A/D data acquisition cards (12 bit digitizers) installed in a Kontron portable computer. Each card "stored" 4000 samples of data per channel with the RC1 card operating at 16 μs per sample and RC2 at 1 ms per sample. This sampling rate approach provided results with adequate data overlap as well as good early and late time signal resolution. Reduced results include Greg (air plus dust), Snob total (air only) and Snob static pressure time history data up to 4 sec after event detonation. Performance for all three measurements was nominal as demonstrated by overall signal output behavior and consistency between pre and post test calibration results. Although the Snob's differential pressure transducer also provided some early time data, it failed due to pressure overload at approximately 12 ms after flow onset. (Note that this 25 psid transducer was sized/selected to accommodate low speed wind tunnel measurements for another DNA research program and therefore was survival limited at the 60-70 psi pressures of the WES 1 experiment).

Figure 2-13 shows raw data time history results for the Greg, Snob total and Snob static pressure measurements as recorded by

RC2. Note the baseline offsets evident in Figure 2-13 due to bridge thermal effects. This is not an unexpected result in view of the severe heating environment associated with the hot combustion gases of the vent's fireball exhaust. The intensity of this thermal environment is highlighted by the post test appearance of probe exterior surfaces which demonstrates that the flexane coatings were substantially ablated/melted during the WES 1 test. The good survival performance and excellent data return, evident in Figure 2-13 for the Snob/Greg probes is considered an important milestone in development of Snob/Greg technology for airblast testing. The success with the WES Snob/Greg probes represents one of the beneficial results of DNA's support over the years for developing this state of the art diagnostics technique.

Thermal offset-corrected Greg, Snob total and Snob static pressure data are presented in Figures 2-14 and 2-15. These data illustrate excellent late time baseline stability (Figure 2-14) and good data overlap (Figure 2-15c). Note that on WES 1 a flow baffle was mounted on the ceiling vent pipe in support of an exhaust contaminant collection system Figure 2-16;Graham, 1993). The rise and maximizing of plume static pressures at a post detonation time of approximately 40 ms evident in Figure 2-15 and consistent with WES 1 vent pipe measurements, are caused by the constricting effects of the noted collector bag chamber.

Reduced Dust Momentum Flux results (DMF $\equiv \rho_D u_D^2$) are presented in Figure 2-17. Maximum DMF's as high as 30 to 50 psi are in evidence with dust flow duration lasting to approximately 1.8 seconds after flow onset. Similar DMF data obtained by PRi from their LDV/LAT diagnostics on WES 2B are also shown for comparison in Figure 2-17. WES 2B was also a 1 lb detonation event with the PRi measurements being made at the vent pipe exit station. Although differences in magnitude between the two measurements are evident in Figure 2-17, test durations and qualitative trends are in favorable agreement.

Corresponding time history data for Mach number (M), dynamic pressure ($q = \rho u^2 / 2$) and dust loading factor ($k = \rho_{dust} / \rho_{air}$) are shown in Figure 2-18. Except for early time, the flow is observed to be subsonic in nature with a loading factor of the order of 1 to 2. For comparison purposes, vent pipe temperatures (TIPI) measured by WES personnel on Event 1 (Graham, 1993) are provided in Figure 2-19. These data have also been used to compute plume velocities (Equation 2.7) from the Snob/Greg Mach number data and results are given in Figure 2-20. Presented also therein are derived velocities for a lower bound approximation based on using an ambient temperature value for the local speed of sound ($T_{amb} = 63°F$). In general, the two Snob/Greg curves are seen to bracket the LDV velocity data measured by PRi at the pipe exit station on WES 2B, a comparable event to WES 1.

Of interest in evaluating overall vent exhaust performance is the use of the Snob/Greg results to determine an approximate measure of total amount of dust discharged during the WES 1 experiment. Such an estimate for mass expelled (M_x) has been made and is based on the double integral of dust mass flux over the jet radius ($0 \le r \le R$) and time ($0 \le t \le T_1$):

$$M_x = \int_o^T \int_o^R (\rho_D u_D)^2 \, \pi \, r \, dr dt \qquad (2.10)$$

By defining the dust mass flux in terms of dust momentum flux ($\rho_D u_D^2$), Mach number (M) and speed of sound (a_o, "assumed" constant), namely,

$$\rho_D u_D = \rho_D u_D^2 / M a_o \qquad (2.11)$$

$$= B / a_o \qquad (2.12)$$

the mass expelled relationship can be written as:

$$M_x = \frac{2\pi R^2 T_1}{a_o} \frac{B_{CL}}{B_{.625}} \int_o^1 (B / B_{CL})(r / R) d(r / R) d(t / T) \qquad (2.13)$$

where R represents the jet outer radius at the 11.6" elevation location ($R \cong 1.25$") and T_1, the test duration ($\simeq$ 1.8 sec). The subscript "CL" and ".625" correspond to radial locations at the jet centerline and at the r = 0.625" location, respectively. For a Gaussian distribution given by:

$$B / B_{CL} = e^{-h^2 (r/R)^2} \qquad (2.14)$$

where $e^{-h^2} = 0.05$ (*5% edge definition*)

it can be shown that:

$h = 1.73,$

$B_{CL} / B_{.625} \cong 2.11$

and $\int_o^1 (B / B_{CL})(r / R)\, d\,(r / R) \cong 0.20,$

The mass expelled formulation then becomes:

$$M_x = \frac{2\,\pi\, R^2 T}{a_o} (2.11)(0.2) \int_o^1 B_{.625}\, d\,(t / T_1) \qquad (2.15)$$

By approximating $B_{0.625}$ in terms of an average value (Figures 2-17 and 2-18),

$$B_{.625} \equiv (\rho_D u_D^2 / M)_{.625}$$
$$\cong 17 psi$$

a mass expelled estimate can be made, namely

$$M_x\, a_o \cong 3606\ lb\ ft / \sec$$

Although several important assumptions have been made to arrive at the noted ($M_x\, a_o$) magnitude (e.g. Gaussian distribution flow

profiles, time independence, jet radius $\cong 1.25$", etc.) they represent assumptions based on measured WES data and/or nominal jet flow characteristics. Conversely, in computing the final estimate for M_x, uncertainty arises when selecting a value for the flow's local speed of sound, since measured data are unavailable with which to approximate a_o. An approach, however, can be made in determining M_x by evaluating max/min limits to M_x based on an estimated range in a_o values. For example, in ambient air the speed of sound is approximately 1140 ft/sec whereas for WES hot plume gases, the speed of sound is of the order of 2150 ft/sec under the assumption that $\gamma \simeq 1.3$, $MW \simeq 14$ and $T \simeq 1000$°R. (Note, e.g., WES measured vent pipe temperatures of Figure 2-19.) With these magnitudes for the speed of sound setting the maximum and minimum values for mass expelled, respectively, it can be shown that

$$M_x = 2.5 \pm 0.75\, lb$$

The noted M_x value is comparable to a similar derived result made by Ganong (1993) and to a total mass loss based on summing up pre/post test mass sample weighing data (2.4 lb, Graham, 1993). Here the estimated weight for carbon soot expelled from the explosive charge is also included ($\simeq$ 0.2 lb). Note that the magnitude of the expelled mass represents approximately 7% of the pretest beads/tracer weight. This modest amount of expelled mass is consistent with the relatively mild experienced by the simulant bed evident in the post test photograph of Figure 2-21. Such a "mild" expulsion result is consistent, however, with dust scouring experiments performed in shock tubes (Batt, et al, 1991). For these tests suspended dust clouds resulted in substantially higher dust movement when impacted with airblast shocks then when dust lofting occurs due to shock induced boundary layer scouring of dry/loose soil beds. Dust/debris sweep up due to airblasts in confined chambers is, thus, a complex process sensitive to charge characteristics (size, location, elevation, etc.), simulant type/layout and vent geometrics.

2.2.2 WES 3 Snob/Greg Data.

For WES 3 (30 April 1993; Graham, 1994) a single Snob/Greg yoke was suspended 11.6" above the vent pipe exit plane with each probe positioned ± 0.625" on either side of the pipe exhaust centerline. Although a centerline T/C probe (Figure 2-7a) was also installed on WES 3 and survived the test event, data return was poor due to time response limitations and signal over-ranging difficulties. Thus, in lieu of using WES 3 measured T/C plume temperatures to calculate jet velocities from Snob Mach number data, approximate velocity results are provided herein based on temperature data from vent pipe flow measurements (TIPI) from WES 7 (Graham, 1994), a virtual repeat of the WES 3 expulsion test (Table 2-1). The WES 3 results as presented correspond to 10 point average data based on a sample rate of 0.35 ms/sample. Note that the WES 3 raw data were recorded by WES at a rate of 16 μs/sample but have been "depopulated" for processing purposes to a rate of 0.35 ms/sample.

WES 3 was a 0.19 lb detonation event with the exhaust flow unconstrained, in contrast to WES 1 wherein a flow baffle constrictor was externally mounted in support of an exhaust contaminant collection system. The pre test layout for WES 3 simulant material (10 lb Spheriglass beads) included "confining" all bead samples in small plastic bottle containers (Figure 2-4). To simulate container "damage" all bottles were cut with horizontal slices so that the incident shock would "hinge open" the individual containers and, hopefully, result in substantial airblast entrainment. This method of simulant layout, however, was found to be unsatisfactory as small to negligible openings of the containers occurred. Expelled material was of the order of only 1% of the original simulant mass (Graham, 1994), a result consistent with the exhaust gas sampling measurements performed by Los Alamos (Mason, 1993) using a collection tube connected to the outlet of TRW's Snob Probe. Note also that WES 3 simulant setup configuration is in contrast to the WES 7 event wherein the glass beads were spread out on the test structure floor in either

individual piles (8 ea) or as a thin layer on the floor (Figure 2-4). The fact that the expelled mass on WES 7 was of the order of 5% of the pre test simulant mass (5 x WES 3 result) demonstrates the significance of simulant layout to the expulsion process.

Figure 2-22 shows WES 3 baseline corrected data for Greg total, Snob total and Snob static pressure measurements. Derived flow field results (Section 2.1) from these data are given in Figure 2-23 in terms of Dust Momentum Flux, Mach Number and Dynamic Pressure. All data correspond to the 0.625" off centerline position which is approximately at the 50% radial location for the WES 3 "expulsion/airblast" jet. Note the evidence that the flow duration and peak pressure for WES 3 (0.2 lb charge; 1.0 sec, 20 psi) are consistently smaller than corresponding values for WES 1 (1 lb charge; 1.8 sec, 70 psi). The duration data, incidentally, are found to correlate favorably on the basis of cube root scaling.

It is also of interest to mention several other features of the Snob/Greg measurements from the WES 3 experiment. The first result concerns the "ambient" nature of the static pressure trace of Figure 2-22c. The noted data illustrate that exhaust pressures for the WES 3 expulsion jet rapidly return to, and remain at, ambient pressure. This finding is in conflict with measurements obtained for the WES 1 event for which measured jet pressures exceeded local ambient. As suggested above in Section 2.2.1, such a protracted overpressure condition was caused by the constricting effect of the collector bag baffle chamber. The current results for WES 3 serve to validate such an explanation.

The second result which seems appropriate to acknowledge is the DMF data of Figure 2-23c. Within the uncertainty spread of ± 2-3 psi, the data indicate that negligible dust/debris was discharged during the WES 3 event. Pre/post test analysis of simulant weight by WES personnel is consistent with this finding (Graham, 1994).

Finally, an estimate has been made of the WES 3 plume velocity (Equation 2.7) based on Snob Mach number data and calculated values for the local speed of sound (Equation 2.8). Such values correspond to a specific heat ratio (γ =) of 1.35, a gas constant ($\bar{R}$) based on air properties (1716 ft/sec^2 °R), local gas temperatures at the 50% radial location (Figure 2-24a) determined from the WES 7 TIPI data and a Guassian profile assumption:

$$\frac{T1P1 - T_{.5}}{T1P1 - T_e} = e^{-h^2(r/R)^2} . \qquad (2.16)$$

Results shown in Figure 2-24 for both the half radius temperature estimate and the ambient air temperature value of 77°F are seen to compare adequately with LDV measured velocities for WES 7 obtained by PRi at the vent pipe exit station. The velocity "hangup" in the WES 7 PRi data versus the steady decay behavior for the WES 3 results evident in Figure 2-24b is considered indicative of the prolong blast wave effects associated with the higher mass expulsion rates for WES 7 as compared to the "lean" discharge rates for the WES 3 event.

2.2.3 WES 5 Snob/Greg Data.

The WES 5 detonation event (24 June 1993; 0.19 lb C_4 explosive charge; Graham, 1994) was the second test at Waterways Experiment Station for which the venting process included both a ceiling discharge opening and a simulated open door "vent" (Table 2-1). For this expulsion experiment, agent simulant consisted of 50 lbs of spheriglass beads laid out on the test structure floor both as a thin layer on the floor and in eight discrete piles (Figure 2-5). On WES 5, TRW fielded four Snob/Greg yokes which were externally mounted on the test chamber with three yokes positioned at the external door location and the fourth one at the vent pipe exit (Section 2.1).

Reduced results from the WES 5 Snob/Greg measurements are presented in Figures 2-25 through 2-35. Results as shown include baseline corrected pressures, T/C temperature (Yoke 2 only) and such "derived" results as Mach number (M), dynamic pressure (q), dust momentum flux (DMF), dust loading factor ($k = \rho_{dust} / \rho_{air}$), local dust mass flux ($\dot{m}$) and approximate plume velocities (u). The raw data processed herein were recorded using TRW's data acquisition computer (Kontron 386/20) at a sampling rate of 1 ms per data sample. All 28 channels of output data (12 transducer chs, 12 thermal compensation chs and 4 T/C chs) were also recorded by WES at a sampling rate of 16 μs per sample. Additional reduction of measured results can therefore be performed to determine finer time resolution features of the data if warranted.

As can be seen in reviewing the current results, the WES 5 test duration was of the order of 40 ms. This flow duration is substantially shorter than flow times for ceiling-vent only experiments (e.g. WES 3, 1000 ms) because of the additional venting relief provided by the open door on WES 5. Except for the Yoke 1 data, Dust Momentum Flux measurements demonstrate that negligible debris/simulant was discharged at Yoke locations 2, 3 and 4 (Figures 2-29c, 2-32c and 2-34c, respectively). Conversely, DMF and Dust Loading Factor (k) results for Yoke 1 (Figure 2-26c and 2-27a, respectively) indicate that measurable dust flow was experienced at this yoke location (elevation: 3"). Since Yoke 1 was installed nearest to the chamber floor, the current Snob/Greg results suggest that dust movement was caused by sweep-up boundary layer and/or airblast "snowplow" phenomena rather than cloud dispersion effects. The high loading factors measured at the near-floor location ($k \simeq 6$) are consistent with this flow model interpretation.

As noted above (Section 2.1), the T/C data of WES 5 are time response limited due to use of sturdy T/C bead designs. However, peak temperatures were found to be consistent with measurements provided by other investigators with faster response

instrumentation at comparable locations and test conditions. Note that the "T11" data of Figure 2-30 correspond to WES measured floor temperatures inside the WES 5 test chamber on the "left" sidewall at the chamber's mid-line location, a distance 34" from the door opening. The ceiling vent temperature data of Figure 2-35a were acquired by SAIC (Doerr, et al, 1994) on the WES 8 event at a probe elevation (above the vent pipe exit plane) of 25". To approximate "door" velocity data (Figure 2-27b), the Yoke 1 Snob Mach number measurements have been combined (Equation 2.7) with speed of sound estimates corresponding to a specific heat ratio of (γ =) 1.35, an air-based value for the local gas constant ($\overline{R}$) and a peak/ambient average temperature. Similar calculations have been performed to estimate plume velocities for the WES 5 vent pipe flow by using either measured TIPI data (Figure 2-35a) or the WES 5 ambient temperature condition (81°F). These vent pipe results (Yoke 4) are presented in Figure 2-35b which also includes WES 8 pipe exit velocities measured by PRi with LDV diagnostics (Modarress, 1993). In general the resultant velocity uncertainty factors due to the noted temperature approximations are of the order of a modest $\pm$ 15%. Clearly a reduction in this uncertainty limitation can be achieved by conducting future expulsion experiments with finer sized (faster responding) T/C probes (0.5 - 2 mils D). SAIC has demonstrated on WES events 7, 8 and 9 that such an approach with shielded probes is effective not only in terms of signal frequency response but also with regard to probe survival. Future expulsion experiments should threfore be conducted with finer sized T/C probes ($\simeq$ .0005 - 1 mils D) to enhance signal frequency response.

An estimate for mass expelled (M_x) for the WES 5 experiment has been made based on time and area integrating mass flux data ($\dot{m} = \rho_D u_D$) from the Snob/Greg measurements. For this approximation, "derived" mass flux results were obtained by ratioing dust momentum flux data ($\rho_D u_D^2$; 3" elevation results only, since S/G's 2, 3 and 4 measured negligible DMF) to the velocity data of Figure 2-27b. A time history plot of so-derived mass flux

data from the 3" elevation results is provided in Figure 2-27c. To determine mass expelled from such mass flux data, the integral relationship given by:

$$M_x = \int_o^{20} \int_o^{7.5} \int_o^{\infty} \dot{m} dt dx dy \qquad (2.17)$$

is used. By assuming that mass flux is invariant with spanwise distance (x) but is exponentially dependent on elevation (y), i.e.:

$$\dot{m} = ae^{-by} \qquad (2.18)$$

it can be shown that

$$M_x \cong 1.2\ lb \quad (Note: WES\ measured\ M_x \cong 1.4\ lb).$$

For the current S/G M_x estimate, the exponential shape factors are based on

$$\int_o^{\infty} \dot{m}_3 dt = 0.82 lb / ft^2 \ (as\ measured\ at\ 3"\ elevation) \qquad (2.19)$$

$$\int_o^{\infty} \dot{m}_6 dt = 0.05 lb / ft^2 \ ("assumed"\ edge\ condition\ at\ 6"\ elevation) \qquad (2.20)$$

If instead of adopting a 6" elevation for matching the 0.05 lb/ft^2 edge definition, elevations of 5" and 7" are used, mass expelled values of 2.61 and 0.7 lb are calculated, respectively.

One observation regarding the WES 5 Snob/Greg data that may warrant some consideration is the indication that primary mass expulsion occurs at "late" airblast times and under conditions of moderate to low temperatures. Note for example the DMF time history trace for S/G 1 (Figure 2-26c) which suggests that the dust outflow is more the result of secondary flow effects rather than the initial airblast interaction. Since high exhaust

temperatures decay at a rapid rate (Figure 2-30), late time expelled simulant/debris is therefore "cold" and may not be dominated by hot buoyancy force phenomena.

Table 2-1. Test matrix for WES expulsion experiments (CY 92 and 93).

TEST NUMBER	DOOR OPENINGS open/closed			BARE EXPLOSIVE		NUMBER OF CONTAINERS	AGENT WEIGHT	DIAGNOSTIC PARTICIPANTS
	NO. OF ROOMS	INNER	OUTER	WEIGHT (C-4) lbs.	LOCATION FROM BACK WALL in.		lbs.	L - LANL N - NRL/ISI P - PRi S - SAIC SR - SRI T - TRW W - WES-IR WES all tests
①	1	CL	CL	0.95	34.25	0	50	SRI,TRW
2A	1	CL	CL	0.19	34.25	0	50	NRL/ISI,PRi,W
2B	1	CL	CL	0.95	34.25	0	50	NRL/ISI,PRi,W
DE13L	4	O	CL	----	34.25	28	--	
DE14L	4	O	CL	----	34.25	14	--	
③	1	CL	CL	0.19	17.00	8	10	LANL,N,TRW,W
4	1	CL	O	0.19	34.25	8(8)	10	WES-IR
⑤	1	CL	O	0.19	17.00	0	50	NRL/ISI,TRW
PIT	--	--	--	----	----	42	50	NRL/ISI,W
6	2	O	CL	0.19	34.25	40(16)	50	LANL,N,W
7	1	CL	CL	0.19	17.00	0	10	PRi,SAIC
8	2	O	O	0.19	34.25	0	10	PRi,SAIC
9	2	O	CL	0.95	17.00	0	10	SAIC,WES-IR
10	2	O	O	0.95	17.00	16(16)	50***	WES-IR

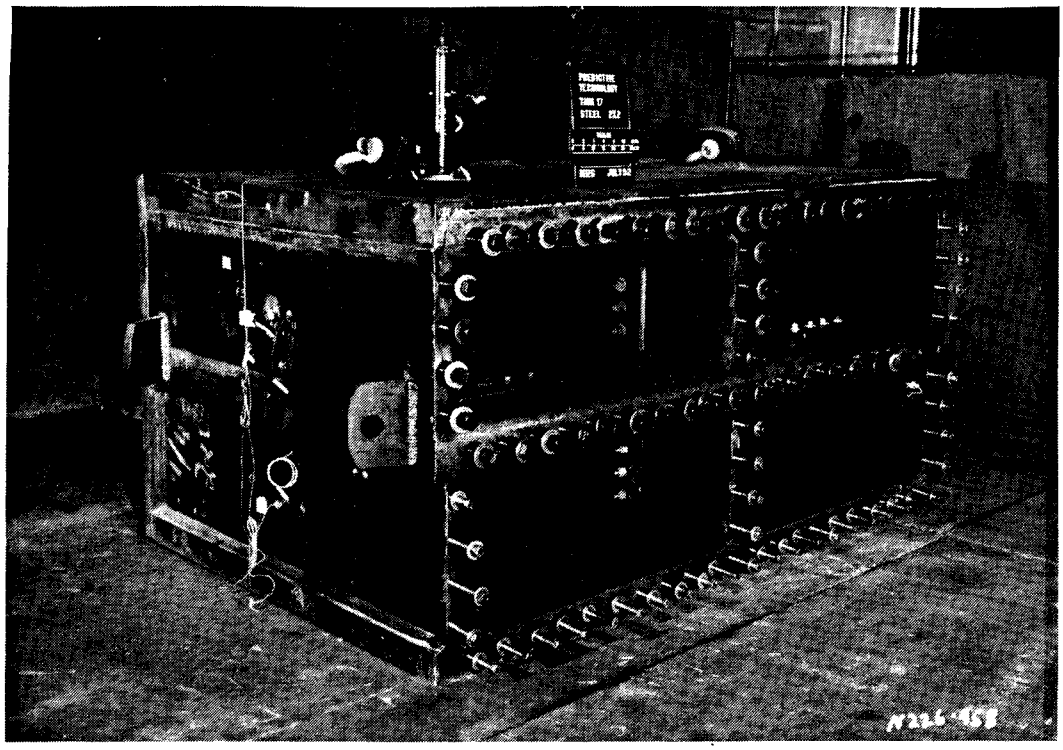

Figure 2-1. View of WES expulsion experiments test facility with front steel door removed.

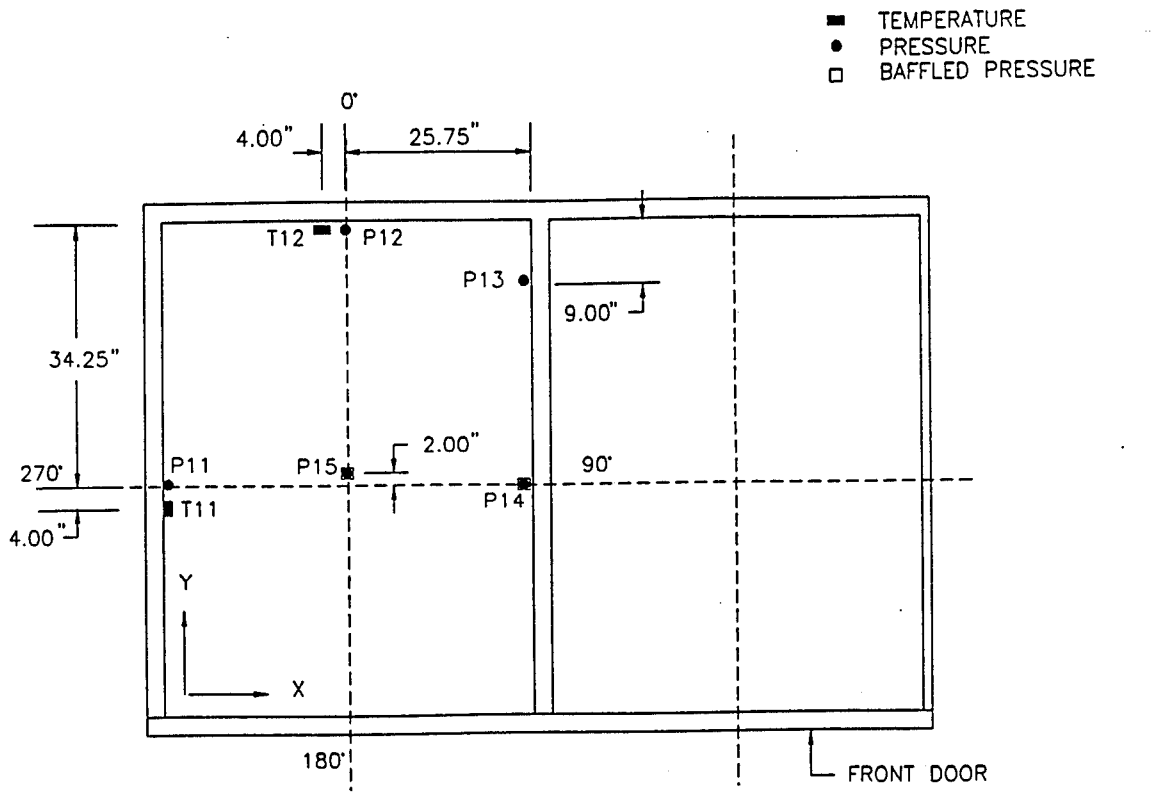

(a) Top view

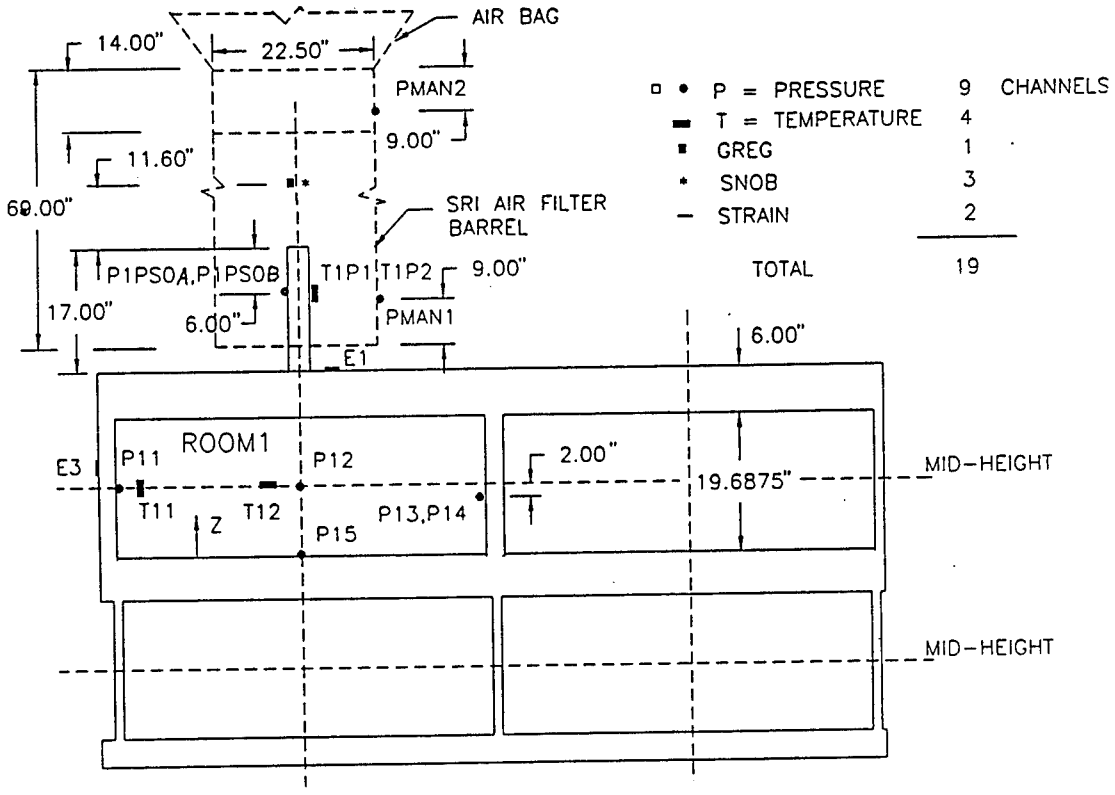

(b) Front view

Figure 2-2. Configuration layout for WES test facility indicating location details for temperature and pressure measurements inside the test chamber.

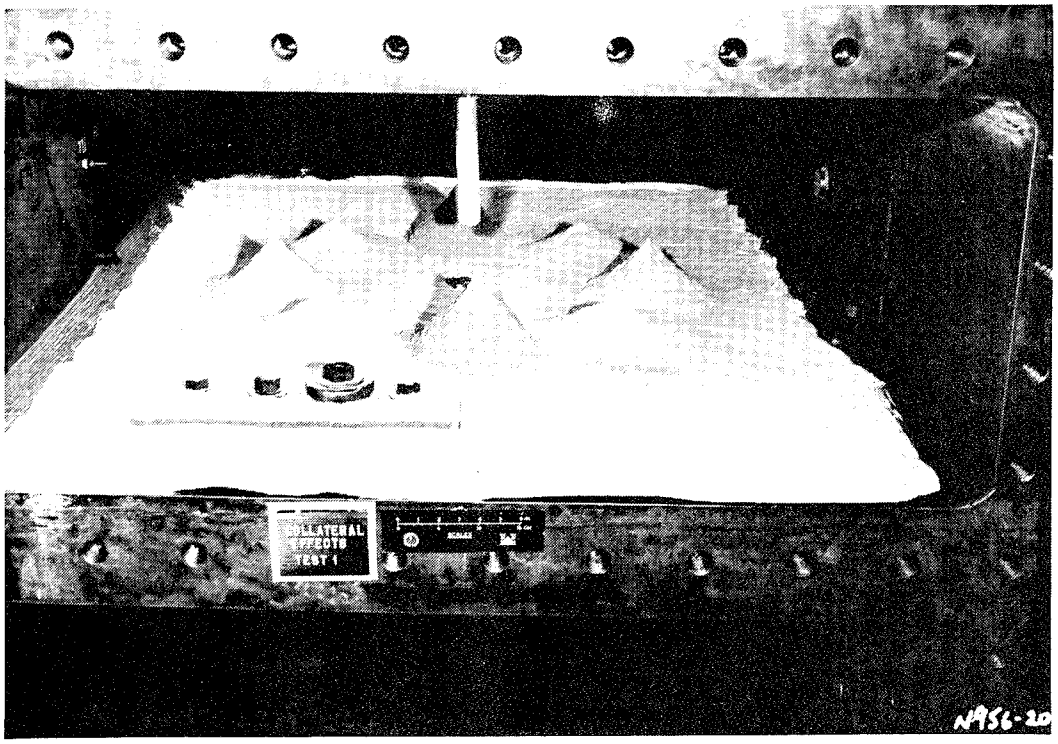

(a) Pre test photograph

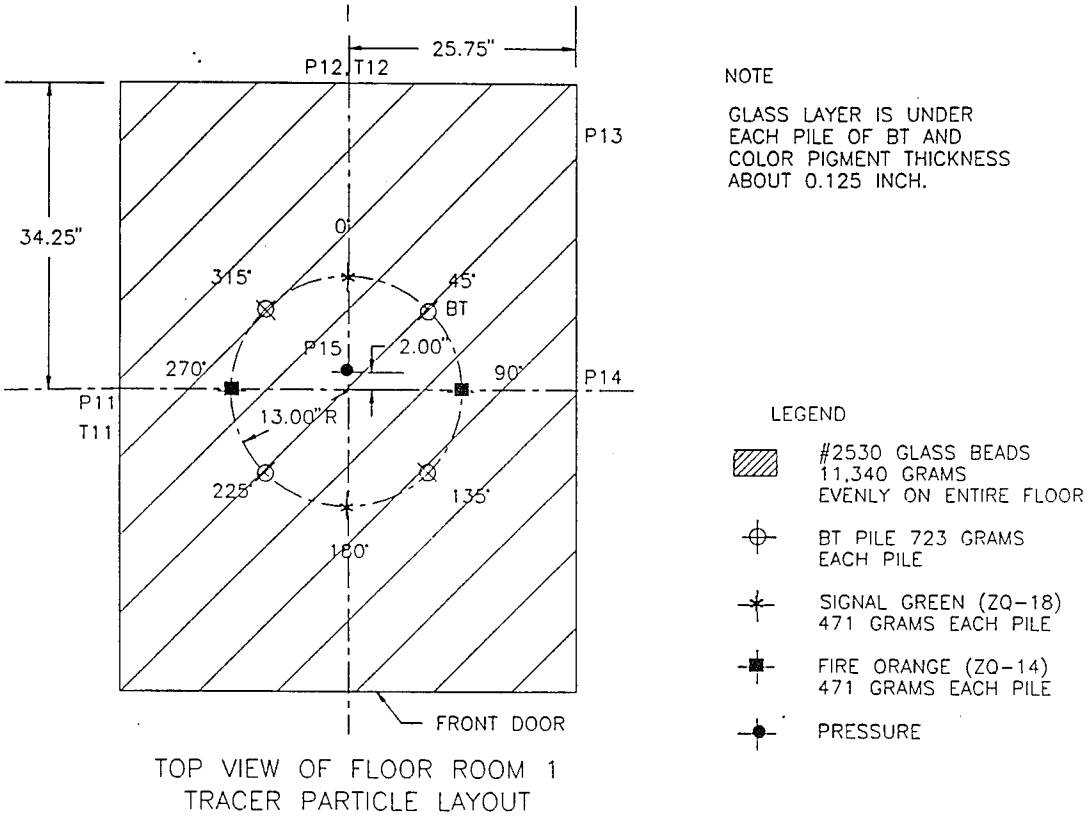

TOP VIEW OF FLOOR ROOM 1
TRACER PARTICLE LAYOUT

(b) Configuration details

Figure 2-3. Tracer material layout for WES 1 event.

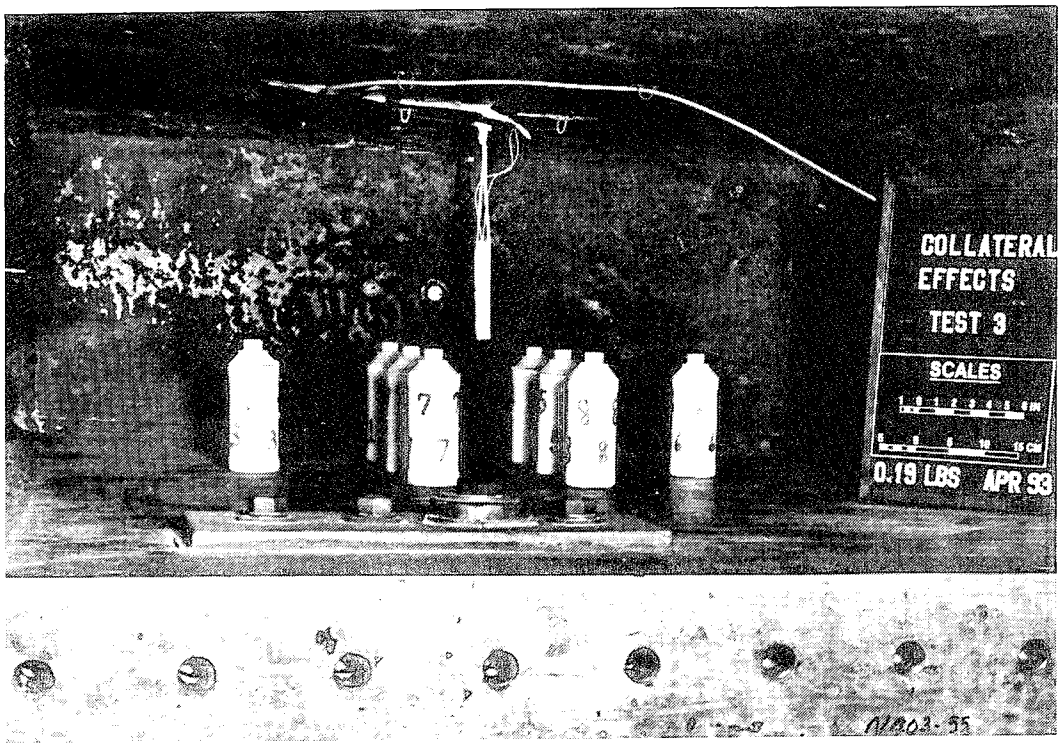

(a) Pre test photograph

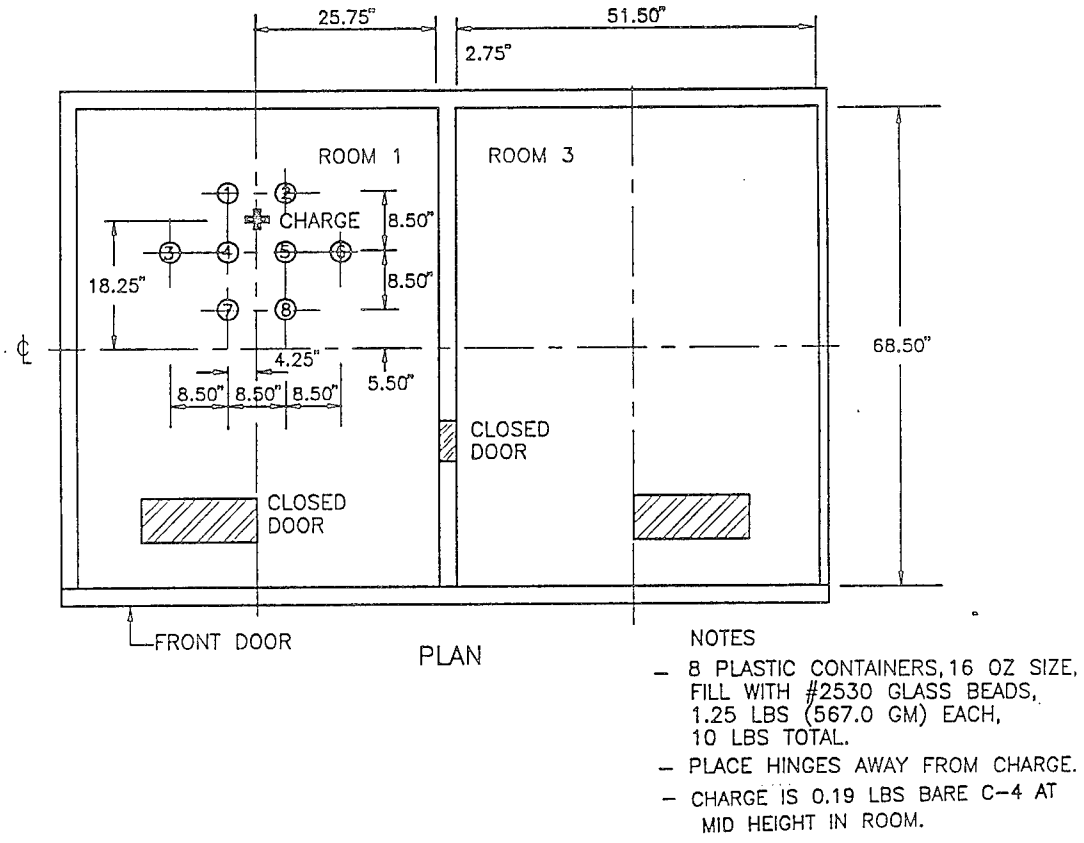

(b) Configuration details

Figure 2-4. Tracer material layout for WES 3 event.

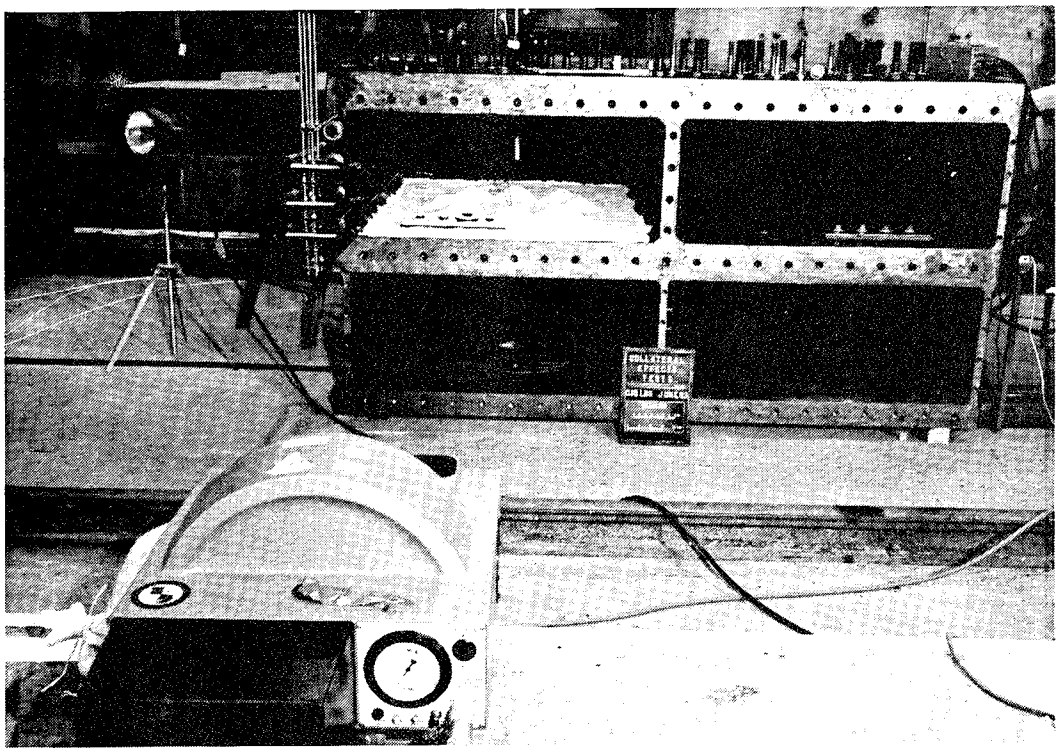

(a) Pre test photograph

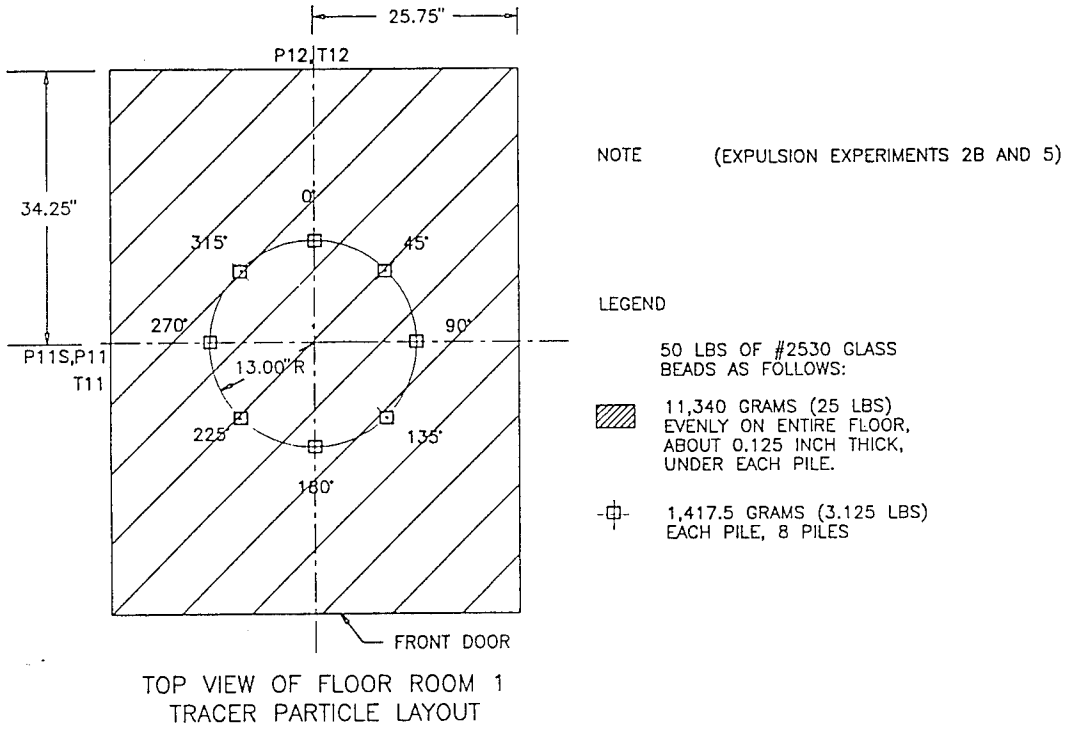

(b) Configuration details

Figure 2-5. Tracer material layout for WES 5 event.

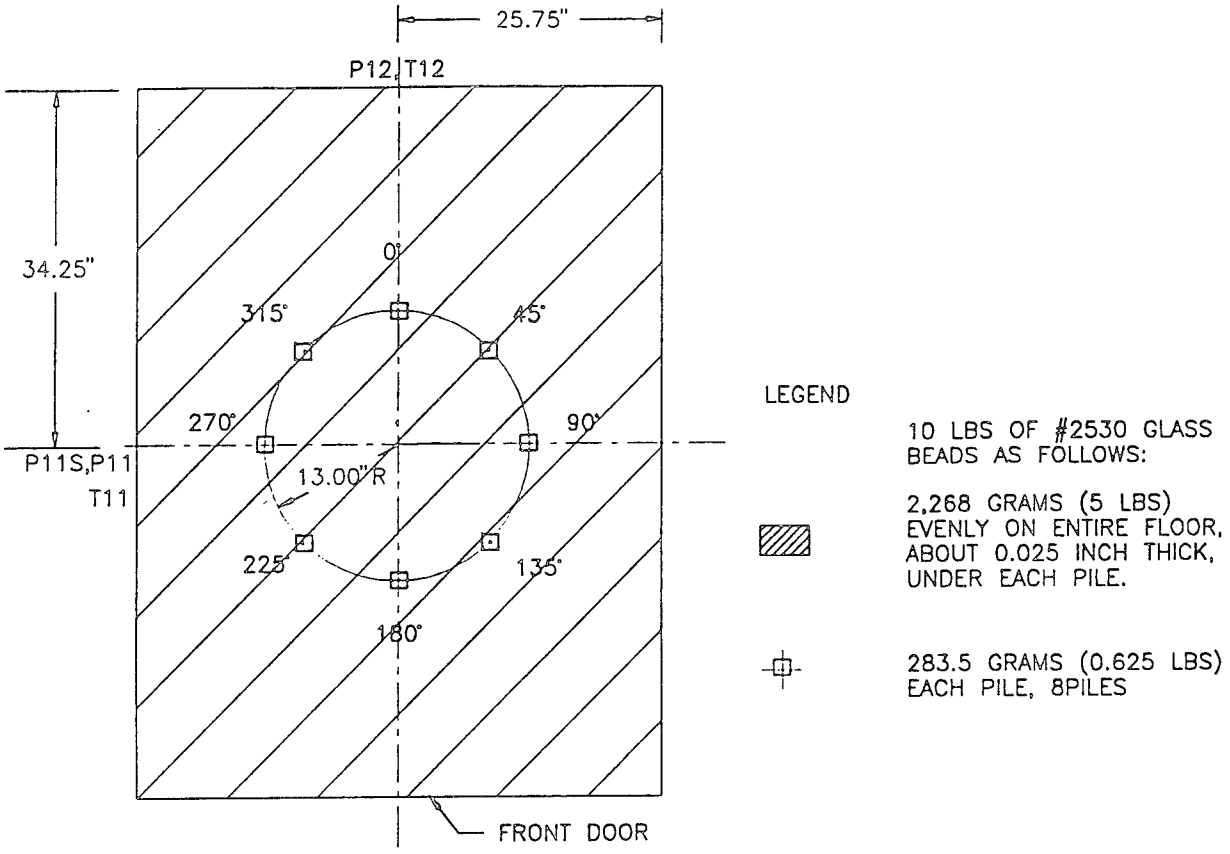

TOP VIEW OF FLOOR ROOM 1
TRACER PARTICLE LAYOUT

Figure 2-6. Tracer material layout for WES 7 event.

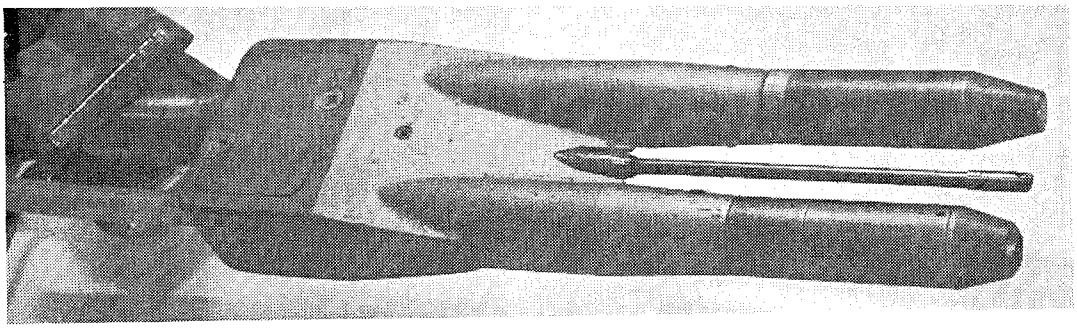

(a) Photograph of Assembled Yoke

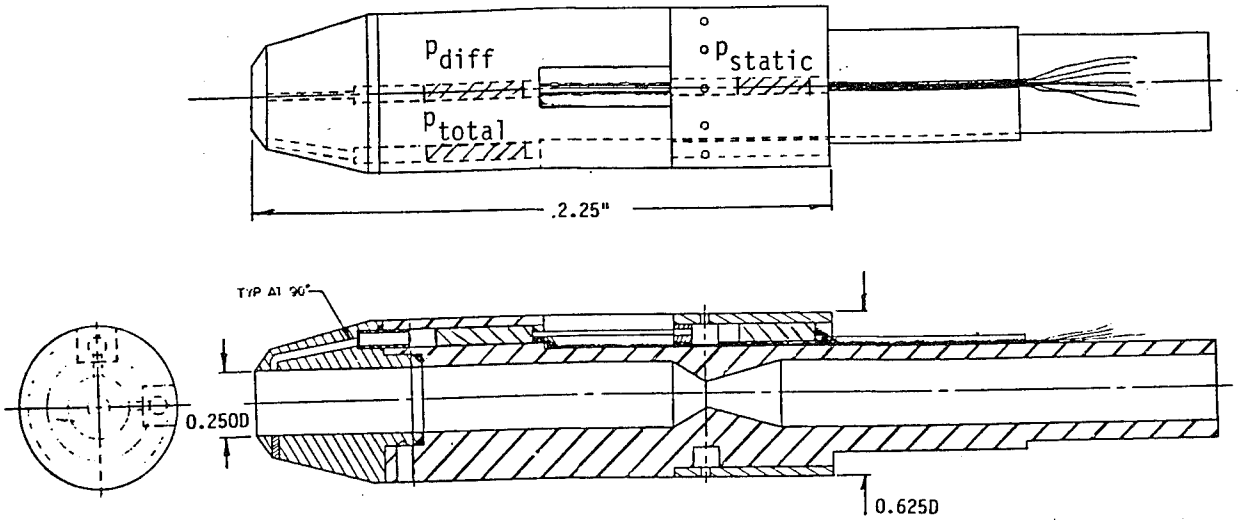

(b) Tri Sensor Snob Probe Configuration

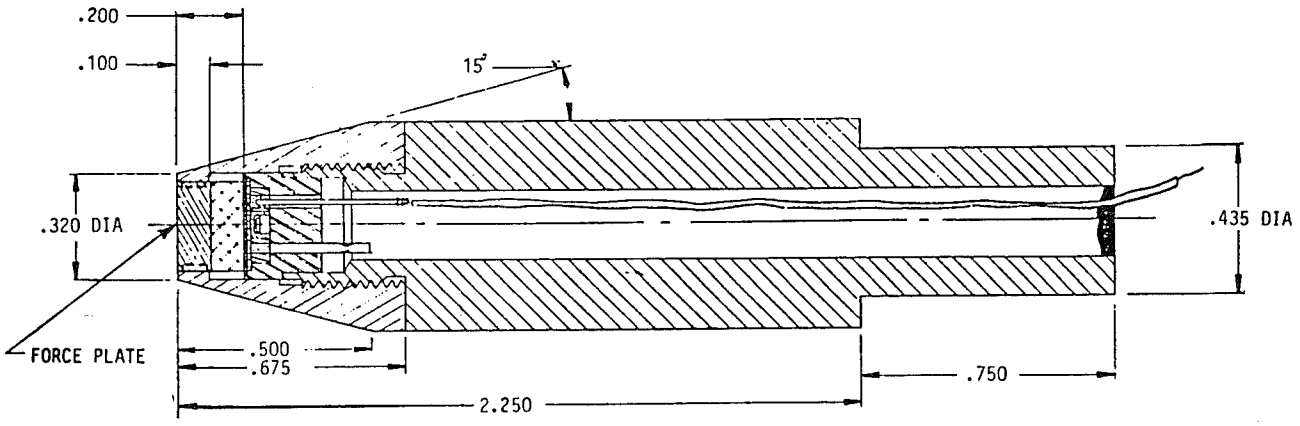

(c) Greg Probe Configuration

Figure 2-7. Snob/Greg probe configuration and yoke mounting holder.

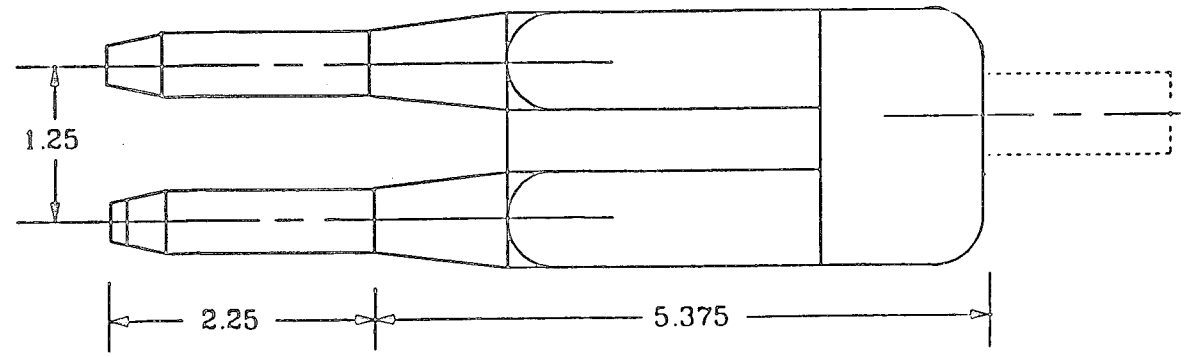

(a) Top view

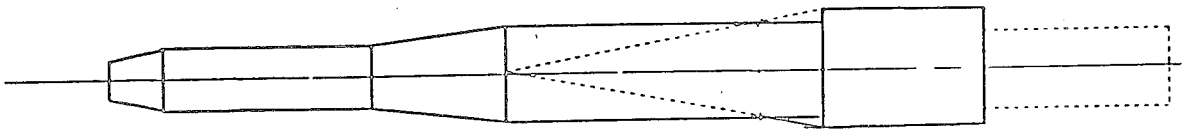

(b) Side view

Figure 2-8. Configuration drawing of Snob/Greg yoke (Dimension: Inches).

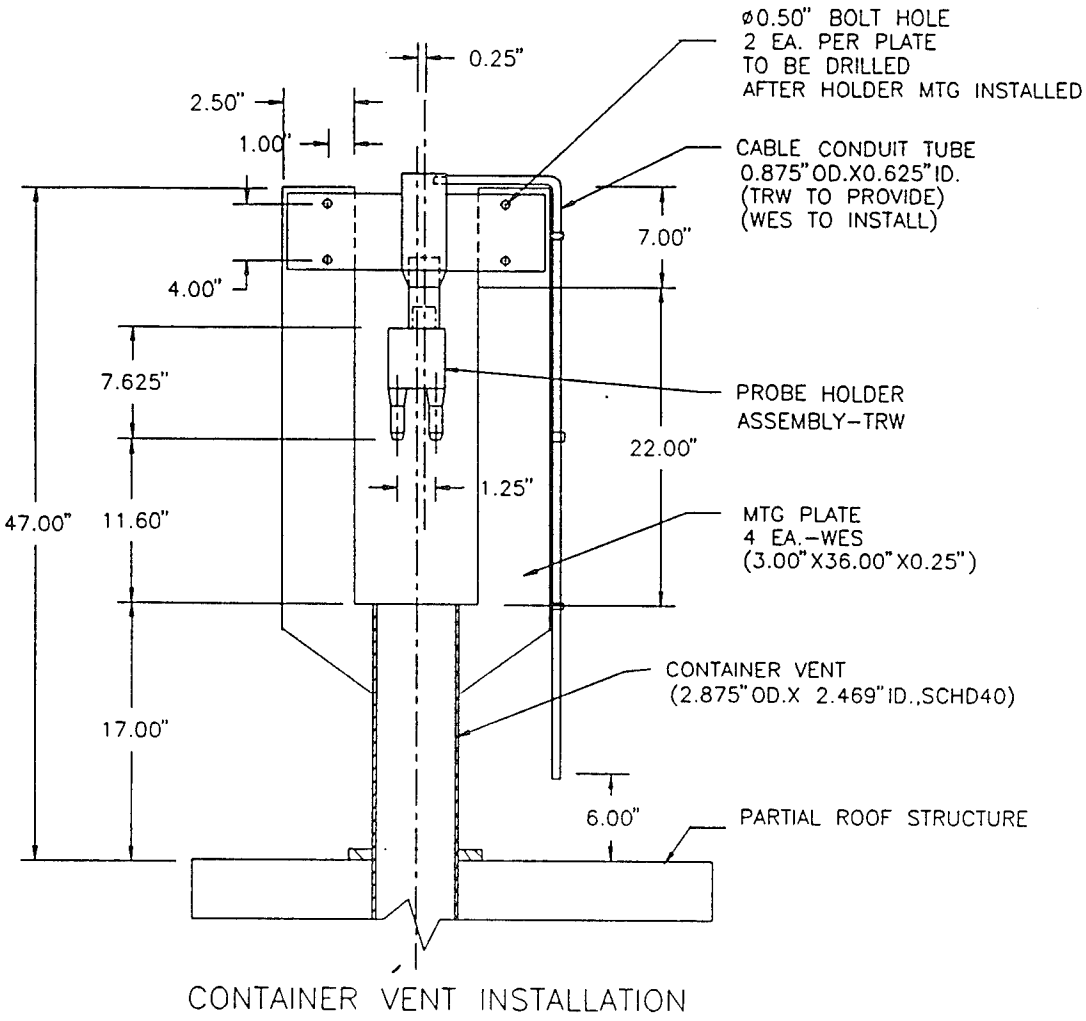

Figure 2-9. Configuration drawing of Snob/Greg probe installation on WES 1.

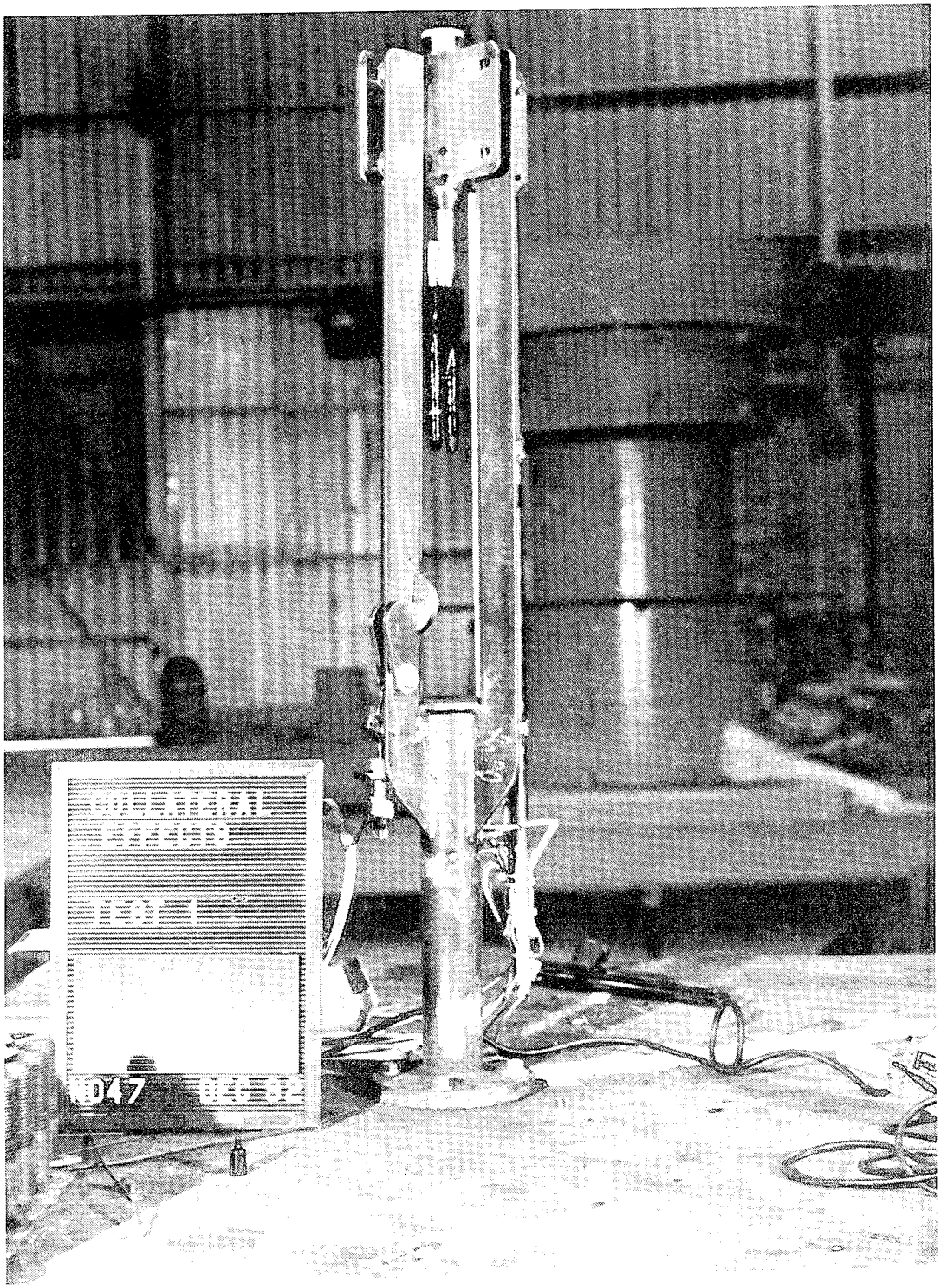

Figure 2-10. Pre test photograph of Snob/Greg probe installation for WES 1 event.

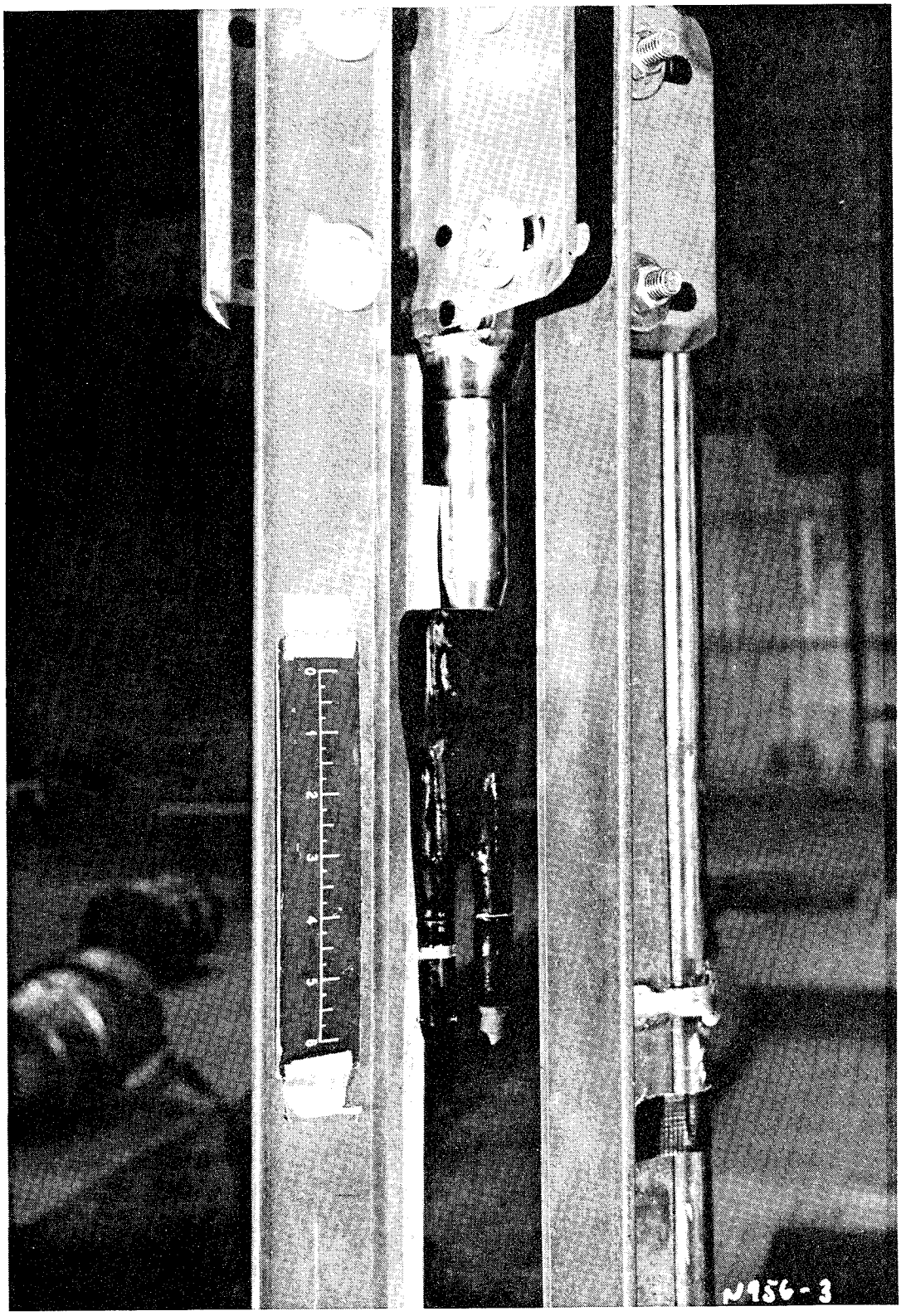

Figure 2-11. Close-up view of Snob/Greg probe installation prior to WES 1 event.

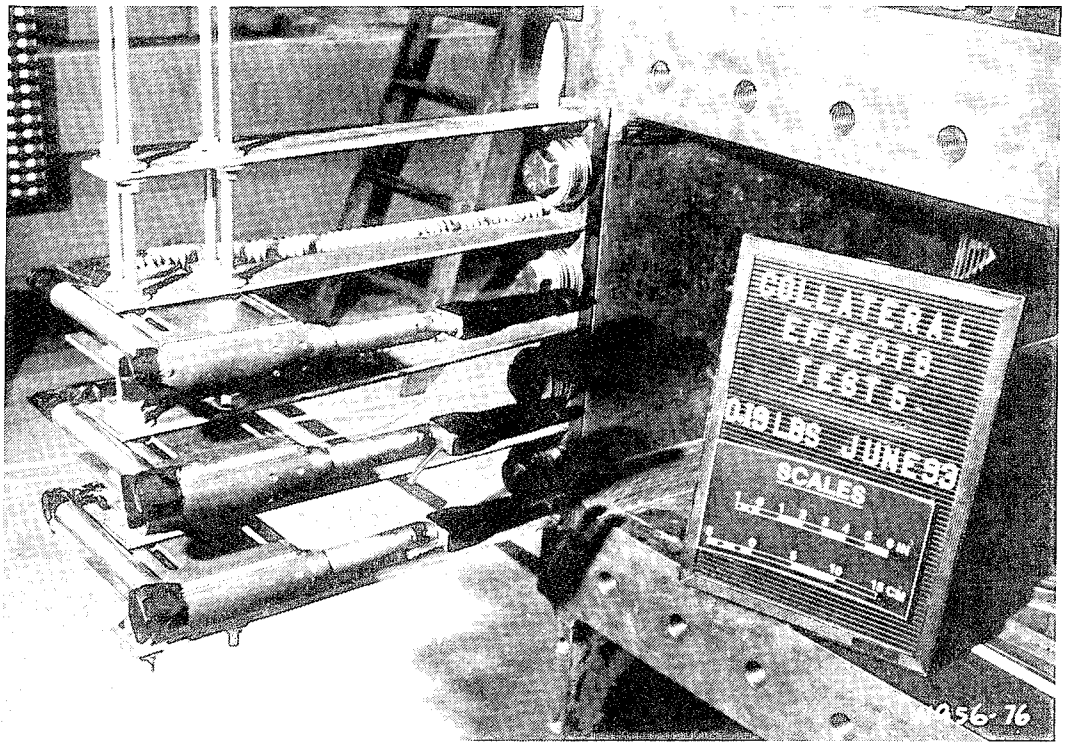

Figure 2-12. Pre test photograph of Snob/Greg rake installation at vent door opening for WES 5 event.

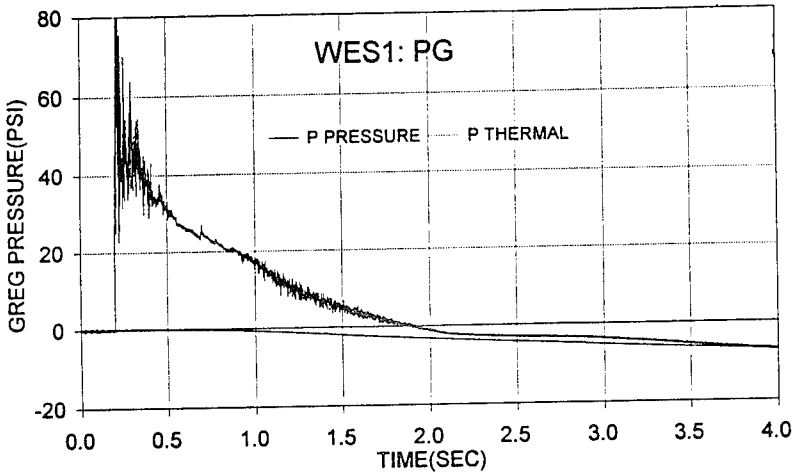

(a) Greg total pressure

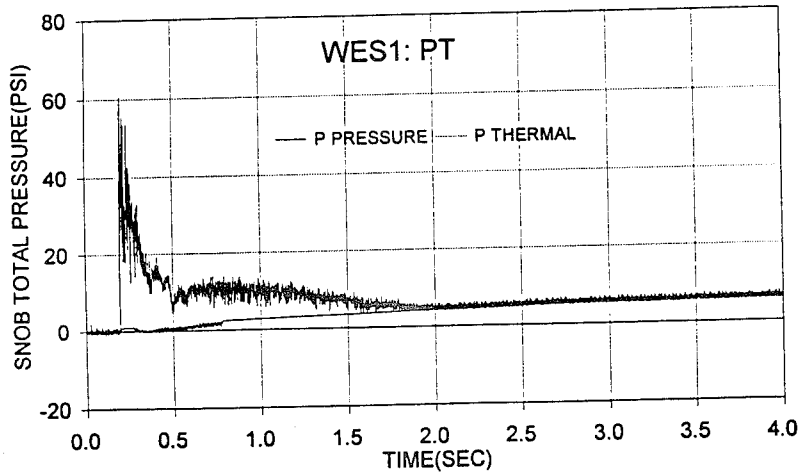

(b) Snob total pressure

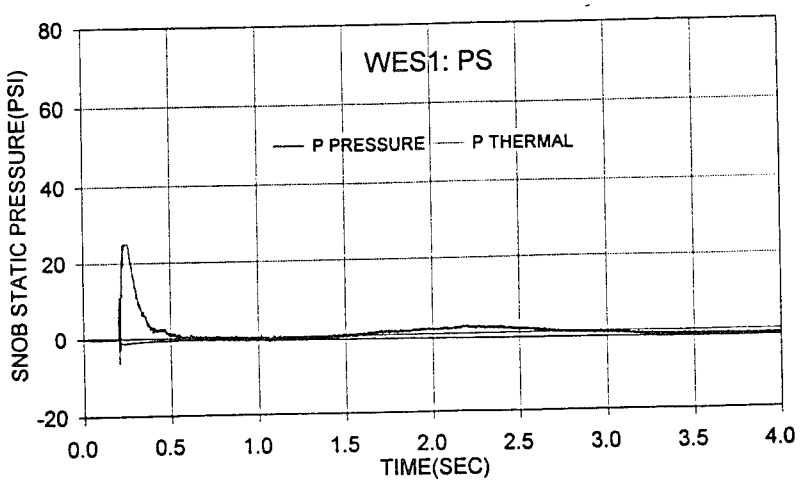

(c) Snob static pressure

Figure 2-13. WES 1 Snob/Greg raw data time histories (1 ms per sample; 11.6" elevation; radial location: ± 0.625").

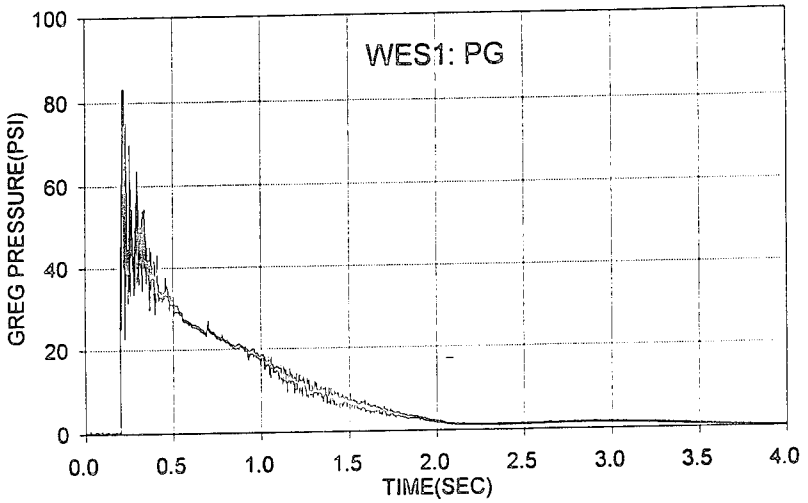

(a) Greg total pressure

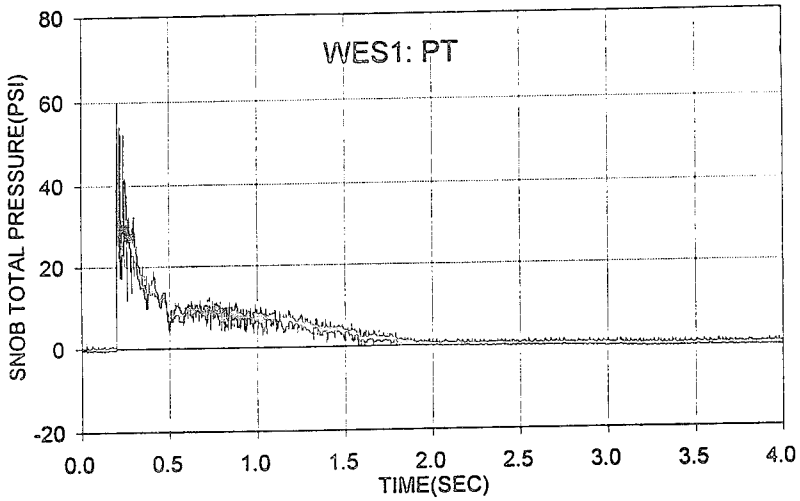

(b) Snob total pressure

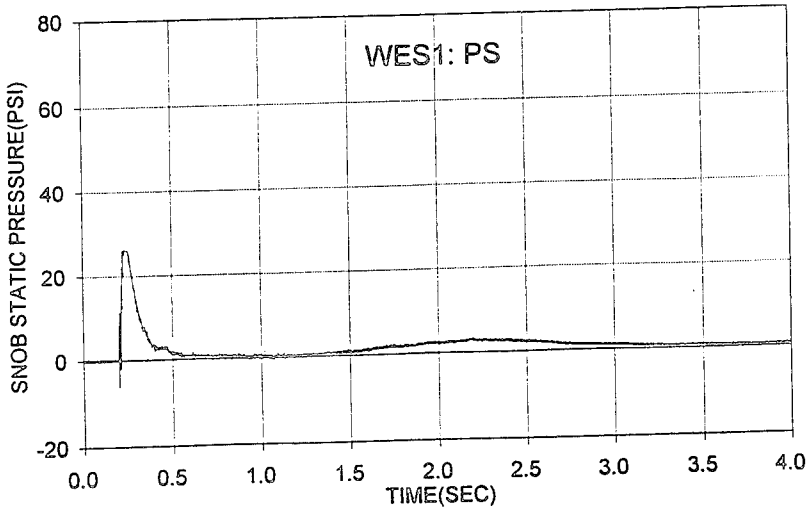

(c) Snob static pressure

Figure 2-14. WES 1 Snob/Greg thermally corrected data (1 ms per sample).

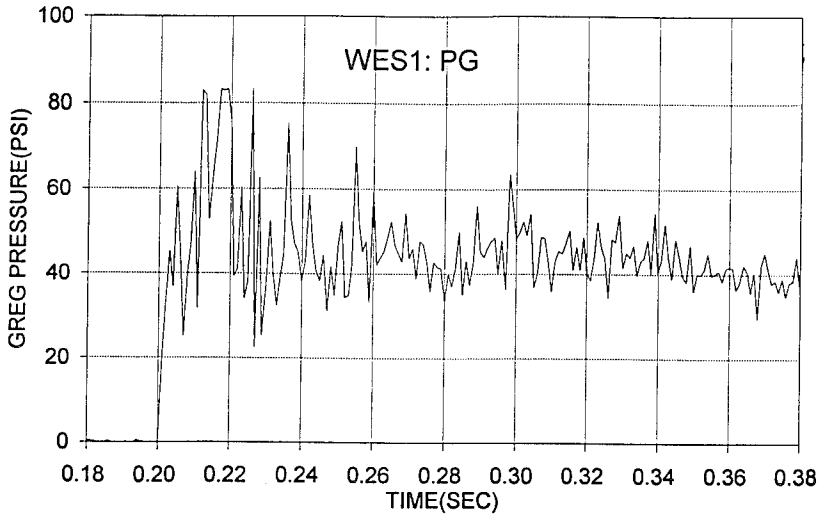

(a) Greg total pressure

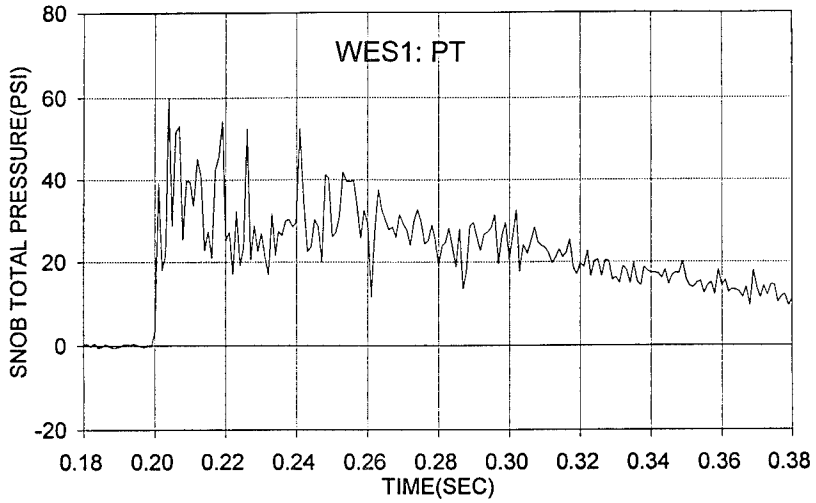

(b) Snob total pressure

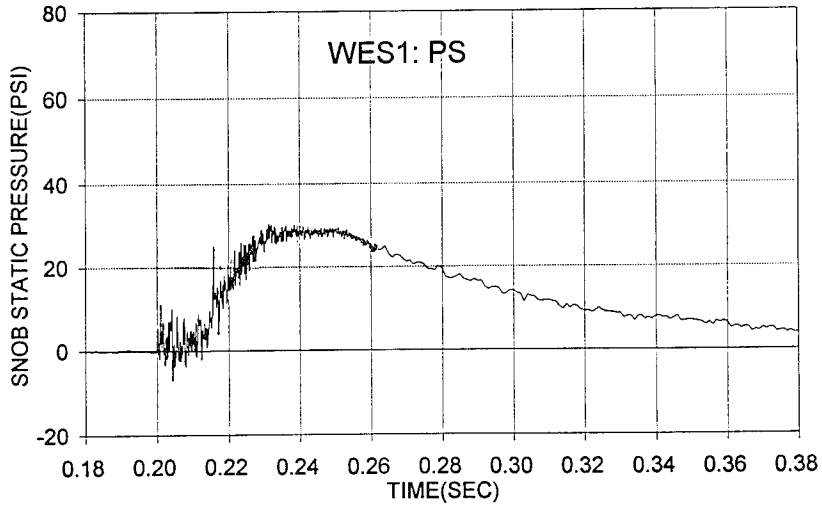

(c) Snob static pressure

Figure 2-15. WES 1 Snob/Greg thermally corrected data (sample rate: 16μs, t < 0.26 sec; 1 ms, t > 0.26 sec).

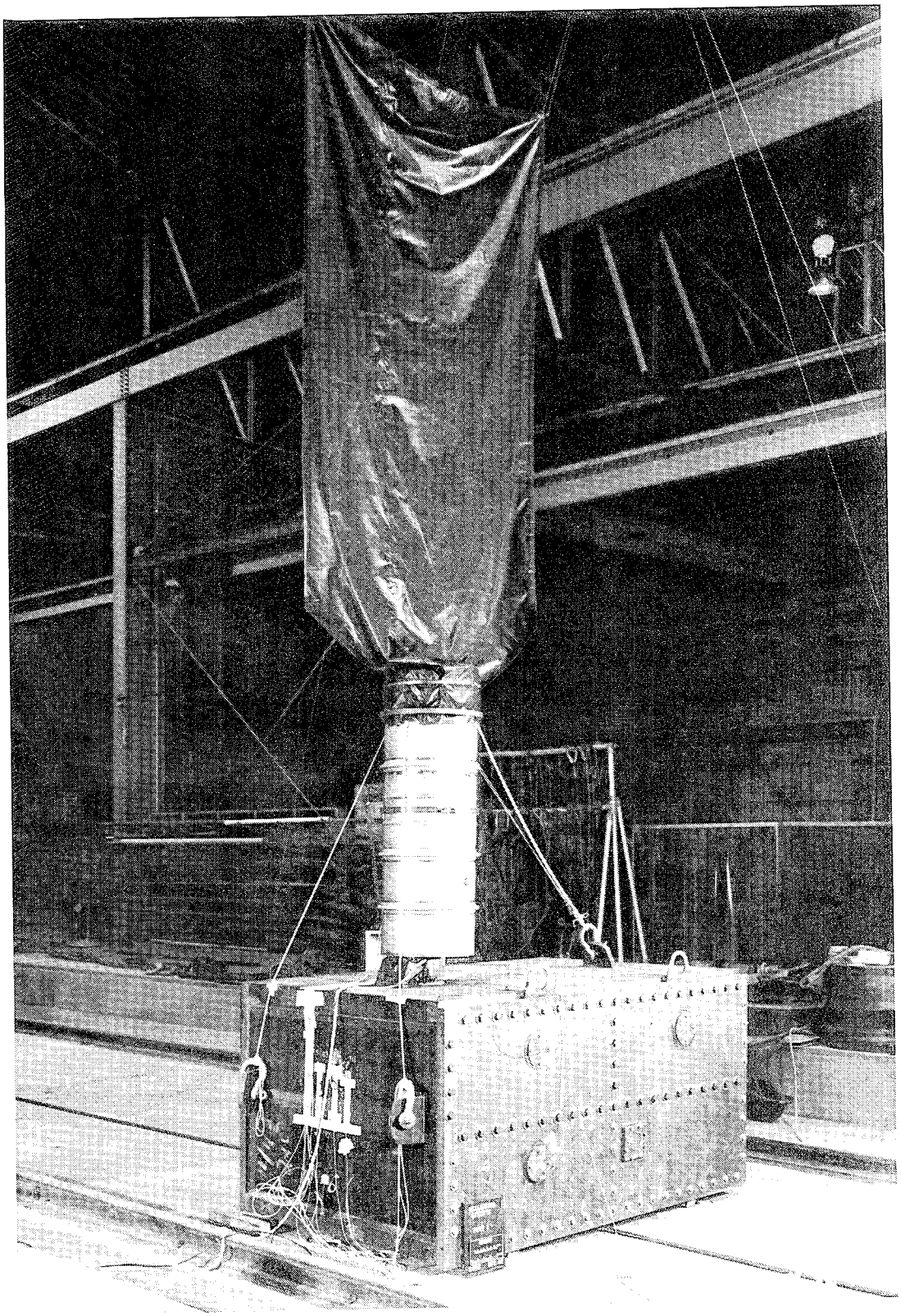

Figure 2-16. Pre test photograph of particle collector assembly for vent discharge flow on WES 1 event.

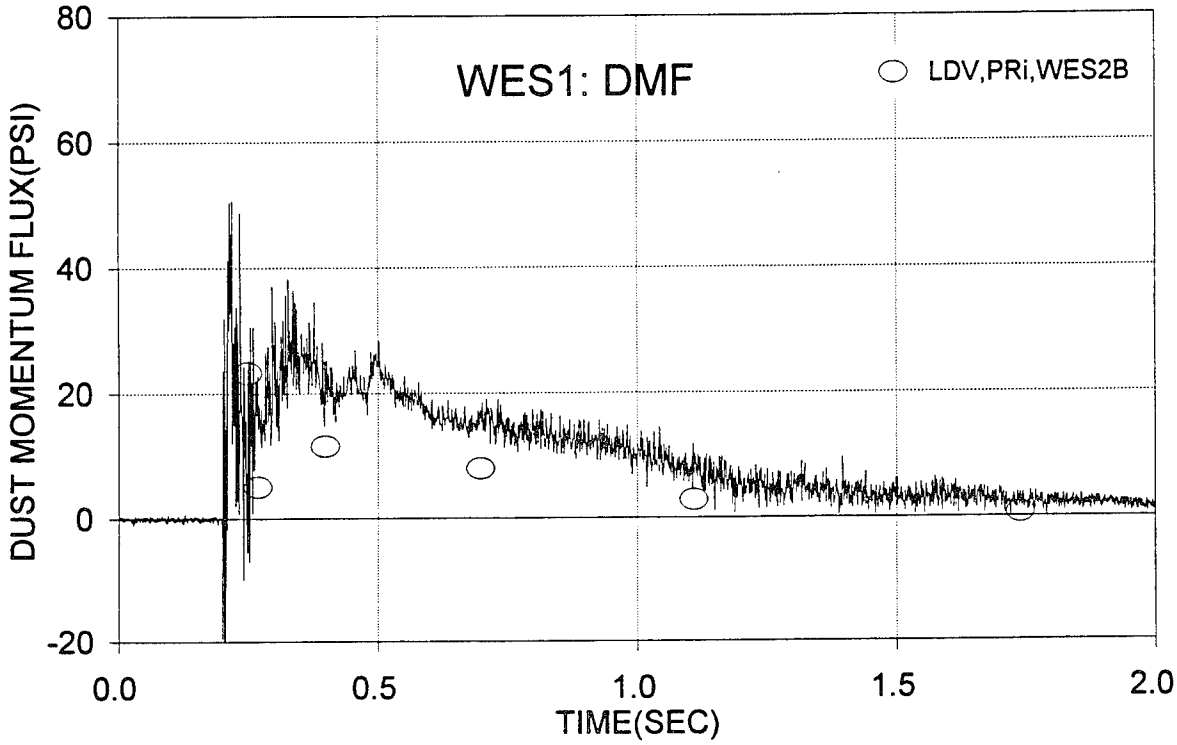

(a) Early time

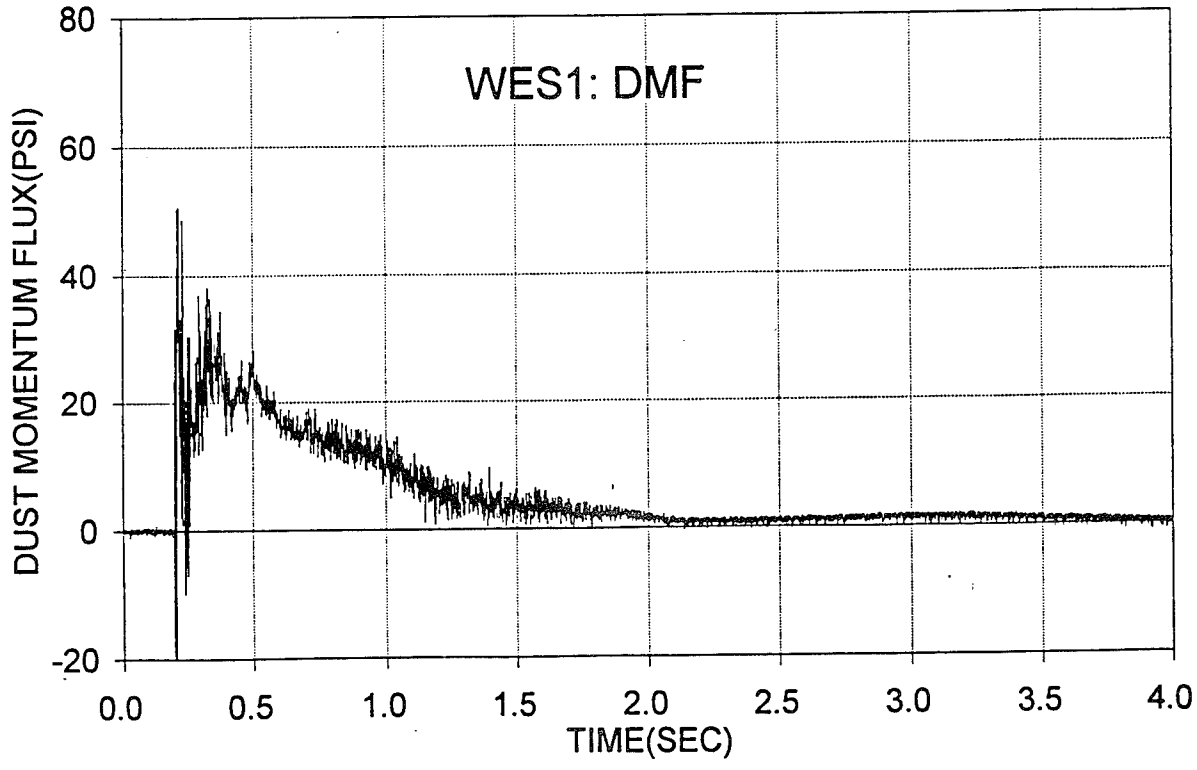

(b) Extended time

Figure 2-17. WES 1 dust momentum flux time history.

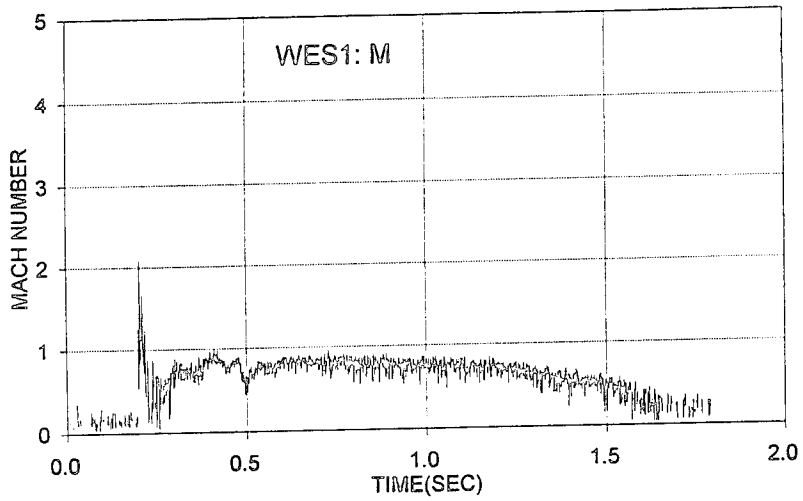

(a) Mach number

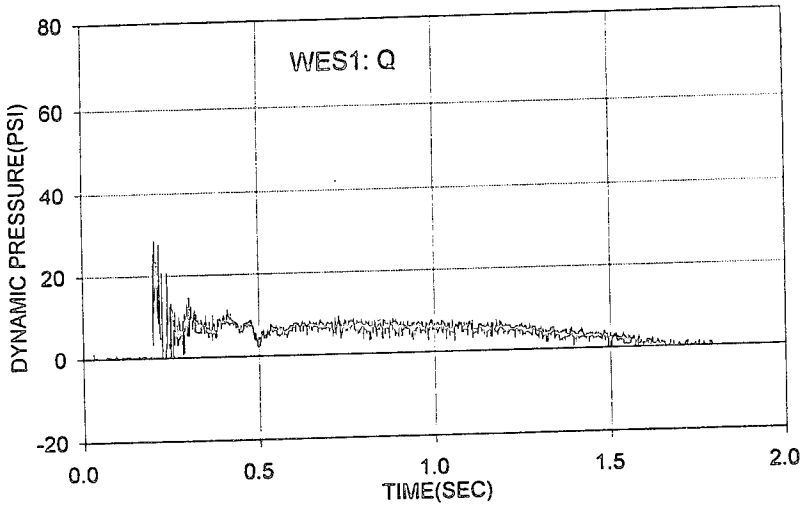

(b) Dynamic pressure

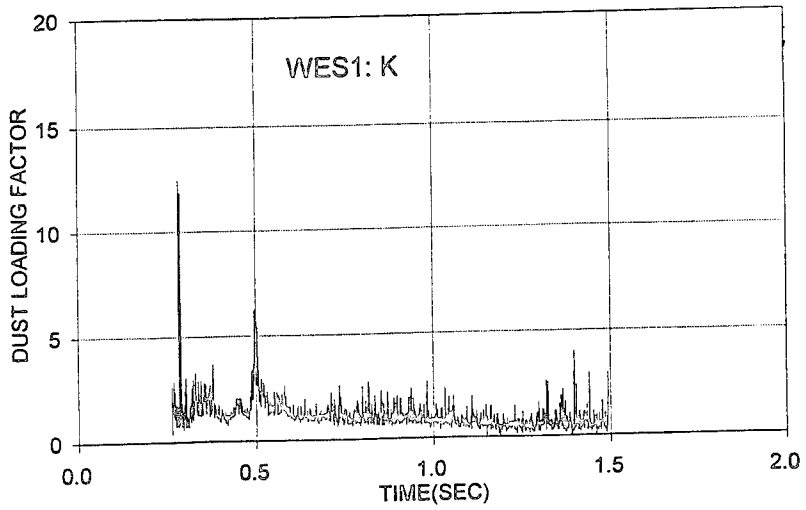

(c) Dust loading factor

Figure 2-18. WES 1 flow field time histories for vent pipe airblast jet (γ = 1.4; 1 ms per sample).

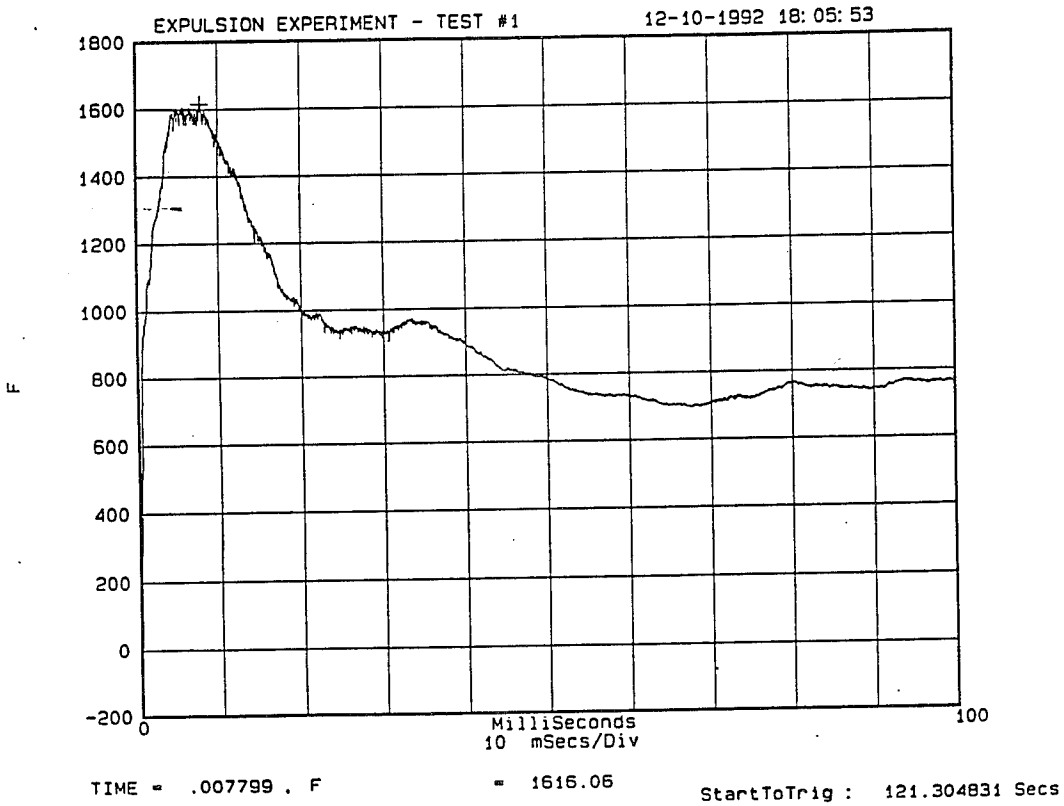

(a) Early time history

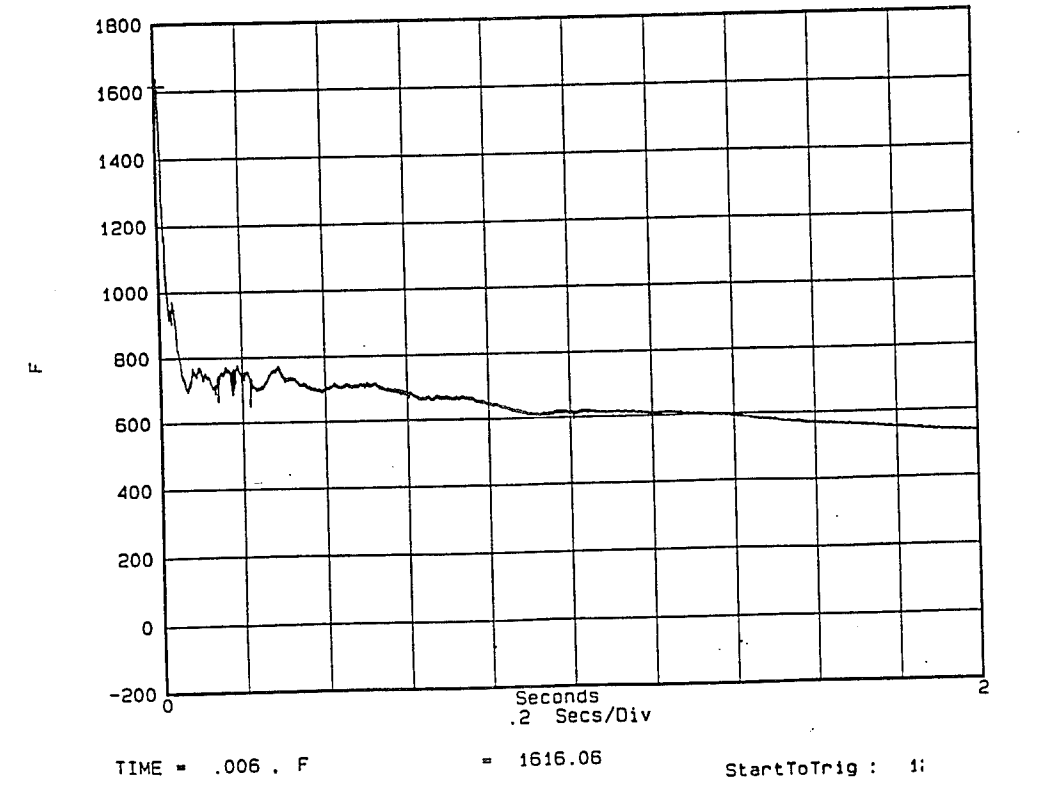

(b) Extended time history

Figure 2-19. WES 1 vent pipe temperature (TIPI).

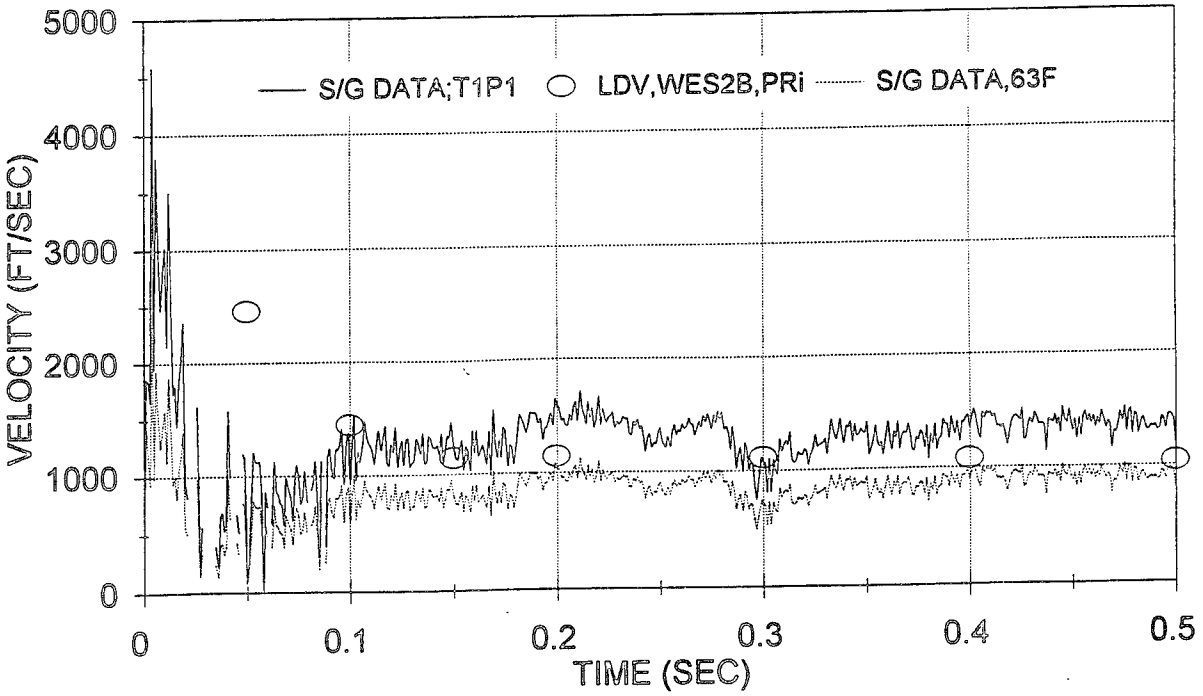

(a) Early time history

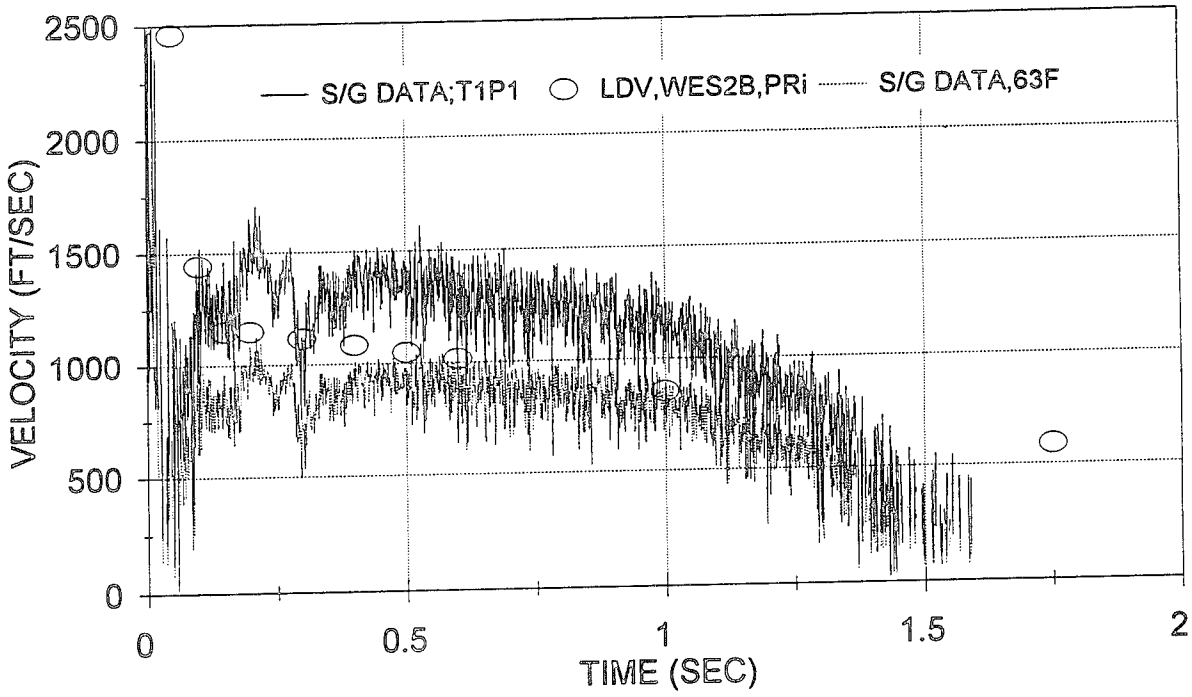

(b) Extended time history

Figure 2-20. Velocity for WES 1 vent pipe flow at Snob/Greg probe location.

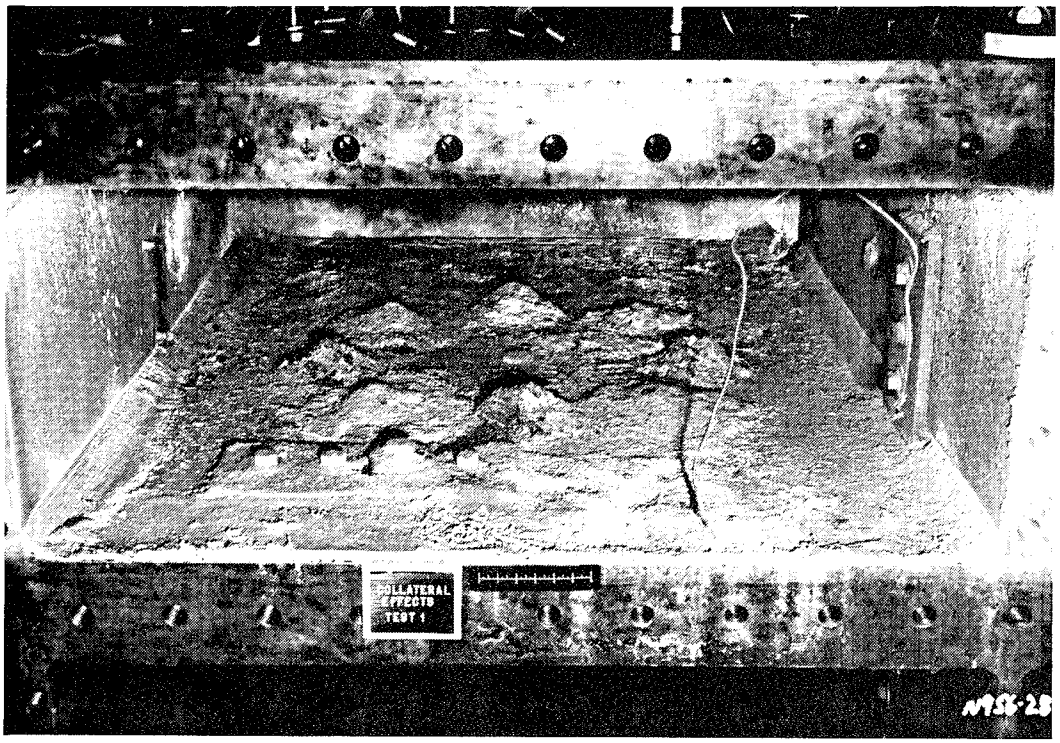

Figure 2-21. Post test photograph of tracer material layout for WES 1 event.

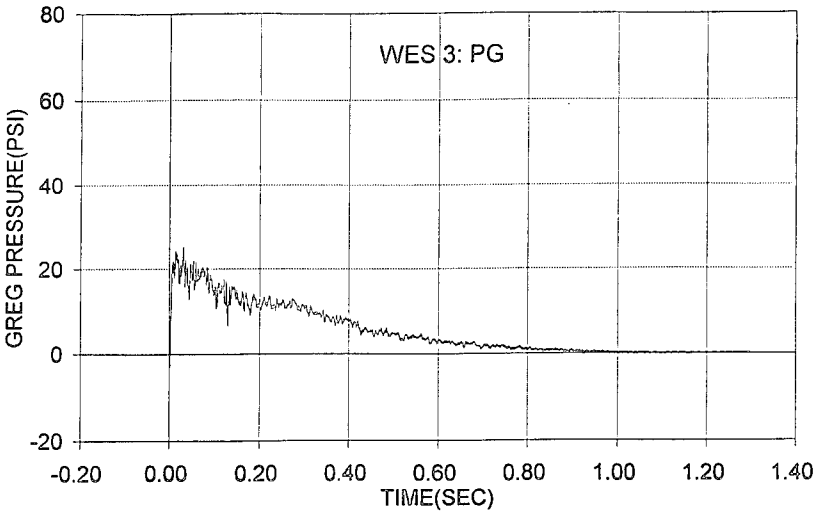

(a) Greg total pressure

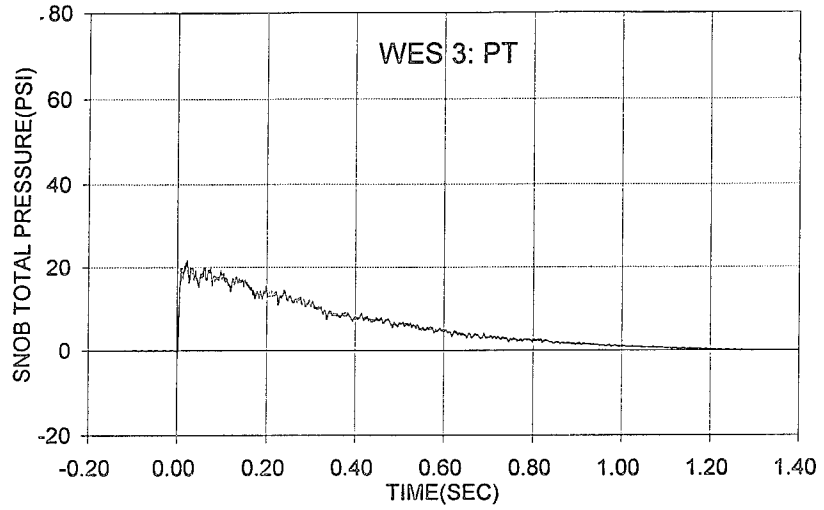

(b) Snob total pressure

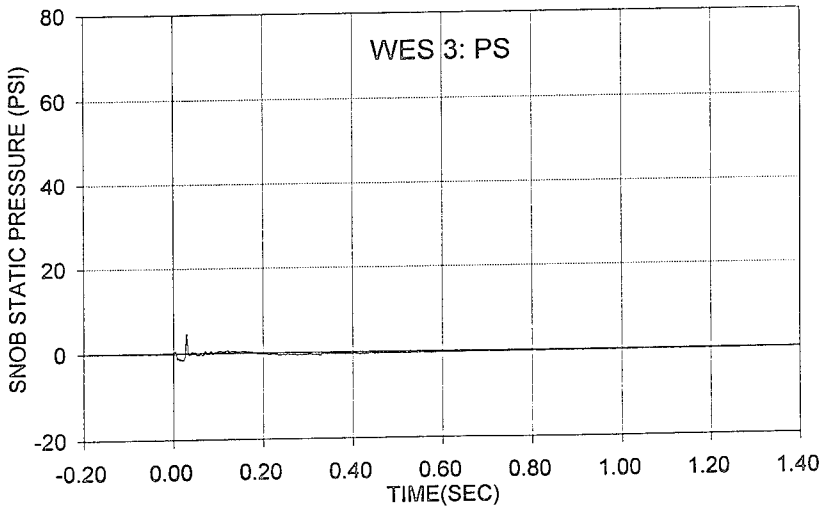

(c) Snob static pressure

Figure 2-22. WES 3 Snob/Greg thermally corrected pressure data (0.35 ms per sample; 10 point average).

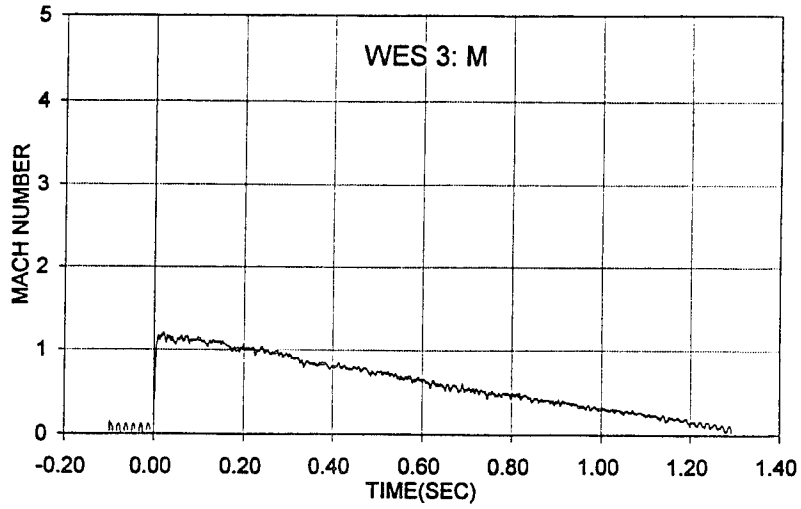

(a) Mach number

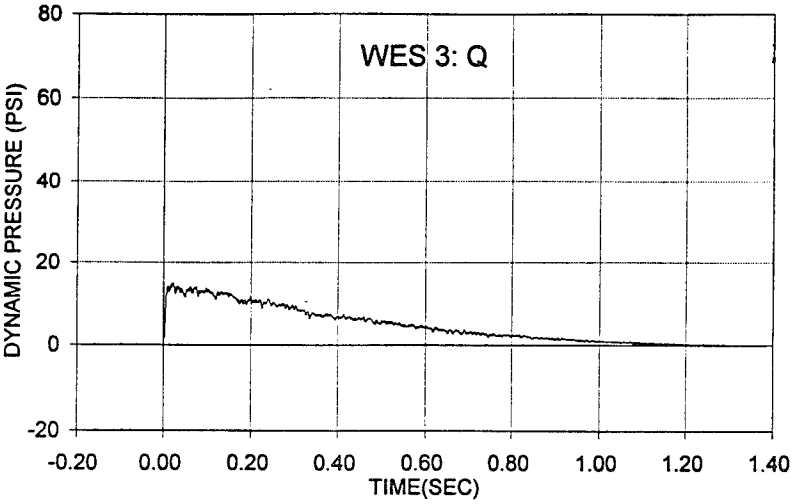

(b) Dynamic pressure

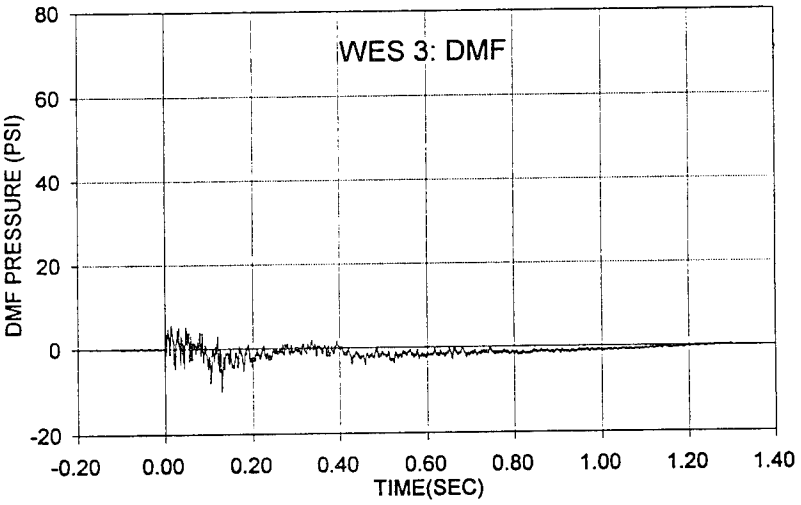

(c) Dust momentum flux

Figure 2-23. WES 3 flow field time histories for vent pipe airblast jet.

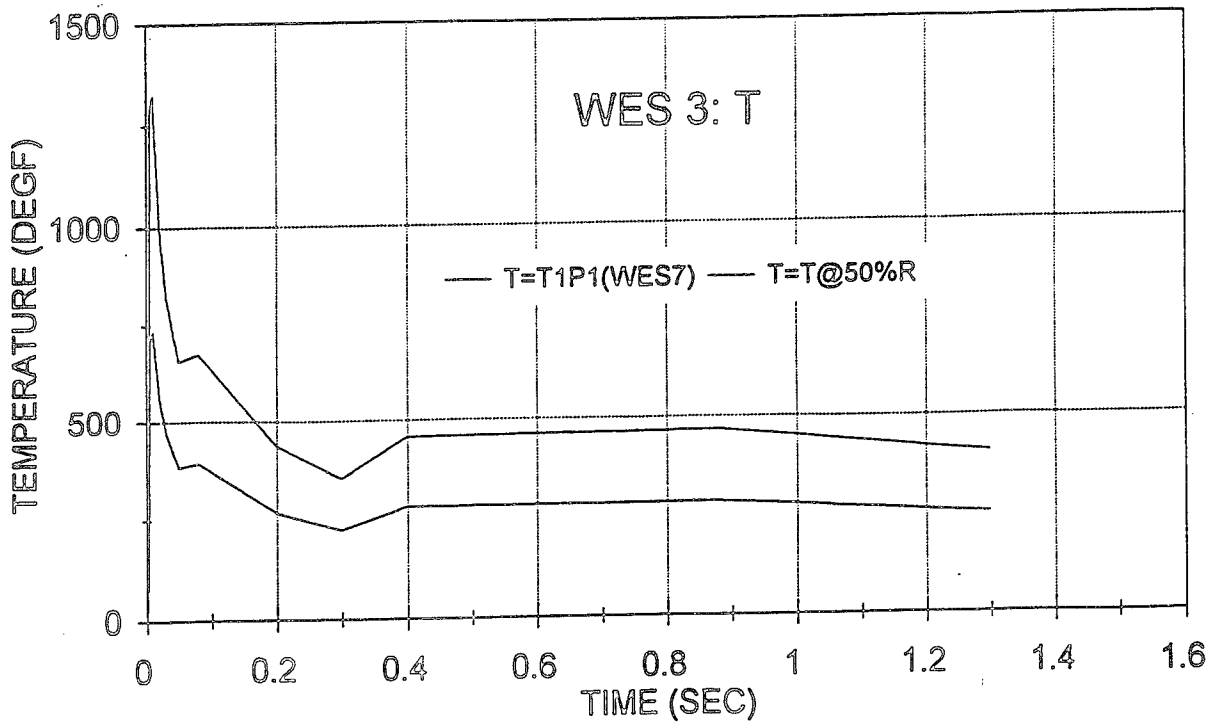

(a) Temperature

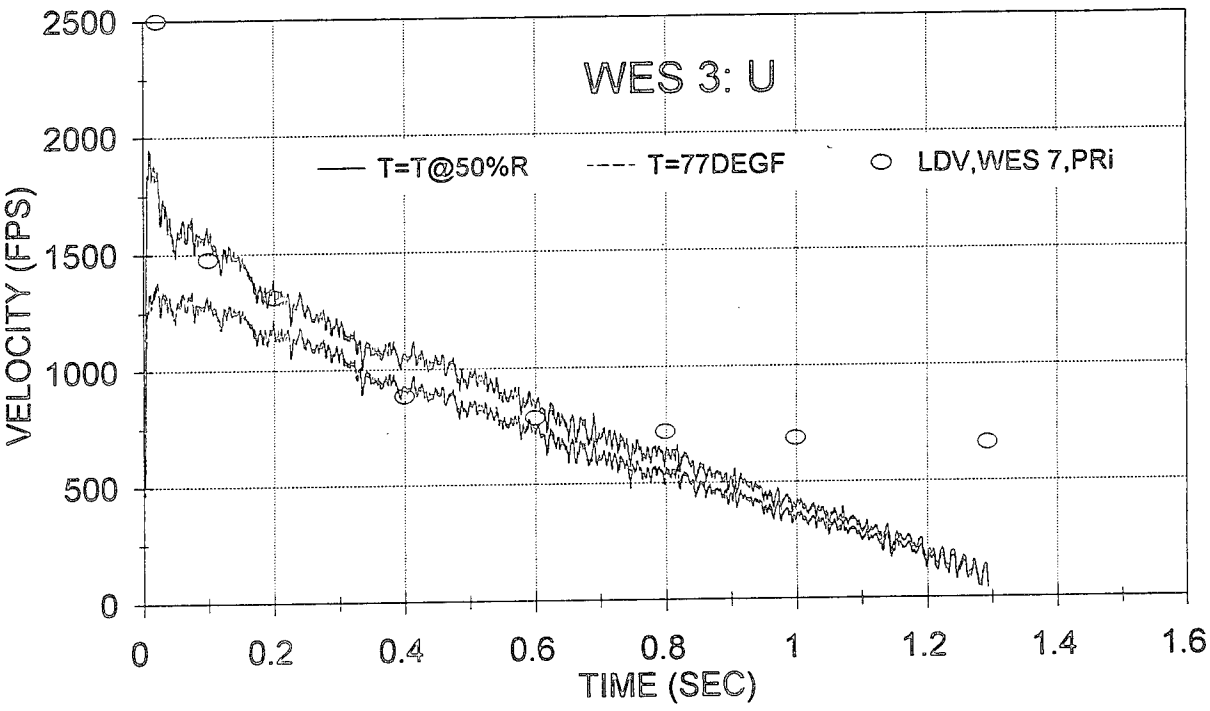

(b) Velocity

Figure 2-24. Estimates of temperature and velocity for WES 3 vent pipe flow at Snob/Greg probe location.

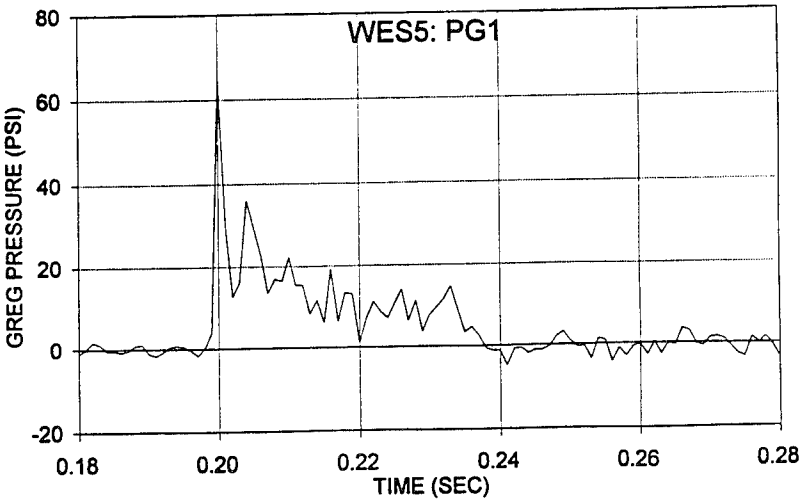

(a) Greg total pressure

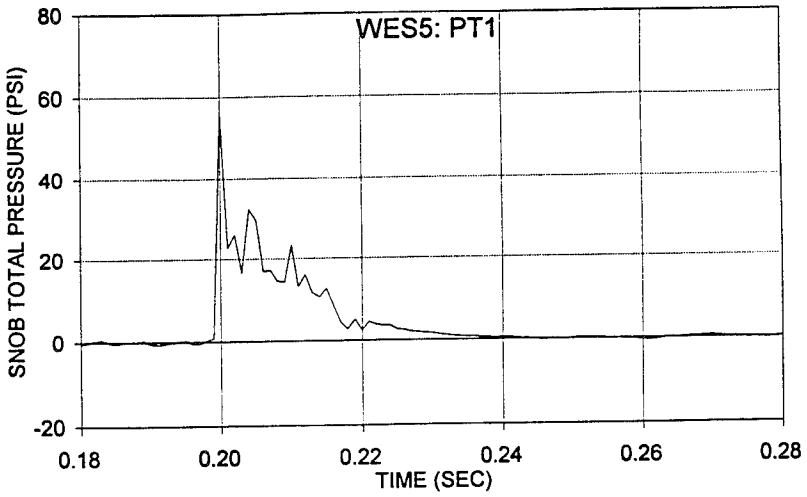

(b) Snob total pressure

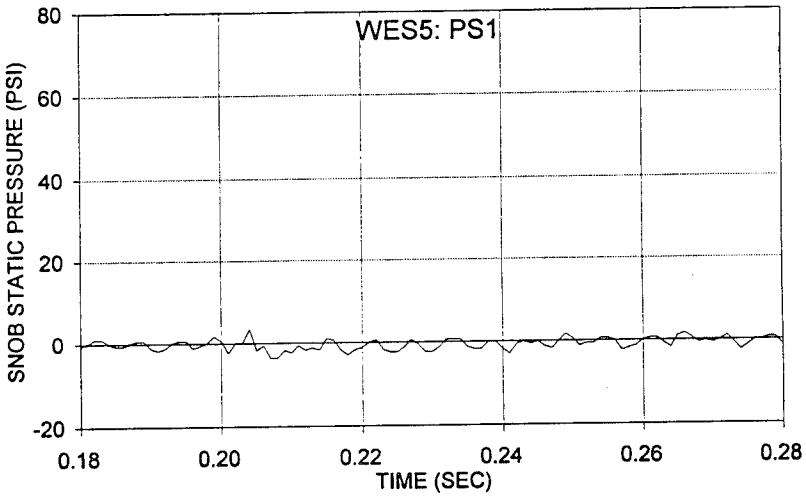

(c) Snob static pressure

Figure 2-25. WES 5/Yoke 1 Snob/Greg pressure measurements at door vent opening (Thermally corrected; 3" elevation).

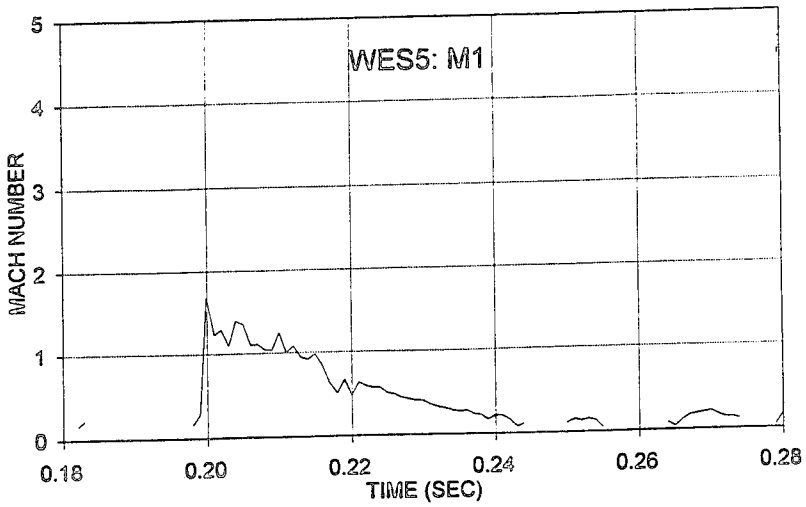

(a) Mach number

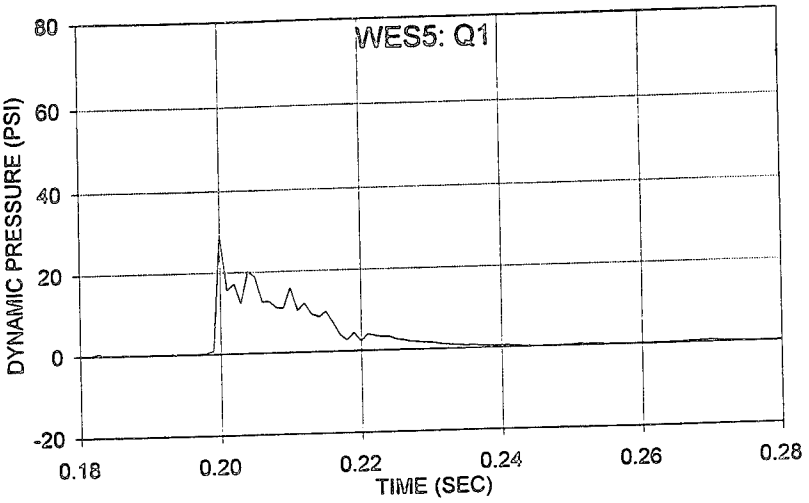

(b) Dynamic pressure

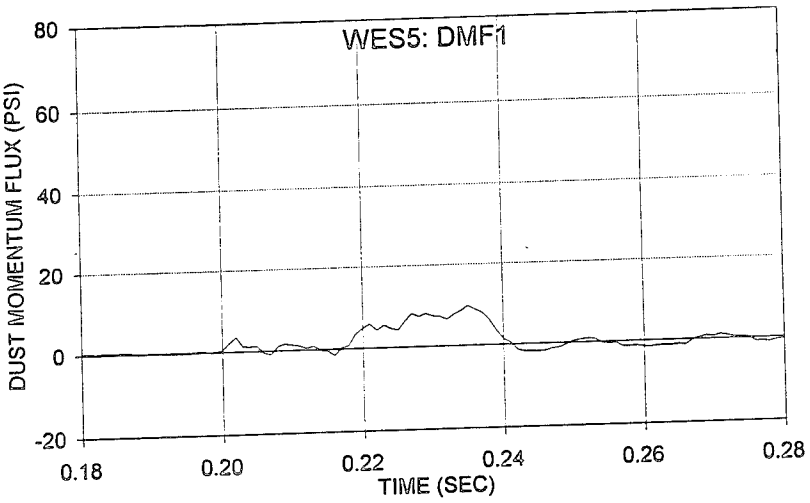

(c) Dust momentum flux

Figure 2-26. WES 5/Yoke 1 flow field time histories for the vent door exit opening.

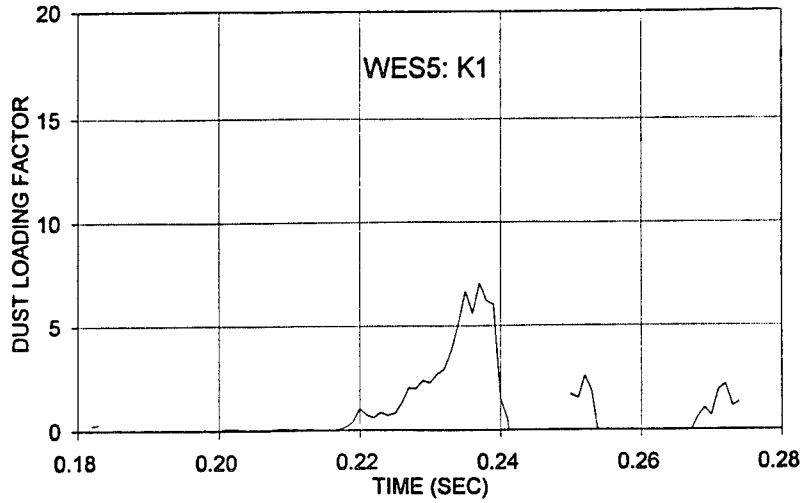

(a) Dust loading factor

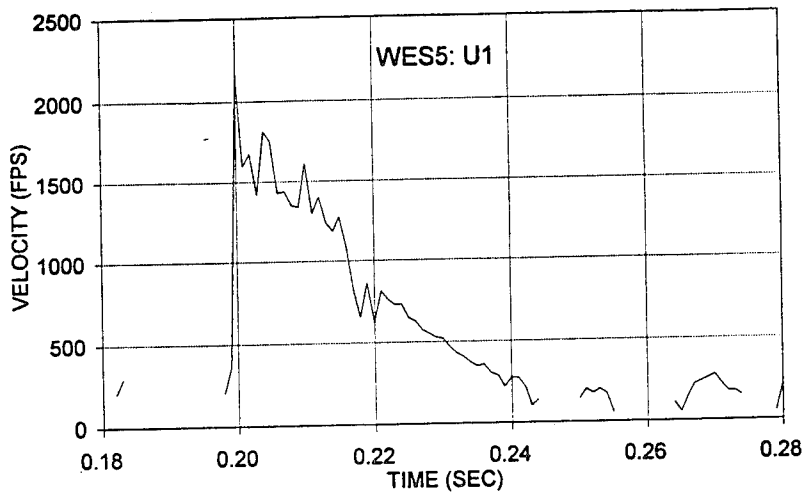

(b) Dust velocity

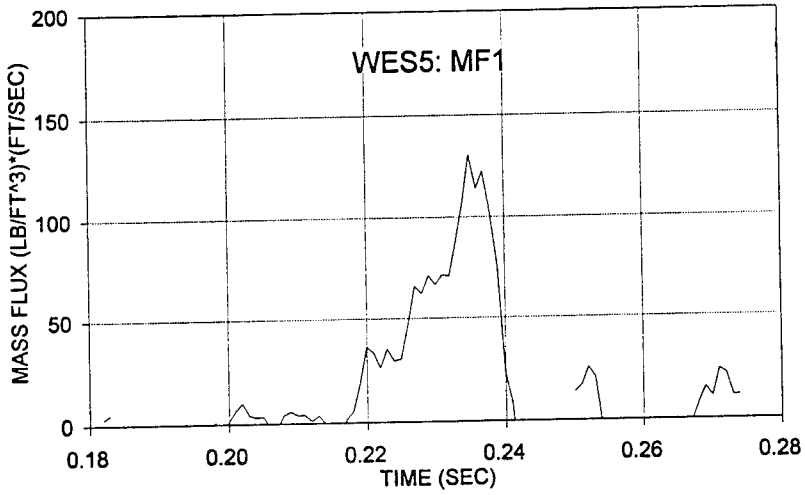

(c) Dust mass flux

Figure 2-27. WES 5/Yoke 1 dust parameter time histories for the vent door exit opening.

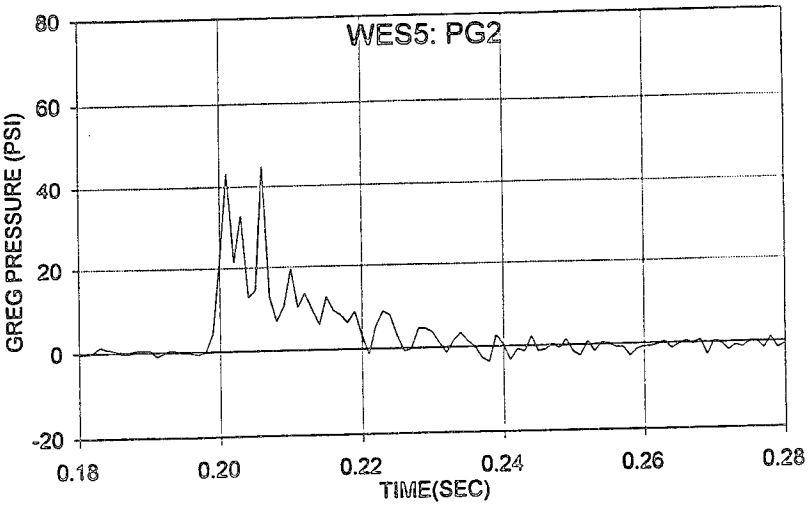

(a) Greg total pressure

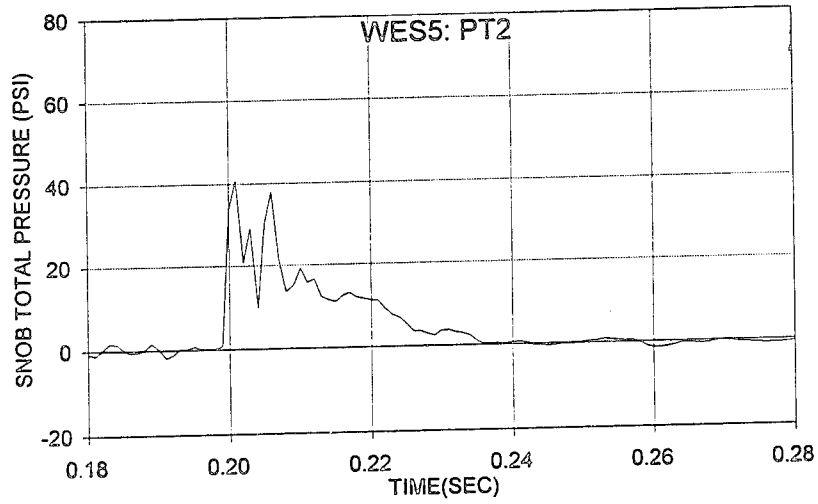

(b) Snob total pressure

Figure 2-28. WES 5/Yoke 2 Snob/Greg pressure measurements at door vent opening (Thermally corrected; 7.5" elevation).

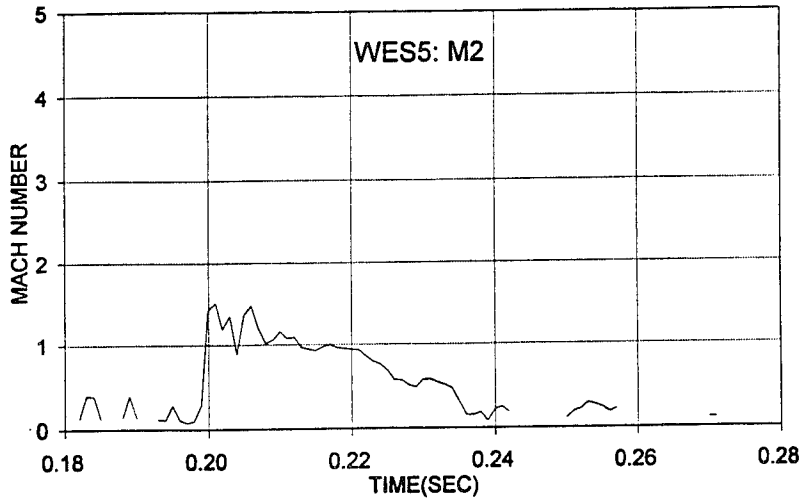

(a) Mach number

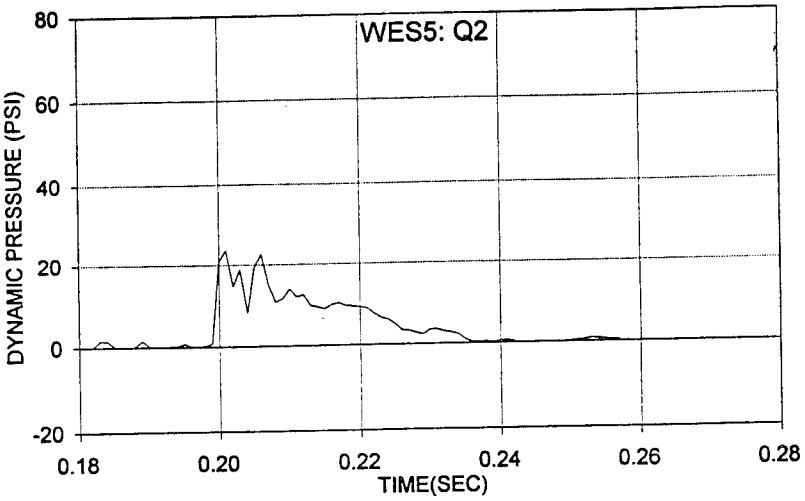

(b) Dynamic pressure

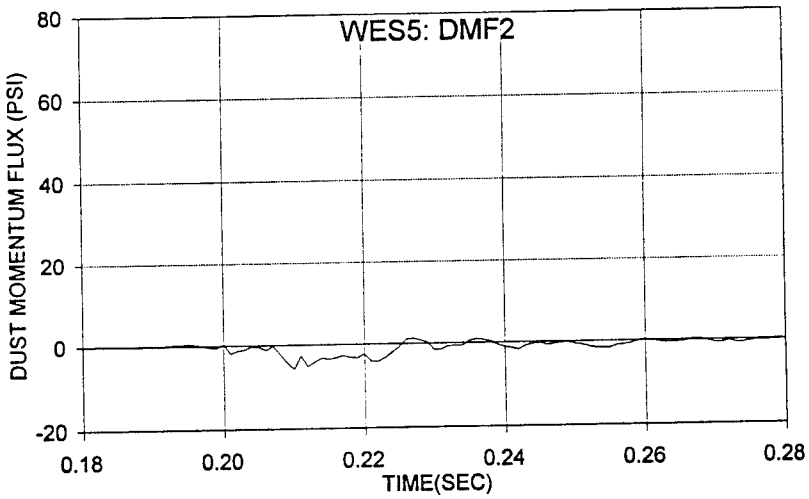

(c) Dust momentum flux

Figure 2-29. WES 5/Yoke 2 flow field time histories for vent door opening.

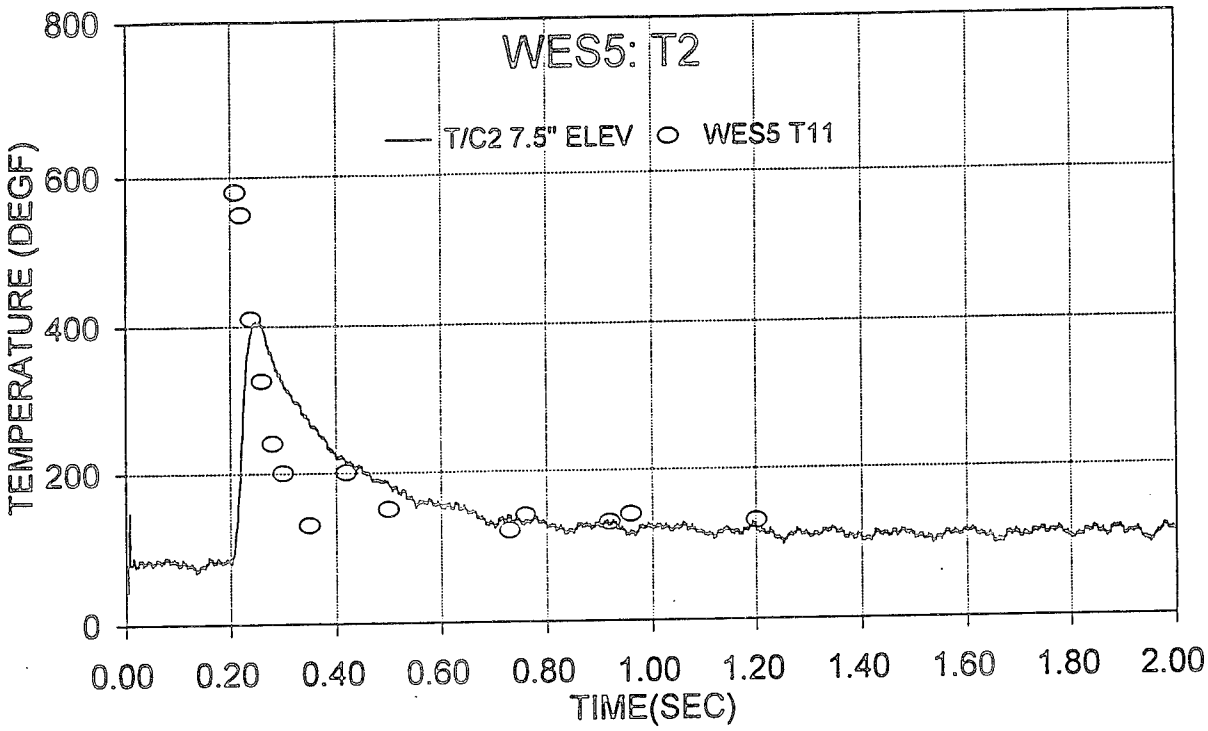

Figure 2-30. Thermocouple temperature data from WES 5/Yoke 2 T/C and comparison with room chamber temperature measurements (T11).

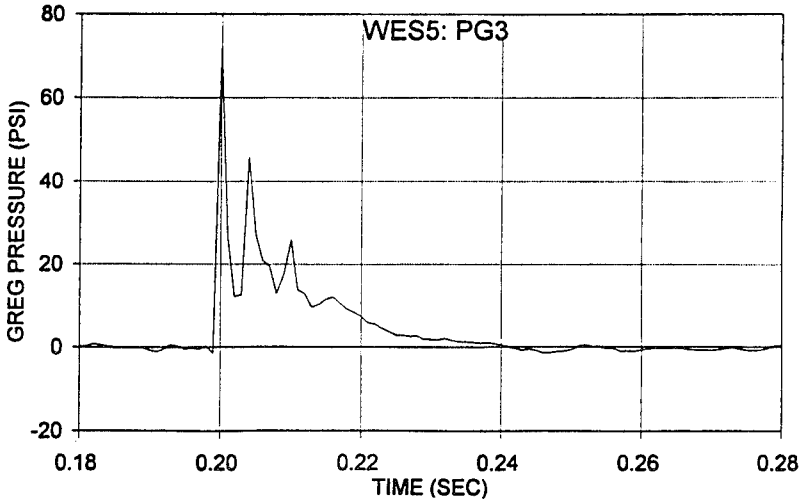

(a) Greg total pressure

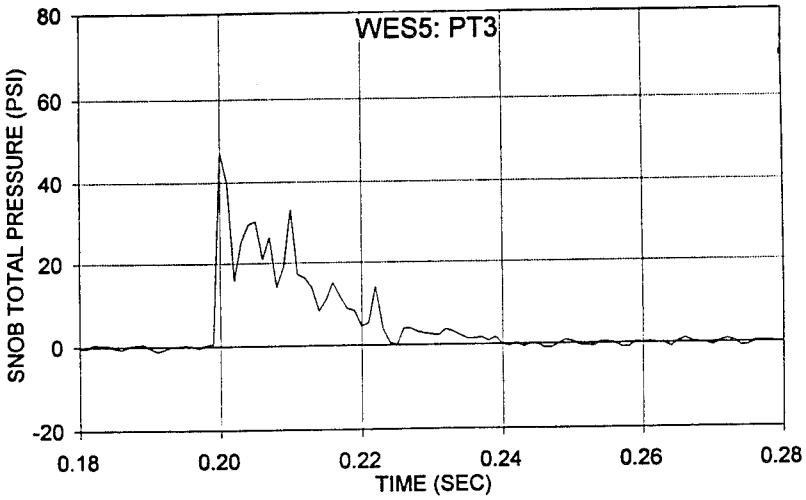

(b) Snob total pressure

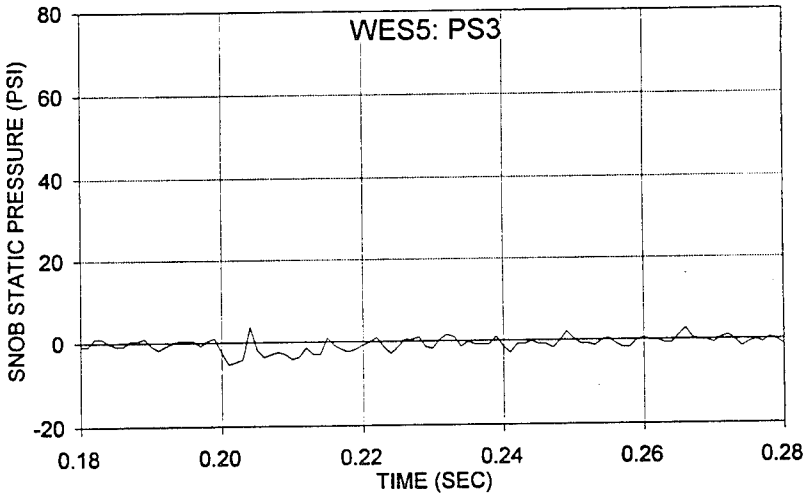

(c) Snob static pressure

Figure 2-31. WES 5/Yoke 3 Snob/Greg pressure measurements at door vent opening (Thermally corrected; 12.5" elevation).

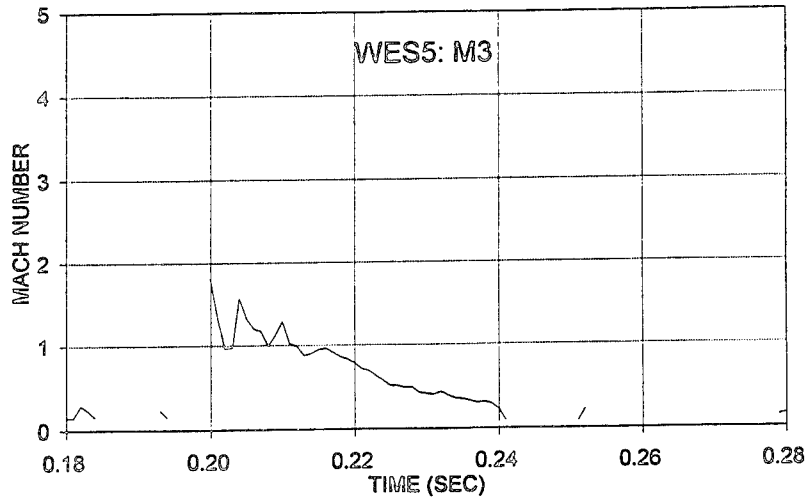

(a) Mach number

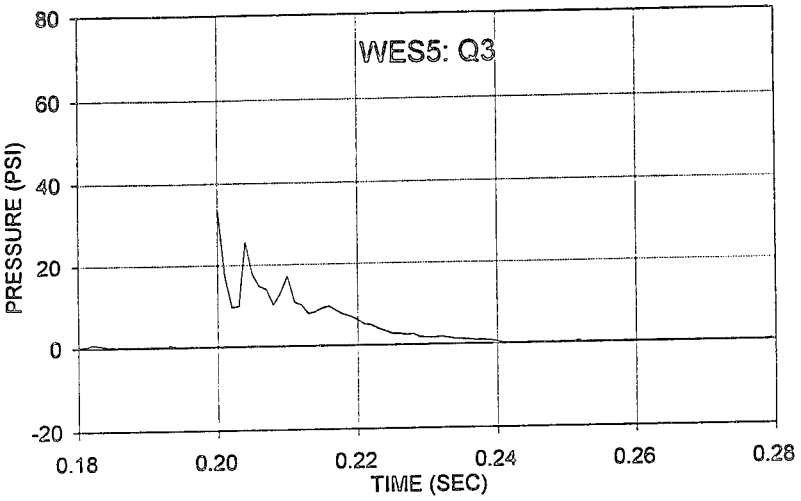

(b) Dynamic pressure

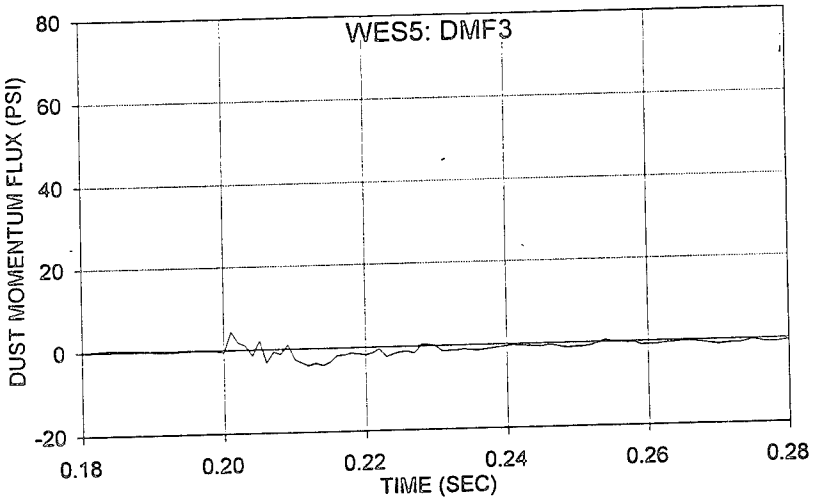

(c) Dust momentum flux

Figure 2-32. WES 5/Yoke 3 flow field time histories for vent door opening.

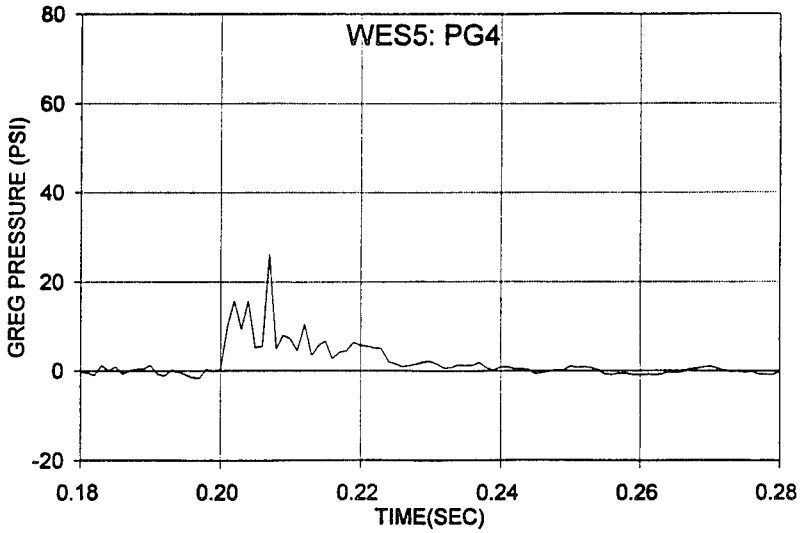

(a) Greg total pressure

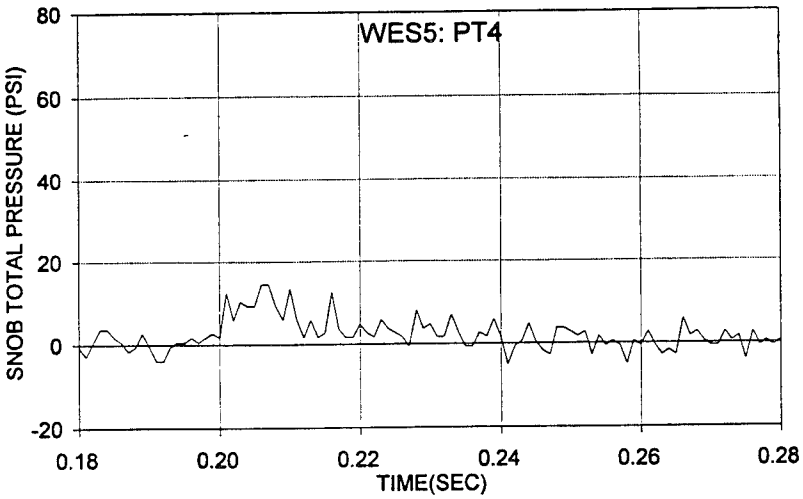

(b) Snob total pressure

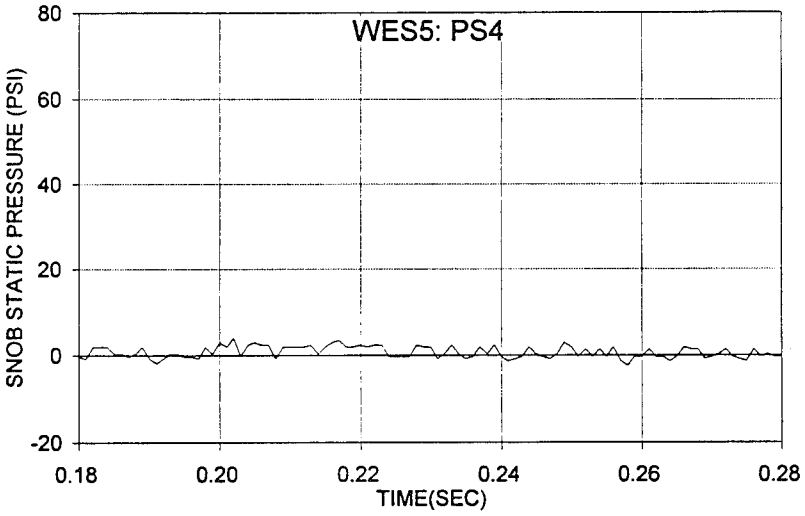

(c) Snob static pressure

Figure 2-33. WES 5/Yoke 4 Snob/Greg pressure measurements at vent pipe exhaust (Thermally corrected; 11.6" elevation).

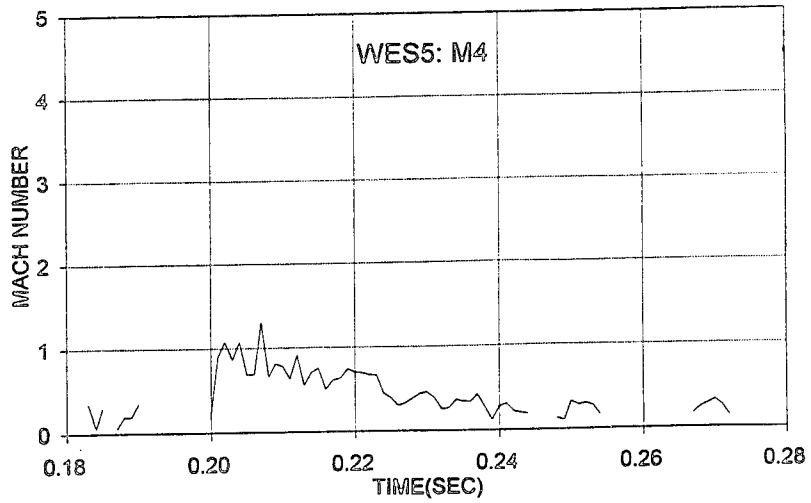

(a) Mach number

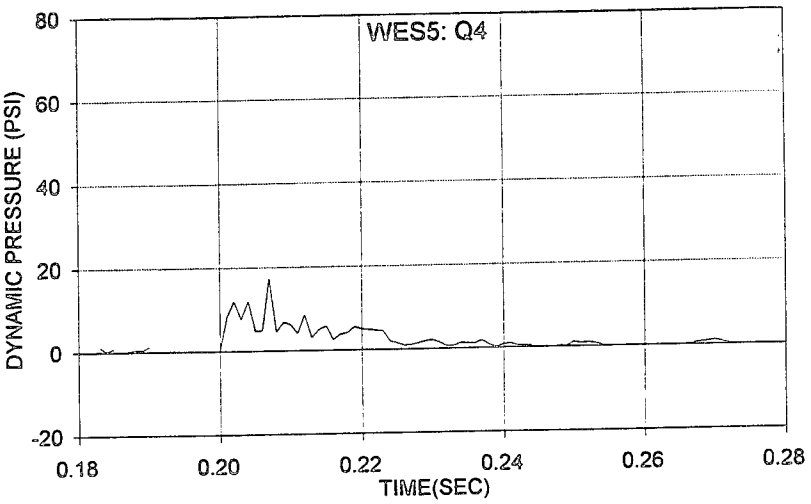

(b) Dynamic pressure

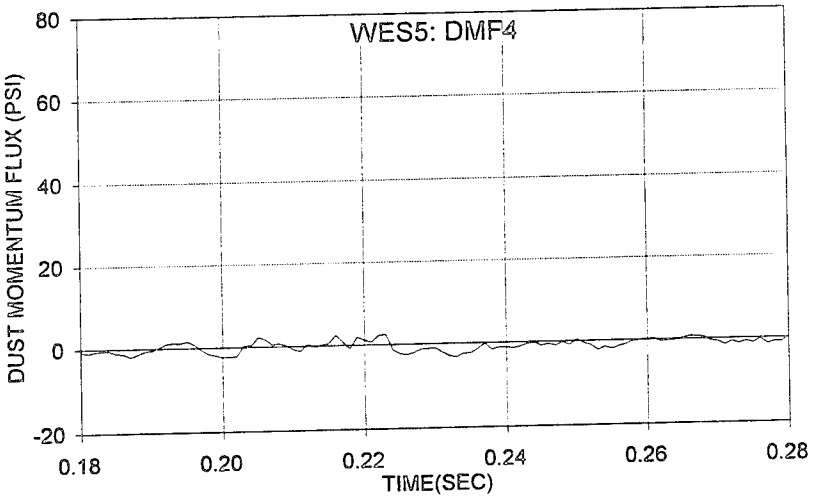

(c) Dust momentum flux

Figure 2-34. WES 5/Yoke 4 flow field time histories for vent pipe exhaust.

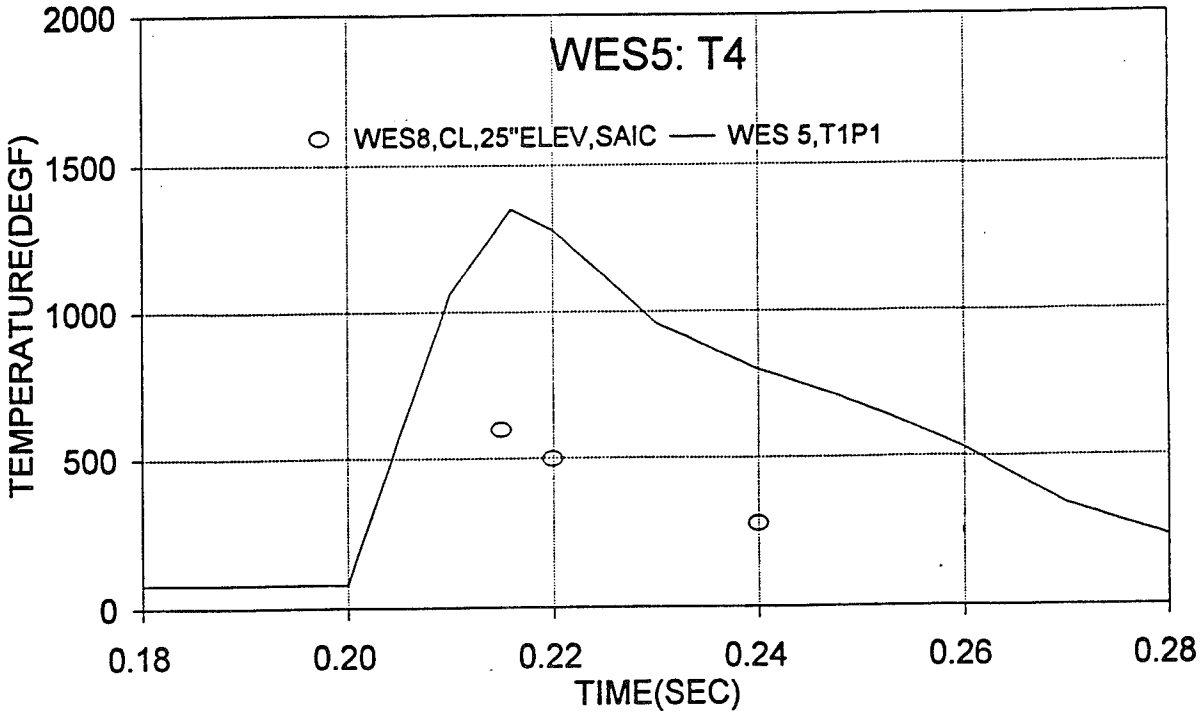

(a) Temperature

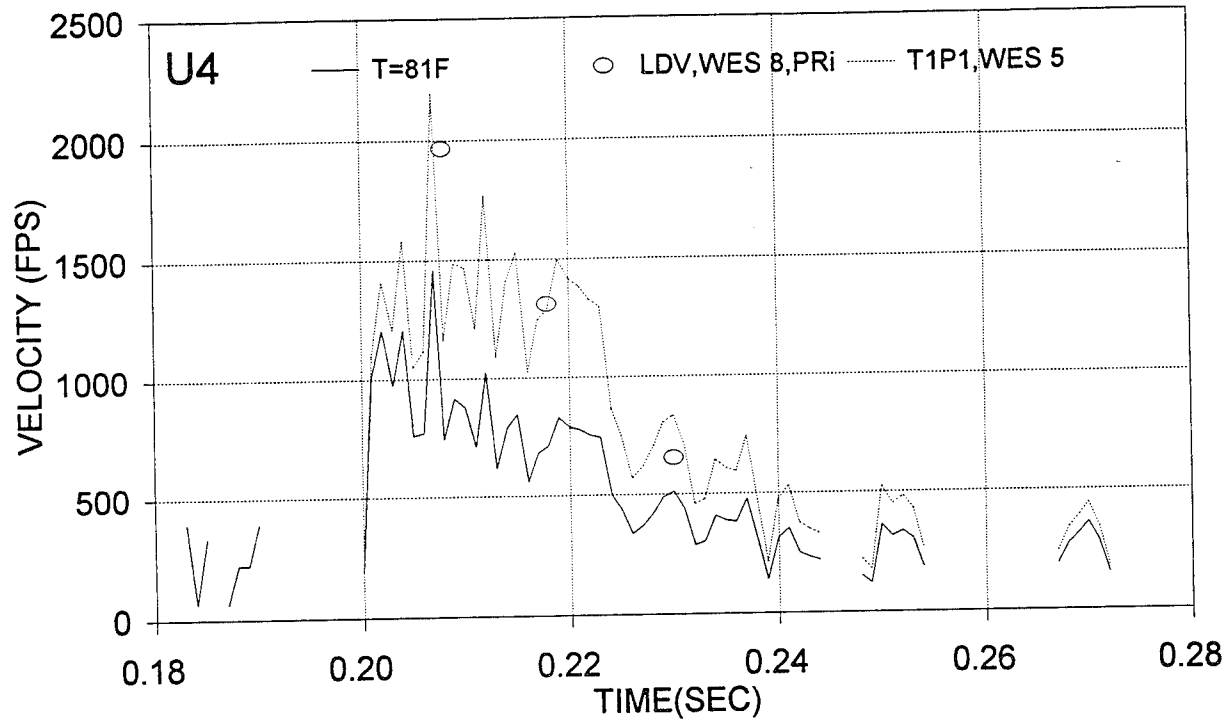

(b) Velocity

Figure 2-35. Estimate for temperature and velocity for WES 5 vent pipe flow at Snob/Greg probe location.

SECTION 3
FURTHER REVIEW OF DSU EXPERIMENTAL RESULTS

Batt, et al (1993) documents results from a series of wind tunnel experiments on dust scouring for White Sands Missile Range (WSMR) and Ottawa sand soil beds. The WSMR dust sample was representative of a natural soil material ($D_{50} \simeq 250$ μm) with a wide particle size distribution whereas Ottawa sand corresponded to a monosized soil type with a 50% finer by weight diameter of ($D_{50} \simeq$) 180 μm. Measurements from this earlier Dust Sweep-Up (DSU) program quantified dependence of scouring rate and profile behavior on soil type, free stream velocity ($\leq$ 370 fps) and bed length ($\leq$ 20 feet). All data correspond to dry, loose, erodible soil beds with flat, smooth surface textures. The results as presented were provided in a data report format with relatively minor analysis/evaluation being performed on the overall data base. The purpose of the current technical effort is to perform a follow-up review and analysis of the DSU measurements with paticular emphasis on scaling considerations.

3.1 CLEAN FLOW VELOCITY SCALING.

Reduced velocity profiles for clean boundary layer flow in the DSU wind tunnel are presented in Figure 3-1a. The data as shown were measured "Pitot-statically" (TRW's thermally compensated Tri Sensor Snob probe) and correspond to flow over a "roughened" floor surface (Astroturf; blade height: 0.625") at flow speeds of 105, 205 and 310 fps. The plotting format used in Figure 3-1 is consistent with the semi-log technique conventionally used to "test" the flow's law of the wall velocity (u) behavior, namely;

$$u = 5.75\, u_f \log (y - y_{surf})/k_o + u_o \qquad (3.1)$$

Here u_f and u_o represent the shear and threshold velocities respectively, k_o is the effective wall roughness height and $y - y_{surf}$ corresponds to elevation above the wind tunnel's steel floor. As expected a "focusing" of the three velocity traces is evidenced (u_o: focus velocity; k_o: focus height) and a linear profile behavior is demonstrated. A replotting of the data in normalized coordinates is presented in Figure 3-1b and the low elevation results are seen to collapse to a common law of the wall scaling. Additional "clean flow" correlation results are provided in Figures 3-2 and 3-3. The data in the noted formats are seen to compare favorably with the Clauser correlation (Clauser, 1956) for rough wall boundary layers when a shear velocity ratio (u_e / u_f) of 12 is adopted.

3.2 SHEAR VELOCITY SCALING OF WSMR/OTTAWA SAND VELOCITY DATA.

Raw data velocity profiles for WSMR and Ottawa sand soil beds are summarized in Figures 3-4 and 3-5, respectively. As was the case for the clean wall profile data discussed above in Section 3.1, the noted dusty flow results demonstrate similar law of the wall behavior for near surface elevations.

Shear velocity values derived from Equation 3.1 for the indicated test cases (as well as the previous clean flow experiments) are summarized in Figure 3-6. For a given bed length, the data indicate (Figure 3-6a) a near linear variation of u_f with the edge velocity (u_e) with the ratio u_e / u_f increasing with axial distance ($10 \leq u_f / u_e \leq 25$). A replotting of the data in Figure 3-6b illustrates that shear velocity tends to decay with distance, a finding which will be discussed further in Section 3.4 where DSU scouring rate data will be reevaluated.

Scaled profile results for both WSMR and Ottawa sand test data are summarized in Figure 3-7. A favorable correlation of the assembled data sets is seen to be in evidence. Such a result supports the dusty law of the wall modeling approach put forward

by Denison and Baum (1986) and others for treating the dusty boundary layer problem.

3.3 DUSTY BOUNDARY LAYER CORRELATIONS.

Since documentation of the DSU raw data measurements, users of the reduced results have pursued various approaches to correlating the overall data base (e.g. Hookham, et al, 1994). Figures 3-8 through 3-13 provide a summary of many of such reduction procedures and include velocity and dusty density profile correlations for both WSMR and Ottawa sand results. The data are plotted both as a function of normalized elevation above the soil surface,

$$\eta = "Eta" = (y / y_{surf}) / \delta_u \tag{3.2}$$

and, as suggested by Kuhl, et al (1990), elevation above the focus point for the dust density profiles (Figures 3-15 and 3-16),

$$\eta_o = "Etao" = (y - y_o) / \delta_u . \tag{3.3}$$

Here, δ_u corresponds to the velocity profile "tangent-slope" edge thickness (in log-log format) and y_o represents the focus elevation, a definition consistent with our previous shock tube experiments on dusty boundary layer scouring (Batt, et al, 1986, 1990 and 1991). The term "KBAR", as seen in Figures 3-17 through 3-20, corresponds to the normalized dust density parameter which approaches 1 at the boundary layer edge and ∞ at the soil surface. It is defined as:

$$\bar{k} = (1 + \rho_{dust} / \rho_{air})^{-1} \tag{3.4}$$

with ρ_{dust} and ρ_{air} representing the density of the local dust flow and air, respectively. Results are presented in log-log, semi-log and lin-lin format to assist other workers in their evaluation/interpretation of the DSU data base.

Comparison of the respective velocity data are made with both power law profile scaling,

$$u/u_e = (y/\delta_u)^n \tag{3.5}$$

and Clauser's rough wall relationship, given by Equation 3.1. The WSMR data are seen to correlate best to a power law slope (n) of 0.5 and a velocity ratio of (u_e/u_f) of 14. Corresponding values for n and u_e/u_f for the Ottawa sand data are 0.75 and 11, respectively. For the shock tube results, a slope of 0.7 was found to best correlate the overall data set for both WSMR dust and Frenchman's Lake fine sand soil. Also shown for completeness purposes herein are earlier velocity results for Ottawa sand profile data (Figure 3-14) measured by Hartenbaum (1971).

3.4 CORRELATION OF DSU SCOURING RATE MEASUREMENTS.

In the final report for the DSU program reference was made to the dependence of scouring rate ("M dot" $\equiv \dot{m}$) on edge mass flux ($\rho_e u_e$), bed length and free stream velocity (Mach number). For each of the nine runs for the two soil types tested, determination of "M dot" as a function of bed length was based on pre/post test soil recession measurements. Typical M dot results as normalized with edge mass flux, are summarized in Figures 3-21a and 3-21b for the WSMR and Ottawa Sand data, respectively. Although the results as shown exhibit moderate correlation with $\rho_e u_e$, there still exists evidence of a dependence on free stream Mach number (M). As noted in the DSU final, this dependence appeared to correspond to Mach number to the one-half power. Figure 3-22 demonstrates that such a correlation approach provides a satisfactory collapsing of the bulk of the scouring rate data.

Evidence of the noted Mach number dependence is illustrated by the summary plot in Figure 3-23 of the soil loss data for the WSMR

soil beds in the DSU wind tunnel. Both profile integrated results (DSU program),

$$Q = \int_o^e \rho_d u_d d_y \tag{3.6}$$

as well as dust throughput data measured with a boundary layer slot collector (Bagnold collector; Section 4) are shown. Note the adequate agreement between the two measurement techniques. A variation of throughput with velocity/Mach number to the 3/2's power is in evidence. Such a sensitivity to local free stream velocity is in contrast to soil loss data for low speed flows as measured by the data of Shao, et al (1993). For this latter flow, a power law dependence to the cube power of velocity is indicated which agrees with the predictions of Bagnold (1941) and Owen (1964) for saltation flow. The noted discrepancy in power law behavior is attributed to the fact that flow regimes differ between the two sets of data. For example, the lower speed results ($u \leq 50$ FPS) reflect a scouring mechanism associated with gravity/collision dominated "saltation" effects whereas the current results correspond to flows controlled by turbulent diffusion processes where drag to weight ratios are large (200 μm: D/W = 300 @ 100 FPS, 1000 @ 350 FPS). It is not surprising then that different scaling laws would apply.

Although the noted Mach number scaling indicates a favorable collapsing of the overall data base, there still exists some sensitivity to soil type and bed length. In an attempt to account for the effects of soil type, both sets of data have been replotted, as suggested by Mazzola (1993), in terms of normalized bed length, namely, x / D_{50}, with D_{50} representing the 50% finer by weight diameter for the respective soil samples. Results are shown in Figure 3-24 and good agreement with this correlation procedure is illustrated. Note that the decrease in scouring rate with bed length, evident in Figures 3-21 and 3-22 was estimated in Batt, et al (1993) to be representative of an exponential decay

process. By replotting the Figure 3-24a results in the semi-log format of Figure 3-24b, the exponential nature of the rate dependence on axial distance is demonstrated.

One final scaling approach to the DSU scouring rate results is illustrated in Figure 3-25. Here the rates have been normalized by a mass flux based on shear velocity (Figure 3-6) rather than edge velocity. It is interesting to note that this scaling procedure, one that has been suggested by various workers investigating the dusty boundary layer problem (e.g. Rosenblatt, et al 1985; Denison and Baum, 1986; Traci, 1988; Pierce, 1989; Gaj and Small, 1989), appears to moderate the bed length dependence noted above and to collapse both sets of data to a universal normalized rate of,

$$\dot{m} / (\rho_e u_f M_e^{0.5}) \simeq 0.3 \pm 0.1. \qquad (3.7)$$

For comparison purposes, Rosenblatt, et al (1985) and Traci (1988) suggested constant values for $\dot{m} / \rho_e u_f$ of 0.4 and 0.33, respectively!

3.5 DUSTY FLOW SCHMIDT NUMBER SCALING.

One consideration which sweep-up modelers have inquired about was the relationship between dust density profiles and velocity profiles. Such a relationship provides information regarding the magnitude of the turbulent Schmidt number for the DSU results. As noted by Denison (Hookham, et al, 1994), this "measure" of mass diffusivity relative to diffusivity of momentum can be determined, approximately, by scaling velocity profiles to dust density profiles as follows:

$$\bar{k} = (u / u_e)^{\sigma} \qquad (3.8)$$

where $\bar{k} = (1 + k)^{-1}$

$$k = \rho_{dust} / \rho_{air}$$

σ = Turbulent Schmidt number

Figures 3-26 and 3-27 show this correlation approach for both WSMR and Ottawa sand data and a value for σ of approximately 0.7 provides favorable agreement with the bulk of the data.

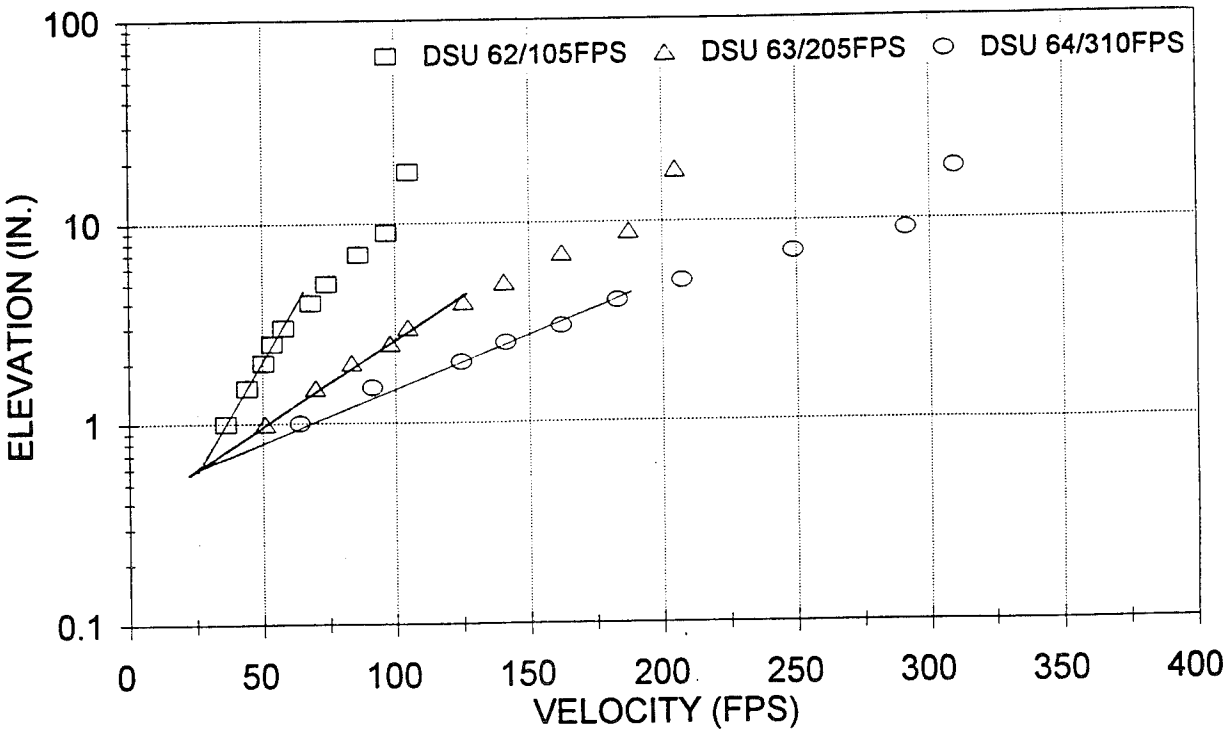

(a) Log height velocity profile data

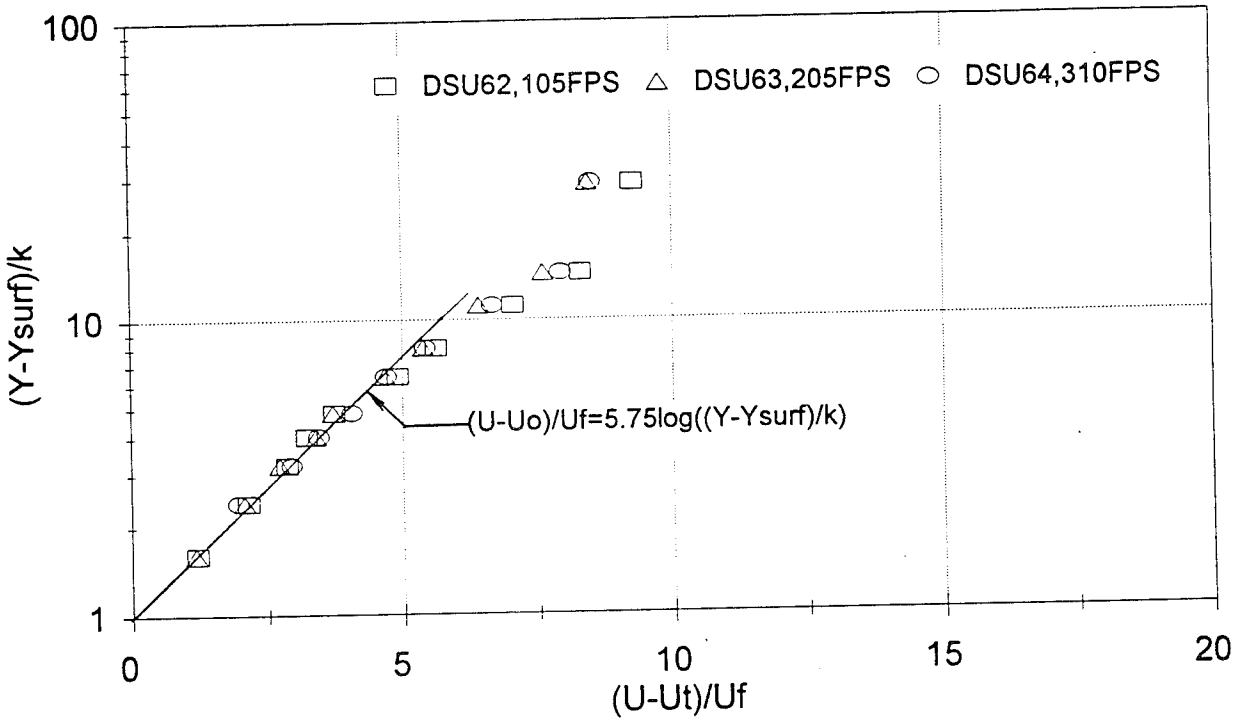

(b) Scaled velocity profiles

Figure 3-1. Velocity profiles for clean "Astroturf" boundary layers (21' 4" location).

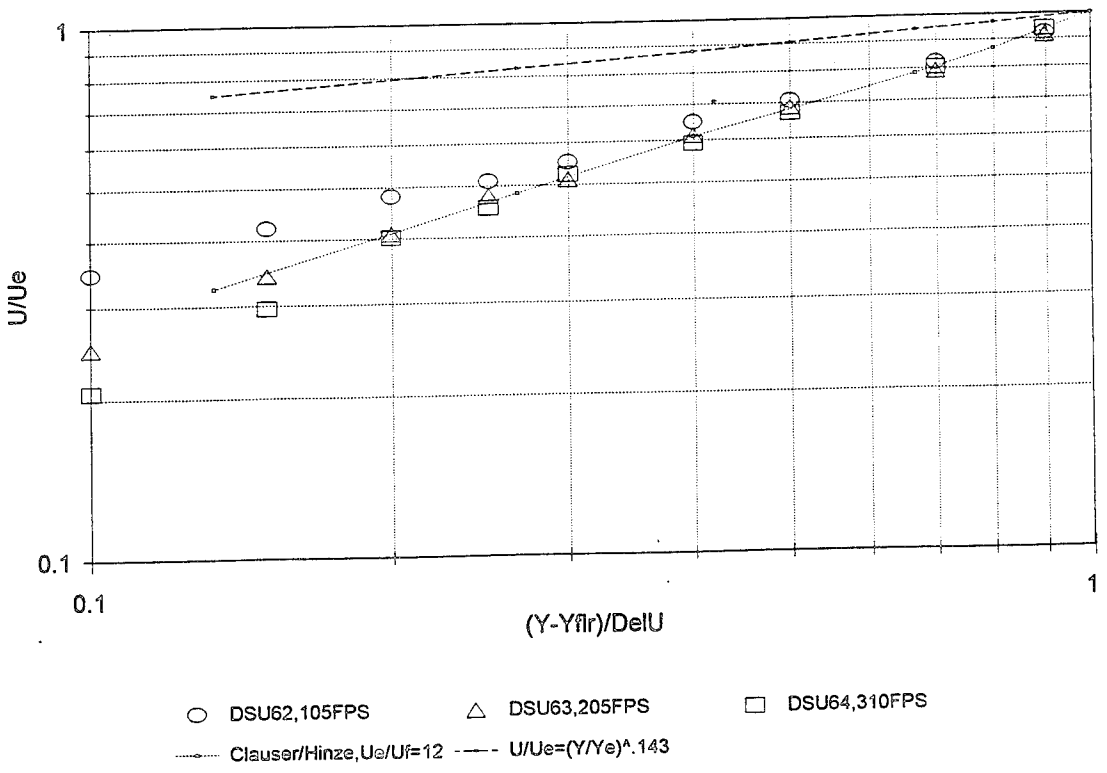

(a) Power law evaluation

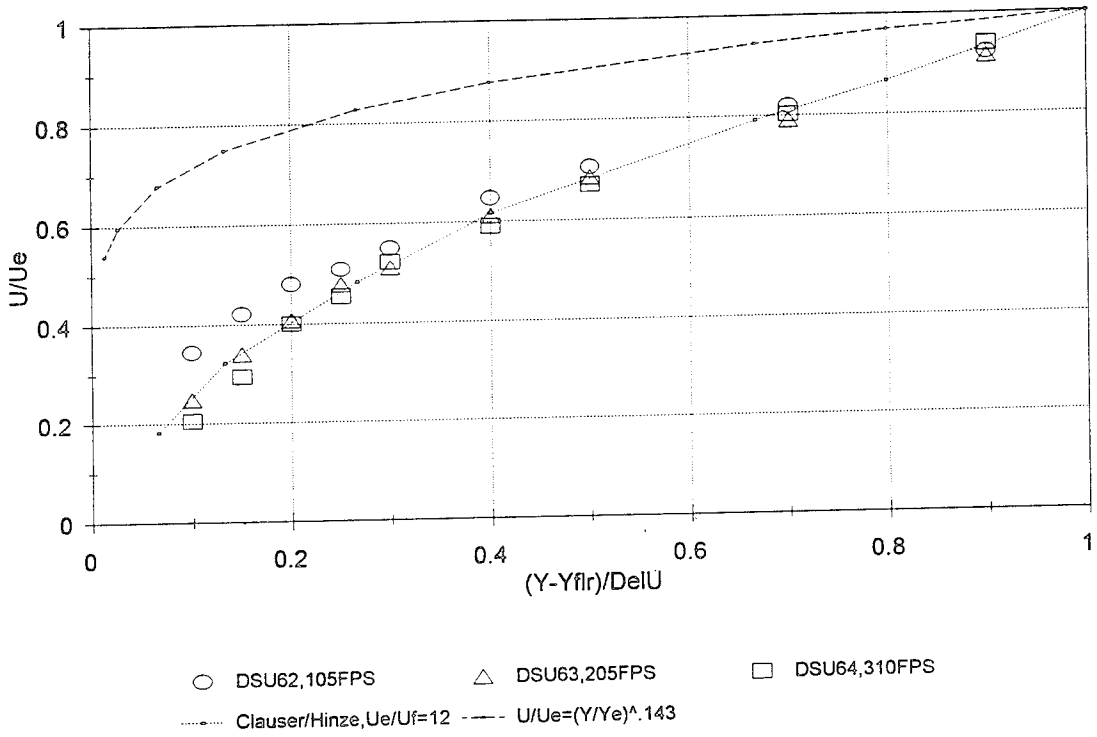

(b) Lin-lin plotting comparisons

Figure 3-2. Velocity profile summary for clean Astroturf boundary layers (21' 4" location).

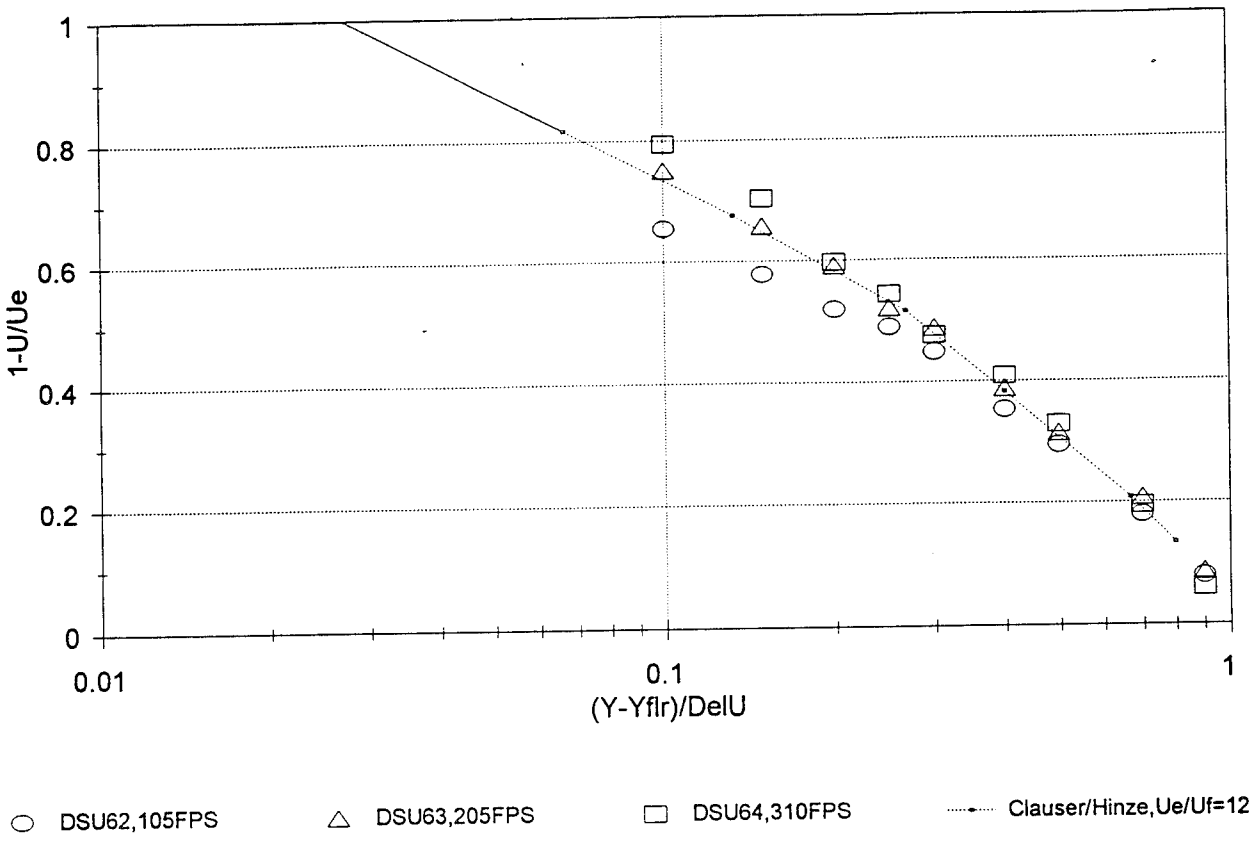

Figure 3-3. Velocity defect profile summary for clean Astroturf boundary layers (21' 4" location).

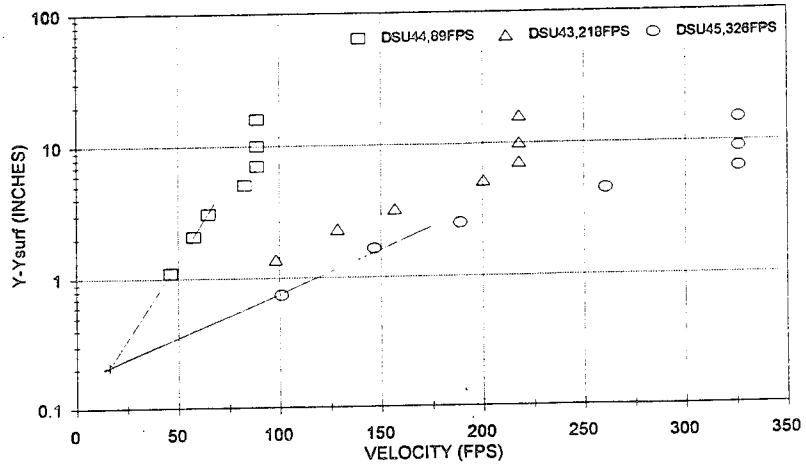

(a) 7 Foot bed length

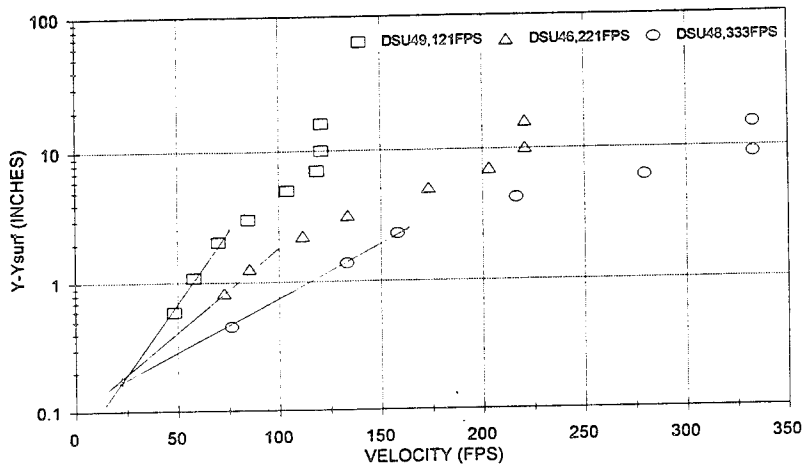

(b) 13 Foot bed length

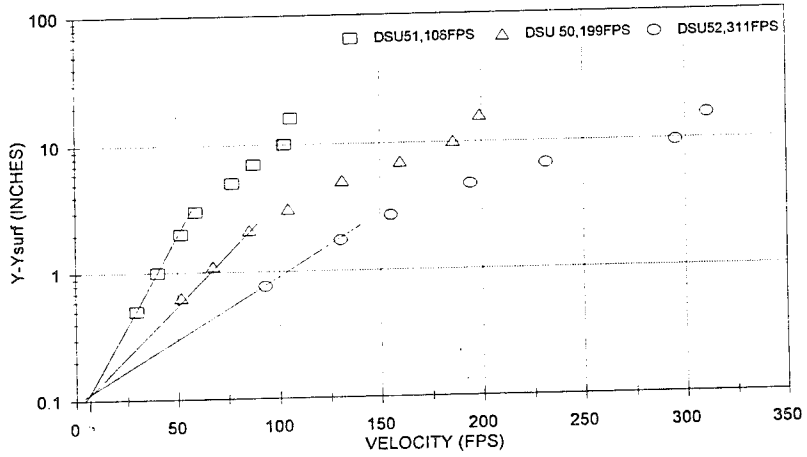

(c) 19 Foot bed length

Figure 3-4. Log height velocity profiles for WSMR DSU experiments.

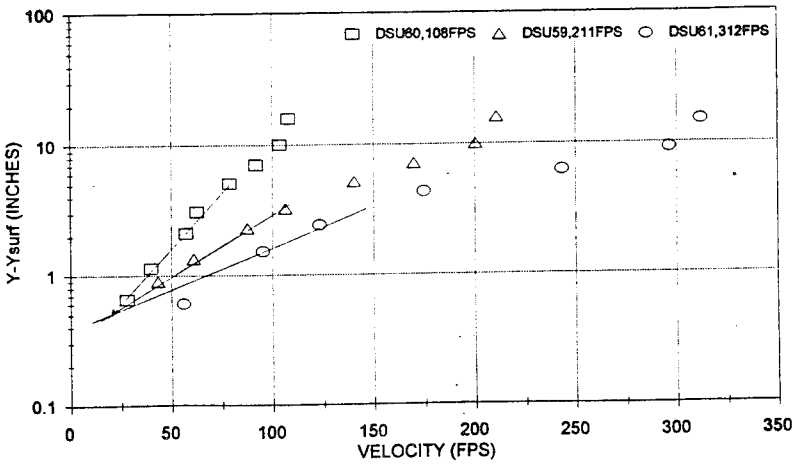

(a) 7 Foot bed length

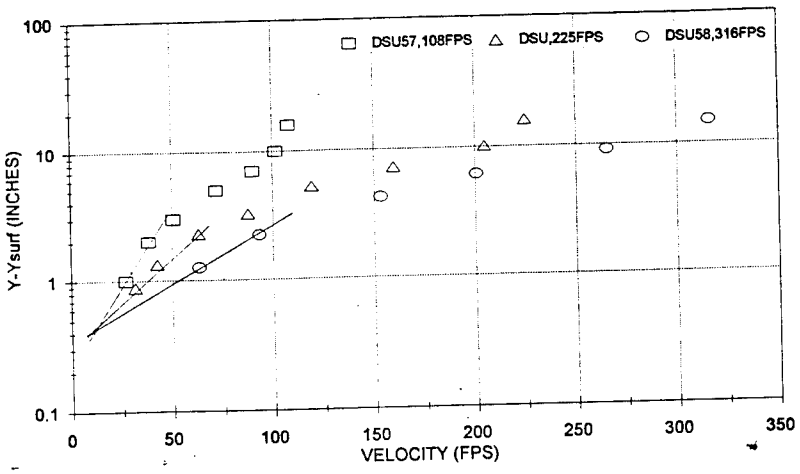

(b) 13 Foot bed length

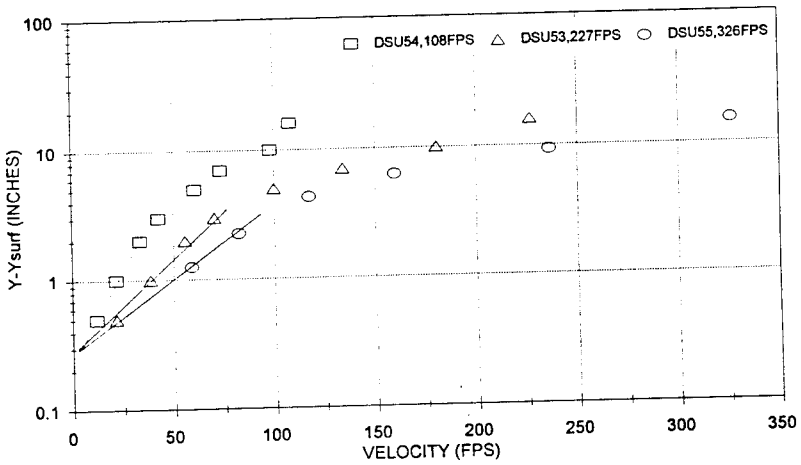

(c) 19 Foot bed length

Figure 3-5. Log height velocity profiles for Ottawa sand DSU experiments.

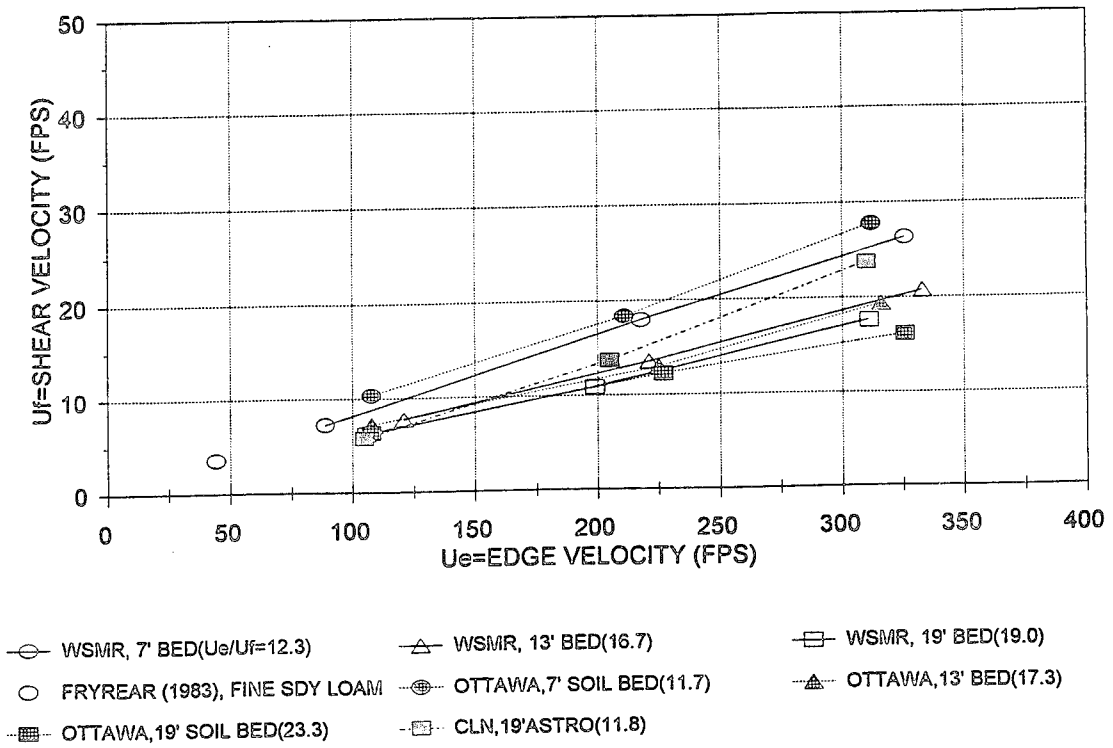

(a) Velocity dependence

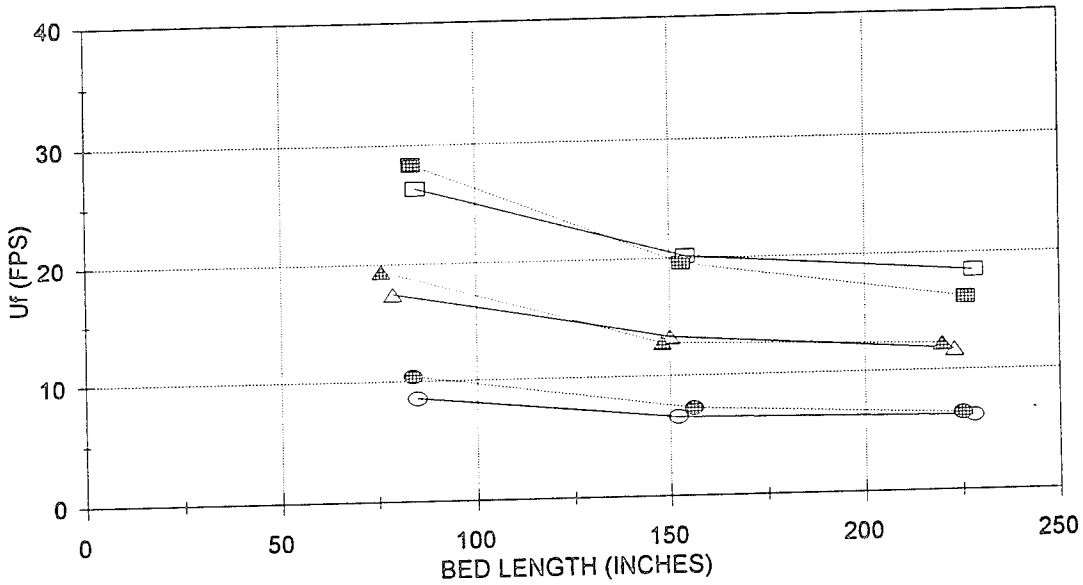

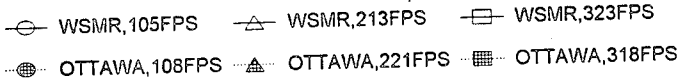

(b) Bed length dependence

Figure 3-6. DSU shear velocity summary.

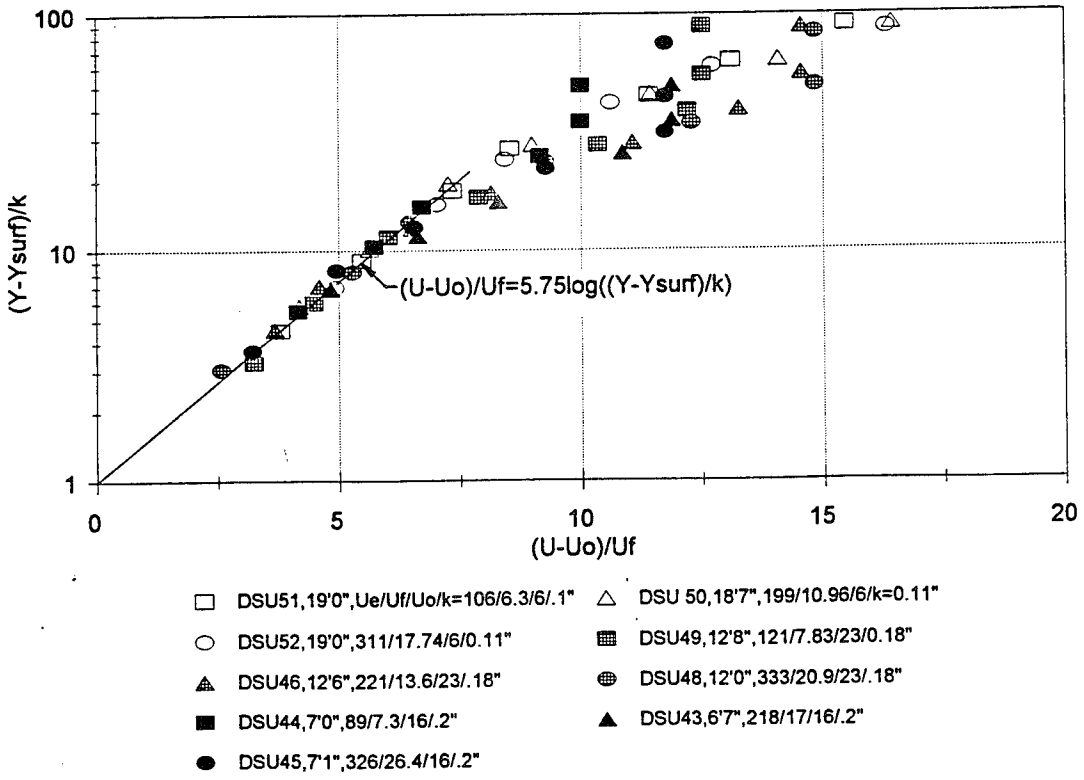

(a) WSMR

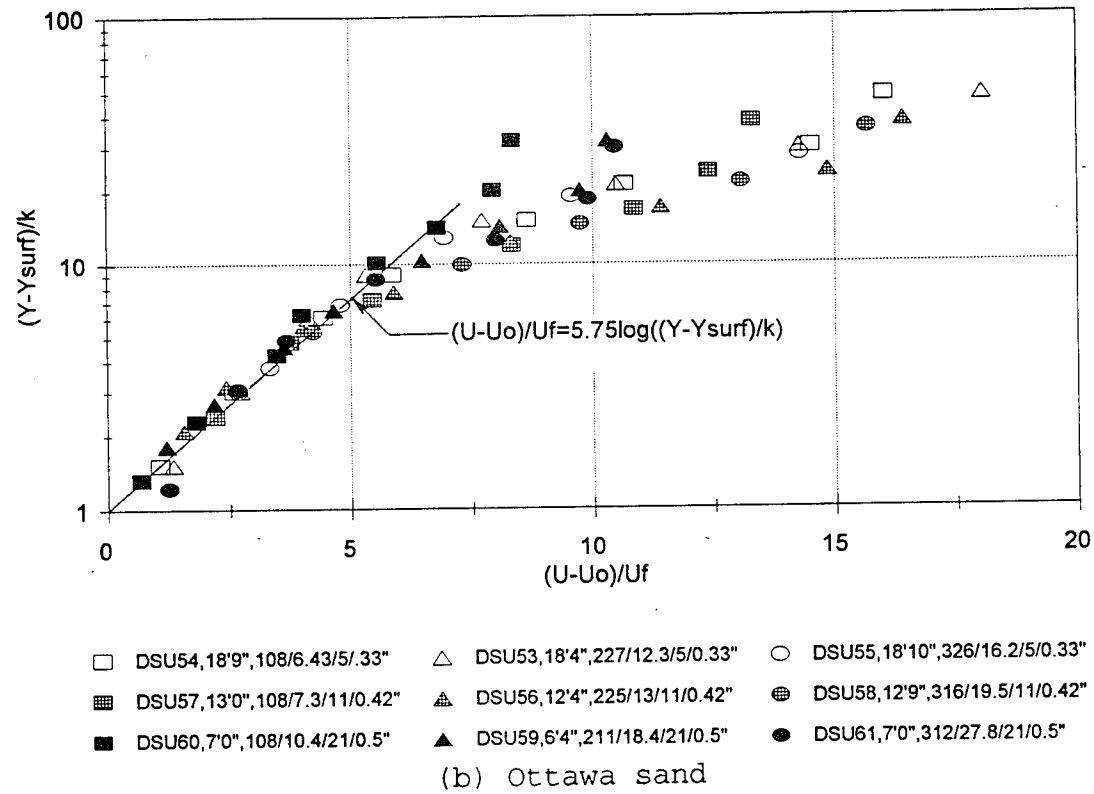

(b) Ottawa sand

Figure 3-7. Velocity scaling summary for DSU experiments.

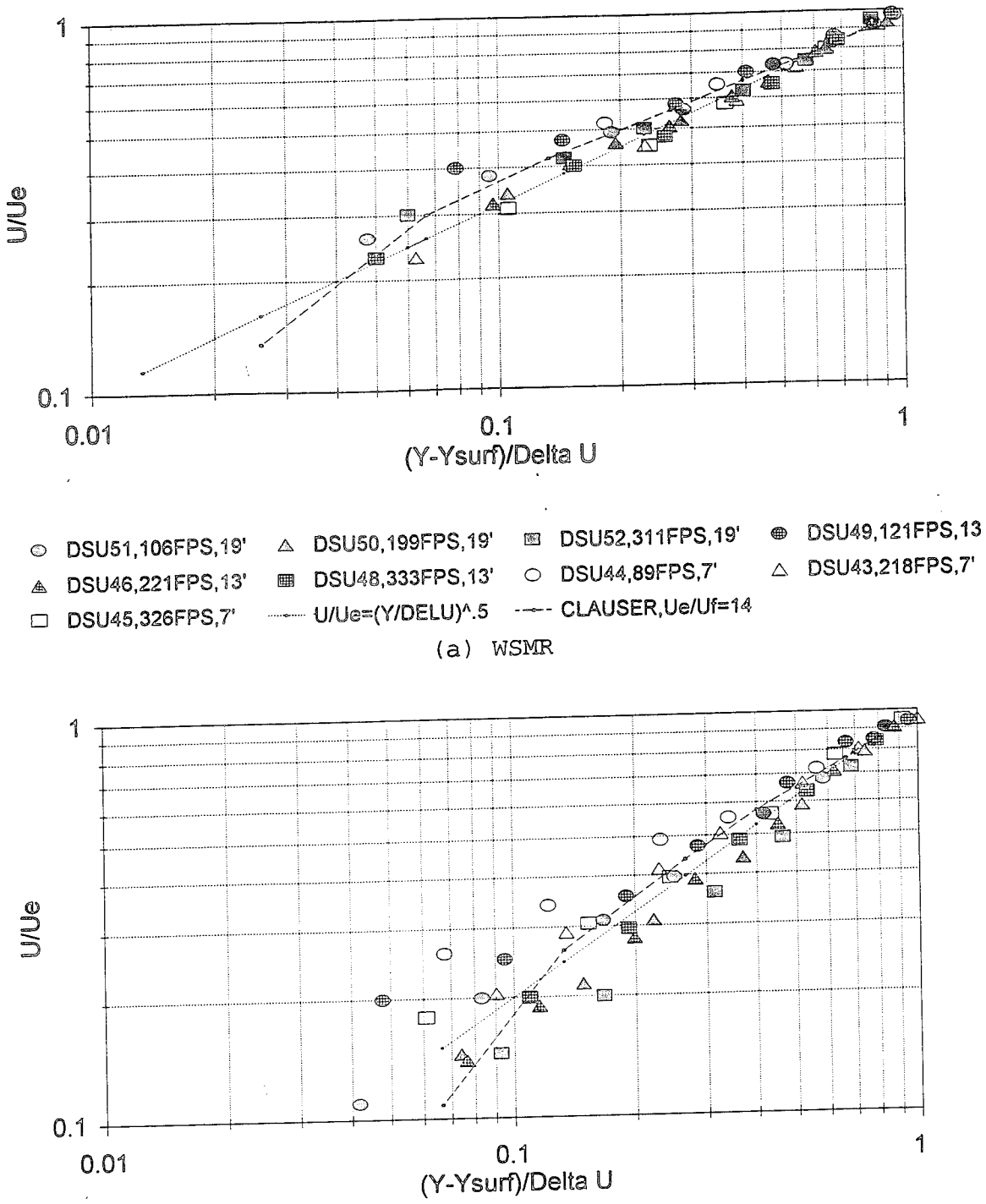

Figure 3-8. Power law velocity scaling summary for DSU experiments (Surface elevation).

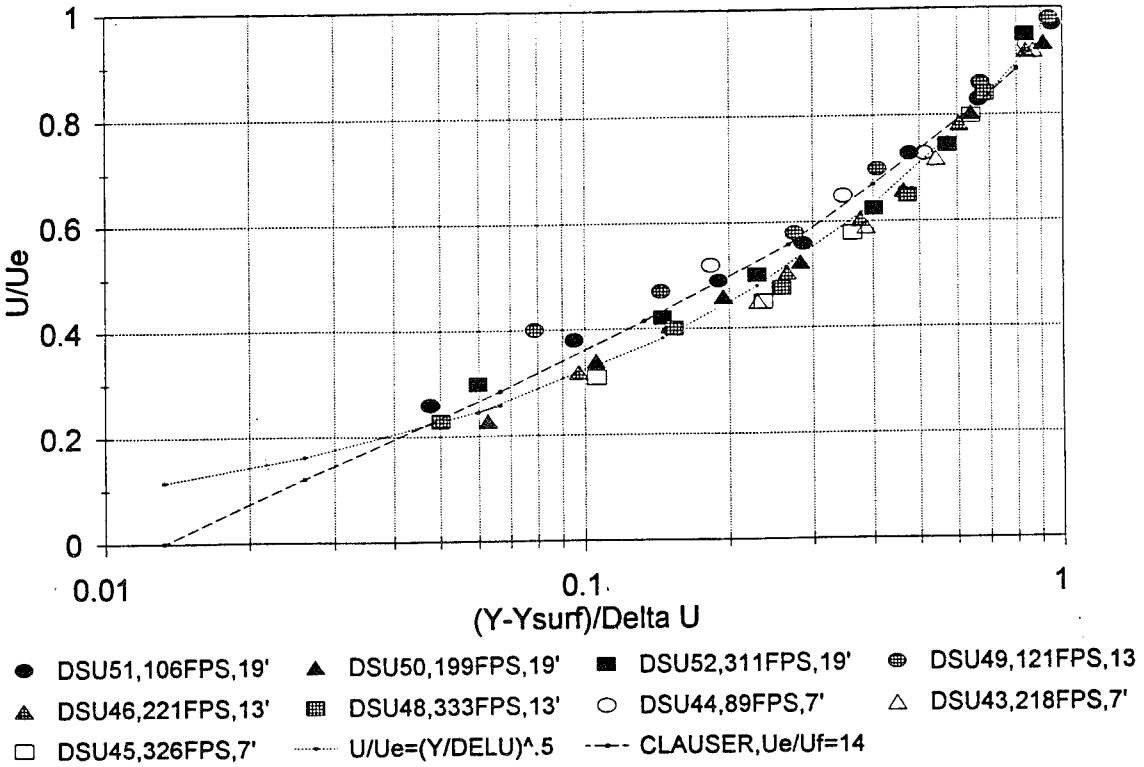

(a) WSMR

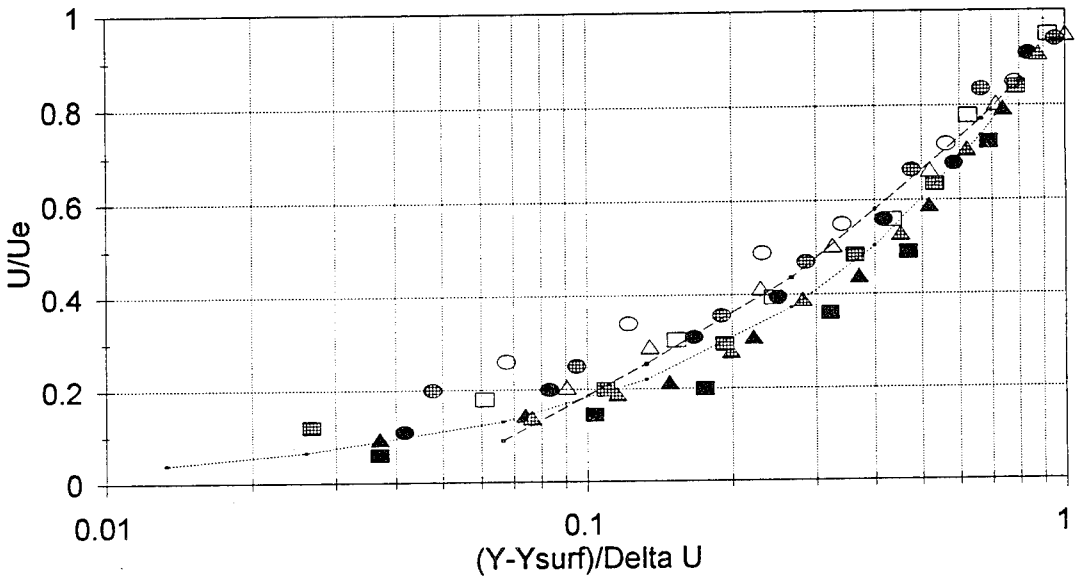

(b) Ottawa sand

Figure 3-9. Semilog velocity scaling summary for DSU experiments (Surface elevation).

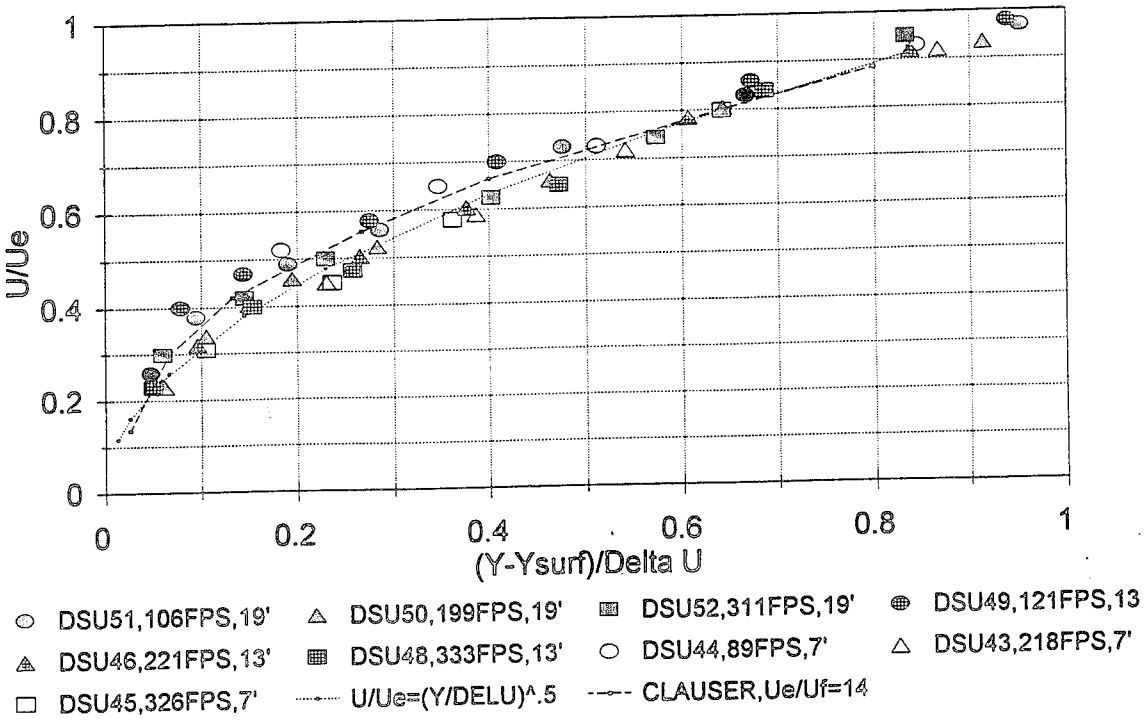

(a) WSMR

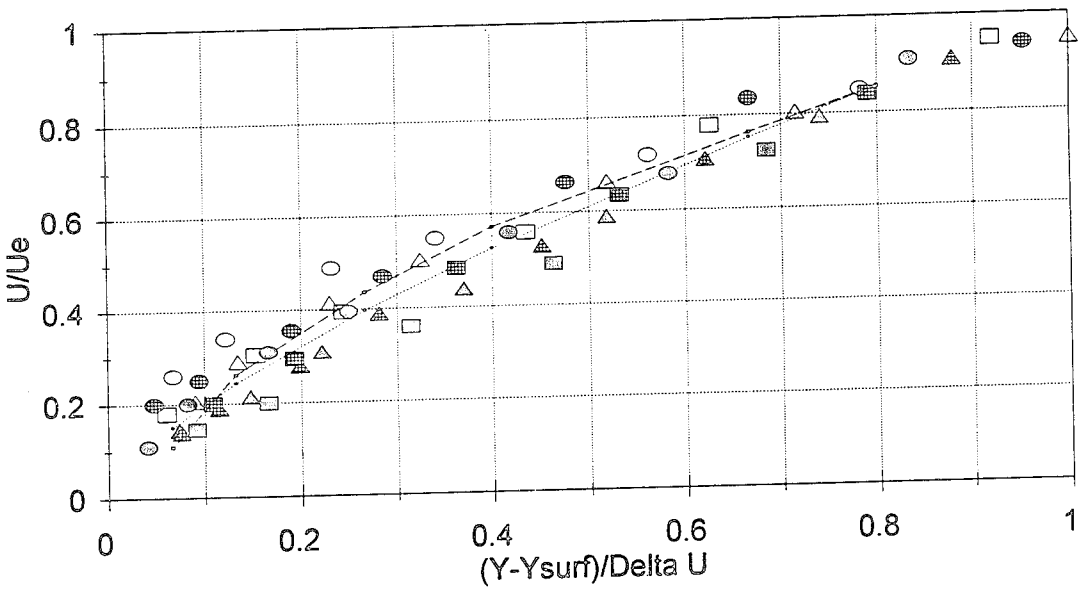

(b) Ottawa sand

Figure 3-10. Lin-lin velocity scaling summary for DSU experiments (Surface elevation).

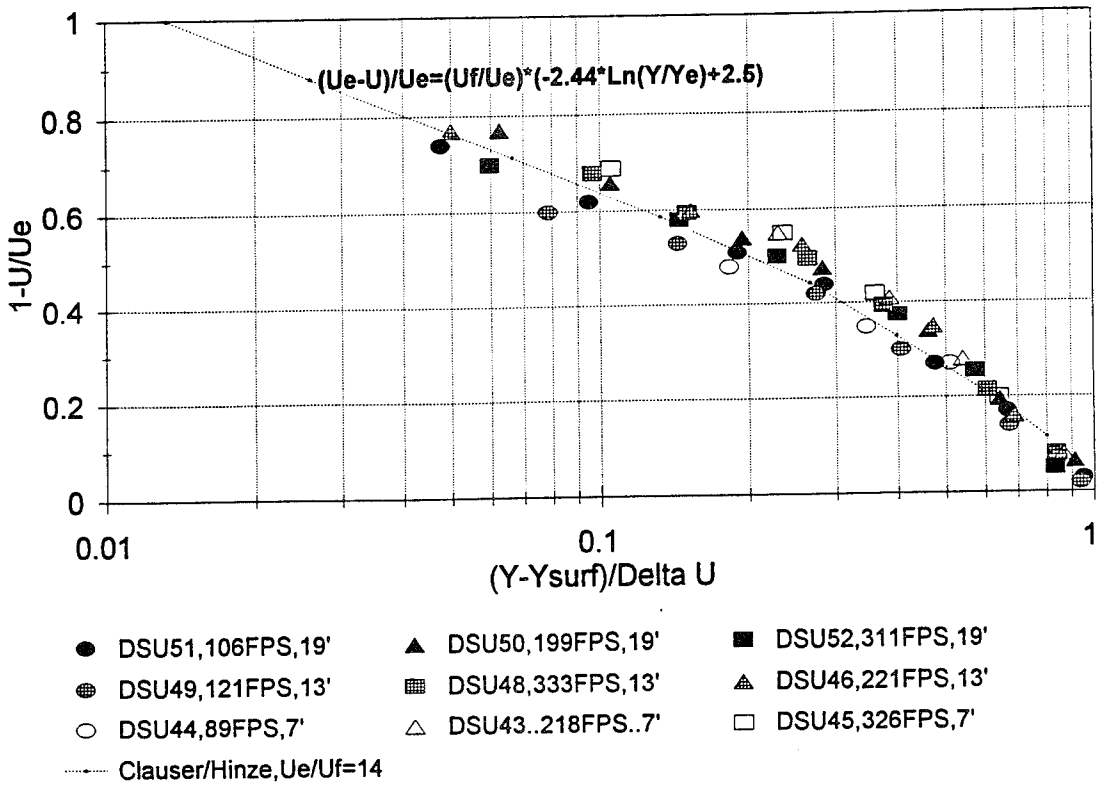

(a) WSMR

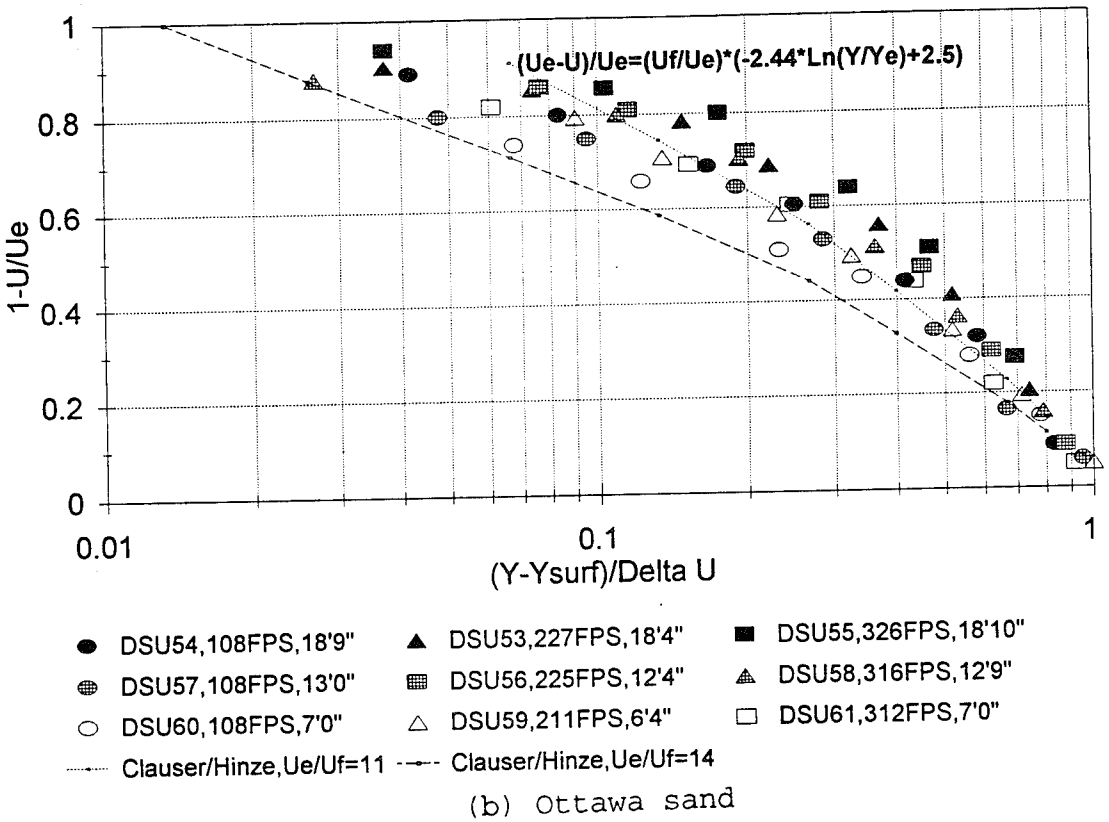

(b) Ottawa sand

Figure 3-11. Velocity defect scaling summary for DSU experiments (Surface elevation).

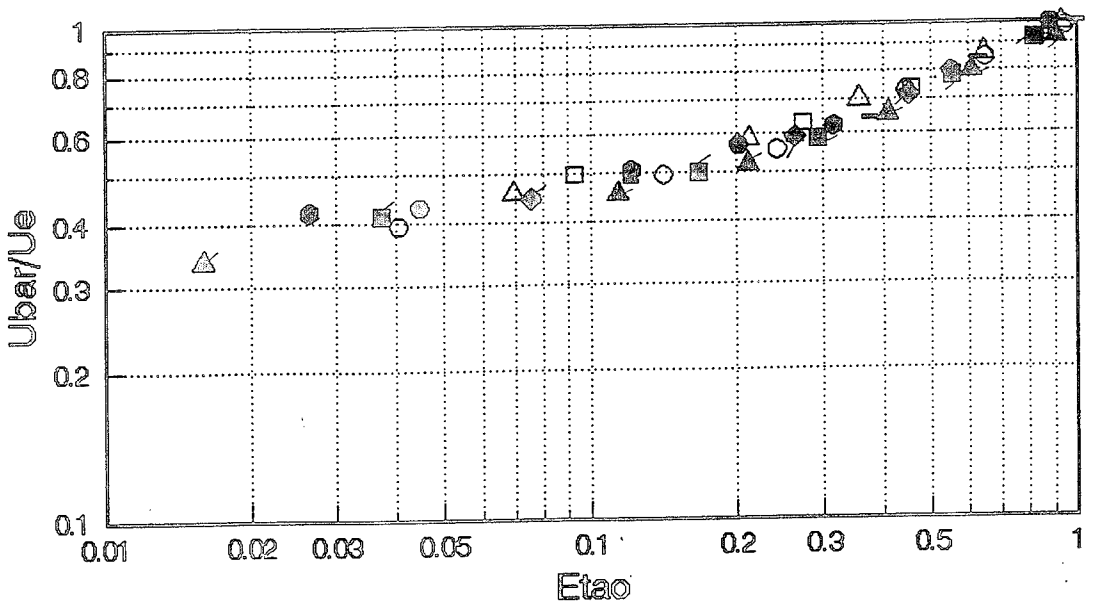

DSU 44/89 FPS	49/121	51/106	43/218	46/221	50/199	45/326	48/333	52/311
0.6"/7'1"	0.6"/12'8"	0.6"/19'0"	1.0"/6'7"	1.0"/12'6"	1.0"/18'7"	1.4"/7'1"	1.4"/12'10"	1.4"/19'0"

(a) WSMR

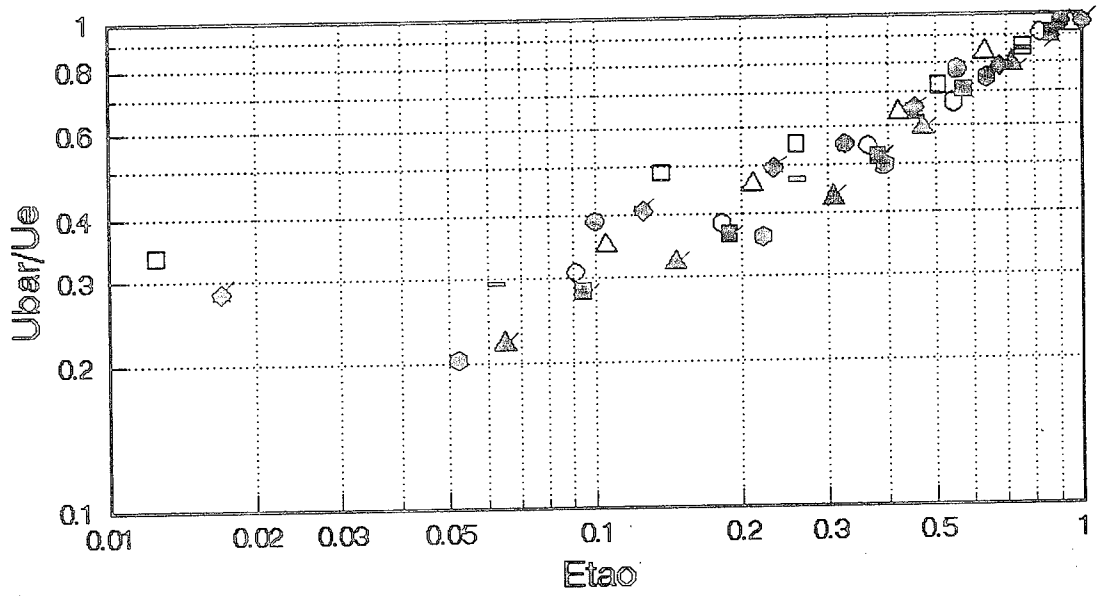

DSU 60/108 FPS	57/108	54/108	59/211	56/225	53/227	61/312	58/316	55/326
1.0"/7'0"	1.0"/13'5"	1.0"/18'9"	1.2"/6'4"	1.2"/12'4"	1.2"/18'4"	1.6"/7'0"	1.6"/12'9"	1.6"/18'10"

(b) Ottawa sand

Figure 3-12. Power law velocity scaling summary for DSU experiments (Profile focus elevation).

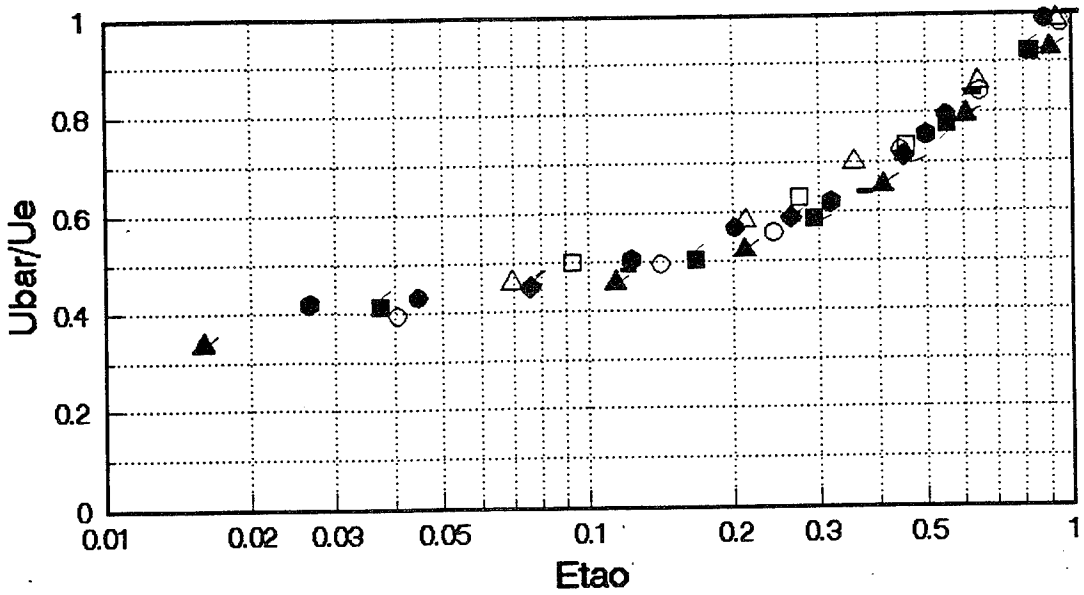

DSU 44/89 FPS	49/121	51/106	43/218	46/221	50/199	45/326	48/333	52/311
0.6"/7'1"	0.6"/12'8"	0.6"/19'0"	1.0"/6'7"	1.0"/12'6"	1.0"/18'7"	1.4"/7'1"	1.4"/12'10"	1.4"/19'0"

(a) WSMR

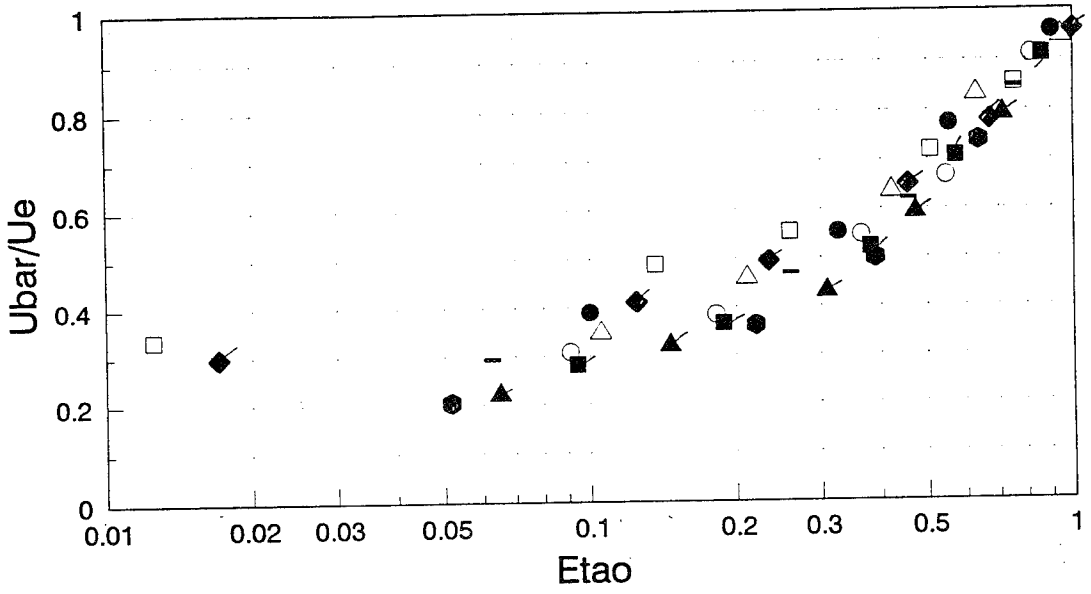

DSU 60/108 FPS	57/108	54/108	59/211	56/225	53/227	61/312	58/316	55/326
1.0"/7'0"	1.0"/13'5"	1.0"/18'9"	1.2"/6'4"	1.2"/12'4"	1.2"/18'4"	1.6"/7'0"	1.6"/12'9"	1.6"/18'10"

(b) Ottawa sand

Figure 3-13. Semilog velocity scaling summary for DSU experiments (Profile focus elevation).

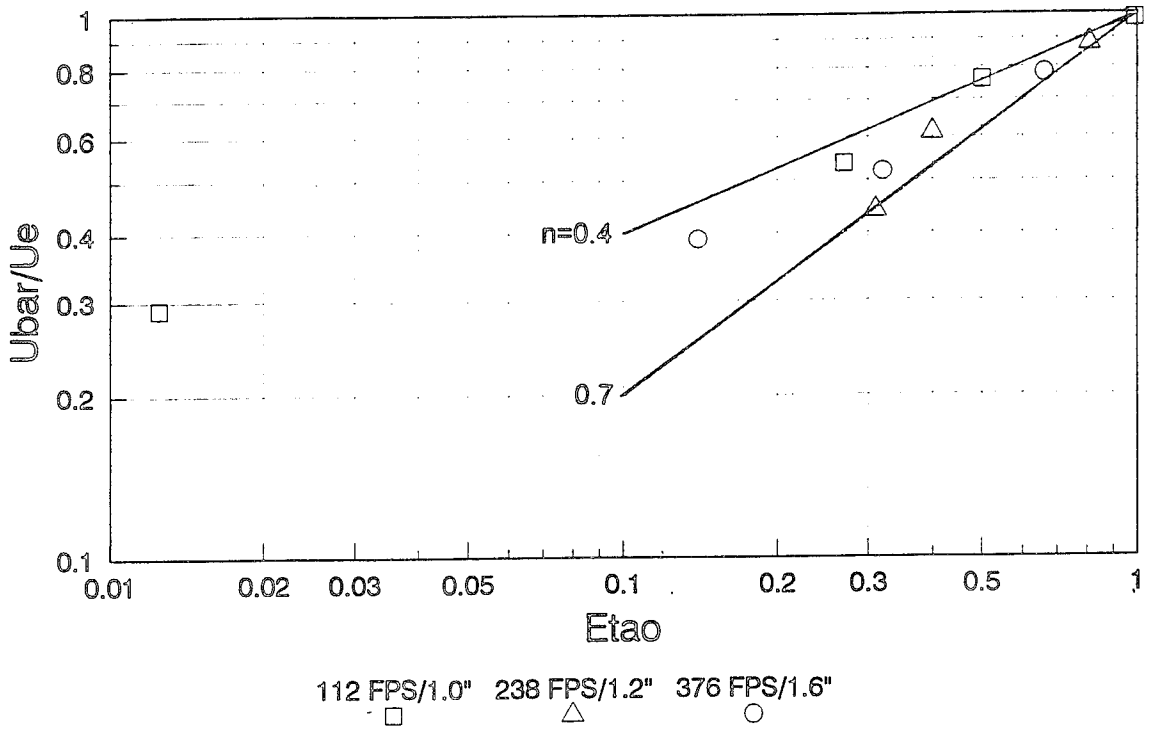

(a) Power law scaling

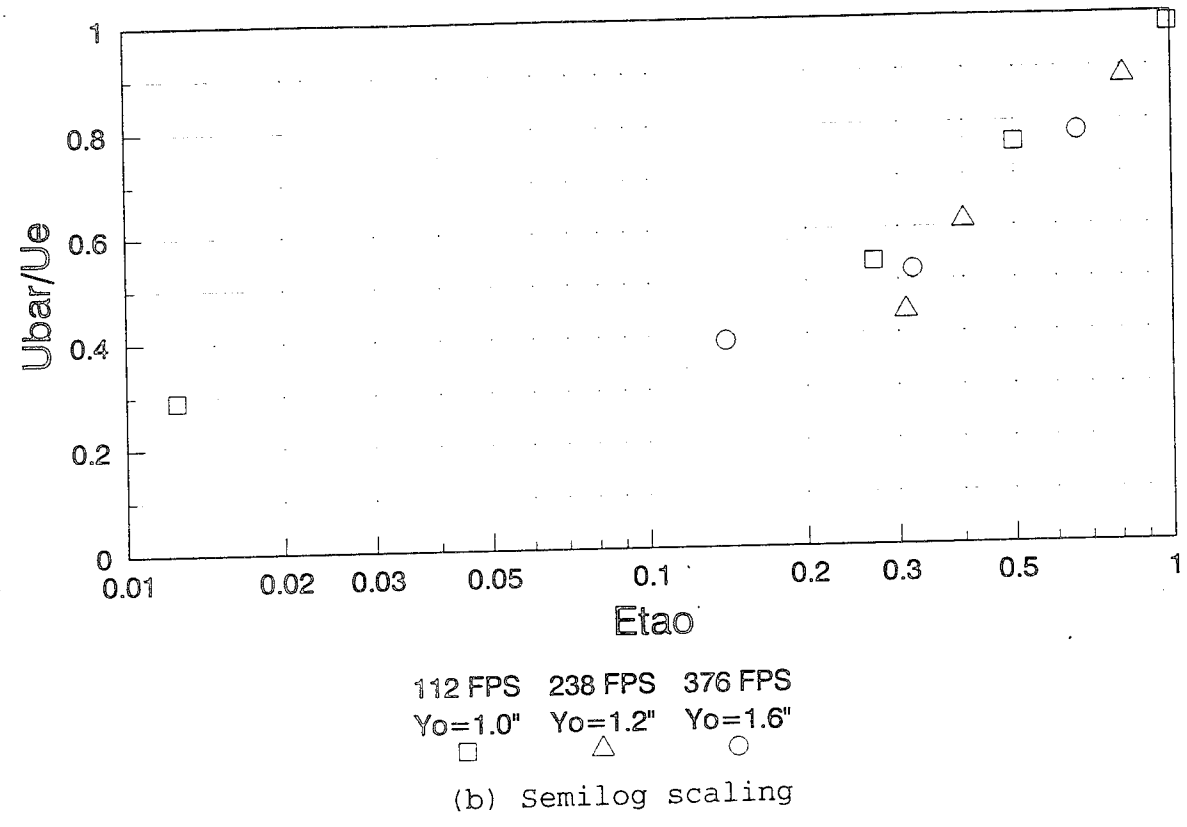

(b) Semilog scaling

Figure 3-14. Velocity profile scaling for Hartenbaum Ottawa sand experiments (17 foot bed length; profile focus elevation).

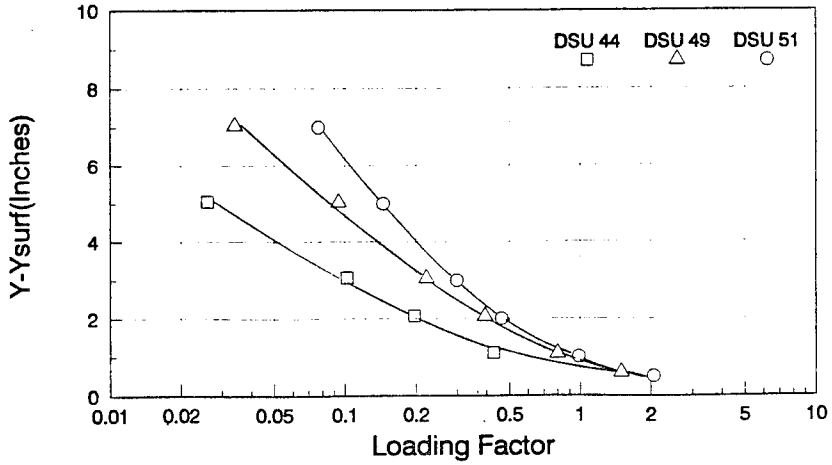

(a) 7 Foot bed length

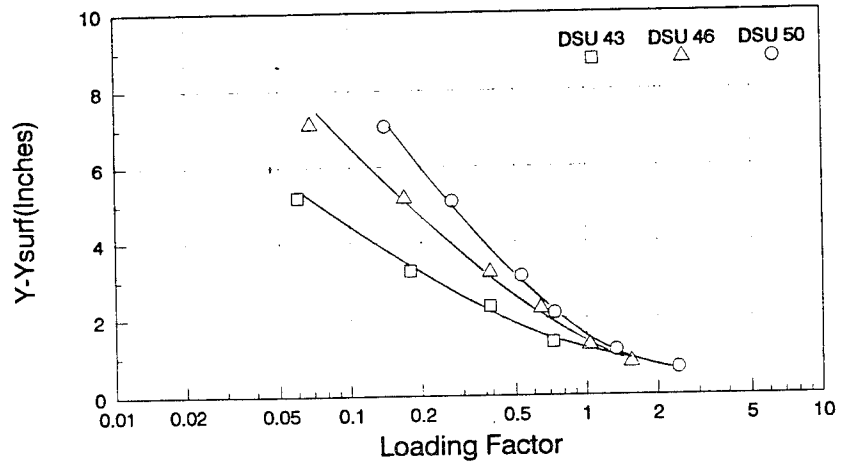

(b) 13 Foot bed length

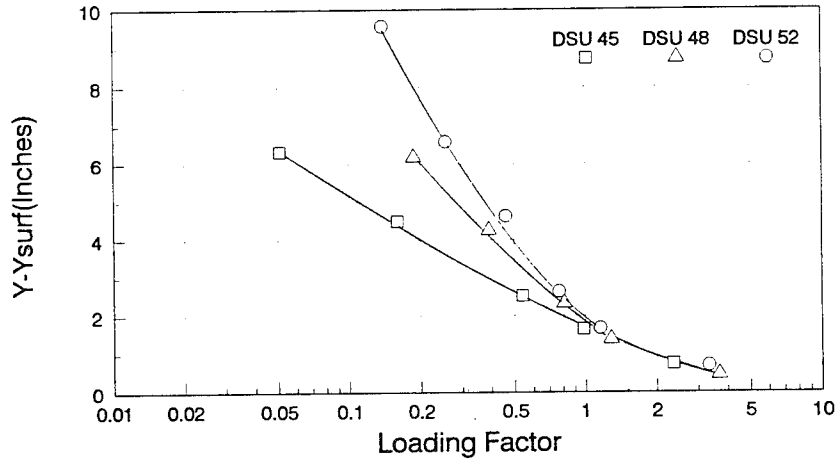

(c) 19 Foot bed length

Figure 3-15. Loading factor profiles for WSMR DSU experiments.

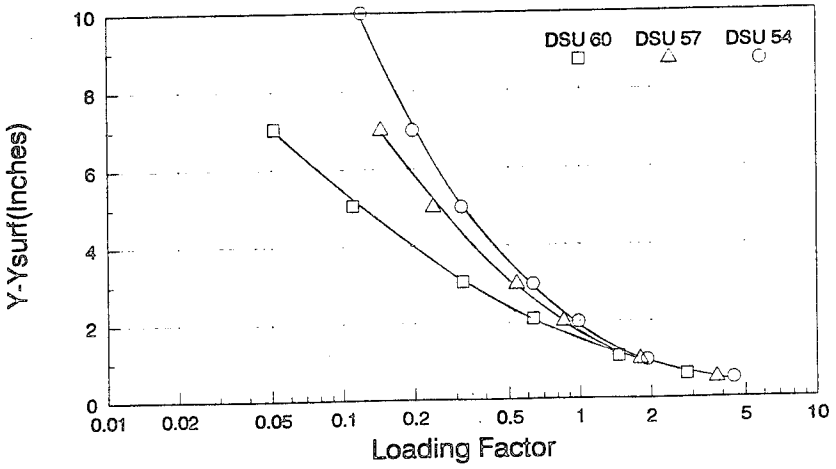

(a) 7 Foot bed length

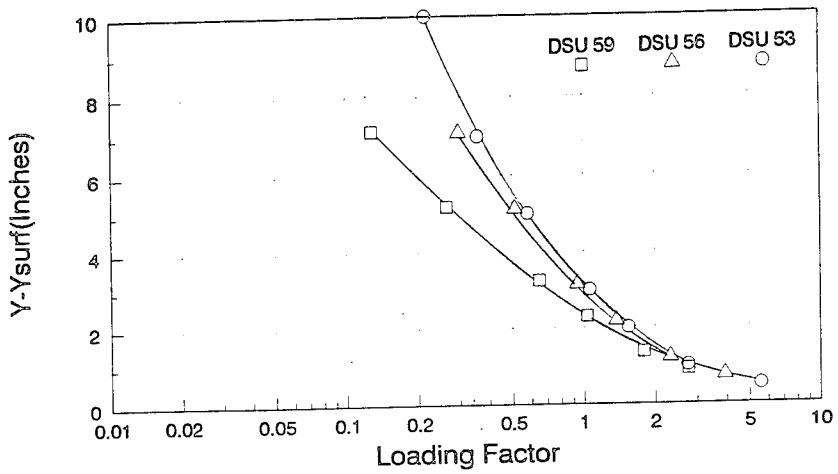

(b) 13 Foot bed length

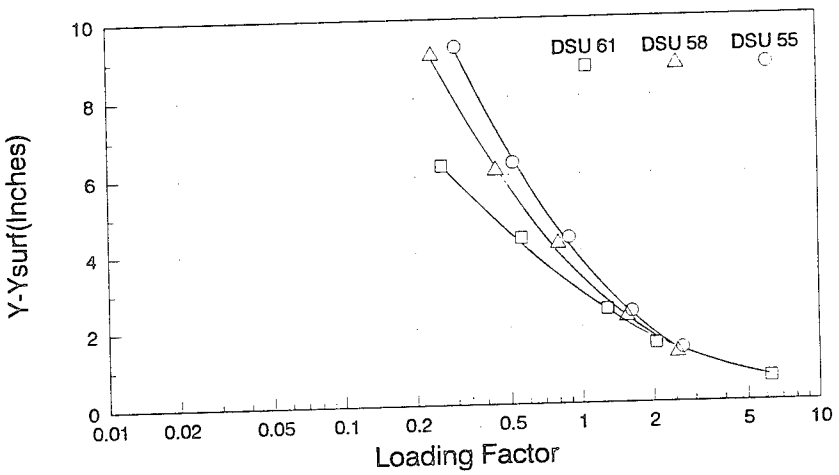

(c) 19 Foot bed length

Figure 3-16. Loading factor profiles for Ottawa sand DSU experiments.

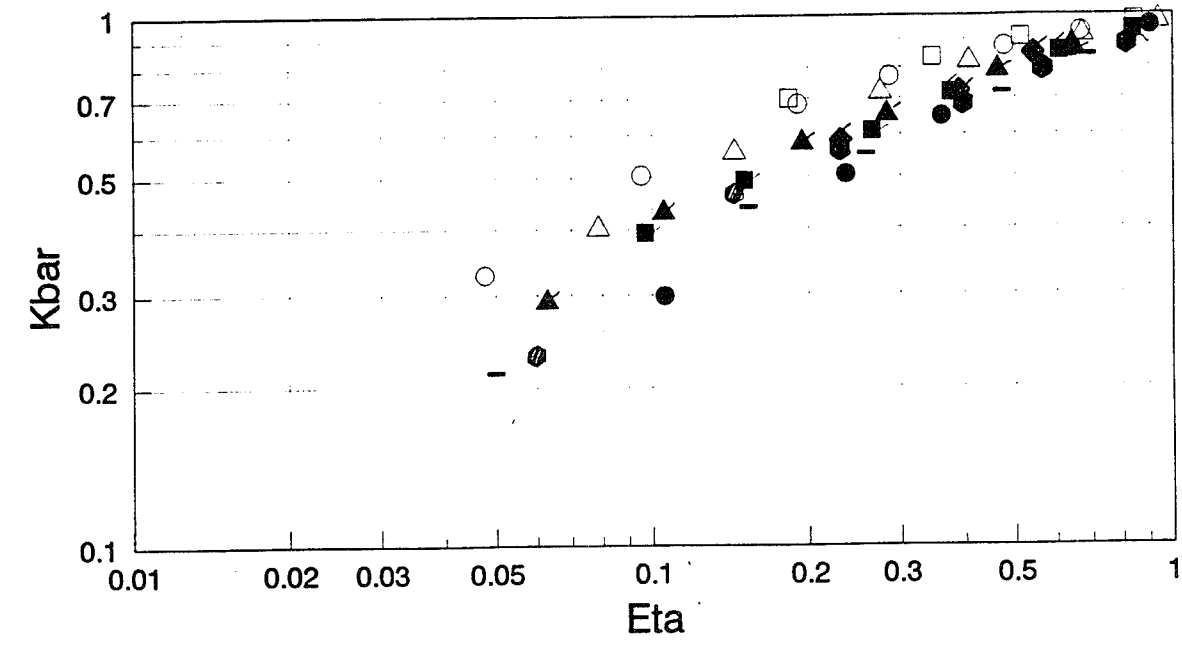

DSU 44/89 FPS	49/121	51/106	43/218	46/221	50/199	45/326	48/333	52/311
7'1"	12'8"	19'0"	6'7"	12'6"	18'7"	7'1"	12'10"	19'0"

(a) WSMR

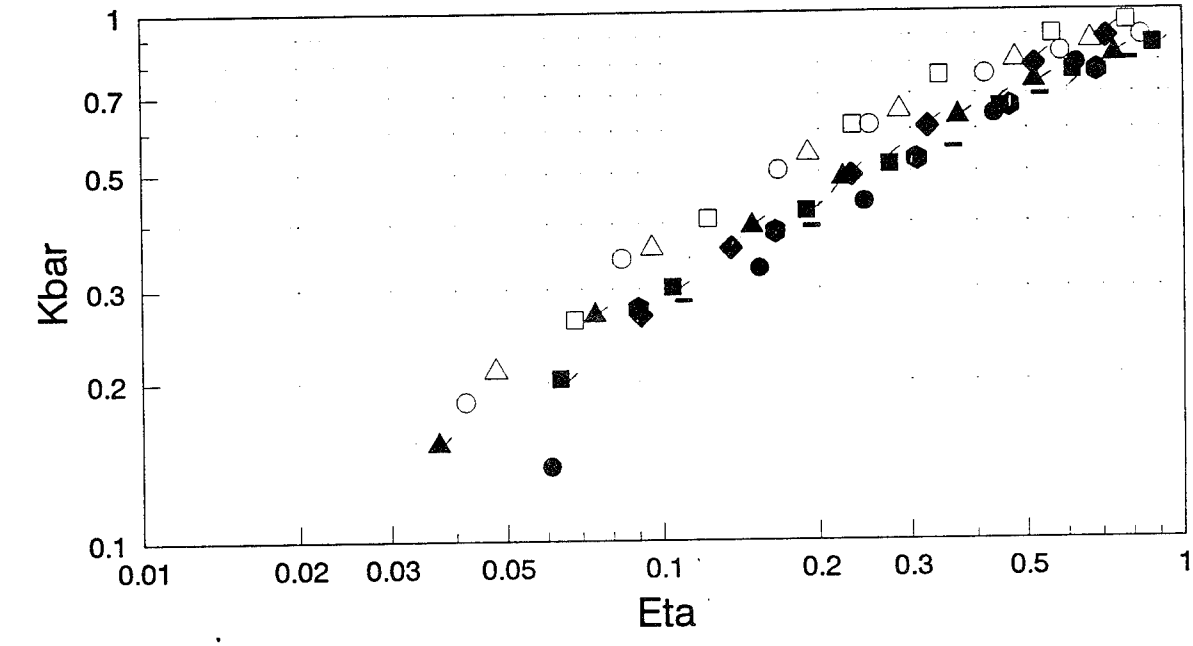

DSU 60/108 FPS	57/108	54/108	59/211	56/225	53/227	61/312	58/316	55/326
7'0"	13'5"	18'9"	6'4"	12'4"	18'4"	7'0"	12'9"	18'10"

(b) Ottawa sand

Figure 3-17. Power law scaling of normalized loading factor profiles for DSU experiments (Surface elevation).

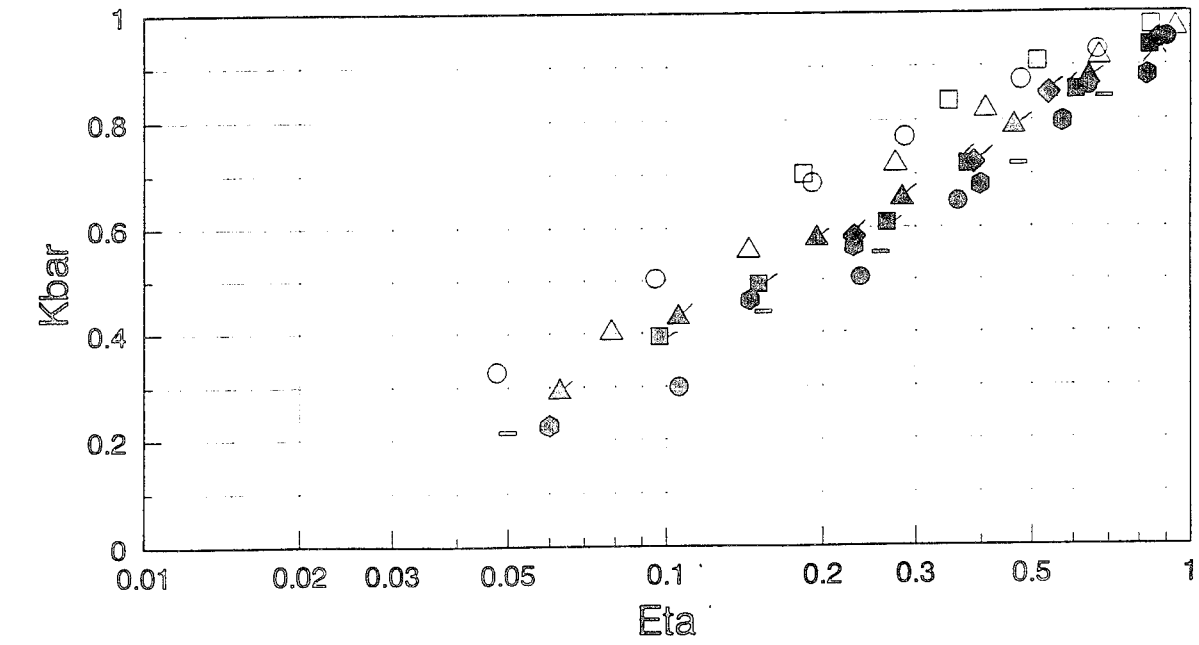

DSU 44/89 FPS	49/121	51/106	43/218	46/221	50/199	45/326	48/333	52/311
7'1"	12'8"	19'0"	6'7"	12'6"	18'7"	7'1"	12'10"	19'0"

(a) WSMR

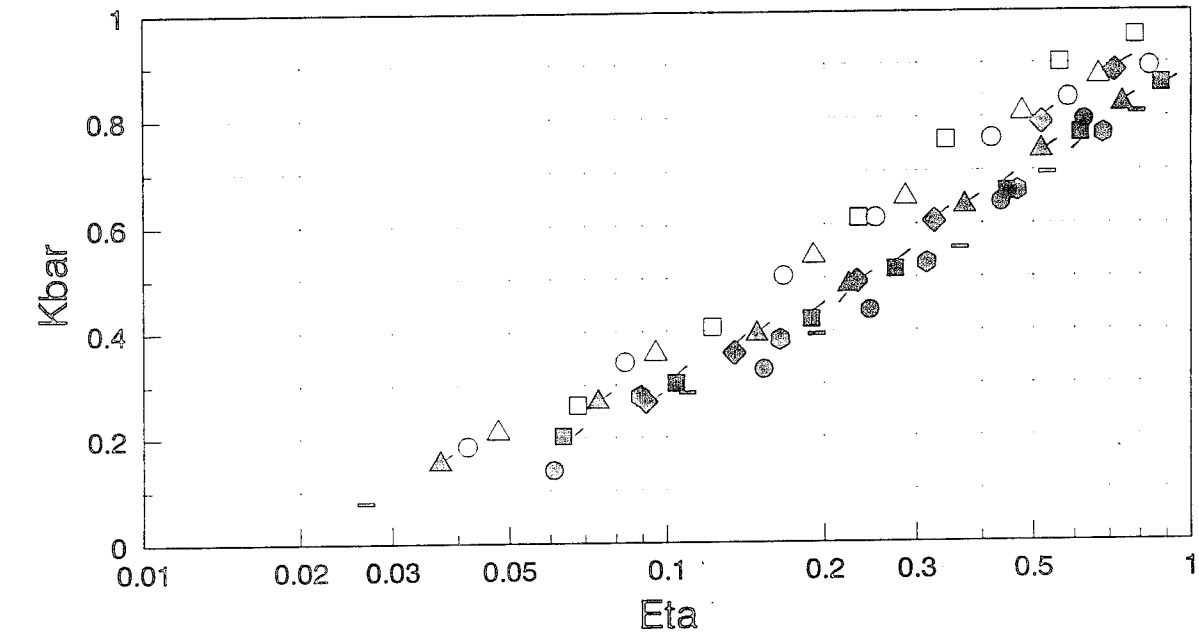

DSU 60/108 FPS	57/108	54/108	59/211	56/225	53/227	61/312	58/316	55/326
7'0"	13'5"	18'9"	6'4"	12'4"	18'4"	7'0"	12'9"	18'10"

(b) Ottawa sand

Figure 3-18. Semilog scaling of normalized loading factor profiles for DSU experiments (Surface elevation).

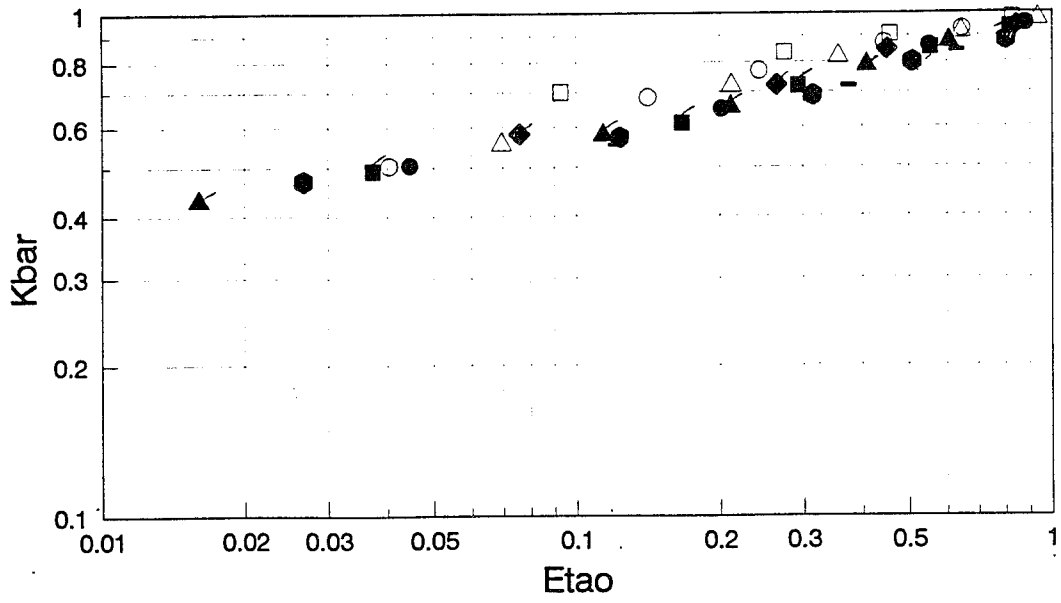

DSU 44/89 FPS	49/121	51/106	43/218	46/221	50/199	45/326	48/333	52/311
0.6"/7'1"	0.6"/12'8"	0.6"/19'0"	1.0"/6'7"	1.0"/12'6"	1.0"/18'7"	1.4"/7'1"	1.4"/12'10"	1.4"/19'0"

(a) WSMR

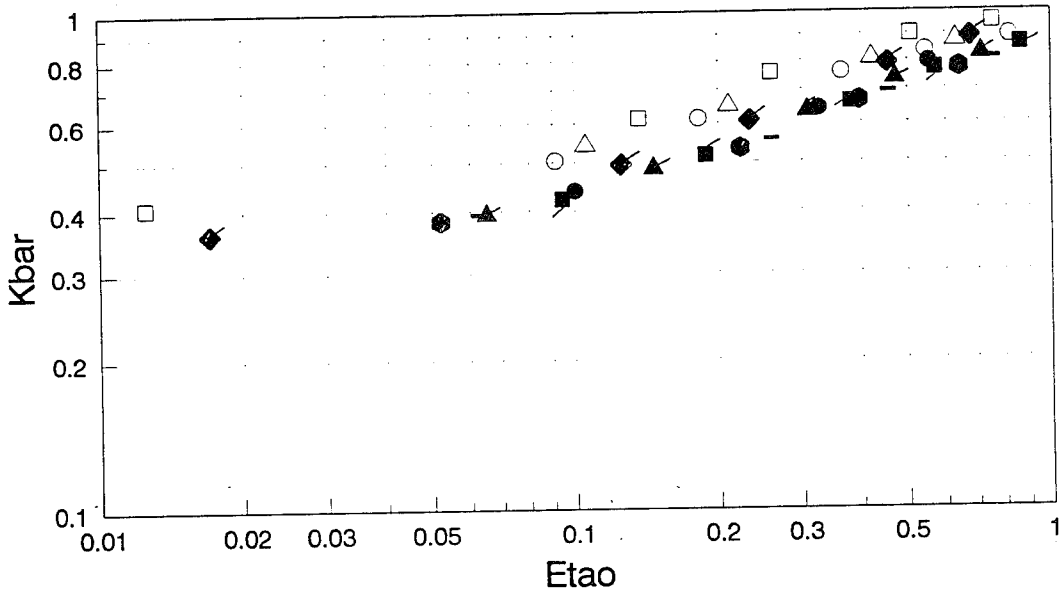

DSU 60/108 FPS	57/108	54/108	59/211	56/225	53/227	61/312	58/316	55/326
1.0"/7'0"	1.0"/13'5"	1.0"/18'9"	1.2"/6'4"	1.2"/12'4"	1.2"/18'4"	1.6"/7'0"	1.6"/12'9"	1.6"/18'10"

(b) Ottawa sand

Figure 3-19. Power law scaling of normalized loading factor profile for DSU experiments (Profile focus elevation).

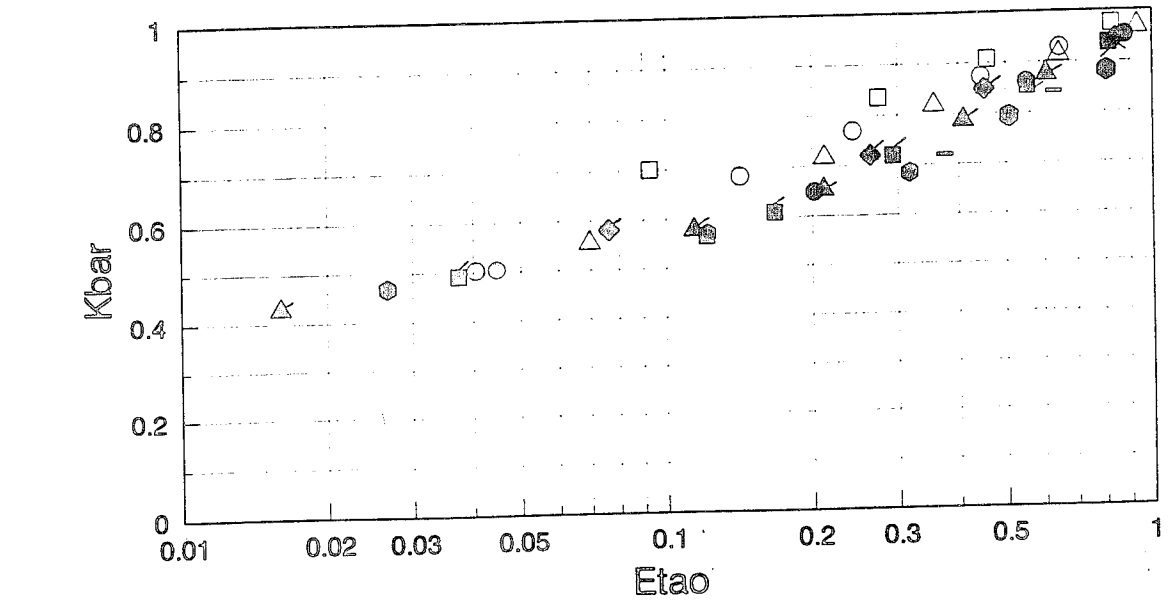

DSU 44/89 FPS	49/121	51/106	43/218	46/221	50/199	45/326	48/333	52/311
0.6"/7'1"	0.6"/12'8"	0.6"/19'0"	1.0"/6'7"	1.0"/12'6"	1.0"/18'7"	1.4"/7'1"	1.4"/12'10"	1.4"/19'0"

(a) WSMR

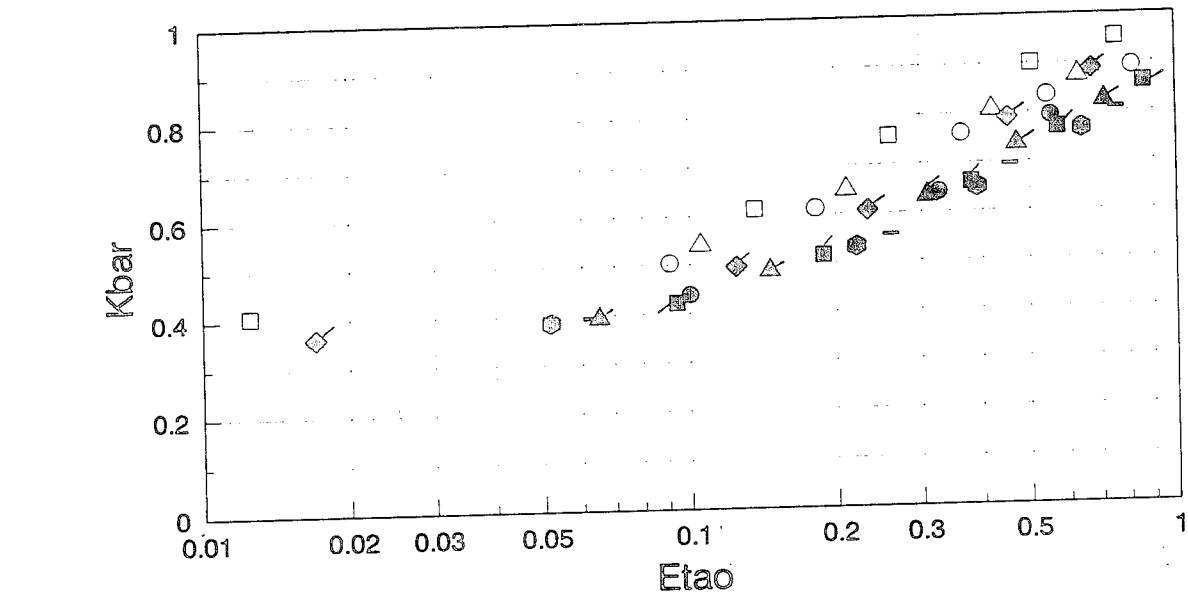

DSU 60/108 FPS	57/108	54/108	59/211	56/225	53/227	61/312	58/316	55/326
1.0"/7'0"	1.0"/13'5"	1.0"/18'9"	1.2"/6'4"	1.2"/12'4"	1.2"/18'4"	1.6"/7'0"	1.6"/12'9"	1.6"/18'10"

(b) Ottawa sand

Figure 3-20. Semilog scaling of normalized loading factor profiles for DSU experiments (Profile focus elevation).

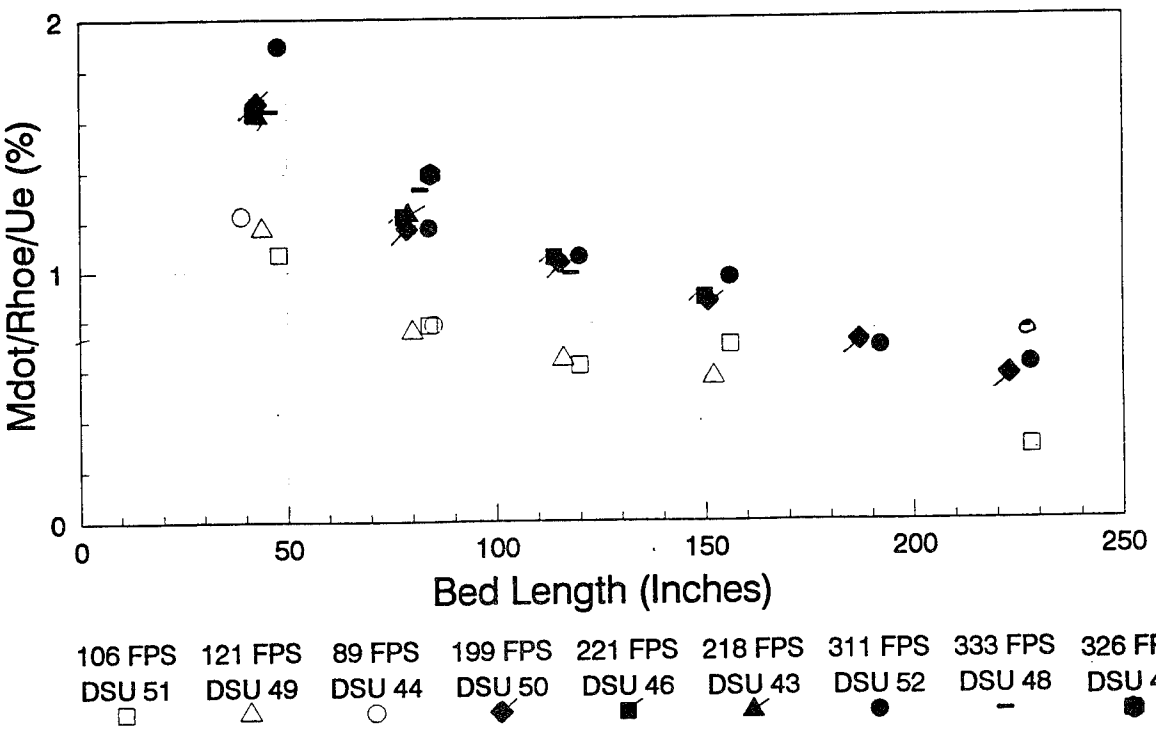

(a) WSMR

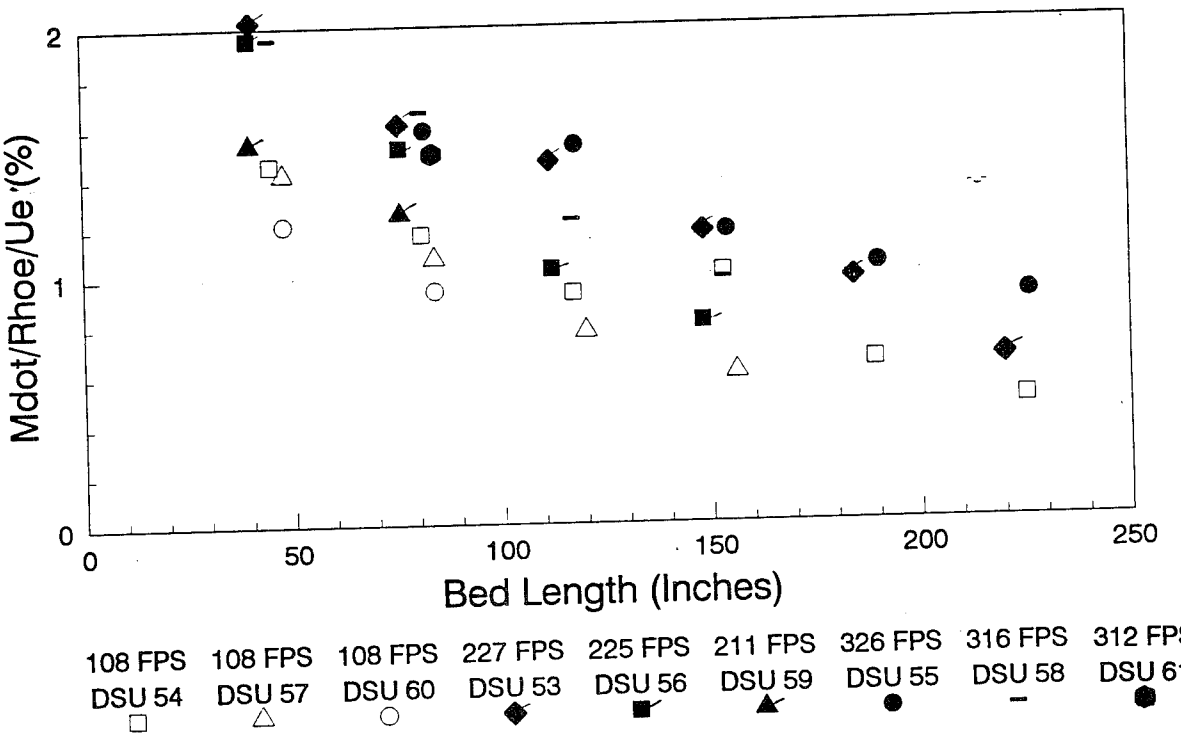

(b) Ottawa sand

Figure 3-21. Scouring rate summaries for DSU experiments.

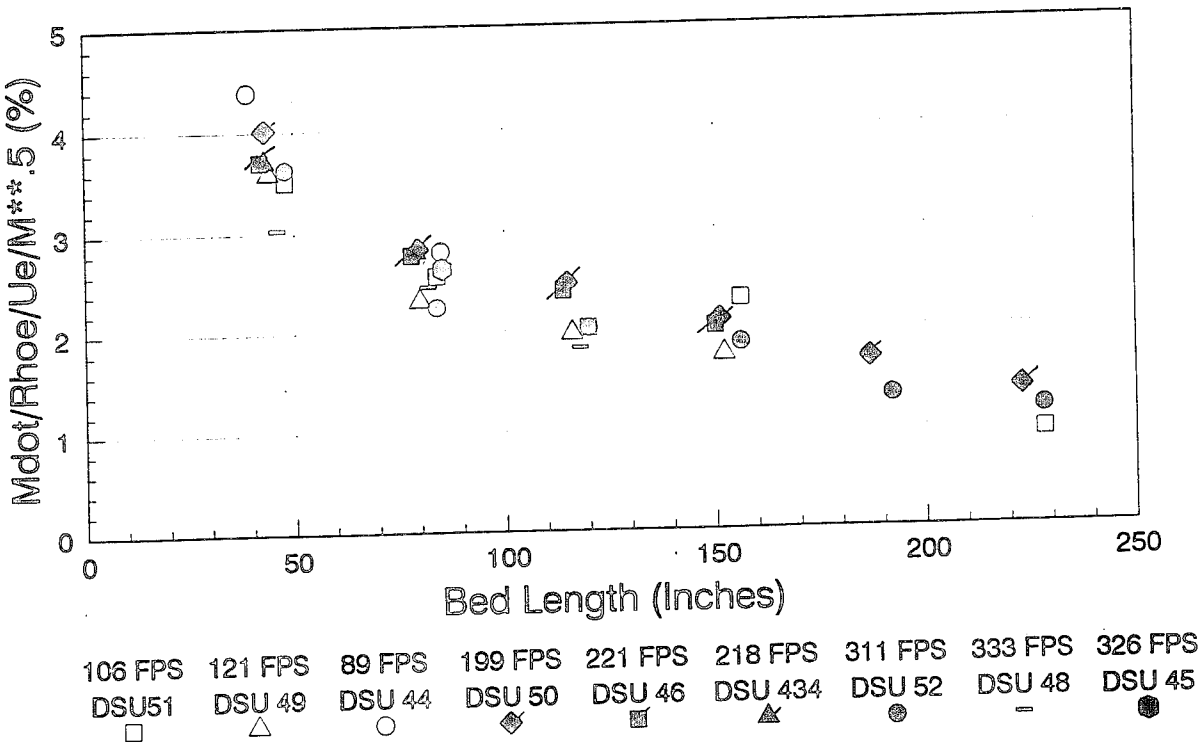

(a) WSMR

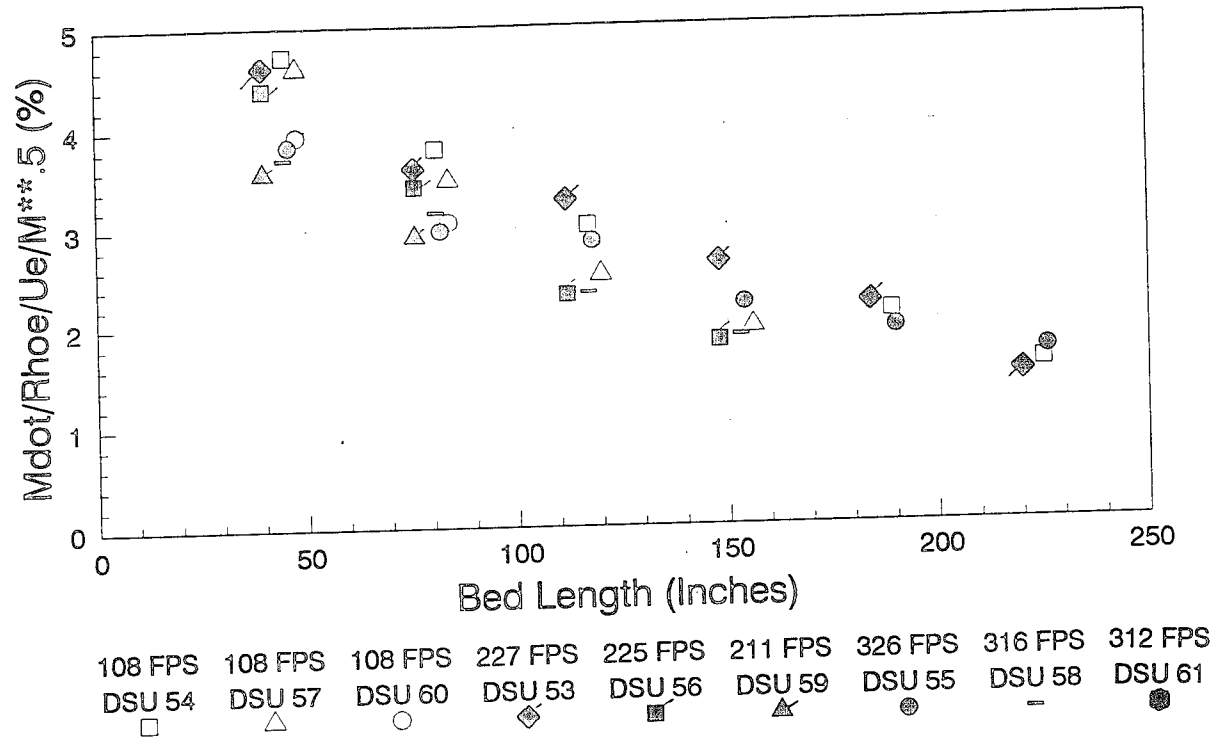

(b) Ottawa sand

Figure 3-22. Mach number scaling of scouring rate data for DSU experiments.

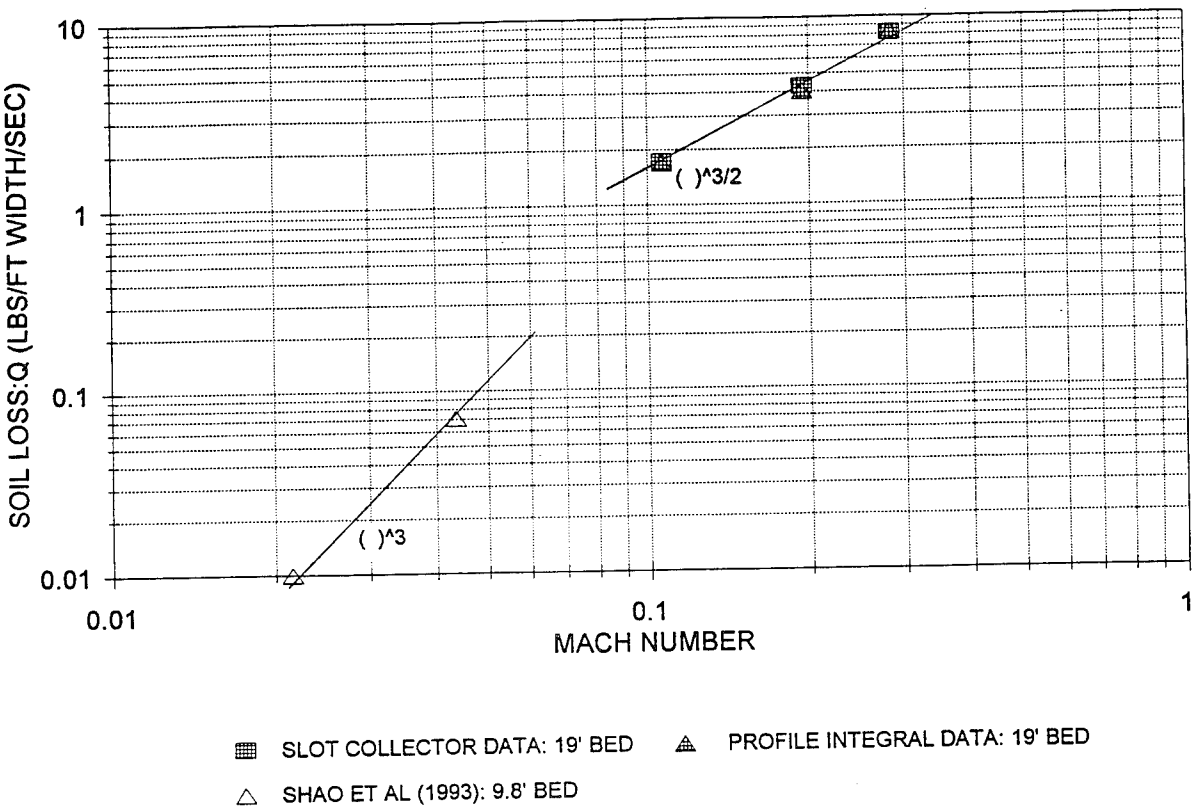

Figure 3-23. Soil loss summary.

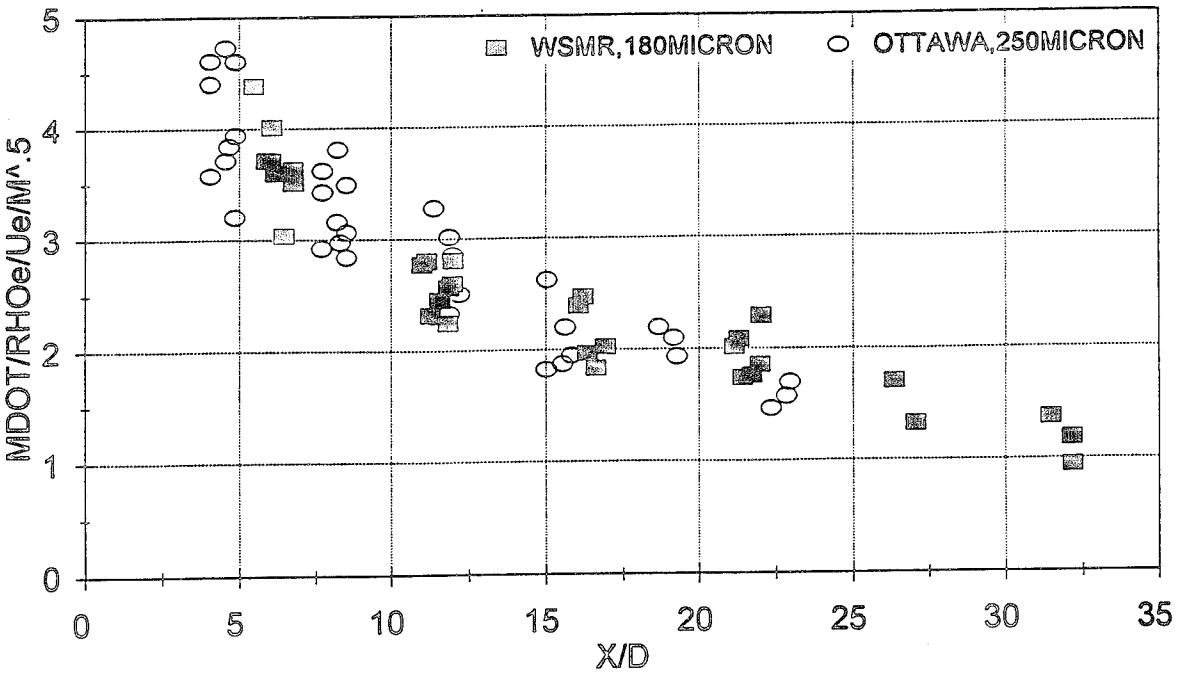

(a) Linear scaling

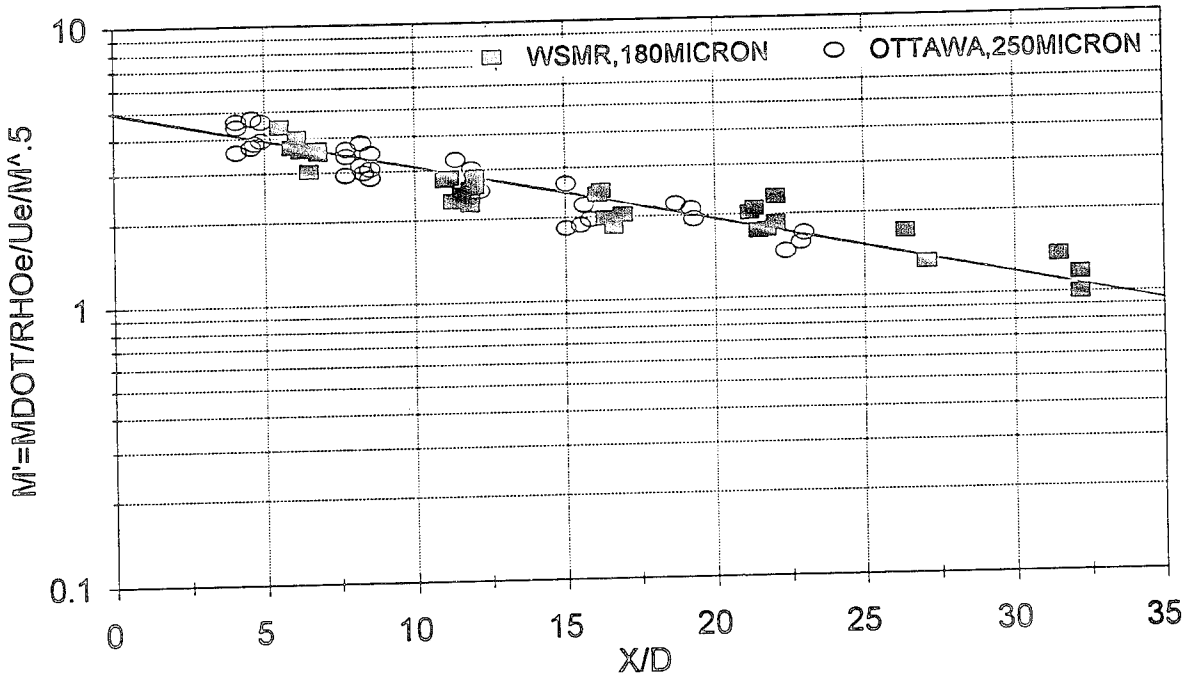

(b) Exponential scaling

Figure 3-24. Particle size scaling of scouring rate data for DSU experiments.

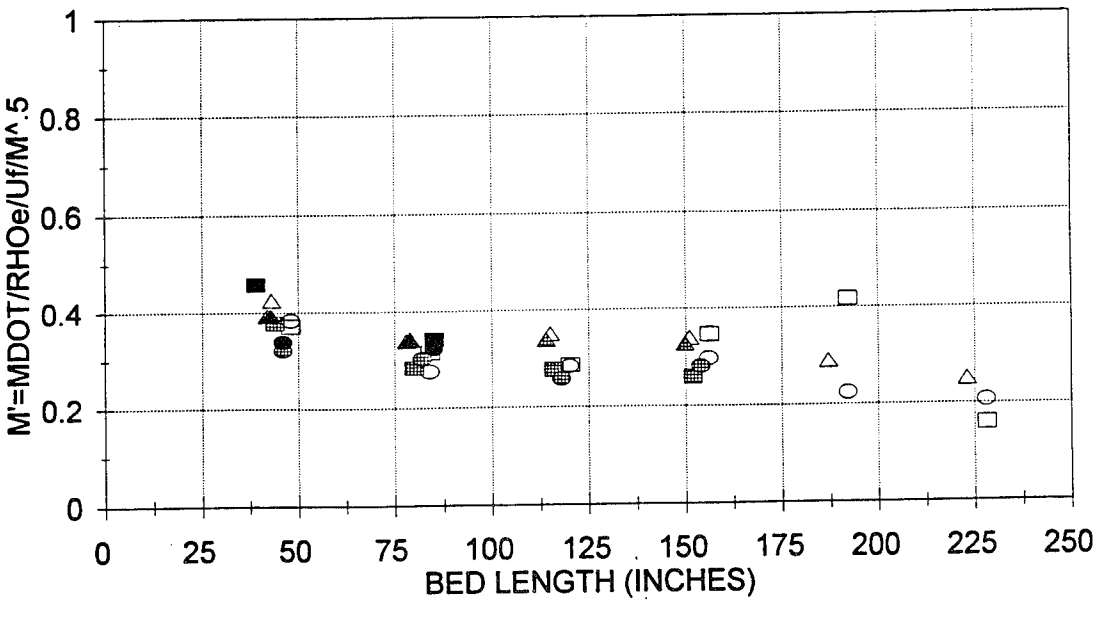

□ DSU51,106/7.1,19'0" ▦ DSU49,121/7.3,12'8" ■ DSU44,89/7.3,7'0",
△ DSU50,199/14.6,18'7" ▲ DSU46,221/16.2,12'6" ▲ DSU43,218/17,6'7"
○ DSU52,311/23.4,19'0" ● DSU48,333/25.7,12'0" ● DSU45,326/26.4,7'0"

(a) WSMR

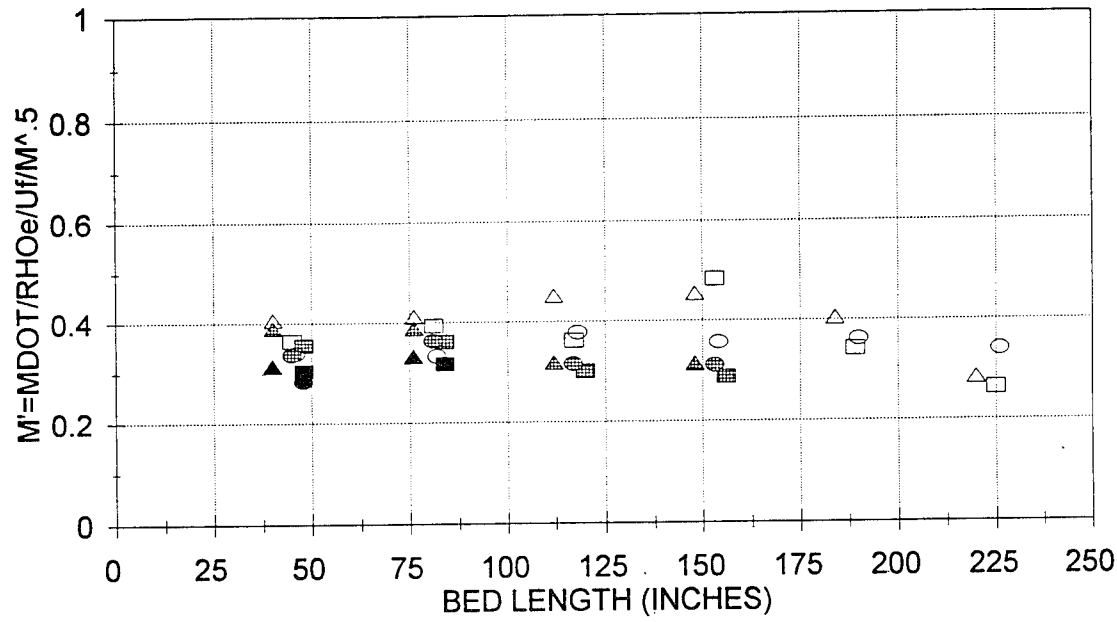

□ DSUDSU54,108/5.7,18'9" ▦ DSU57,108/7.8,13'0" ■ DSU60,108/10.4,7'0"
△ DSU53,227/8.7,18'4" ▲ DSU556,225/13,12'4" ▲ DSU59,211/18.4,6'4"
○ DSU55,326/10.8,18'10" ● DSU58,316/19.5,12'9" ● DSU61,312/27.8,7'0"

(b) Ottawa sand

Figure 3-25. Shear velocity scaling of scouring rate data for DSU experiments.

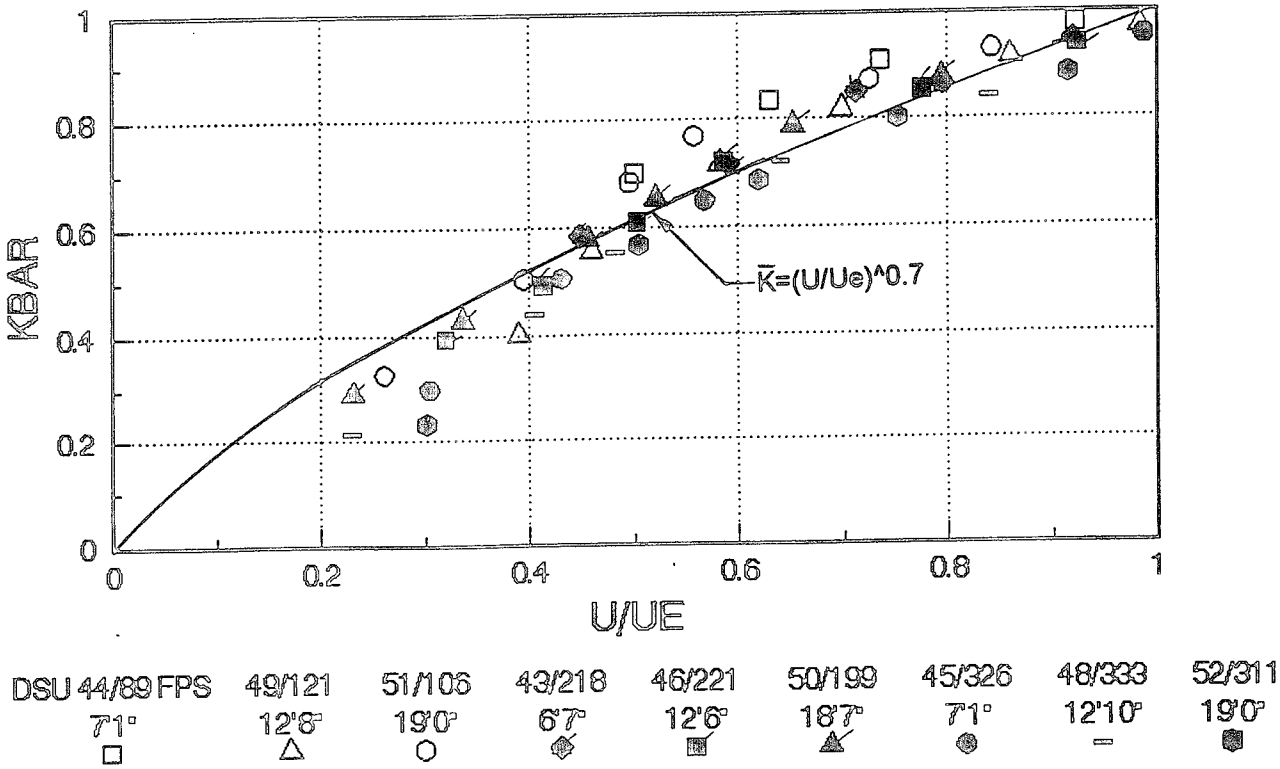

(a) WSMR

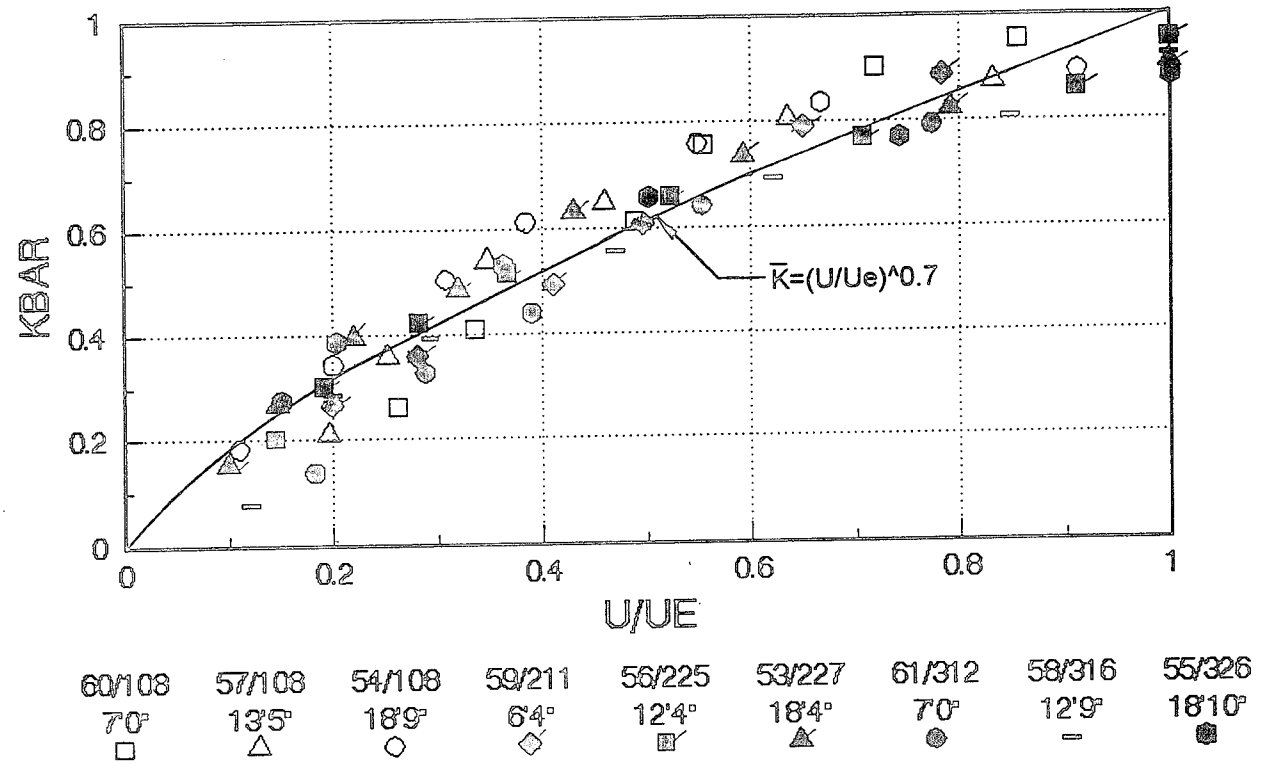

(b) Ottawa sand

Figure 3-26. Schmidt number scaling for DSU experiments (Normalized loading factor).

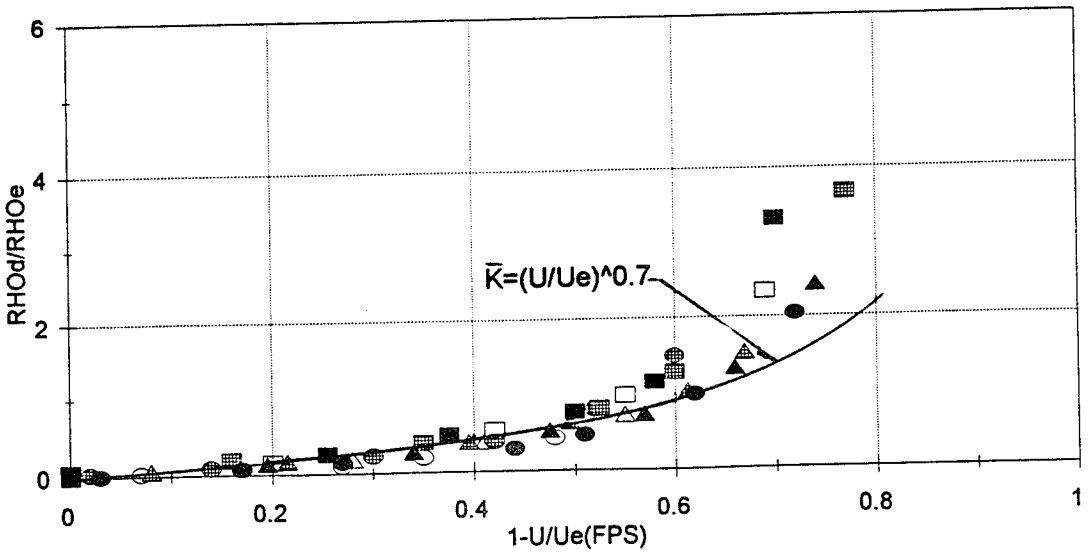

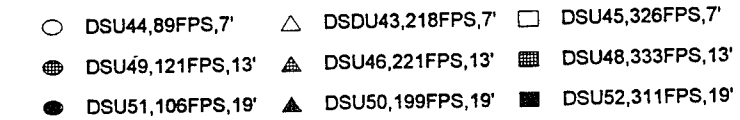

(a) WSMR

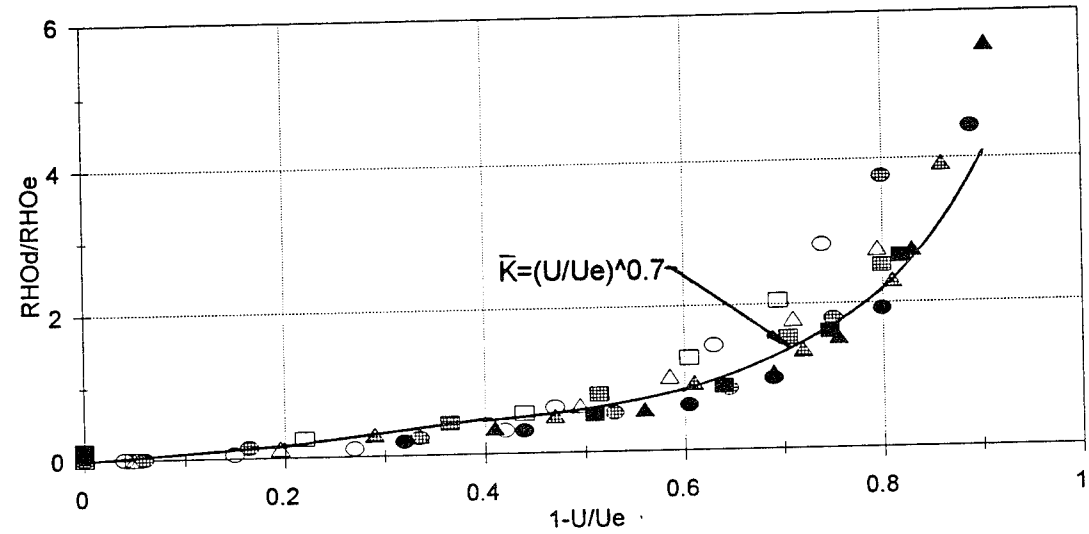

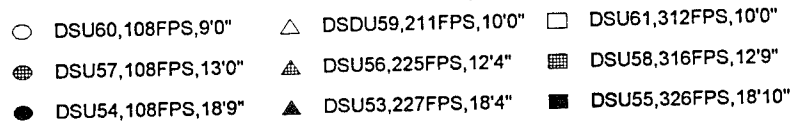

(b) Ottawa sand

Figure 3-27. Schmidt number scaling for DSU experiments (Loading factor).

SECTION 4
REAL SURFACE (RS) DUST LOFTING EXPERIMENTS

As noted above (Section 3.0), results from the erodible soil experiments under the DSU program (Batt, et al, 1993) are necessarily limited in that such "real surface" effects as cultivation ridges, soil clods, vegetation stubble, surface texture roughness, moisture content, etc. are unaccounted for in the data base. The current documentation extends the DSU measurements to real soils by presenting WSMR dust lofting results for simulated realistic surfaces. Conditions studied include: "ordered" roughness (Ridges/Clods/Stubble; Section 4.1), random roughness (Gravel Seeded WSMR, 4.2), discrete roughness (Leading Edge Disturbance, 4.3), threshold velocities for large particles (Gravel "Soil" Beds, 4.4) and moisture content (Effect on Threshold Velocity, 4.5). Table 4-1 lists the RS Test Matrix and summarizes test conditions of interest for the individual run cases.

All results to be presented were obtained in the DSU wind tunnel (18"W x 34"H x 20'L, Figure 4-1, Batt, et al, 1993) at flow speeds up to 370 fps. In addition to tunnel monitoring instrumentation (free stream dynamic/static pressure, temperature, etc.), boundary layer diagnostics were also installed at the tunnel's 21'4" axial station. Such instrumentation consisted of a fixed rake of Snob/Greg probe "pairs" (4 ea; dusty flow pressures), a traversing narrow beam x-ray system (spanwise averaged dust density) and one dust flow slot collector ("Bagnold" collector; temporal measurement of lofted dust mass; Bagnold, 1991). Pre and post test photographs of bed appearance were also obtained for each test as well as close-up video film of typical near surface flow conditions.

It should be noted that all RS photography was performed with color film. As a result, the resolution of the black and white velox prints enclosed herein (Appendix) is limited relative to the

the original color prints. For those interested in greater detail regarding the structure of post test bed surfaces, reference should be made to the color originals. Although the current photographic "results" are not "data" in the quantitative sense, they should provide assistance to investigators because they document the surface scouring "signature" as a function of roughness type. It is hoped that such photographs will therefore prove useful in evaluating boundary layer dust lofting models and the physics of the scouring process.

As noted in Batt, et al (1993), the Snob probe (Figure 2-7b) measures gas-only pressures whereas the Greg gauge (Figure 2-7c) measures the full effects of the gas stagnation pressure and the local dust momentum flux. The Snob probe illustrated in Figure 2-7b has been configured as a "tri" sensor pressure diagnostic in that it uses three transducers to measure total, static and differential pressure. Because of its differential pressure measurement capability, it performs as a dusty Pitot-static probe and thus provides a direct measure of local boundary layer velocities. A detailed review of the Snob/Greg diagnostics as well as the x-ray attenuation technique for measuring local dust densities (Figure 4-2) is given in Batt, et al (1993).

Post test photographs of the Bagnold collector unit are provided in Figure 4-3 as viewed looking downstream for one of the Gravel-Seeded-WSMR test cases (Section 4.2). In the collector, captured dust in each slot chamber (0.5"W x 1"H) is first directed aft to a common vertically oriented duct and then fed through a below-floor tube into a light weight paper vacuum bag. Time resolution of this soil loss "measure" is made possible via use of 5 vacuum pumps and a computer controlled traverse system which moves the five vacuum inlets in a rapid stop-hold-move fashion. Time "hold" steps varying from 2 seconds (for the 350 fps data) to 6 seconds (for the 120 fps measurements) have been used for the current results. The importance of time-resolved data for total dust lofted (often termed soil loss and/or dust throughput) is that

after 1 to 2 time increments, reduction in lofted dust is observed. Such a finding was expected, however, since real surface soils with rough surface textures tend to be self-limiting in dust sweep-up due to the onset with erosion of the "desert pavement" effect (shielding of fines by surface roughness). Unless otherwise noted, all soil loss data provided herein correspond to initial soil loss values. In this way, surface textures are still at pre test conditions and the effects of surface changes due to local sand motion (eroding/filling) are minimized.

4.1 RIDGES/CLODS/STUBBLE.

For the initial Real Surface (RS) experiments an array of non-erodible ridges was mounted on the DSU wind tunnel floor to simulate a cultivated field with hard packed (non-erodible) ridges (Figure 4-4). Steel angles of 4" leg length were used for this simulation. The inverted angles were oriented orthogonal to the flow direction at 12" spacings and spanned the width of the tunnel (18"). All floor and side wall joints were made leak tight though use of RTV sealant. The ridge array extended downstream from the 6' Test Section location to the 20' station with the diagnostics installed at a 21'4" axial distance. Because some leading edge erosion, i.e. aft movement, occurred for each test, soil beds were "laid out" such that each experiment corresponded, approximately, to a nominal overall bed length of 19 feet. Dust beds consisting of WSMR soil were used for all measurements with RS elevations (bed height to ridge top) varying from 0 to 2" (bed depth: 3" - 1"). As noted by Fryrear (1984) use of non-erodible ridge material for the current experiments is an appropriate simulation technique since often field ridges are hardpacked with clods/rock and thus exhibit erosion resistant behavior.

Typical pre and post test side view photographs for a non-erodible ridge soil bed are given in Figures 4-5. The RS 33 results shown (flow is from left to right) correspond to a 2" pre

test RS elevation at a freestream velocity of 124 fps. The effect of stagnating flow on the windward side of each ridge and the leeward side soil deposition due to the inter-ridge vortices is clearly evident. The noted leeward side dust buildup, a phenomena common to drifting snow, is also demonstrated in the upstream overview photograph of Figure 4-6b. Additional pre/post test photographs for the ridge experiments are provided in the Appendix (Figures A-1 through A-18).

A summary of collected dust results from these non erodible ridge experiments is provided in Figure 4-7a in terms of dust throughput, as measured by the Bagnold collector (Section 4.0). As discussed in Section 3.3 (Figure 3-23), soil loss data from the Bagnold collector compare favorably with corresponding Q data developed under the DSU program using integrated profile results,

$$Q = \int_o^e \rho_d u_d d_y. \tag{4.1}$$

Such agreement represents an independent verification of previous results as well as validation of the slot collector's performance. Note also that this boundary layer soil loss measure is also equivalent to the integral of local scouring rate <u>over</u> the soil bed length,

$$Q \equiv \int_o^L \dot{m}\ dx \tag{4.2}$$

and to first order,

$$Q \cong \dot{m}_{avg} L \tag{4.3}$$

where $\dot{m}_{avg}$ = average scouring rate.

Thus soil loss, in effect, corresponds to an approximate "measure" of a soil's scouring potential and therefore has been used

historically to characterize the dust lofting performance of "real" surface soils.

The data shown in Figure 4-7a are presented with leading edge contribution to total throughput subtracted out and as normalized by a given velocity's flat surface soil loss ("zero" ridge elevation data). The leading edge contribution noted was fixed for all results for a given velocity and was equal, approximately, to the corresponding soil loss amount that occurred for a non-ridged soil bed. An estimate of this soil loss term was made by testing only with a leading edge dust bed, i.e. dust bed extending downstream just to the first ridge (6' Test Section location). Values of this "baseline" soil loss term $(Q/\rho_e u_e)_o$ were approximately 0.60, .90 and 1.10 inches for the 120, 220 and 320 fps cases, respectively.

In plotting the data in the manner shown in Figure 4-7, a direct evaluation can be made of the effect of ridges on soil scouring relative to flat surface dust sweep-up. Not only do the results scale well with the selected normalization procedure, but the data show a substantial fall-off in dust lofting with ridge elevation. This finding indicates that the 2" RS elevation test cases are nearly representative of the "Desert Pavement", i.e. wind stabilized, limiting condition.

In pursuing approaches to enhance soil scouring, several tests were also conducted for a real surface of "erodible" ridges. Such ridges were prepared from loose WSMR dust and configured to duplicate the shape geometrics of the non-erodible ridges. Soil loss results for these "erodible" experiments are summarized in Figure 4-7b. The data as shown illustrate that even for these maximum ridge scouring conditions, soil loss, although enhanced over non-erodible ridge conditions, is still less than flat surface scouring (most probably because of inherent surface contouring effects). Such data suggest that dust lofting from dry/loose/erodible flat surfaces may in fact represent the maximum

scouring to be expected for a given soil type. Typical velocity profile data from the erodible ridge experiments are also presented here (Figure 4-8) and fair agreement with previous non-erodible data is evidenced.

Late in the DSUE program a set of follow-up experiments were performed for non-erodible ridge soil beds to investigate the effects of ridge separation on soil loss. These latter tests, suggested by Kubota (1993), were conducted for a ridge separation distance of 24" in contrast to the original ridge separation of 12". Both sets of results are summarized in Figures 4-9a where soil loss for the 24" ridge spacing is seen to be larger for a given elevation than corresponding data for a 12" separation. However, the different data sets are seen to collapse favorably (Figure 4-6b) when results are scaled with normalized elevation (RSEL/SEP). It is interesting to note that soil loss reduces to approximately 10% of non-ridge levels for normalized elevation of 0.10 or greater. Such a finding highlights a well established approach for moderating wind induced soil erosion as often used by agricultural workers.

The normalized soil loss parameter incorporated in Figures 4-7 and 4-9 can be characterized as, for purposes of definition, a Soil Erodibility Factor (SEF). It varies from 1 to 0 depending on the real surface conditions of interest and is a parameter popular with soil erosion investigators. The favorable collapsing of results in Figure 4-9b suggests that perhaps scouring for other surface types (clods, stubble, etc.) can similarly be correlated, thus leading to a straightforward approach to relating a given soil texture to scouring potential. Once a soil's surface characteristics are known, prediction of mass of dust lofted can then be made by "adjusting" flat erodible results for the SEF value of interest.

Subsequent to the original experiments on dust lofting for surfaces with simulated ridges, testing in the DSU wind tunnel was

directed towards evaluating the effects on soil scouring of clods and residue stubble. For the "clod" experiments, 3" diameter PVC caps (3 1/2 inch elevation) were mounted on the wind tunnel floor at 6 inch spanwise spacing and 12 inch axial separation in a diamond pattern (Figure 4-10). The bed of clods extended from the tunnel's 6 foot station downstream to the 19 foot location. A corresponding layout was adopted for the simulated stubble experiments by using 16d nails (0.133" diameter; 3 1/2 inch long) in a "plus" pattern within a 3 inch diameter circle (Figure 4-11). Dust bed depths were set at levels necessary to establish the required pre test real surface elevation (either 1 or 2 inches). As was the case for our previous non-erodible ridge experiments test speeds were varied from 120 to as high as 370 fps. Also measurements again consisted of velocity and dust density profile data (Snob/Greg probe rake; x-ray diagnostics) as well as soil loss results (Bagnold slot collector) at the 19 foot bed length location.

A reduction of the clod/stubble measurements has been made and results for soil loss data are presented herein in Figure 4-12a. For completeness, data are shown for the three non-erodible test series: ridges, clods and simulated stubble. Corresponding velocity profile results and pre/post test photographs from selected experiments are shown in Figures 4-13 and A-19 through A-35, respectively.

The current soil loss data (Figure 4-12a) show a consistent reduction in soil scouring with increase in real surface elevation. The ridge beds are seen to provide the strongest attenuation in boundary layer scouring with the data for the clod soil beds exhibiting a less pronounced effect. These findings are again supportive of the view that scouring from flat-dry-loose soil beds corresponds to the most severe real surface dust lofting condition.

The velocity data in Figure 4-13 are plotted as a function of elevation above a given disturbance "top". In general such a procedure is seen to collapse the measurements for a given free stream velocity. Some profile sensitivity to velocity is evidenced in Figure 4-13, however, by noting the trend of increasing edge thickness (δ) and profile slope with velocity. In terms of power law behavior, wherein the normalized velocity data (u/u_e) are related to boundary layer elevation (y/δ) by:

$$u/u_e = (y/\delta)^n, \qquad (4.4)$$

the present results correspond to a range in power law slope (n) of 0.35 to 0.50, in reasonable agreement with the flat surface results from our previous DSU program.

4.2 RANDOM ROUGHNESS RESULTS (GRAVEL SEEDED WSMR).

Of concern since the start of the DSUE program was the question of how does one go about setting up and performing "real surface" experiments under controlled and repeatable test conditions. The range of soil types and surface texture features is literally infinite in scope. In an attempt to bring order to this complex problem, the first series of RS experiments were scoped out to study specific real surface effects which could be evaluated on an individual basis. Using dry, loose "erodible" WSMR soil (dry to avoid soil moisture considerations and to maximize soil scouring) these first experiments included tests with non-erodible ridges, clods and residue stubble (Section 4.1).

For the three initial RS "soils" (Ridges/Clods/Stubble) the roughness was of an ordered nature, i.e. patterned in a prescribed manner. Obviously the question arises as to how results for such simulated real surfaces compare with, say, random roughness surfaces. To evaluate this issue, tests were performed with soils prepared with random textured surfaces by seeding WSMR soil with pebble rocks (smooth mountain stream pebble) of 1.5 $\pm$ 0.5 inch

diameter. All tests (RS70 - 74) were conducted in the DSU wind tunnel with gravel-seeded beds extending from the test section's six foot location to the twenty foot station with nominal (i.e., unseeded) WSMR dust being used for the bed leading edge. The seeded beds were prepared on a 3:1 basis (450 lb WSMR/150 lb gravel) resulting in a 25% total mix ratio by weight which is approximately the area coverage ratio (the corresponding "clod" area ratio was approximately 11%). As was the case for the measurements for the Section 4.1 results, the present random roughness experiments consisted of velocity and dust density profile data (Snob/Greg probe rake; x-ray diagnostics) as well as soil loss results (Bagnold slot collector) at the 19 foot bed length location.

Figures 4-14a and 4-14b show typical pre and post test photographs, respectively, of the gravel seeded WSMR test bed. For this test, RS70 (130 FPS), the run duration was 26 sec and negligible gravel (pebble) motion is seen to occur. In fact, even for a run speed of 227 FPS (RS73, 38 sec) little movement of gravel took place (Figure 4-15). Conversely, the photographic results for RS74 (367 FPS, 24 sec, Figure 4-16) illustrate that substantial gravel was "lofted" as is evidenced by the close up photographs of the diagnostics station in Figures 4-3 and 4-17, the mass of collected pebble downstream of the 20 foot station (55 lb), and the impact summary diagram of Figure 4-18. Note that impacts are observed at elevations as high as 25 inches above the dust bed, a result which dramatically illustrates that gravel particles "lofted" well above the boundary layer proper ($\simeq$ 12") and accelerated to high velocities. Mention should be made that all Snob/Greg probes (4 Snob, 4 Greg) survived the RS 74 run and retained pre test calibration values! Such a result further illustrates the performance capabilities of the Snob/Greg probes under high impact test conditions and serves to validate the ruggedized design approach adopted for probe construction.

Video replay of the scouring motion for RS74 at the 9 foot station showed that pebble lofting did not take place initially but occurred approximately 12 sec after run start. By this time the local soil surface had receded substantially thereby exposing rock surfaces and enabling drag forces to overcome the effects of gravity. Note that the drag to weight ratio (qC_DA/W) for a 1 inch diameter "rock" at 367 FPS is approximately 10. It is therefore not surprising that significant pebble scouring did in fact occur for RS74. Additional photographs further illustrating the nature of soil scouring for RS 74 and for the other gravel-seeded dust experiments are provided in Figures A-36 through A-63.

As a side note, threshold shear velocities (i.e., the log height velocity at which particles first become lofted) is well established for dust sized particles (Bagnold, Gillette, etc.). Such results are currently unavailable, however, for large particles, e.g., the 1 - 2 inch diameter pebbles used for the RS70 - 74 experiments. To date investigators have focused primarily on low speed ($u \leq 50$ FPS) conditions and dust particle sizes of the order of 100 - 1000 μm. As a result of the RS73 and 74 measurements, large gravel "particles" are seen to become lofted at a free stream velocity between 227 FPS (RS73) and 367 FPS (RS74). Experiments to determine the corresponding threshold shear velocity for such rock samples have been performed under DSUE and results, representing an important extension of the existing data base to "large" particles are discussed in Section 4.4.

From the soil loss measurements obtained by the Bagnold collector, normalized throughput results have been calculated for all gravel WSMR runs. Tests RS70, 73 and 74 correspond to initial "covered" pebble surfaces (i.e. simulated non-eroded surfaces). Conversely, runs RS71 and 72 were tests, performed with initial surfaces "conditioned" to represent typical "eroded/weathered" soil beds, with the RS70 and 71 post test surfaces used as the pre test beds for RS71 and 72, respectively. In this manner "long"

test times could be accommodated thereby providing a means to study "desert pavement" effects on soil scouring.

As was the case for results discussed in Section 4.1, the current dust throughputs (soil loss at 19 foot bed length location) have been ratioed herein to the corresponding flat surface data. The effects of leading edge scouring have also been subtracted out to provide a direct "measure" of the effects of surface roughness on scouring. The present gravel WSMR data are shown in Figure 4-19 along with our previous results for the ridge and clod experiments. The data are shown as a function of RS elevation with the gravel results being associated with an RS elevation value of 1 inch. On a preliminary basis, the gravel data are seen to compare favorably with the 1 inch clod results. Such a finding, which further validates the importance of roughness height, suggests that the clod simulation approach may indeed represent a fair approximation to a random roughness surface.

The "desert pavement" phenomena refers to that soil condition wherein the surface roughness texture, due to non-erodible particles/roughness, "shields" fine particles from being lofted. For surfaces initially covered with fines with imbedded large non-erodible particles, lofting will occur initially but slowly attenuate as more and more "non-erodibles" start shielding the smaller particles. The RS70 - 74 runs were performed to also explore this "desert pavement" effect with the WSMR soil and results are presented in Figures 4-20 and 4-21.

The first of these figures (Figure 4-20) shows the variation of normalized soil loss for the gravel WSMR tests as a function of total flow exposure time. As expected from desert pavement considerations, Figure 4-20a illustrates that a falloff in soil loss with time occurs for all three velocity conditions. An approximate scaling of this fall off process has been made by "stretching" the time scale by velocity (Mach Number) to the 3/2's

power. This scaling approach was considered based on results from the DSU program which showed that soil loss varied, approximately, with velocity to the 3/2's power (Figure 3-23). Figure 4-20b shows such a scaling approximation and the results are seen to be encouraging.

Finally some total (integrated) soil loss data are presented in Figure 4-21. Gravel WSMR data only are presented in Figure 4-21a with Figure 4-21b showing "scaled" results for both flat and gravel surface soil beds. The spread between flat and gravel data illustrates the relative effects of particle shielding occurring with increasing time. Again favorable correlation of the data is seen to take place. Note that the 367 FPS gravel results include only Bagnold collector soil loss data and not those mass losses associated with lofted gravel. If allowances were made for such losses the throughput data in Figure 4-21b for the last three time steps for the 367 FPS run case would need to be increased by approximately 20% with corresponding increases in the results of Figure 4-20b. A better correlation would then be in evidence.

4.3 DISCRETE ROUGHNESS (LEADING EDGE DISTURBANCE).

During initial testing on the DSU program, there were indications that bed leading edge disturbances could generate persistent and intense vortices which extended downstream over the full length of the dust bed. Such phenomena were recognized as significant sources for dust scouring and potentially could cause increased scouring over nominal flat (undisturbed) soil beds. Several tests were therefore conducted in the DSU wind tunnel in an attempt to clarify this issue.

As noted in Table 1, three types of leading edge disturbance were investigated. These include: 1. Single and double rows of clods (1-7" RS elevation), 2. A single row of flat plate vortex generators (1-2" RS elevation), and 3. A single leading edge ridge (1 - 1.5" RS elevation). Tunnel free stream velocities ranged

from 120 to 370 FPS and again measurements were performed with the same diagnostics already discussed for the other RS experiments. Typical pre and post test photographs of the soil bed set up for these leading edge experiments are given in Figures A-64 through A-89.

Results for these leading edge disturbance surveys are summarized in Figure 4-12b for all three types of disturbance. In general, the combined data set illustrates that soil losses associated with dust beds experiencing substantial leading edge vorticity appear to be either equivalent to or less than corresponding soil losses for flat soil beds. Post test characteristics of dust bed surfaces, however, suggested that local scouring enhancement did in fact occur at or immediately downstream of disturbance locations. But, because of the mass limited nature of dusty boundary layers and soil redeposition phenomena, soil loss measurements at "far" downstream stations were unaffected. Although additional testing of different types and sizes of vortex generators could be pursued to further explore this initial vorticity issue, such experimentation does not seem warranted in view of the current "non-enhancement" results. The present evidence that even leading edge disturbance effects do not cause increased scouring, further substantiates the view that flat dry dust beds composed of loose erodible particles constitute that soil type which will produce maximum scouring for a given flow condition. Such a finding, if additionally confirmed with further testing and analysis, therefore suggests that flat dry loose soil beds represent upper bound limits of dust scouring sources for dust cloud hydrocode calculations.

4.4 THRESHOLD VELOCITY FOR LARGE PARTICLES (GRAVEL SOIL BEDS).

As noted in the Test Matrix of Table 4-1, threshold shear velocity measurements have been performed in the DSU wind tunnel for both "coarse" gravel ($D \simeq 1 - 2$") and "P" gravel ($D \simeq 0.25$") bed samples. For these experiments, beds extending from the DSU

tunnel's 7' test station to the probe rake measurement location (21'4") were laid out on the steel floor of the facility's test section. Bed depths of 1.5" and 3" were used for the P gravel and coarse gravel, respectively. Typical pre and post test photographs for the prepared beds are given in Figures 4-22 through 4-25. Primary measurements consisted of free stream Pitot-static pressures, side view video photography (15' station), fixed elevation x-ray attenuation and a Snob probe rake (4 probe pairs) at the 21'4" location. Each test was run under variable speed conditions using the tunnel's diesel engine's throttle to vary the facility's fan RPM from low to high until the onset of particle motion. In keeping with historical precedence, the shear velocity just prior to particle movement, as indicated by video and x-ray results, is designated herein as the "threshold" shear velocity (u_{ft}). Because available results on threshold velocities correspond only to particle sizes up to 1 mm in diameter, the present measurements serve to clarify the scouring behavior of large "particles" at high velocities.

Figures 4-26 through 4-31 show time trace histories (at station 21'4") for edge velocity (ceiling mounted Pitot static probe) and fixed elevation x-ray attenuation for the two gravel sizes tested. The onset of sustained x-ray down spikes represents the "signature" of gravel motion suggesting freestream threshold velocities (u_{et}) of 125 - 150 and 275 - 300 FPS for the P gravel and coarse gravel beds, respectively.

Typical log height velocity profiles are provided in Figure 4-32. These data have been used to determine the near surface shear velocity (u_f) as a function of freestream condition in the conventional manner:

$$u = 5.75\, u_f \log (y / y_o). \qquad (4.5)$$

A compilation of so-determined shear velocities is provided in Figure 4-33. Indicated therein by "solid" and "half-solid"

symbols are fully developed and intermittent gravel "lofting" conditions, respectively. Annotation markings are also shown specifying selected values for threshold "shear" velocities (9.5 and 21.5 FPS for P gravel and coarse gravel, respectively) and threshold "freestream" velocities (140 and 295 FPS, respectively). Note that extrapolation of the Bagnold threshold shear velocity correlation (Bagnold, 1941; Owen, 1964) to "high" speed and "large" particles suggests that coarse gravel lofting should have occurred at a free stream velocity of approximately 80 FPS! An overall summary for the present gravel shear velocity results is given in Figure 4-34 and a value of shear velocity ratio (u_e/u_f) of approximately 15 is indicated.

Some further analysis and interpretation of the current shear velocity data has also been pursued. Typical results from this review process are the velocity data plotted in Figure 4-35a. Shown therein as a function of particle diameter (d) are particle terminal (settling) velocities (u_T), measured threshold shear velocities, measured threshold edge velocities, Bagnold's empirical formulation for threshold shear velocity for beginning of saltation,

$$u_f \equiv u_{ft\ salt} = 0.1 \sqrt{\frac{\rho_p}{\rho}\, gd} \qquad (4.6)$$

and Owen's definition for suspension onset,

$$u_{susp} = 1.0 \sqrt{\frac{\rho_p}{\rho}\, gd}\,. \qquad (4.7)$$

In the above ρ_p and ρ correspond to the particle and air density, respectively. When reviewing the Figure 4-35a results, several observations are of interest to note: 1. Measured values for threshold shear velocities for large particles exceed Bagnold's empirical "extrapolation" by a factor of 2 to 3. This finding implies that hydrocode calculations based on the Bagnold

approximation will overpredict scouring for large particles. 2. Both smooth and rough wall boundary layer measurements (Hinze, 1959) indicate that vertical eddy velocities (v') are of the order of the wall shear velocity. Thus particle suspension will set in when u_f (i.e., v') velocities start approaching terminal velocities (u_T). This result, it should be noted, is consistent with the Owen's specification for the upper boundary between the saltation and suspension regimes given approximately by: $u_{ft\ susp} = 10\ X\ u_{ft\ salt}$. Lofting experiments under the DSU program were conducted for both WSMR and Ottawa sand soil samples whose mean particle sizes were 180 and 250 μm, respectively. Nominal freestream velocities for these experiments were 120, 220 and 320 fps corresponding to, approximately, vertical eddy velocities of ($v' \simeq .05\ u_e$), 6, 11 and 16 FPS, respectively. From Figure 4-35a, it is seen that these velocities all exceed terminal velocities for corresponding particle sizes implying, therefore, that the bulk of the DSU results are representative of the suspension regime for particle motion.

In Figure 4-35b particle drag-to-weight ratio results (D/W) are shown as a function of freestream (edge) velocity with particle diameter used as the free parameter. The noted drag values are based on edge velocities and established drag coefficient data for spheres in air (Schlicting, 1955). Also plotted therein are the threshold data from our current gravel experiments and threshold results obtained by Bagnold (1941) and Gillette (1988) for 250 μm and 1 mm particles, respectively. It is interesting to note that saltation onset is seen to occur at freestream D/W ratios of the order of 3 ± 1 for particles ranging in size from 250 μm to as large as 1.5". Is it possible that the operative parameter to assess particle scouring potential (saltation onset) is in fact a freestream-based particle D/W ratio? If in fact the D/W correlation proves to be the most appropriate predictor of scouring onset than a revision to those hydrocode empirical "fits", which now use Bagnold's threshold shear velocity formulation, would seem to be in order. Such a

revision may be of interest since calculations based on D/W threshold velocities, for size and mass of lofted particles, result in less predicted mass scoured to altitude than corresponding estimates based on Bagnold's correlation approach.

Finally, for the velocity range associated with the DSU experiments (120 - 370 FPS) note the magnitude of the D/W ratios (> 100). It is not surprising, therefore, that even for the DSU lowest speed case, substantial drag forces exist wherein the bulk of the boundary layer flow consists of particles which have entered into suspension.

4.5 THRESHOLD VELOCITIES FOR MOIST WSMR SOIL BEDS.

To date, investigations into the effects of moisture content on soil scouring have, in general and understandably, been focused on the soil erosion concerns of the agricultural community (e.g., Chepil, 1956). As a result measured results have been limited to low speed flows (< 50 fps) with substantial uncertainty existing relative to the scouring performance of moist soils at high speeds. The available data base suggests that negligible scouring takes place once the moisture content exceeds a soil's "wilting point" condition (Chepil, 1956). For sandy soils similar to WSMR, the wilting point corresponds, approximately, to a water-to-soil mass ratio of 2-3%. The intent of the current investigation was to validate these previous results for moist WSMR soil and to demonstrate that negligible scouring would indeed take place at speeds associated with high airblast flow conditions.

All moist soil tests were performed with a 5/8" deep WSMR bed extending from the DSU tunnel's 12 foot location to downstream of the primary diagnostics station (21'4"). To achieve turbulent boundary layer flow and repetitive/controlled test conditions, Astroturf matting was bonded to the steel floor of the wind tunnel upstream of the 12 foot station. As was the case for the gravel

threshold experiments (Section 4.4) primary measurements again consisted of edge velocity (freestream Pitot-static probe), side view video photography (15' station), fixed elevation x-ray attenuation (0.5" above surface) and a Snob probe rake at the 21' 4" location. Each test was run under increasing speed conditions until the onset of particle motion or, as for some cases, maximum tunnel speed was reached without achieving scouring onset (350-370 fps). After laying and leveling each bed, water was added by fine mist spraying to provide a selected moisture content of 5 to 25%. Tests were run with "cure" times varying from 1 to 48 hours. For the 10, 15 and 25% moisture cases (RS 119, 117 and 115 respectively; 24 hour cure) all beds were damp/moist to the touch throughout the bed depth. One 5% case at a 1 hour cure time (RS 124) was damp down to a 0.25" depth and two test cases at 5% moisture content (RS 125 , 24 hour; RS120, 48 hour) had a "dry" texture feel just prior to test time. Additional test details are provided in the test matrix of Table 4-1.

A typical set of output time traces histories for one of the current moist soil experiments is given in Figure 4-36 . For this test case (RS 120) the soil bed corresponds to an initial moisture content of 5% and a cure time of 48 hours. At the time of the RS 120 test, evaporation effects had reduced the surface moisture level to approximately 1% causing the soil to appear dry to the touch and to develop a frangible surface crust of 0.25" thickness. In Figure 4-36 the onset of soil scouring is evidenced by the initial downspike (attenuation) in the x-ray time trace (Figure 4-36a) at a fan rotation speed of 800 RPM (Figure 4-36b; freestream velocity: 45 fps, Figure 4-36c). Note that the threshold edge velocity for dry/"erodible" WSMR soil is of the order of 10 fps (Section 4.4), a value substantially lower than the current measured value for moist/crusted WSMR. This finding points out the important (and complicating) effects of crust formation due to water evaporation (cure time) on assessing scouring potential for moist soils. Additional testing would therefore seem warranted to separate out the roles of crusting as distinct from moisture

content only. This issue would seem to be especially relevant in view of the fact that surface crusting most likely will be significantly compromised for airblasts of interest due to the crushing effects of high overpressure shocks which will tend to catastrophically break up near surface crusts.

A consistency check on the RS 120 threshold velocity "measure" is provided in Figure 4-37 wherein results for a 24 hour 5% moist test case (RS125) are presented. The onset of scouring is seen to occur at similar freestream velocities for each of the 5% moist WSMR experiments (~ 45 fps). This result is most probably due to the fact that near surface crusts were formed for each and moisture content values at test times were comparable (~ 1-2%). Also shown in Figure 4-37c are rake measured velocity profile data plotted in semi log format in order to determine conventional shear velocity results. The data illustrate that measured shear velocities at onset are larger than dry/erodible sand data ($\simeq$ 1 fps) but that the velocity ratio, u_e/u_f, is similar to established measurements for rough wall turbulent boundary layers (Hinze, 1959). The current threshold shear velocity data (~ 2.5 fps) are also found to be in good agreement with results obtained by Gillette (1988) for "crusty"/sandy soils.

In an attempt to further clarify the interplay between moisture content, crusting, cure time and scouring onset, a 5% moist WSMR experiment (RS 124) was performed for a soil bed allowed to cure for only <u>one</u> hour prior to test. Results are provided in Figure 4-38 which indicate that modest soil motion first occurred at an edge velocity of approximately 150 fps. For this case no crust was formed, the soil felt slightly damp to the touch and the moisture content at test time was of the order of 5%. As indicated in Figure 4-38c, a "high" value for threshold shear velocity (~ 8 fps) was measured and the velocity ratio (u_e/u_f) was approximately 18 again in fair agreement with existing results for turbulent boundary layers.

For tests run at 10% moisture content or higher, soil scouring was essentially negligible even up to an edge velocity of 370 fps (Figures 4-39, 4-40 and 4-41). Corresponding velocity ratios (u_e / u_f) of approximately 24 are higher than nominal and illustrate that shear velocities tend to be on the small side suggesting that some velocity slip at the surface may be occurring due to moisture effects. The fact that no lofting took place at these higher moisture test cases reaffirms the view that soils moist to the touch will indeed not erode even under substantially high velocity conditions.

The current results demonstrate that just a nominal amount of moisture effectively eliminates dust lofting. It thus may be appropriate, to treat the soil moisture issue in code calculations of dust mass lofted to altitude on the basis of an either/or approximation, namely, the soil surface is either moist or dry corresponding to an SEF of 0 or 1, respectively.

Table 4-1. Test matrix for RS dust lofting experiments.

RS TYPE	TEST	DATE	VELOCITY	BED DEPT	RS ELEV	FLO TIME
	RS NO		FPS	IN	IN	SEC
NON EROD RIDGES/1'	26	3/25/93	237	3	0	33
NON EROD RIDGES/1'	27	3/30/93	237	RS26	RS26	31
NON EROD RIDGES/1'	28	3/30/93	236	RS27	RS27	31
NON EROD RIDGES/1'	29	3/31/93	102	3	0	40
NON EROD RIDGES/1'	30	4/2/93	114	2	1	42
NON EROD RIDGES/1'	31	4/2/93	118	2	1	39
NON EROD RIDGES/1'	32	4/5/93	116	2	1	40
NON EROD RIDGES/1'	33	4/6/93	124	1	2	40
NON EROD RIDGES/1'	34	4/6/93	225	1	2	30
NON EROD RIDGES/1'	35	4/13/93	120	0	3	40
NON EROD RIDGES/1'	36	4/13/93	233	0	3	40
NON EROD RIDGES/1'	37	4/13/93	116	2.5	0.5	41
NON EROD RIDGES/1'	38	4/14/93	227	2	1	32
NON EROD RIDGES/1'	39	6/3/93	367	2	1	26
NON EROD RIDGES/1'	40	6/5/93	374	0	3	27
NON EROD RIDGES/1'	65	8/30/93	129	1	2	20
NON EROD RIDGES/1'	66	8/31/93	361	1	2	17
NON EROD RIDGES/1'	67	9/1/93	238	1	2	18
NON EROD RIDGES/2'	126	6/14/94	116	1	2	
NON EROD RIDGES/2'	127	6/14/94	238	1	2	28
NON EROD RIDGES/2'	128	6/15/94	124	2	1	28
NON EROD RIDGES/2'	129	6/15/94	240	2	1	27
NON EROD RIDGES/2'	130	6/16/94	372	2	1	27
NON EROD RIDGES/2'	131	6/16/94	376	1	2	18
EROD RIDGES	41	7/7/93	114	2	1	28
EROD RIDGES	42	7/14/93	120	1	2	25
EROD RIDGES	43	7/15/93	120	1	2	27
EROD RIDGES	44	7/16/93	118	2	1	24
NON EROD CLODS	45	7/23/93	112	2.5	1	24
NON EROD CLODS	46	8/3/93	120	2.5	1	24
NON EROD CLODS	47	8/4/93	234	2.5	1	30
NON EROD CLODS	48	8/5/93	361	2.5	1	24
NON EROD CLODS	49	8/6/93	127	1.5	2	22
NON EROD CLODS	50	8/9/93	222	1.5	2	25
NON EROD STUBBLE	56	8/17/93	121	1.5	2	21
NON EROD STUBBLE	57	8/18/93	231	1.5	2	24
NON EROD STUBBLE	58	8/19/93	121	1.5	1	22
NON EROD STUBBLE	59	8/20/93	230	1.5	1	19
NON EROD STUBBLE	60	8/23/93	335	2.5	1	20
NON EROD STUBBLE	61	8/24/93	356	1.5	2	18
LE CLODS(DBL ROW)	51	8/10/94	127	2.5	1	21
LE CLODS(DBL ROW)	52	8/11/93	235	2.5	1	21
LE CLODS(DBL ROW)	53	8/11/93	122	1.5	2	21
LE CLODS(DBL ROW)	54	8/12/93	232	1.5	2	22
LE CLODS(SGL ROW)	55	8/12/93	122	1.5	2	22
LE RIDGE	62	8/25/93	124	1.5	1.5	17
LE RIDGE	63	8/26/93	229	1.5	1.5	19
LE RIDGE	64	8/27/93	124	2	1	17
LE CLDS(SGL ROW)	68	9/2/93	129	2	7	19
LE CLDS(SGL ROW)	69	9/2/93	234	2	7	19
LE VORT GEN	75	9/21/93	122	2.25	1	27
LE VORT GEN	76	9/22/93	234	2.25	1	21
LE VORT GEN	77	9/23/93	364	2.25	1	17
LE VORT GEN	78	9/24/93	120	2.25	2	28
LE VORT GEN	79	9/24/93	232	2.25	2	19
LE VORT GEN	80	9/27/93	367	2.25	2	18
GRVL SDD WSMR	70	9/8/93	130	3	1	26
GRVL SDD WSMR	71	9/9/93	122	3	1	37
GRVL SDD WSMR	72	9/9/93	134	3	1	46
GRVL SDD WSMR	73	9/10/93	227	3	1	38
GRVL SDD WSMR	74	9/14/93	367	3	1	24
LG GRVL SHR VEL	90	10/15/93	VAR	3	1	56
LG GRVL SHR VEL	91	10/15/93	VAR	3	1	56
LG GRVL SHR VEL	92	10/18/93	VAR	3	1	59
LG GRVL SHR VEL	93	10/19/93	VAR	3	1	90
LG GRVL SHR VEL	95	10/19/93	VAR	3	1	80
LG GRVL SHR VEL	96	10/20/93	VAR	3	1	52
LG GRVL SHR VEL	97	10/20/93	VAR	3	1	72
P GRVL SHR VEL	103	10/25/93	VAR	1.5	0.25	60
P GRVL SHR VEL	104	10/25/93	VAR	1.5	0.25	75
P GRVL SHR VEL	105	10/26/93	VAR	1.5	0.25	80
P GRVL SHR VEL	107	10/26/93	VAR	1.5	0.25	75
MOIST WSMR/25%/24HR	114	4/6/94	VAR	0.625	NA	87
MOIST WSMR/25%/24HR	115	4/6/94	VAR	0.625	NA	86
MOIST WSMR/15%/24HR	116	4/7/94	VAR	0.625	NA	85
MOIST WSMR/15%/24HR	117	4/7/94	VAR	0.625	NA	85
MOIST WSMR/10%/24HR	118	4/8/94	VAR	0.625	NA	85
MOIST WSMR/10%/24HR	119	4/8/94	VAR	0.625	NA	74
MOIST WSMR/5%/48HR	120	4/10/94	VAR	0.625	NA	80
MOIST WSMR/5%/24HR	121	5/17/94	VAR	0.625	NA	80
MOIST WSMR/5%/24HR	122	5/17/94	VAR	0.625	NA	95
MOIST WSMR/5%/24HR	123	5/17/94	VAR	0.625	NA	75
MOIST WSMR/5%/1HR	124	5/18/94	VAR	0.625	NA	80
MOIST WSMR/5%/24HR	125	5/20/94	VAR	0.625	NA	84

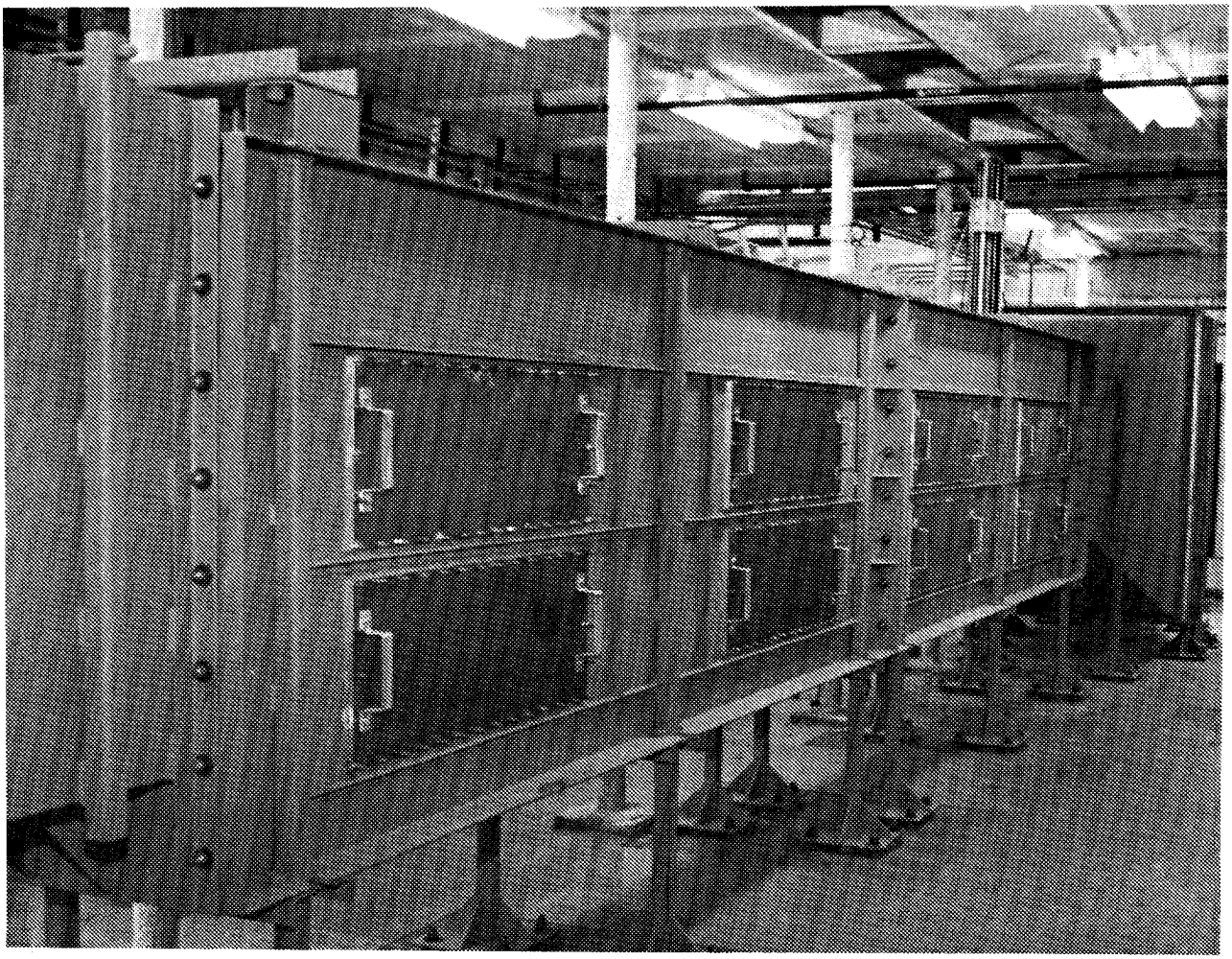

Figure 4-1. DSU Wind Tunnel test section (north side view looking upstream towards facility contraction section).

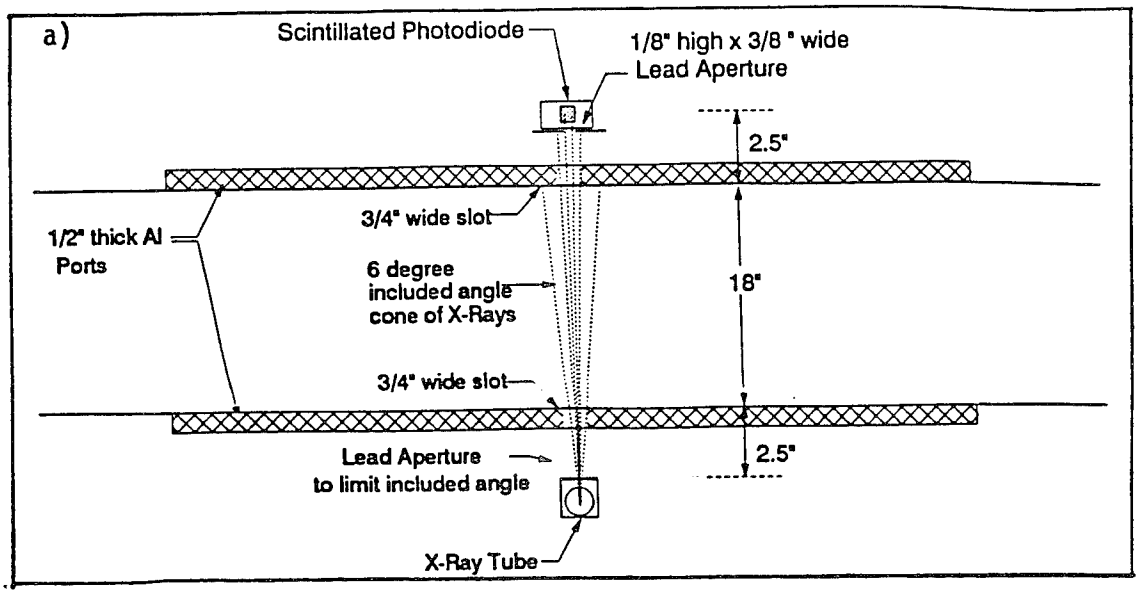

(a) Plan view

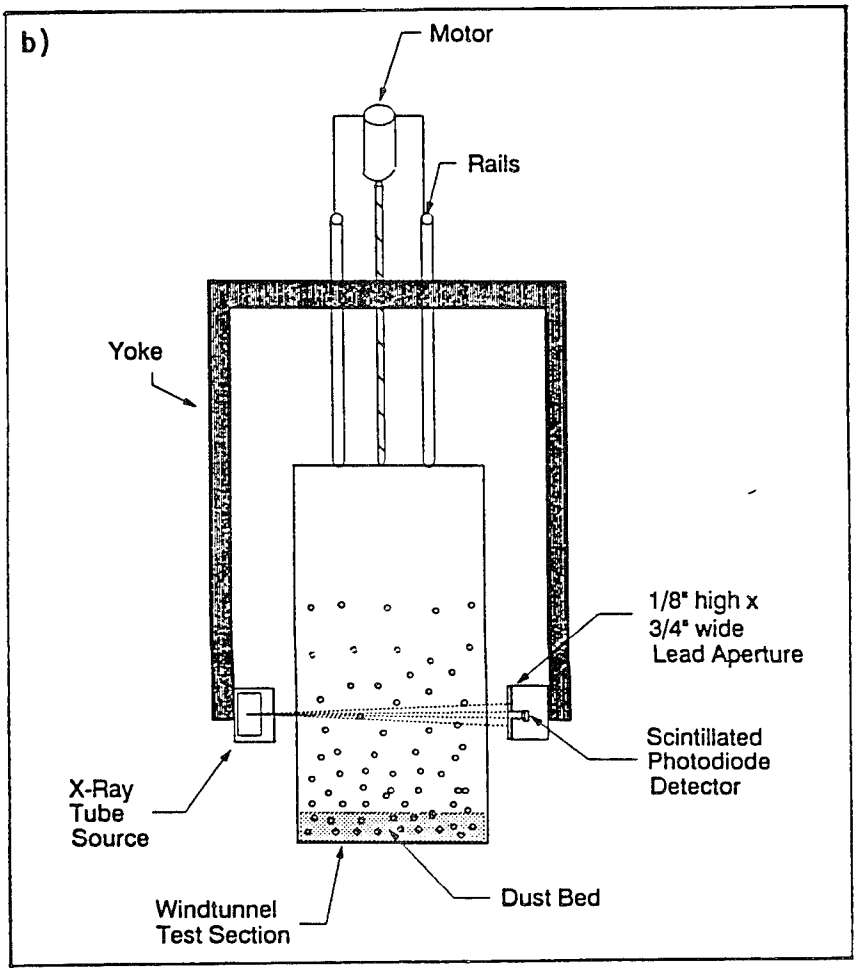

(b) View looking upstream

Figure 4-2. X-Ray dust density diagnostics schematic.

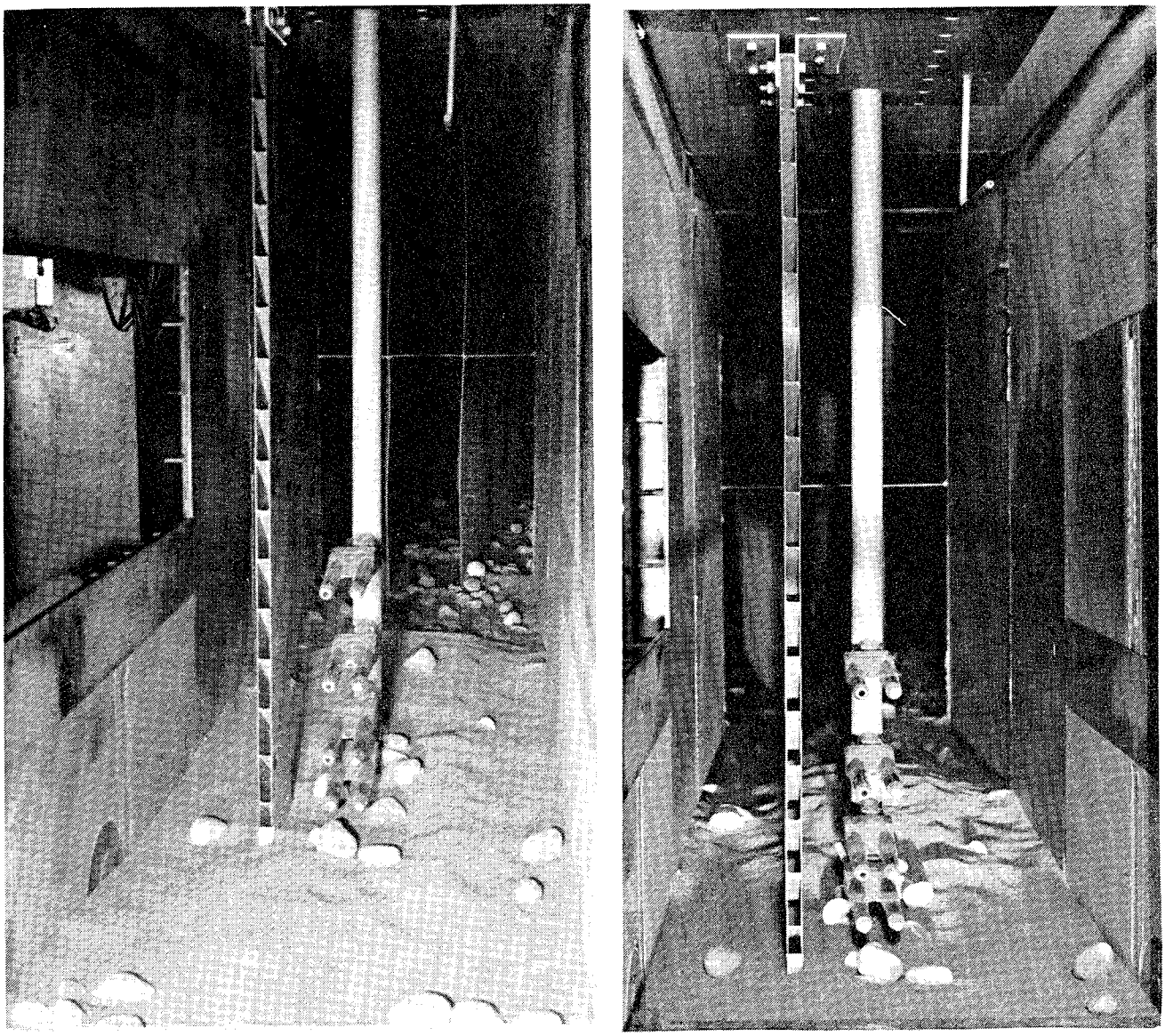

(a) "South" side view of diagnostics station

(b) "North" side view of diagnostics station

Figure 4-3. Post test photographs of Gravel Seeded WSMR dust bed: RS74, 367 FPS.

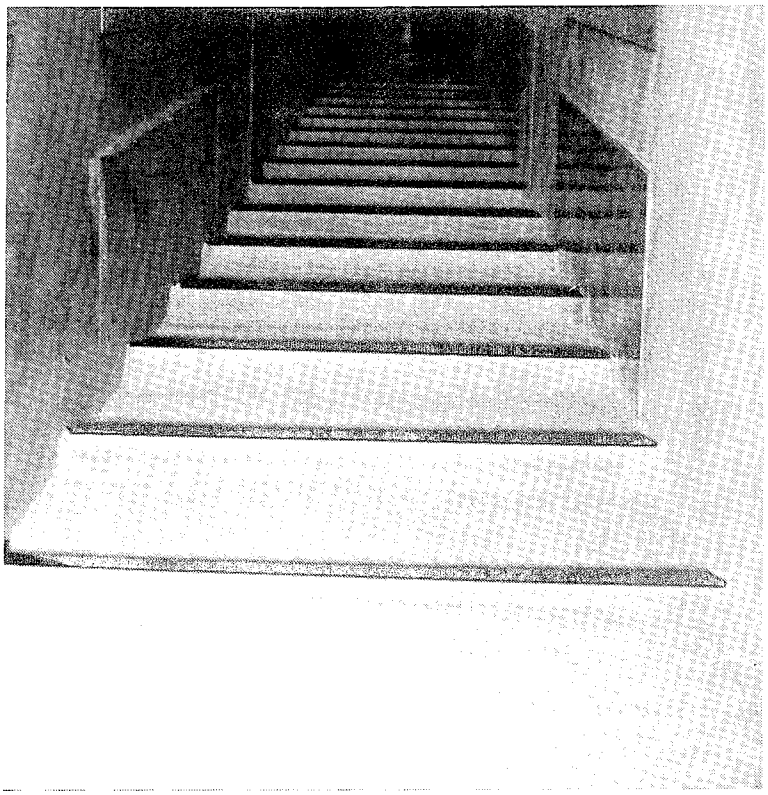

(a) Downstream view

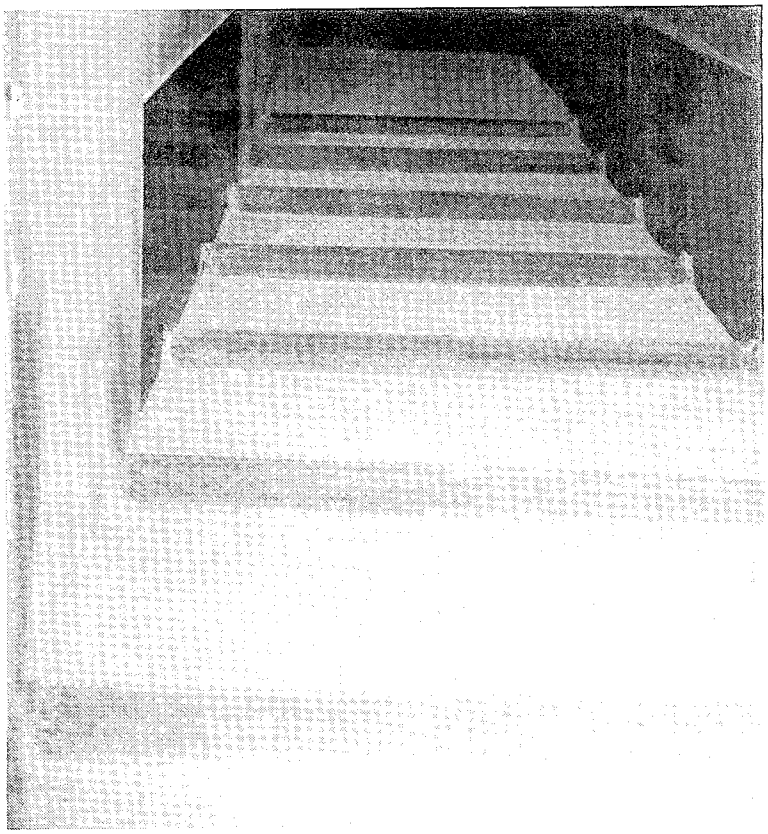

(b) Upstream view

Figure 4-4. Pre test photographs of ridge dust bed.

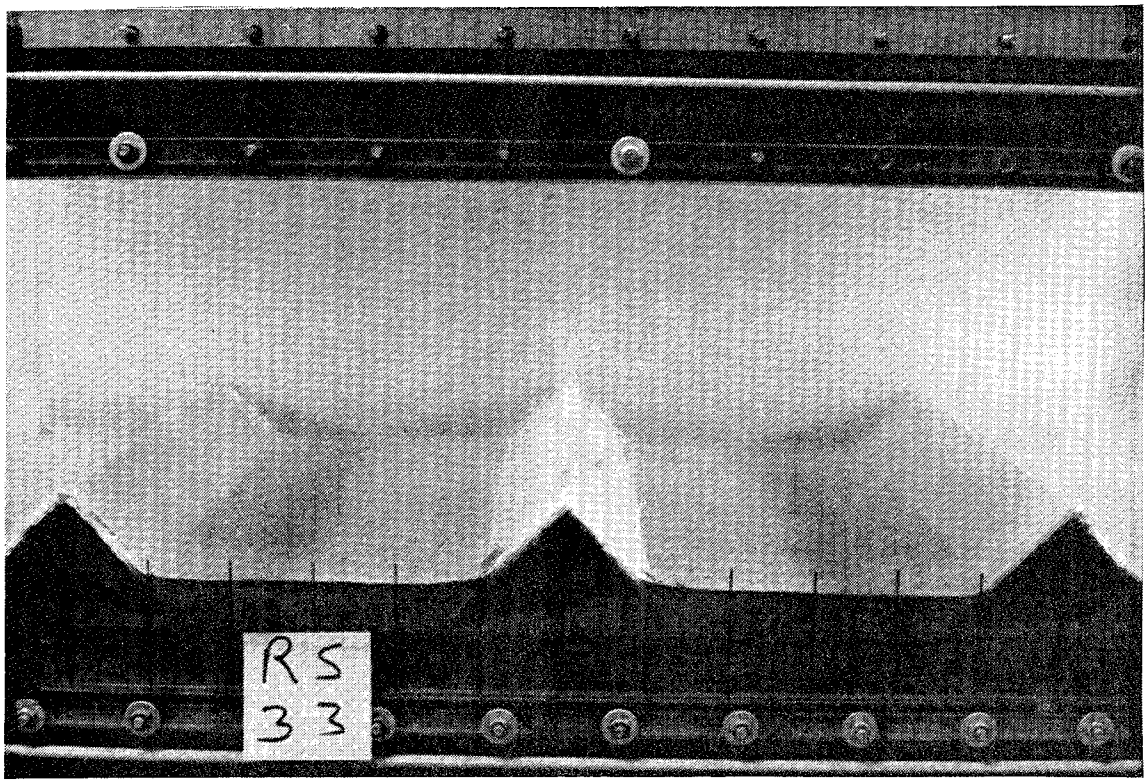

(a) Pre test view

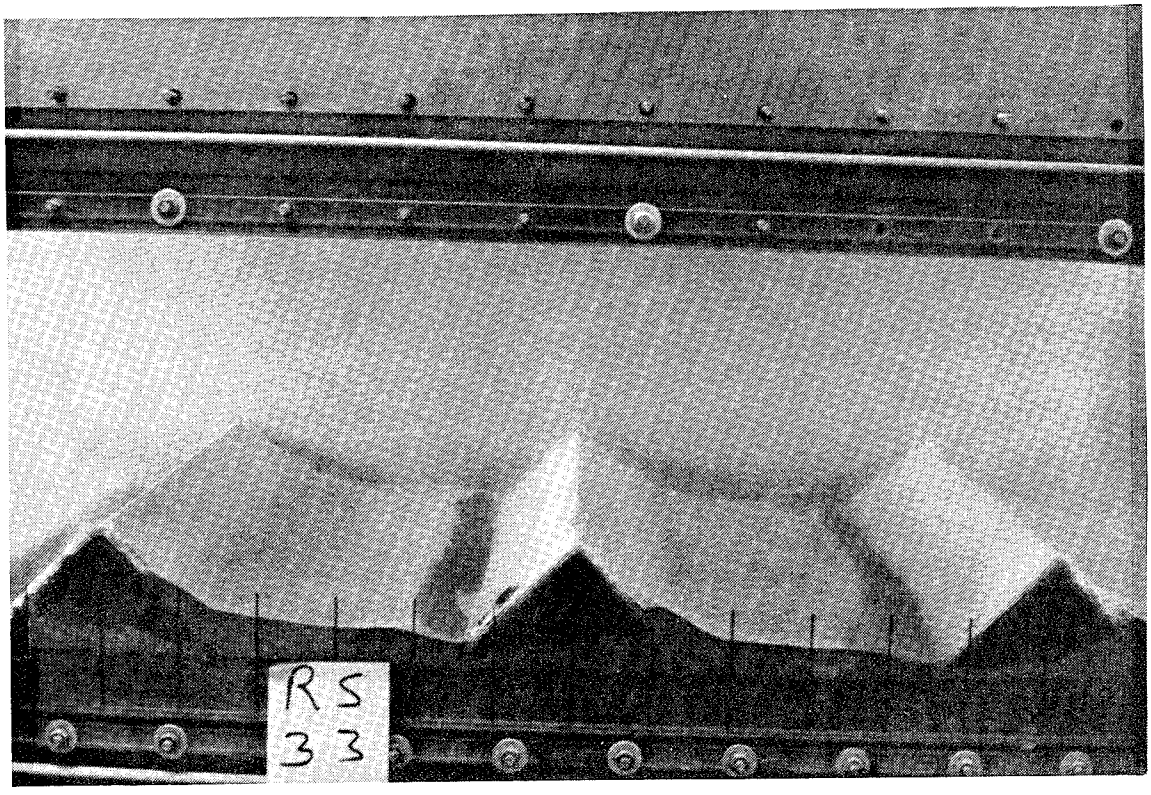

(b) Post test view

Figure 4-5. Side view photographs at 9' test station of ridge dust bed: RS33, 124 FPS, 2" elevation.

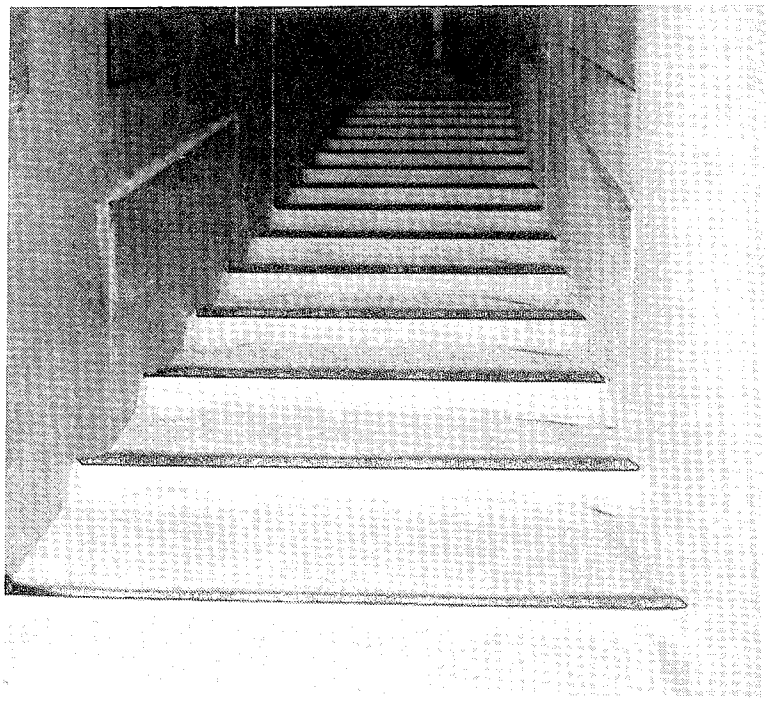

(a) Downstream view

(b) Upstream view

Figure 4-6. Post test photographs of ridge dust bed: RS32, 116 FPS, 1" elevation.

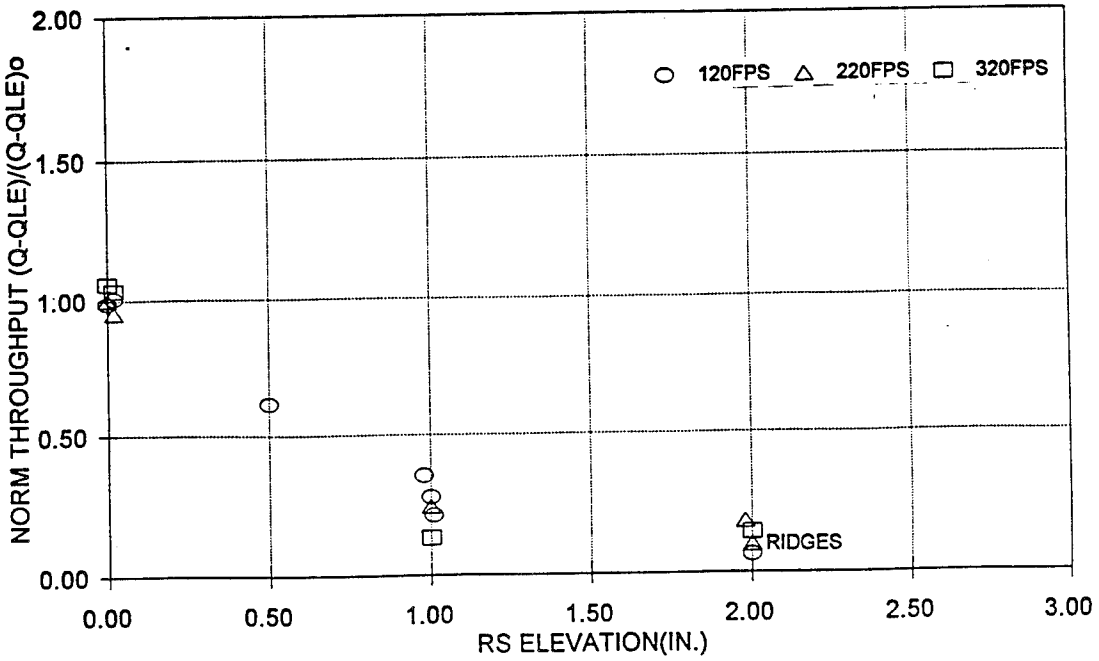

(a) Non-erodible ridge data

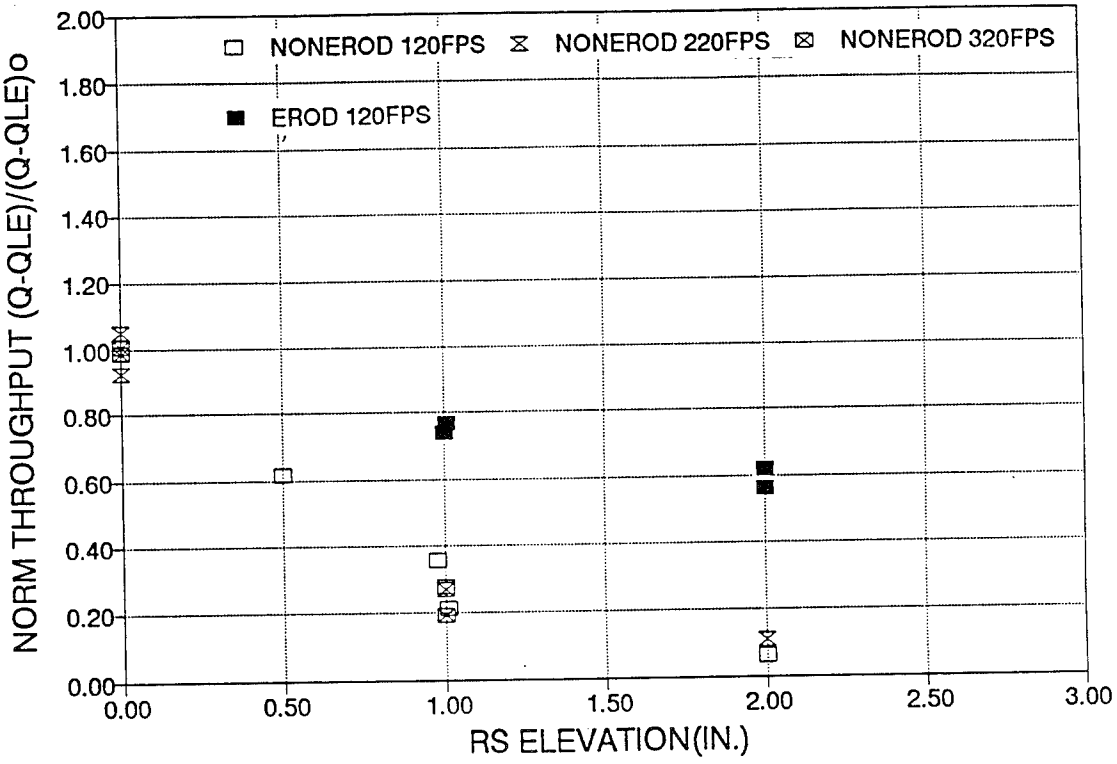

(b) Erodible ridge data

Figure 4-7. Dependence of normalized soil loss on ridge elevation (Ridge separation: one foot).

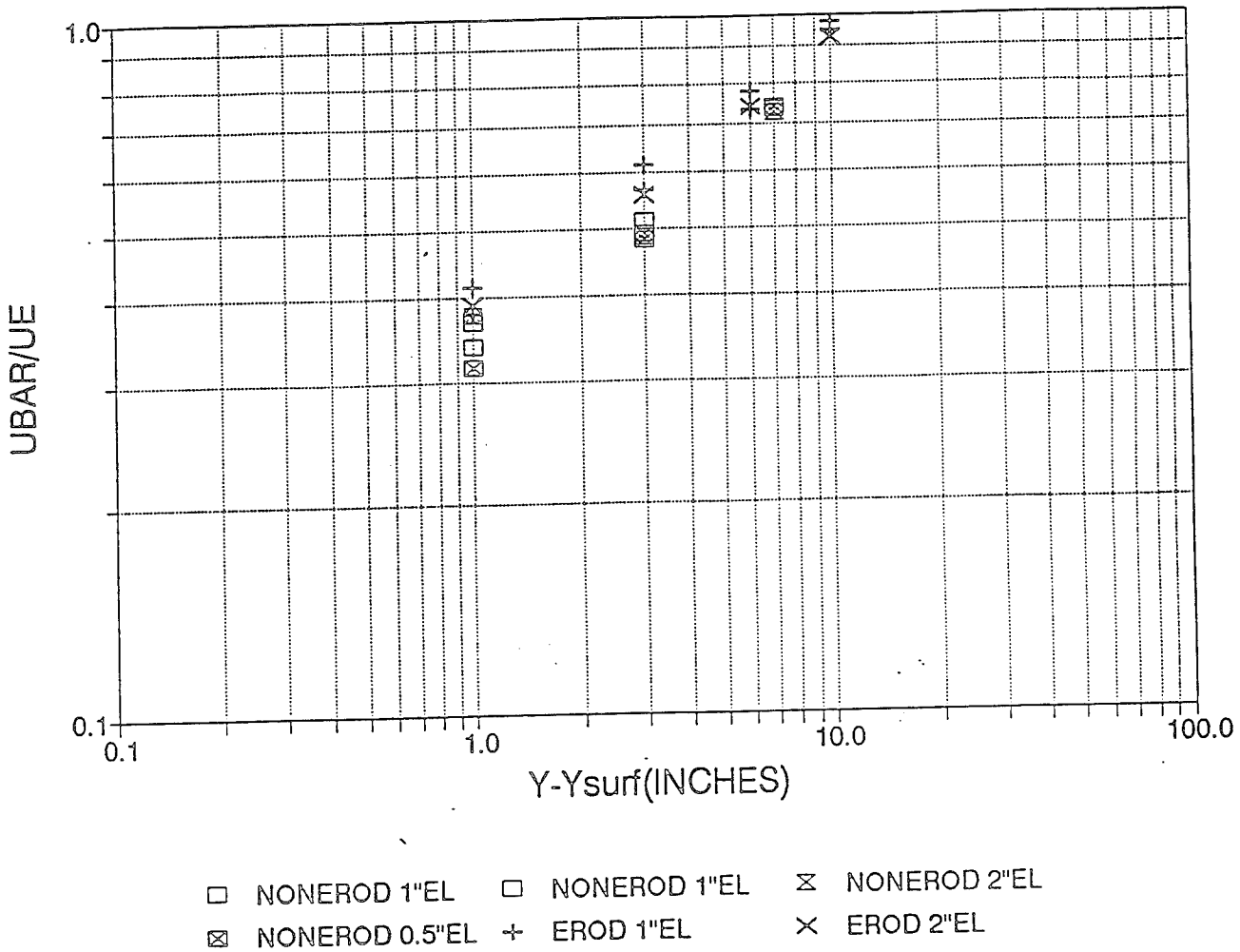

Figure 4-8. Real surface velocity profiles at 21' 4" station for ridge soil beds.

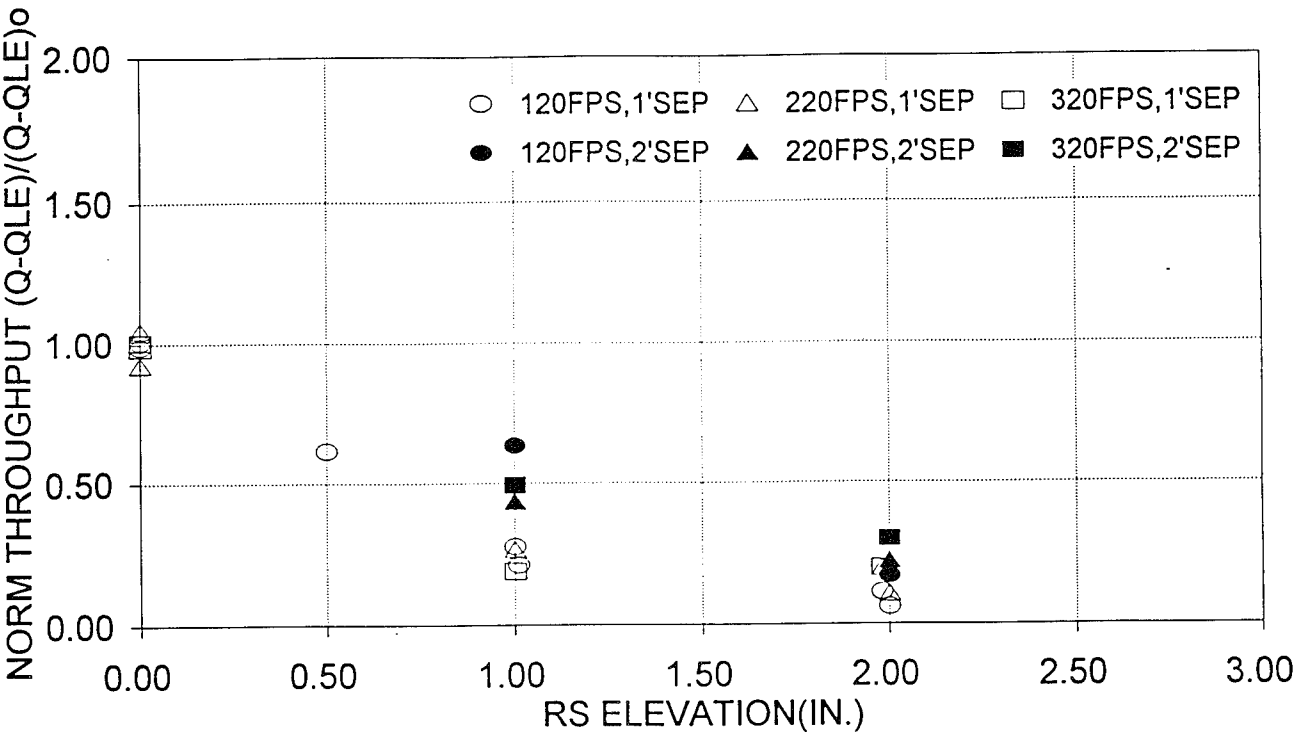

(a) Measured elevation

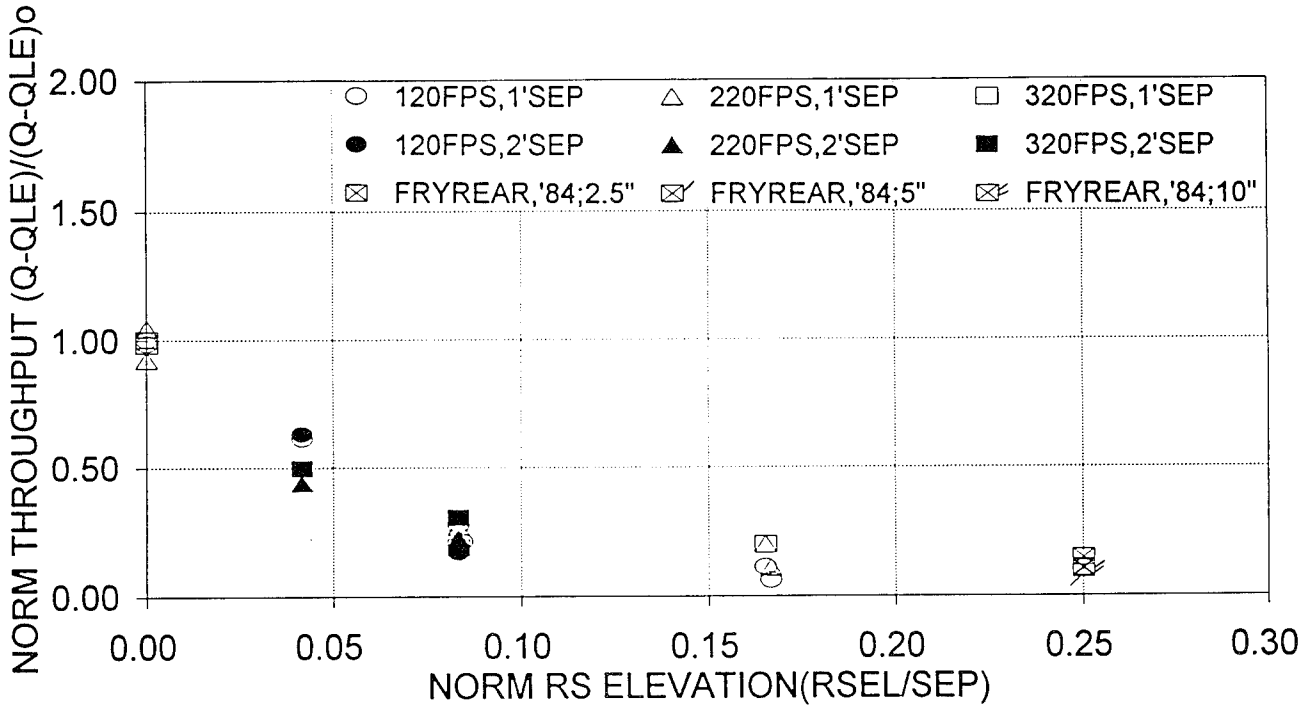

(b) Normalized elevation

Figure 4-9. Dependence of normalized soil loss on ridge separation.

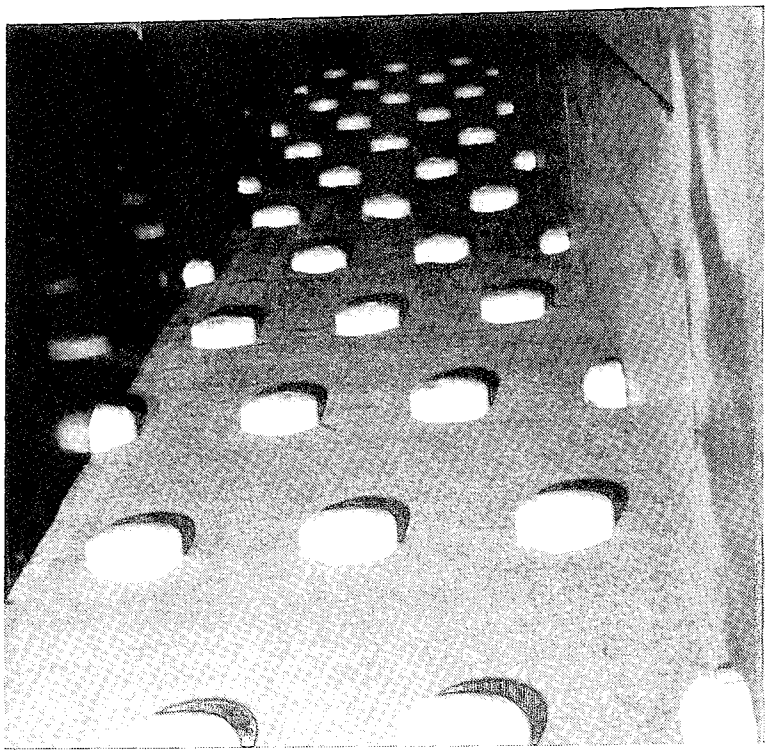

(a) One inch clod elevation

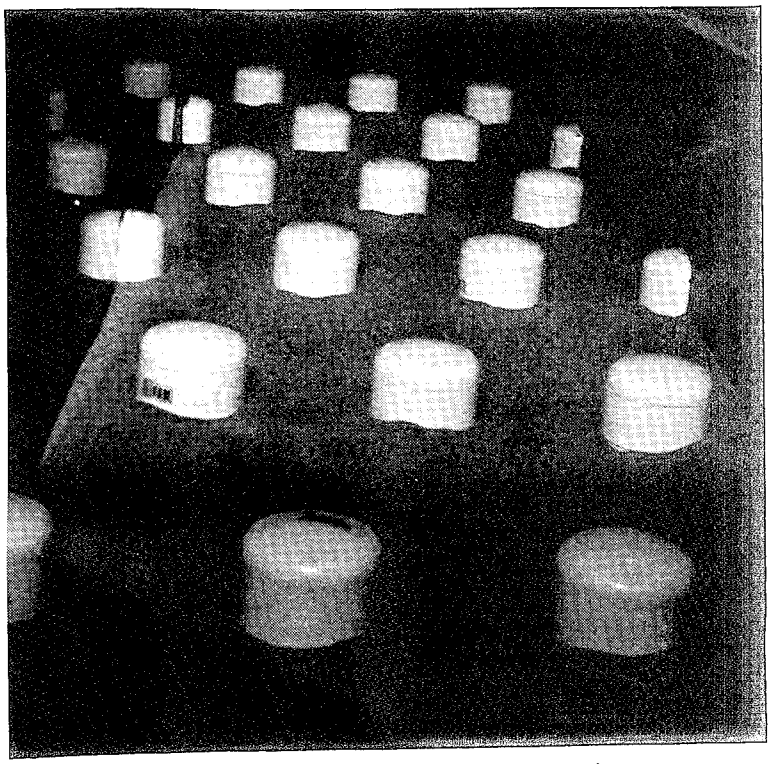

(b) Two inch clod elevation

Figure 4-10. Pre test photographs of clod dust bed looking upstream.

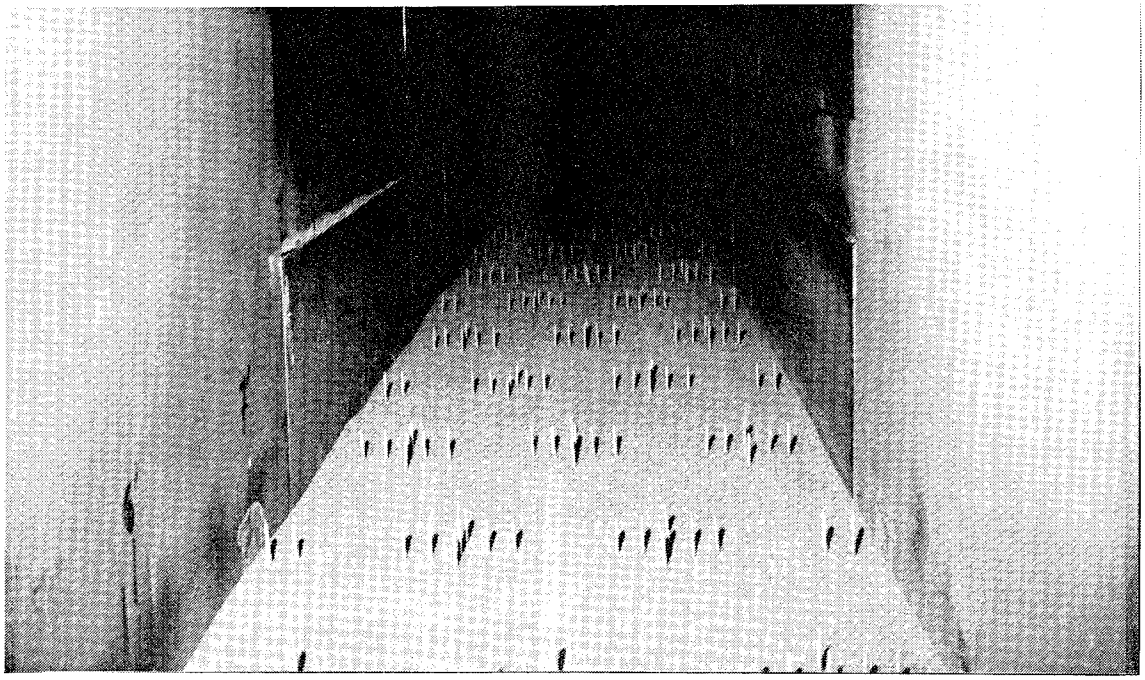

(a) One inch stubble elevation

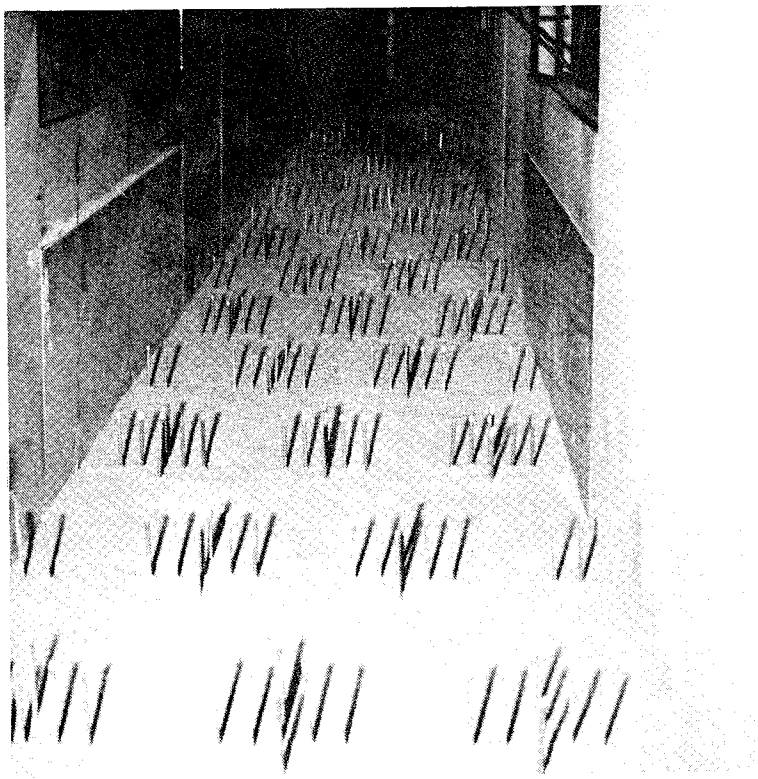

(b) Two inch stubble elevation

Figure 4-11. Pre test photographs looking downstream of stubble dust bed.

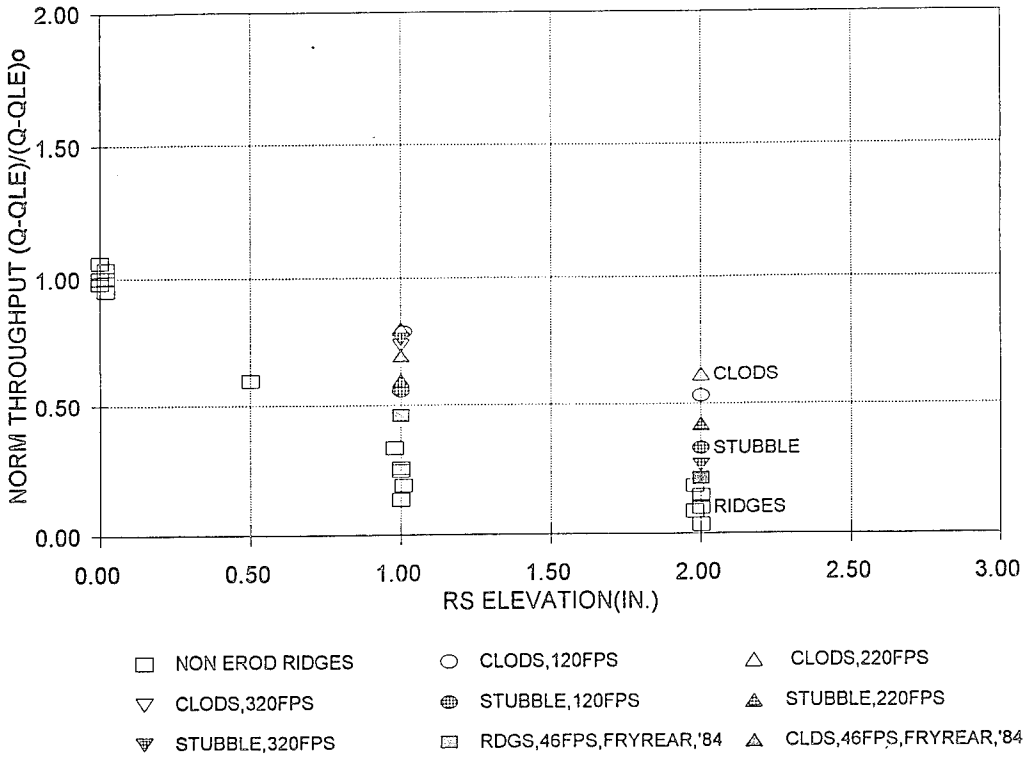

(a) Distributed real surface disturbances

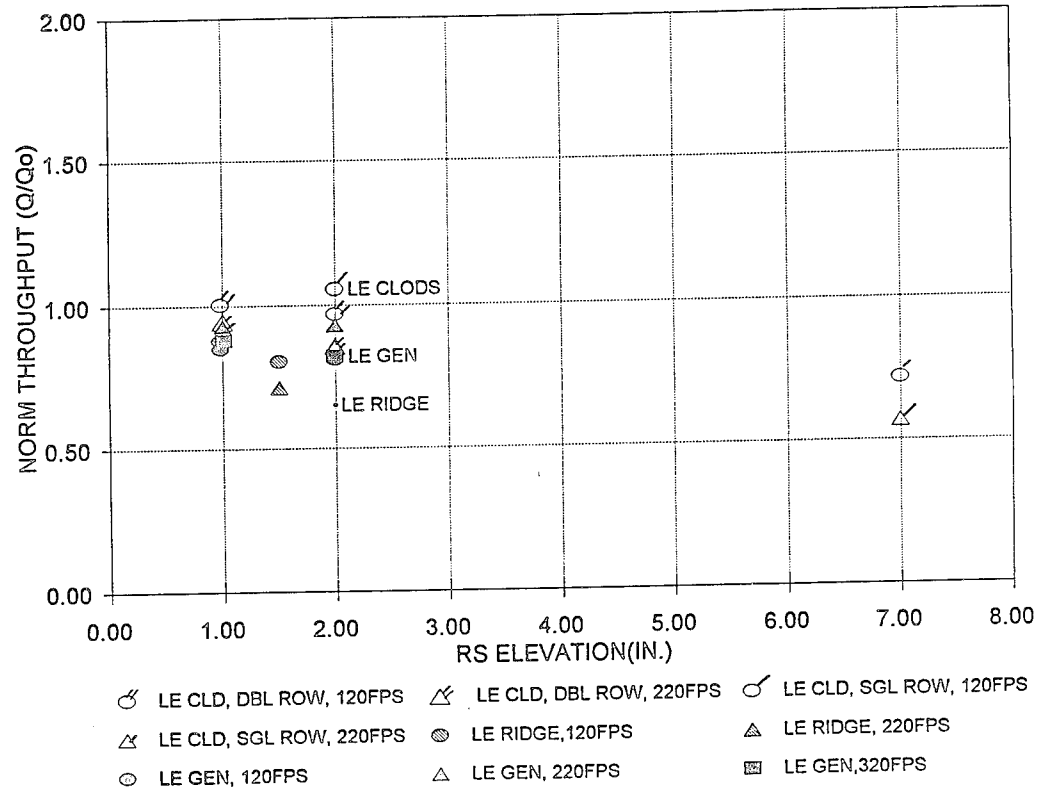

(b) Leading edge disturbances

Figure 4-12. Soil loss versus non-erodible real surface elevation (Axial separation: one foot).

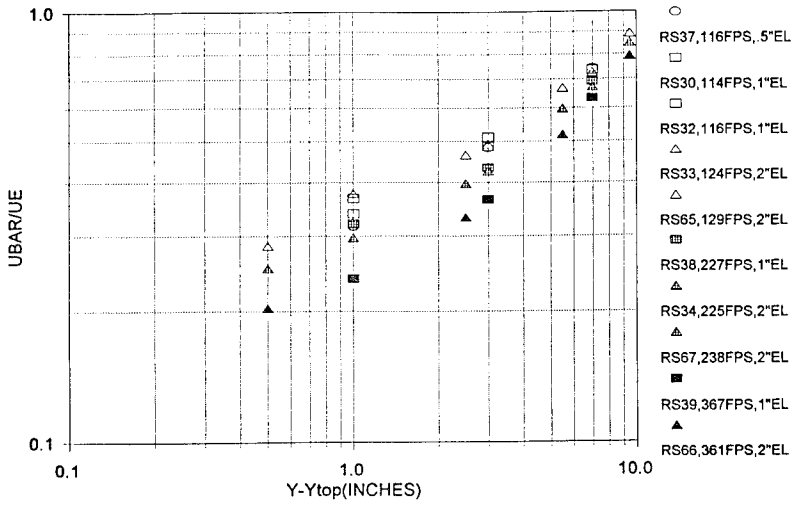

(a) Non-erodible ridge soil beds

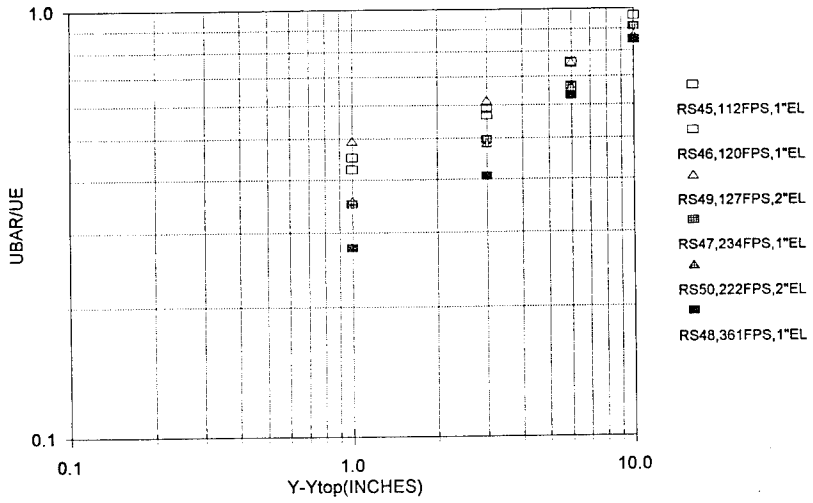

(b) Non-erodible clod soil beds

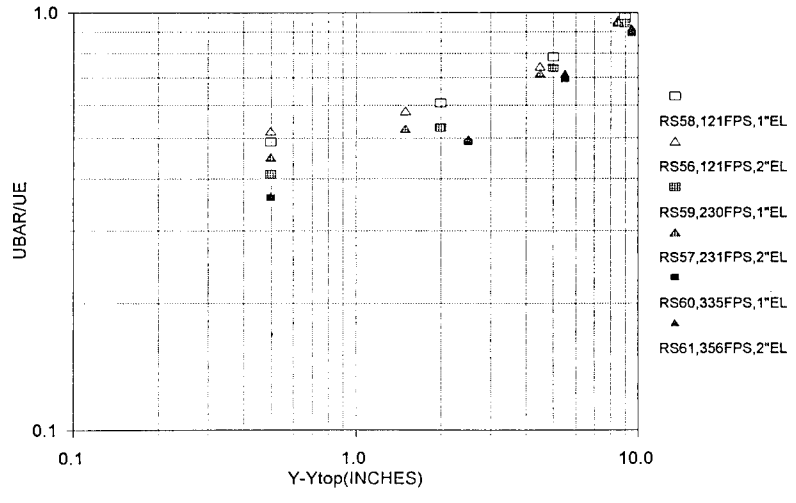

(c) Non-erodible stubble soil beds

Figure 4-13. Real surface velocity profiles at 21' 4" station.

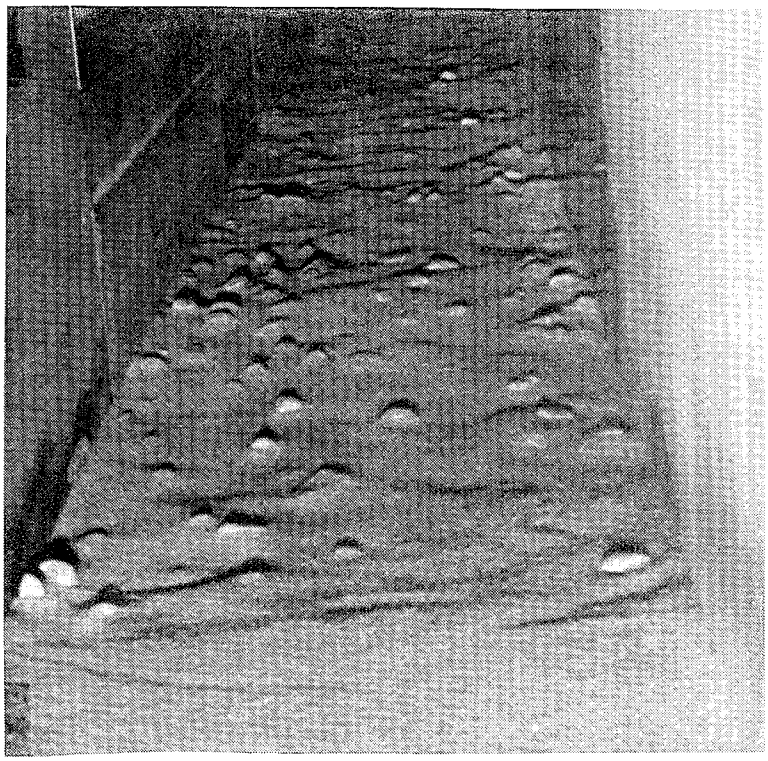

(a) Pre test

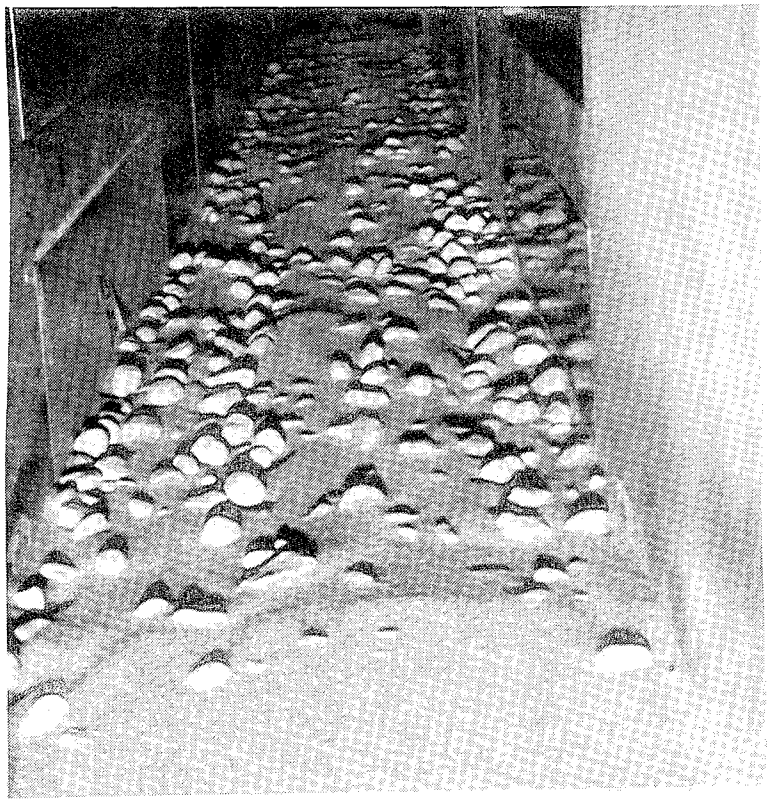

(b) Post test

Figure 4-14. Downstream view photographs of Gravel Seeded WSMR dust bed: RS70, 130 FPS.

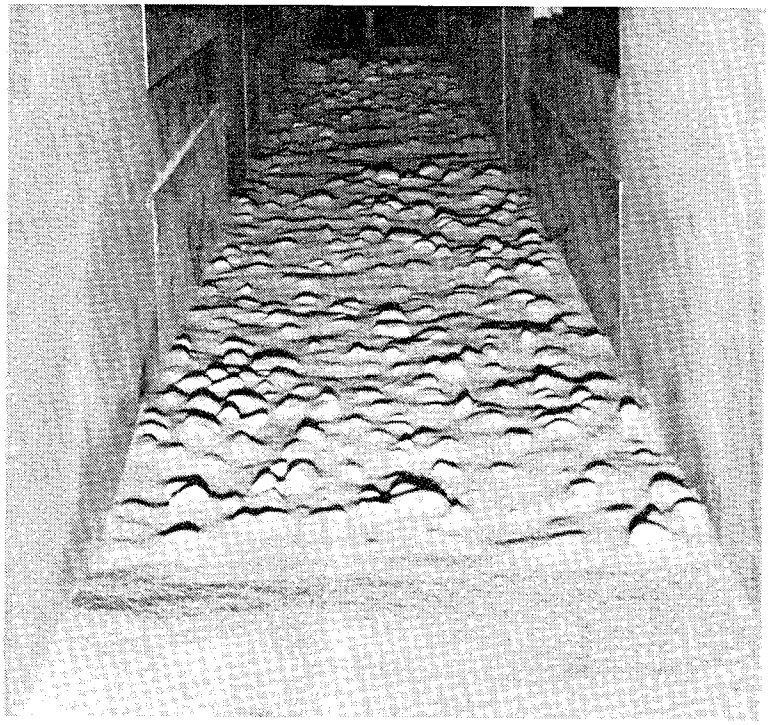

(a) Pre test

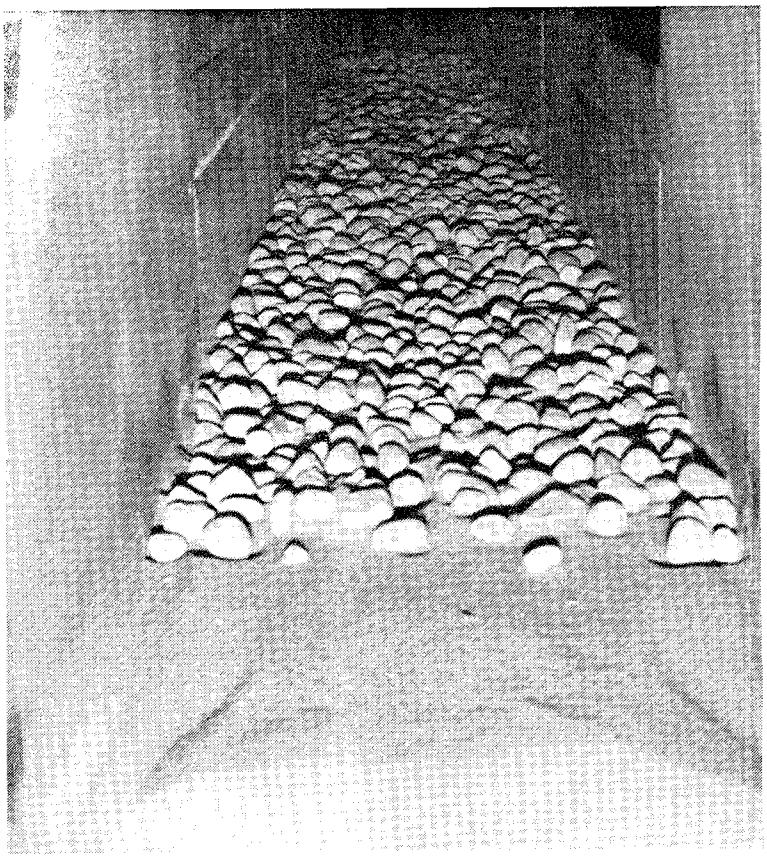

(b) Post test

Figure 4-15. Downstream view photographs of Gravel Seeded WSMR dust bed: RS73, 227 FPS.

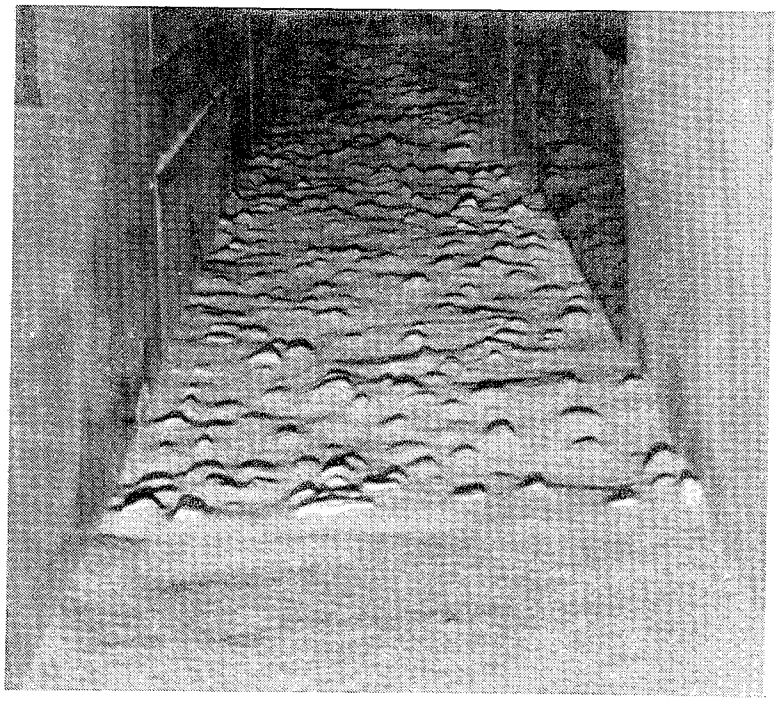

(a) Pre test

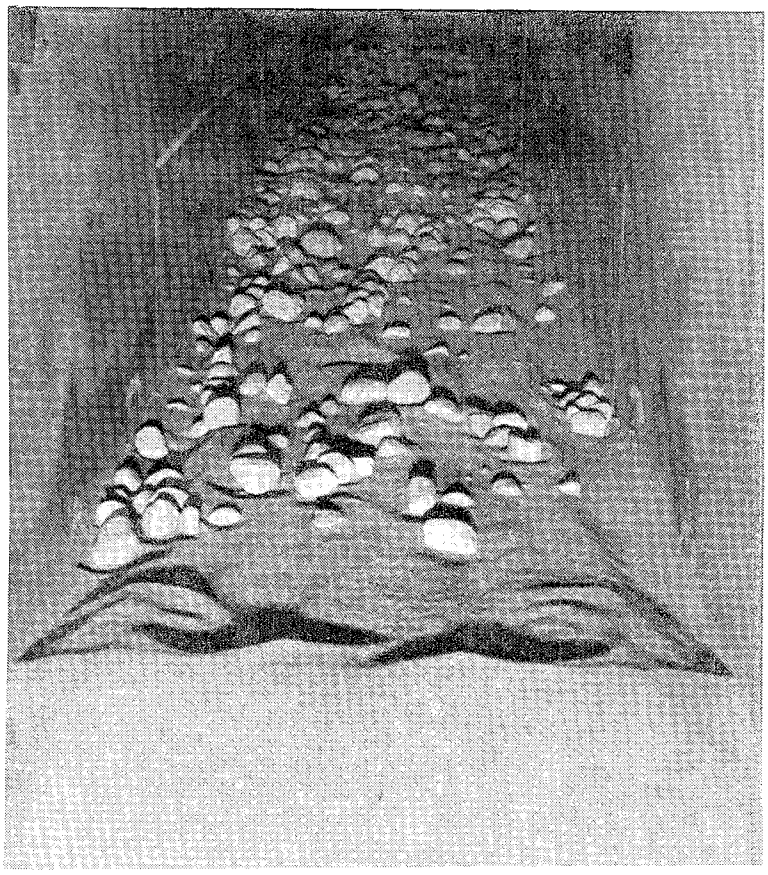

(b) Post test

Figure 4-16. Downstream view photographs of Gravel Seeded WSMR dust bed: RS74, 367 FPS.

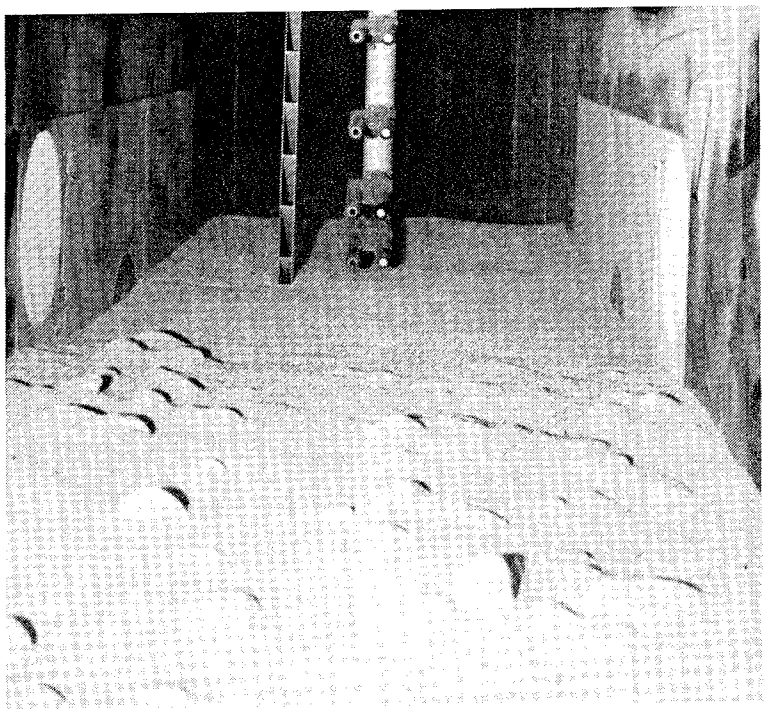

(a) Pre test

(b) Post test

Figure 4-17. Downstream view photographs of Gravel Seeded WSMR dust bed at diagnostics station: RS74, 367 FPS.

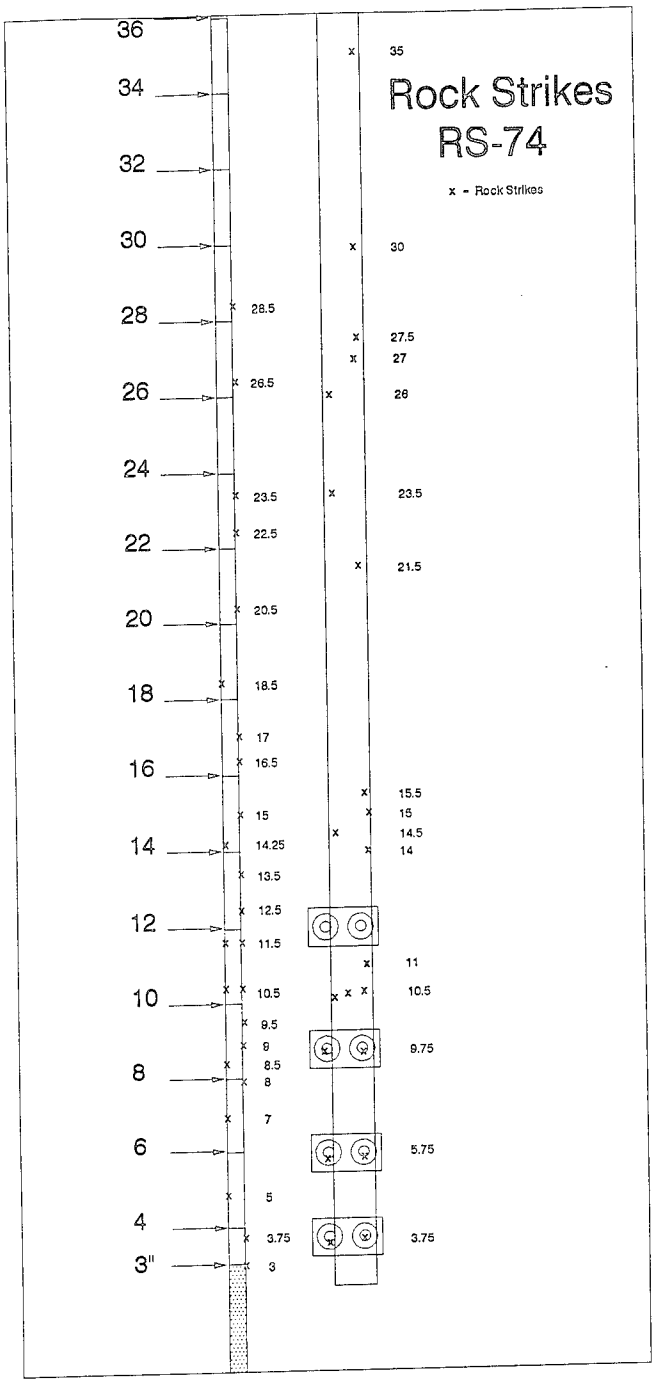

Figure 4-18. Summary of gravel impacts on Bagnold collector and probe strut.

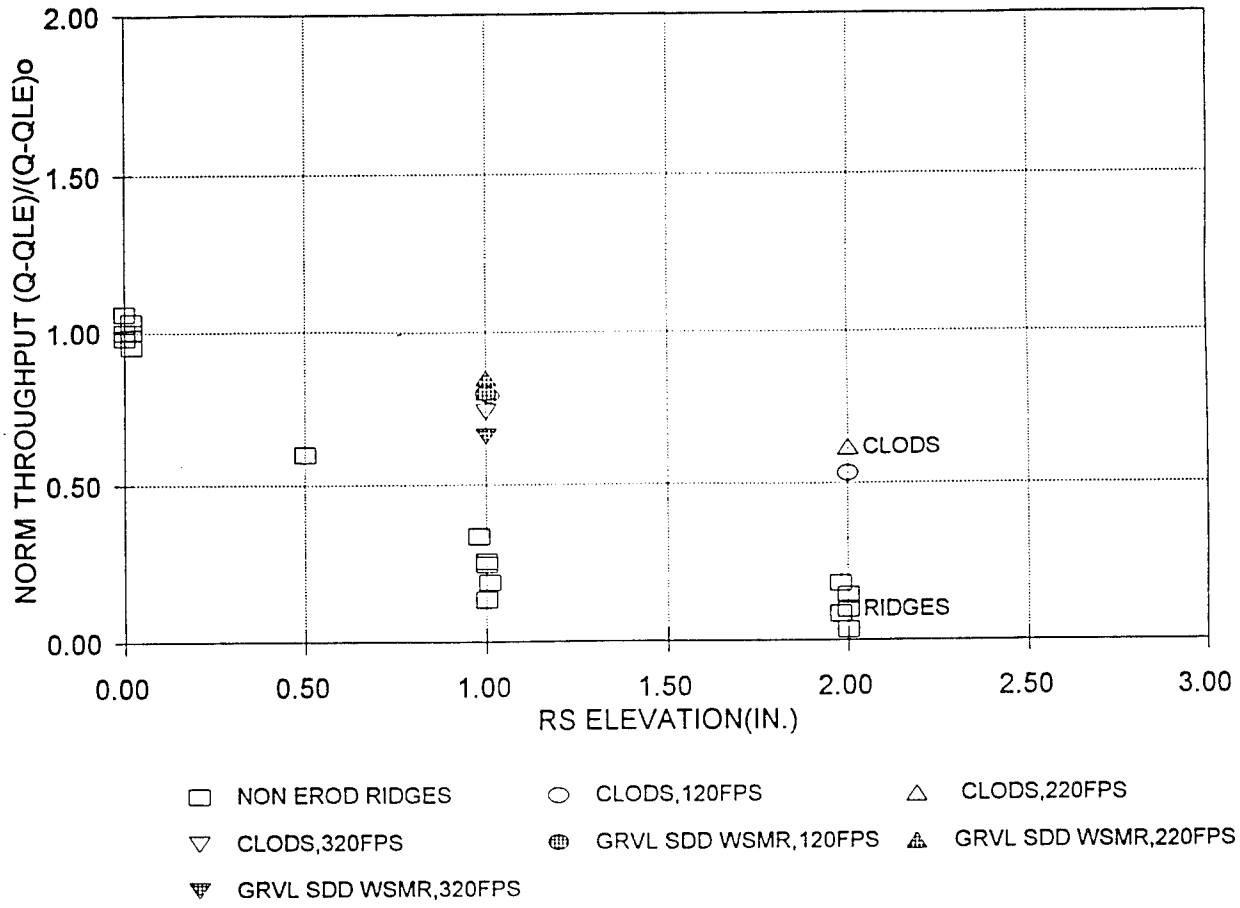

Figure 4-19. Soil loss for Gravel Seeded WSMR dust beds.

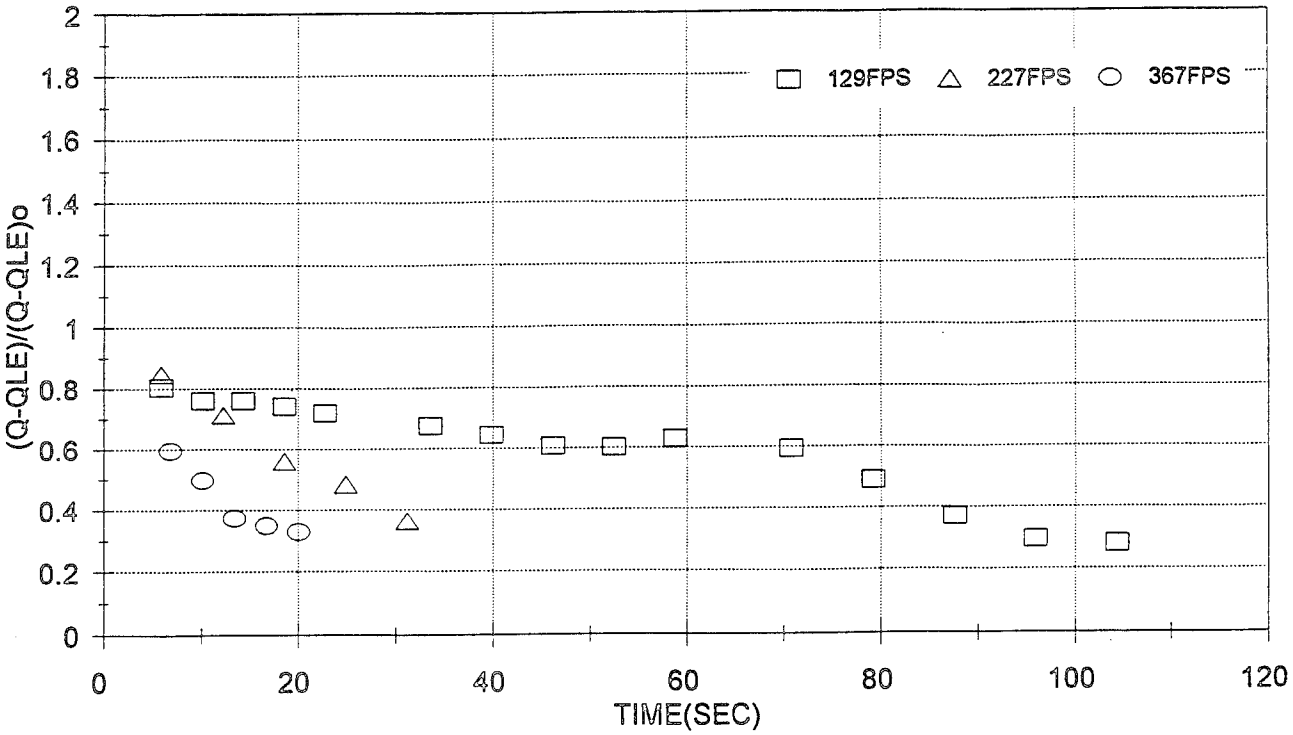

(a) Time from flow onset

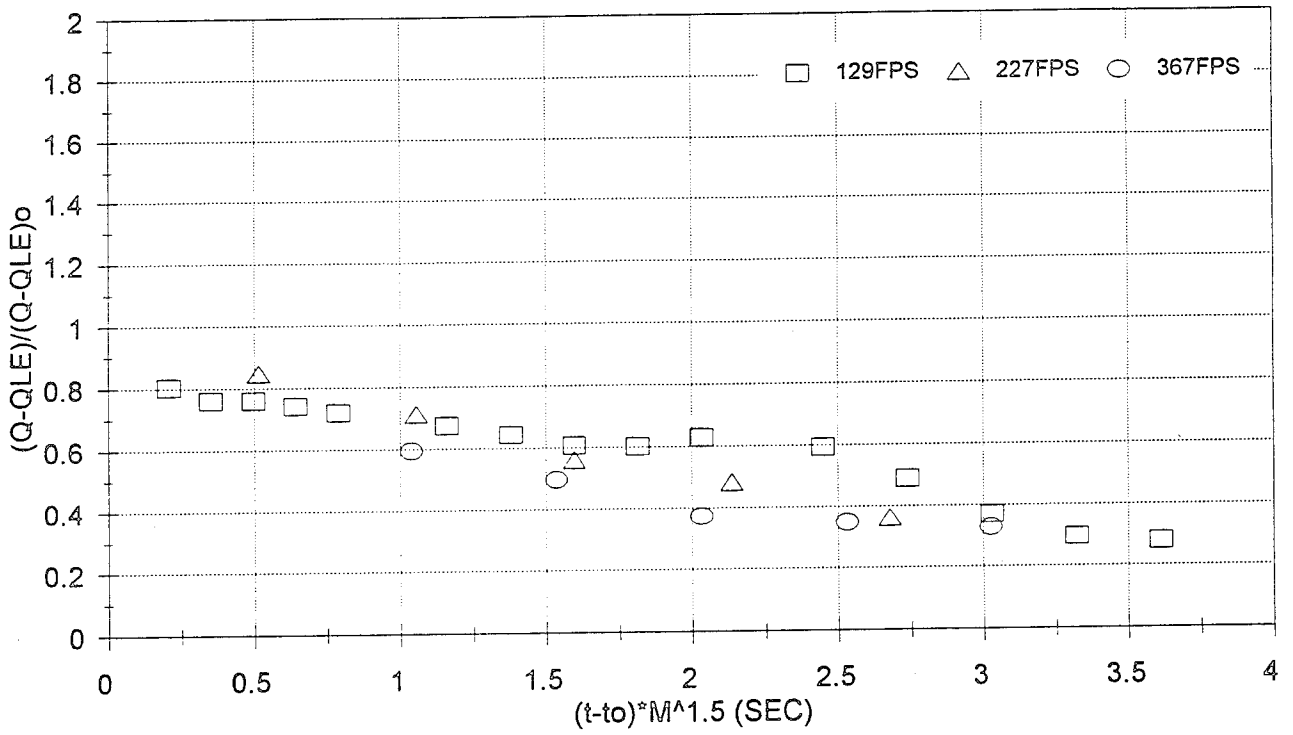

(b) Scaled time

Figure 4-20. Dependence of soil loss on flow exposure time for Gravel Seeded WSMR dust beds.

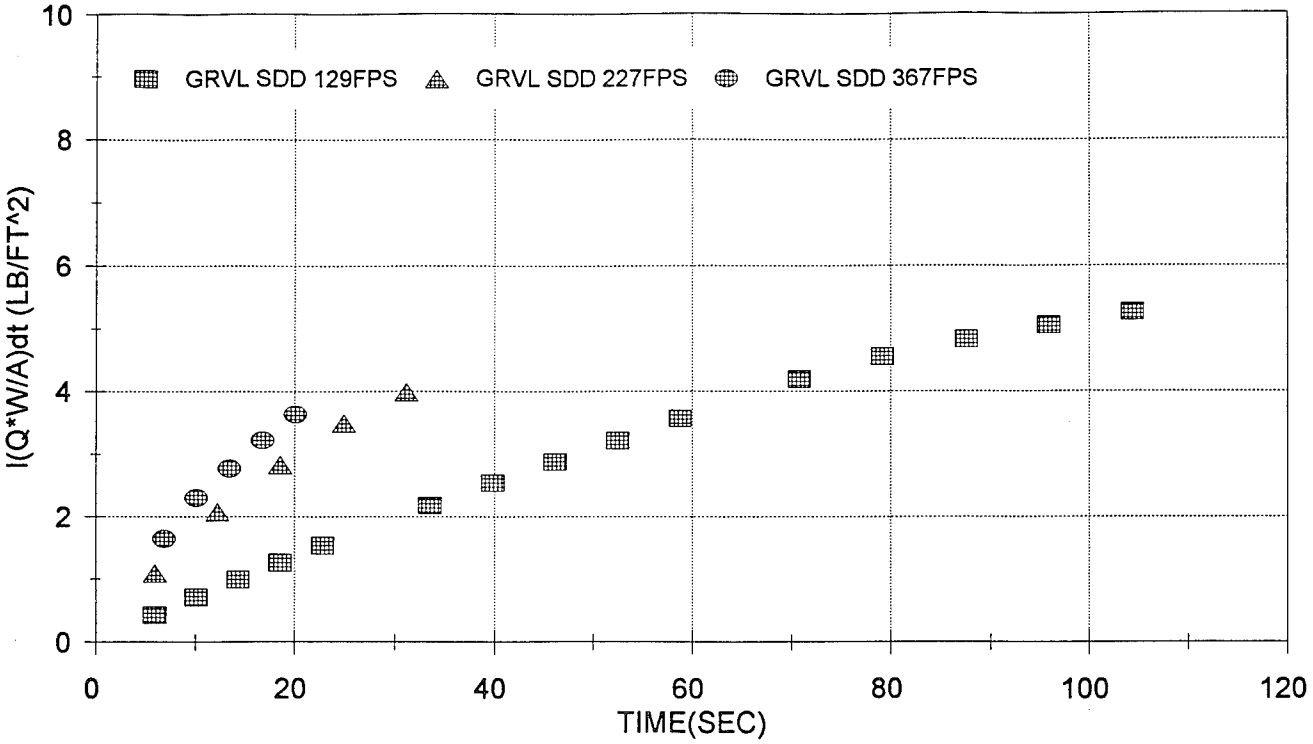

(a) Time from flow onset

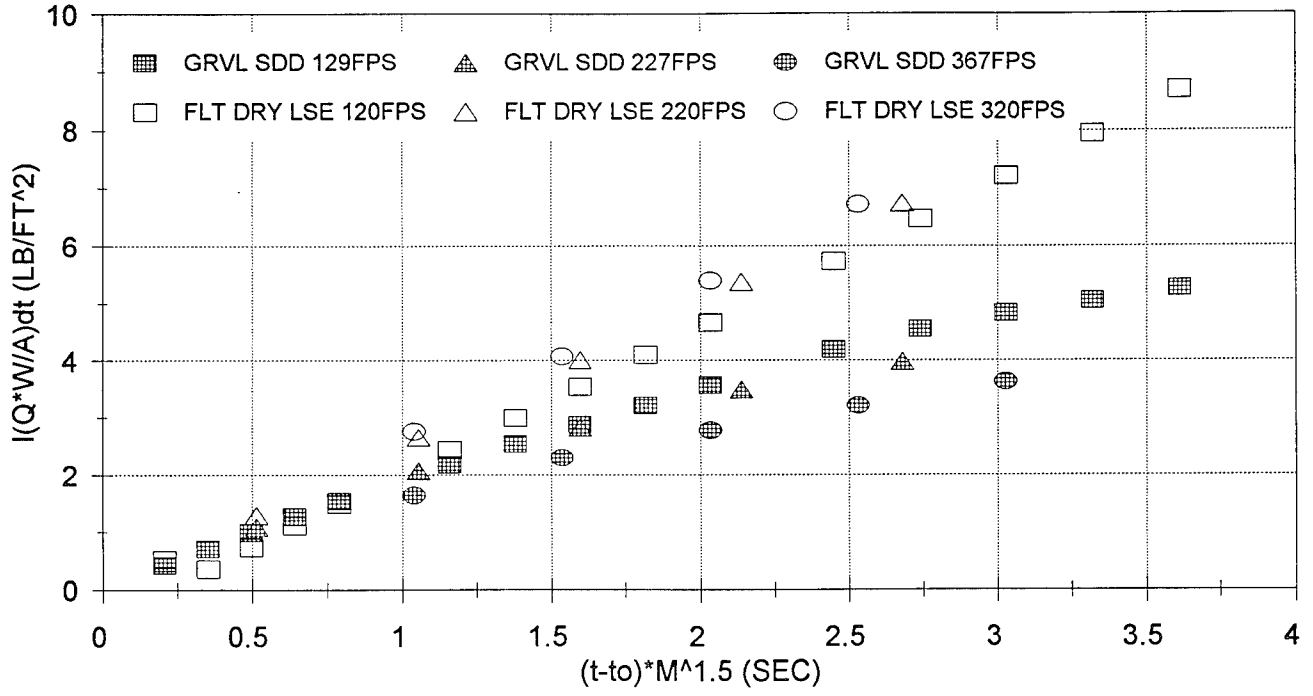

(b) Scaled time

Figure 4-21. Integrated soil loss as a function of flow exposure time for Gravel Seeded WSMR dust beds.

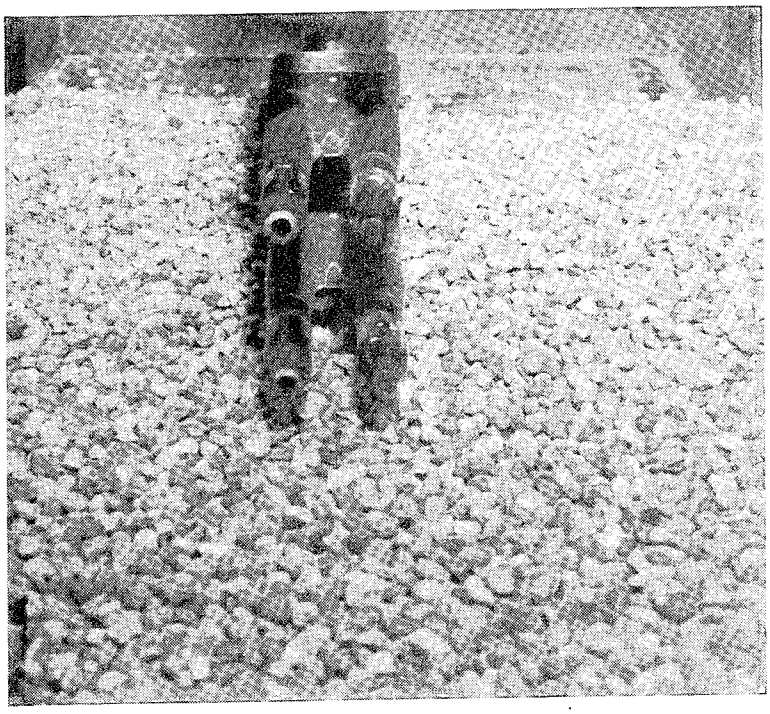

(a) Close up view of Snob/Greg yoke

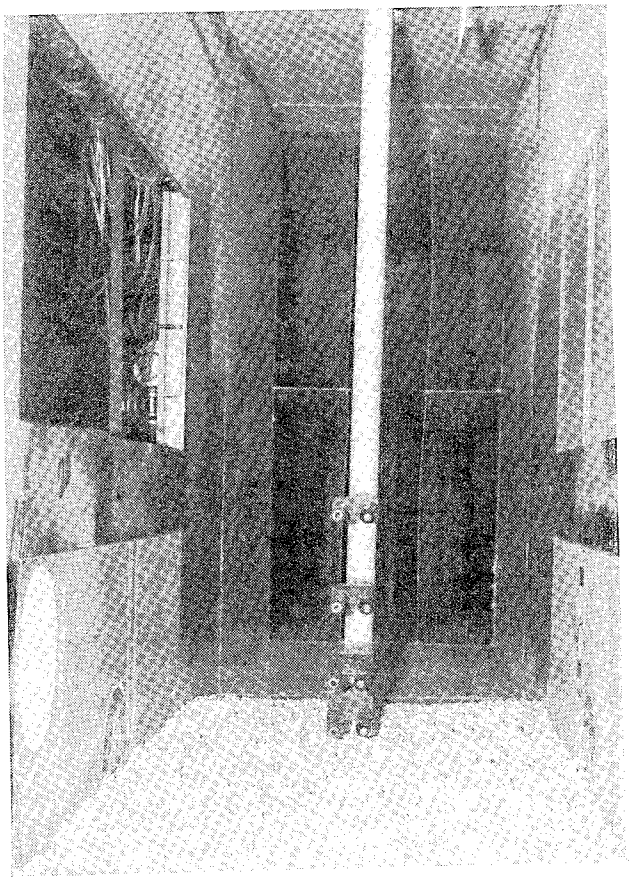

(b) View at 21'4" station

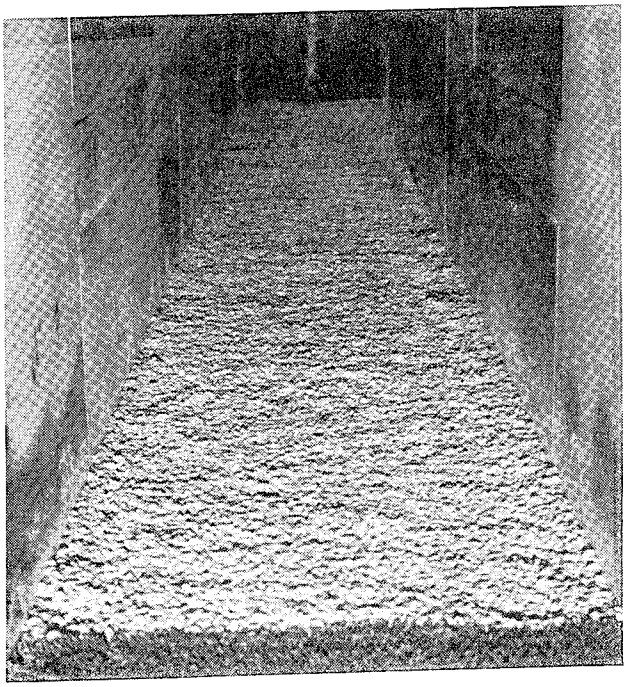

(c) Downstream view from bed leading edge

Figure 4-22. Typical photographs of P Gravel "dust" bed, RS 102 - 107: Pre test.

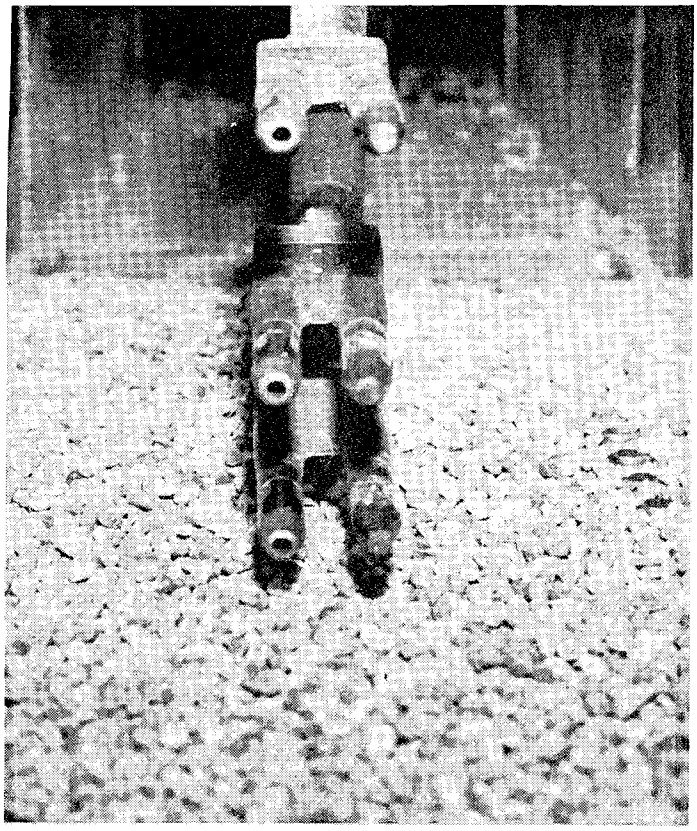

(a) Close up view of Snob/Greg yoke

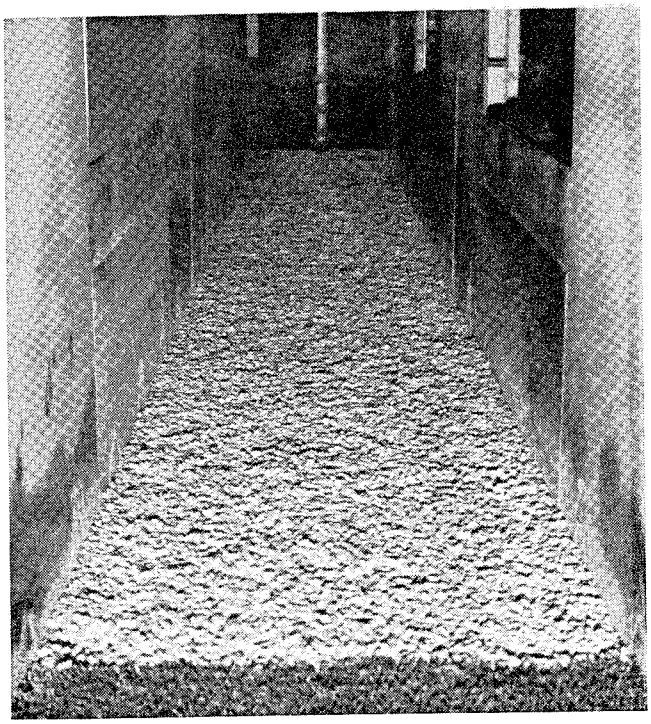

(b) Downstream view from bed leading edge

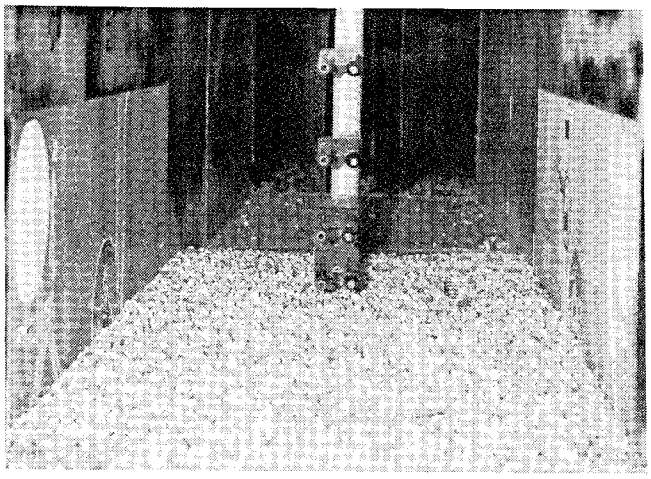

(c) View at 21' 4" station

Figure 4-23. Typical photographs of P Gravel "dust" bed, RS102 - 107: Post test.

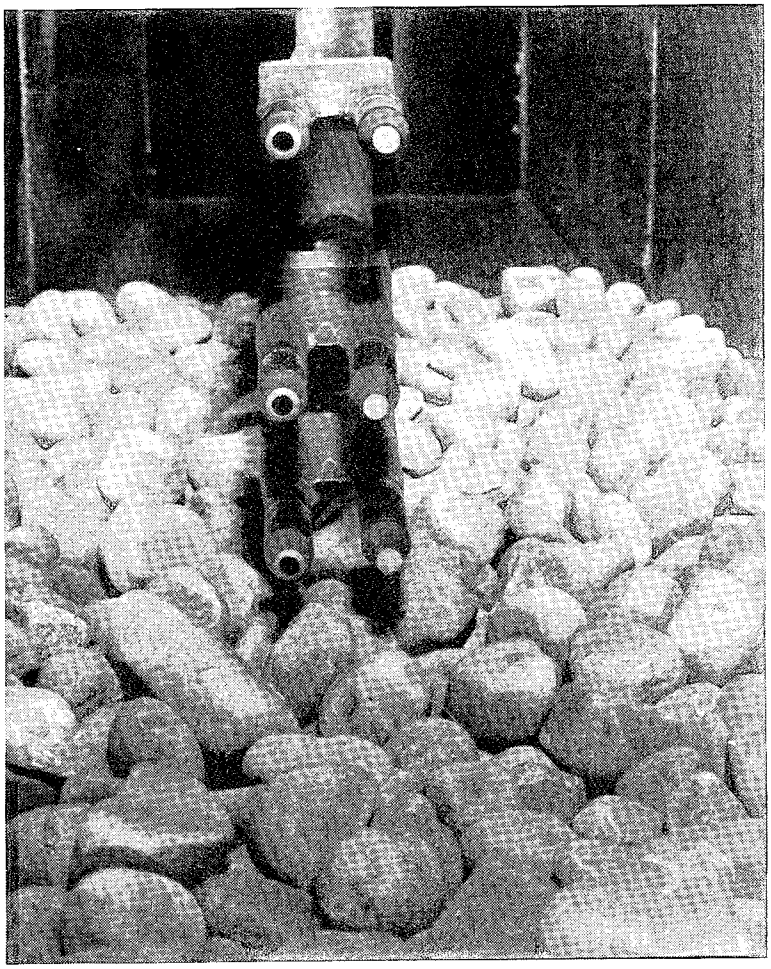

(a) Close up view of Snob/Greg yoke

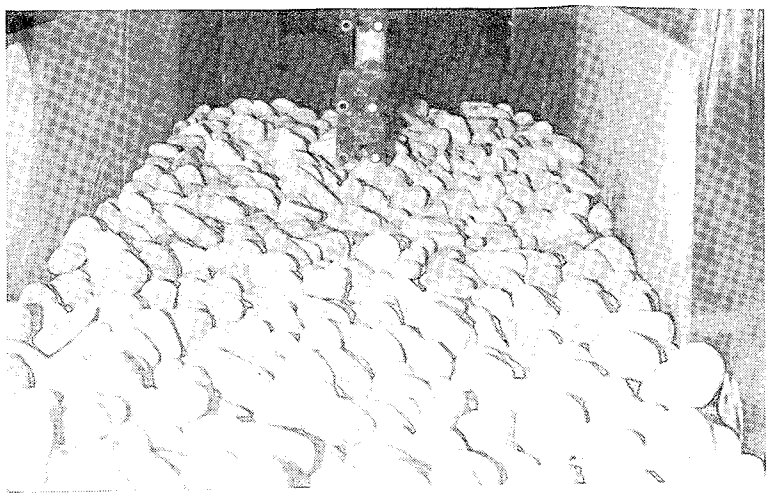

(b) View at 21'4" station

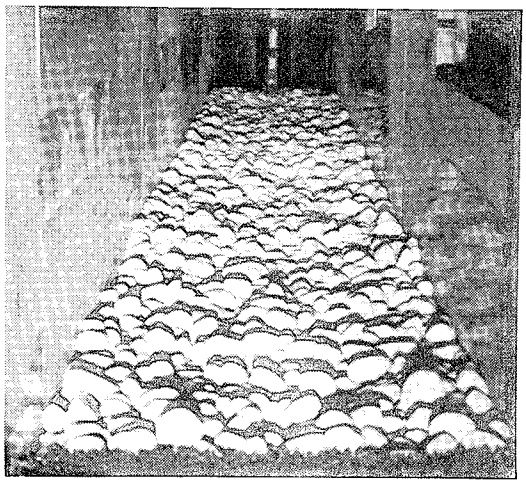

(c) Downstream view from bed leading edge

Figure 4-24. Typical photographs of Coarse Gravel "dust" bed, RS93 - 97: Pre test.

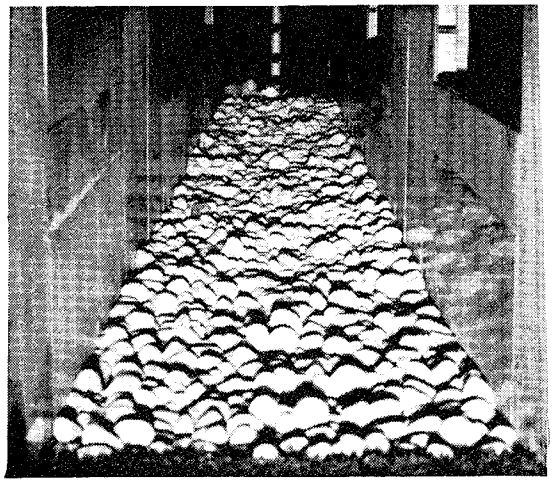

(a) Downstream view from bed leading edge

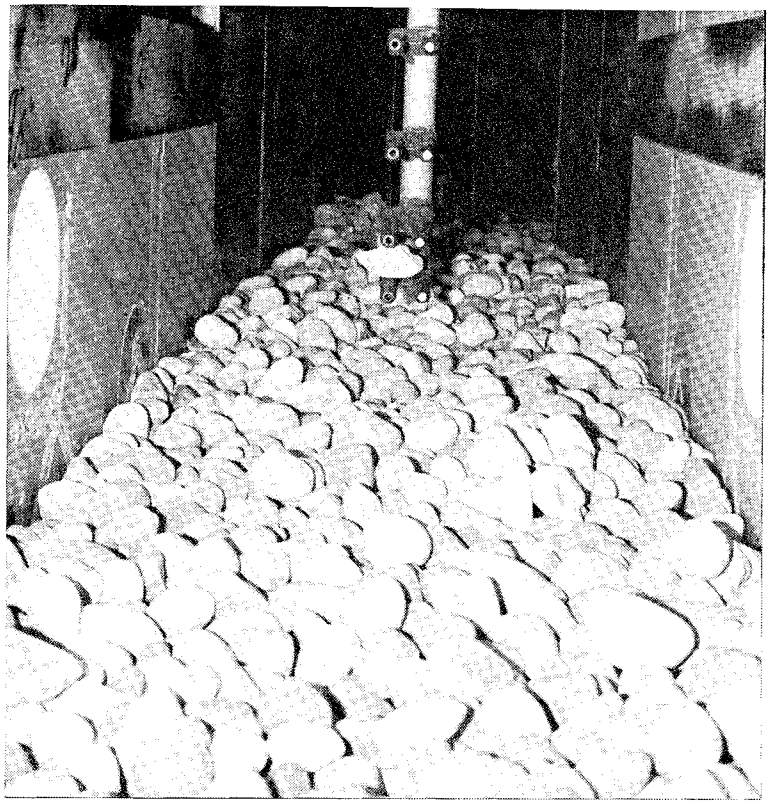

(b) View at 21'4" station

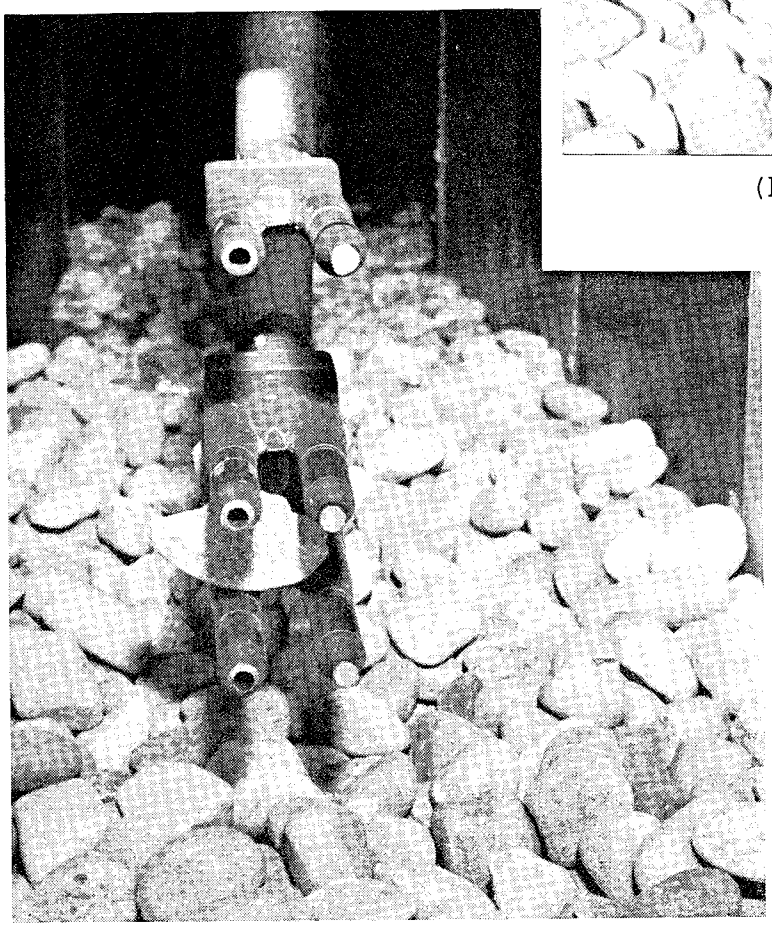

(c) Close up view of Snob/Greg rake

Figure 4-25. Typical photographs of Coarse Gravel "dust" bed, RS93 -97: Post test.

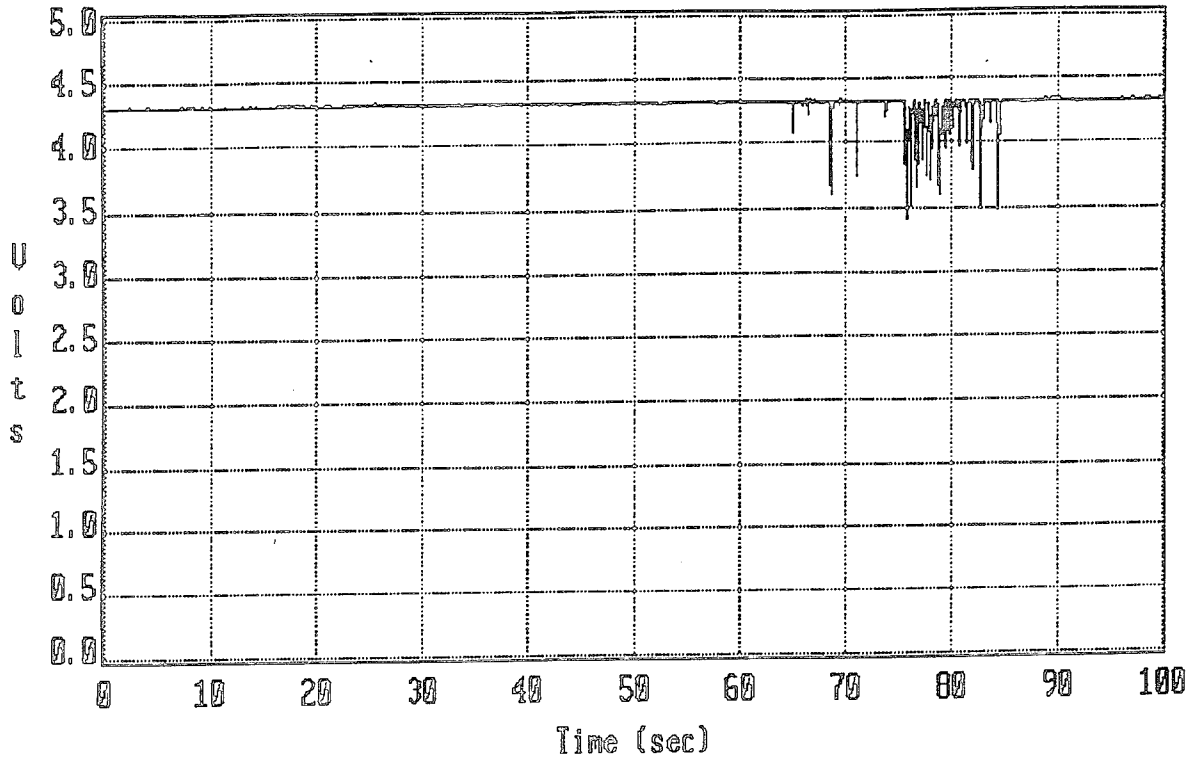

(a) Transmitted x-ray signal at 2" elevation

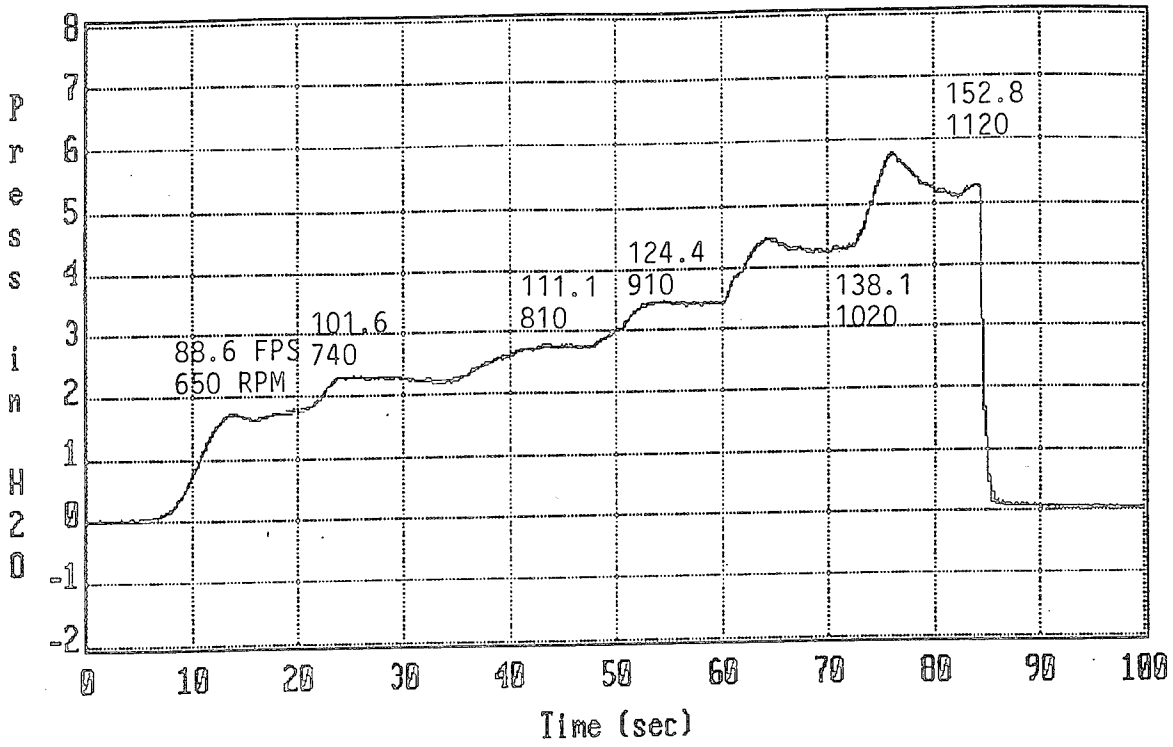

(b) Free stream dynamic pressure

Figure 4-26. Flow field time histories at 21' 4" station for "P" gravel lofting onset experiments: RS104.

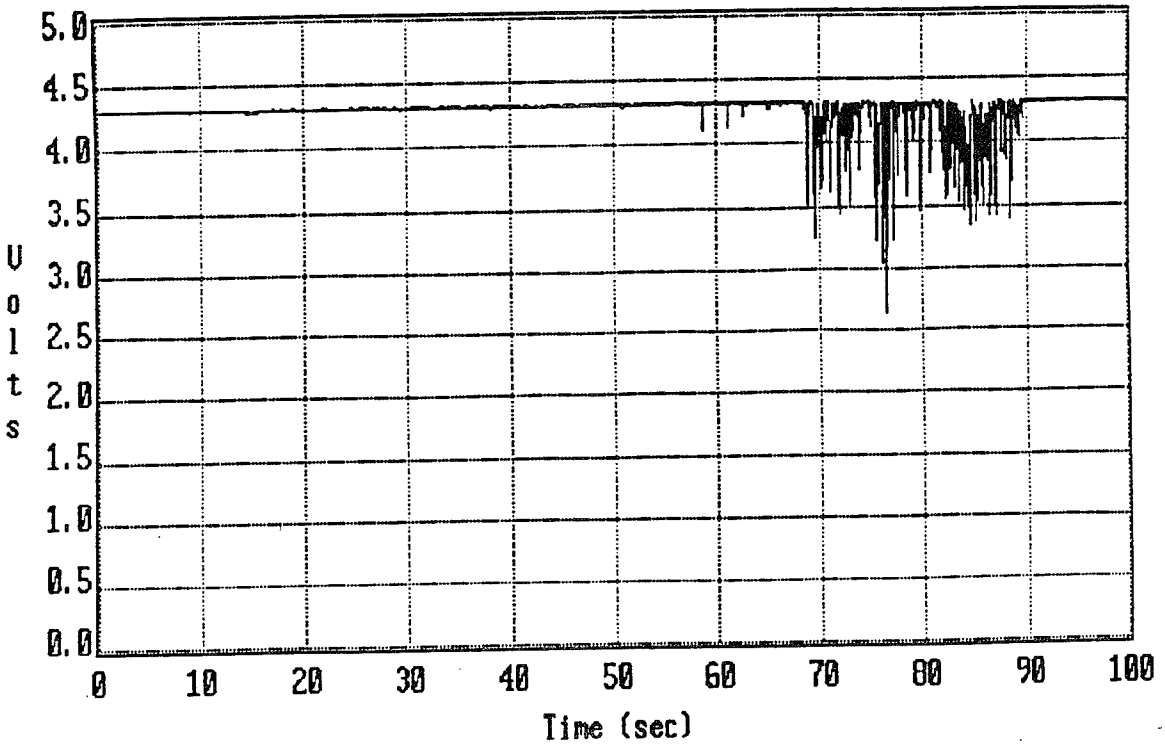

(a) Transmitted x-ray signal at 2" elevation

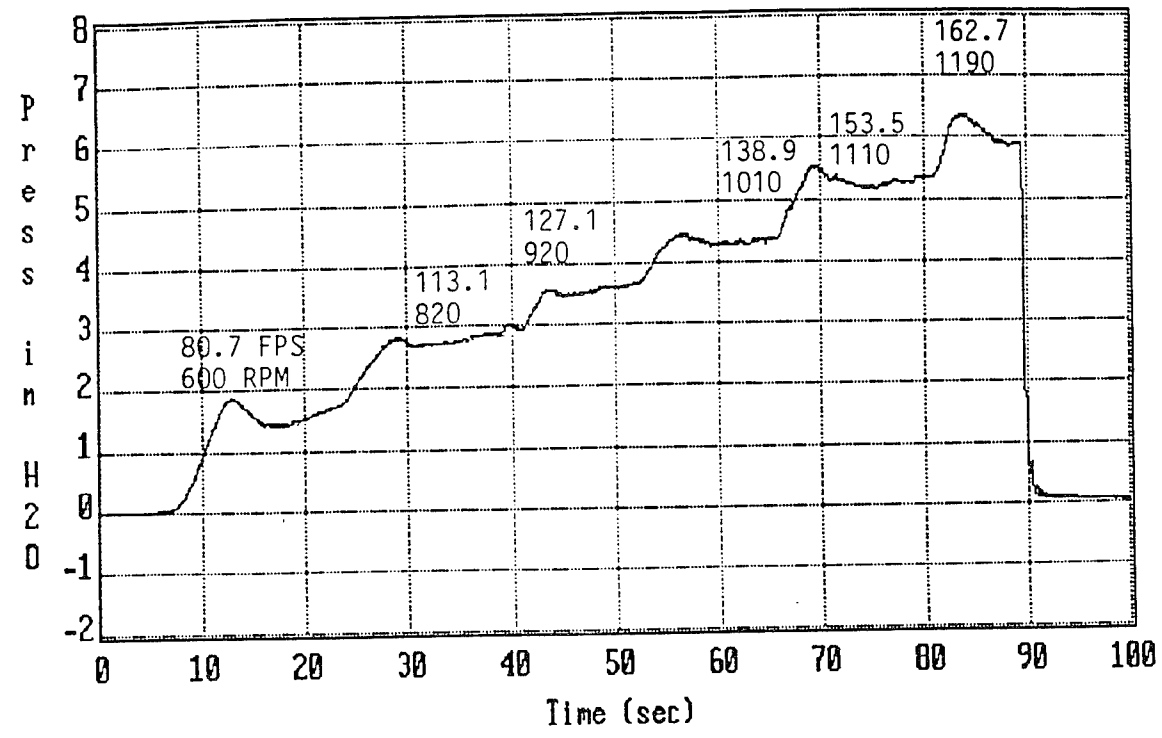

(b) Free stream dynamic pressure

Figure 4-27. Flow field time histories at 21' 4" station for "P" gravel lofting onset experiments: RS105.

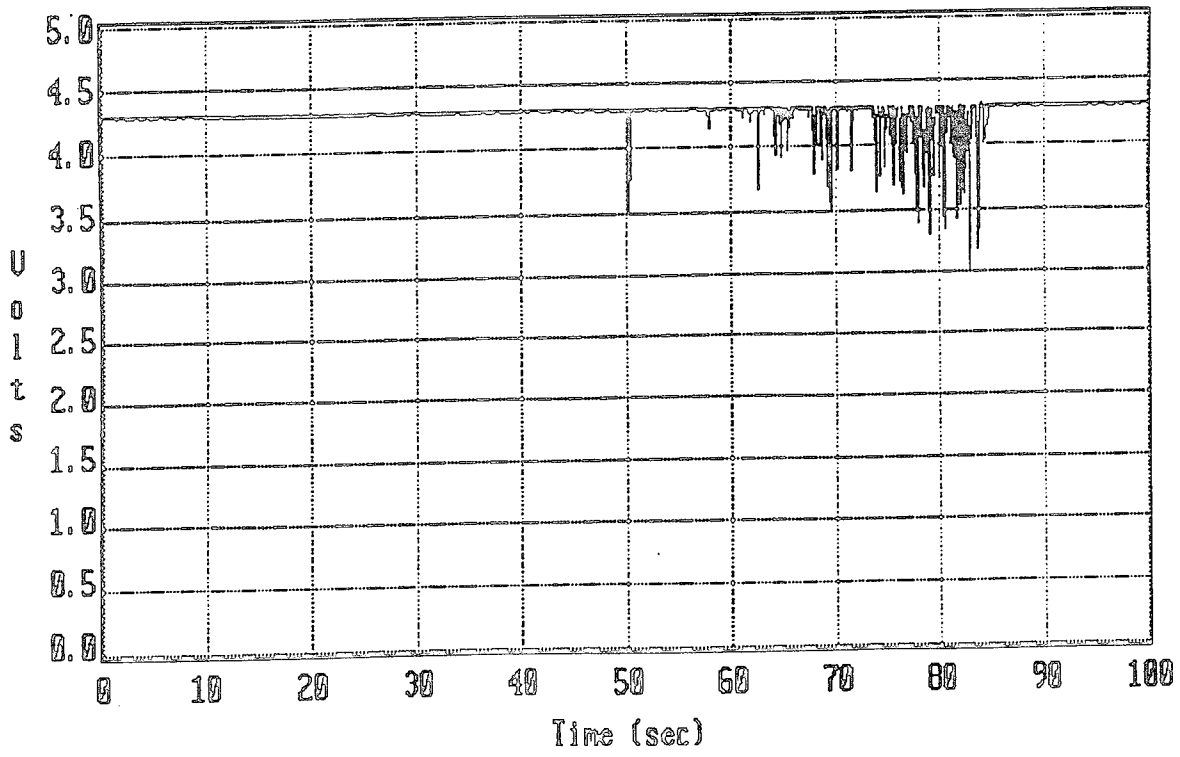

(a) Transmitted x-ray signal at 2" elevation

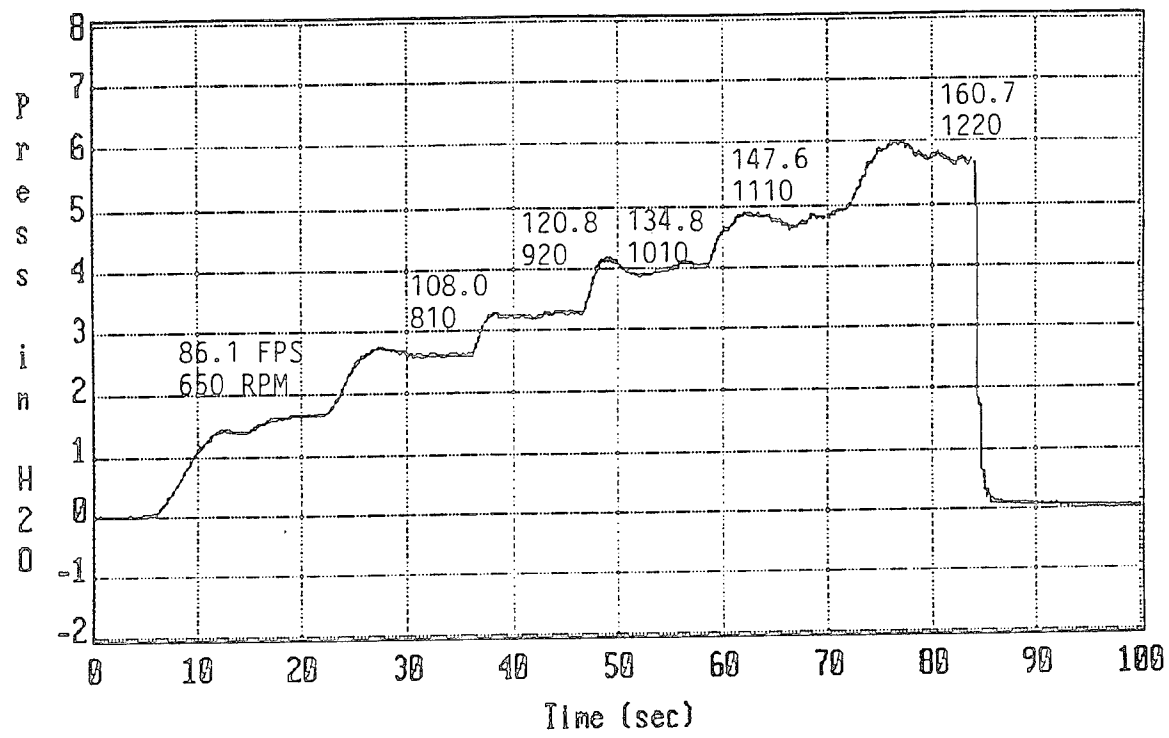

(b) Free stream dynamic pressure

Figure 4-28. Flow field time histories at 21' 4" station for "P" gravel lofting onset experiments: RS107.

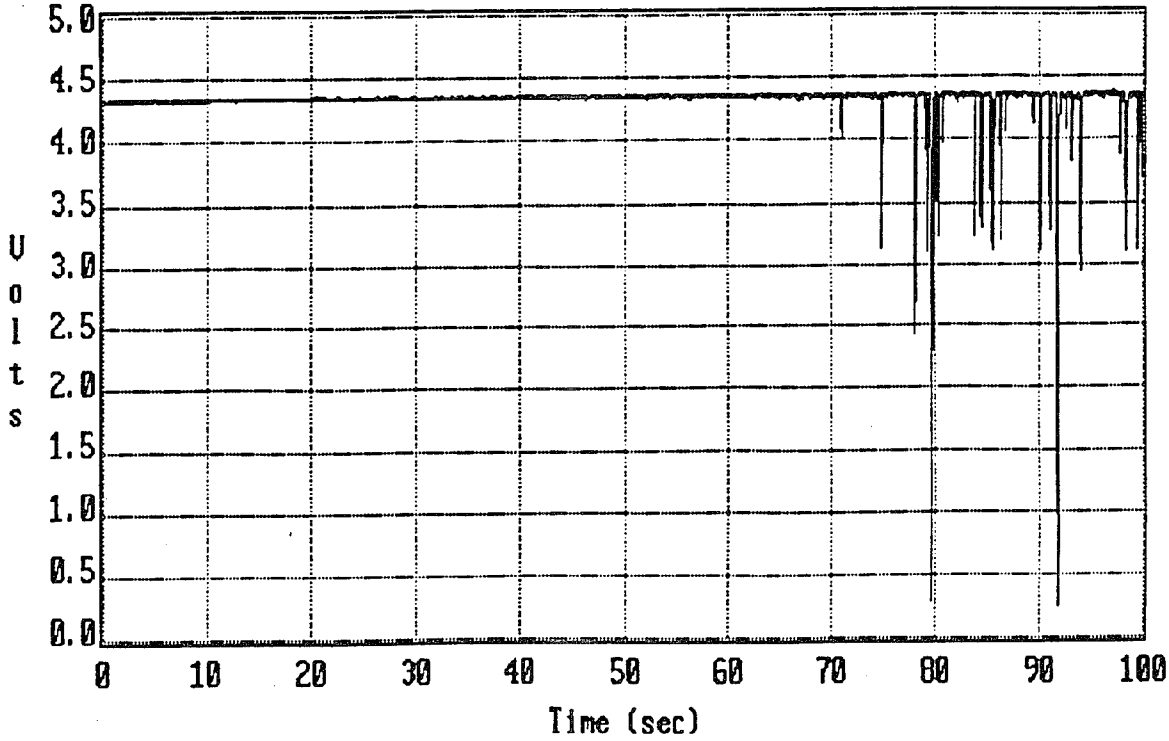

(a) Transmitted x-ray signal at 3" elevation

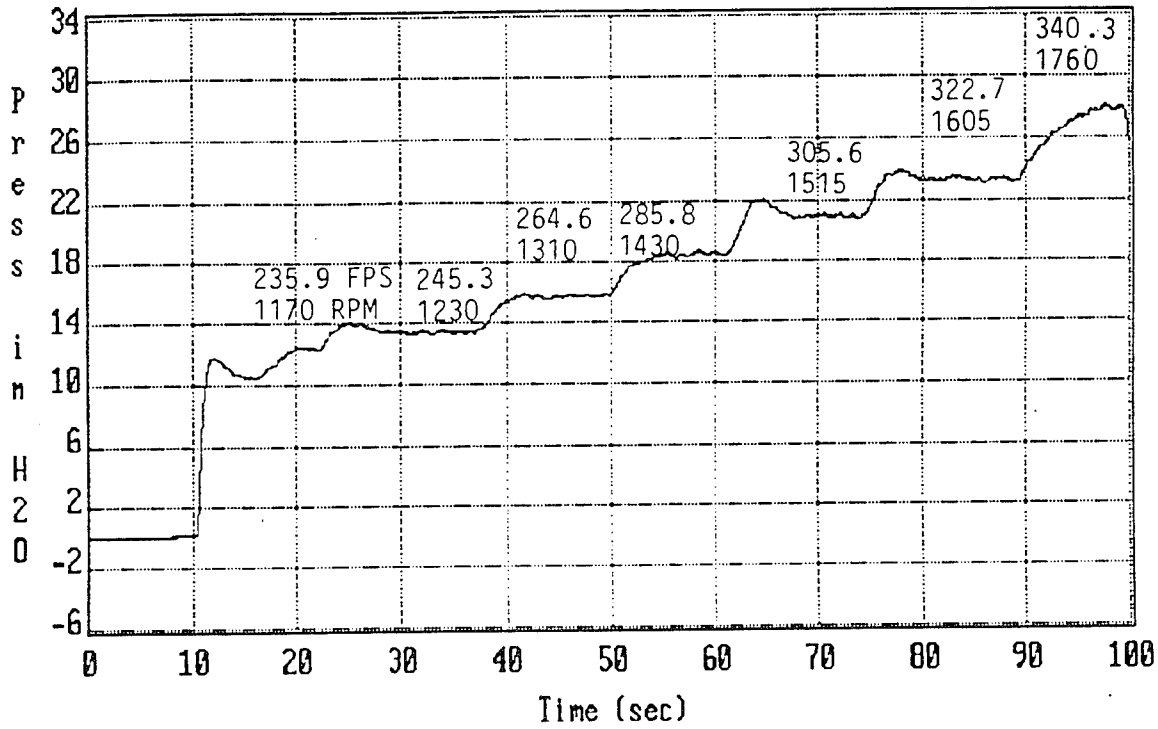

(b) Free stream dynamic pressure

Figure 4-29. Flow field time histories at 21' 4" station for "Coarse" gravel lofting onset experiments: RS93.

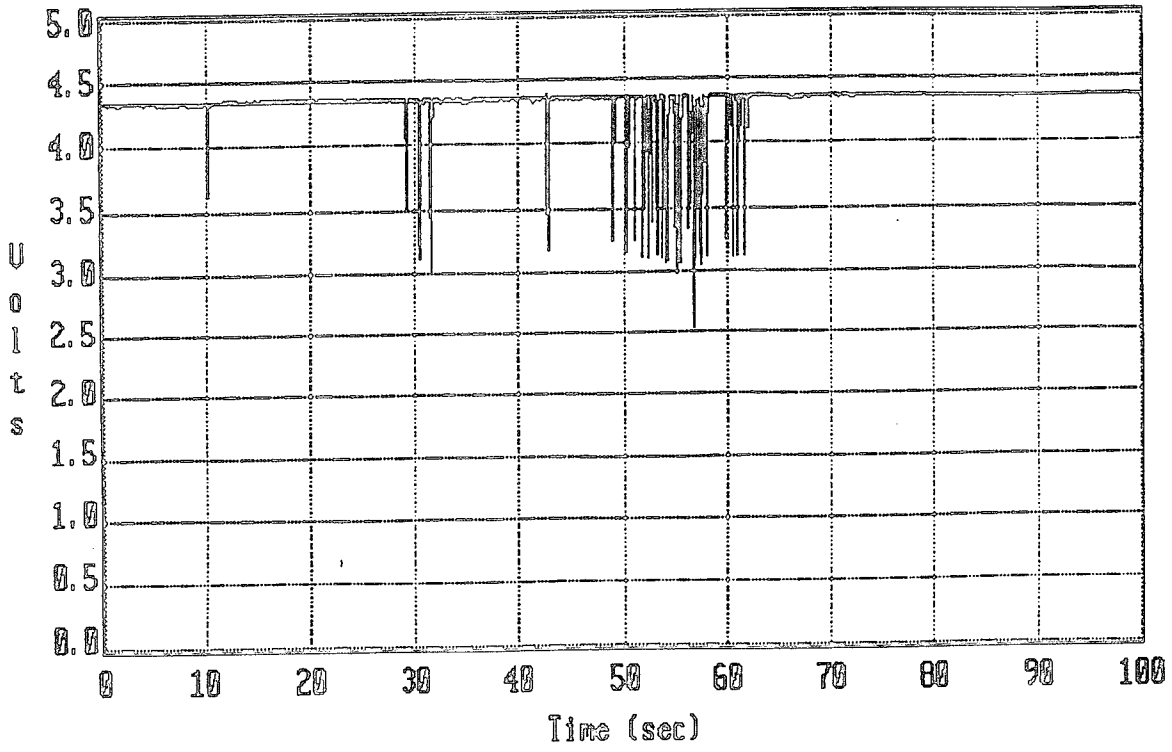

(a) Transmitted x-ray signal at 3" elevation

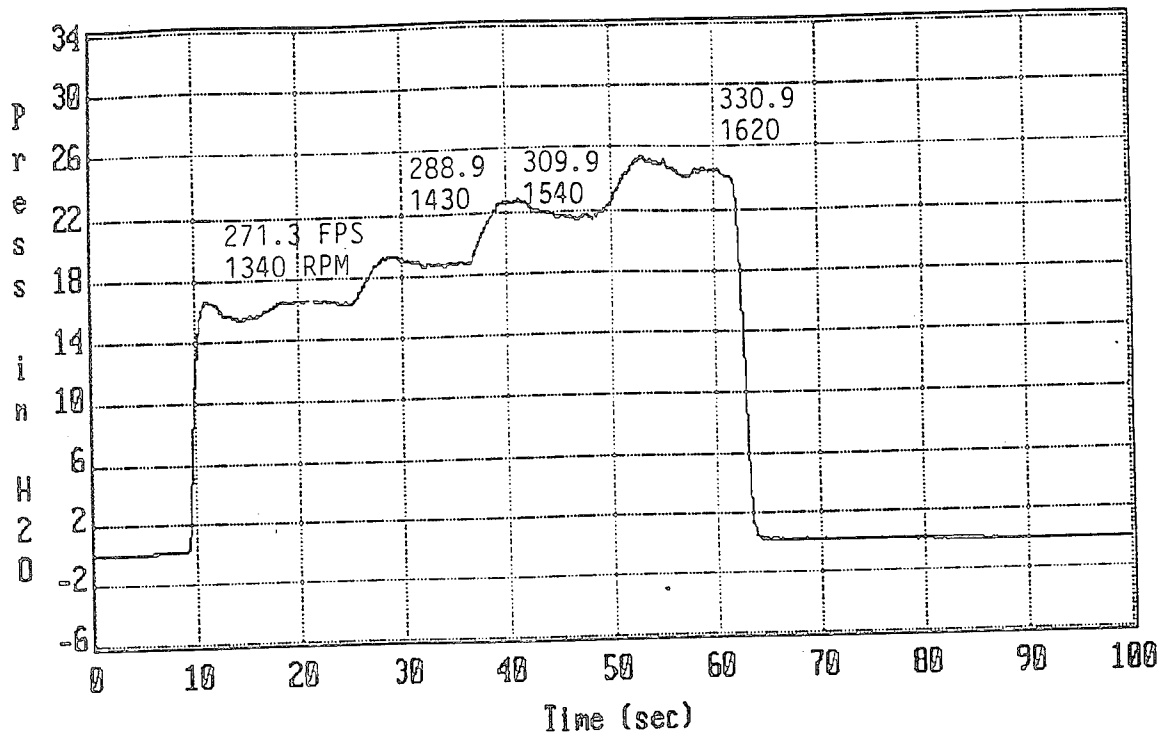

(b) Free stream dynamic pressure

Figure 4-30. Flow field time histories at 21' 4" section location for "coarse" gravel lofting onset experiments: RS96.

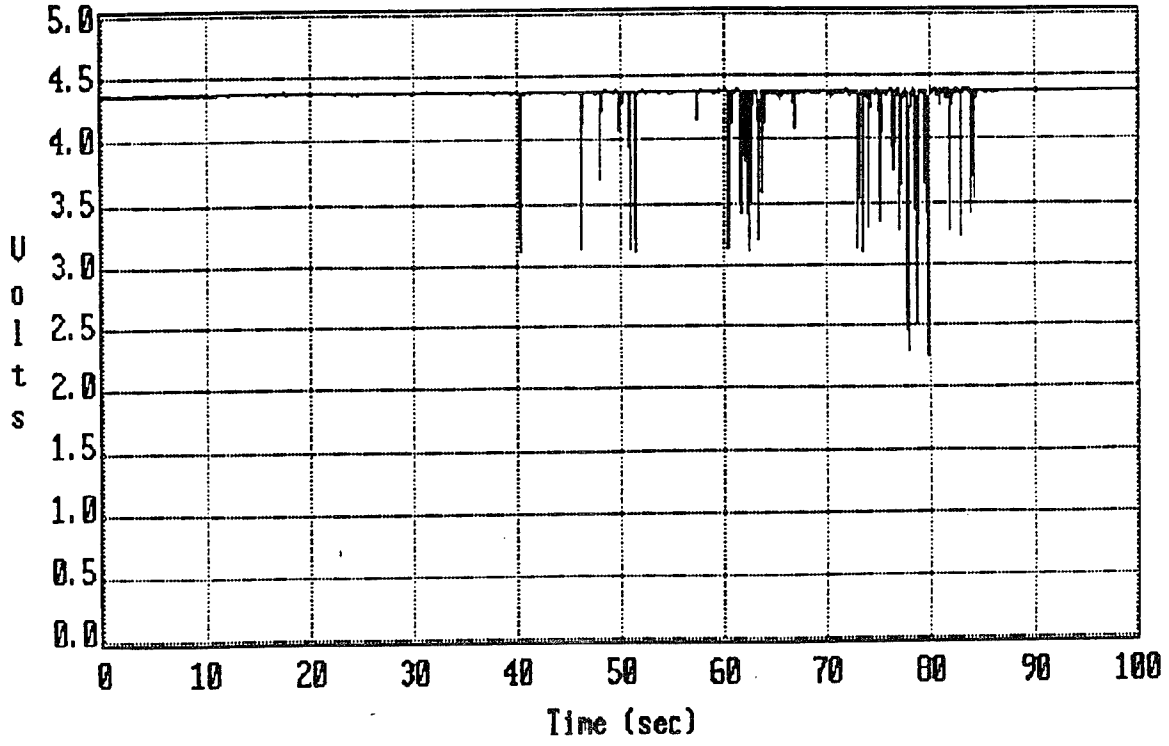

(a) Transmitted x-ray signal at 3" elevation

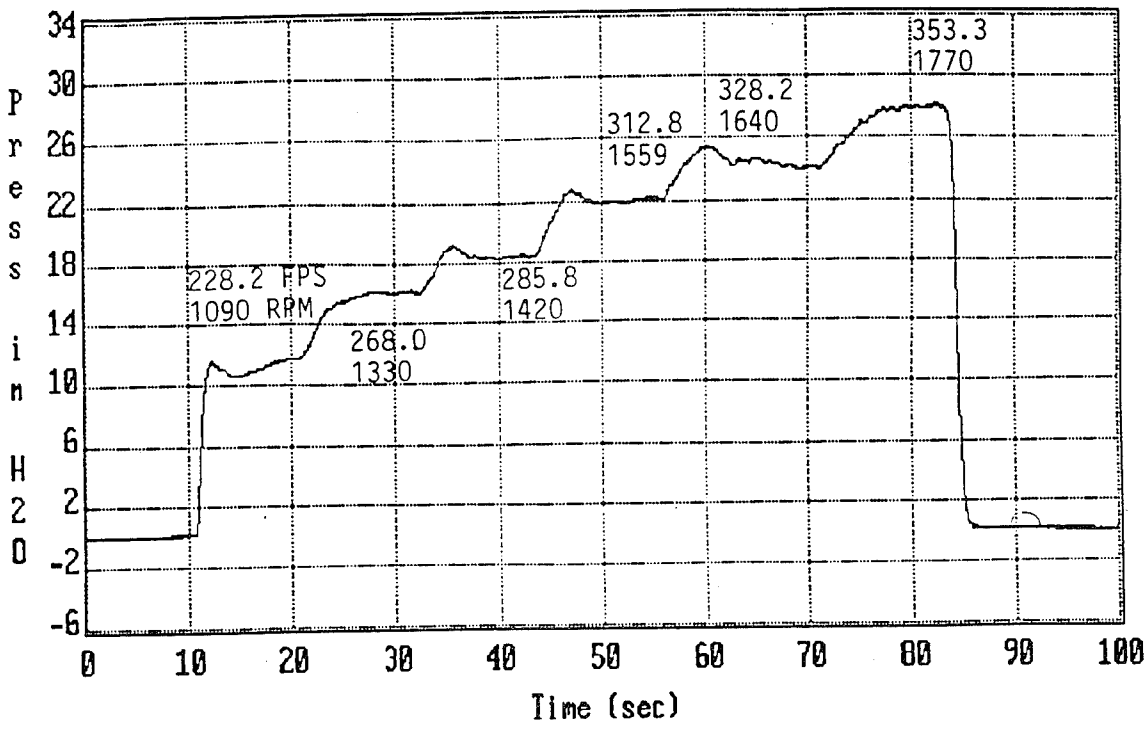

(b) Free stream dynamic pressure

Figure 4-31. Flowfield time histories at 21' 4" station for "Coarse" gravel lofting onset experiments: RS97.

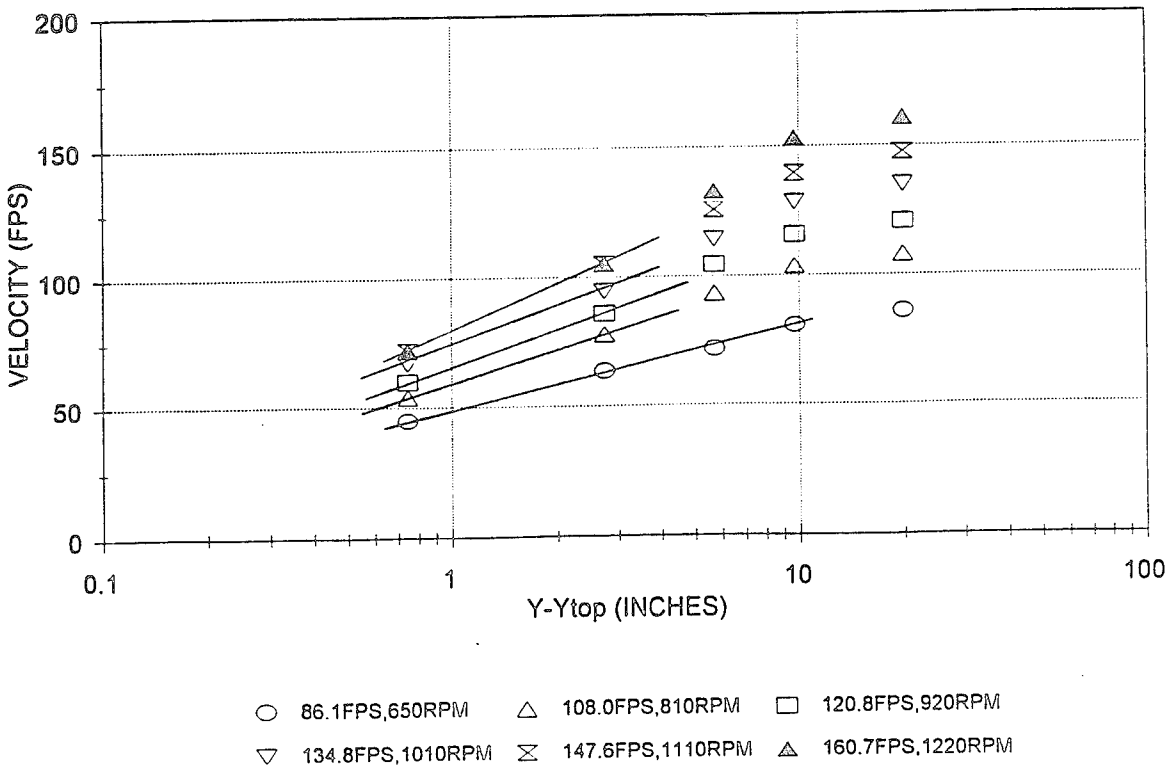

(a) "P" gravel (RS107)

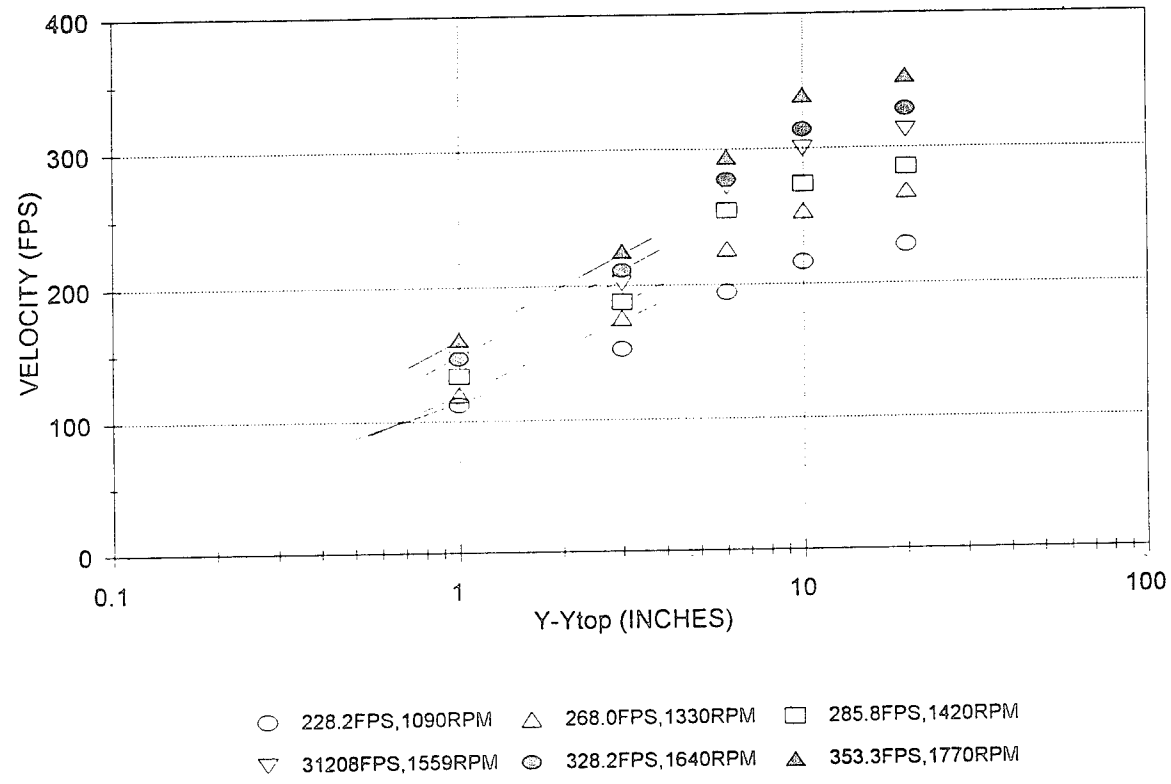

(b) "Coarse" gravel (RS97)

Figure 4-32. Typical log height velocity profiles for gravel lofting onset experiments.

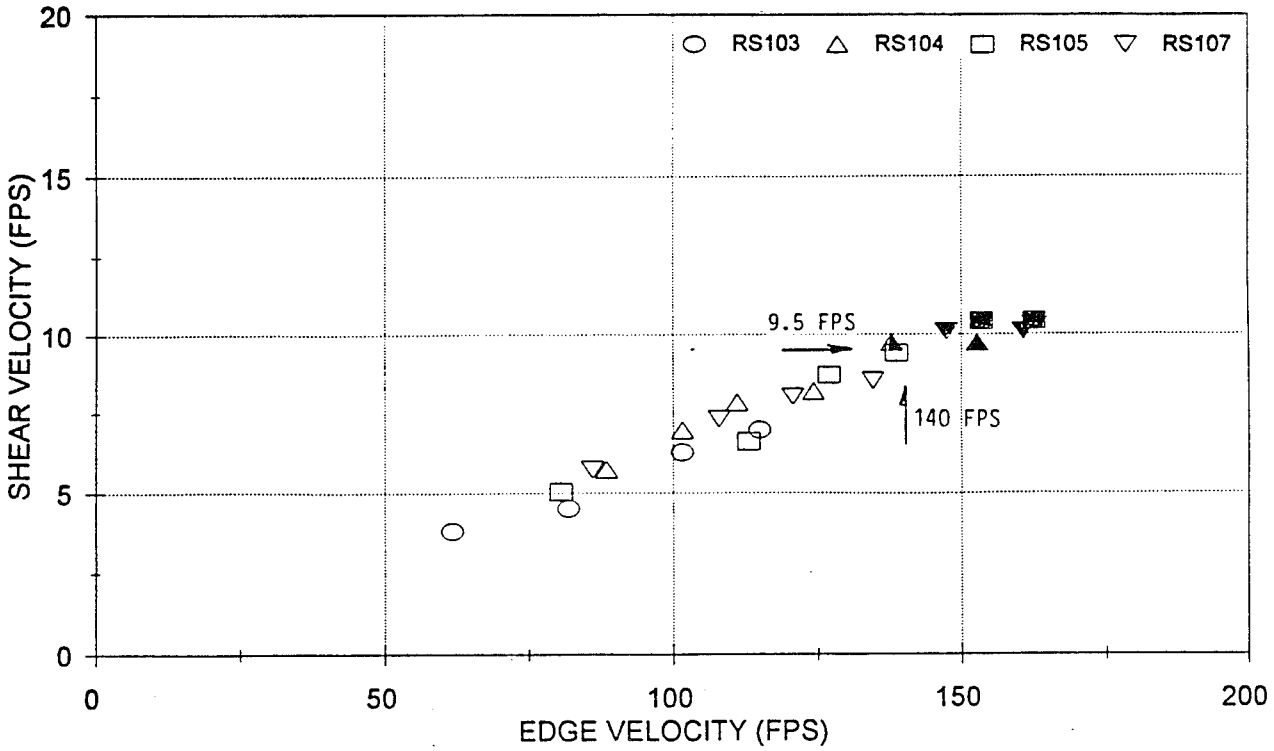

(a) "P" gravel scouring

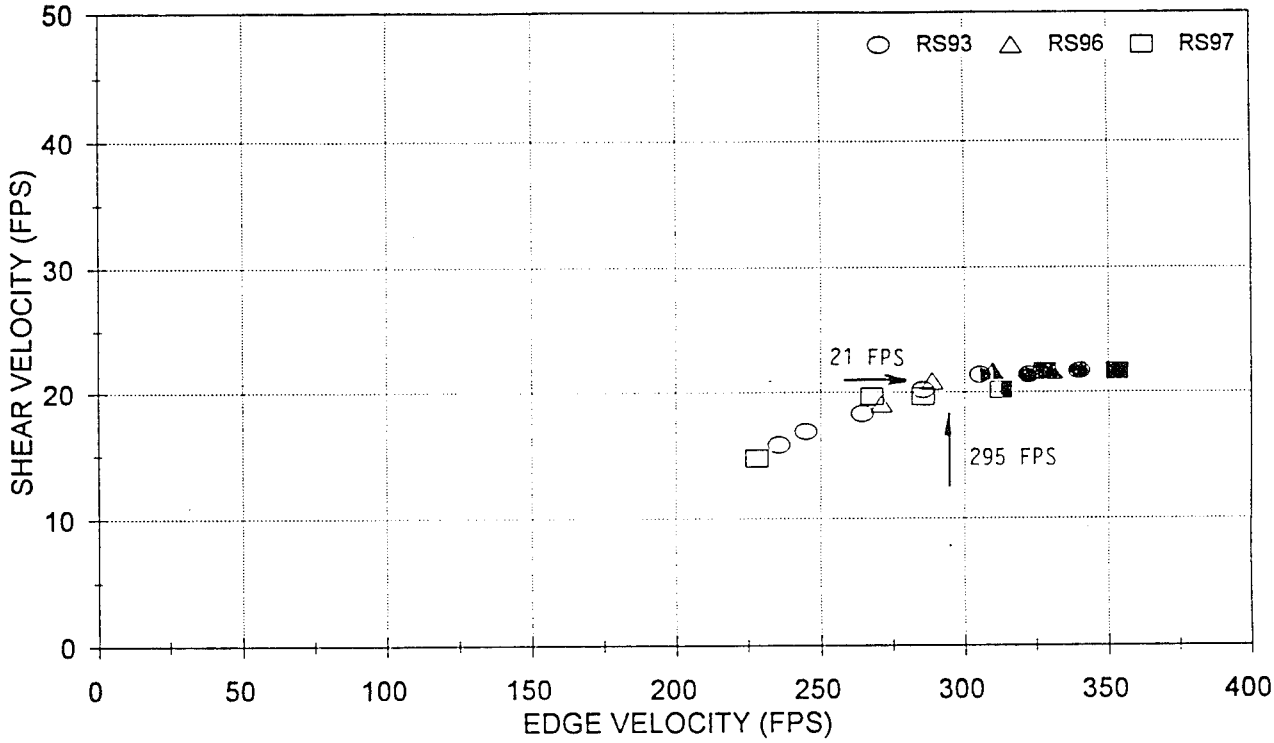

(b) "Coarse" gravel scouring

Figure 4-33. Shear velocity summary.

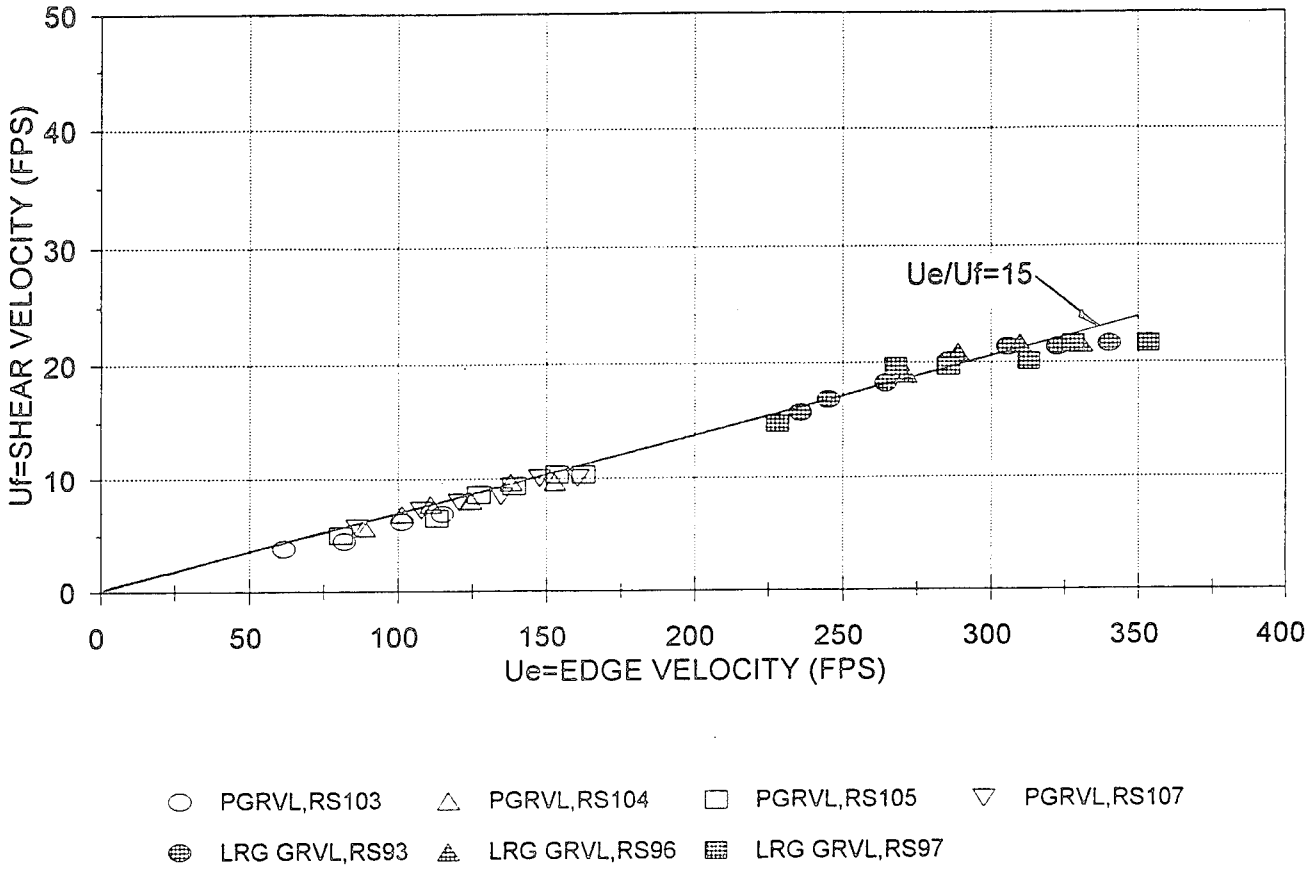

Figure 4-34. Combined shear velocity summary.

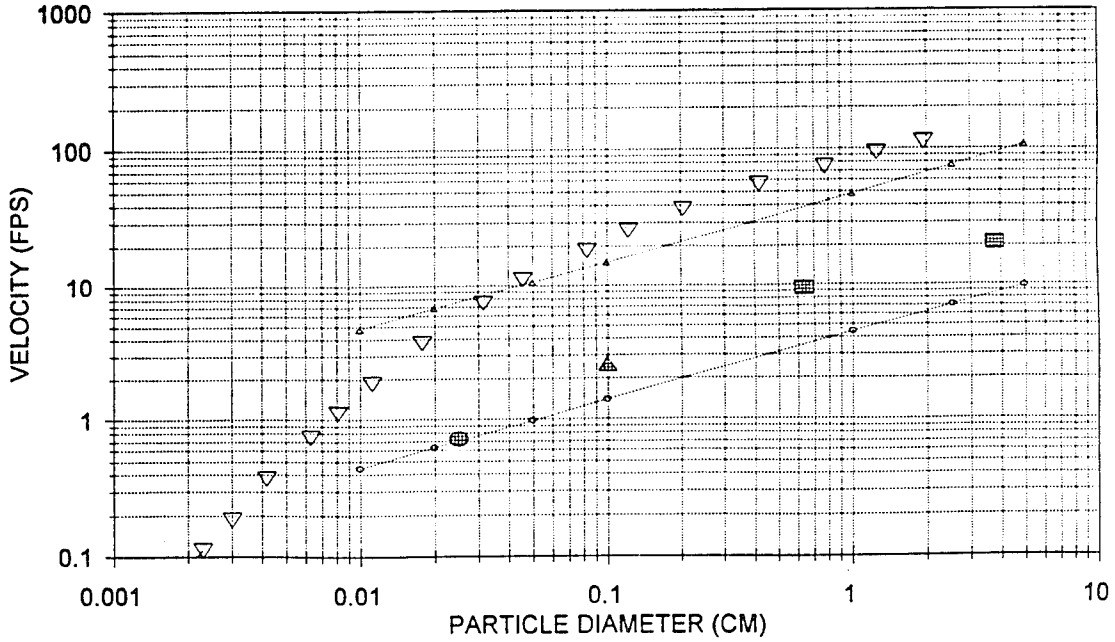

U*thresh salt calc:Bagnold/Owen
Terminal/Settling Velocity
U*thresh salt meas: Bagnold
U*thresh salt meas:Gillette
U*thresh salt meas:TRW
U*thresh suspension calc: Owen

(a) Characteristic velocity

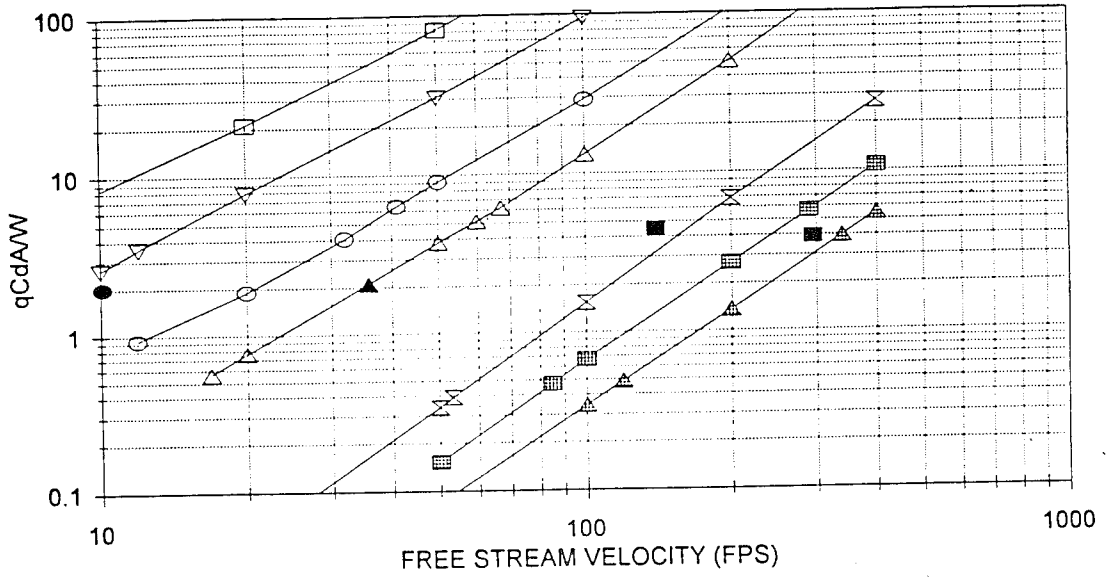

D=.01CM
D=.02CM
D=.05CM
D=.1CM
D=1CM
D=2.54CM
D=5CM
Ue thresh salt: Bagnold
Ue thresh salt:Gillette
Ue thresh salt: TRW

(b) Drag-to-weight ratio

Figure 4-35. Particle velocity scaling.

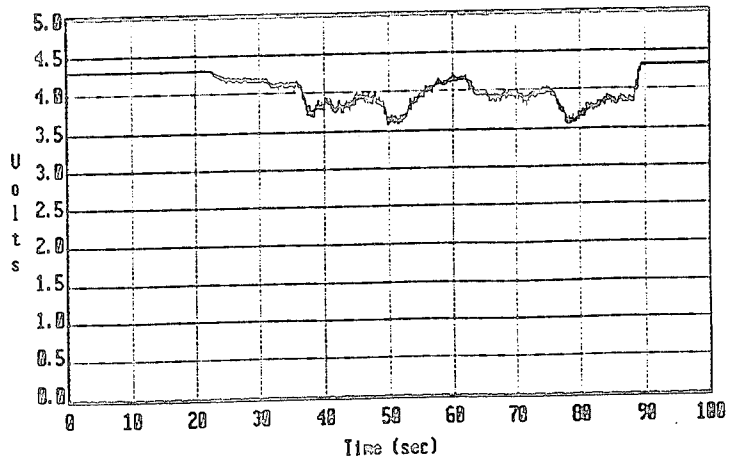

(a) Transmitted x-ray signal at 0.5" elevation

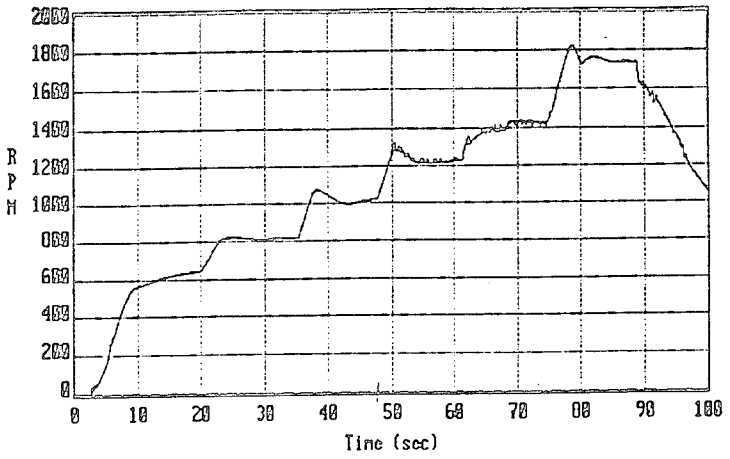

(b) Free stream dynamic pressure

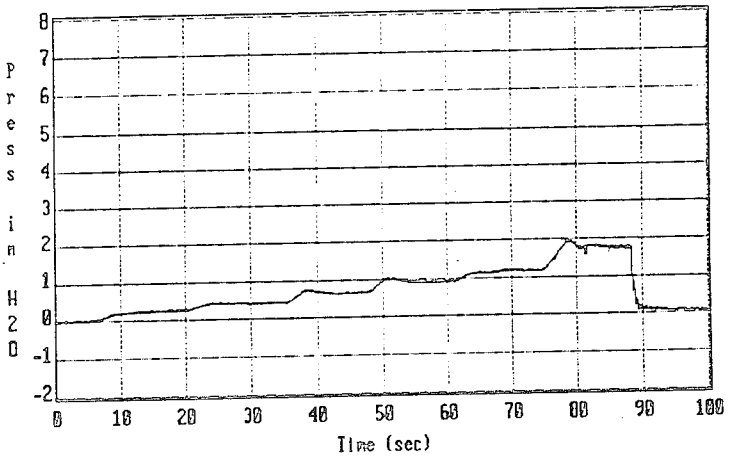

(c) Velocity profiles at 21'4" station

Figure 4-36. Threshold velocity experiments (RS120, 5%/1% soil moisture, 48 hour cure).

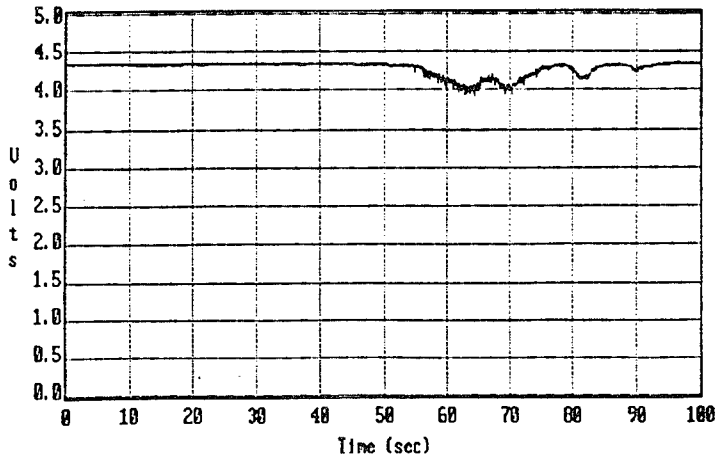

(a) Transmitted x-ray signal at 0.5" elevation

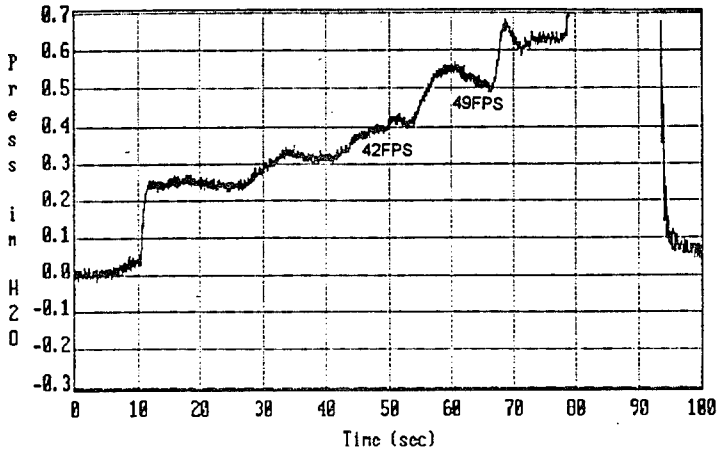

(b) Free stream dynamic pressure

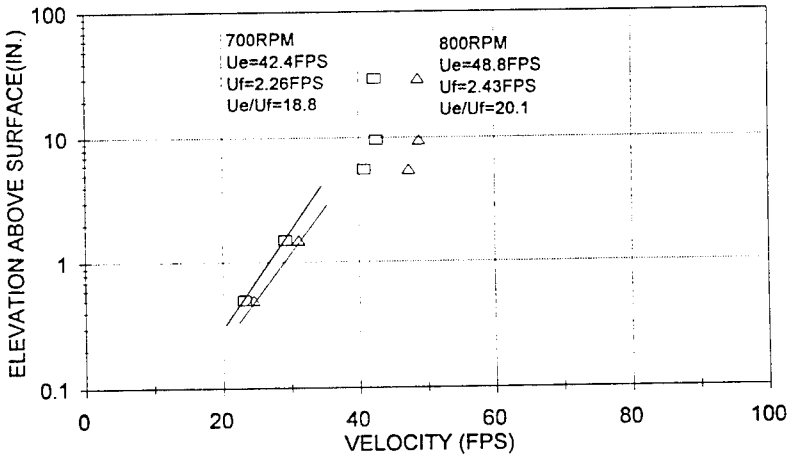

(c) Velocity profiles at 21'4" station

Figure 4-37. Threshold velocity experiments (RS125, 5%/2% soil moisture, 24 hour cure).

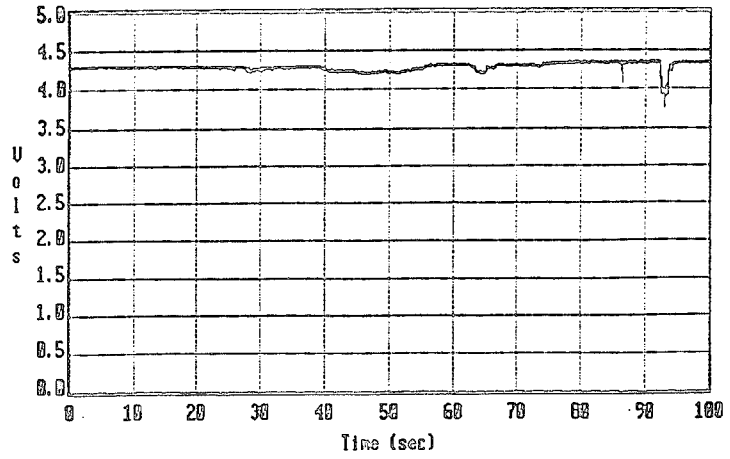

(a) Transmitted x-ray signal at 0.5" elevation

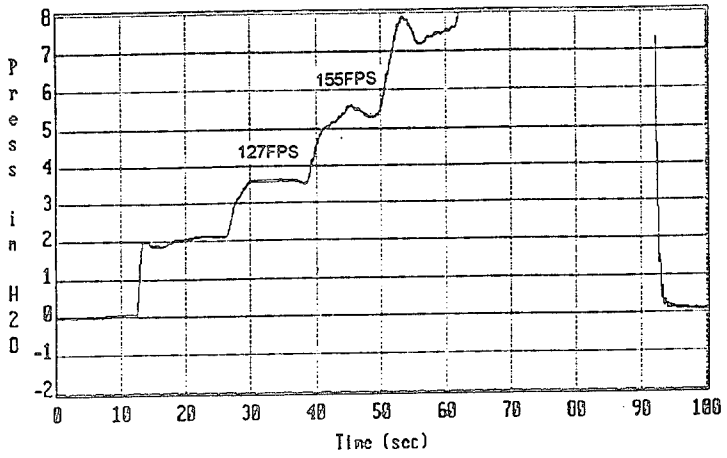

(b) Free stream dynamic pressure

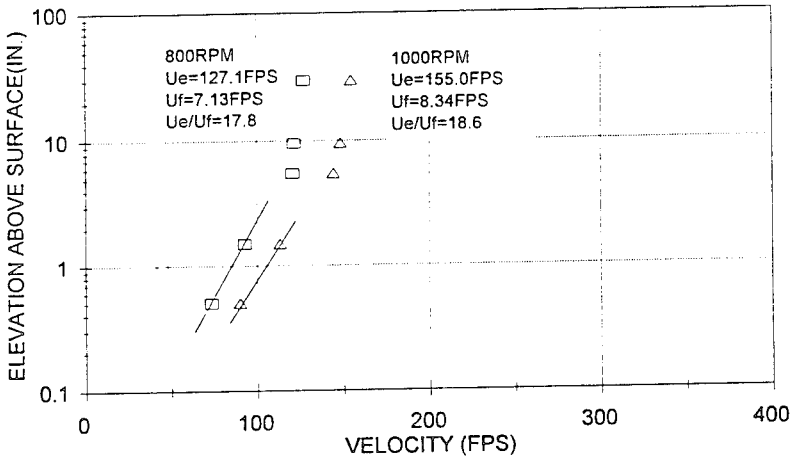

(c) Velocity profiles at 21'4" station

Figure 4-38. Threshold velocity experiments (RS124, 5%/5% soil moisture, 1 hour cure).

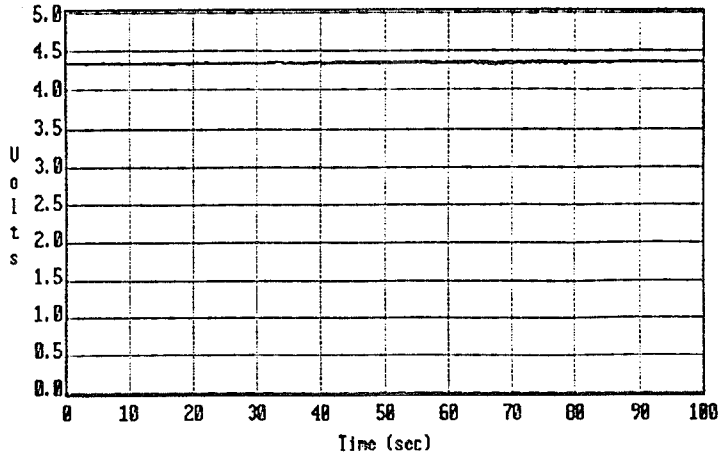

(a) Transmitted x-ray signal at 0.5" elevation

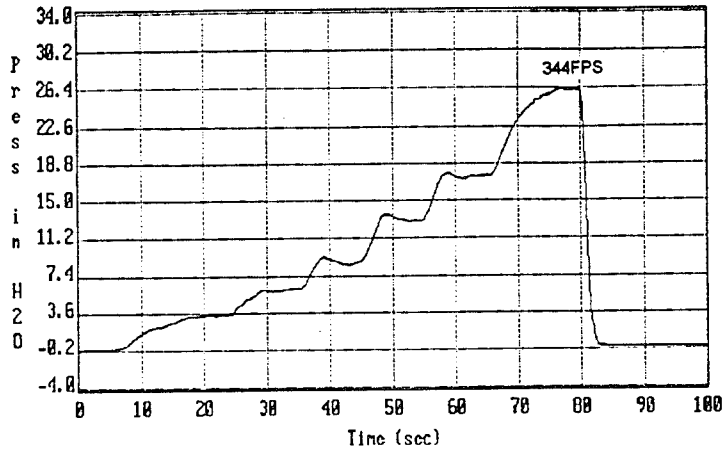

(b) Free stream dynamic pressure

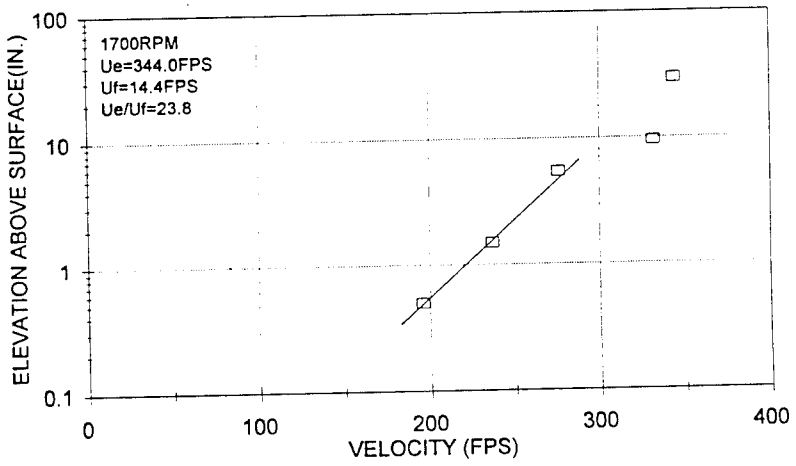

(c) Velocity profiles at 21'4" station

Figure 4-39. Threshold velocity experiments for moist WSMR soil bed (RS119, 10%/8% soil moisture, 24 hour cure).

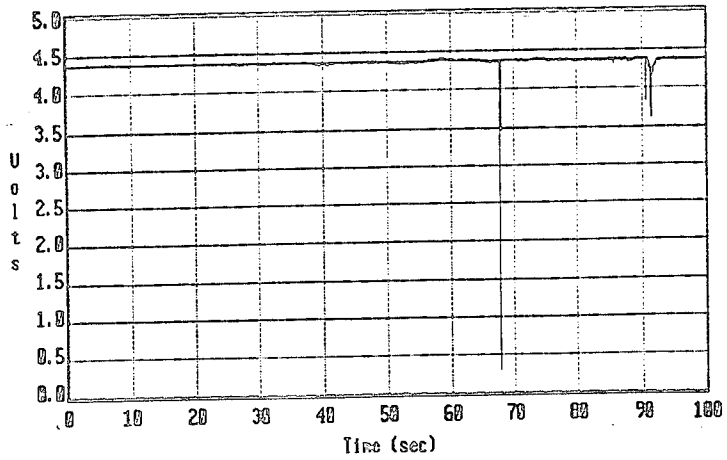

(a) Transmitted x-ray signal at 0.5" elevation

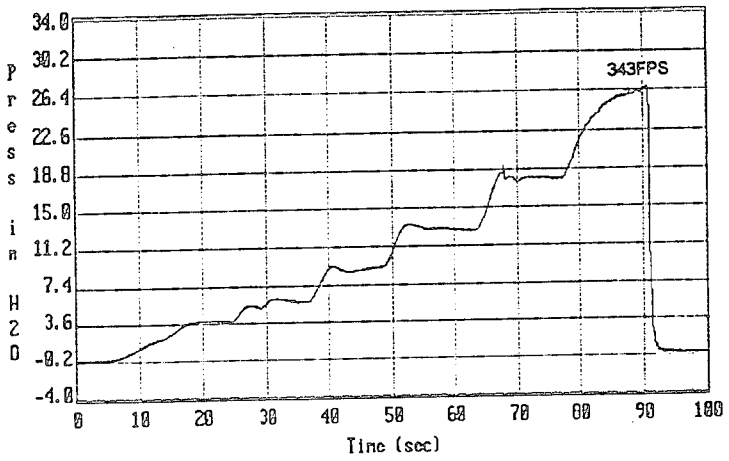

(b) Free stream dynamic pressure

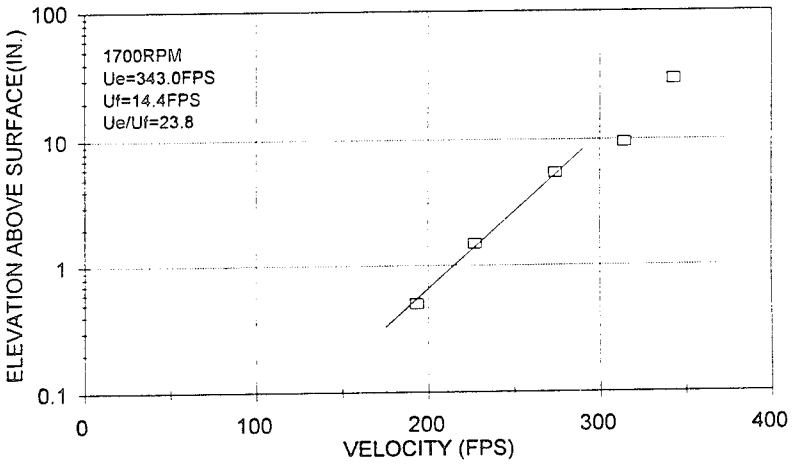

(c) Velocity profiles at 21'4" station

Figure 4-40. Threshold velocity experiments for moist WSMR soil bed (RS117, 15%/12% soil moisture, 24 hour cure).

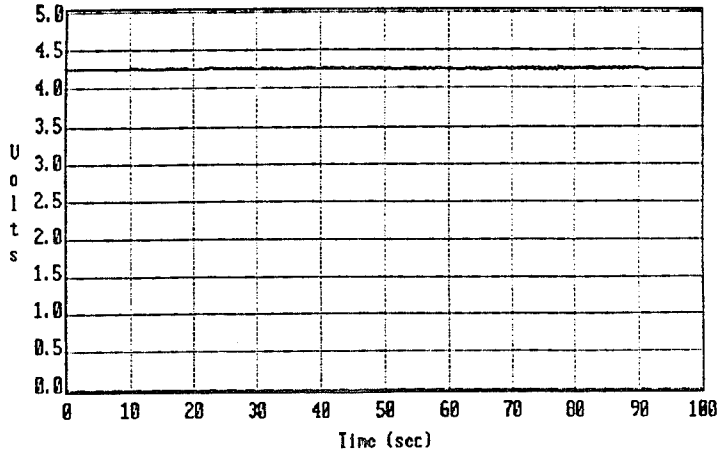

(a) Transmitted x-ray signal at 0.5" elevation

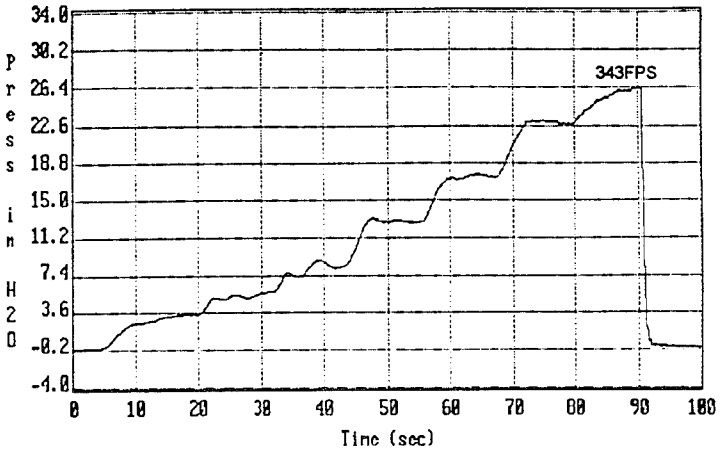

(b) Freestream dynamic pressure

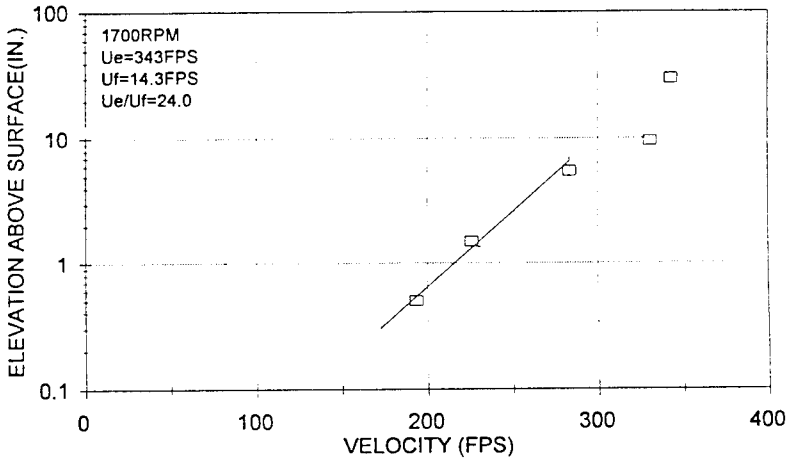

(c) Velocity profiles at 21'4" station

Figure 4-41. Threshold velocity experiments for moist WSMR soil bed (RS115, 25%/18% soil moisture, 24 hour cure).

SECTION 5
CONCLUSIONS

A technical study, both experimental and analytical, has been conducted to investigate the phenomenology of several aspects of high speed dust lofting. The areas investigated include: mass expulsion from confined chambers due to interior detonations (Collateral Effects Diagnostics Support), additional analysis and evaluation of boundary layer scouring data from wind tunnel experiments of erodible soil beds (Further Review of Dust Sweep-Up Experimental Results) and experimental investigation of soil scouring for realistic surface conditions (Real Surface Dust Lofting Experiments).

Important findings from the investigation are as follows:

5.1 COLLATERAL EFFECTS DIAGNOSTICS SUPPORT - SNOB/GREG MEASUREMENTS ON WATERWAYS EXPERIMENT STATION (WES) EVENTS 1, 3, AND 5.

For the three WES events on which Snob/Greg diagnostics were fielded, a total of six Snob/Greg probe pairs were operated. All data (Greg total, Snob Total and Snob static pressure) were acquired successfully and, after thermal compensation, demonstrated favorable baseline performance. On each of the three noted WES events one probe pair was installed to measure vent pipe exhaust flow at a 11.6" elevation above the pipe exit (2.5" diameter). These yoke mounted probes straddled the vent flow centerline at radial displacements of $\pm$ 0.625". In addition, a rake of vertically aligned probe pairs (3 each) were also mounted at the WES 5 door vent opening (7"W x 20"H) to measure door exit flow properties. The probes were positioned 4" downstream of the vent exit plane and at elevations above the chamber floor (52"W x 68"DP) of 3", 7.5" and 12.5".

Specific results for each of these events are:

5.1.1 WES 1 (1 lb charge; vent pipe discharge only; 35 lb exposed simulant on chamber floor; particle collector assembly attached to pipe exhaust).

- From the Dust Momentum Flux (DMF) measurements (40 psi peak; 1.8 sec duration) an estimate for total discharged mass has been made based on double integrating the DMF data over time and space (assuming a Gaussian profile distribution). The so-calculated result (2.5 $\pm$ 0.75 lb) compares favorably with the pre-post test weighing value of 2.4 lb.

- An early time "spike" in the WES 1 Snob static pressure signal is attributed to the use of a baffle chamber on the vent pipe exhaust flow. This chamber was installed as part of a particle collection assembly and resulted in moderate constriction of the WES 1 airblast jet.

- For WES 1, exhaust flow Mach numbers were relatively constant at approximately (M =)0.75 for a major portion of the flow duration. Corresponding dust loading factors were similarly constant at values of (k =)1.5 to 2.0.

- Derived vent pipe velocities agreed favorably with LDV velocities measured by PRi at the vent pipe exit on WES 2B (a comparable event to WES 1).

5.1.2 WES 3 (0.2 lb charge; vent pipe exhaust only; 10 lb simulant confined in pre damaged containers).

- As expected, the flow duration and peak pressure for WES 3 (0.2 lb charge; 1.0 sec, 20 psi) are consistently smaller than corresponding values for WES 1 (1 lb charge; 1.8 sec, 60-80 psi). The duration data are found to correlate favorably on the basis of cube root scaling.

- Reduced DMF data indicate that negligible dust mass was discharged during the WES 3 event. This result is in

agreement with WES measurements of pre-post test simulant weights and reflects the finding that the simulant was not effectively dispersed by the interaction of the airblast with the simulant containers.

- The pressure spike observed on WES 1 at early times did not occur for WES 3. This result supports the conclusion cited above that flow constriction effects caused the noted WES 1 pressure enhancement at early time.

- Derived WES 3 velocity data based on Snob pressure measurements and approximate temperature data show good agreement with LDV velocities as measured by PRi on WES 7 (an event comparable to WES 3).

5.1.3 WES 5 (0.2 lb charge; vent pipe and door vent discharge; 50 lb exposed simulant on chamber floor).

- Of the four Snob/Greg probe pairs fielded on WES 5 only the S/G pair at the 3" elevation location at the door vent measured detectable dust flow. Integrating this location's DMF data over both time and space, it is estimated that 1.2 $\pm$ 0.25 lb of simulant mass was discharged at the vent opening (pre-post test mass result: 1.4 lb). The fact that only the lowest elevation location (3") showed measurable dust flow, illustrates that when simulant is distributed in exposed layers/piles on the chamber floor, dust movement is caused primarily by boundary layer scouring phenomena rather than cloud dispersion effects. Also there exists a moderate delay in the DMF signal ($\simeq$ 20 ms) suggesting that the dust outflow is more the result of secondary flow effects rather than the initial airblast interaction.

- Because of the open vent door, the WES 5 blow down duration was substantially reduced over that for WES 3 (40 ms versus 1 sec).

- Derived vent pipe velocities compared favorably with LDV velocities measured by PRi at the vent pipe exit on WES 8 (a comparable event to WES 5).

- Dust loading factors for the door vent measurements at the 3" elevation location increased to a maximum of 5-6 towards the end of the airblast's positive phase duration. This result indicates that significant dust flow occurred at late time and low speed, a finding consistent with video/film evidence of delayed mass expulsion for the WES 5 event. Since exhaust temperatures decay at a rapid rate, late time expelled simulant/debris is therefore "cold" and may not be dominated by hot buoyancy force phenomena.

5.2 FURTHER REVIEW OF DSU EXPERIMENTAL RESULTS.

A follow-up review and analysis of measured results from the DSU test program, a wind tunnel dust lofting program conducted just prior to DSUE, has been made. Detailed profile data (velocity and dust density) as well as dust scouring results for WSMR dust and Ottawa sand soil beds have been reexamined. Both law of the wall scaling and conventional correlation comparisons have been applied to the data.

Specific findings from the study include:

- The tunnel's clean flow boundary layer demonstrated a law of the wall behavior and scales favorably with Clauser's correlation for rough wall boundary layers when a shear velocity ratio (u_e / u_f) of 12 is used.

- Similarly, measured dust profiles exhibit typical law of the wall characteristics and correlate satisfactorily using a velocity ratio of 14 and 11 for the WSMR and Ottawa sand data, respectively. This result further substantiates the

dusty law of the wall model put forward by Denison (1986) and others for treating the dusty boundary layer problem.

- Deduced shear velocities are found to increase linearly with edge velocity but decay with bed length distance in an approximate exponential manner.

- Normalized dust velocity profile data collapse approximately to a power law correlation,

$$u/u_e = (y/\delta_e)^n$$

based on either surface elevation or height above the profile "focus" point. The average power law slope (n) for the WSMR and Ottawa sand data was 0.5 and 0.75, respectively. These results are comparable to previous shock tube measurements of dust sweep-up wherein slope values of the order of 0.7 were found to best correlate the data.

- Boundary layer soil loss as measured either by profile integrated results or with a boundary layer slot collector (both measurements agree favorably), was found to increase to the 3/2's power of edge velocity. This high speed result, which also implies that scouring rates vary in a similar way, is in contrast with established low speed data where a power law dependence to the cube power of velocity is indicated. This discrepancy is attributed to flow regime differences between the two sets of data. For example, the lower speed results (u < 50 fps) are representative of a scouring mechanism (saltation) dominated by gravity/collision effects whereas the current wind tunnel data correspond to flow controlled by turbulent diffusion processes (particle suspension) where drag-to-weight ratios are large (300-1000).

- Scouring rate data collapse favorably when rates are normalized with edge Mach number to the 3/2's power.

- Scaling of lofting rate data with soil type is favorable when the data are correlated in terms of bed length as normalized by a soil's mean particle size.

- Because shear velocities decay exponentially with axial distance, the observed decay behavior in scouring rate with bed length is substantially reduced when lofting rates are normalized by a mass flux based on shear velocity rather than edge velocity. This correlation result corresponds to an approximate constant scouring rate value for both WSMR and Ottawa sand soil beds and for bed lengths up to 20 feet in extent. This "universal" rate is given by:

$$\dot{m}/(\rho_e u_f M^{0.5}) = 0.3 \pm 0.1.$$

- An approximate turbulent Schmidt number of 0.7 is derived when the DSU velocity profile data are correlated with corresponding dust density results. This finding is valid for both WSMR and Ottawa sand measurements.

5.3 REAL SURFACE DUST SCOURING EXPERIMENTS.

- Soil loss from a dry erodible bed of WSMR dust is always reduced when the soil bed is "textured" with ridges, clods and/or stubble. For comparable bed length spacing, ridges are found to be most effective in reducing soil scouring, with stubble the least.

- Normalized soil loss data (Soil Erodibility Factor - SEF) collapse/correlate favorably with normalized ridge elevation (H/L, ridge elevation ratioed to ridge spacing). Near linear decay of SEF from 1 to 0.1 with elevation is demonstrated for a range in elevation from a dry loose flat soil bed (surface

without ridges, H/L = 0%) to a 10% elevation condition. A constant soil loss of the order of 10% is suggested for elevation ratios greater than 10%. These findings highlight a well established approach for moderating wind-induced soil erosion commonly used by agricultural workers.

- The favorable collapsing of the noted ridge results suggests that scouring for other surface types (clods, stubble, etc.) can similarly be correlated, thus leading to a straightforward approach to relating a given soil texture to scouring potential. Once a soil's surface characteristics are known, prediction of mass of dust lofted can then be made by "adjusting" flat erodible results for the SEF value of interest.

- Isolated (leading edge) roughness elements (ridges/clods/vortex plate generators) produced persistent axially aligned vortex flows but only minor to negligible reduction in soil loss over that for flat undisturbed soil beds. Although localized soil scouring enhancement was evident from post test photographs of soil bed surfaces, increase in <u>overall</u> soil loss did not occur. In fact, for the complete range of real surface conditions tested under DSUE, scouring enhancement was never observed!

- Current results support the view that scouring from flat-dry-loose "undisturbed" soil beds corresponds to the most severe dust lofting condition. The primary effect of "real surface" textures is apparently to attenuate soil scouring over that for dry erodible soil beds. This finding validates those approaches which calculate upper bound limits of lofted mass from code predictions based on dry loose soil beds without real surface disturbances.

- Soil loss results for WSMR dust beds seeded with "coarse" gravel to simulate a random rough real surface, compare

satisfactorily with "ordered" (clod) surface disturbance measurements. As exposure time increased, soil loss was progressively reduced illustrating the effect of "desert pavement" phenomena (shielding of fines by non-erodibles). Correlation of this decay process with "scaled time" based on edge Mach number to the 3/2's power was favorable.

- Unique measurements of threshold velocities for large gravel particles (0.25 - 2") at high speed have been performed herein. Results indicate that velocities required to initiate particle movement are greater ($\simeq$ x 3) than predictions based on extrapolating low speed/small-particle data. Correlations of overall results is favorable when motion onset is determined based on a threshold value for particle drag-to-weight ratio of 3 $\pm$ 1. This scaling prediction for scouring onset suggests that revision to those empirical fits currently in use for hydrocode calculations of dust lofting may be in order. Such a revision merits consideration since calculations based on a D/W threshold criteria results in <u>less</u> predicted mass scoured to altitude than corresponding estimates using extrapolated velocities from low speed experiments.

- For the velocity range associated with the DSU/DSUE experiments (100 - 370 fps), drag-to-weight ratios are of the order of 100 or greater. Substantial drag forces are therefore imposed on individual particles such that the bulk of the boundary layer flow consists of particles which have entered into full turbulent suspension. Further support for this conclusion is illustrated by noting that vertical velocity intensities typically and substantially exceed particle terminal/fall velocities for the test conditions investigated.

- Threshold velocity experiments for moist soil beds demonstrated that all soils "moist" to-the-touch produced

- Threshold velocity experiments for moist soil beds demonstrated that all soils "moist" to-the-touch produced negligible soil loss (10-25% moisture content, 24 hour cure; 5%, 1 hour cure) for velocities up to as high at 370 fps. Only when a soil's moisture content was less ($\leq$ 1 - 2%) and adequate "cure" time was allowed did soil scouring take place (5%; 24, 48 hour cure). As soils "dried out" thin frangible crusts were formed in the bed surface ($\simeq$ 0.1 - 0.2" thick) which were dry to the touch. Threshold velocities as measured for these "crust" surfaces were substantially larger than corresponding dry erodible results ($\simeq$ x 8). The present findings suggest that code predictions, where moisture content may be a factor, might best be accommodated by assuming an either/or approximation, e.g., moist (zero scouring, SEF = 0) or dry (fully erodible, SEF = 1).

SECTION 6

REFERENCES

Bacon, D.P., Dunn, T.J., Sands, M.P., and Sarma, R.A., "SingleBurst Nuclear Cloud Data Base: Volume I. Cloud Rise and Stabilization Modeling", SAIC 90/1150, DNA-TR-90-36-VI, June 1991 (Unclassified).

Bagnold, R.A., "The Physics of Blown Sands and Desert Dunes", Methyen and Co., Ltd., London 1941 (Unclassified).

Barthel, J.R., "2D Hydrocode Computation using a K-ε Turbulent Model: Model Description and Test Calculations", DNA-TR-89-220, May 1990 (Unclassified).

Batt, R.G., Kulkarny, V.A., Behrens, H.W., and Rungaldier, H., "Non-Ideal Airblast Phenomenology Program, Vol. 3, Laboratory Scale Shock Tube experiments", DNA-TR-87-3-V3, 31 Dec 1986 (Unclassified).

Batt, R.G., Behrens, H.W. and Rungaldier, H., "Non-Ideal Airblast Phenomenology Experiments (NIAPE) Program, Vol. 1, Shock Induced Dusty Boundary Layer Experiments", DNA-TR-89-48-V1, Feb 1990 (Unclassified).

Batt, R.G. and Peabody, S.A., II, "Rail Garrison Instrumentation Development", DNA-TR-91-126, 31 March 1991 (Unclassified).

Batt, R.G., Petach, M.B., Peabody, S.A II, and Batt, R.R., "Experimental Investigation of Vegetation and Dust Sweep-Up", DNA-TR-92-53, January 1993 (Unclassified).

Chepil, W.S., "Influence of Moisture on Erodibility of Soil by Wind", Soil Science Proceedings, 1956, pp 288-292 (Unclassified).

Clauser, F.H., "Advances in Applied Mechanics", Vol 4, p 1, New York, 1956 (Unclassified).

Denison, M.R. and Baum, E., "Engineering Research Support to Defense Nuclear Agency ICBM Basing Program, Vol. III - Dusty Boundary Layer Modeling", DNA-TR-84-355-V3, 5 Dec 1984 (Unclassified).

Denison, M.R. and Baum, E., "Non-Ideal Airblast Subscale Phenomenology Experimentation Program, Volume 1 - Boundary Layer Analysis", DNA-TR-87-3-VI, 15 September 1986 (Unclassified).

Doerr, S., Schaeffer, B. and Simmons, J., "DNA Collateral Effects Program - Task Report", SAIC, Contract No.DNA001-88-C-0105, January 1994 (Unclassified).

Dussard, J.L. and Shapiro, A.H., "A Deceleration Probe for Measuring Stagnation Pressure and Velocity of a Particle-Laden Gas Stream", Jet Propulsion, January 1958, pp 24-34 (Unclassified).

Fryrear, D.W., "Soil Ridges - Clods and Wind Erosion", Transaction of the ASAE, 1984, pp 445-448 (Unclassified).

Gaj, R.A. and Small, R.D., "Target Area Operating Condition: Vol. 4 Dust Lofting from Natural Surfaces", PSR Report 1817, 30 November 1989 (Unclassified).

Ganong, G.P., "Collateral Effects Program Review - Analysis of Data from First Shot and Plans for Other Shots", Logicon RDA, 10 February 1993, p 405 - 426 (Unclassified).

Gillette, D.A., "Threshold Friction Velocities for Dust Production for Agricultural Soils", J. of Geophysical Research, Vol. 97, No. D10, pp 12645-12662, October 20, 1988 (Unclassified).

Graham, P.W. and Dallriva, F., "Test Results for Laboratory Expulsion Experiment Number 1 in Support of the Collateral Effects Environment Program", Waterways Experiment Station, January 21, 1993 (Unclassified).

Graham, P.W., "Test Results for Laboratory Expulsion Experiments 2A and 2B in Support of the Collateral Effects Environment Program", Waterways Experiment Station, May 18, 1993 (Unclassified).

Graham, P.W., "Test Results for Laboratory Expulsion Experiments 3, 4, 5, 6, 7, 8, 9, and 10 in Support of the Collateral Effects Environment Program", Waterways Experiment Station, January 5, 1994 (Unclassified).

Hartenbaum, B., "Lofting of Particles by a High Speed Wind", DNA2737, Sept 1971 (Unclassified).

Hinze, J.O., "Turbulence", McGraw-Hill Book Co., Inc., 1959 (Unclassified).

Hookham, P.A., Denison, M.R. and Schlamp, R.J., "Near Surface Dust Sweep-Up Modeling", Titan Corp., DNA001-91-C-0154, February 1994 (Unclassified).

Kuhl, A.L., Chien, K.Y., Ferguson, R.E., Collins, J.P., Glaz, H.M., and Colella, P., "Simulation of a Turbulent Dusty Boundary Layer behind a Shock", Current Topics in Shock Waves, American Institute of Physics Press, New York, 1990, pp 762 - 769 (Unclassified).

Kuhl, A.L., Ferguson, R.E., Chien, K.Y., and Collins, J.P., "Turbulent Dusty Boundary Layer in a Surface Explosion"; 13th Military Applications of Blast Simulation (MABS) Symposium; Denlaag, Netherlands; 13-17 September 1993 (Unclassified).

Mason, A.S., "Expulsion Gas Sampling on WES Events 3 and 6", Los Alamos National Laboratory, Letter INC9-93-705, October 27, 1993 (Unclassified).

Modarress, D. and Hoeft, T., "Dusty Flow Diagnostics Using Laser Doppler Velocimetry and Laster Attenuation Technique in Support of WES Expulsion Experiments", PRi, Final Report, September 28, 1993 (Unclassified).

Owen, P.R., "Saltation of Uniform Grains in Air", J. Fluid Mechanics, Vol. 20, Part 2, pp 225-242, 1964 (Unclassified).

Pierce, T.H., "Turbulence and Real-Surface Submodels in S-Cubed Hydrocodes", S-Cubed Final Report, 1989 (Unclassified).

Rosenblatt, M., Hatfield, D., Hassig, P., and Gaj, R., "Real Surface Airblast Calculations Using a Modified Mixing Length Model (Case H-503; 1Mt SHOB = 200 ft/Ktl/3)", presented at Non-Ideal Airblast Environment Review, RDA, Marina del Rey, CA 10 January 1985 (Unclassified).

Schlamp, R.J., Schuckman, K.L. and Rosenblatt, M., "Sweep-Up Layer Characteristics after a 1 Megaton Burst at HOB = 1000 Feet", CRT 5300-1T, California Research and Technology, 1982 (Unclassified).

Schlicting, H., "Boundary Layer Theory", McGraw-Hill, New York, 1955 (Unclassified).

Schneider, K.D., Needham, C.E. and Kennedy, L.W., "Calculational Results for TRW Laboratory - Scale Multiburst Experiments", S-Cubed/Maxwell Laboratories, SSS-DPR-92-13535/R-1 (Unclassified).

Shao, Y., Raupach, M.R. and Findlater, P.A., "Effect of Saltation Bombardment on the Entrainment of Dust by Wind", J. of Geophysical Research, Vol 98, No. D7, July 1993, pp 12,719 - 12,726 (Unclassified).

Traci, R.M. and Su, F.Y., "Turbulent, Twophase Flow Modeling for Dusty Boundary Layer Analyses", Inc., FPI R88-06-05, June 1988 (Unclassified).

APPENDIX A

PRE/POST TEST PHOTOGRAPHS OF DUST BED SURFACES FOR REAL SURFACE EXPERIMENTS

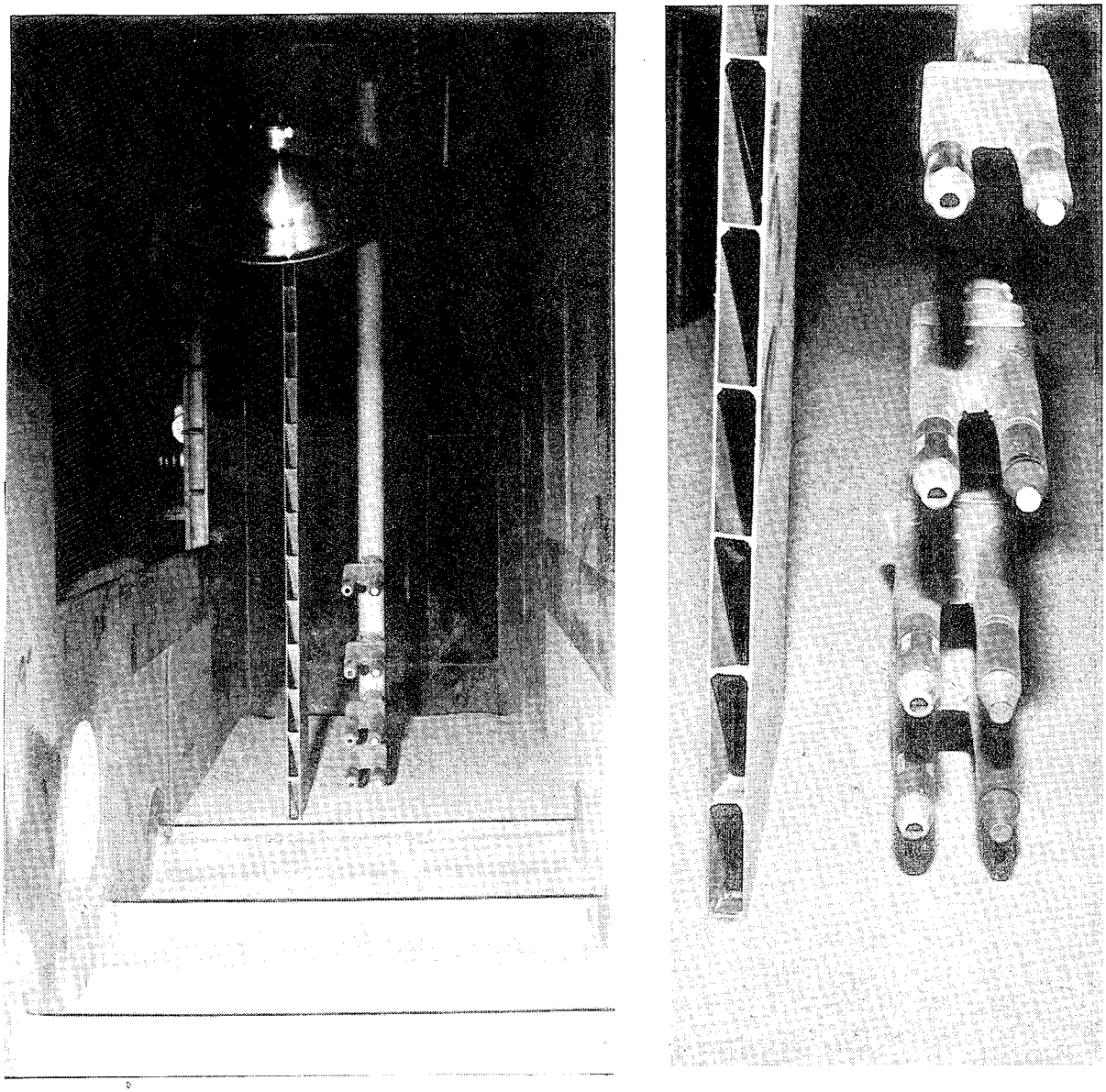

a) Wide angle view

b) Close up view

Figure A-1. Photographs of Bagnold slot collector and Snob/Greg probe rake - 21'4" test section location.

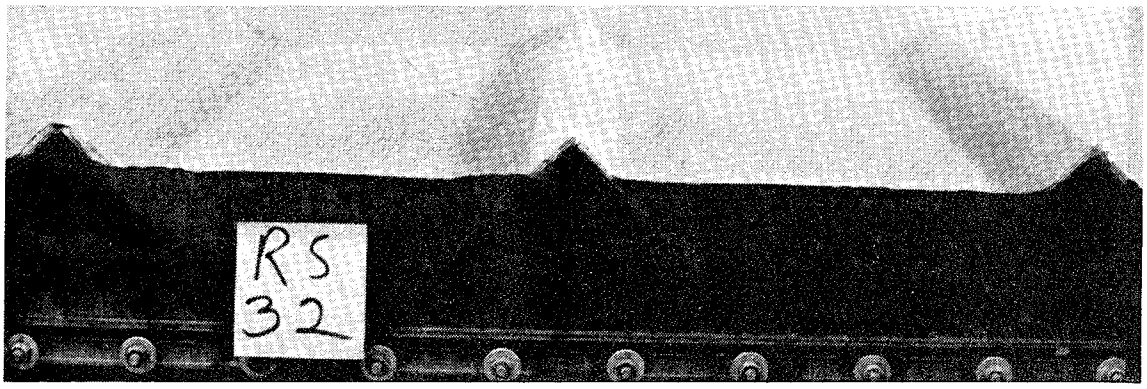

a) Pre test side view,

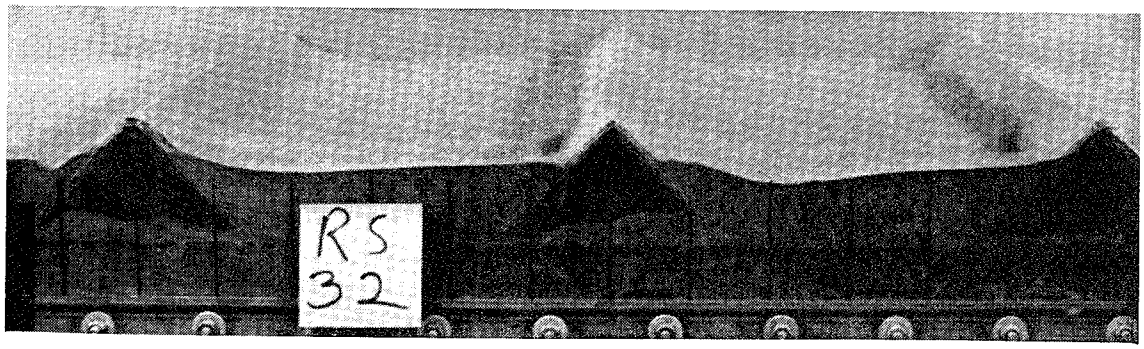

b) Post test side view

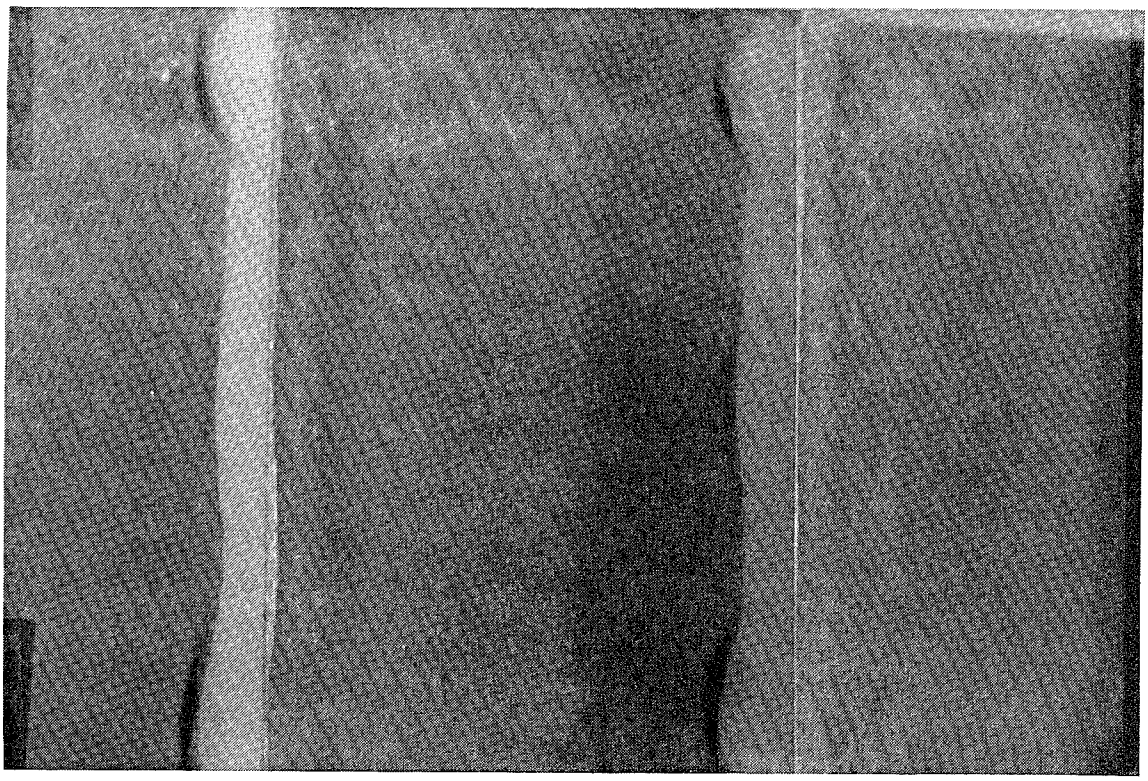

c) Post test overhead view

Figure A-2. Photographs at 9' test section location of ridge dust bed: RS 32, 116 fps, 1" elevation .

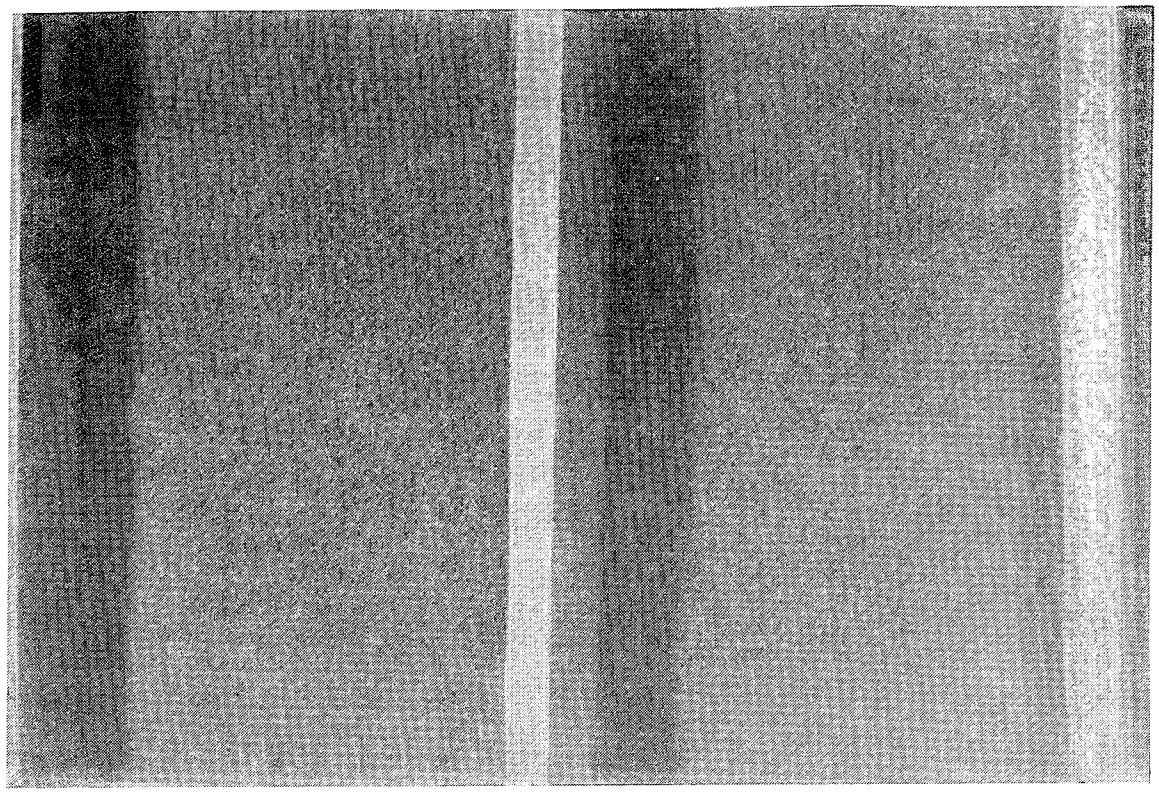

a) Pre test view

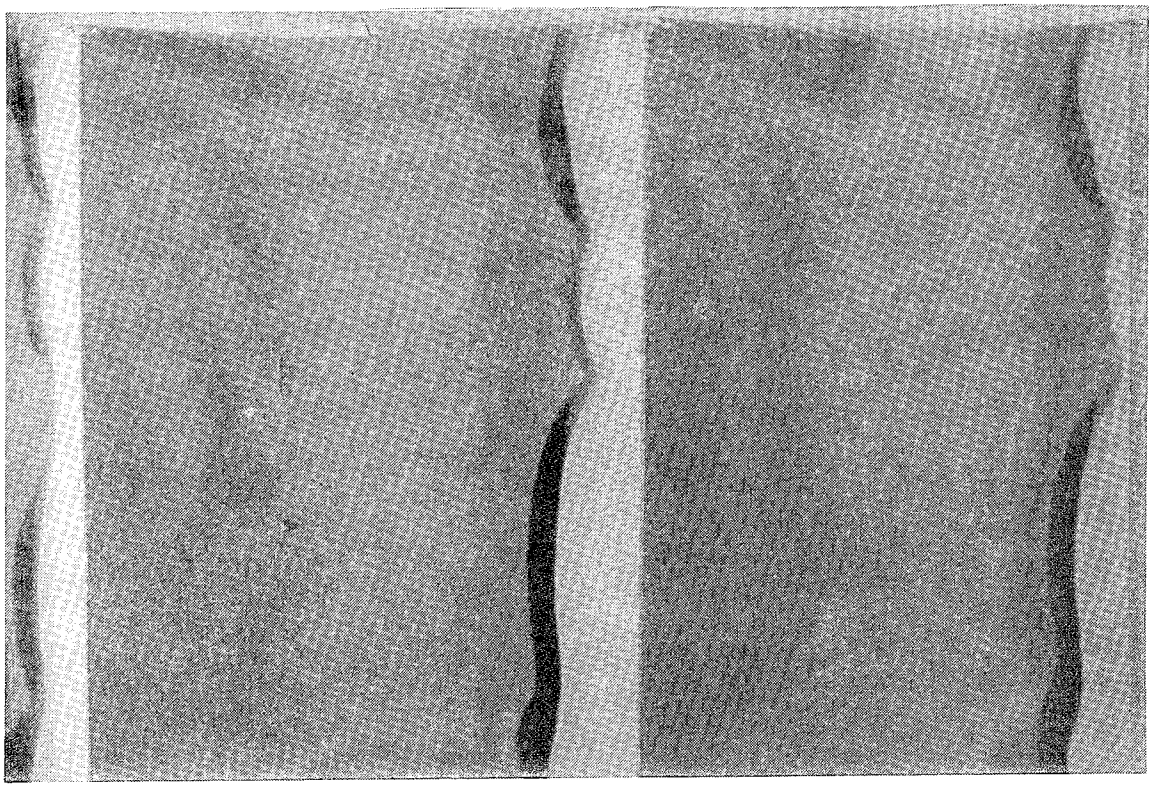

b) Post test view

Figure A-3. Overhead photographs at 9' test section location of ridge dust bed: RS 38, 227 fps, 1" elevation .

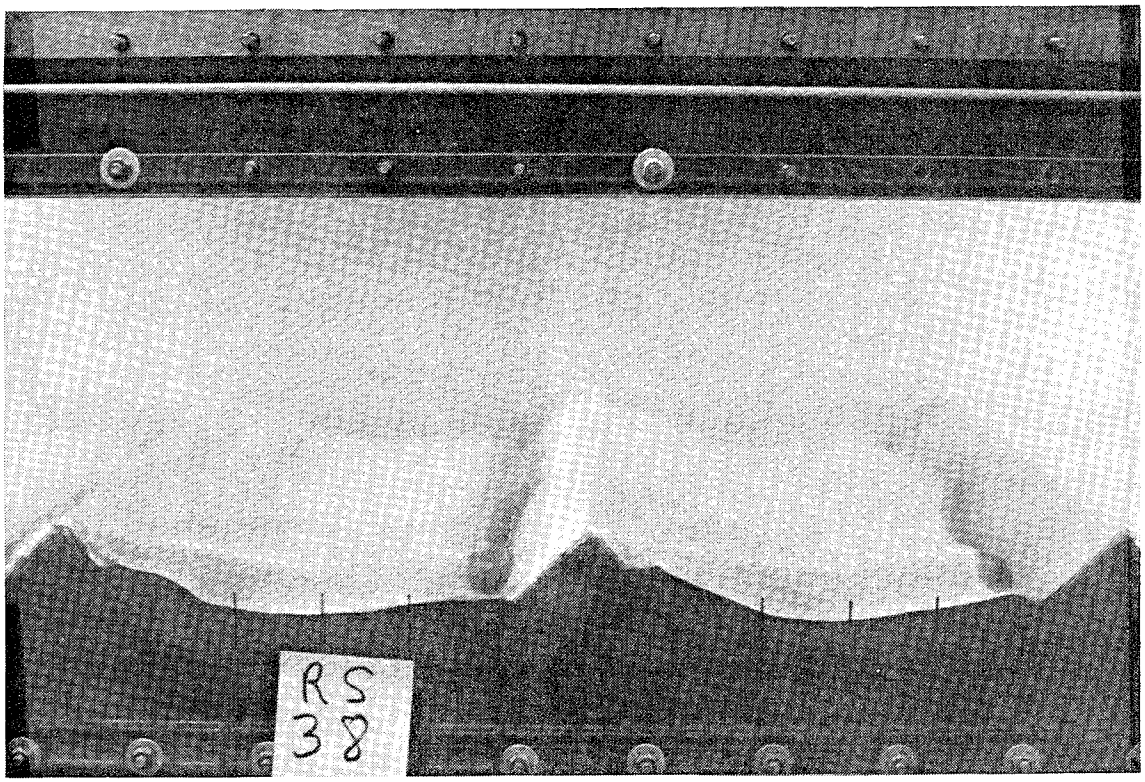

Figure A-4. Post test side view photograph at 9'test section location of ridge dust bed: RS 38, 227 fps, 1" elevation.

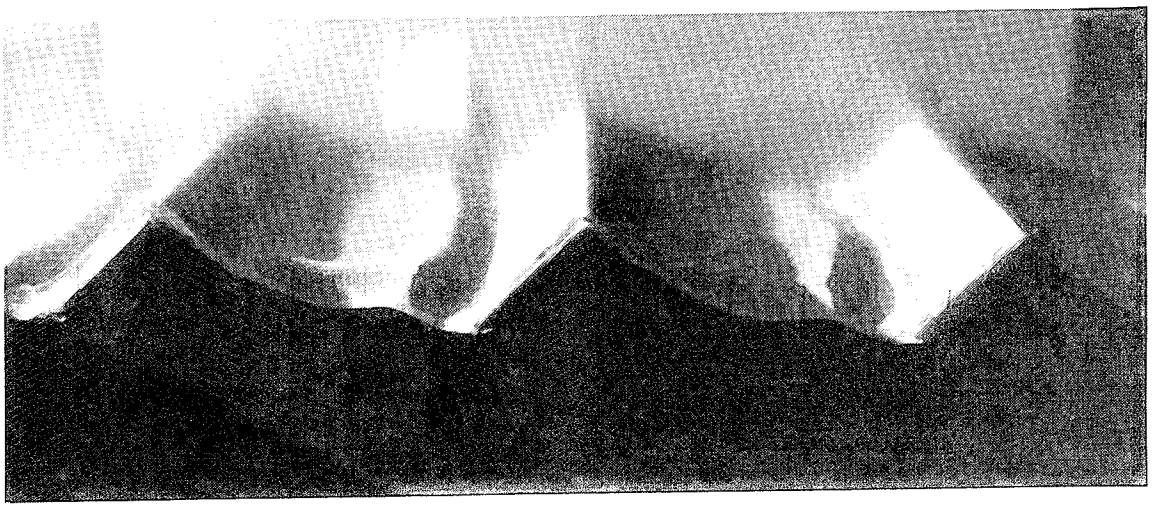

a) 9' station side view, RS 67, 238 fps

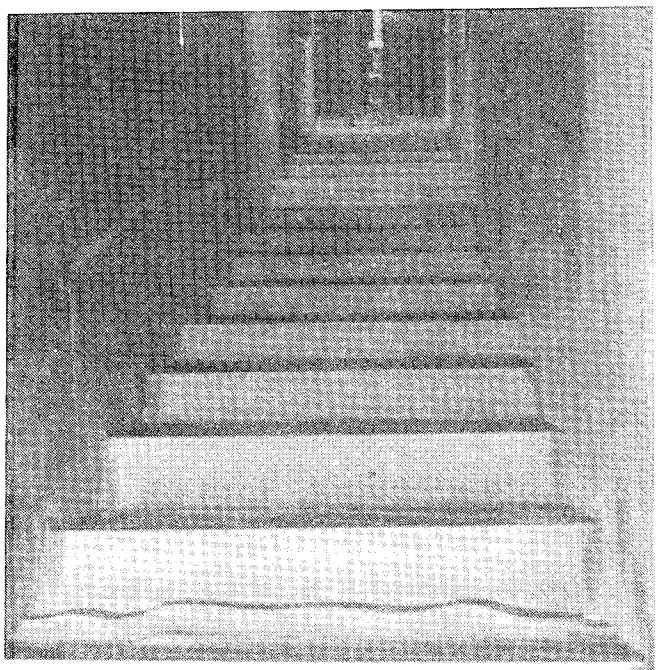

b) Downstream view, RS 67, 238 fps

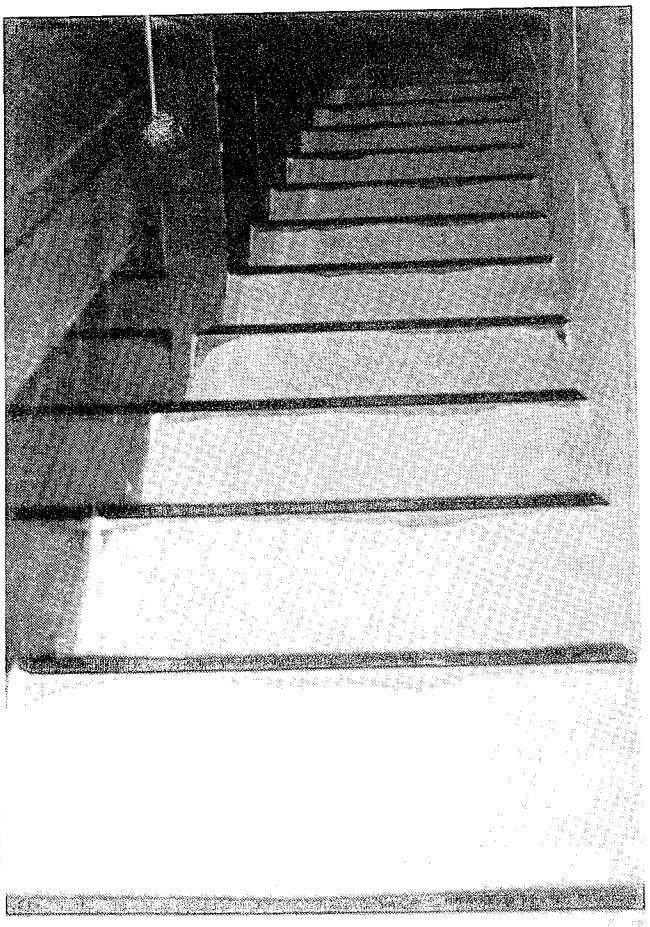

c) Upstream view, RS 34, 225 fps

Figure A-5. Post test photographs of ridge dust bed: 230 fps, 2" elevation.

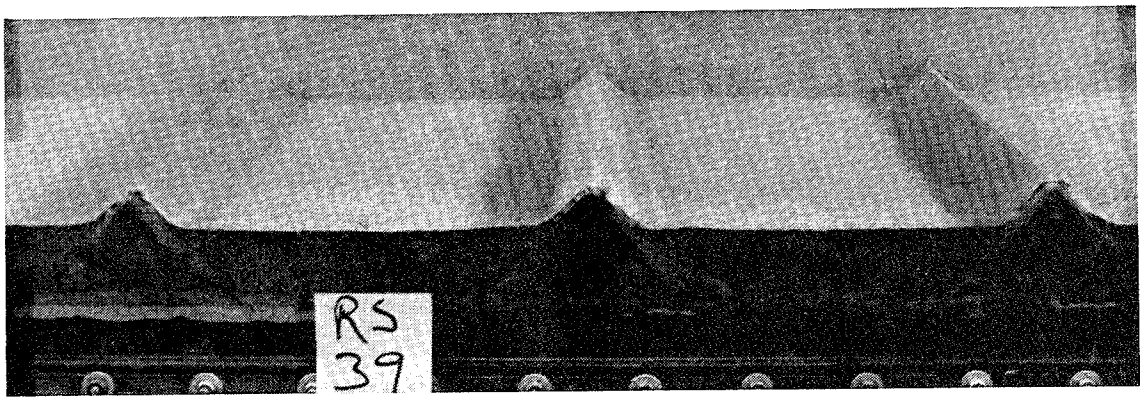

a) Pre test

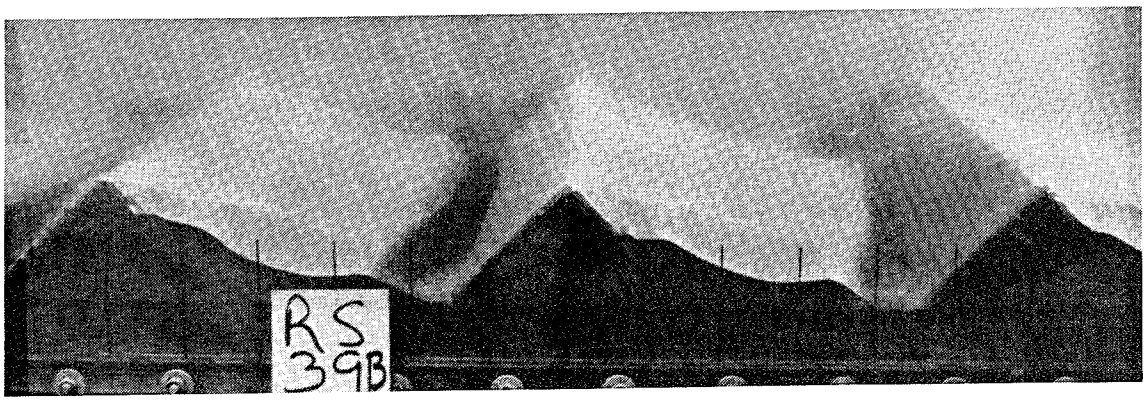

b) Post test

Figure A-6. Side view photographs at 9' test section location of ridge dust bed: RS 39, 367 fps, 1" elevation.

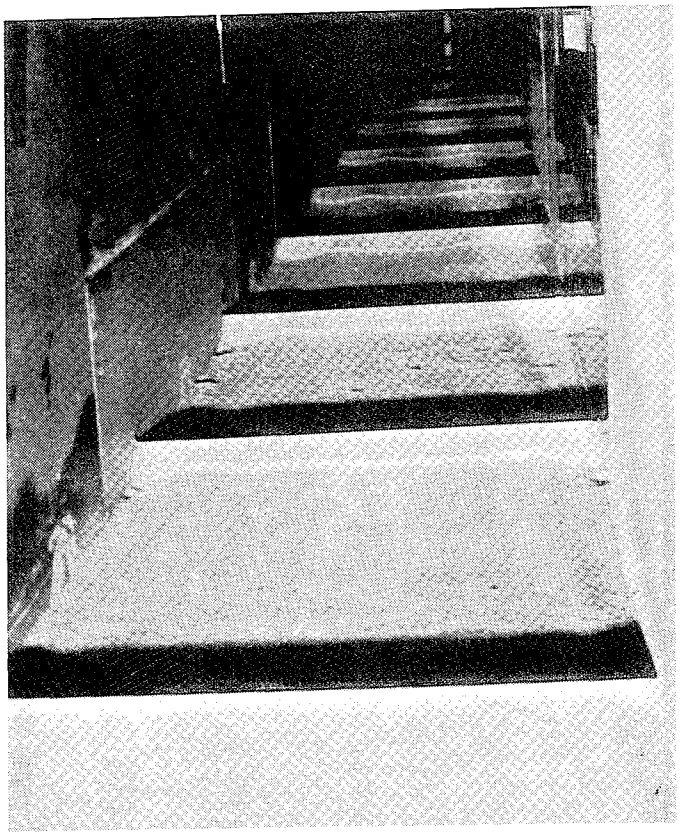

(a) Post test downstream view

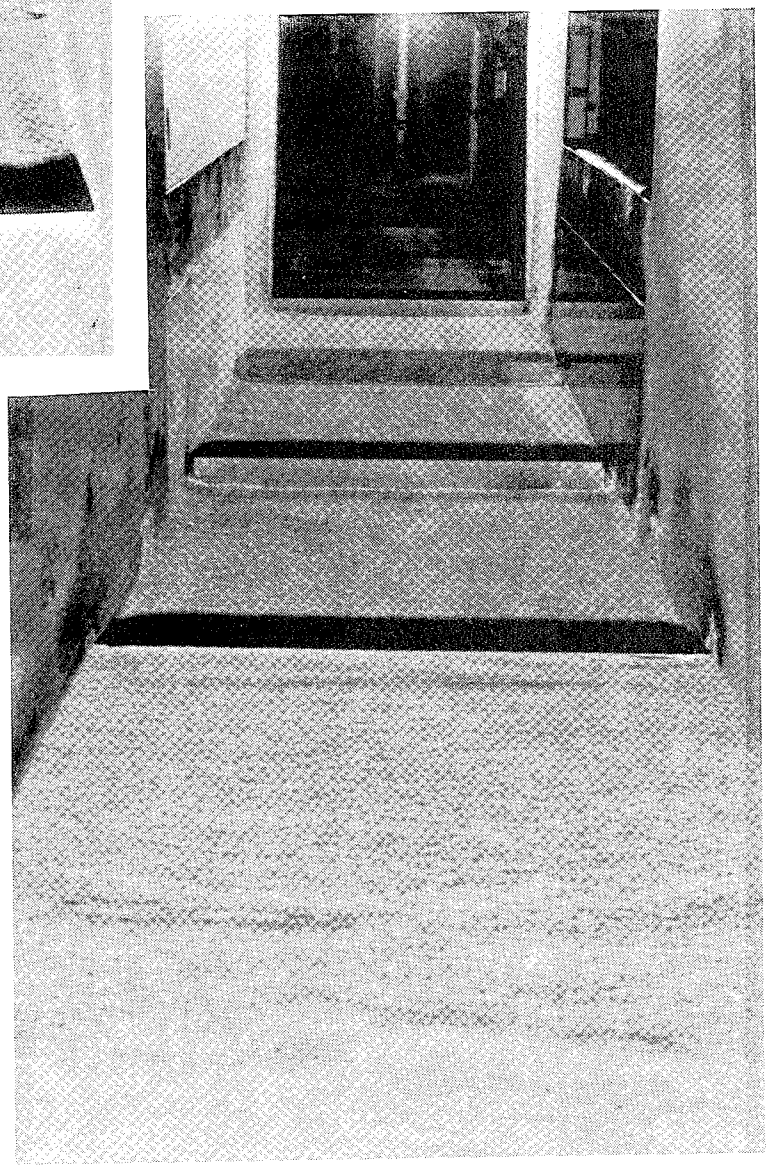

(b) Pre test downstream view

Figure A-7. Photographs of ridge dust bed: RS128, 124 fps, 1" elevation; 2' separation.

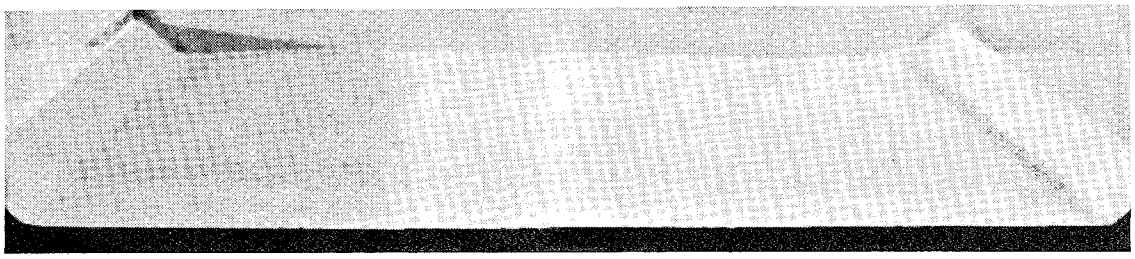

(a) Pre test side view

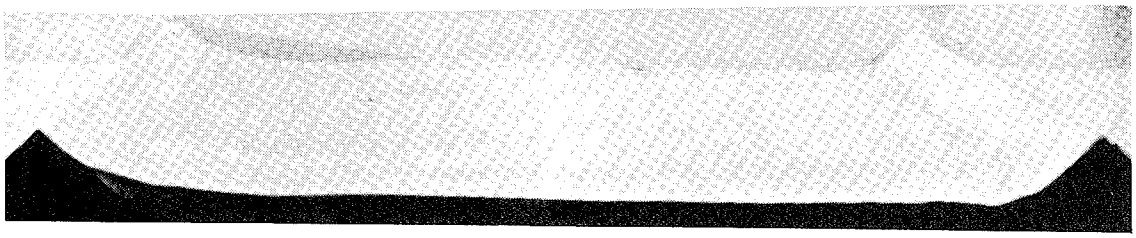

(b) Post test side view

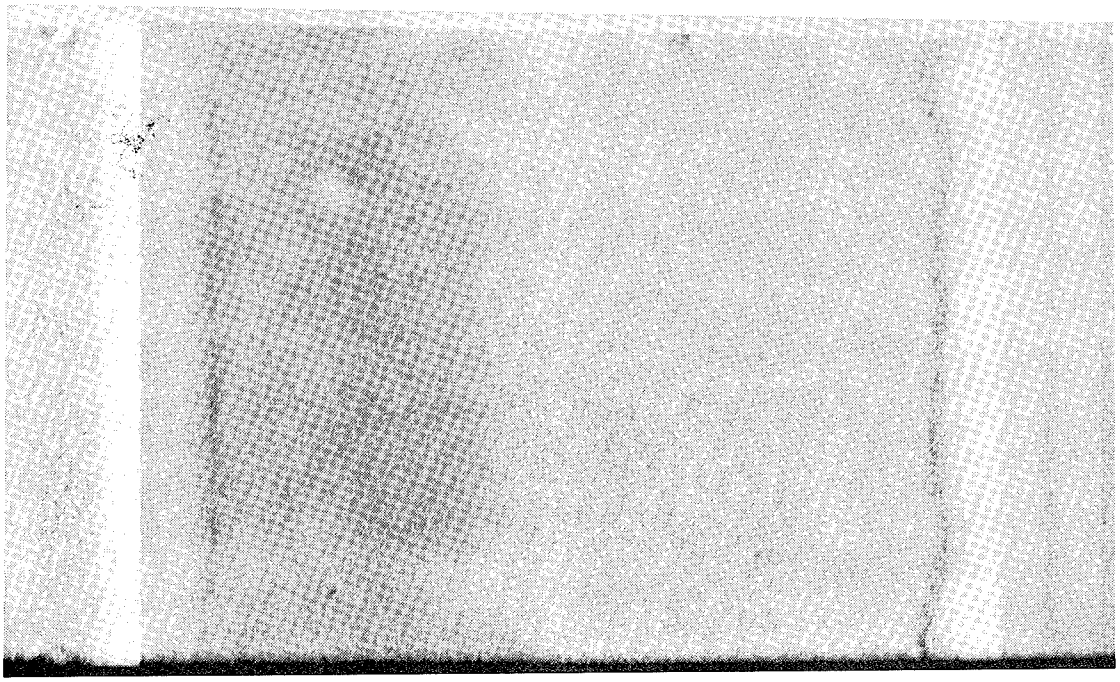

(c) Post test overhead view

Figure A-8. Photographs of ridge dust bed at 9' station: RS128, 124 fps, 1" elevation, 2' separation.

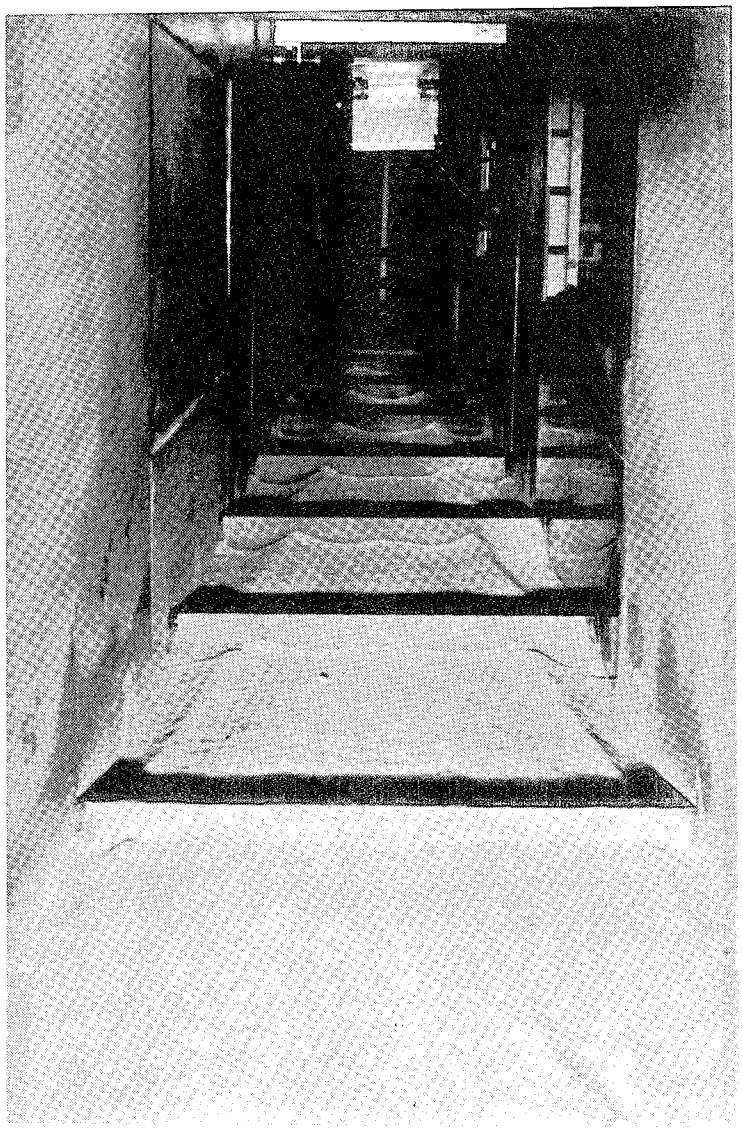

Figure A-9. Post test photograph looking downstream of ridge dust bed: RS129, 240 fps, 1" elevation, 2' separation.

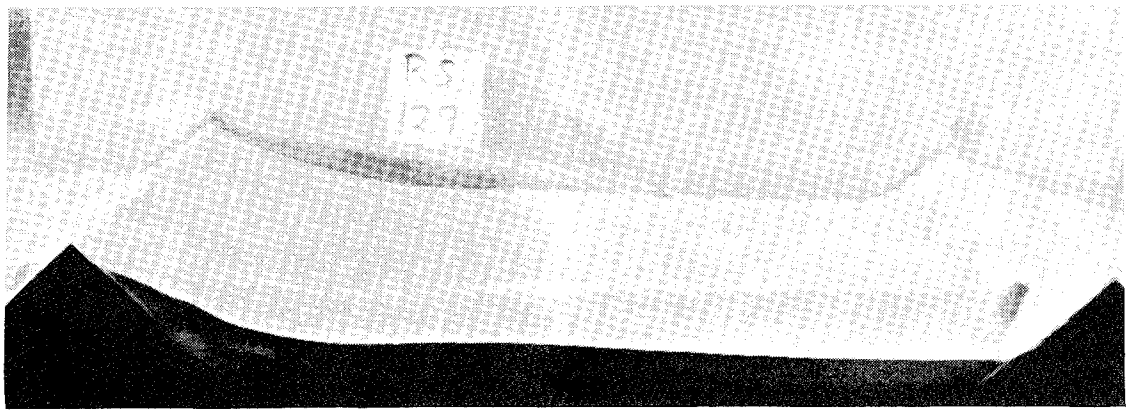

(a) Side view

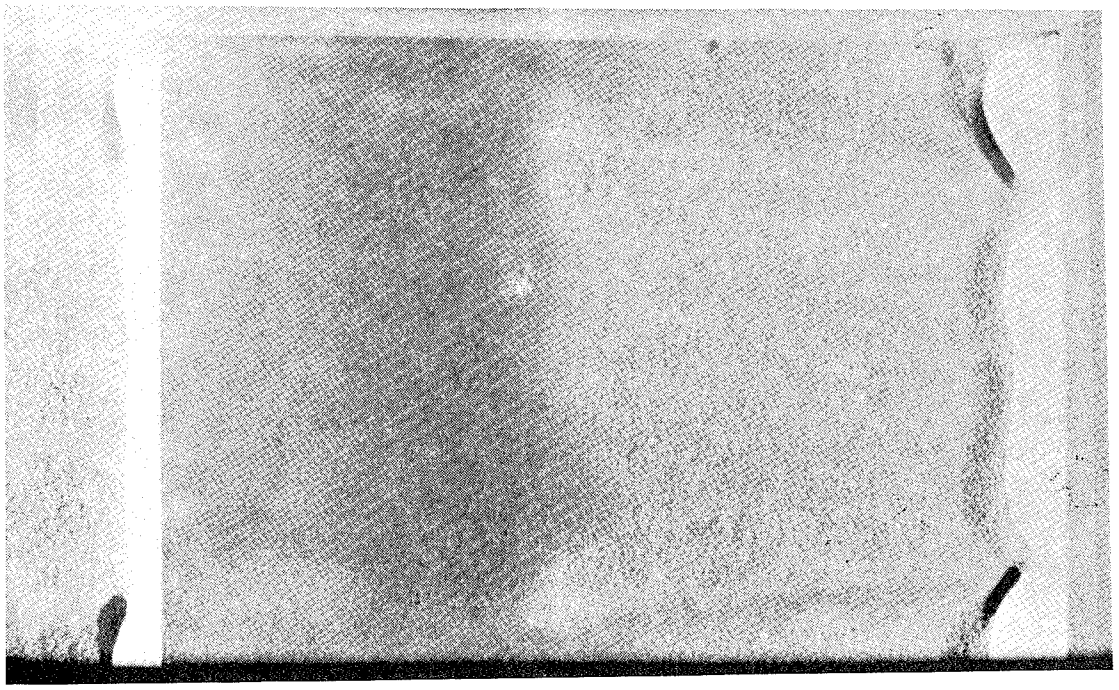

(b) Overhead view

Figure A-10. Post test photographs of ridge dust bed at 9' station: RS129, 240 fps, 1" elevation, 2' separation.

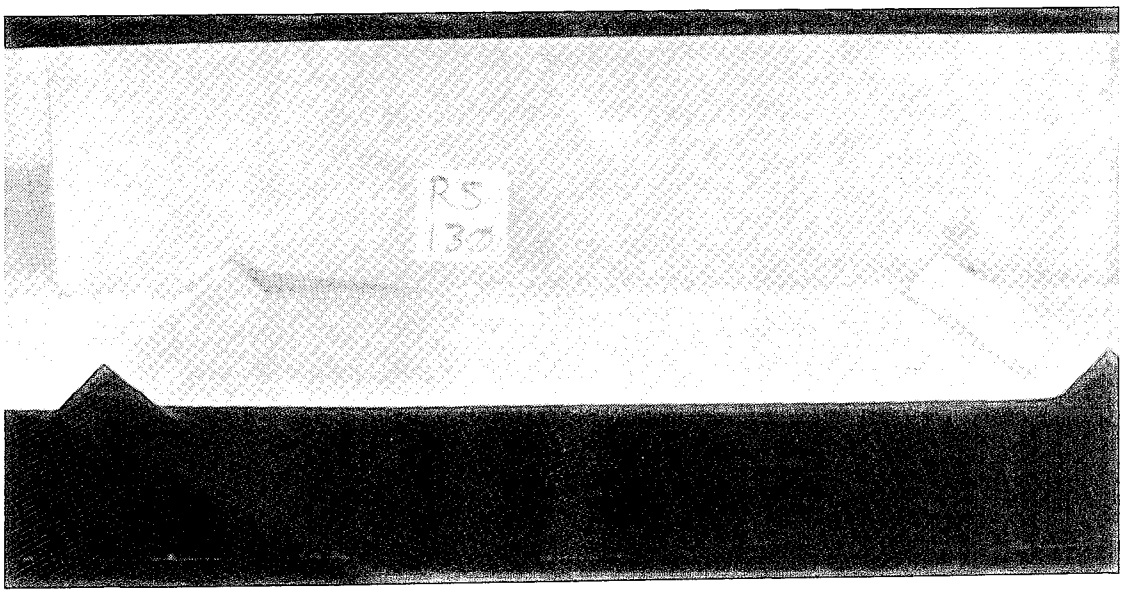

(a) Pre test side view

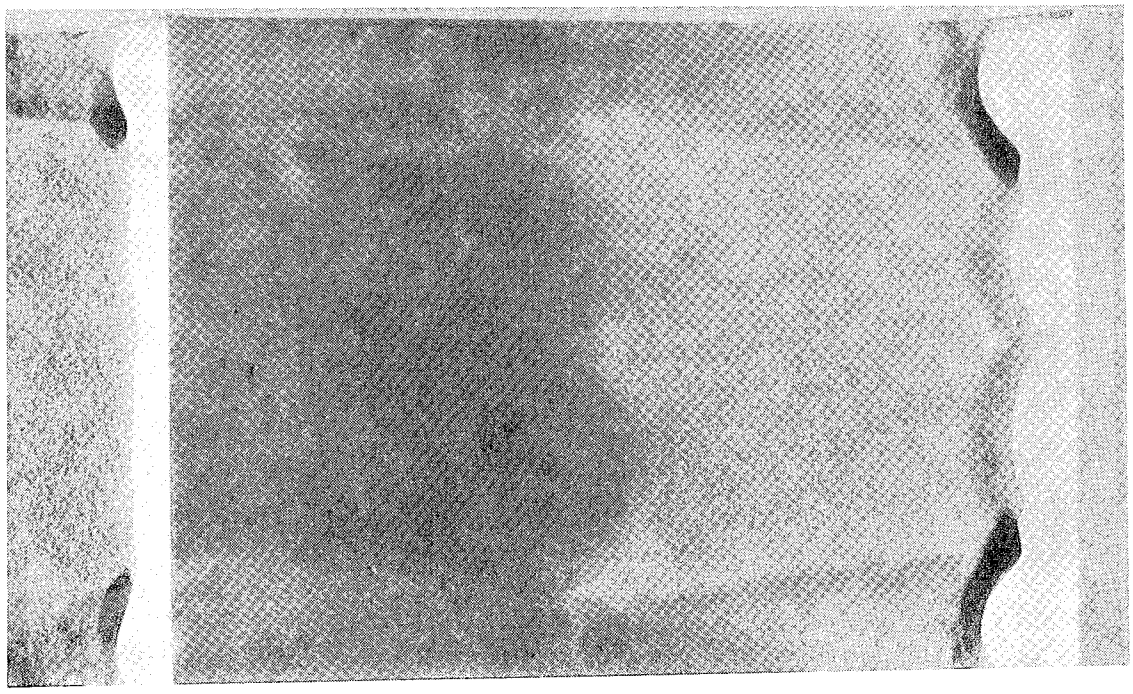

(b) Post test overhead view

Figure A-11. Photographs of ridge dust bed at 9' station: RS130, 372 fps, 1" elevation, 2' separation.

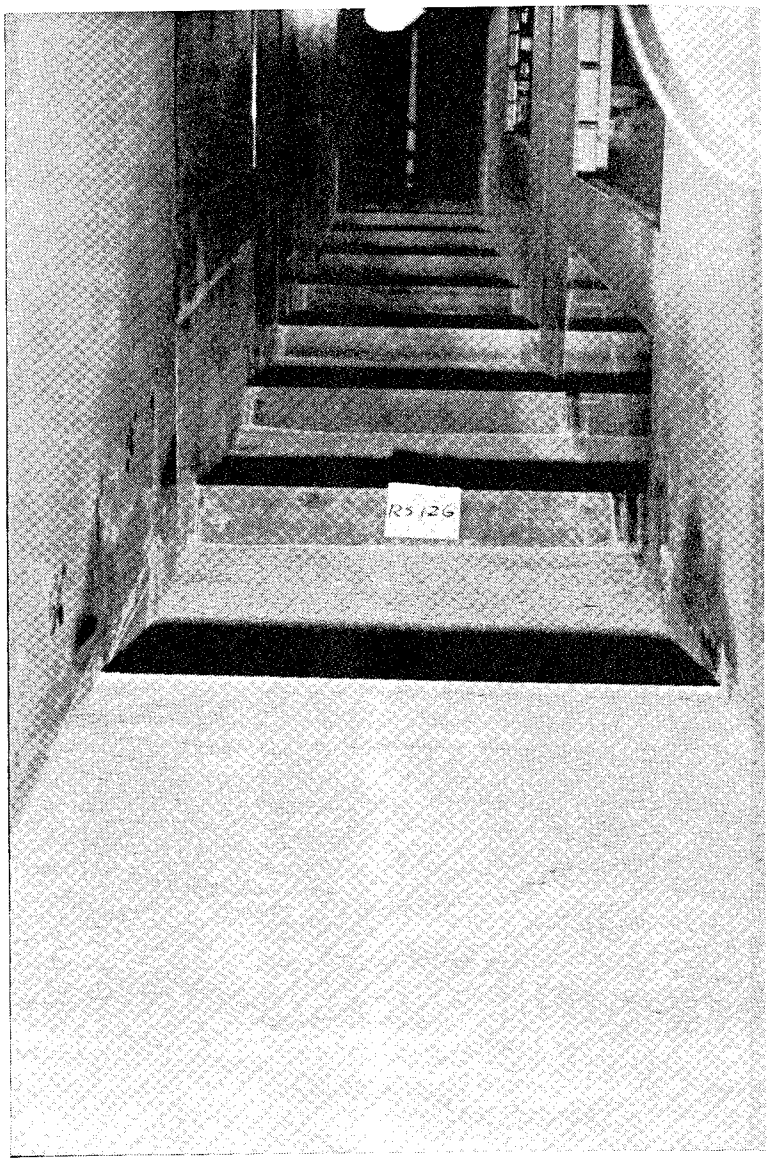

Figure A-12. Pre test photograph looking upstream of ridge dust bed: RS126, 116 fps, 2" elevation, 2' separation.

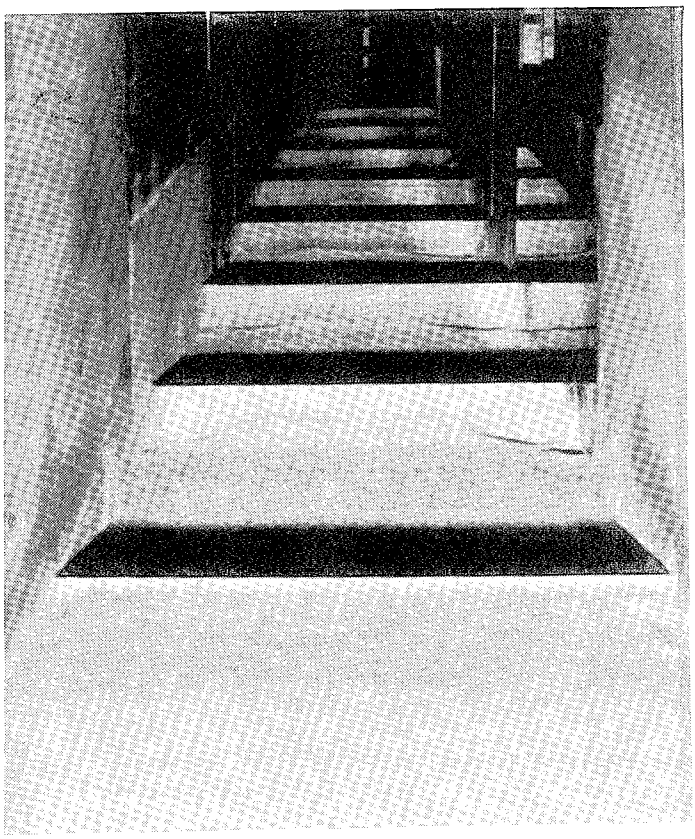

(a) Downstream view

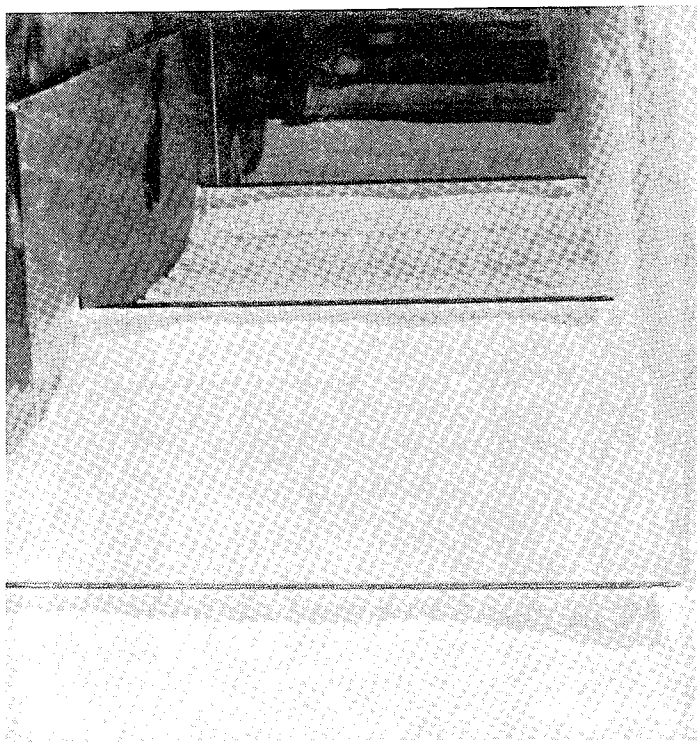

(b) Upstream view

Figure A-13. Post test photographs of ridge dust bed: RS126, 116 fps, 2" elevation, 2' separation.

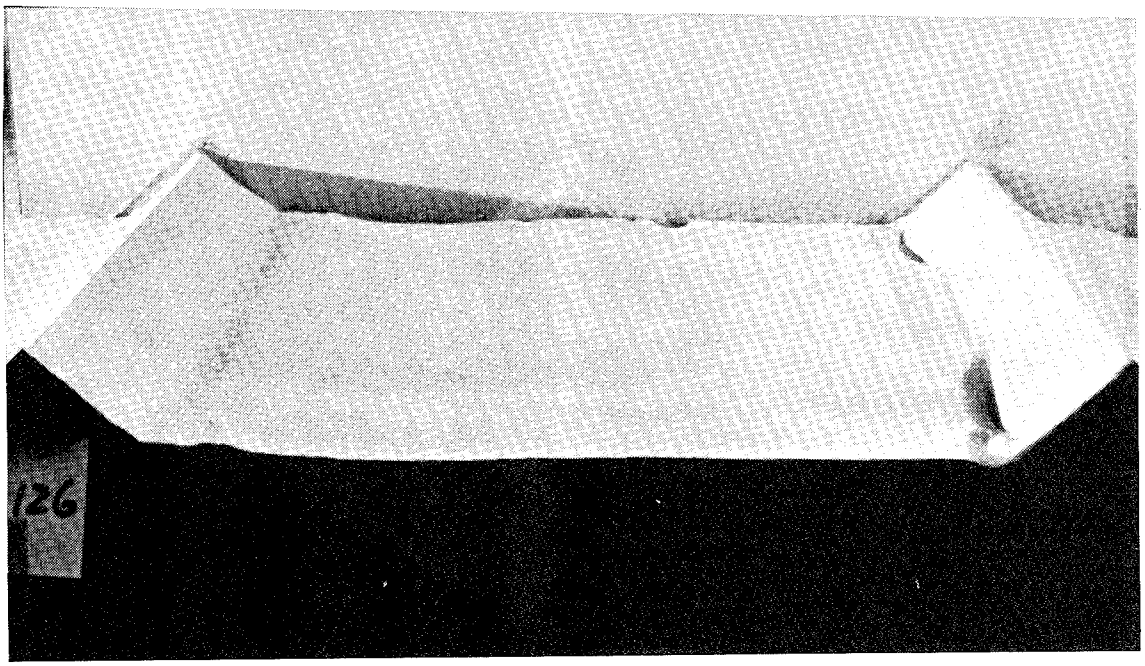

(a) Side view

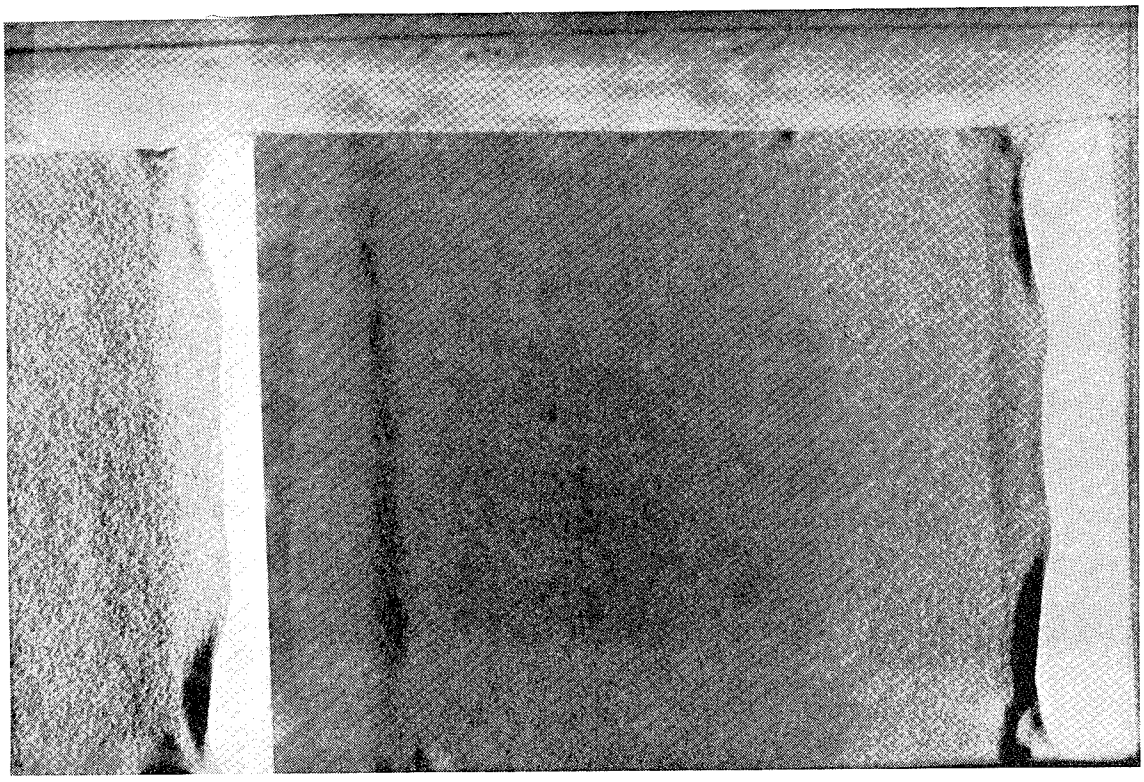

(b) Overhead view

Figure A-14. Post test photographs of ridge dust bed at 9' station: RS126, 116 fps, 2" elevation, 2' separation.

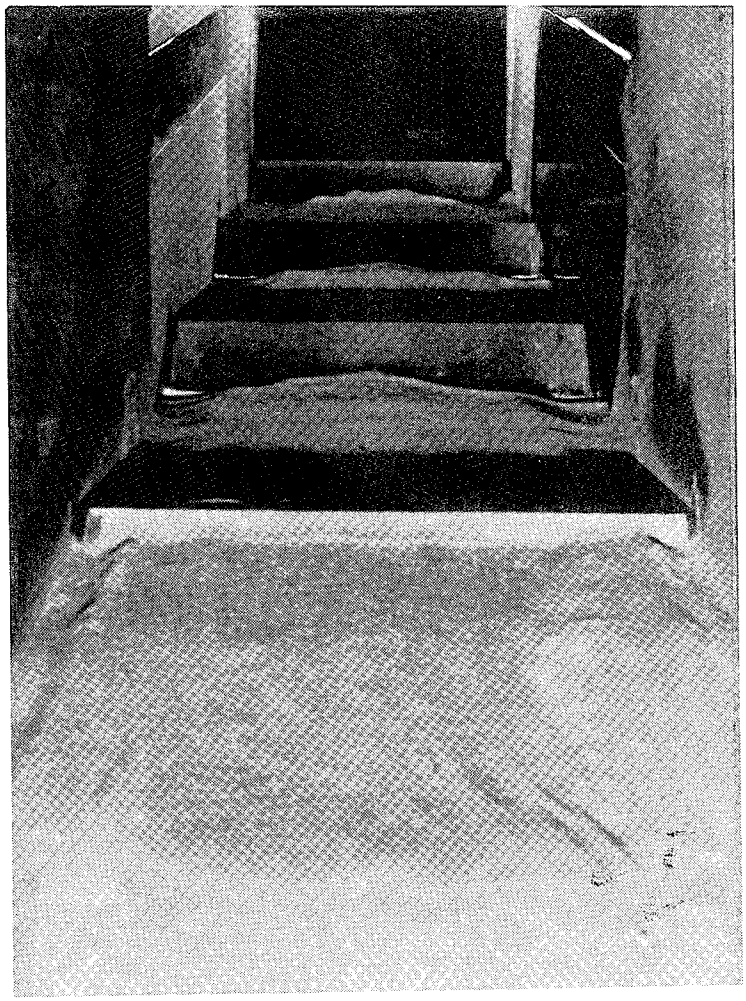

(a) Post test view

(b) Pre test view

Figure A-15. Photographs of ridge dust bed looking downstream: RS127, 238 fps, 2" elevation, 2' separation.

(a) Pre test side view

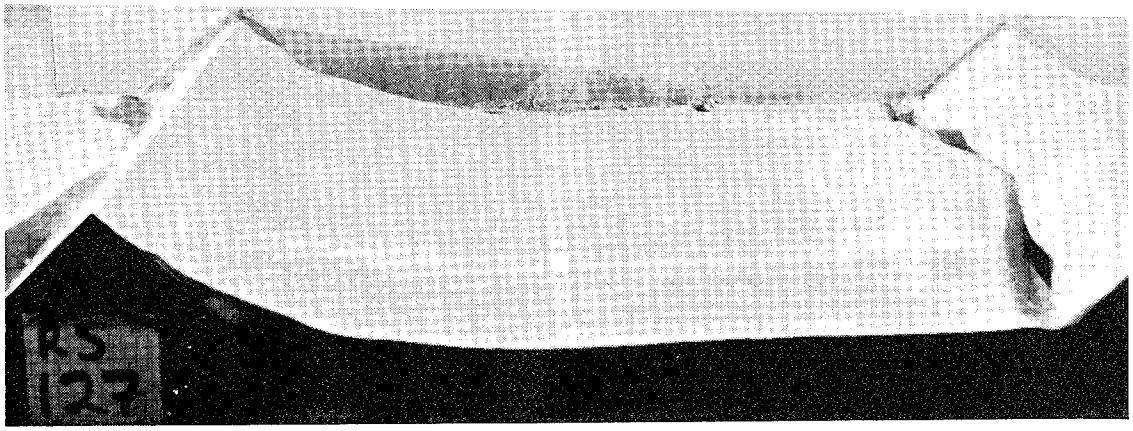

(b) Post test side view

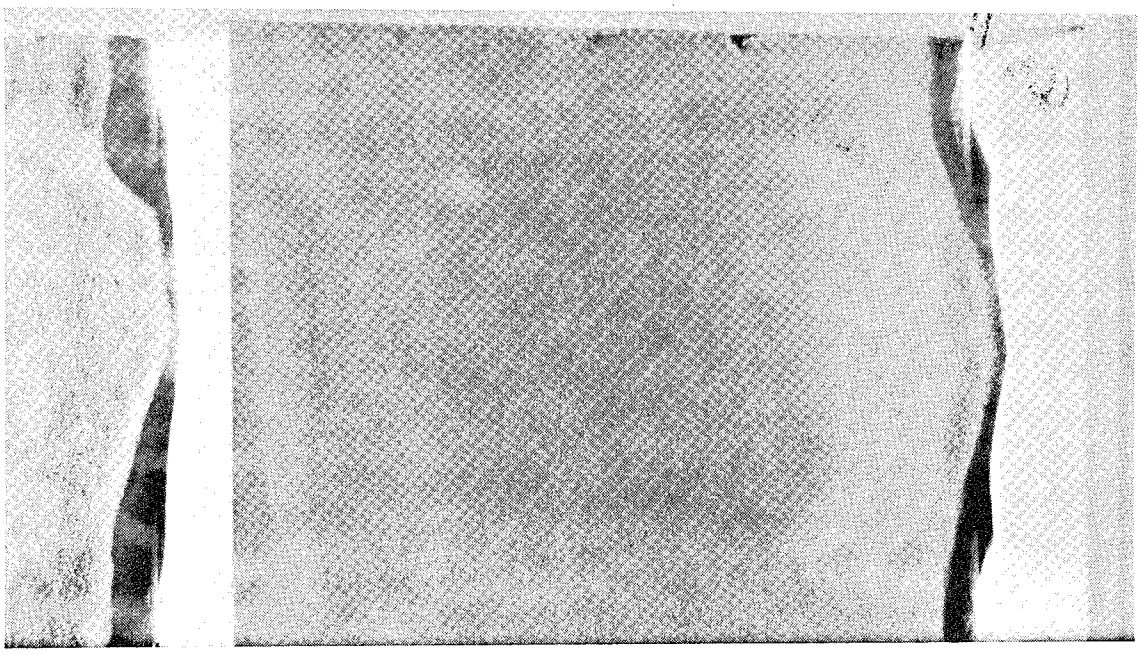

(c) Post test overhead view

Figure A-16. Photographs of ridge dust bed at 9' station: RS127, 238 fps, 2" elevation, 2' separation.

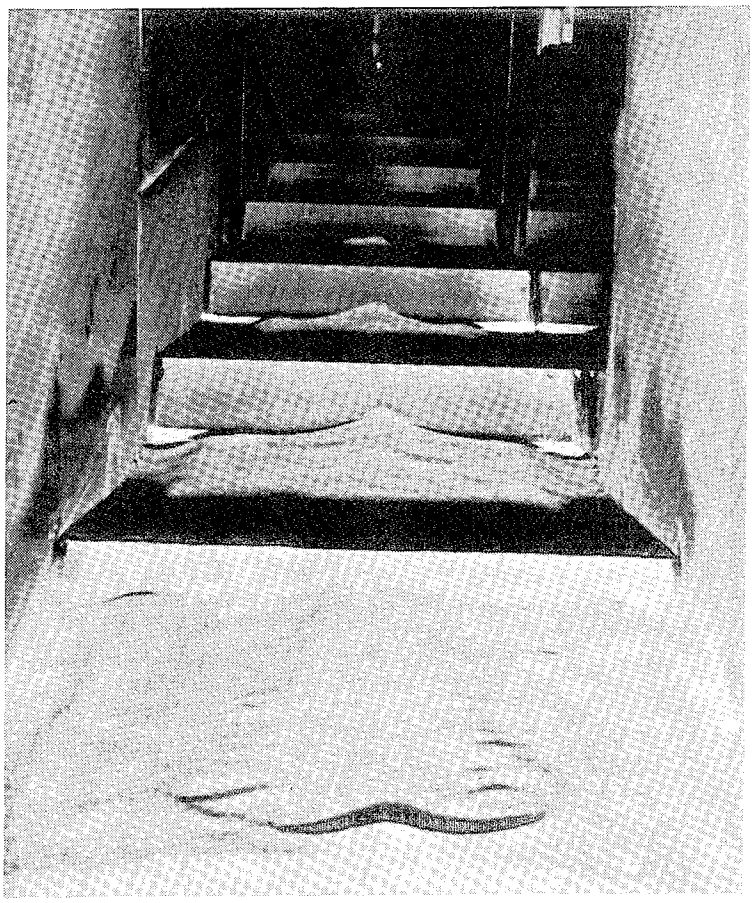

(a) Downstream view

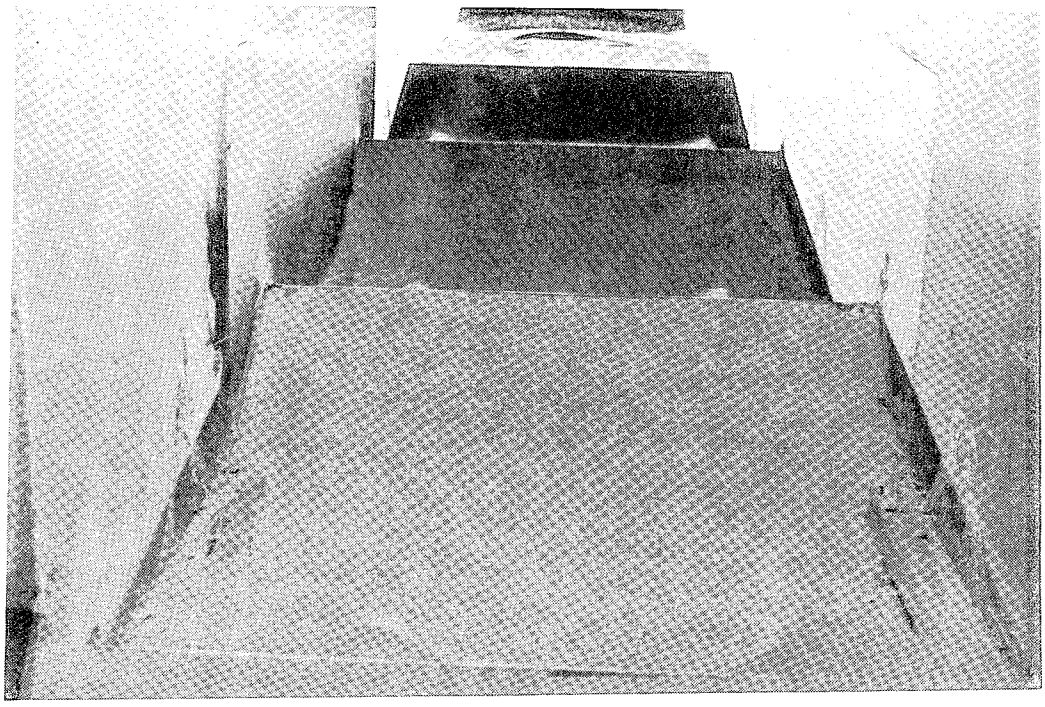

(b) Upstream view

Figure A-17. Post test photographs of ridge dust bed: RS131, 376 fps, 2" elevation, 2' separation.

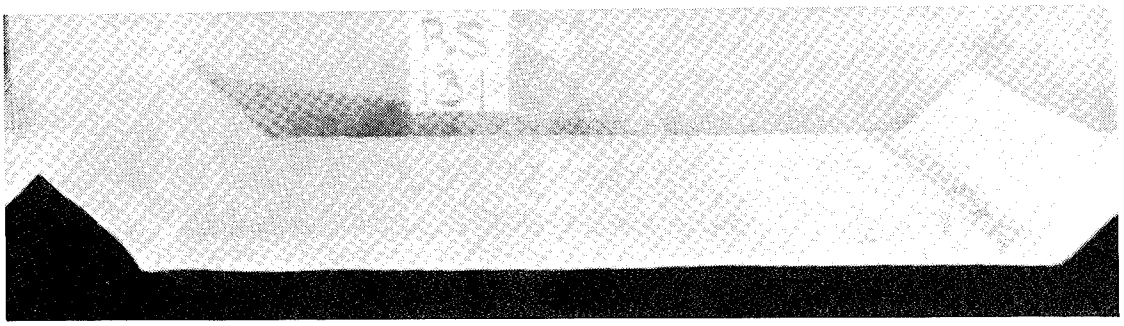

(a) Pre test side view

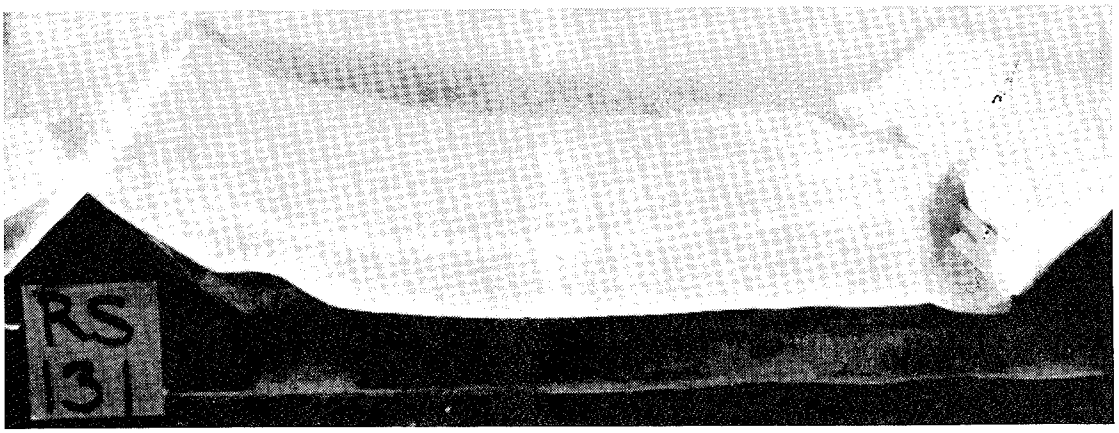

(b) Post test side view

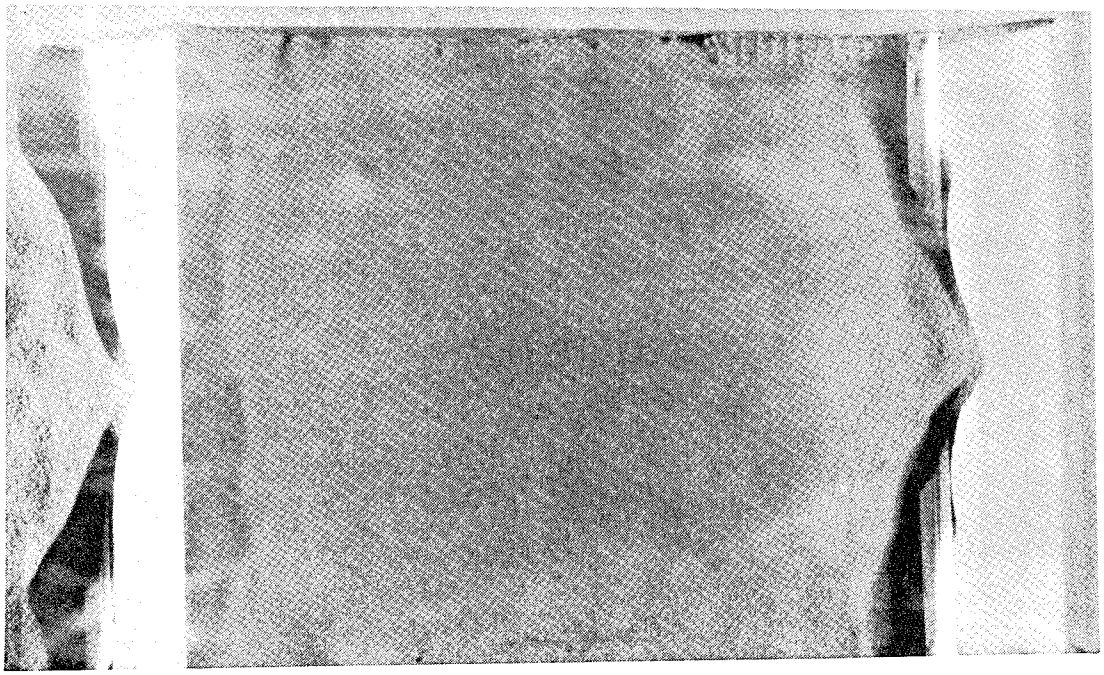

(c) Post test overhead view

Figure A-18. Photographs of ridge dust bed at 9' station: RS131, 376 fps, 2" elevation, 2' separation.

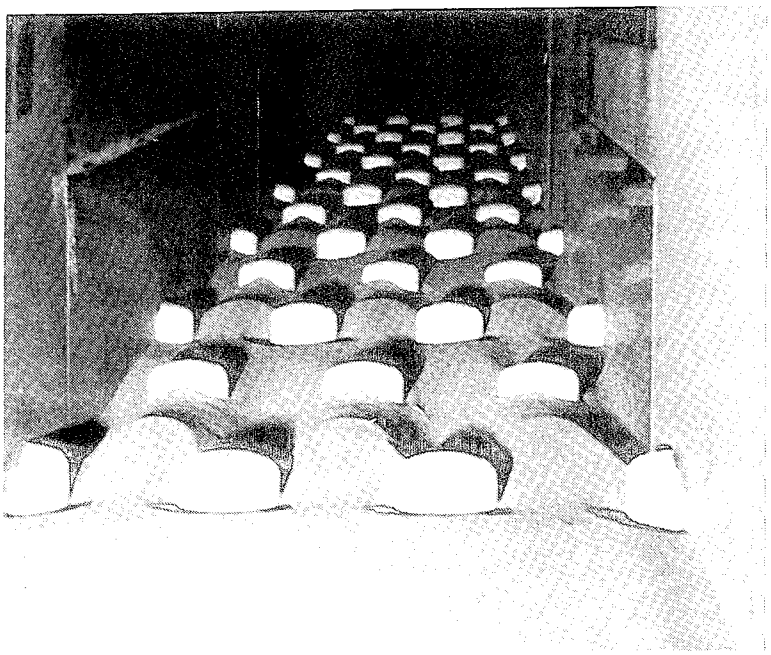

a) Downstream view

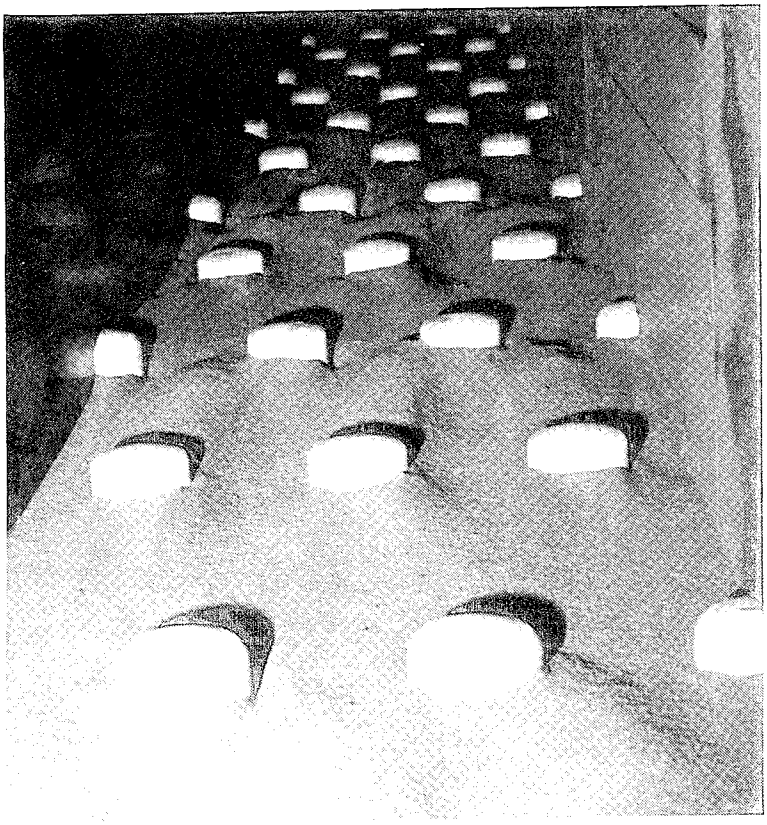

b) Upstream view

Figure A-19. Post test photographs of clod dust bed: RS 46, 120 fps, 1" elevation.

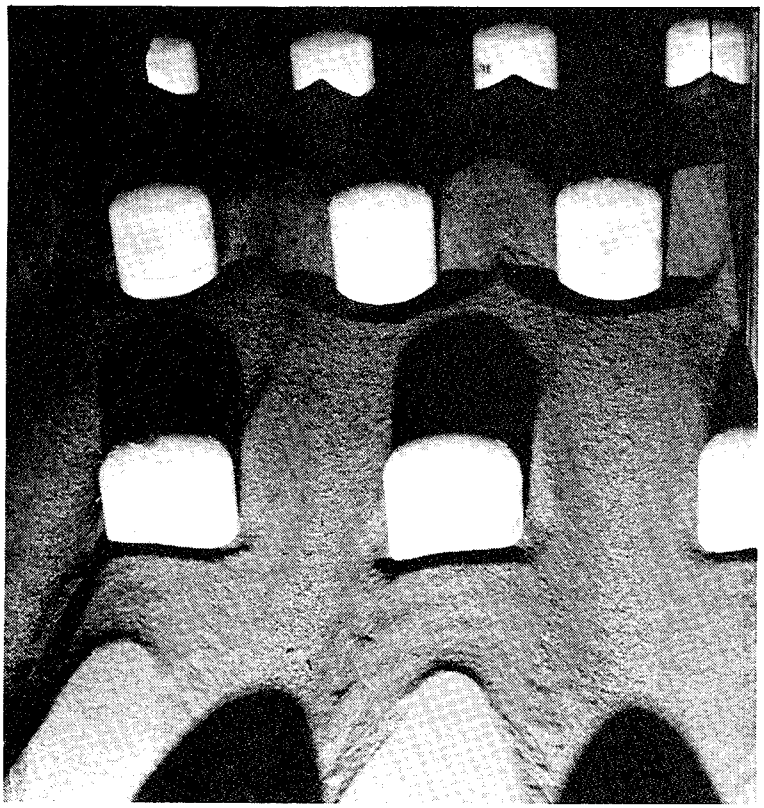

a) Downstream view

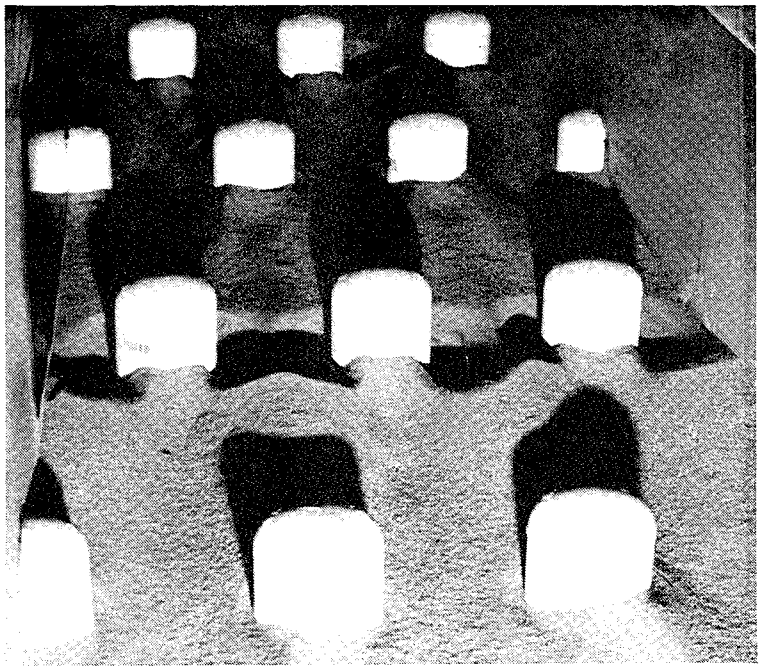

b) Upstream view

Figure A-20. Post test photographs of clod dust bed: RS 49, 127 fps, 2" elevation .

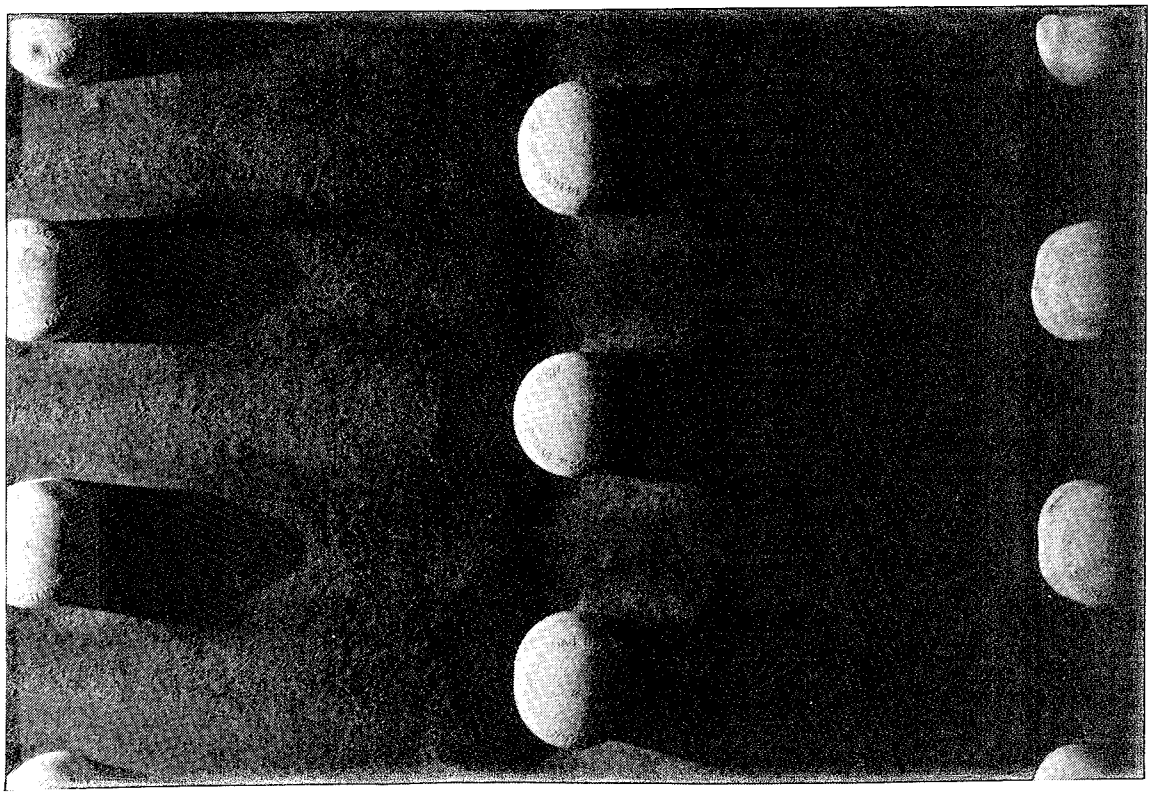

a) Overhead view

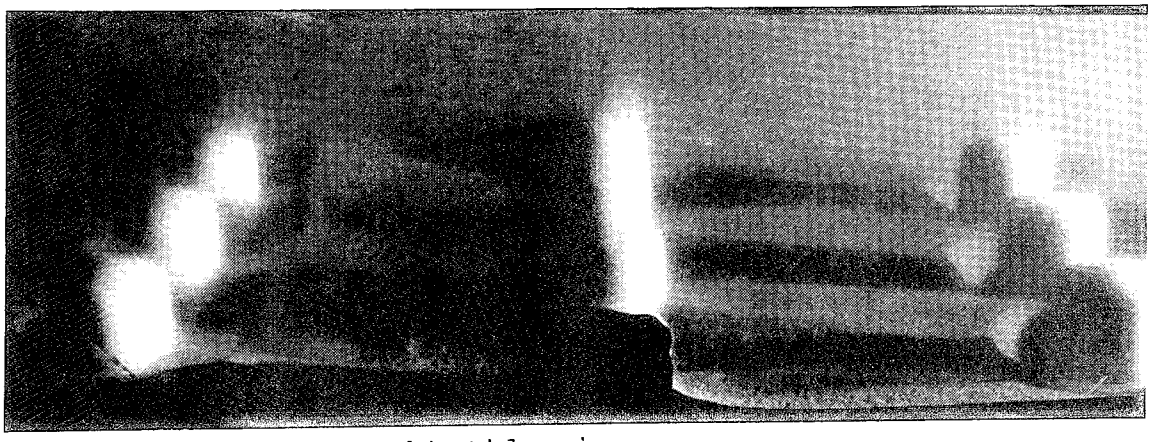

b) Side view

Figure A-21. Post test photographs of clod dust bed: RS 49, 127 fps, 2" elevation.

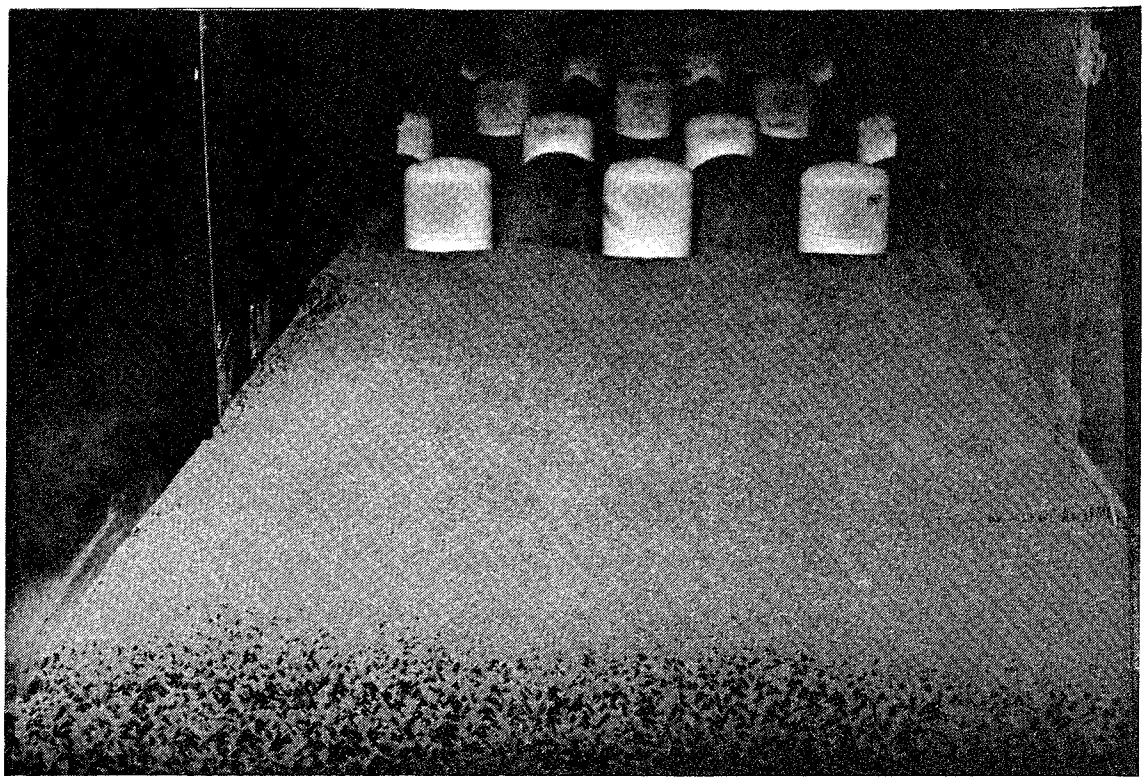

Figure A-22. Post test photograph of clod dust bed: RS 49, 127 fps, 2" elevation - Leading edge view looking downstream, 6' test section location.

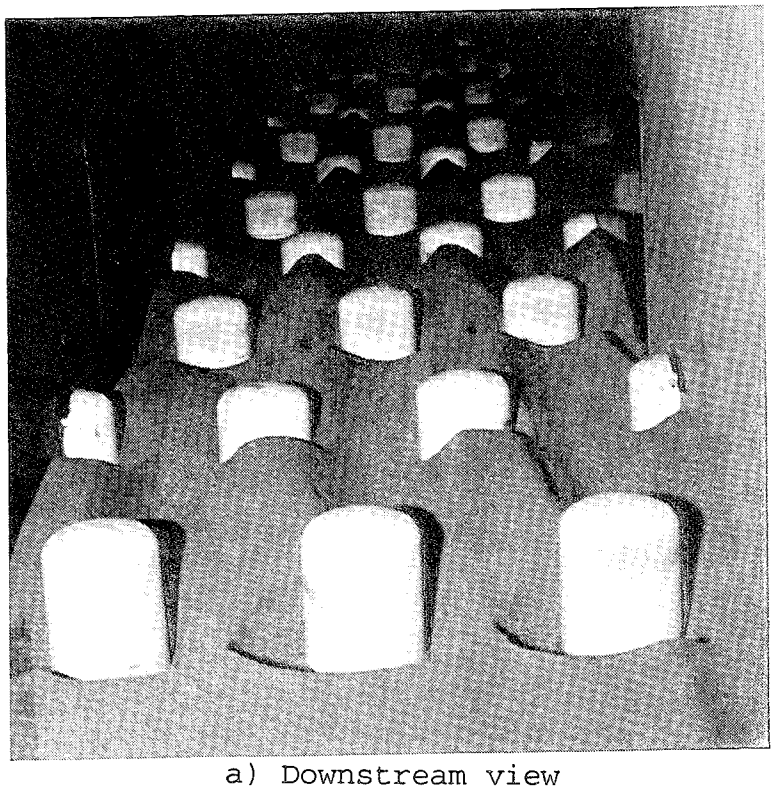

a) Downstream view

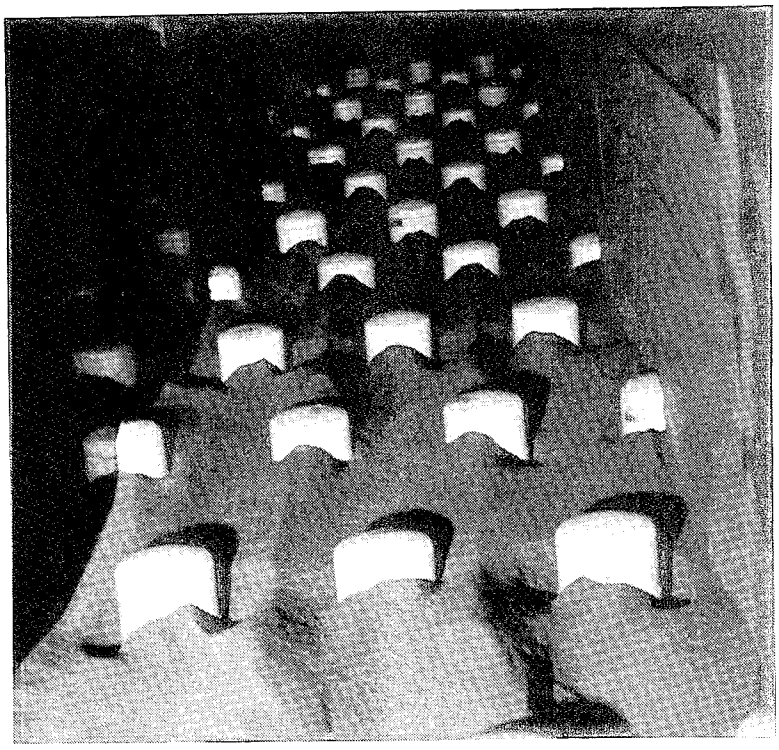

b) Upstream view

Figure A-23. Post test photographs of clod dust bed: RS 47, 234 fps, 1" elevation.

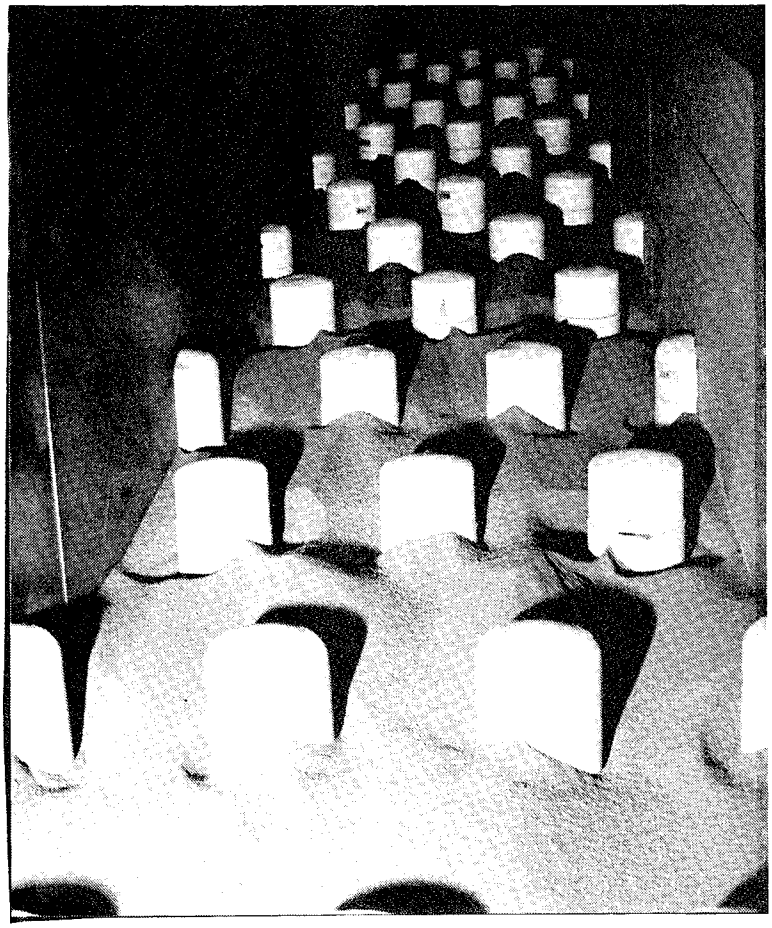

Figure A-24. Post test photograph of clod dust bed: RS 50, 222 fps, 2" elevation - Upstream view.

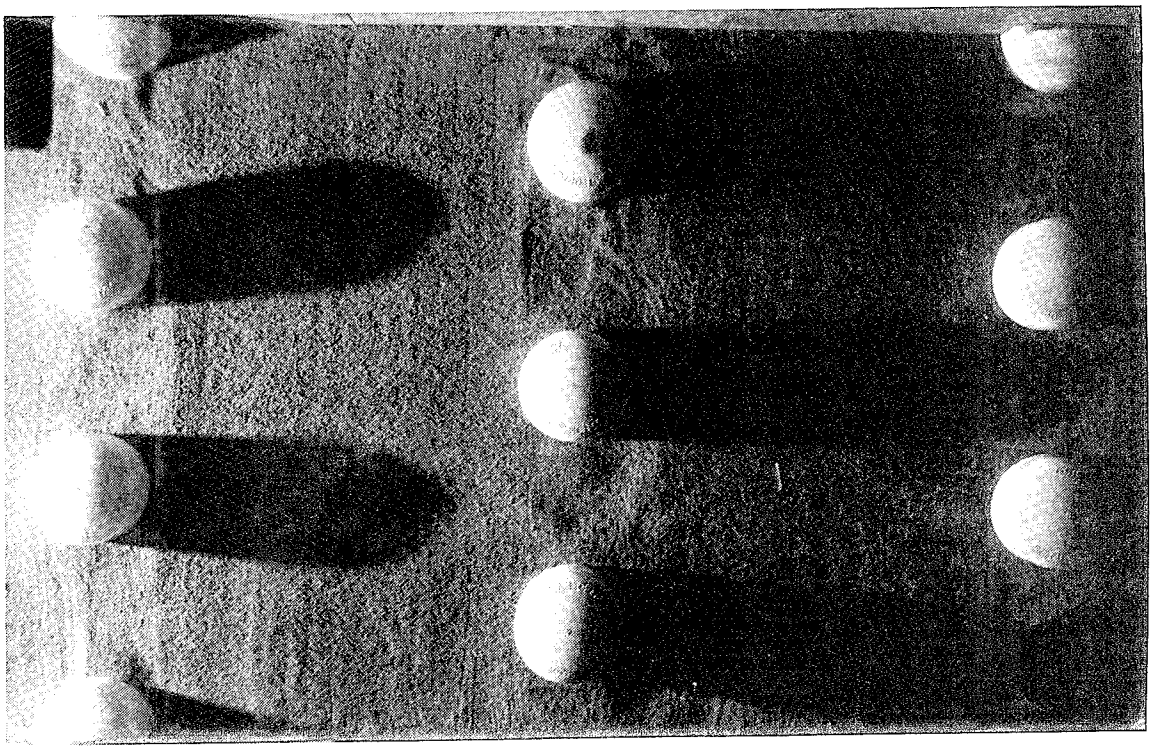

Figure A-25. Pre test close up photograph at 9' station of clod dust bed: RS50, 222 FPS, 2" elevation.

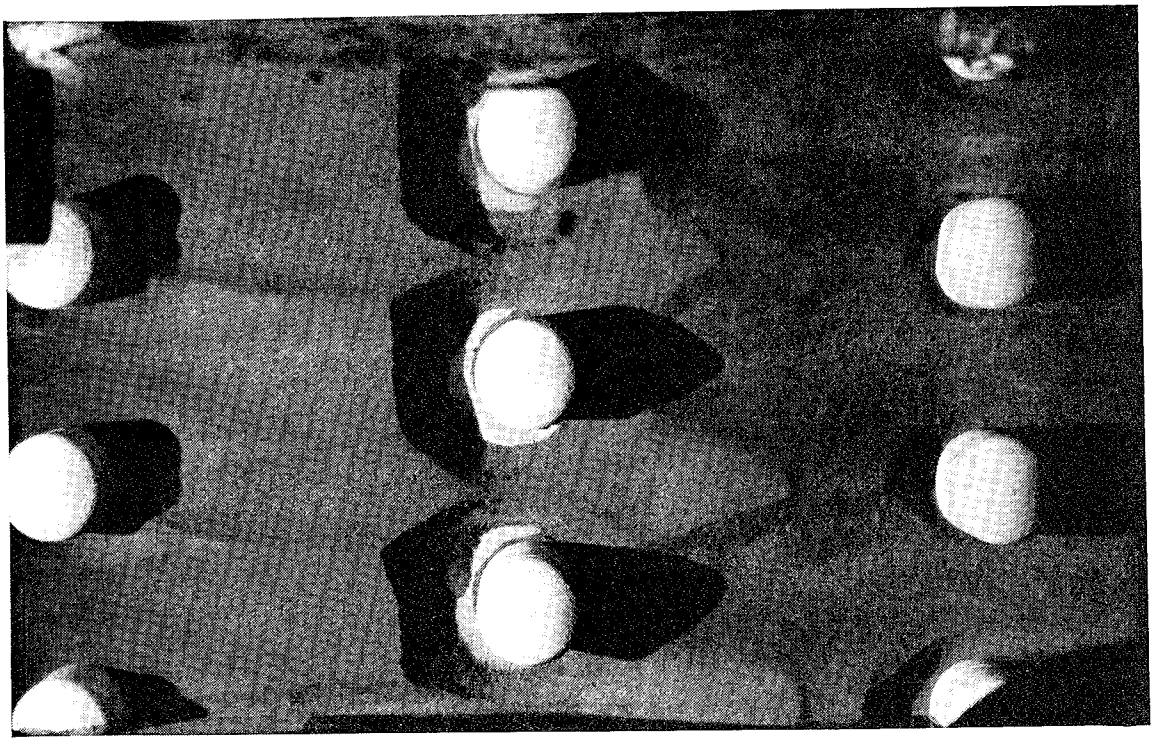

(a) Overhead view

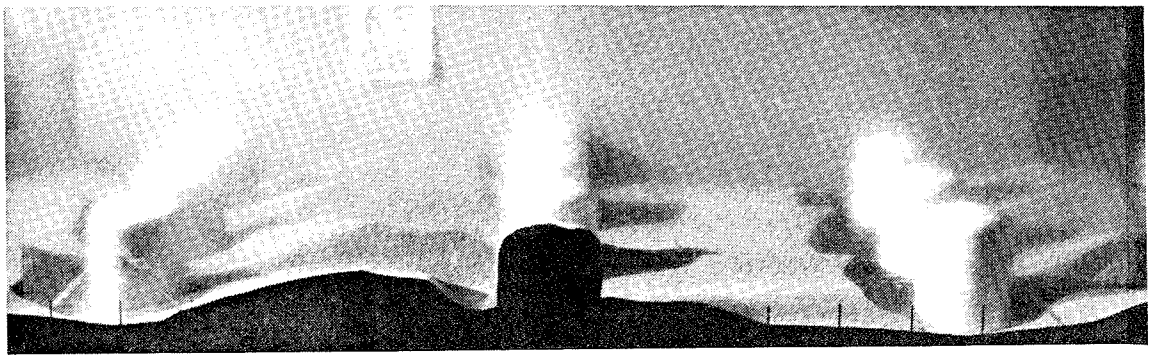

(b) Side view

Figure A-26. Post test photographs at 9' station of clod dust bed: RS50, 222 FPS, 2" elevation.

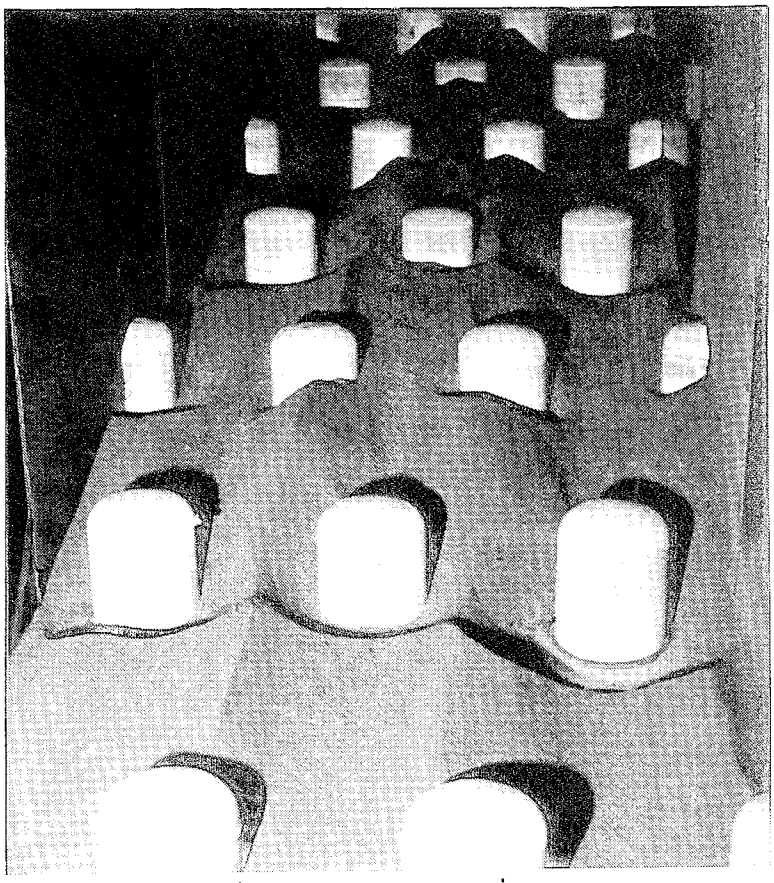

a) Downstream view

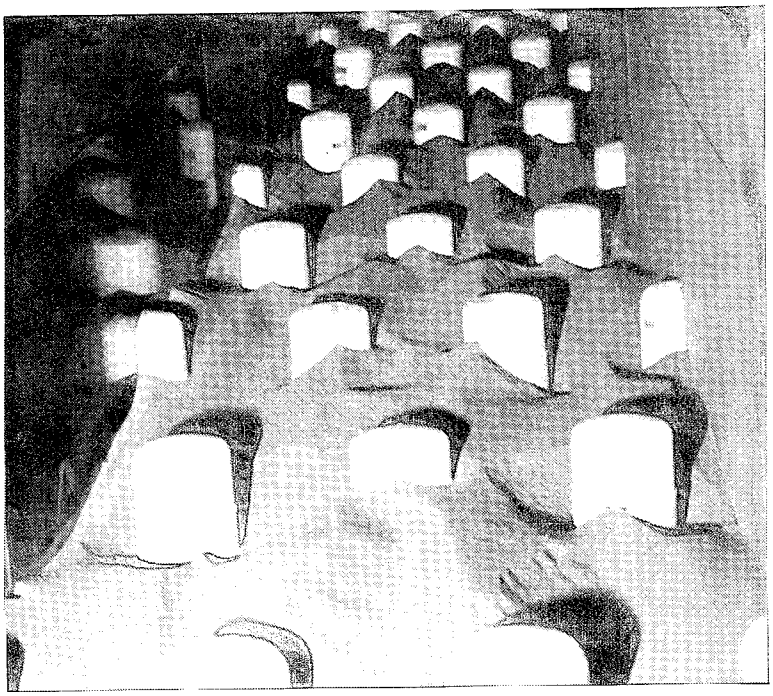

b) Upstream view

Figure A-27. Post test photographs of clod dust bed: RS 48, 361 fps, 1" elevation .

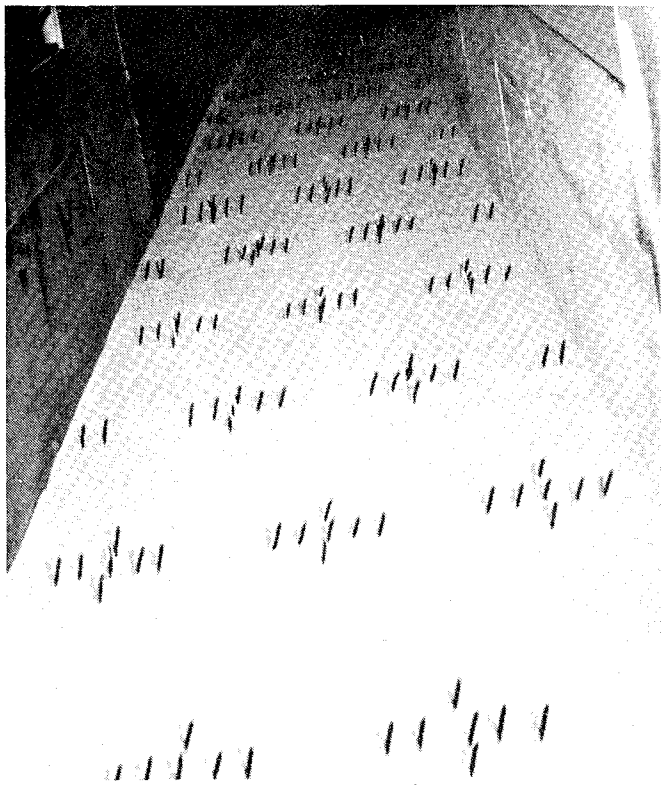

a) Pre test view

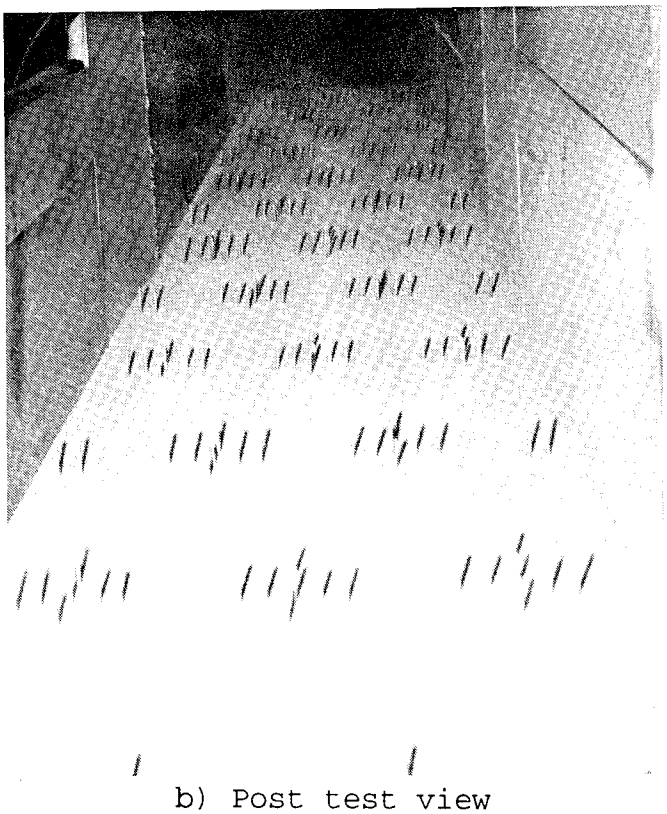

b) Post test view

Figure A-28. Photographs looking upstream of stubble dust bed: RS 58, 121 fps, 1" elevation .

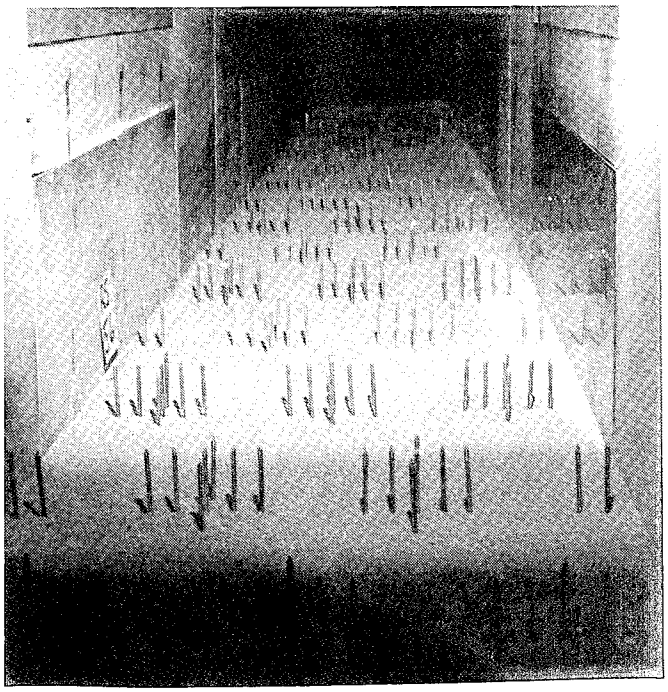

a) Pre test downstream view

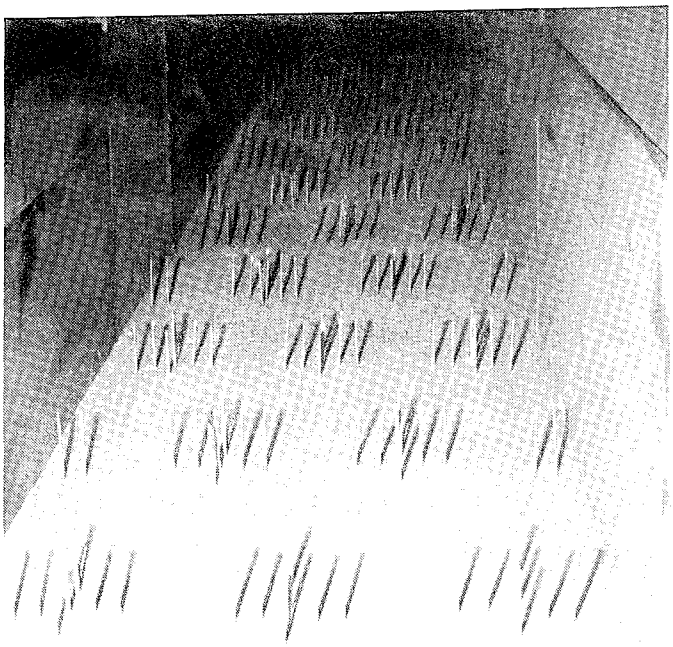

b) Post test upstream view

Figure A-29. Photographs of stubble dust bed: RS 56, 121 fps, 2" elevation .

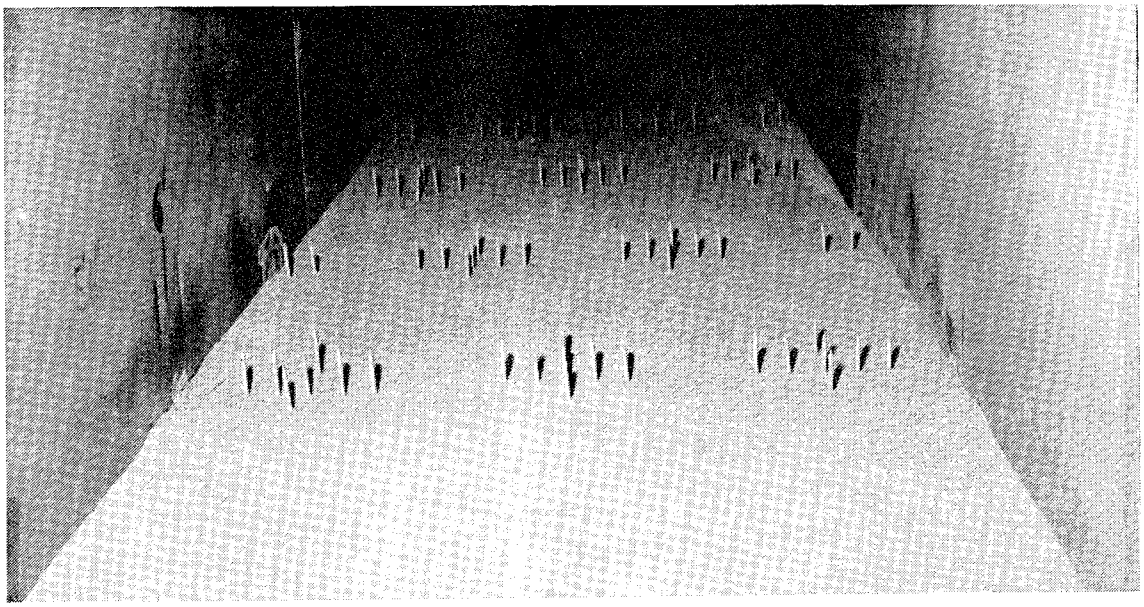

a) Pre test view

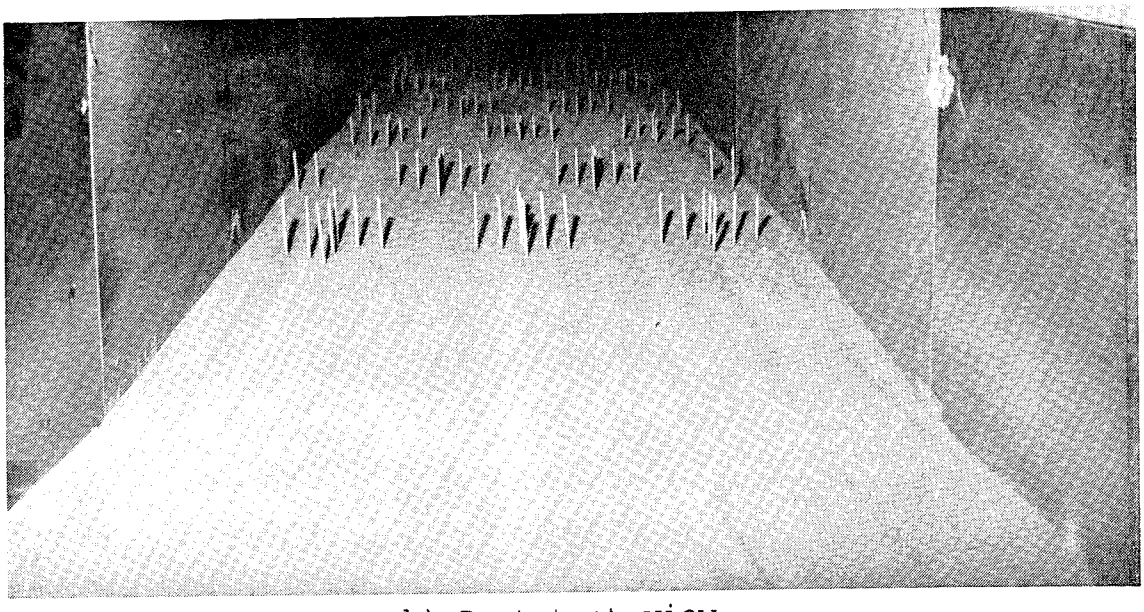

b) Post test view

Figure A-30. Photographs of stubble dust bed leading edge - 6' test section location: RS 59, 230 fps, 1" elevation.

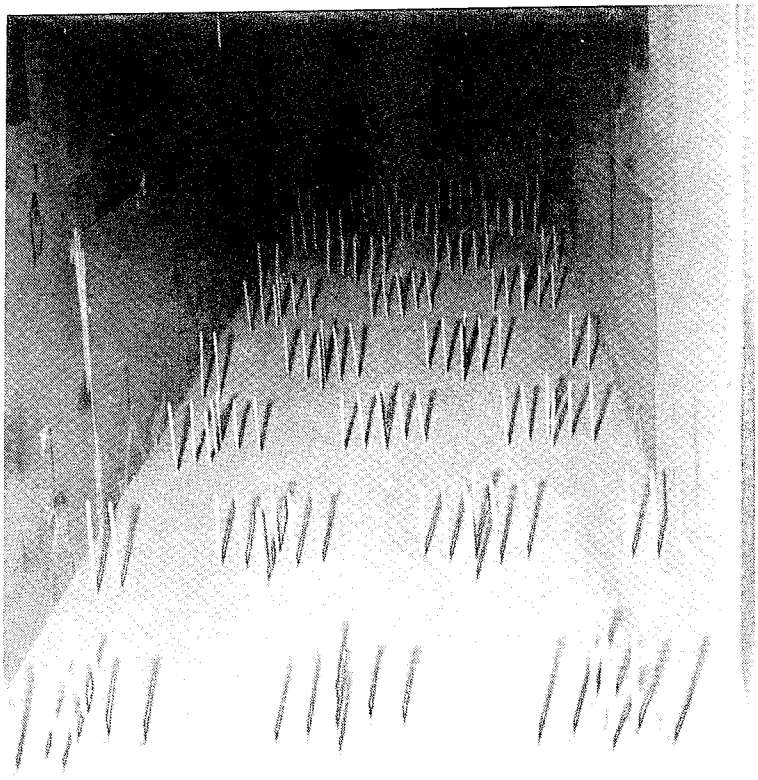

a) Post test downstream view

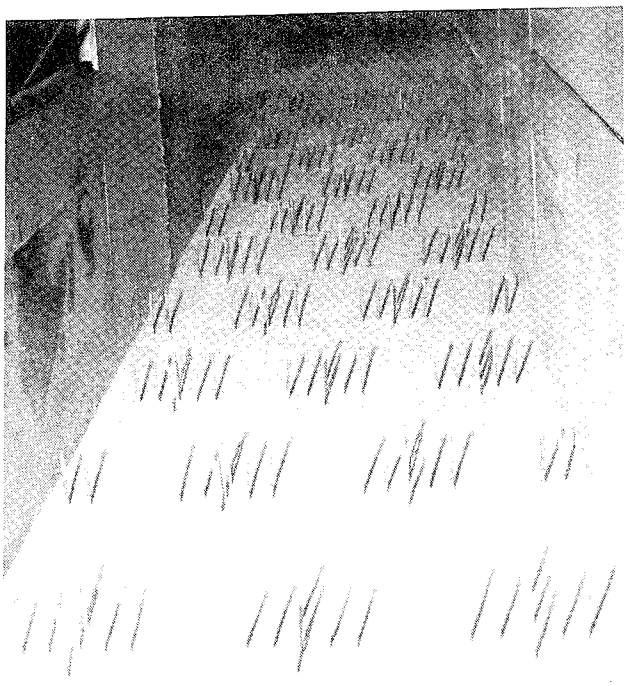

b) Pre test upstream view

c) Post test upstream view

Figure A-31. Photographs of stubble dust bed: RS 57, 231 fps, 2" elevation.

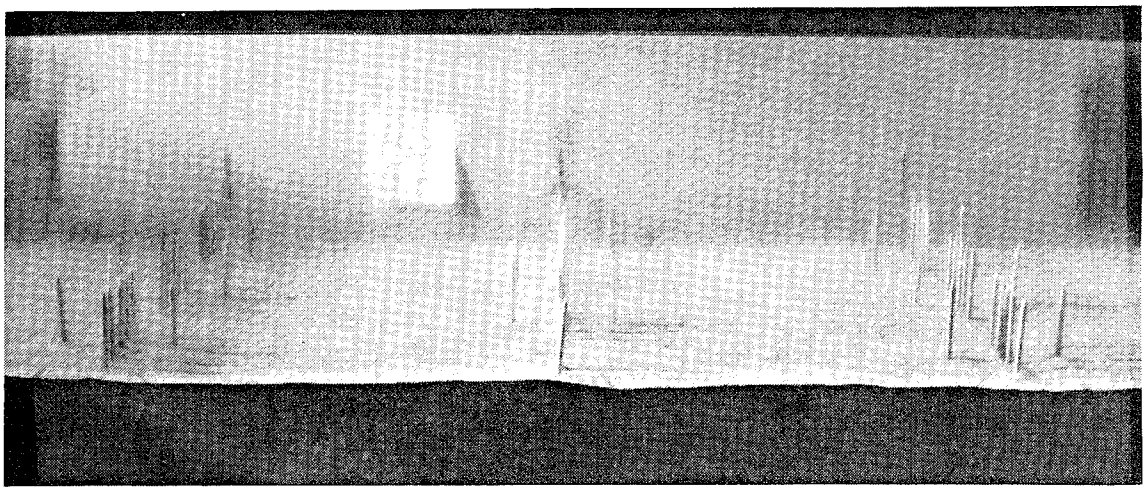

a) Pre test view

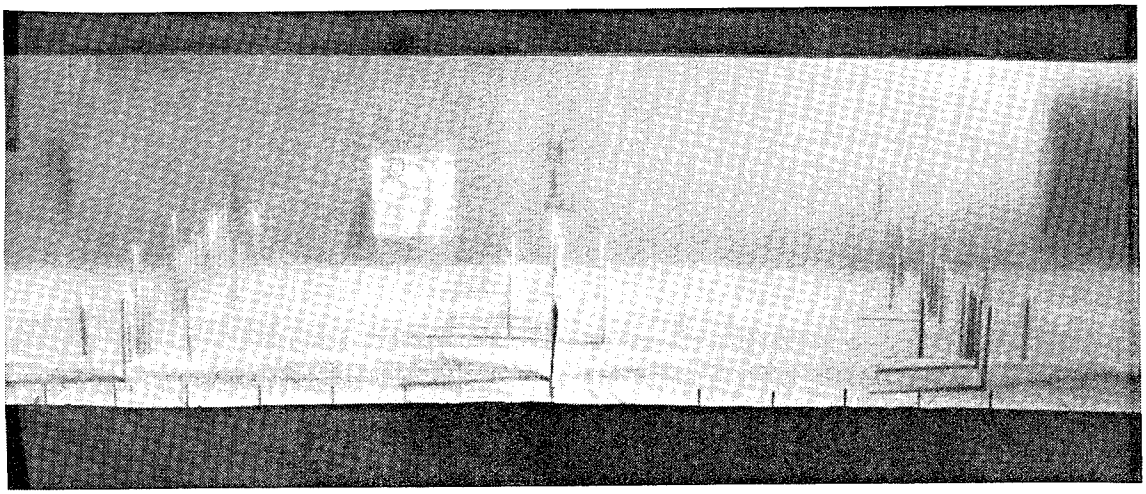

b) Post test view

Figure A-32. Side view photographs at 9' test section location of stubble dust bed: RS 57, 231 fps, 2" elevation.

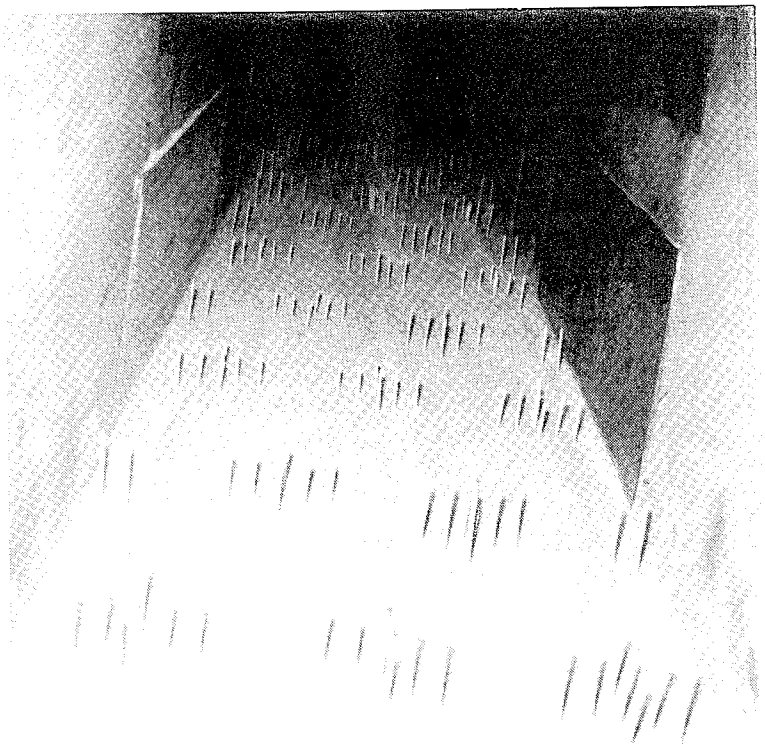

a) Downstream view

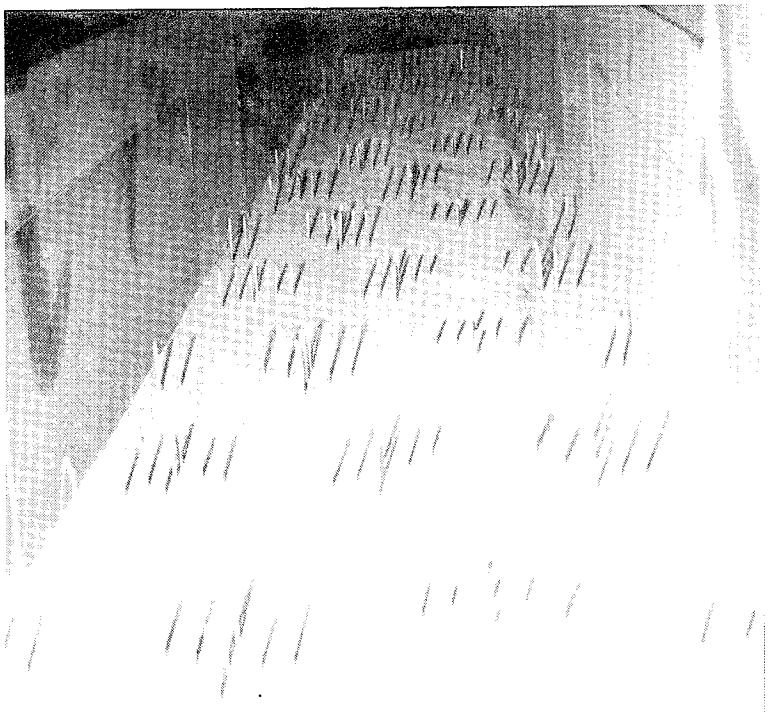

b) Upstream view

Figure A-33. Post test photographs of stubble dust bed: RS 60, 335 fps, 1" elevation .

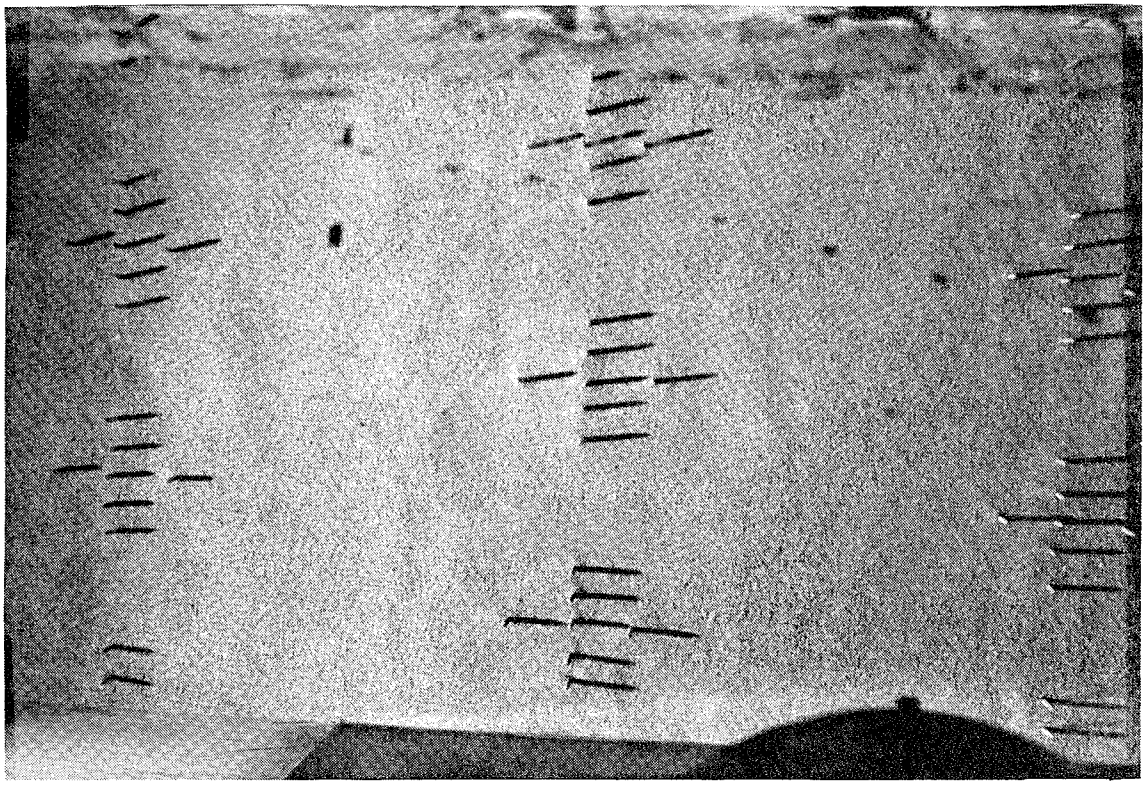

a) Pre test view

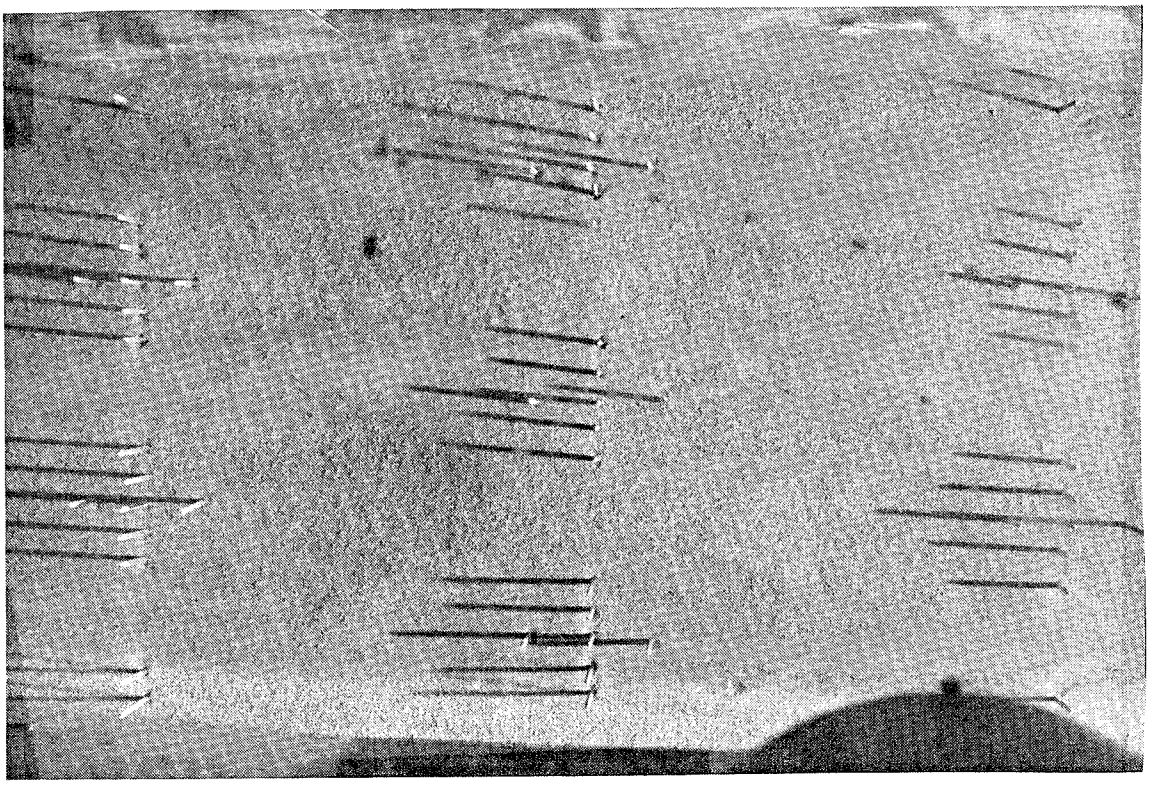

b) Post test view

Figure A-34. Overhead view photographs at 9' test section location of stubble dust bed: RS 60, 335 fps, 1" elevation.

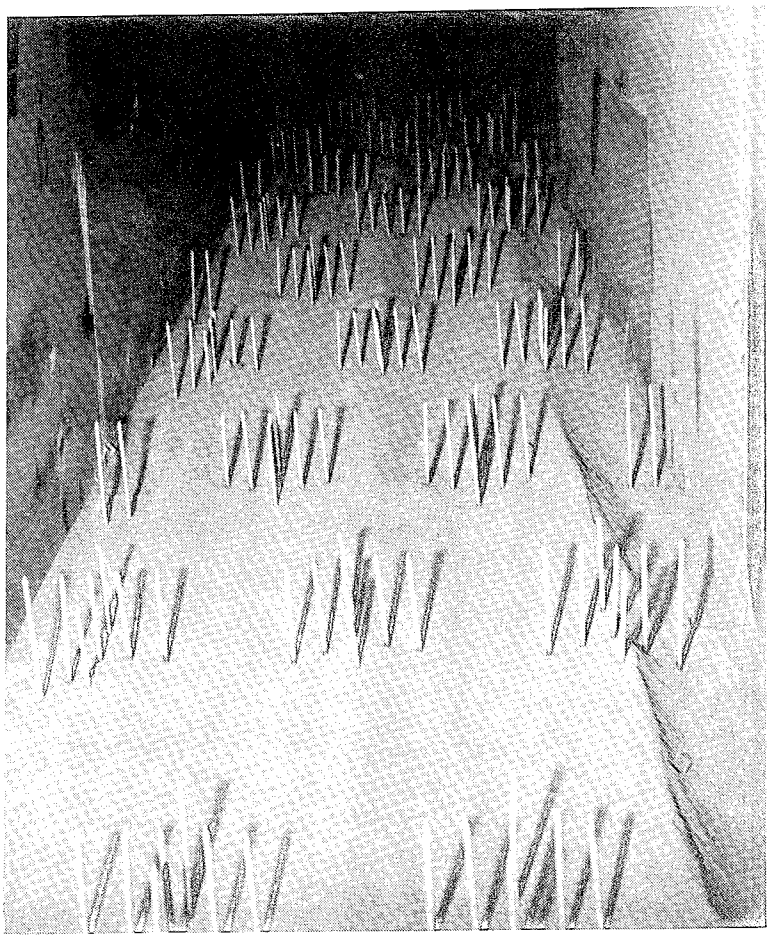

a) Downstream view

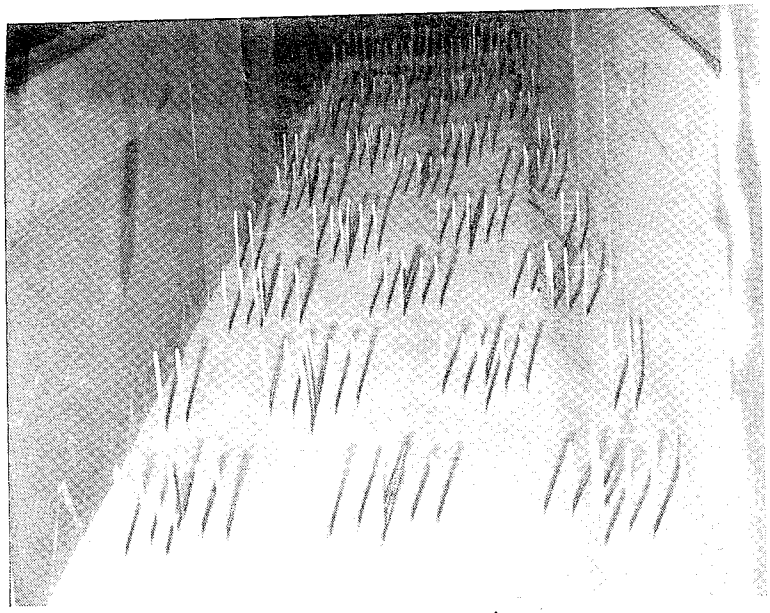

b) Upstream view

Figure A-35. Post test photographs of stubble dust bed: RS 61, 356 fps, 2" elevation.

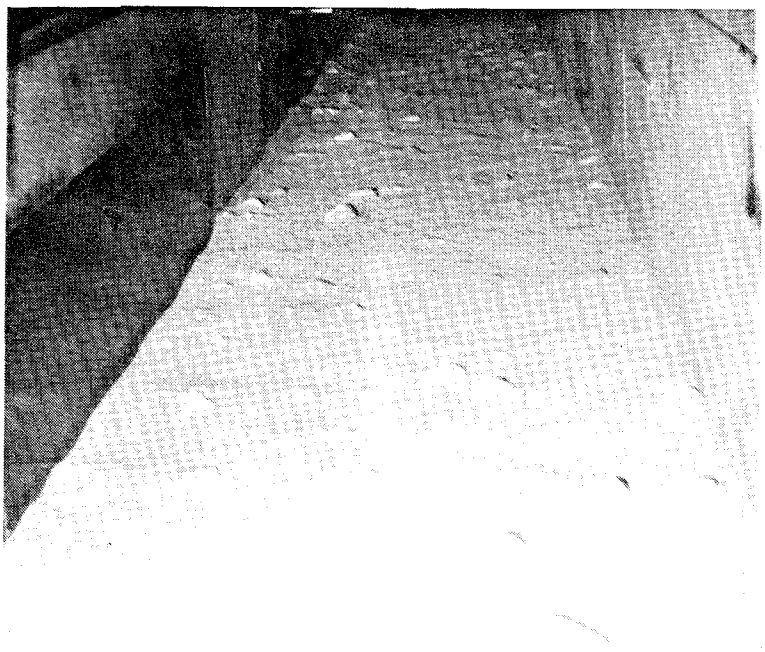

a) Pre test

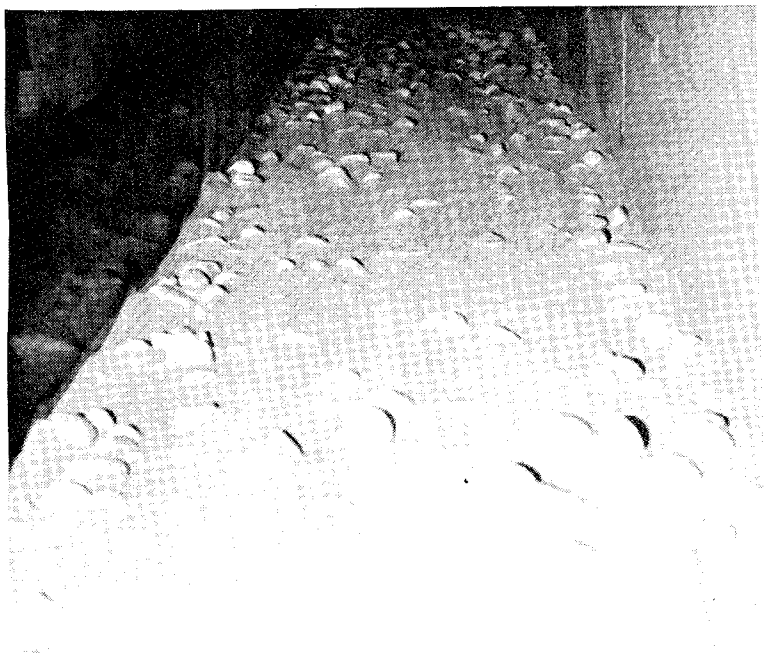

b) Post test

Figure A-36. Upstream view photographs of Gravel Seeded WSMR dust bed: RS 70, 130 fps.

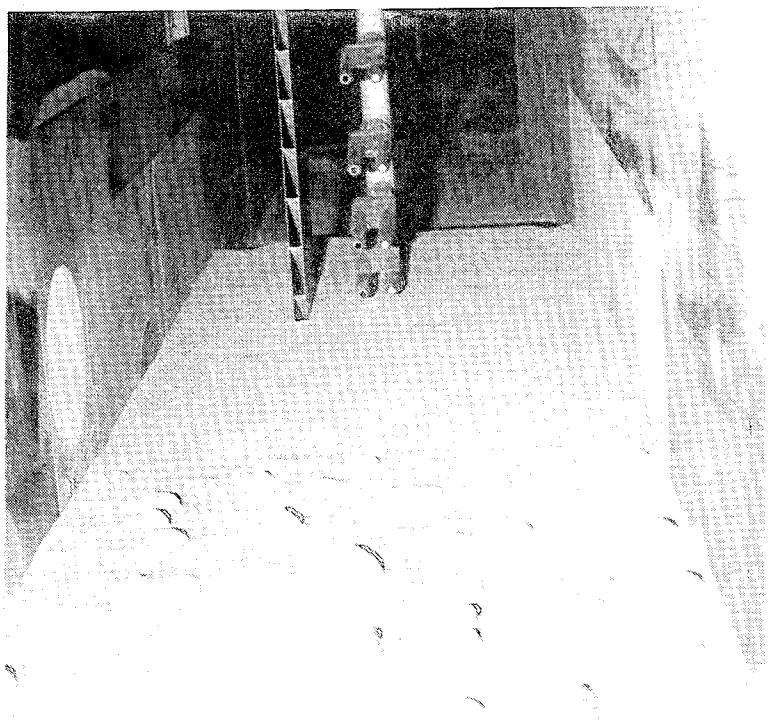

a) Pre test

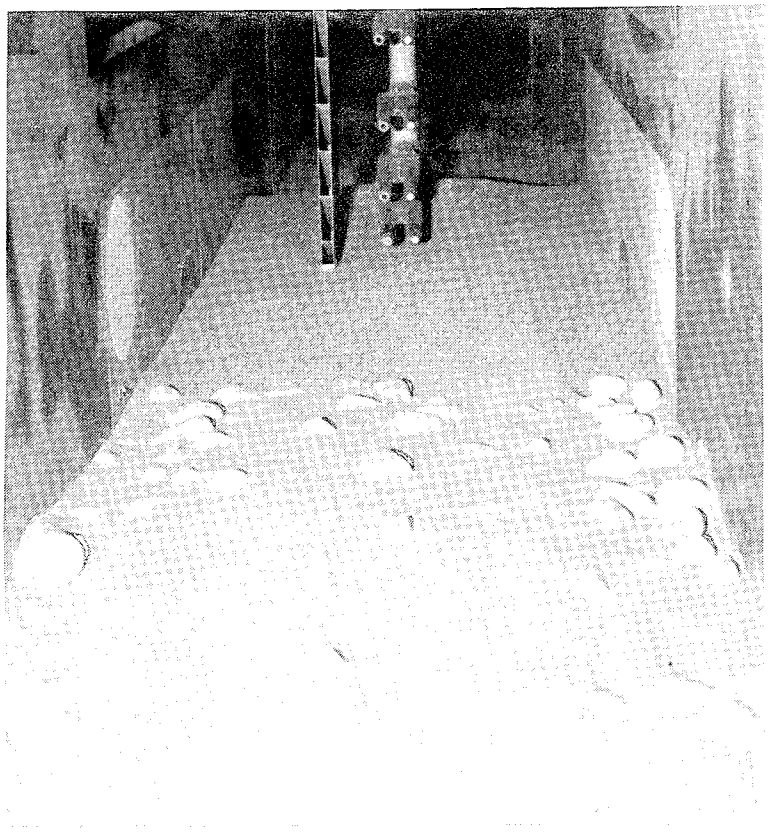

b) Post test

Figure A-37. Downstream view photographs of Gravel Seeded WSMR dust bed at diagnostics station: RS 70, 130 fps.

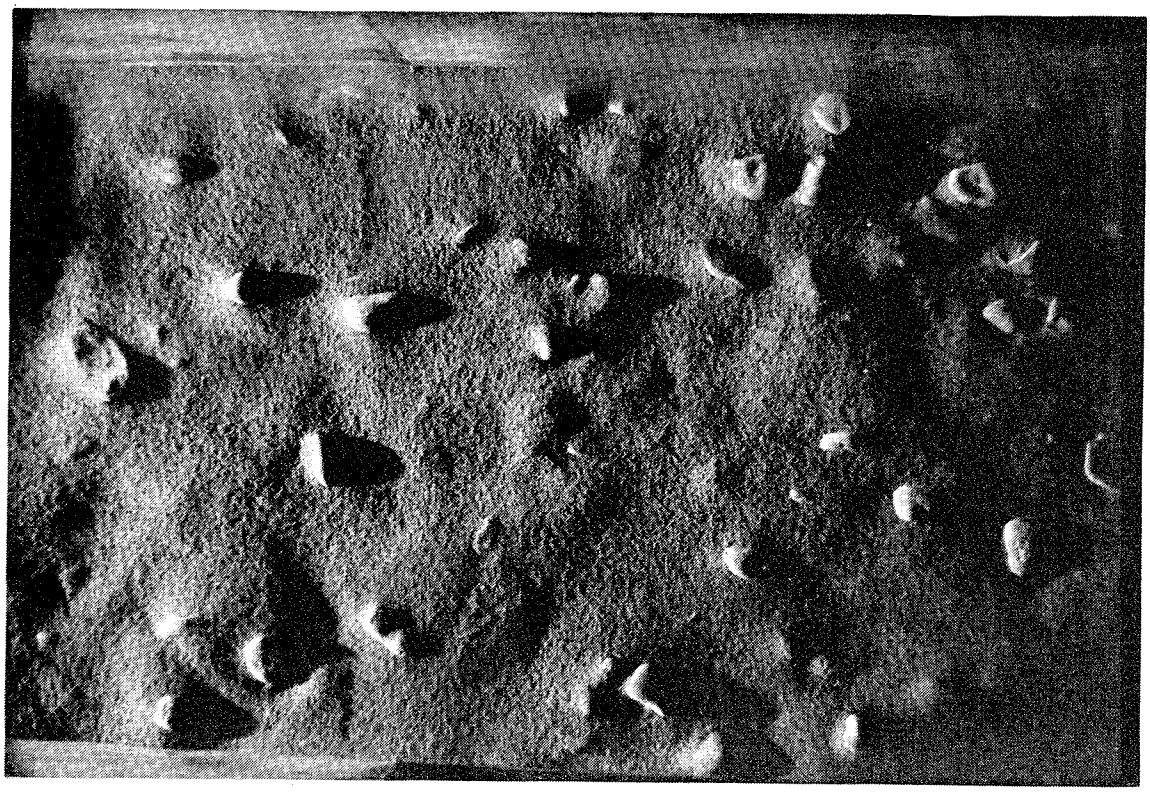

a) Pre test,

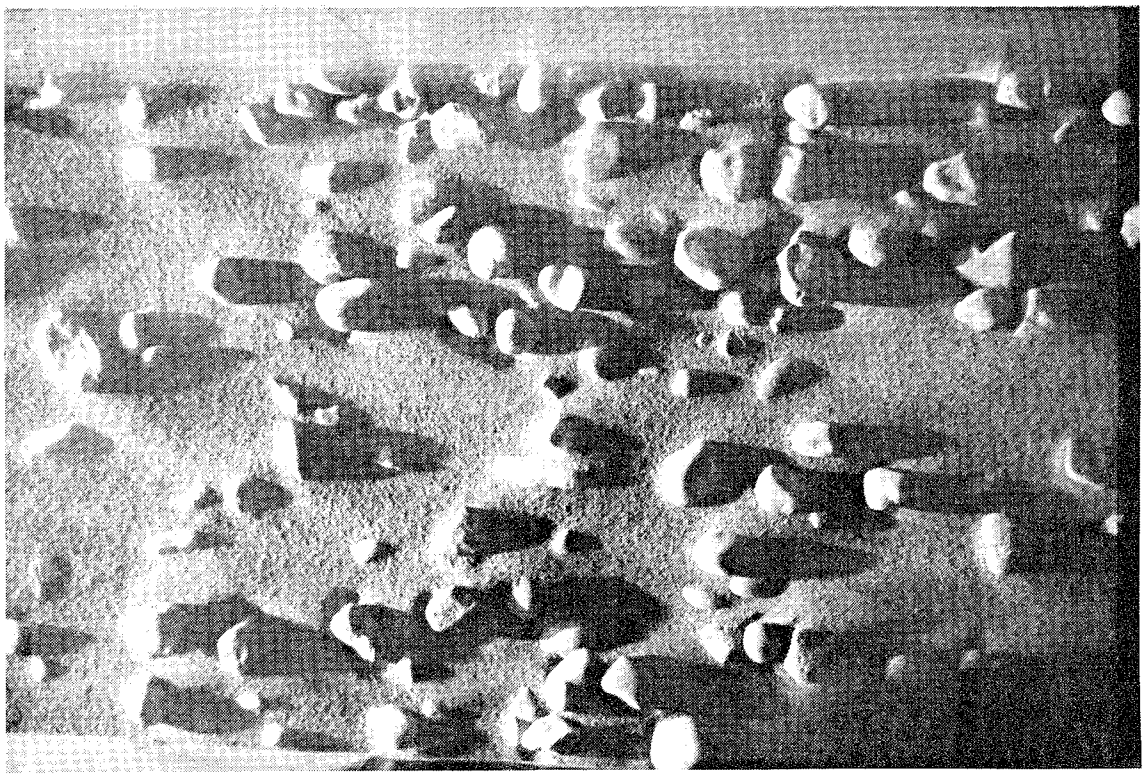

b) Post test

Figure A-38. Overhead view photographs of Gravel Seeded WSMR dust bed at 9' location: RS 70, 130 fps.

Figure A-39. Post test photograph of Gravel Seeded WSMR dust bed: RS 70, 130 fps - Overhead view at 9' location looking upstream.

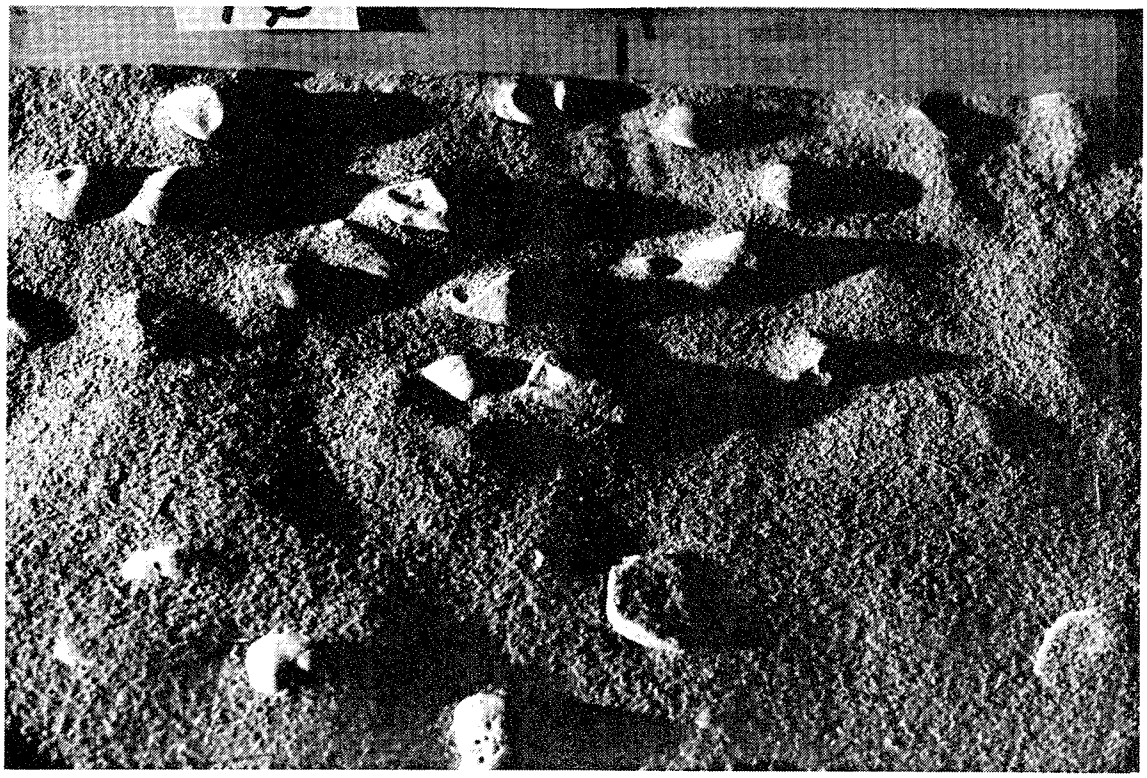

a) Pre test

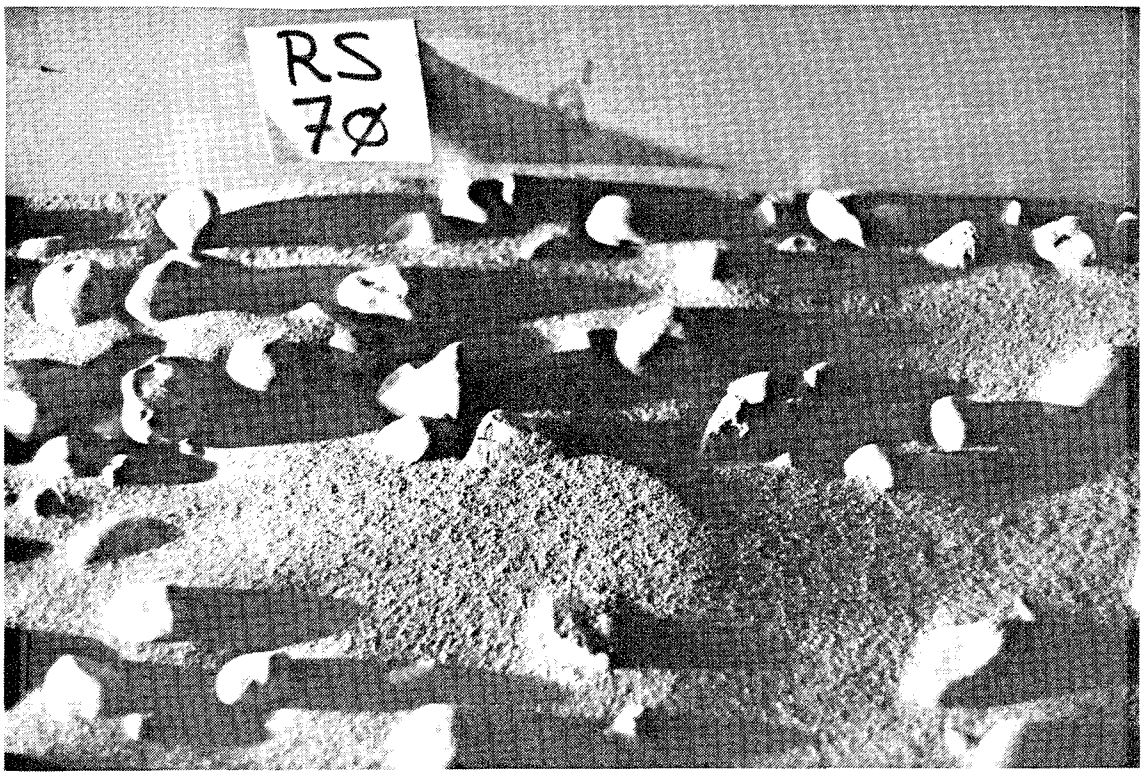

b) Post test

Figure A-40. Overhead close up view photographs of Gravel Seeded WSMR dust bed at 9' location: RS 70, 130 fps.

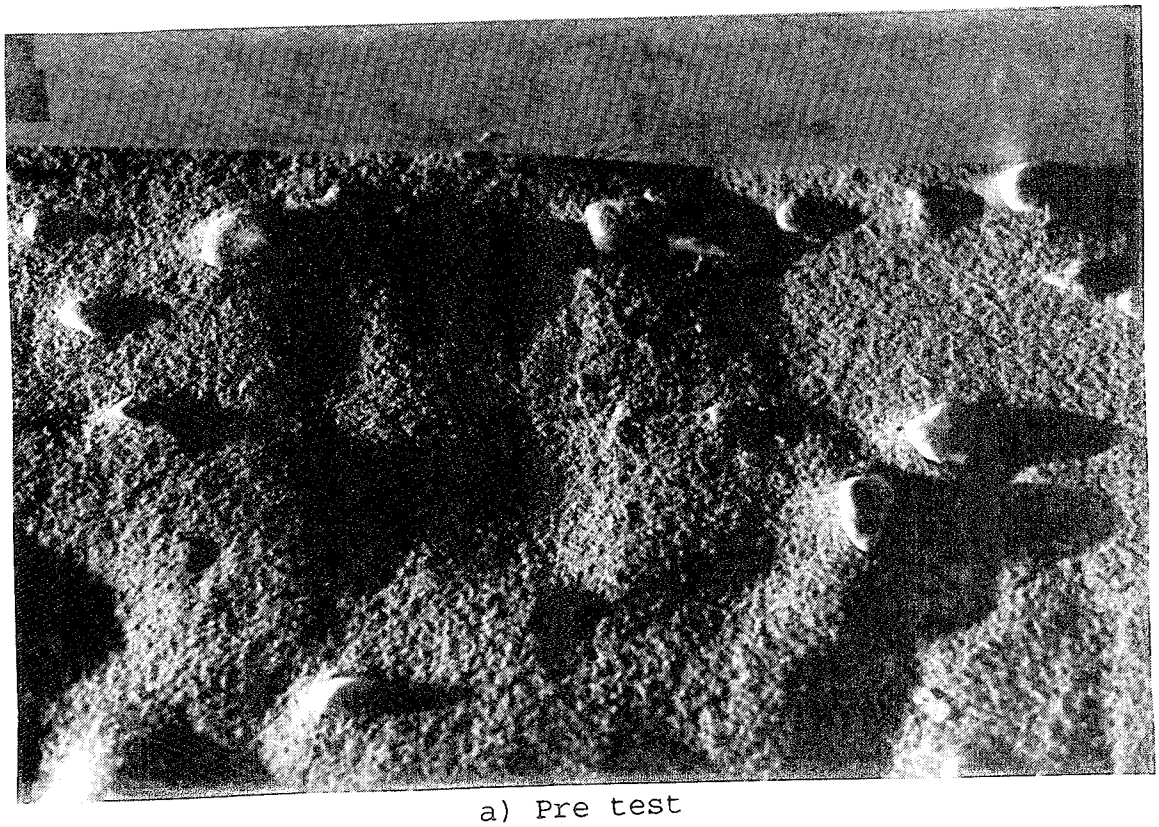

a) Pre test

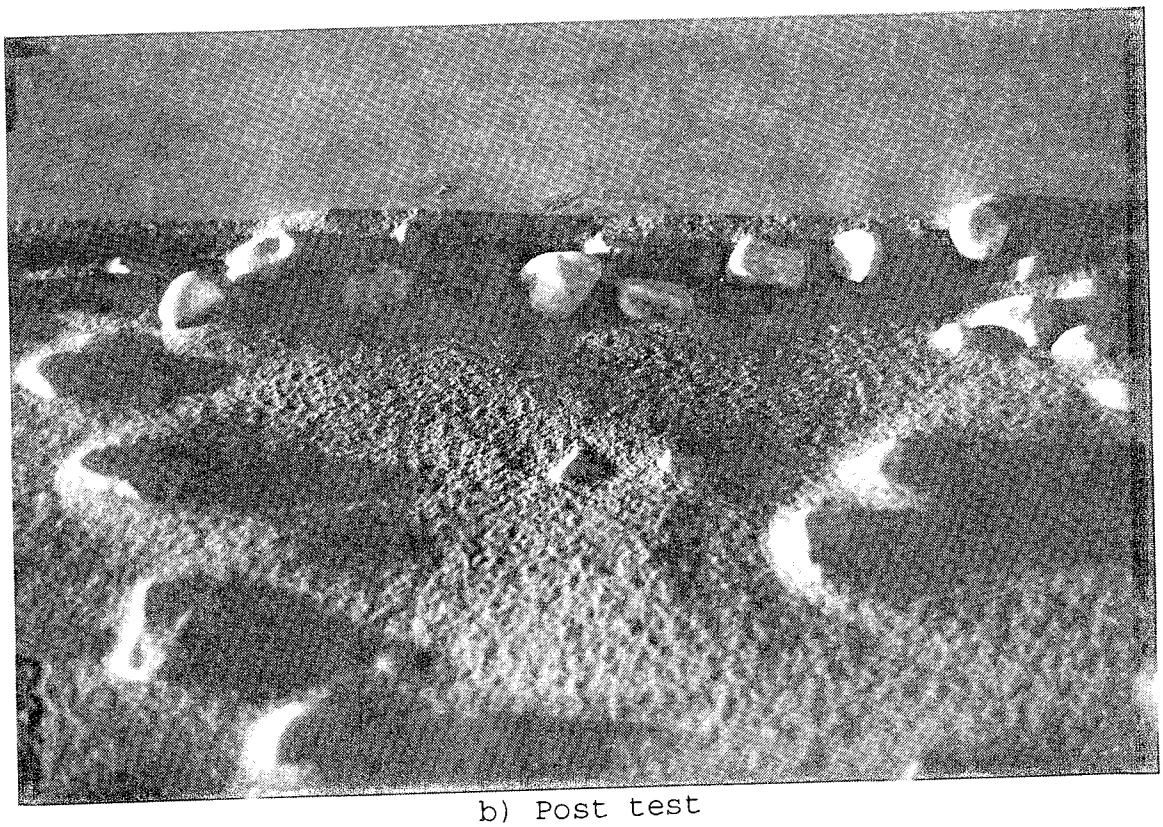

b) Post test

Figure A-41. Overhead close up view photographs of Gravel Seeded WSMR dust bed at 15' location: RS 70, 130 fps.

Figure A-42. Post test photograph of Gravel Seeded WSMR dust bed: RS 70, 130 fps - Side view at 9' location.

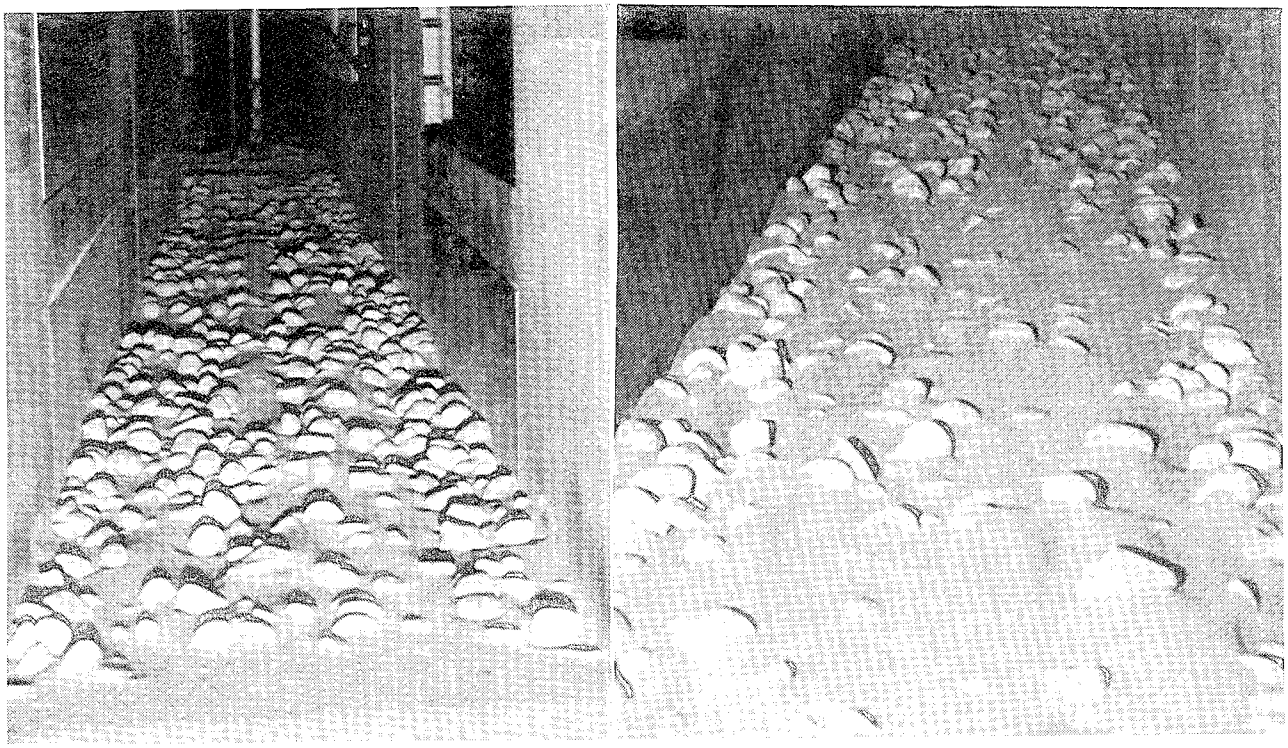

a) Downstream view

b) Upstream view

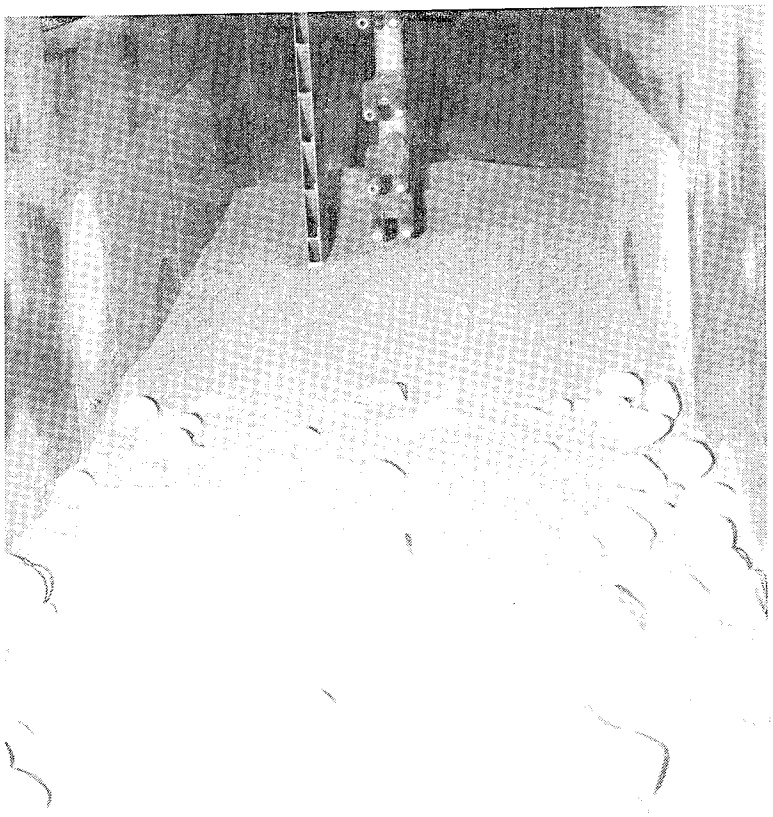

c) Close up view at diagnostics station

Figure A-43. Post test photographs of Gravel Seeded WSMR dust bed: RS 71, 122 fps.

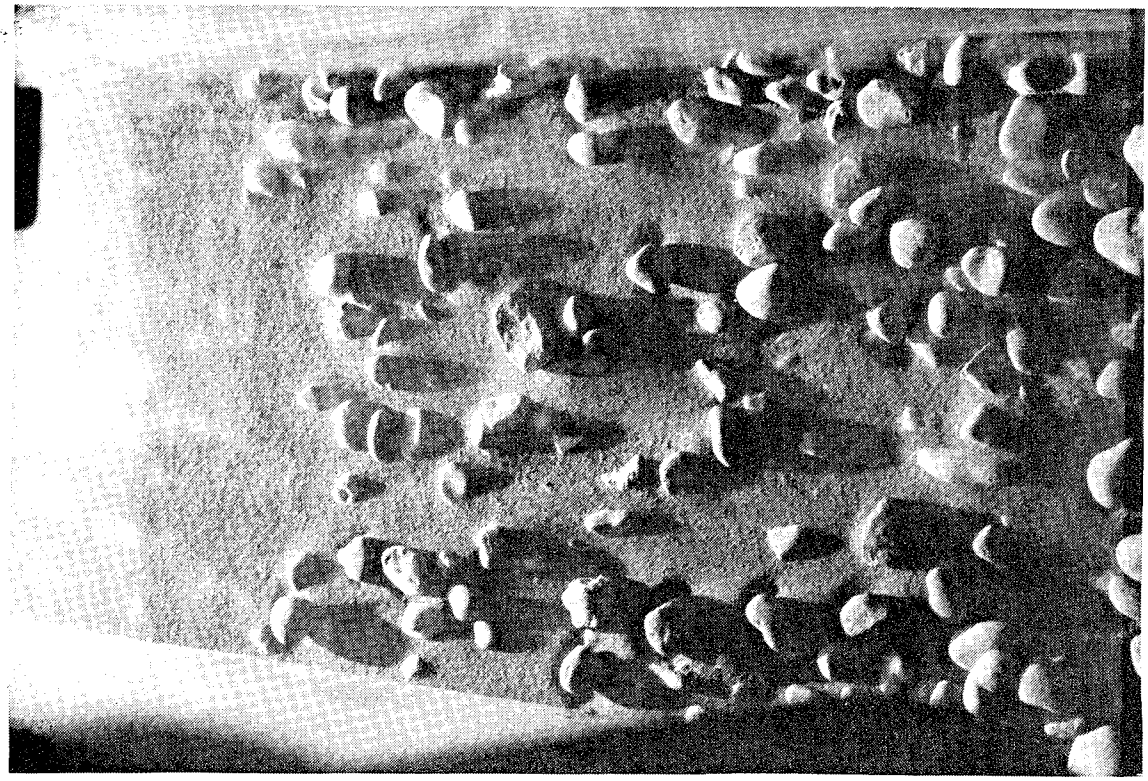

a) Overhead view at 9' location looking upstream

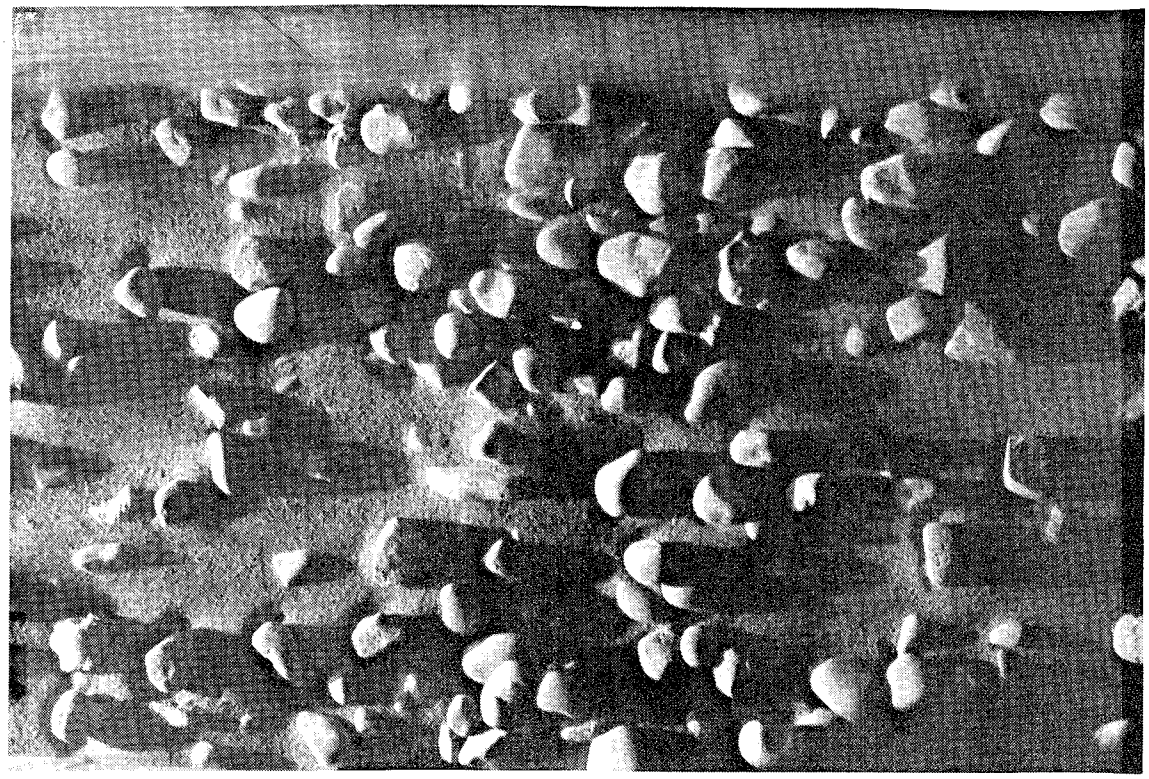

b) Overhead view at 9' location

Figure A-44. Post test photographs of Gravel Seeded WSMR dust bed: RS 71, 122 fps.

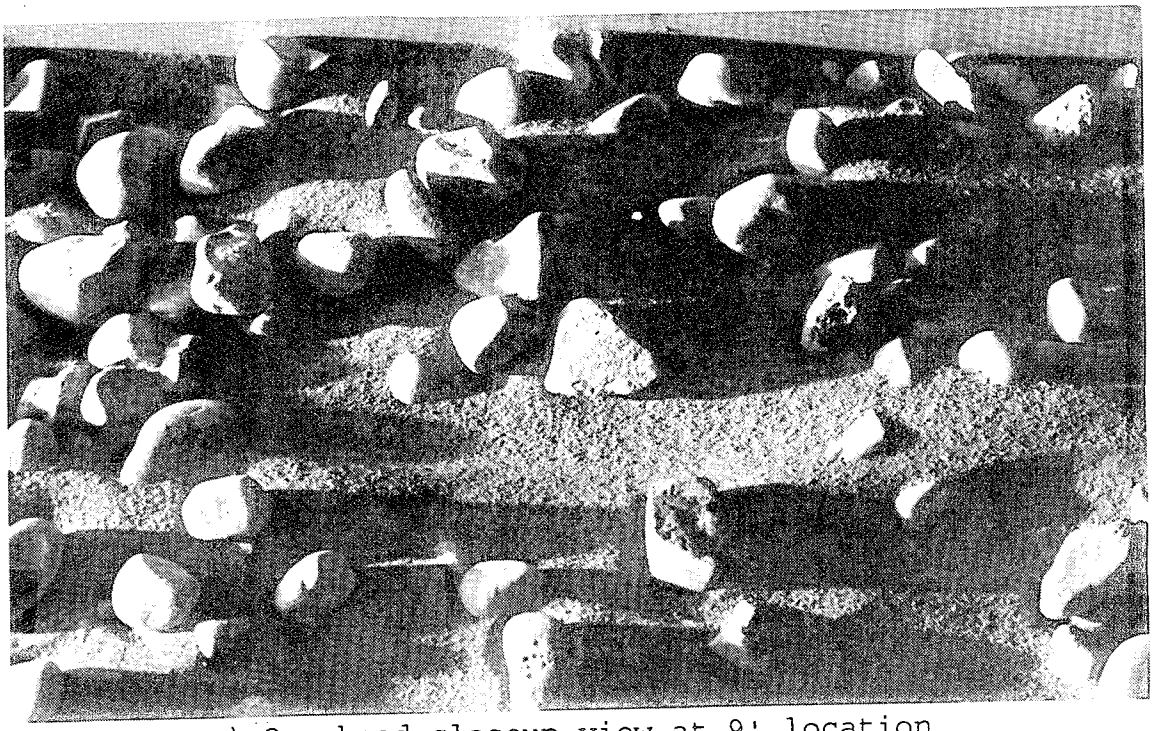

a) Overhead closeup view at 9' location

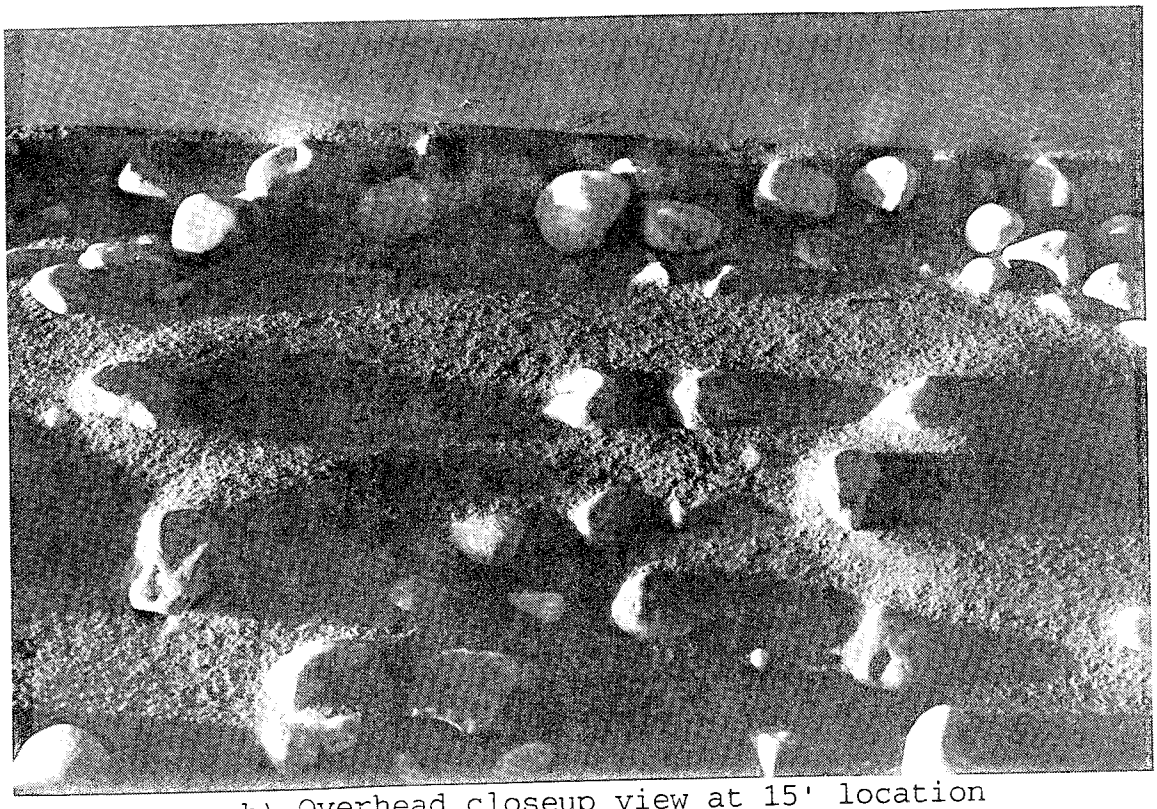

b) Overhead closeup view at 15' location

Figure A-45. Post test photographs of Gravel Seeded WSMR dust bed: RS 71, 122 fps.

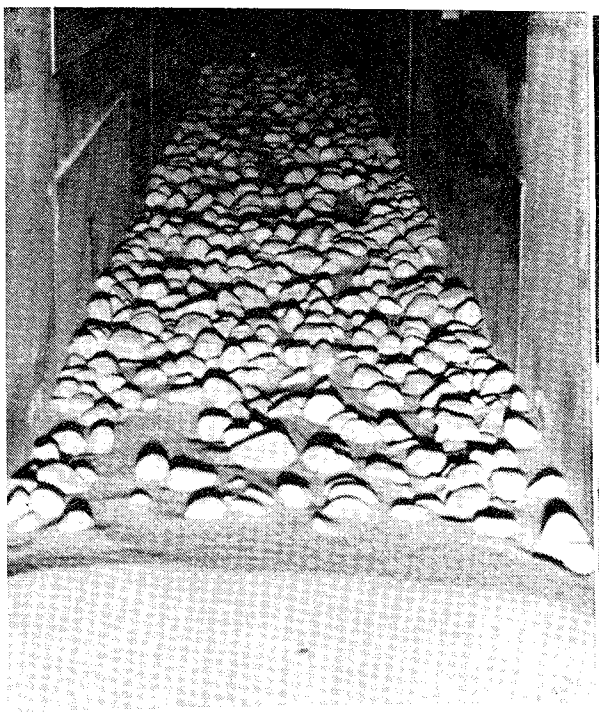

a) Downstream view

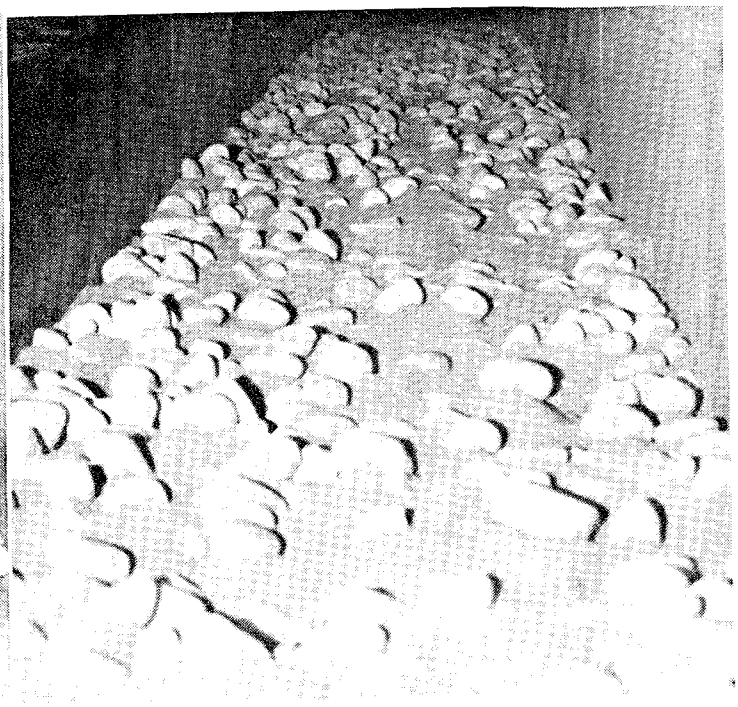

b) Upstream view

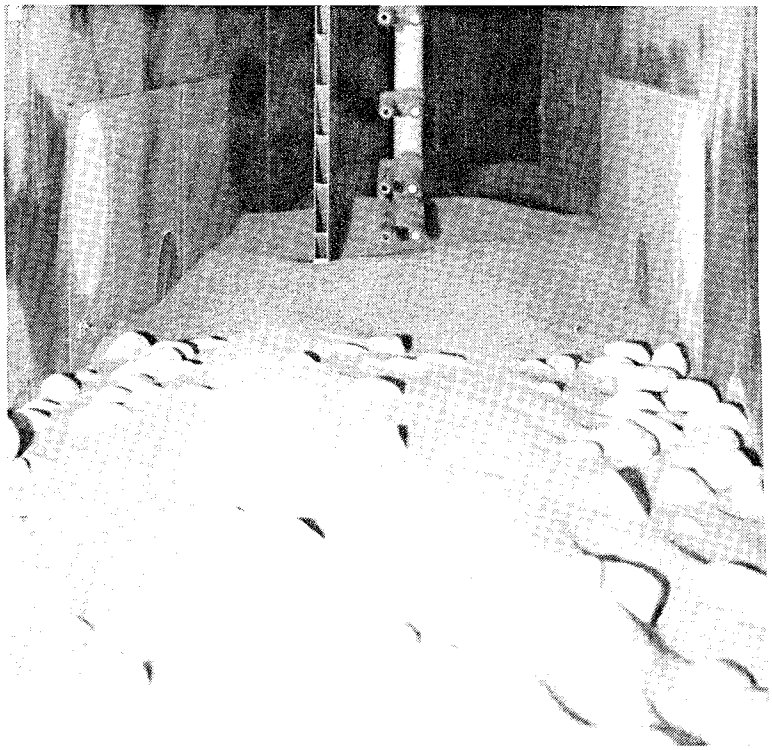

c) Close up view at diagnostics station

Figure A-46. Post test photographs of Gravel Seeded WSMR dust bed: RS 72, 134 fps.

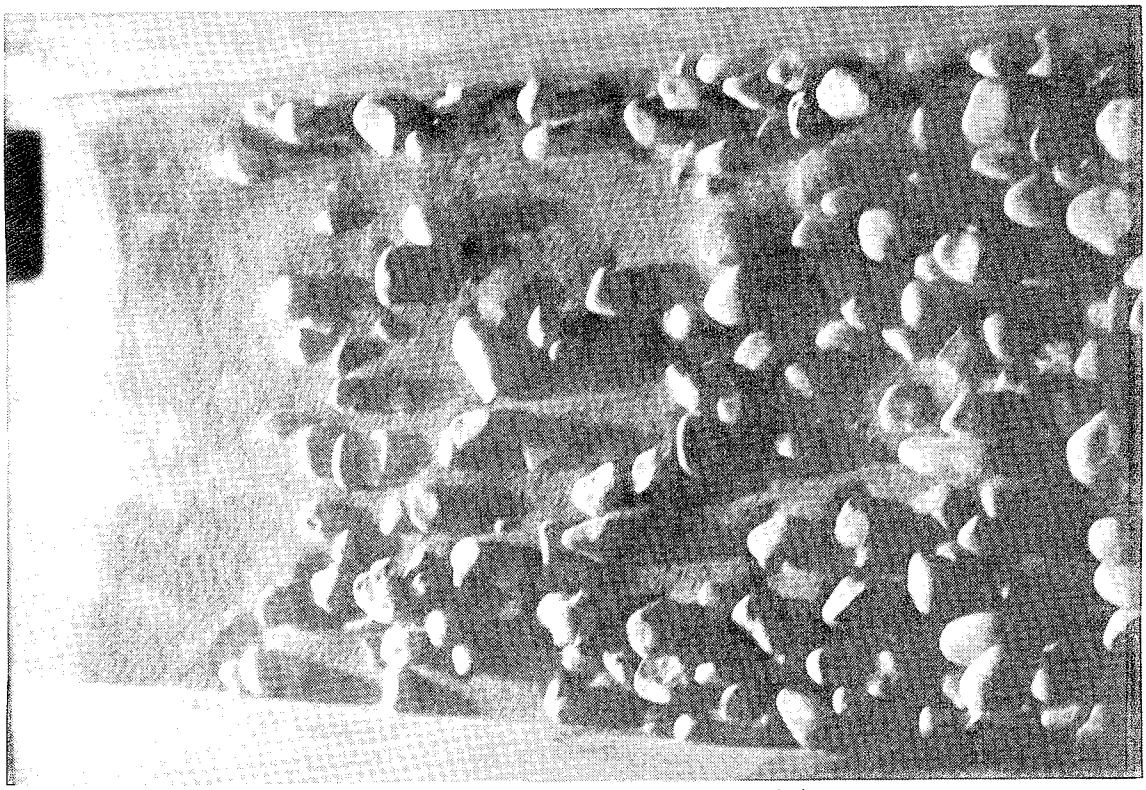

a) Overhead view at 9' location looking upstream

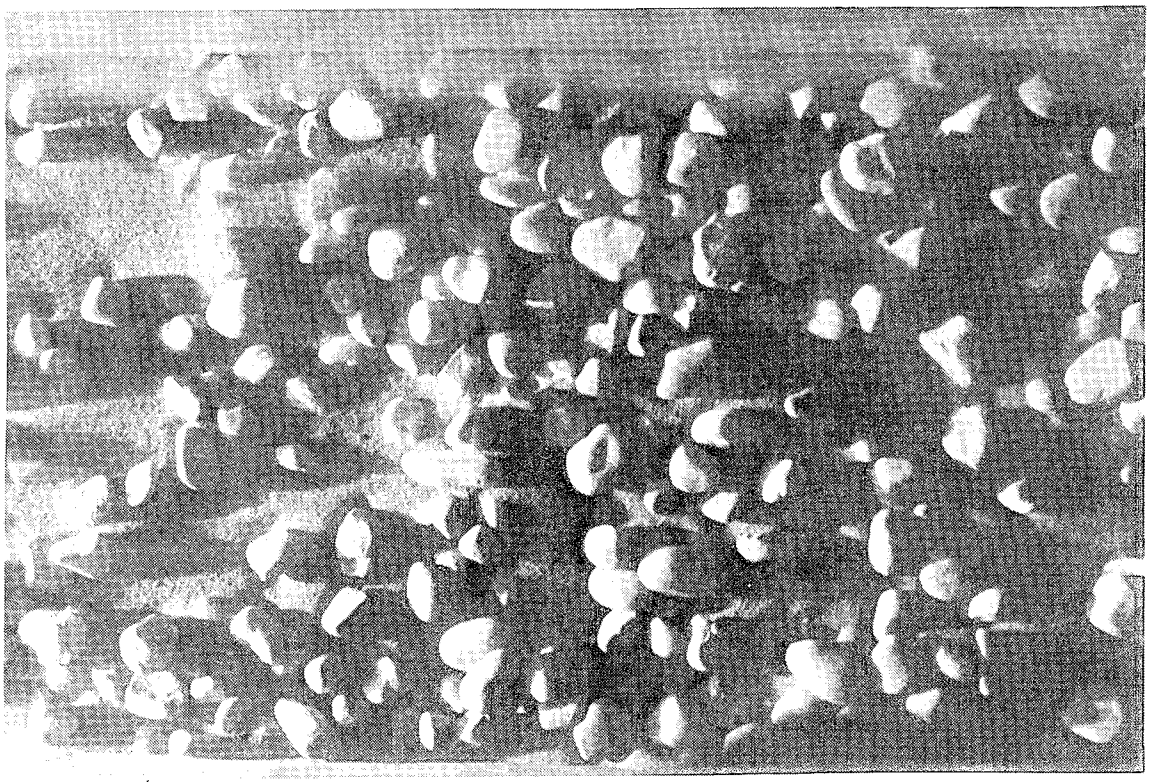

b) Over-head view at 9' location

Figure A-47. Post test photographs of Gravel Seeded WSMR dust bed: RS72, 134 fps.

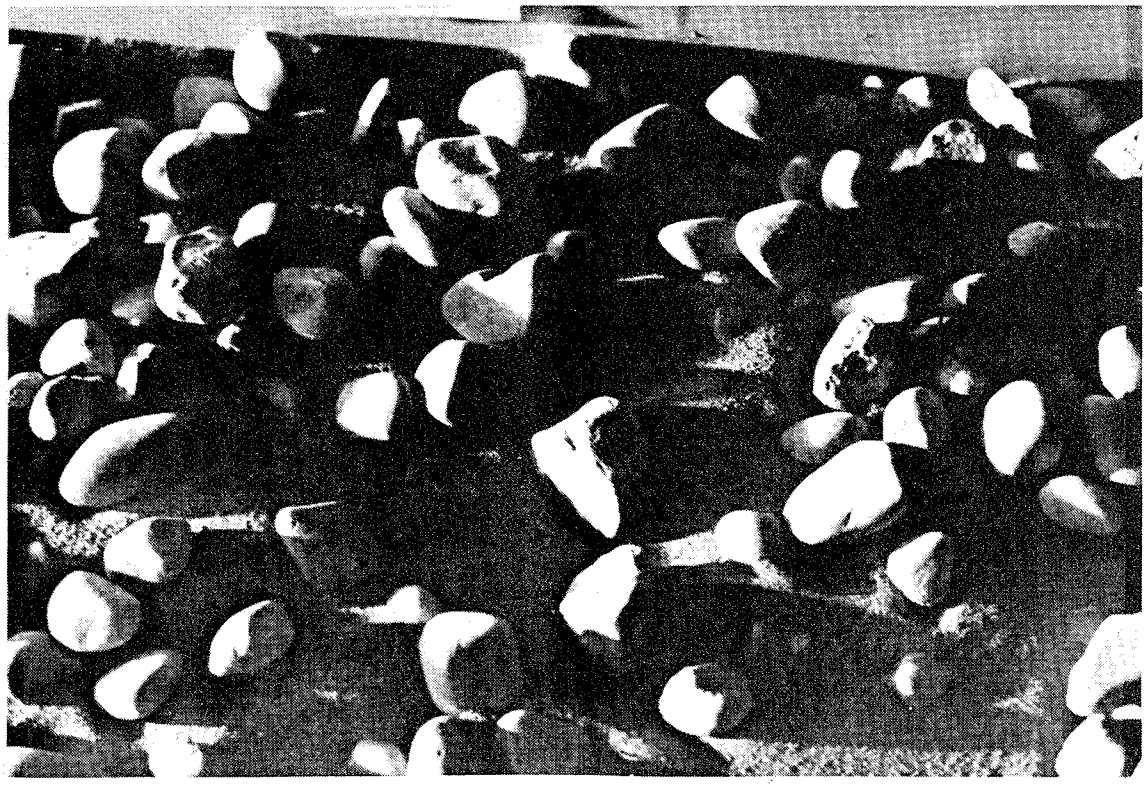

a) Overhead close up view at 9' location

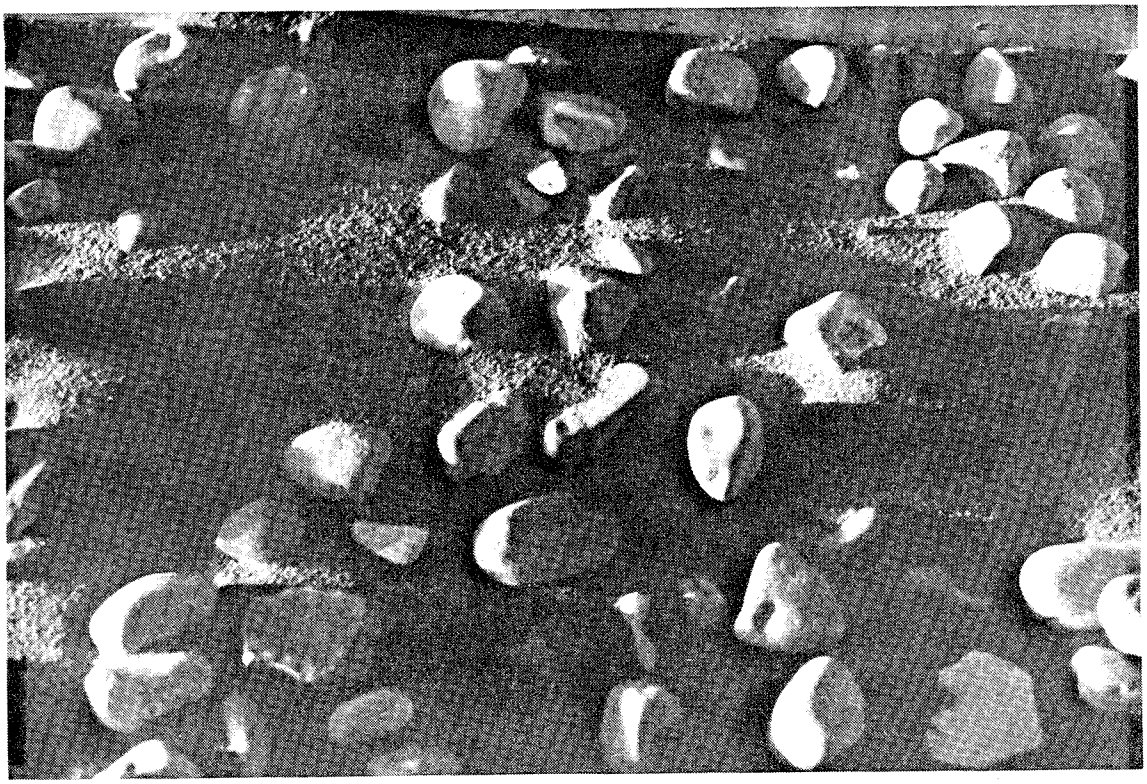

b) Over-head close up view at 15' location

Figure A-48. Post test photographs of Gravel Seeded WSMR dust bed: RS 72, 134 fps.

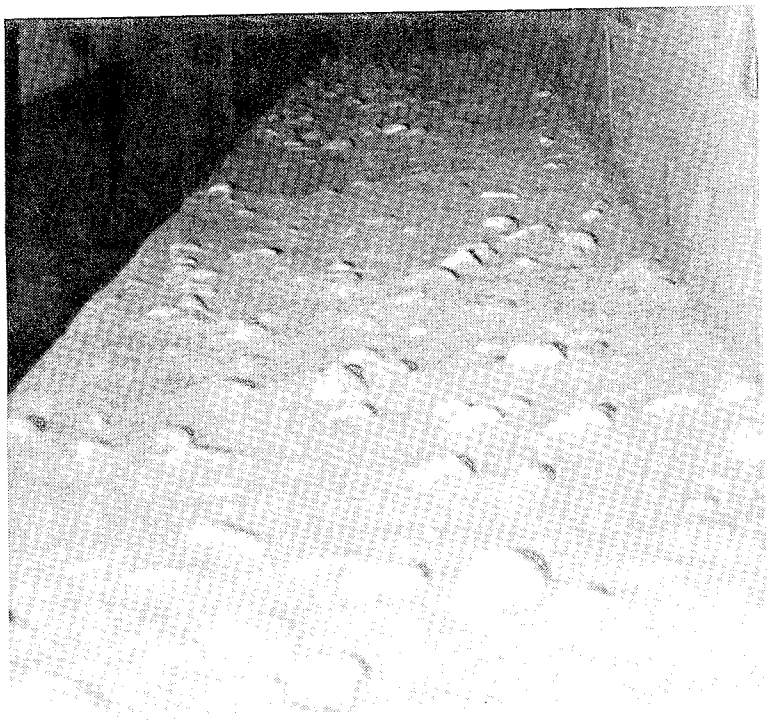

a) Pre test

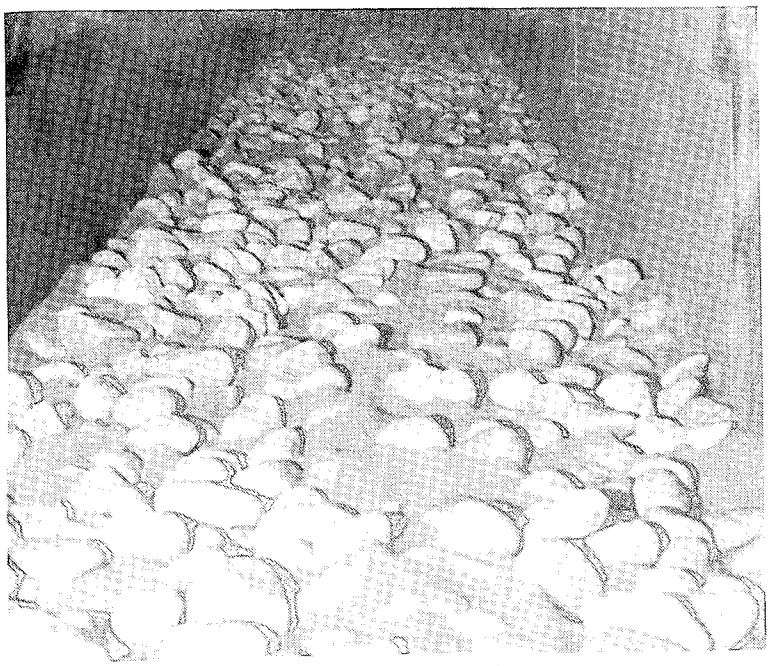

b) Post test

Figure A-49. Upstream view photographs of Gravel Seeded WSMR dust bed: RS 73, 227 fps.

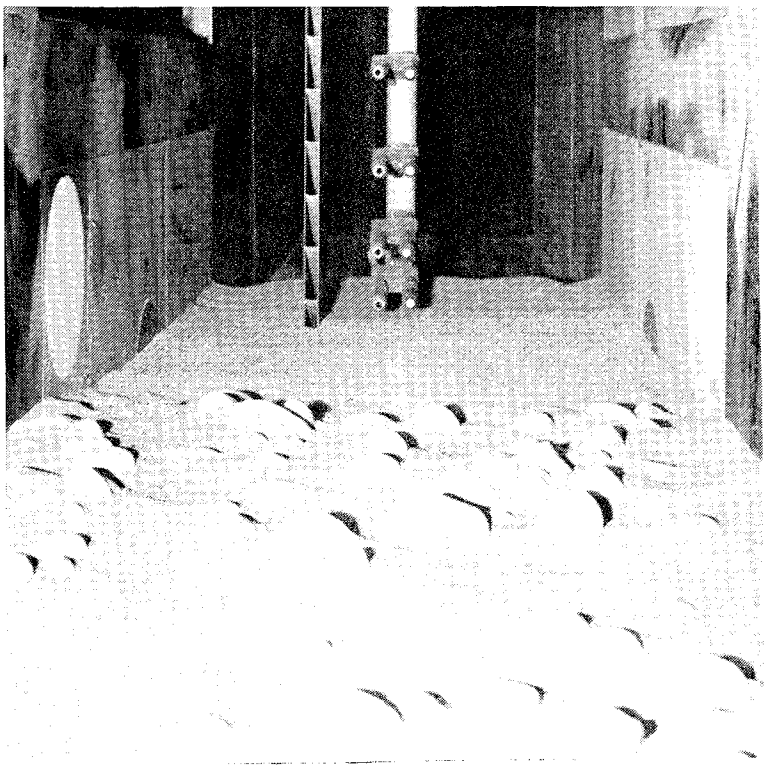

a) Pre test

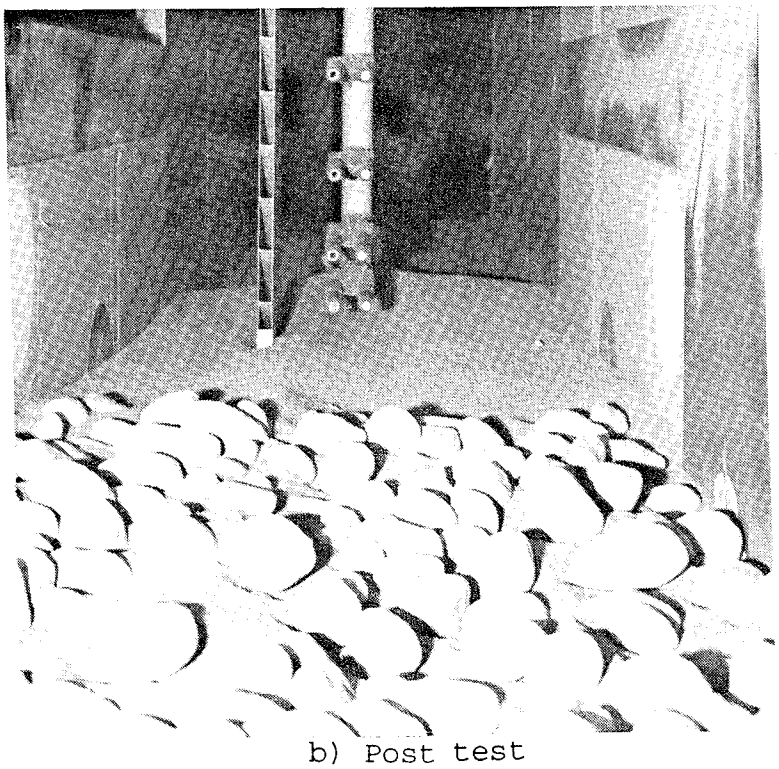

b) Post test

Figure A-50. Downstream view photographs of Gravel Seeded WSMR dust bed at diagnostics station: RS 73, 227 fps.

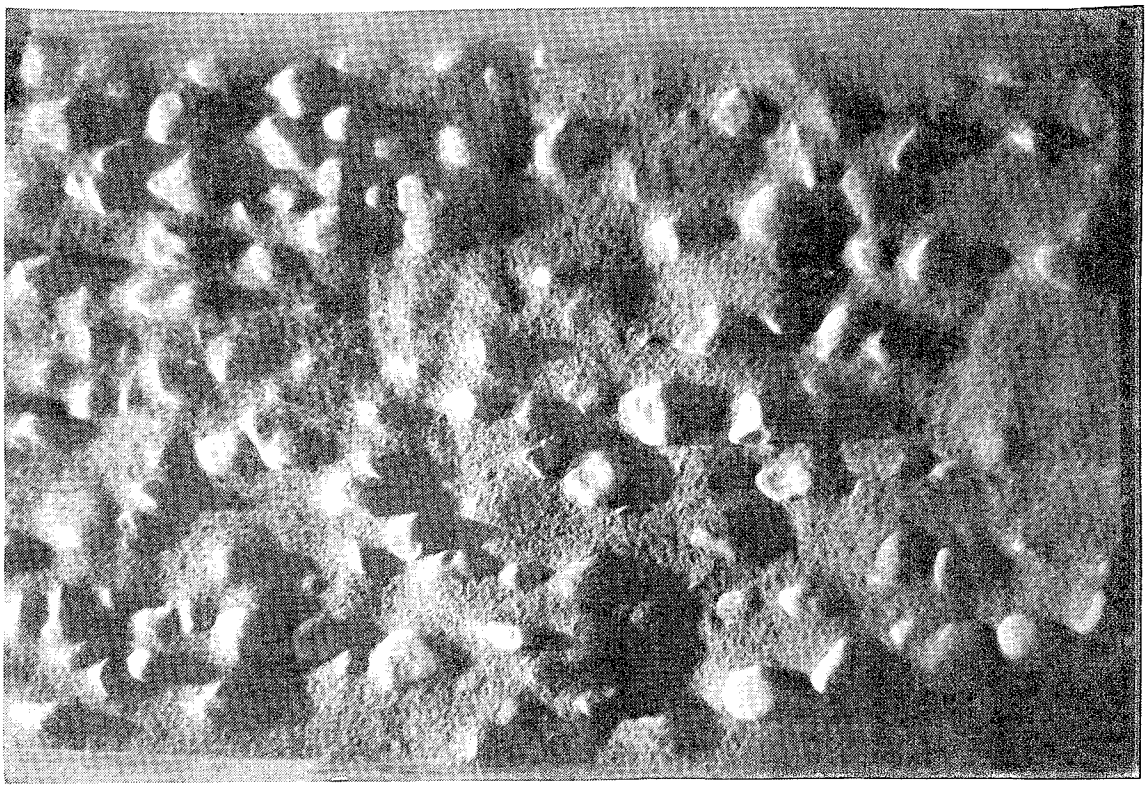

a) Pre test

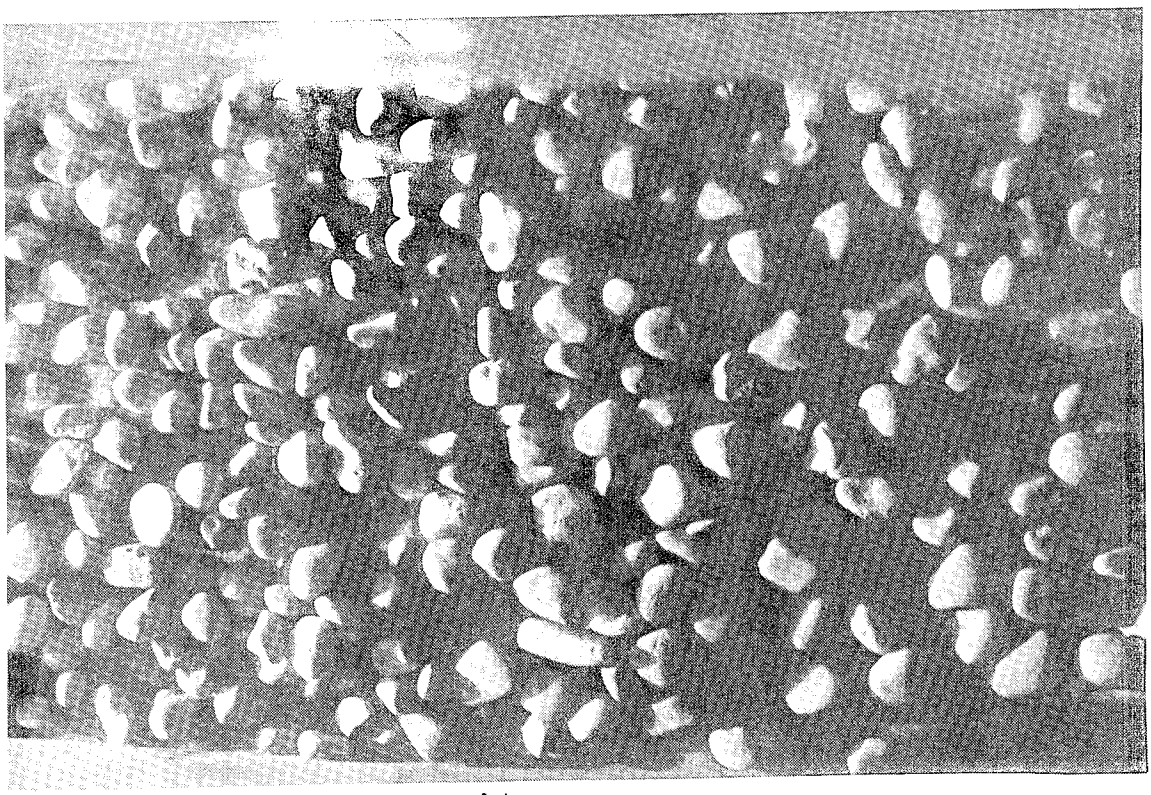

b) Post test

Figure A-51. Overhead photographs of Gravel Seeded WSMR dust bed at 9' location: RS 73, 227 fps.

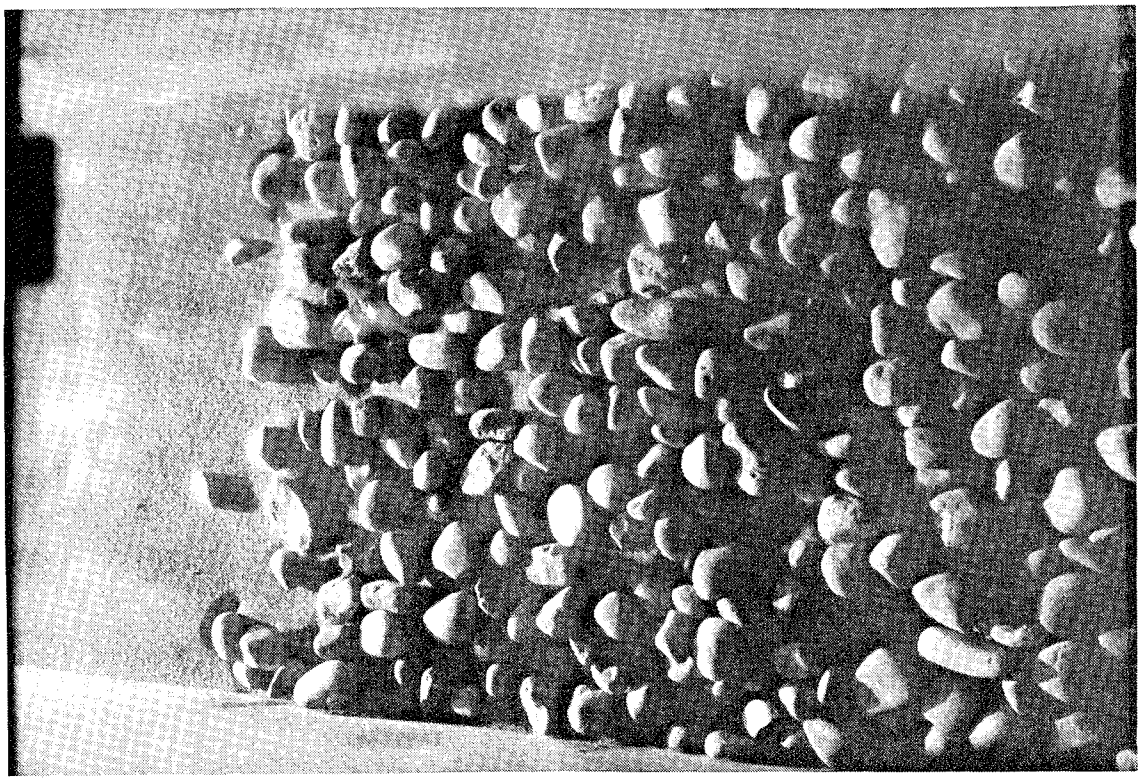

Figure A-52. Post test overhead view photograph of Gravel Seeded WSMR dust bed looking upstream at 9' location: RS 73, 227 fps.

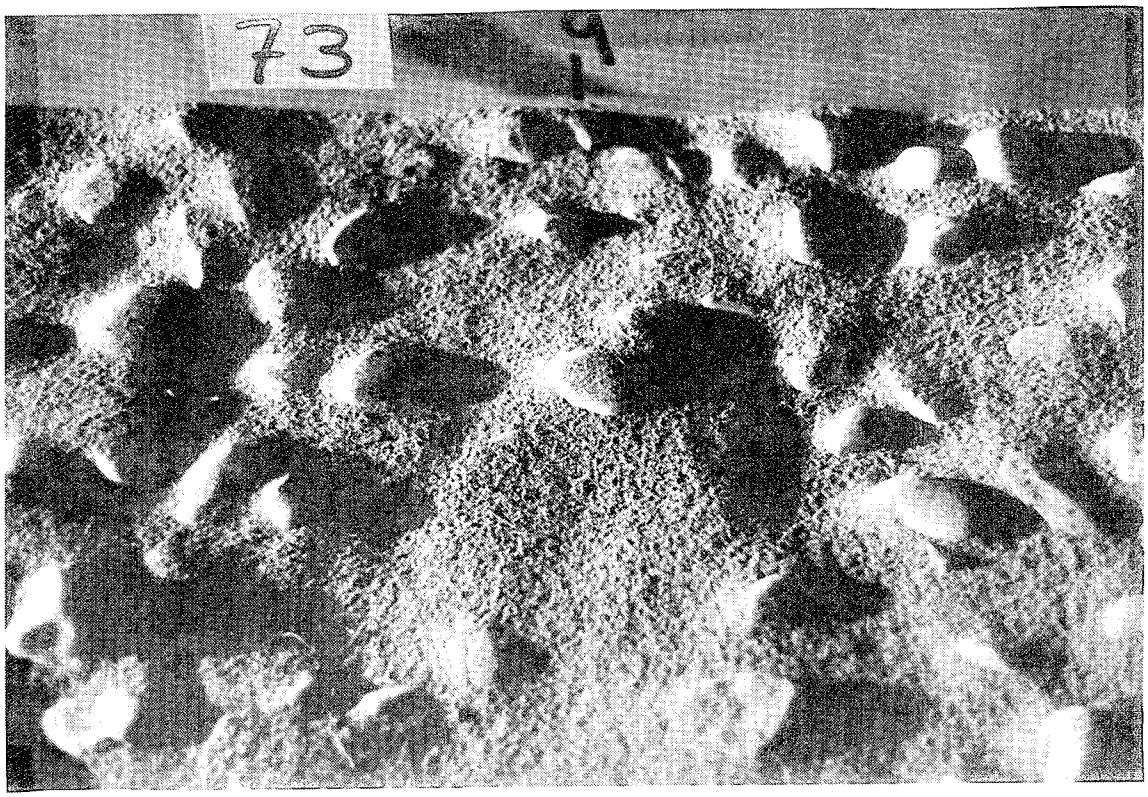

a) Pre test

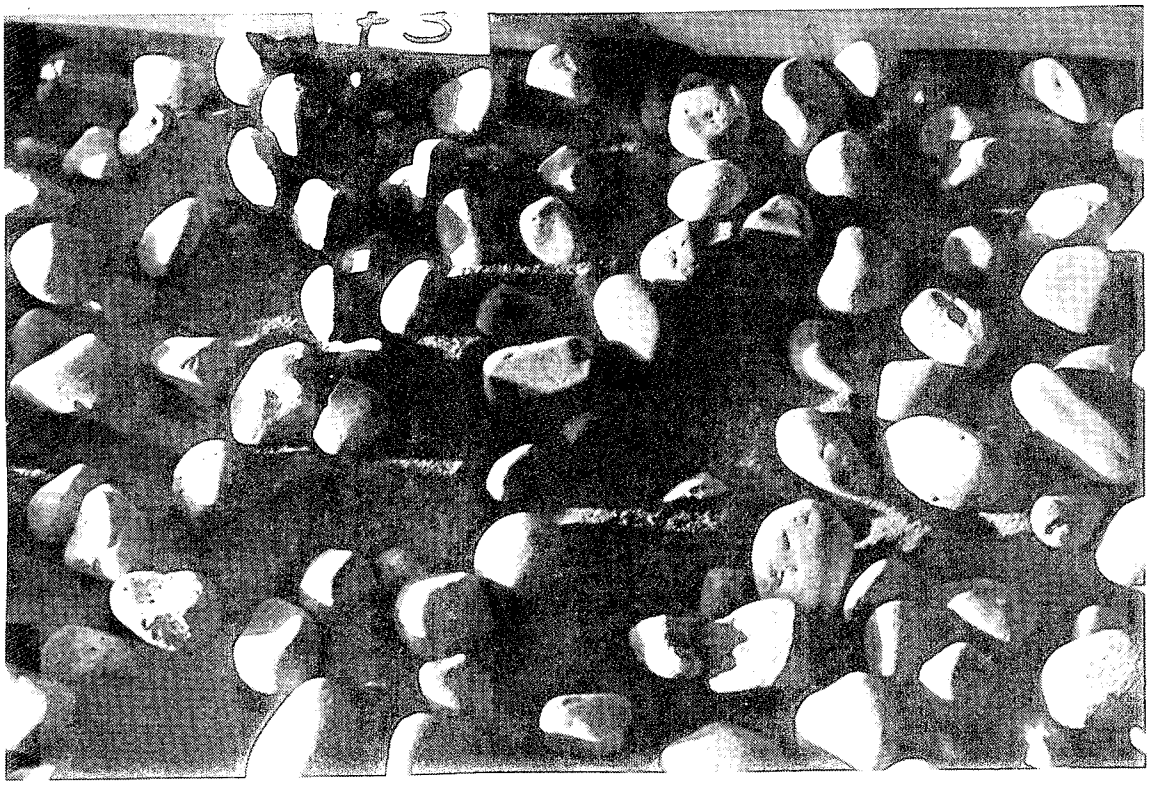

b) Post test

Figure A-53. Overhead close up view photographs of Gravel Seeded WSMR dust bed at 9' location: RS 73, 227 fps.

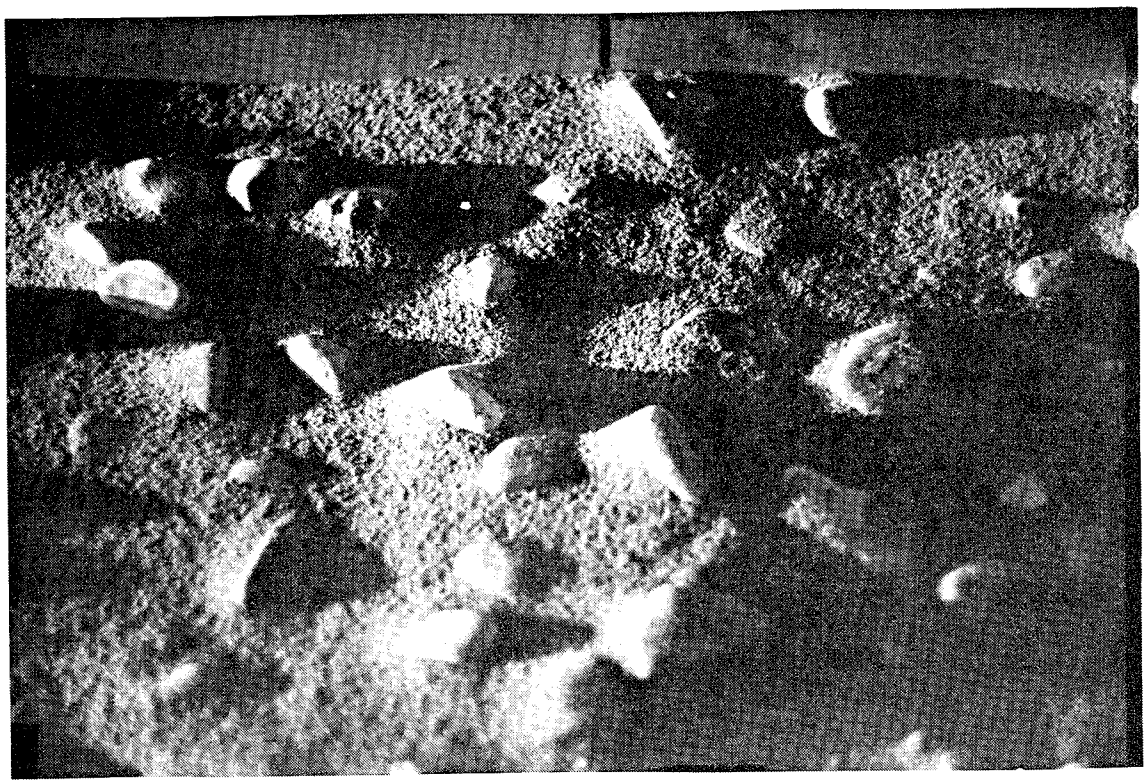

a) Pre test

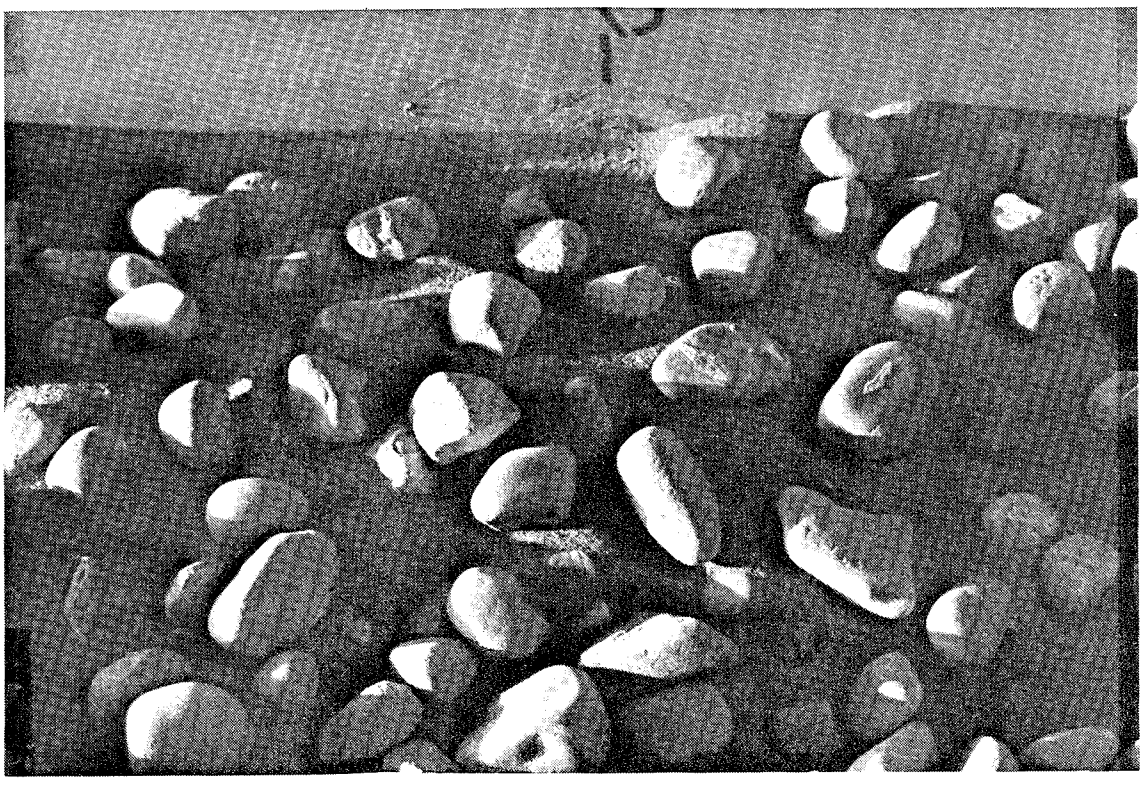

b) Post test

Figure A-54. Overhead close up view photographs of Gravel Seeded WSMR dust bed at 15' location: RS 73, 227 fps.

a) Pre test

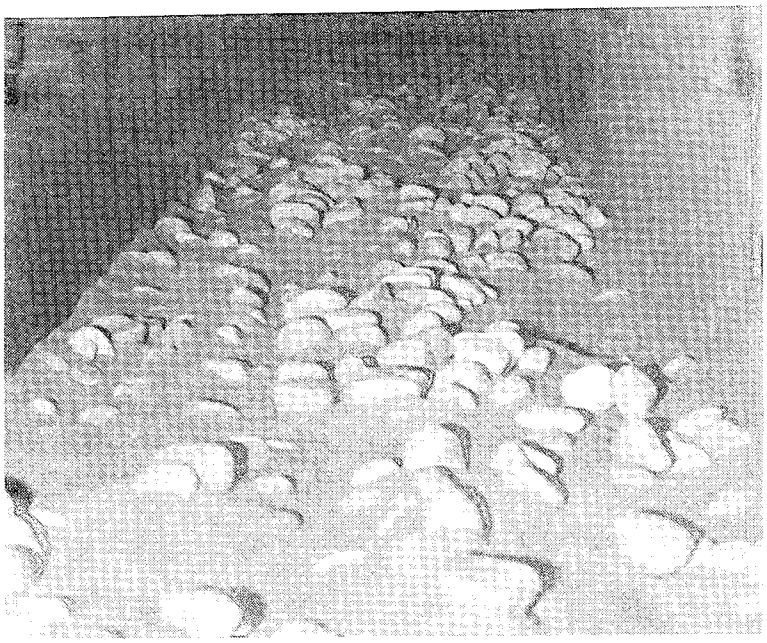

b) Post test

Figure A-55. Upstream view photographs of Gravel Seeded WSMR dust bed: RS 74, 367 fps.

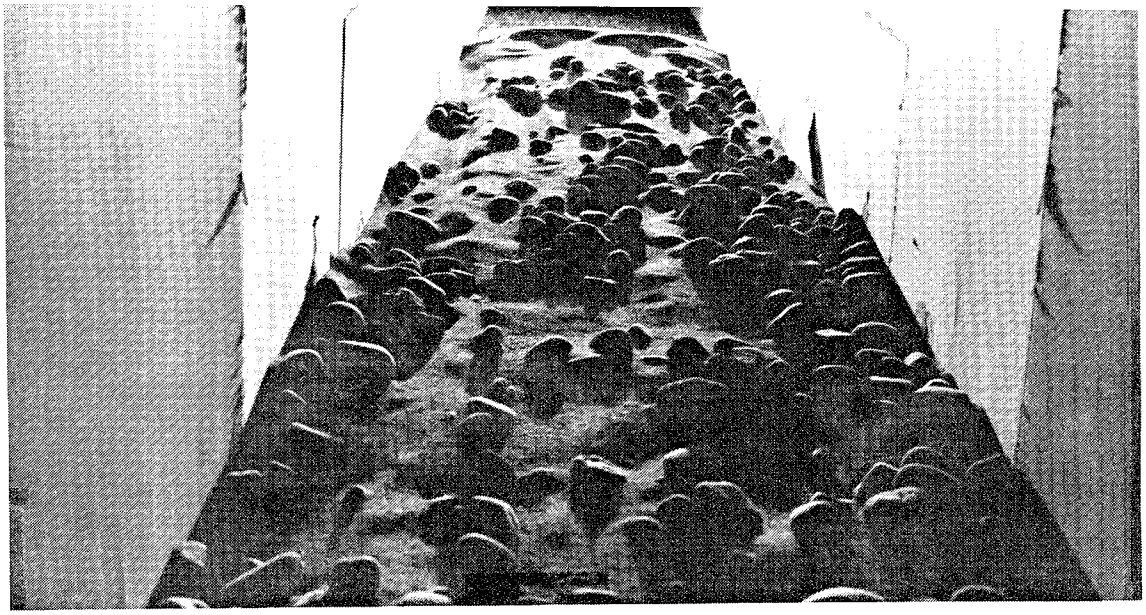

Figure A-56. Post test upstream view of Gravel Seeded WSMR dust bed: RS74, 367 fps.

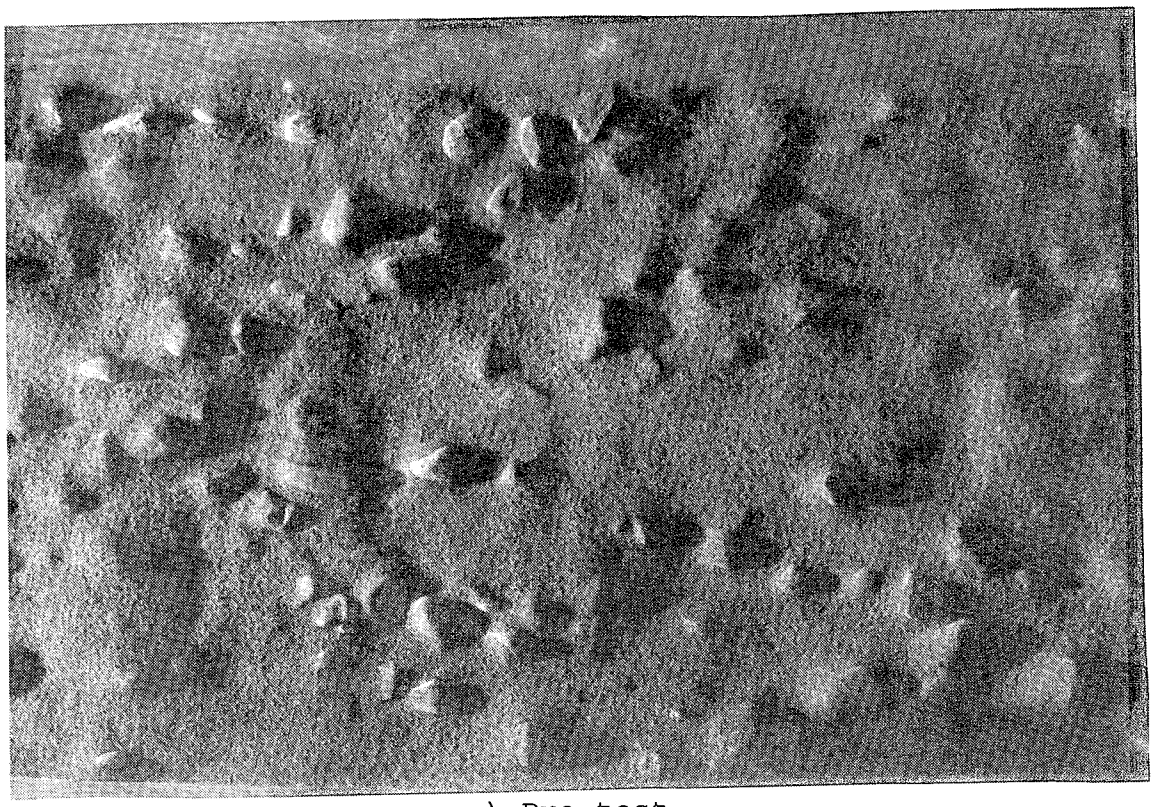

a) Pre test

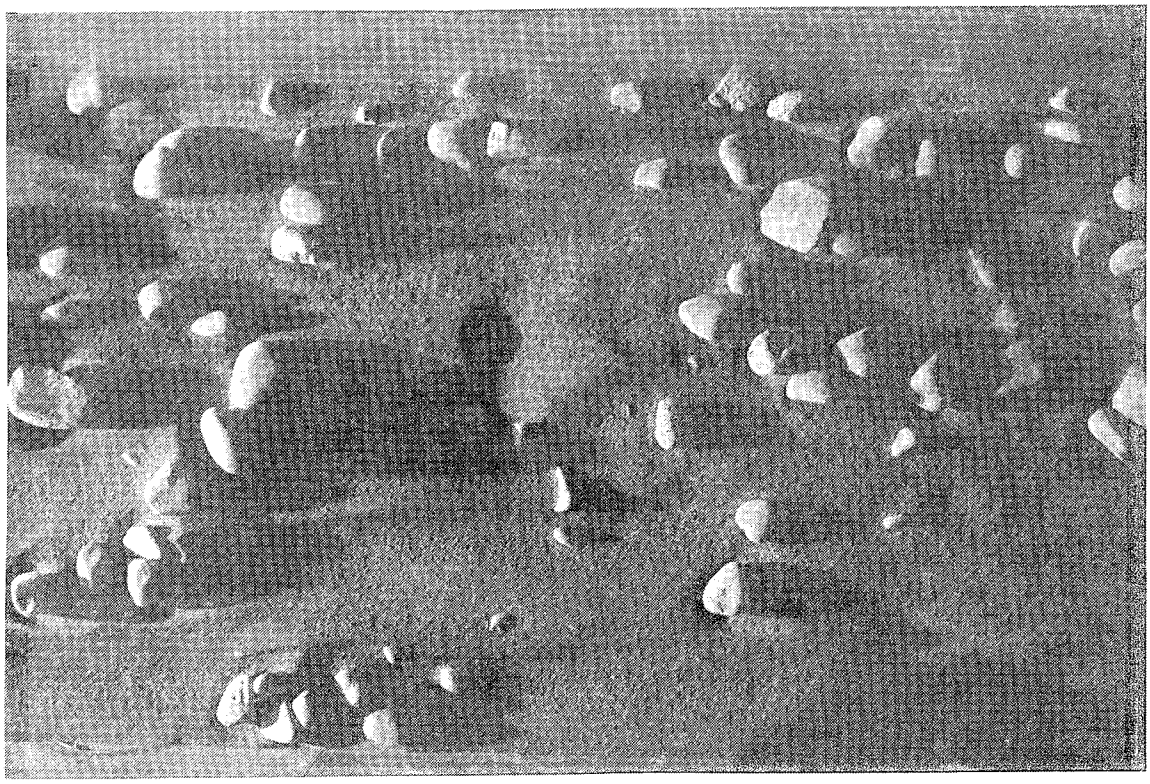

b) Post test

Figure A-57. Overhead view photographs of Gravel Seeded WSMR dust bed at 9' location: RS 74, 367 fps.

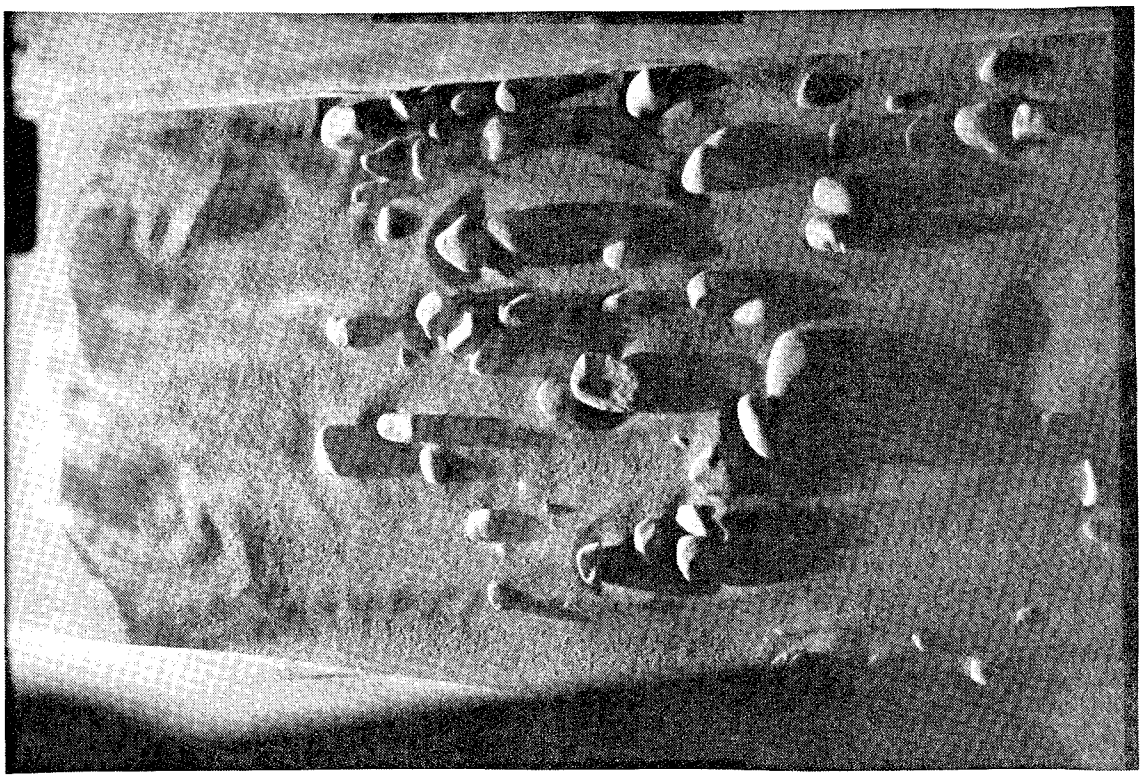

Figure A-58. Post test overhead view photograph of Gravel Seeded WSMR dust bed looking upstream at 9' location: RS 74, 367 fps.

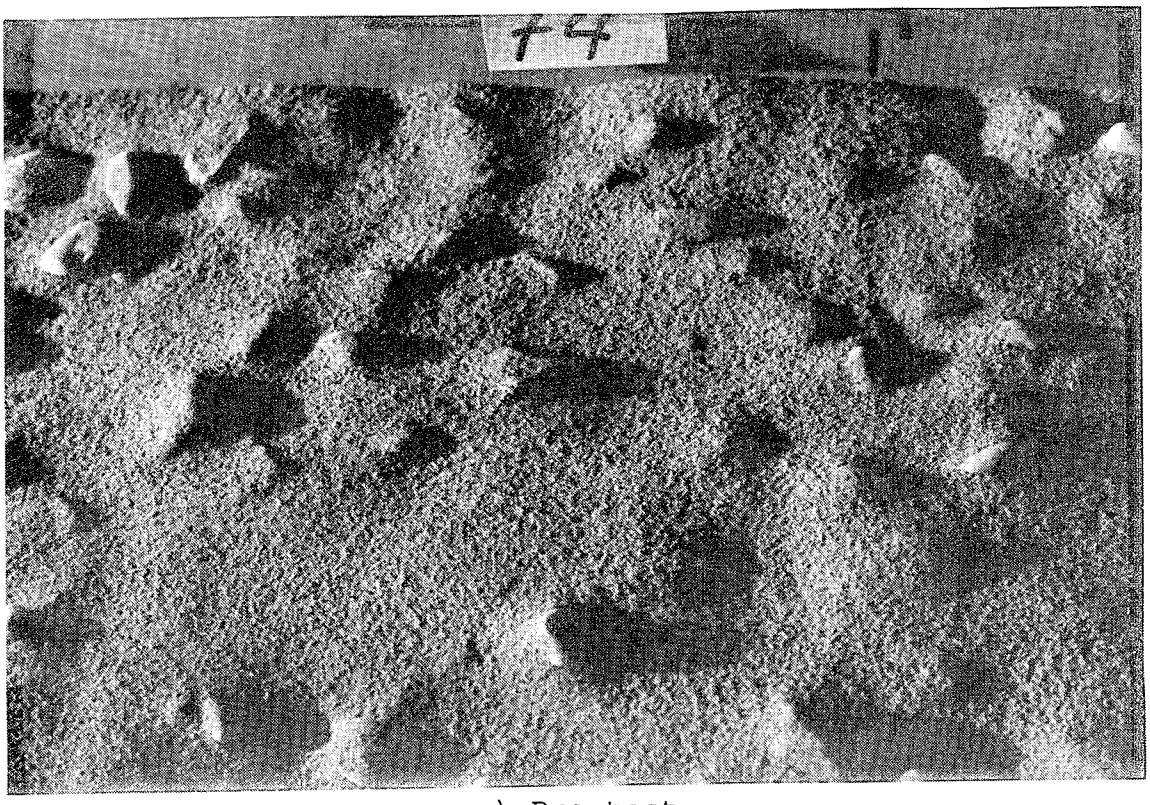

a) Pre test

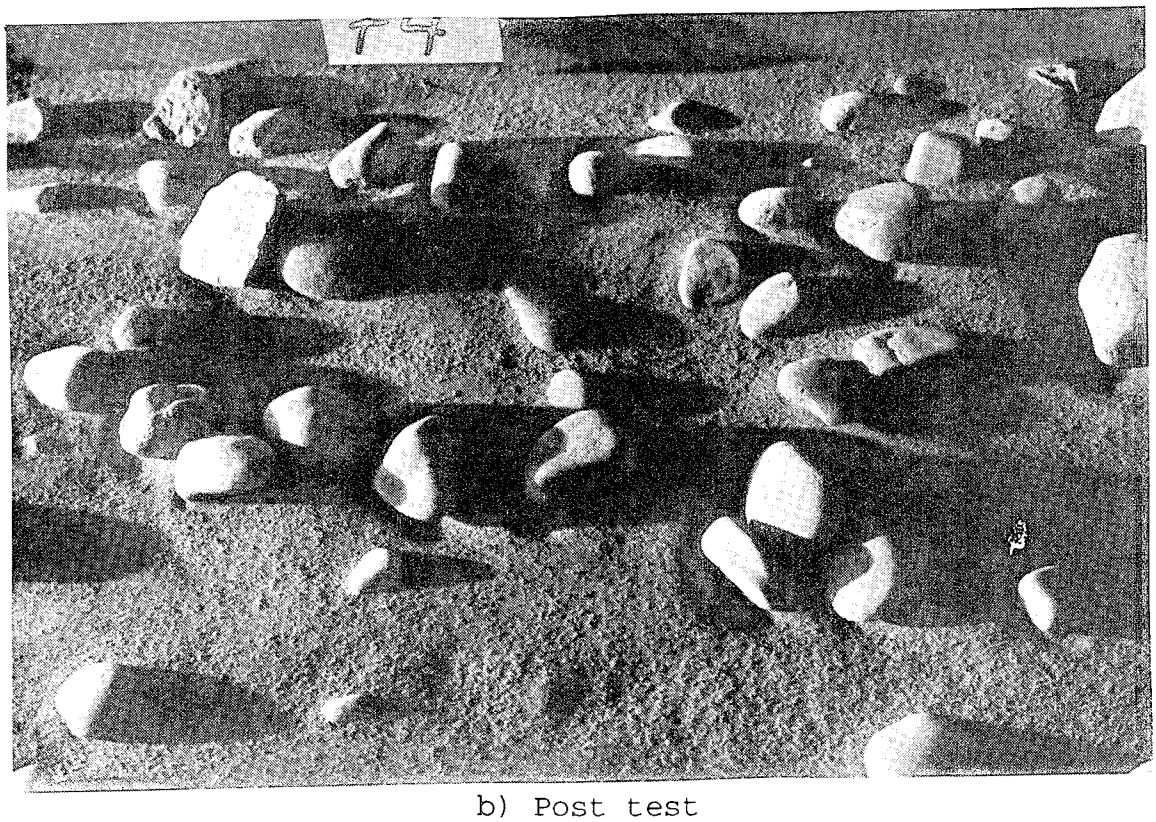

b) Post test

Figure A-59. Overhead close up view photographs of Gravel Seeded WSMR dust bed at 9' location: RS 74, 367 fps.

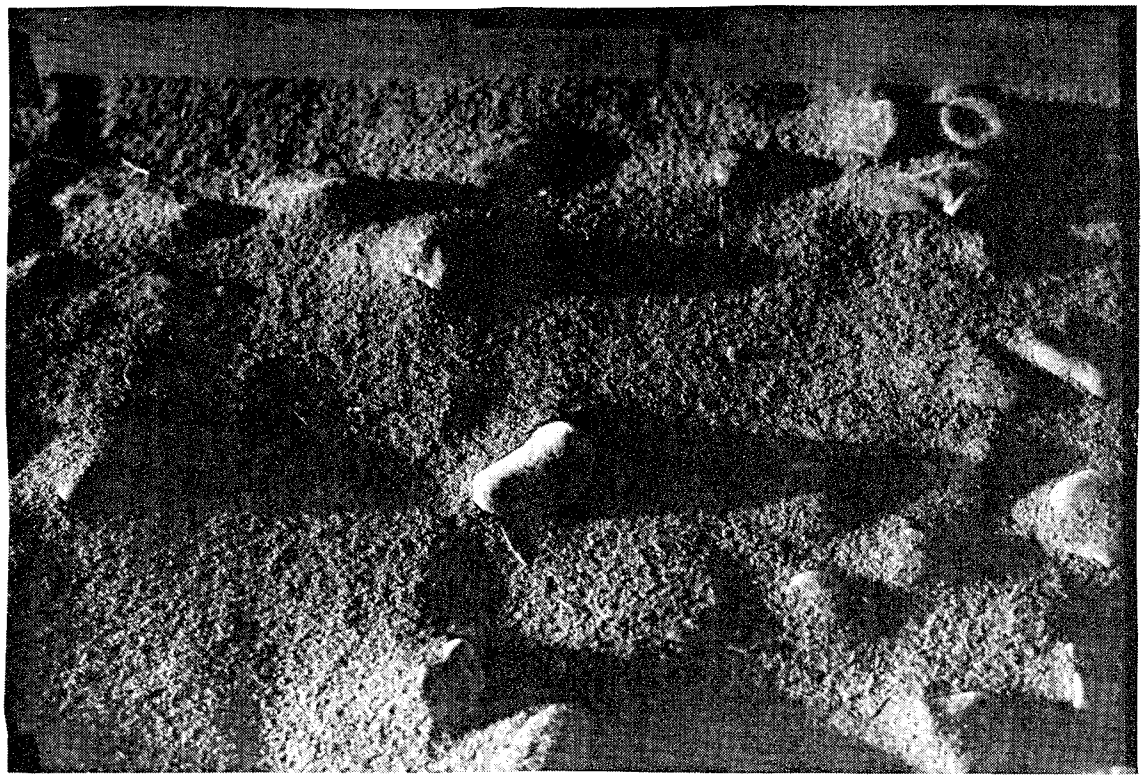

a) Pre test

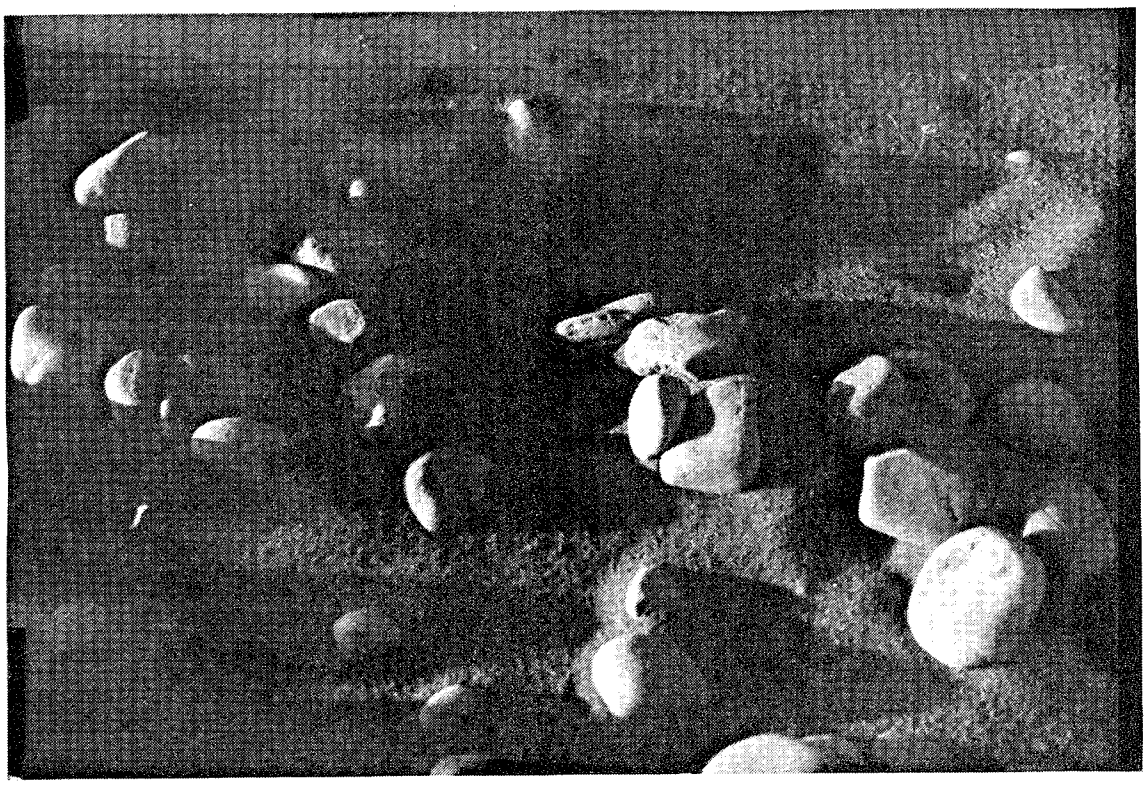

b) Post test

Figure A-60. Overhead close up view photographs of Gravel Seeded WSMR dust bed at 15' location: RS 74, 367 fps.

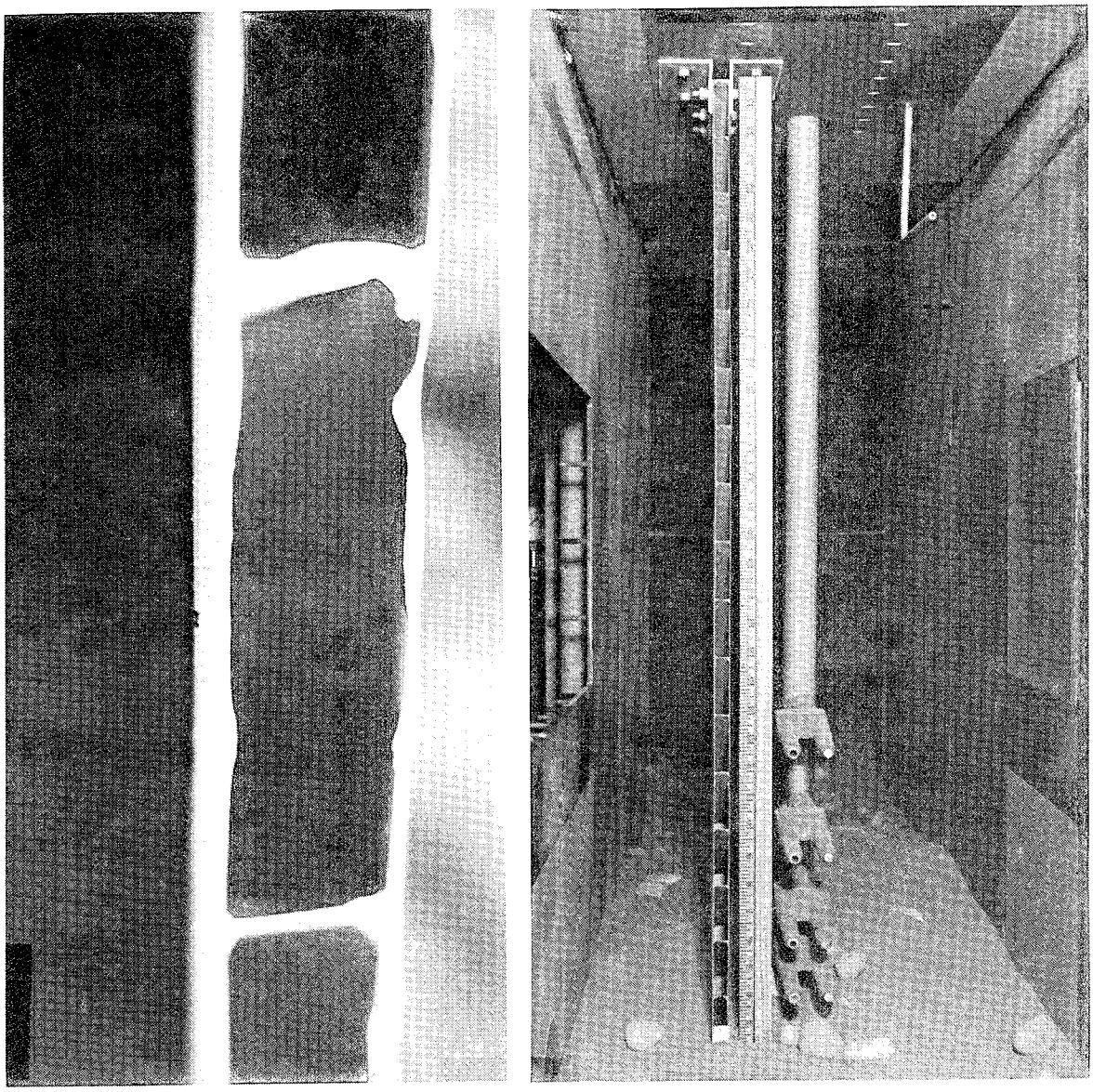

a) Close up view of collector inlet

b) Overview of diagnostics station.

Figure A-61. Post test photographs of Snob/Greg probe rake and Bagnold collector: RS 74, 367 fps.

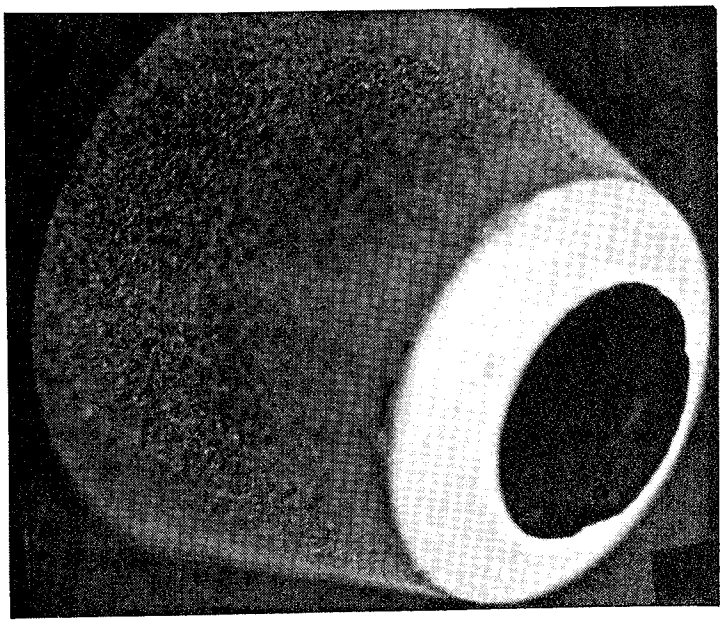

(a) Snob probe inlet

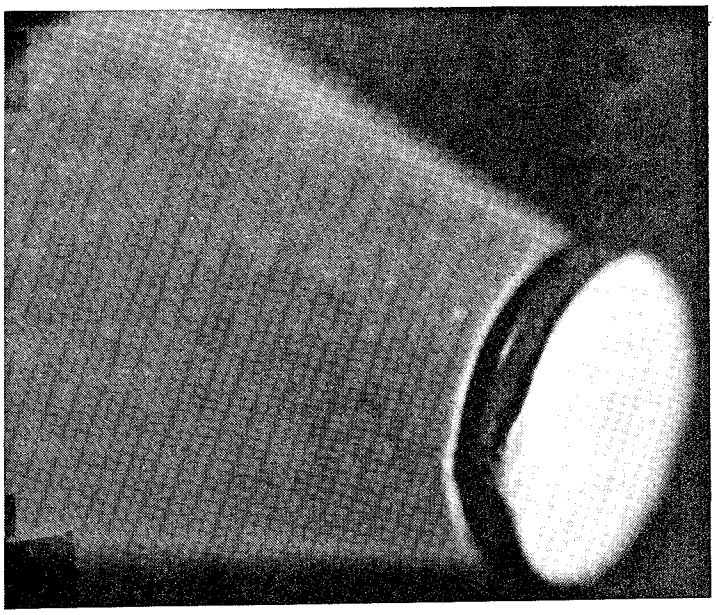

(b) Greg probe force plate

Figure A-62. Post test photographs of Snob/Greg probe nose tips (RS74, 367 FPS).

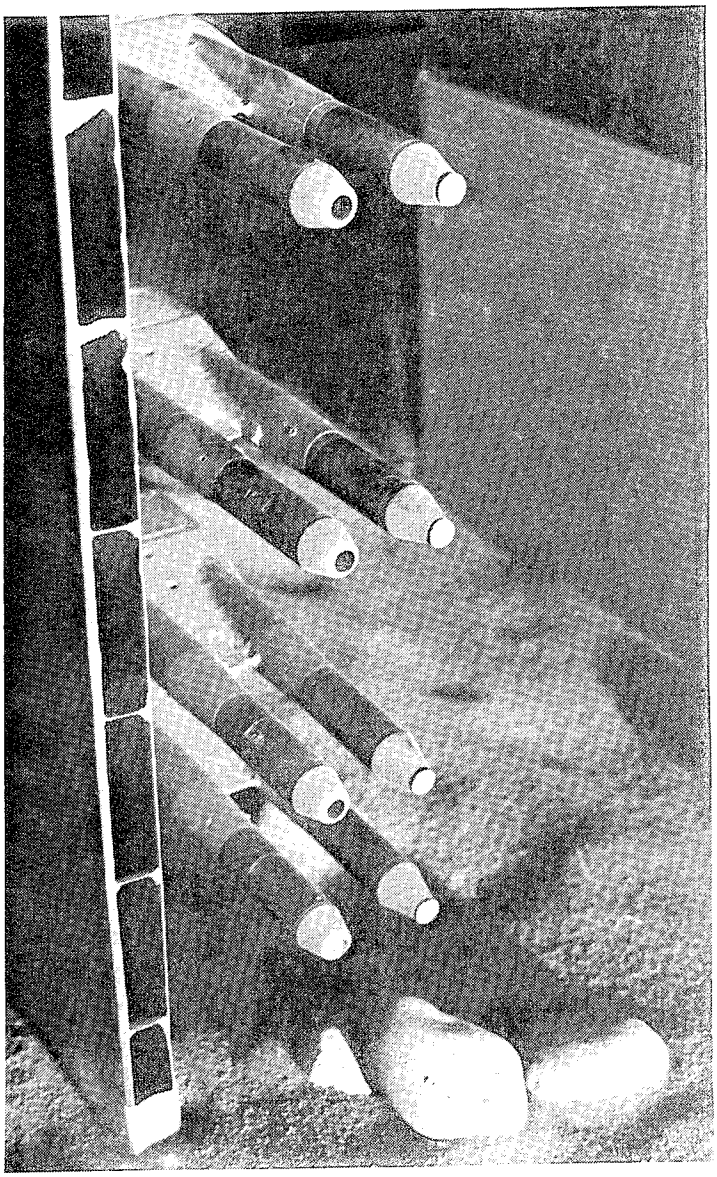

Figure A-63. Post test photograph of Snob/Greg proke rake and Bagnold collector (RS74, 367 fps).

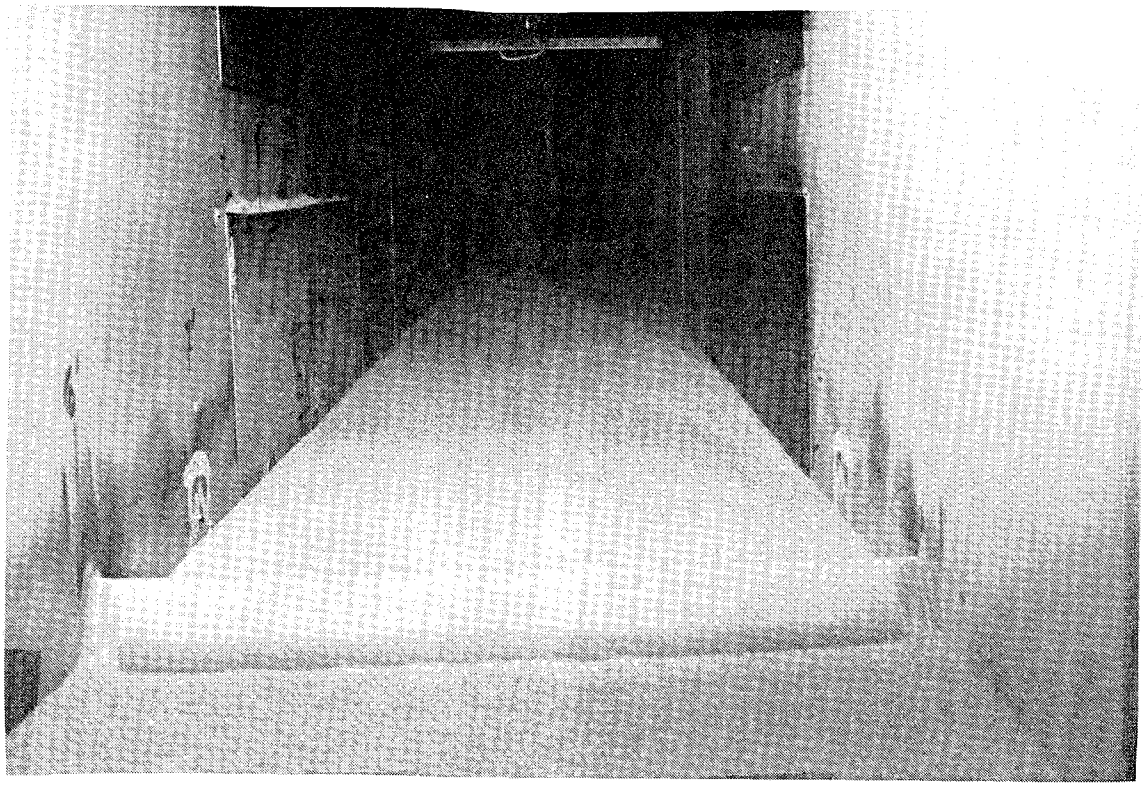

a) Downstream view

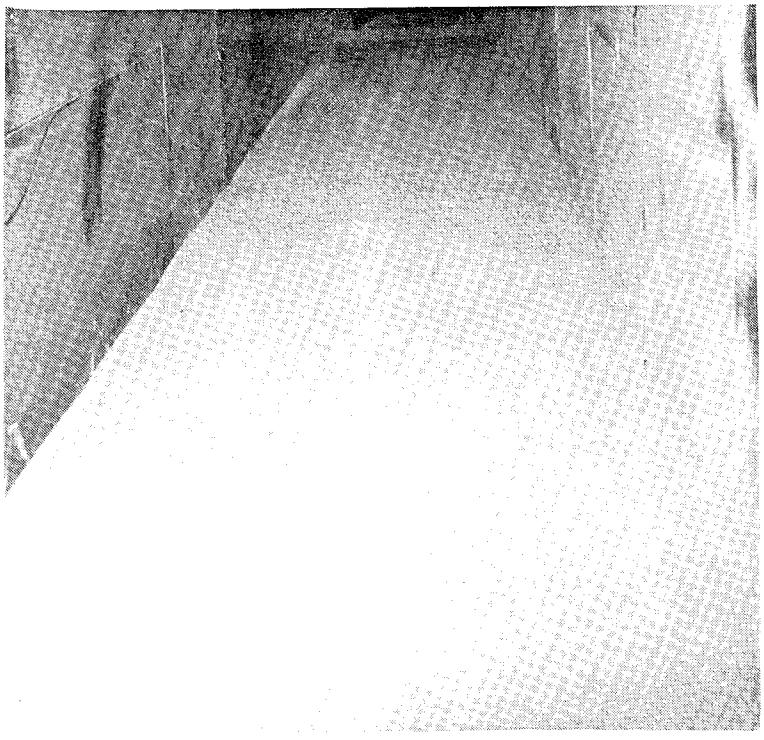

b) Upstream view

Figure A-64. Pre test photographs of WSMR dust bed with leading edge disturbance - 1.5" ridge: RS 62, 124 fps.

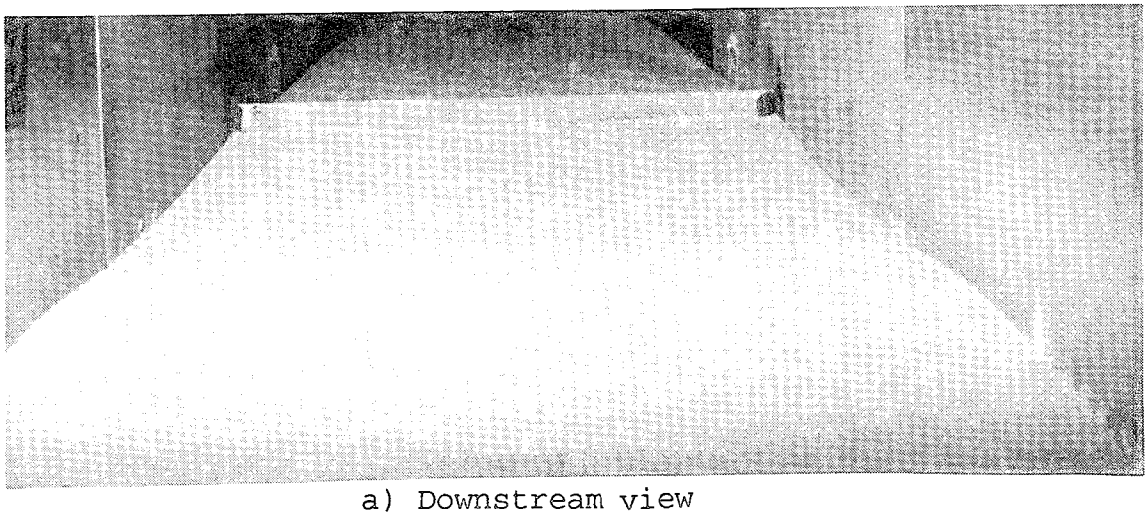

a) Downstream view

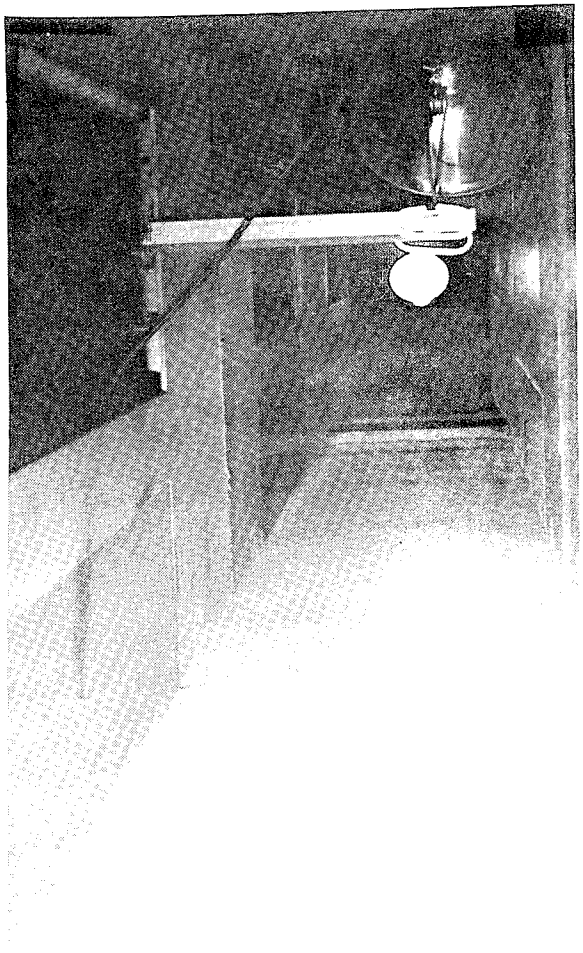

b) Upstream view

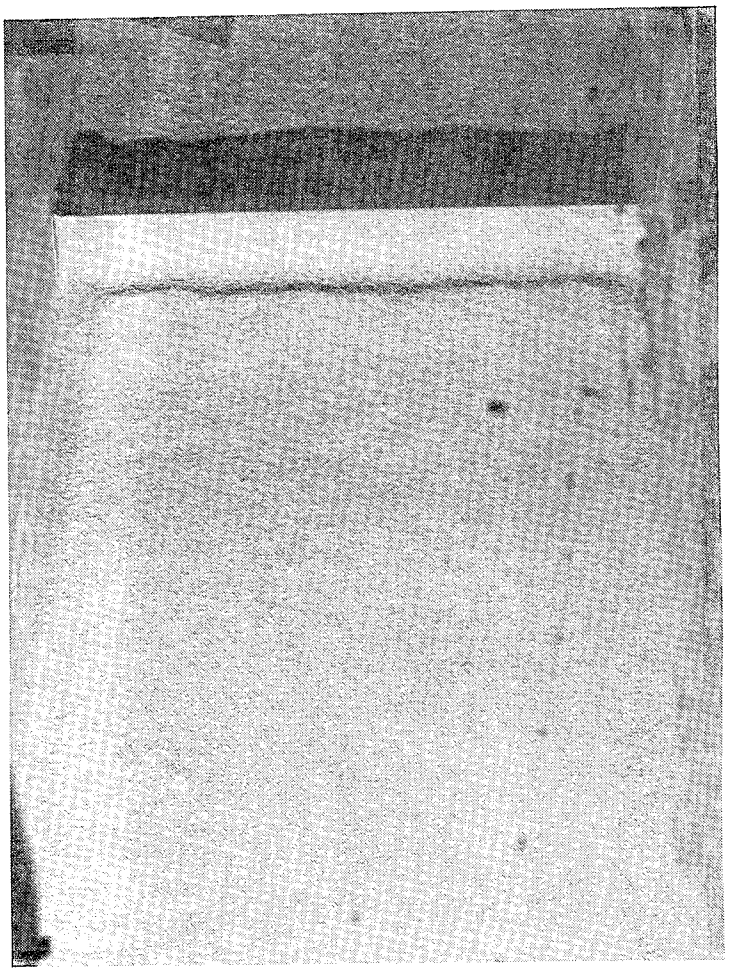

c) Overhead view

Figure A-65. Post test photographs of WSMR dust bed with leading edge disturbance - 1" ridge: RS 64, 124 fps.

a) Downstram close up view

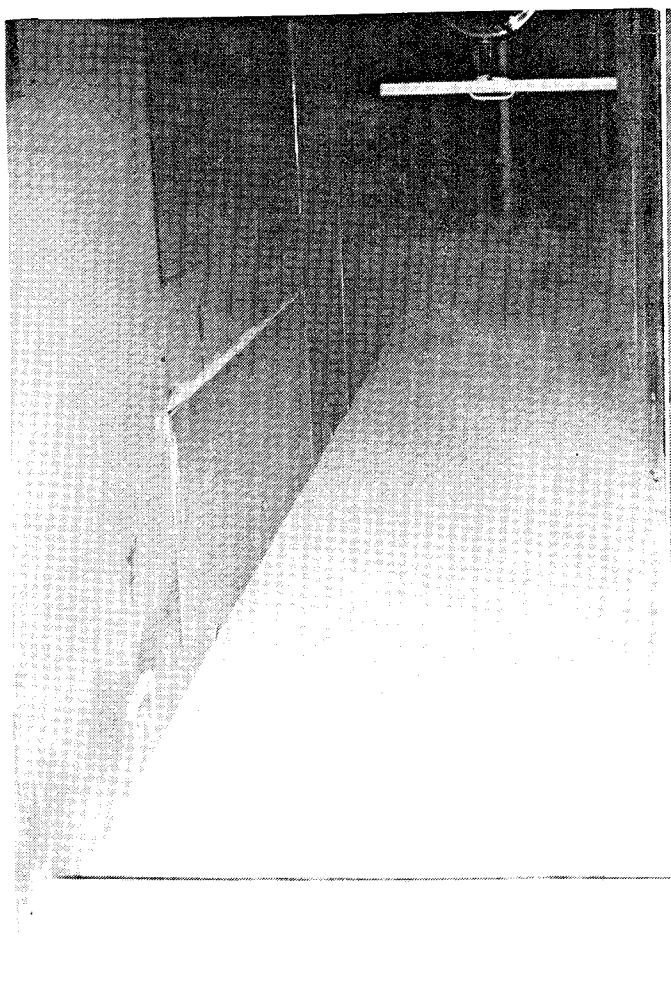

b) Downstream view

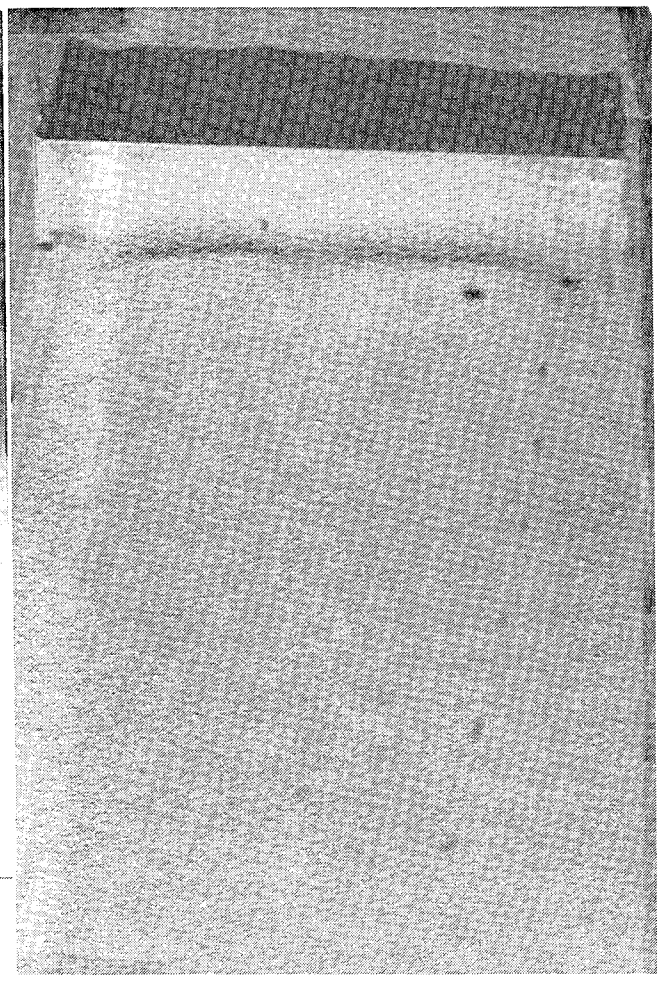

c) Overhead view

Figure A-66. Post test photographs of WSMR dust bed with leading edge disturbance - 1.5" ridge: RS 62, 124 fps.

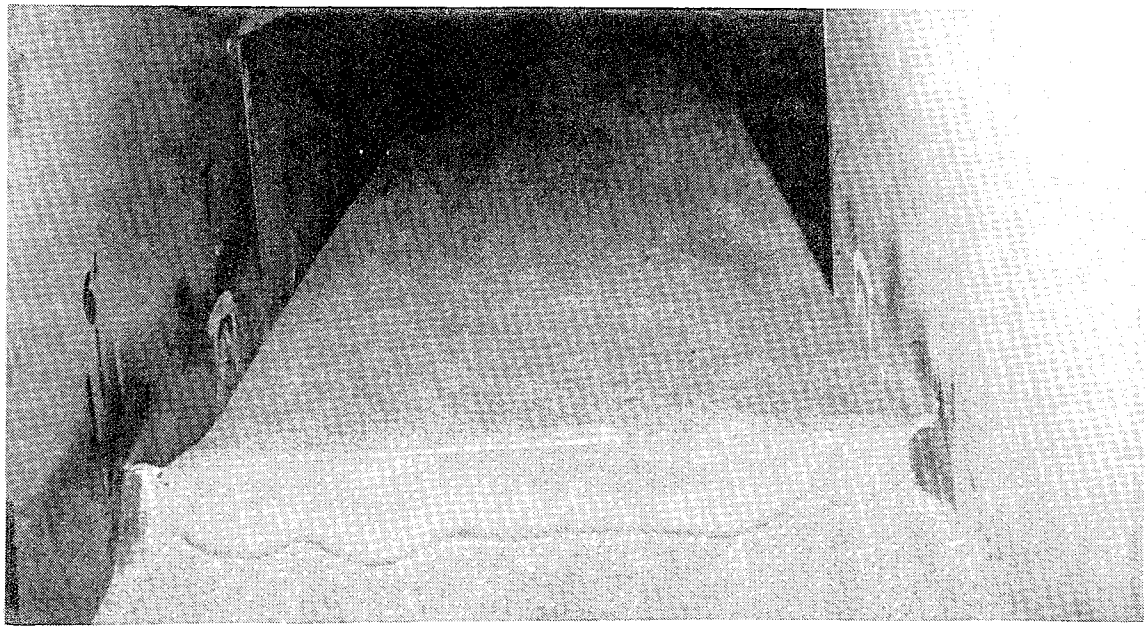

a) Downstream view

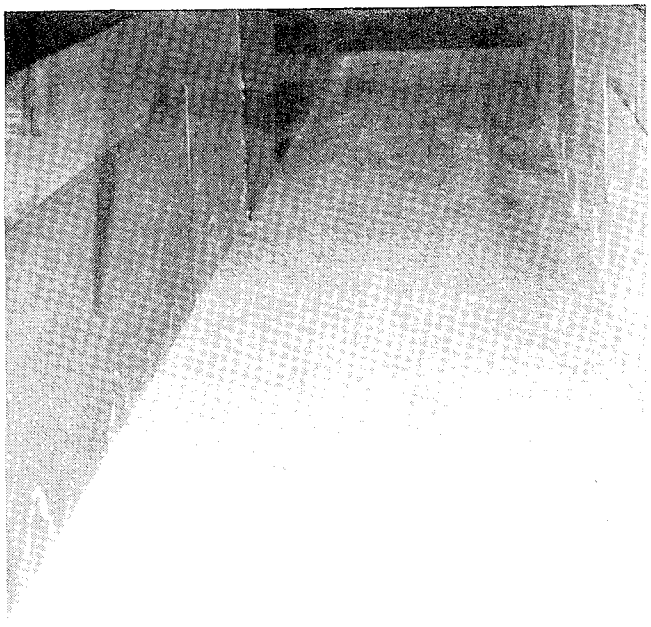

b) Upstream view

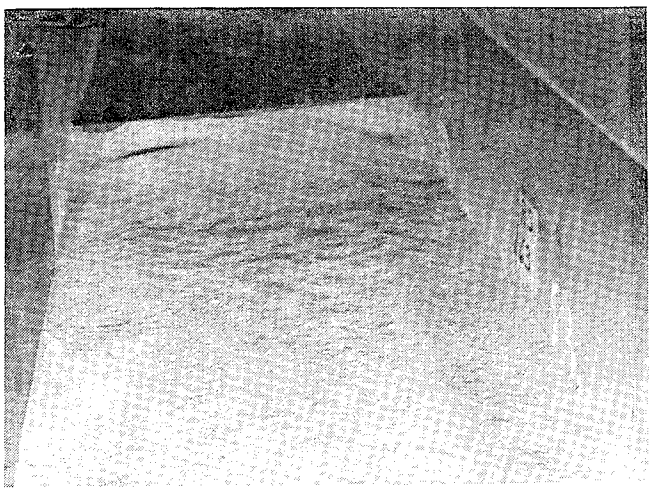

c) Upstream close up view

Figure A-67. Post test photographs of WSMR dust bed with leading edge disturance - 1.5" ridge: RS 63, 229 fps.

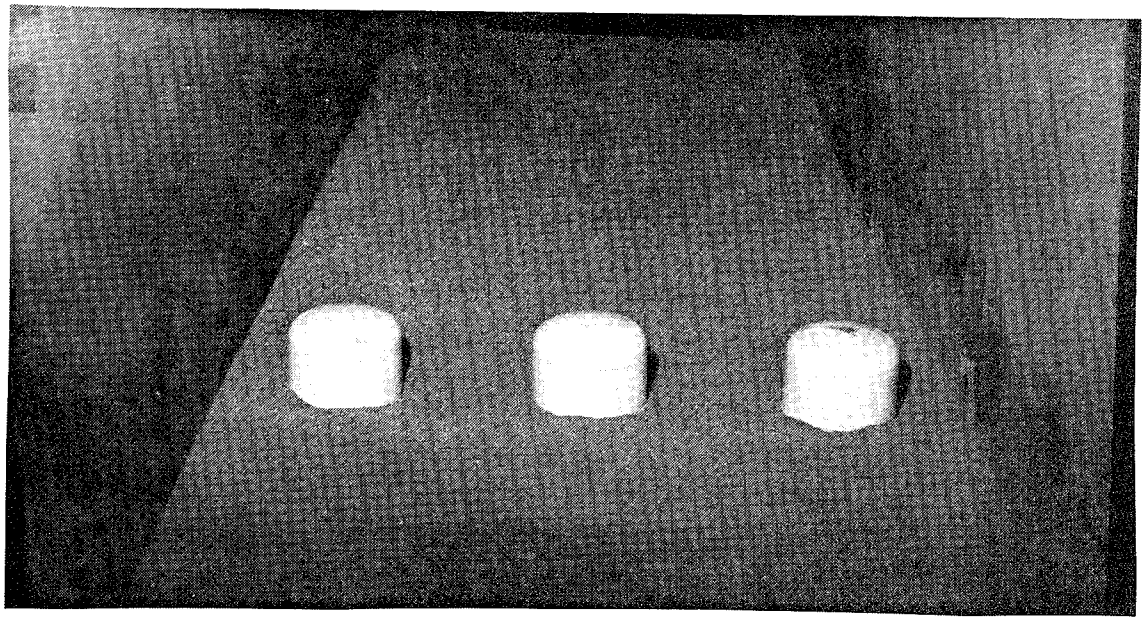

a) Downstream view

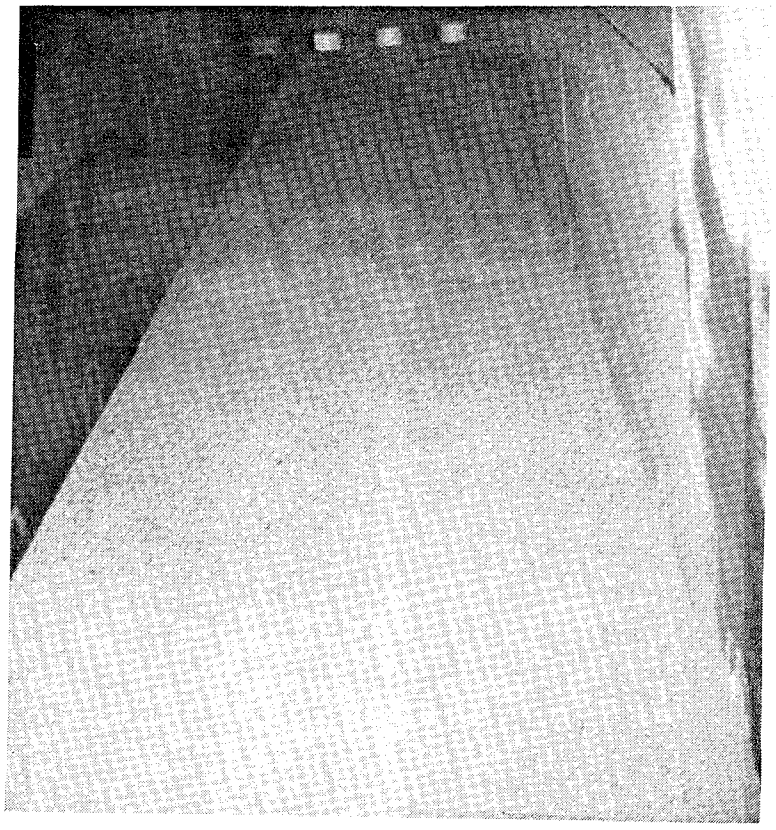

b) Upstream view

Figure A-68. Pre test photographs of WSMR dust bed with leading edge disturbance - Single row clods: RS 55, 122 fps, 2" RS elevation .

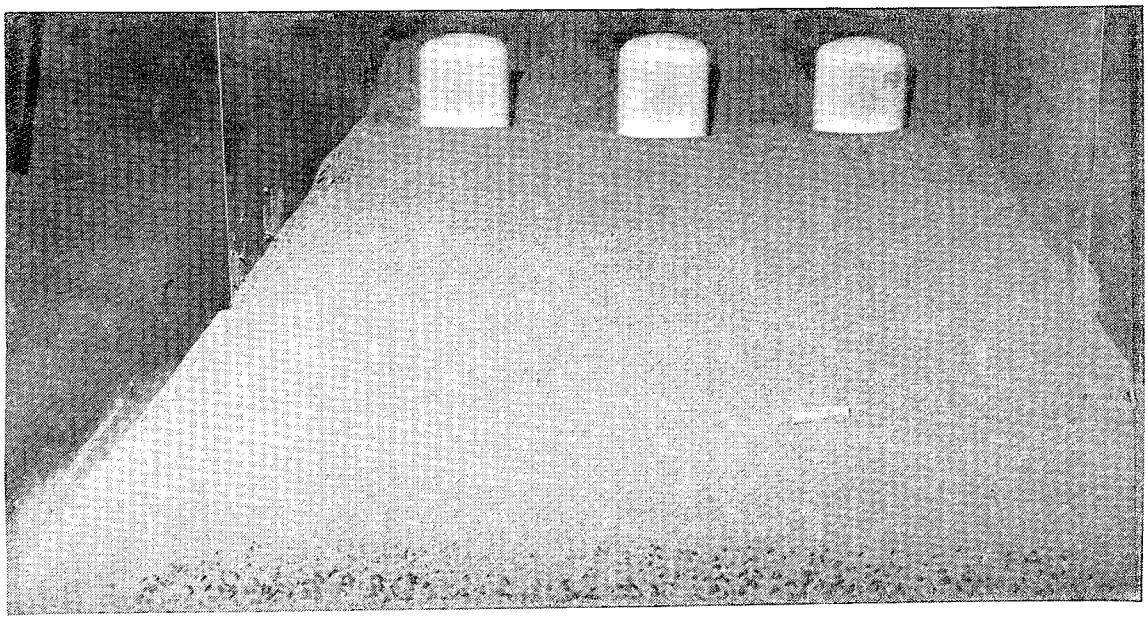

a) Downstream view

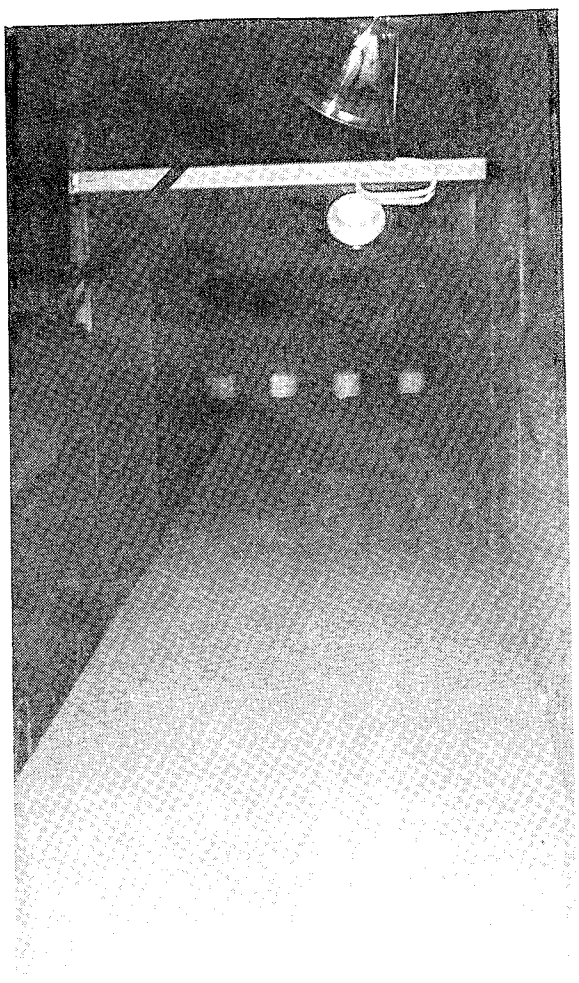

b) Upstream view

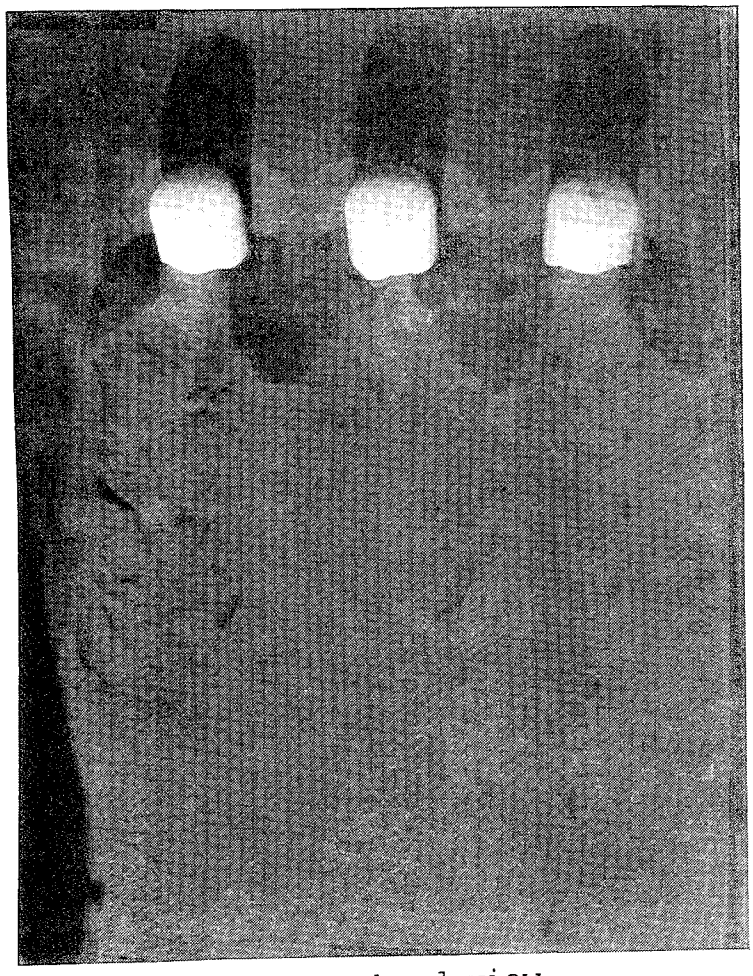

c) Overhead view

Figure A-69. Post test photographs of WSMR dust bed with leading edge disturbance - Single row clods: RS 55, 122 fps, 2" RS elevation.

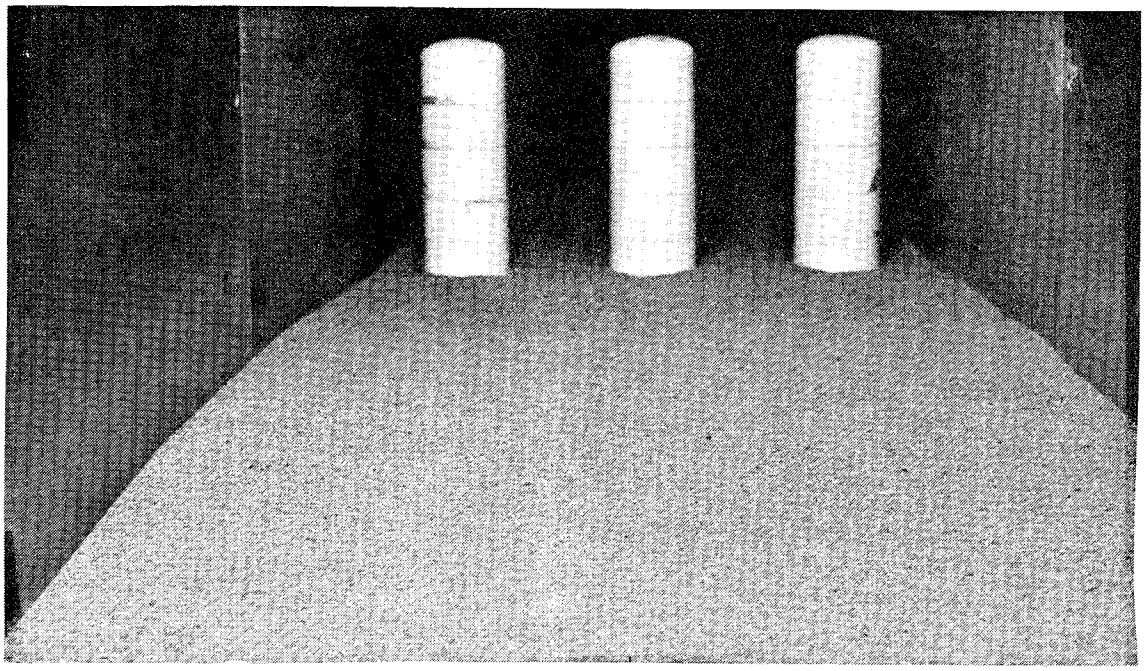

a) Downstream view

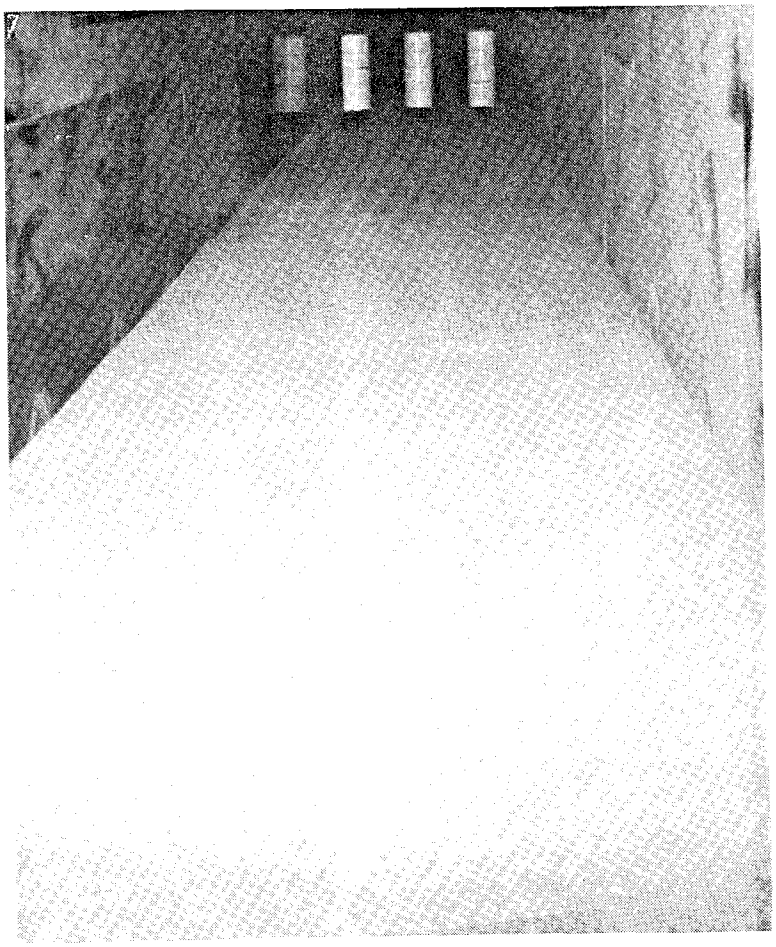

b) Upstream view

Figure A-70. Pre test photographs of WSMR dust bed with leading edge disturbance - Single row clods: RS 68, 129 fps, 7" RS elevation.

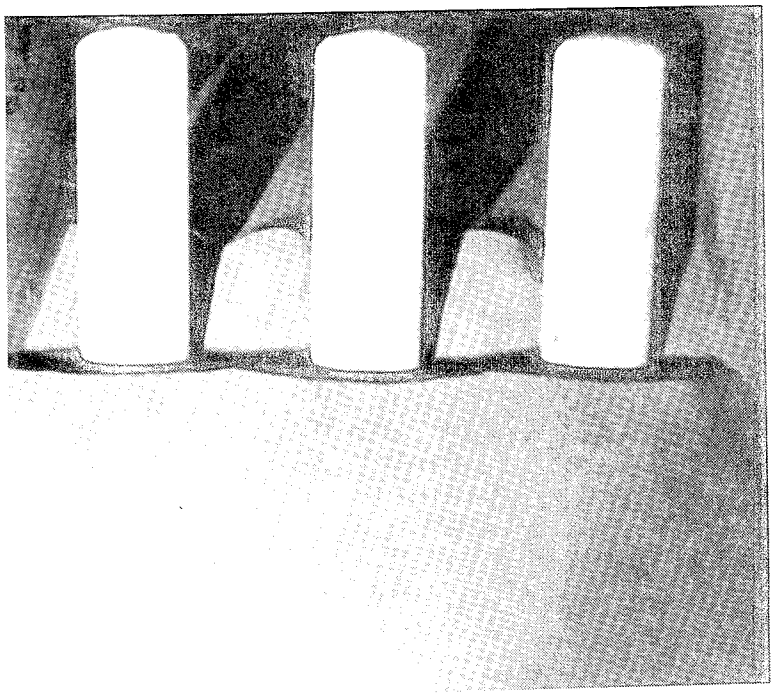

a) Downstream view

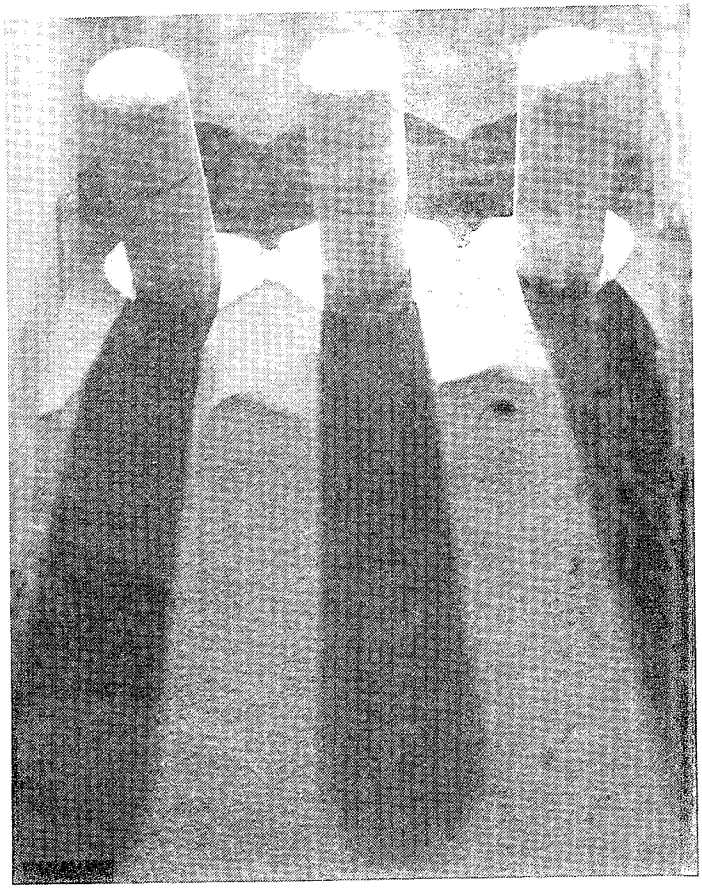

b) Overhead view

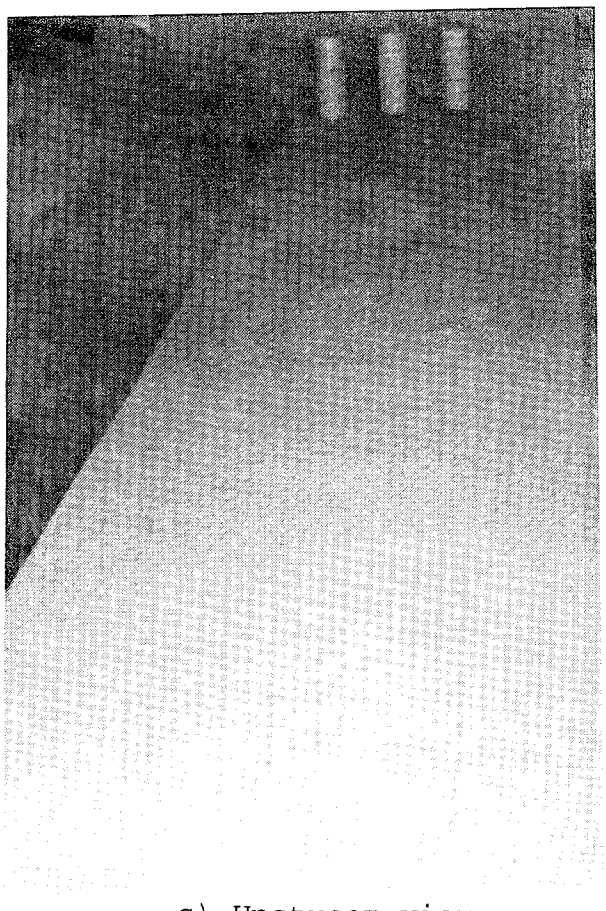

c) Upstream view

Figure A-71. Post test photographs of WSMR dust bed with leading edge disturbance - Single row clods: RS 68, 129 fps, 7" RS elevation.

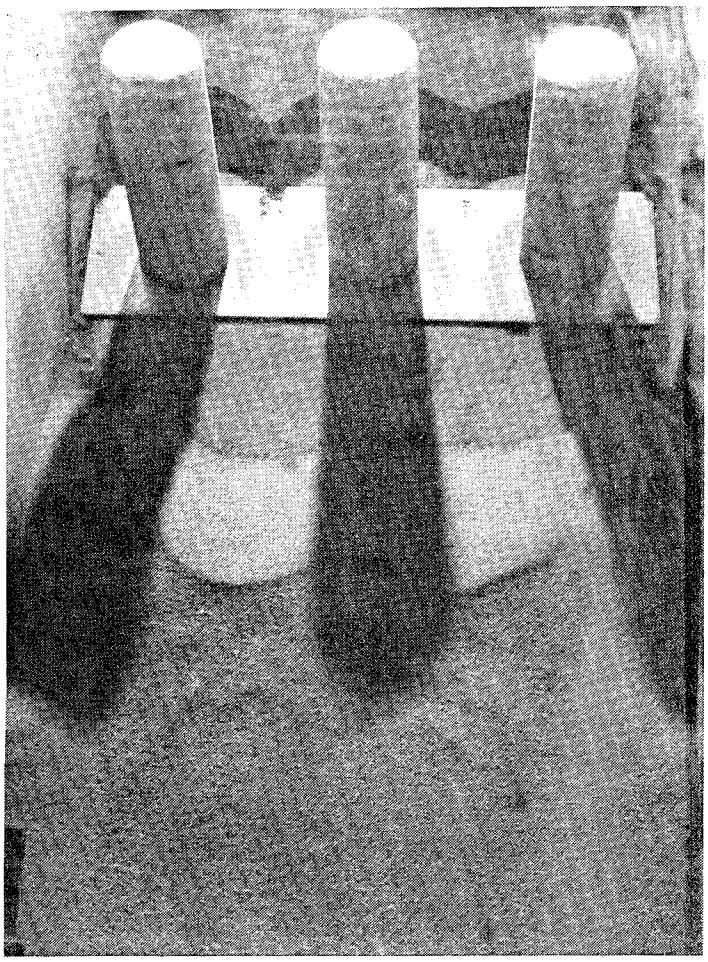

a) Overhead view

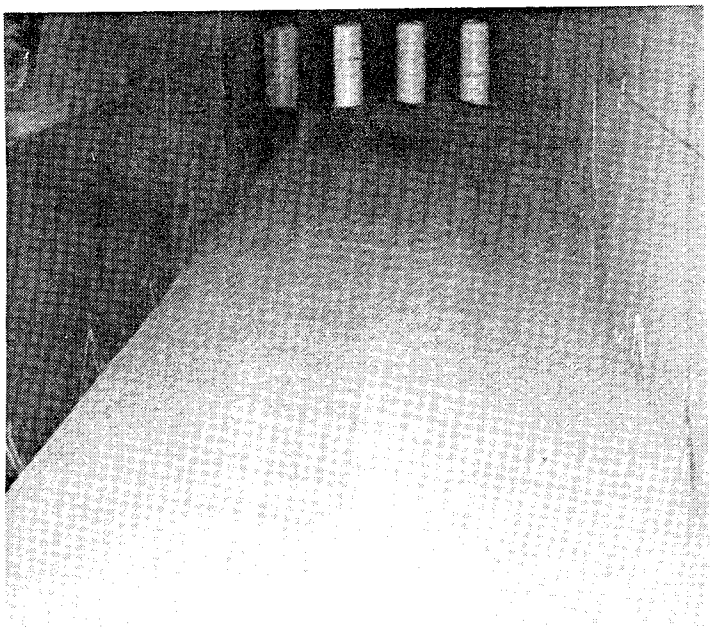

b) Upstream view

Figure A-72. Post test photographs of WSMR dust bed with leading edge disturbance - Single row clods: RS 69, 234 fps, 7" RS elevation.

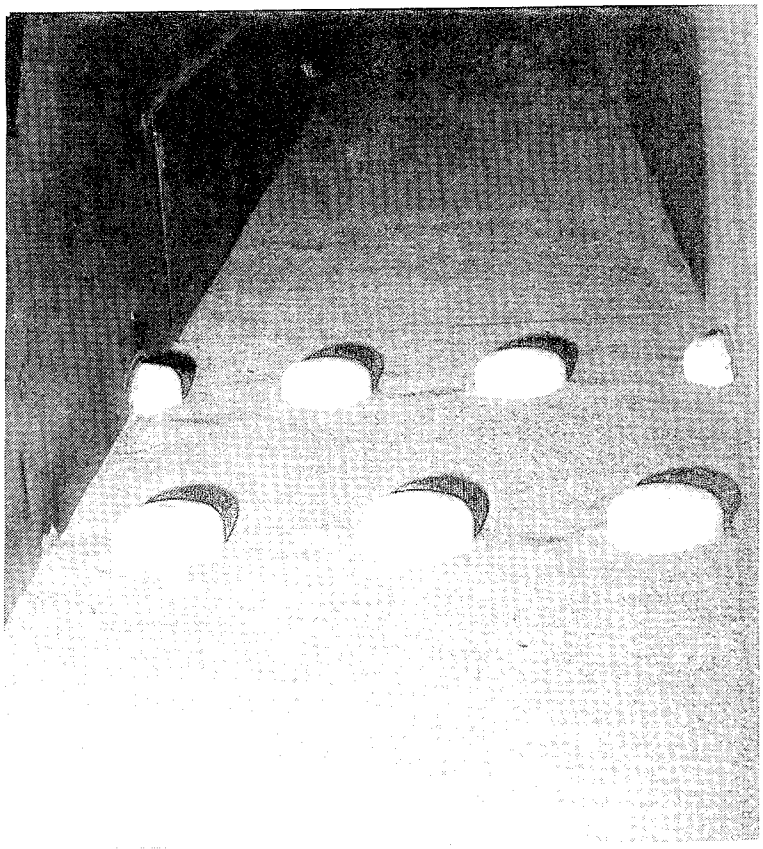

a) Downstream view

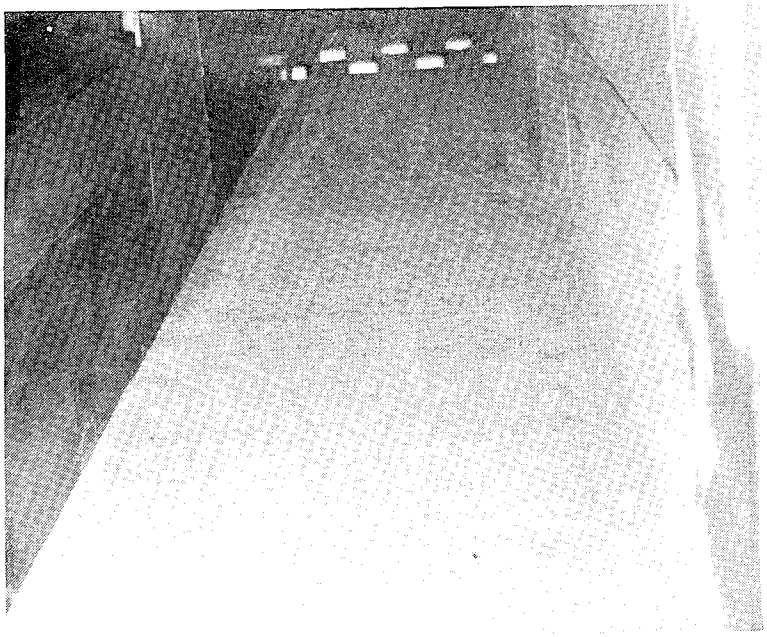

b) Upstream view

Figure A-73. Pre test photographs of WSMR dust bed with leading edge disturbance - Double row clods: RS 52, 235 fps, 1" RS elevation .

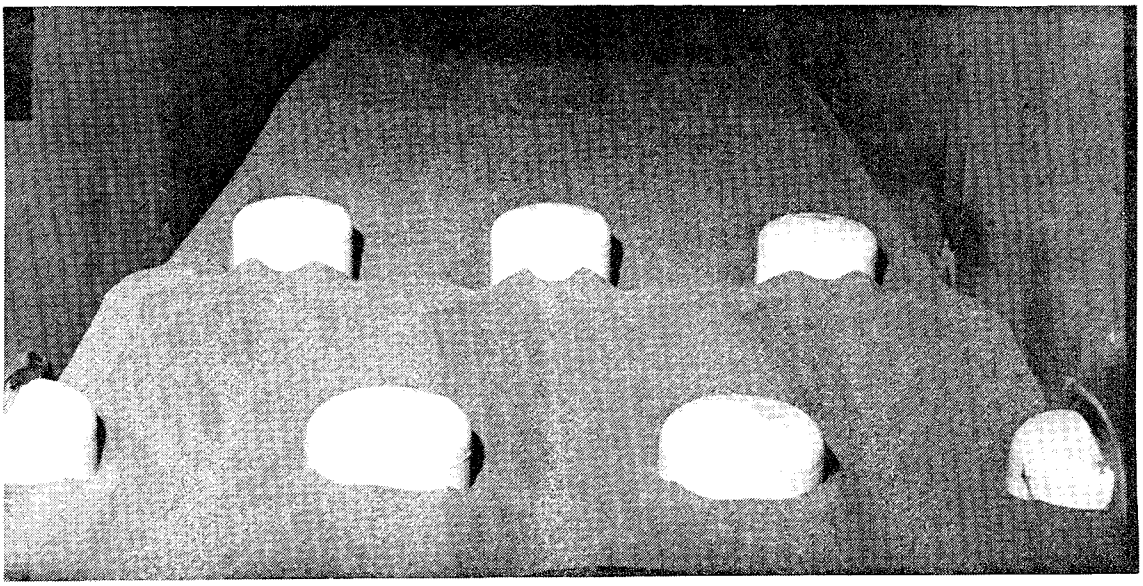

a) Downstream close up view

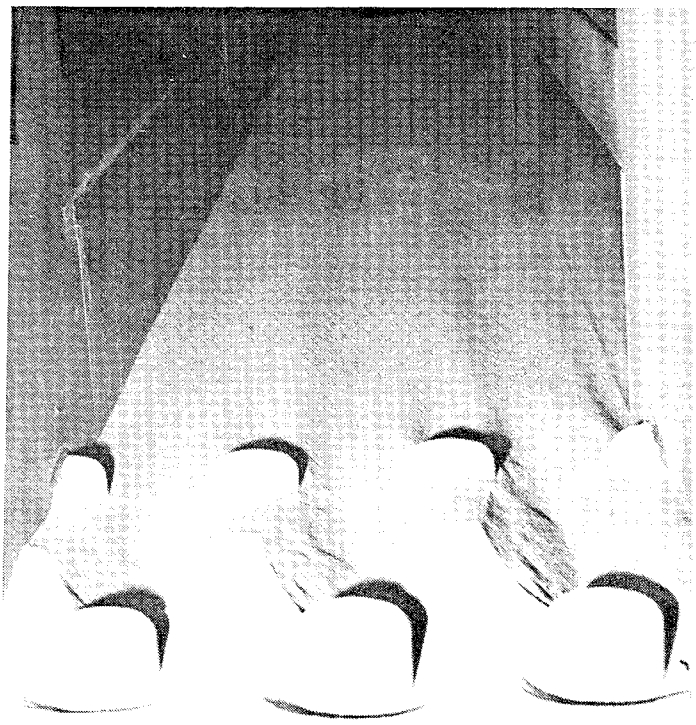

b) Downstream view

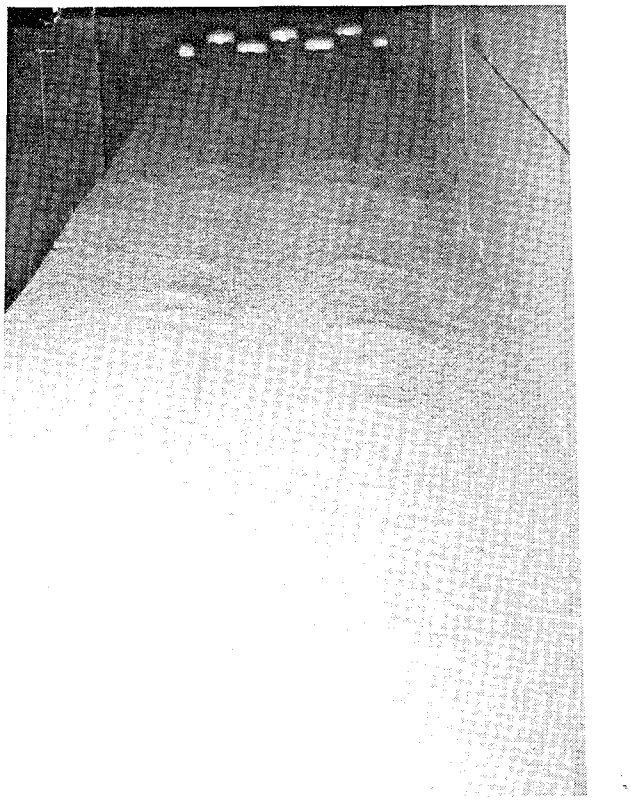

c) Upstream view

Figure A-74. Post test photographs of WSMR dust bed with leading edge disturbance - Double row clods: RS 51, 127 fps, 1" RS elevation.

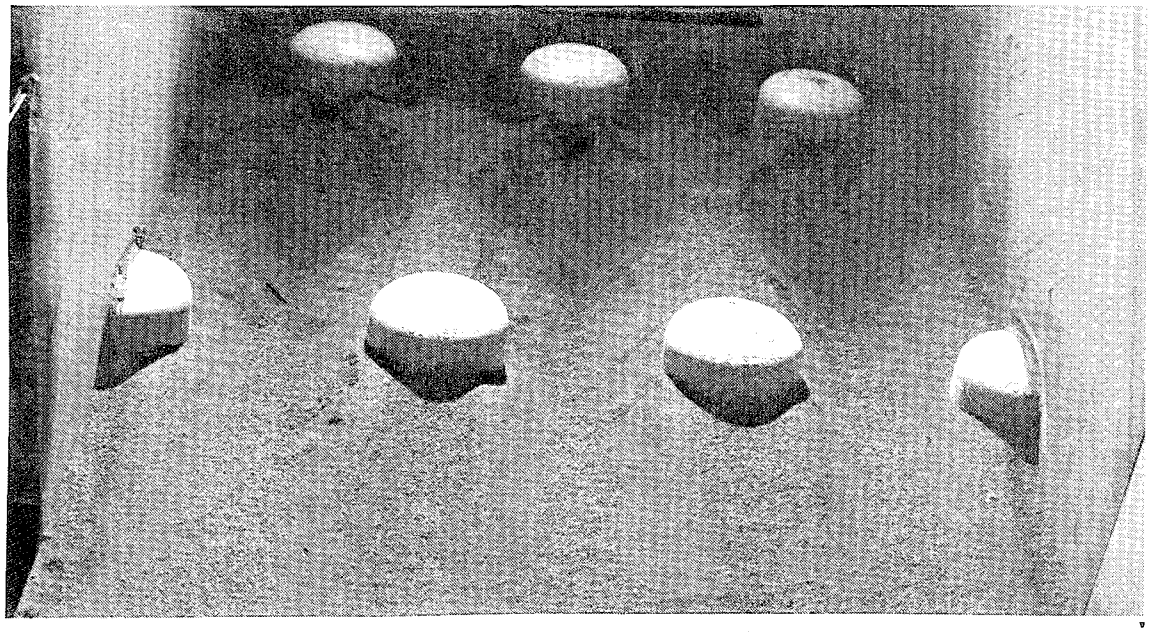

a) Upstream close up view

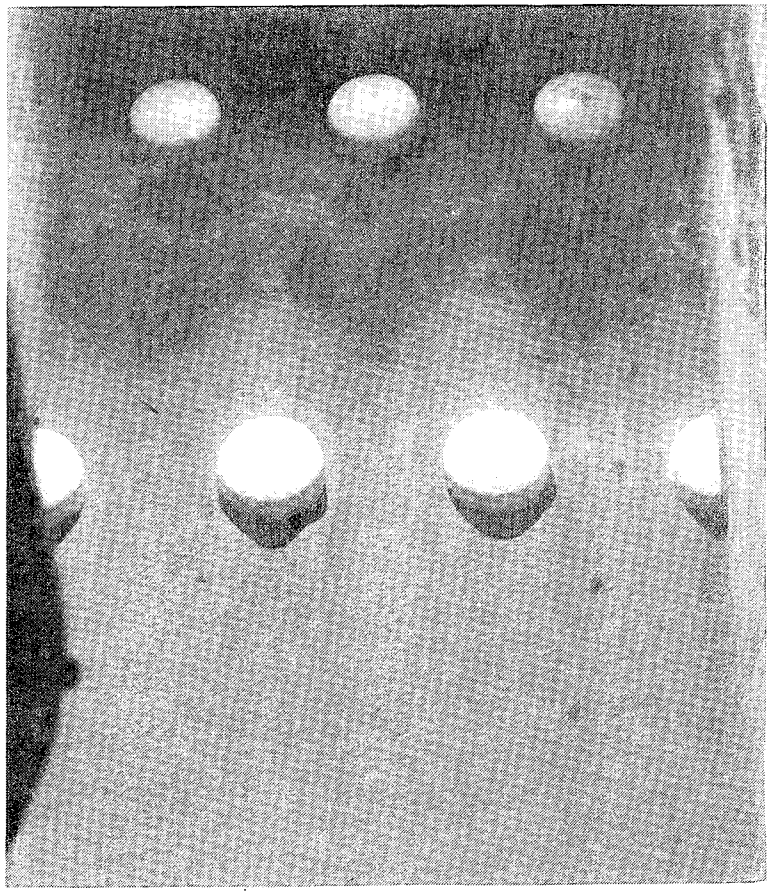

b) Overhead view

Figure A-75. Post test photographs of WSMR dust bed with leading edge disturbance - Double row clods: RS 51, 127 fps, 1" RS elevation.

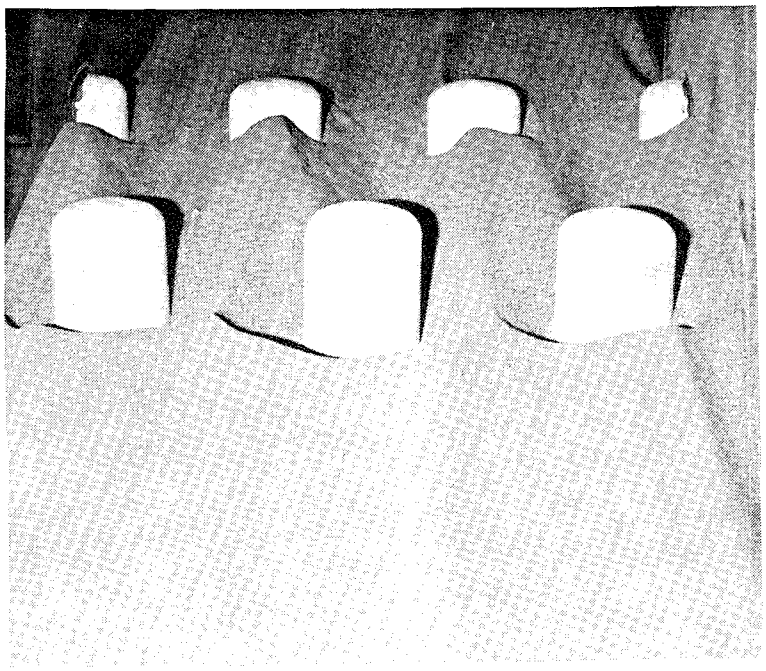

a) Downstream view

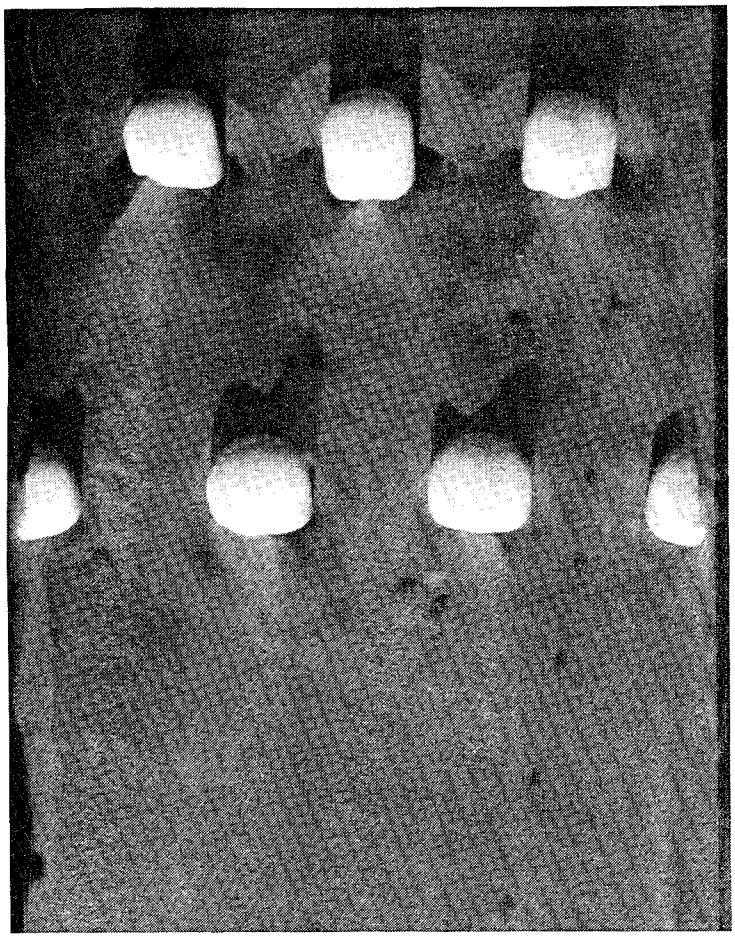

b) Overhead view

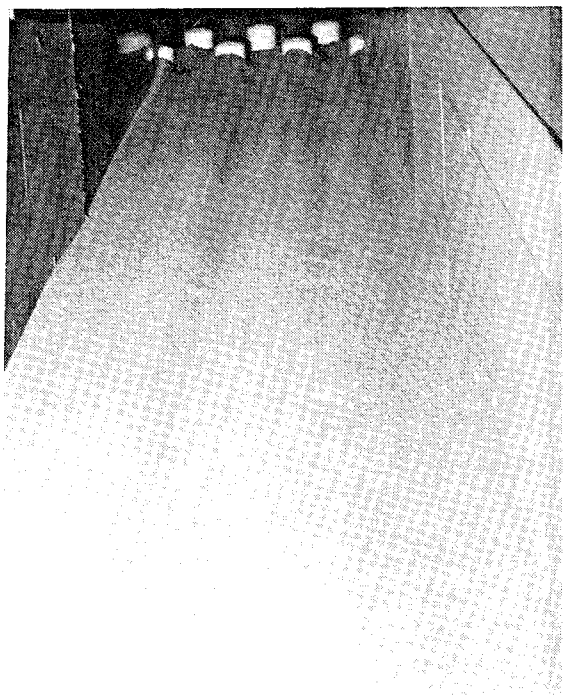

c) Upstream view

Figure A-76. Post test photographs of WSMR dust bed with leading edge disturbance - Double row clods: RS 52, 235 fps, 1" RS elevation.

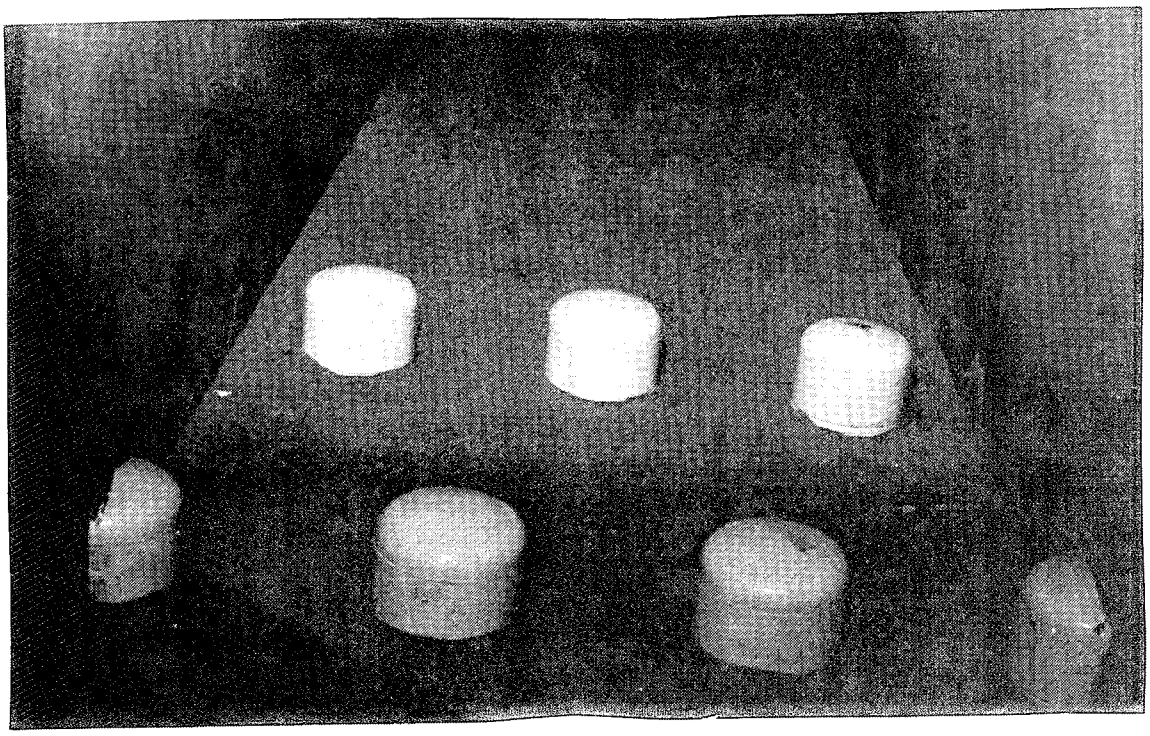

a) Upstream close up view

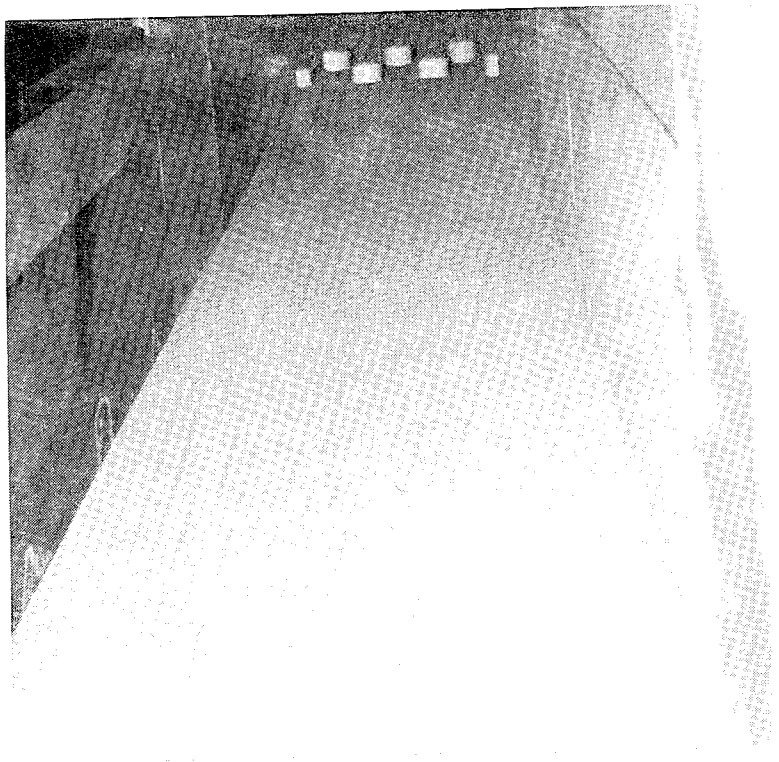

b) Upstream view

Figure A-77. Pre test photographs of WSMR dust bed with leading edge distributions - Double row clods: RS 53, 122 fps, 2" RS elevation.

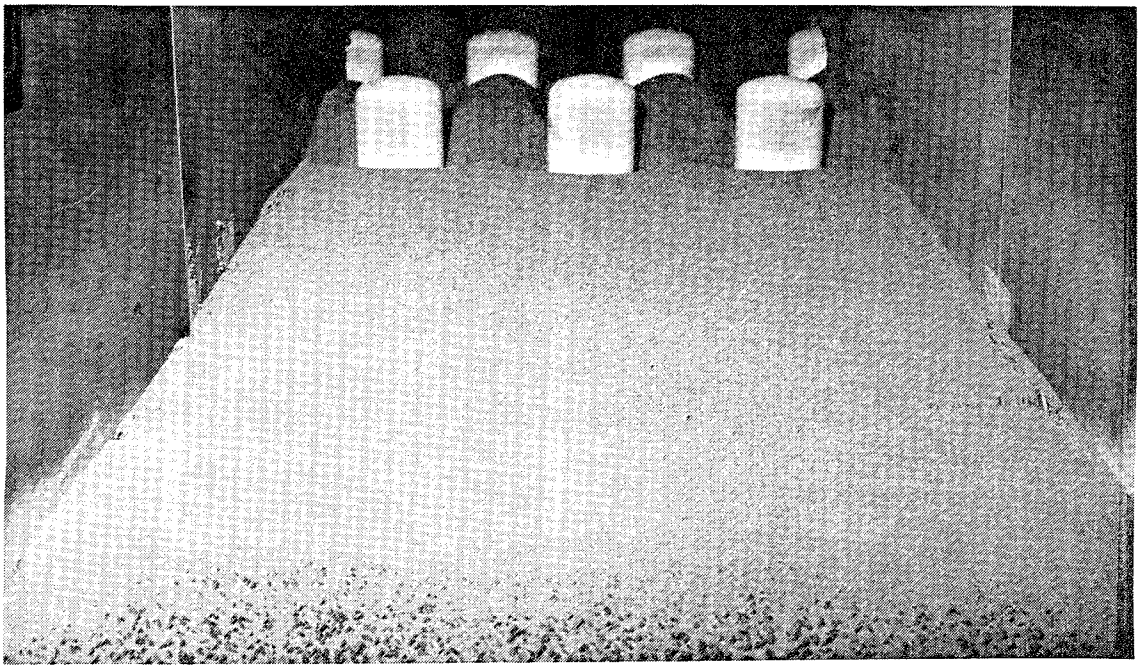

a) Downstream view

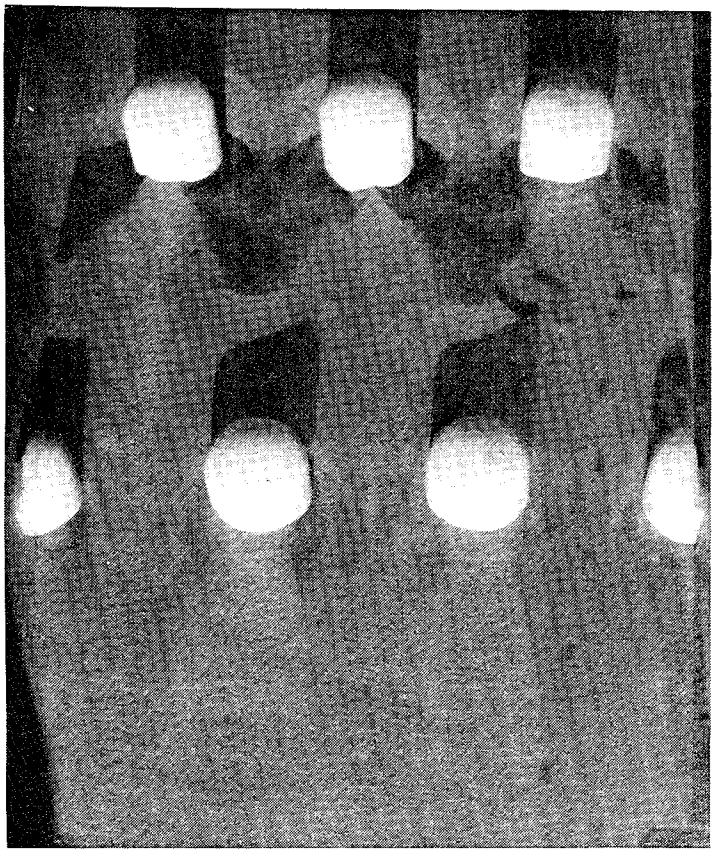

b) Overhead view

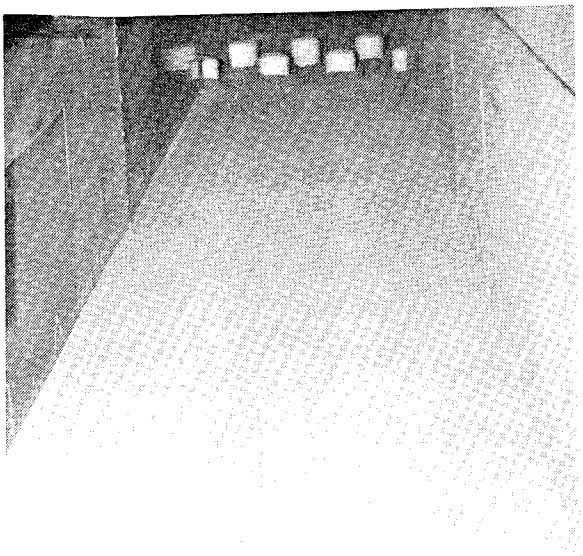

c) Upstream view

Figure A-78. Post test photographs of WSMR dust bed with leading edge disturbance - Double row clods: RS 53, 122 fps, 2" RS elevation.

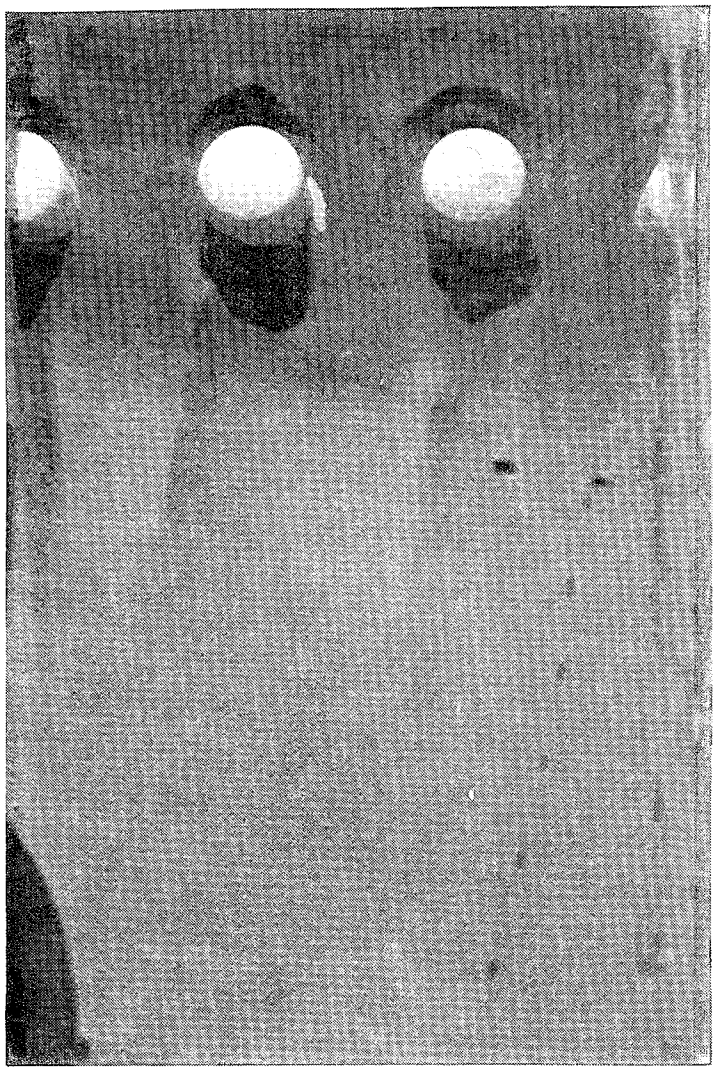

a) Overhead view

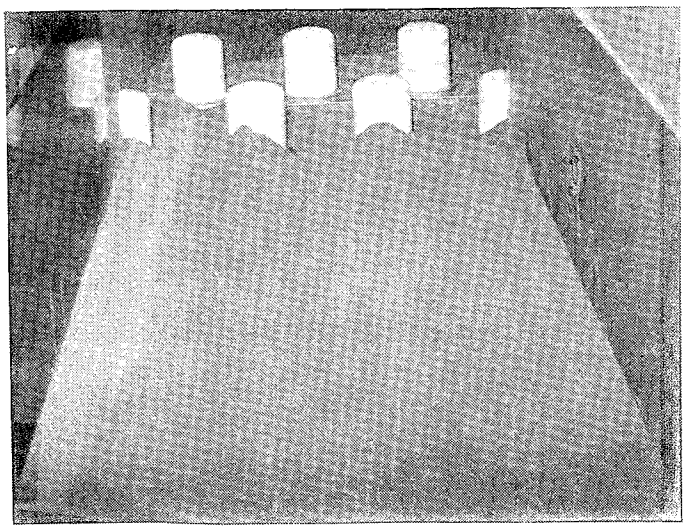

b) Upstream view

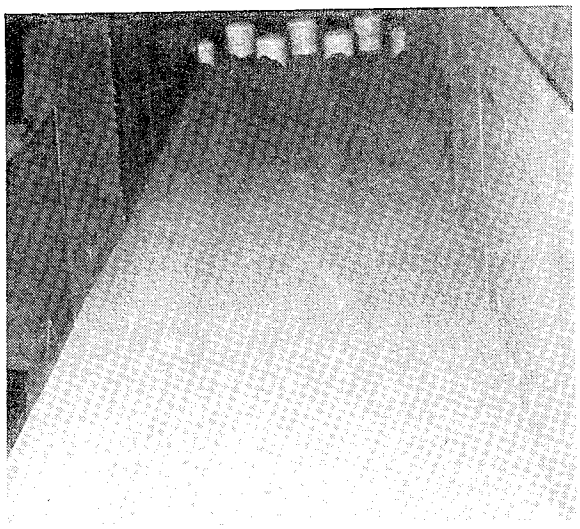

c) Upstream close up view

Figure A-79. Post test photographs of WSMR dust bed with leading edge disturbance - Double row clods: RS 54, 232 fps, 2" RS elevation.

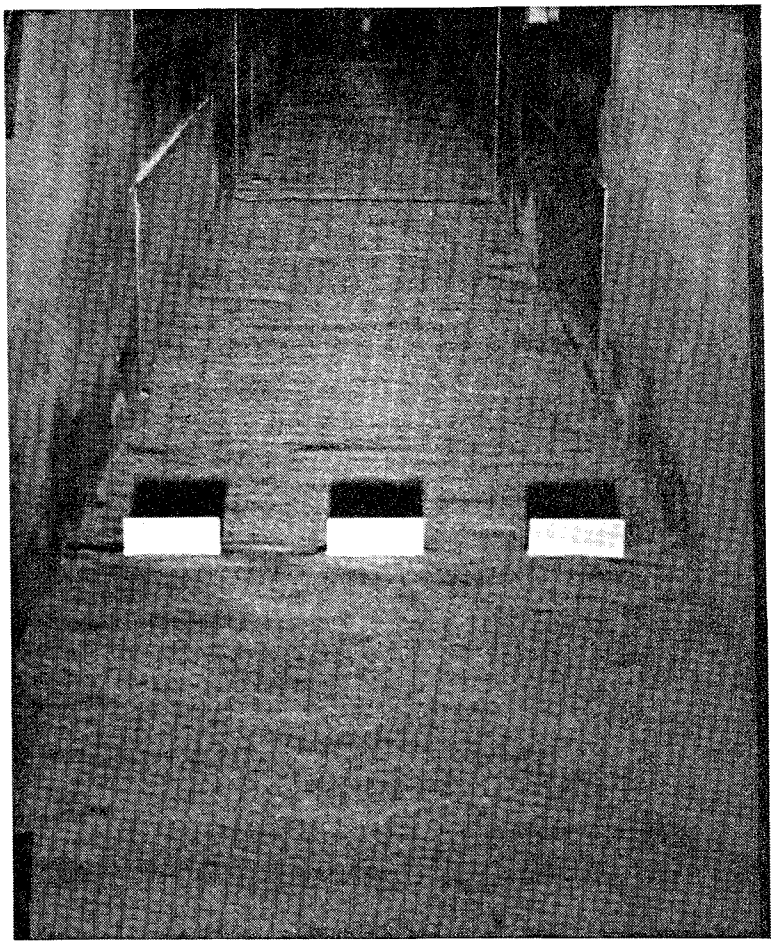

a) Downstream view

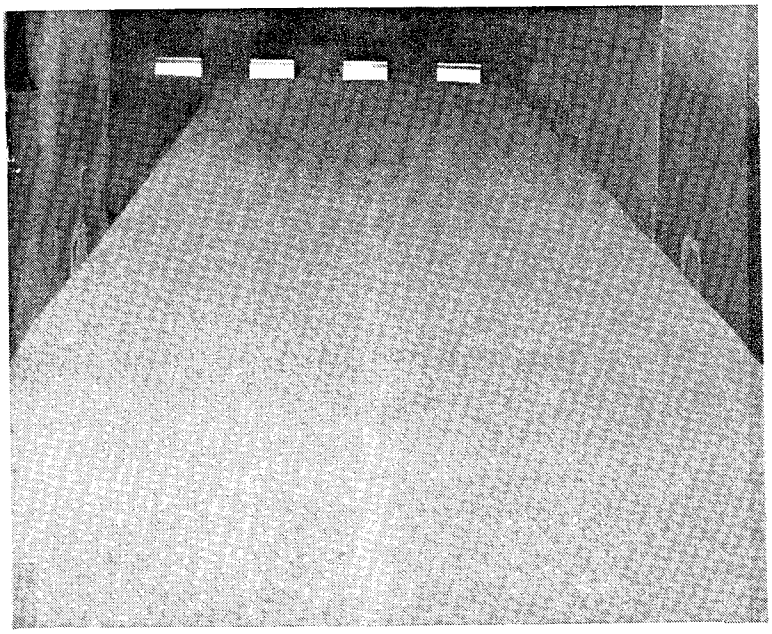

b) Upstream view

Figure A-80. Pre test photographs of WSMR dust bed with leading edge disturbance - Vortex generator array: RS 76, 234 fps, 1" RS elevation.

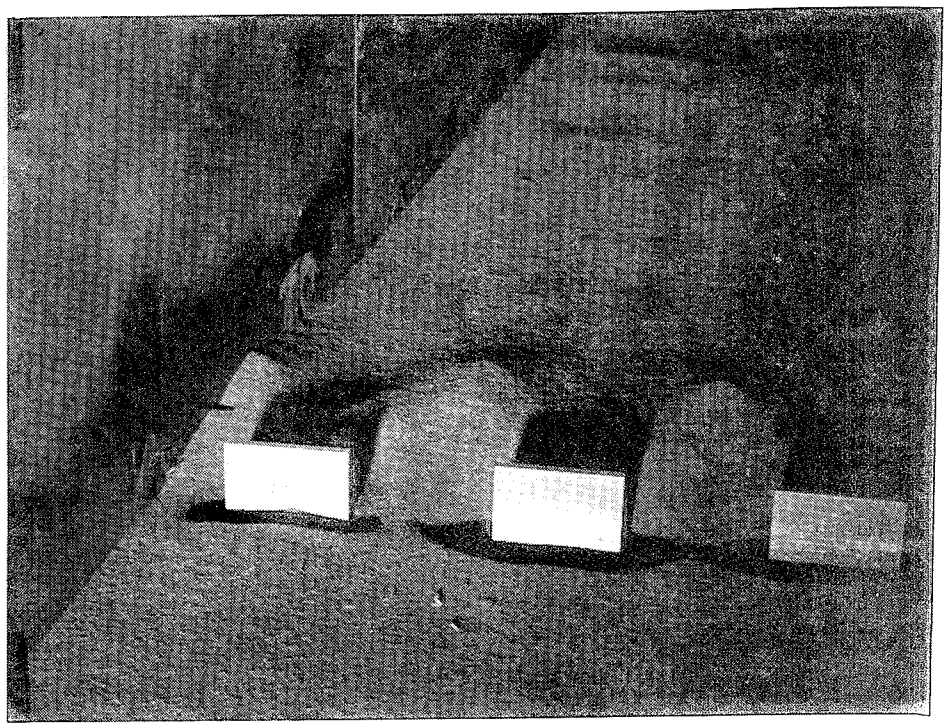

a) Downstream close up view

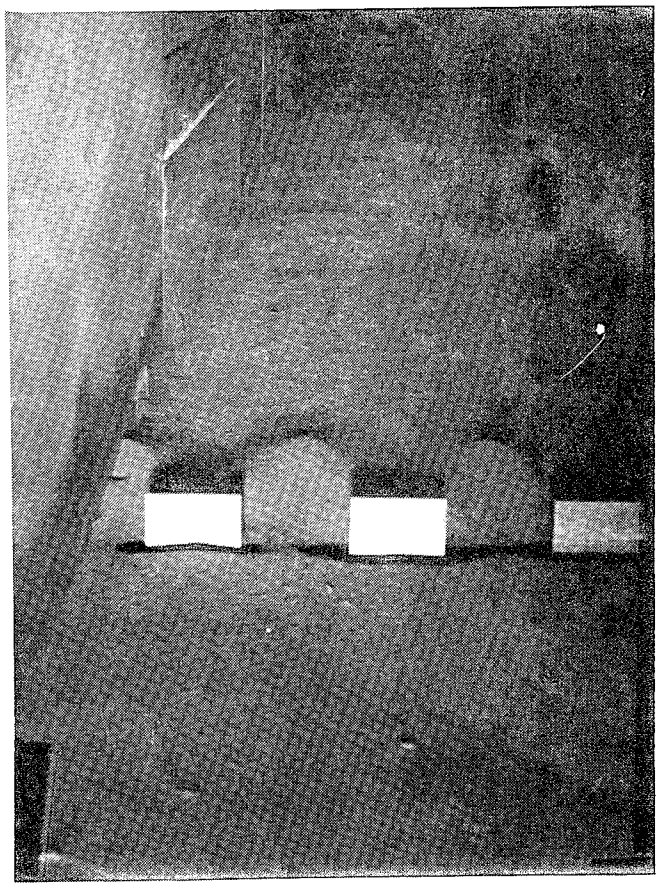

b) Downstream view

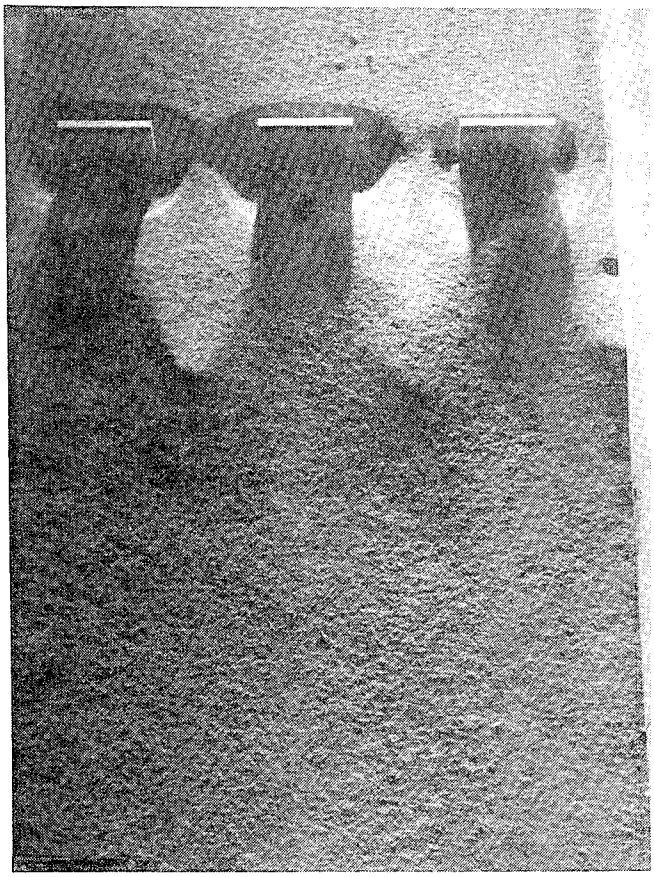

c) Overhead view

Figure A-81. Post test photographs of WSMR dust bed with leading edge disturbance - Vortex generator array: RS 75, 122 fps, 1" RS elevation.

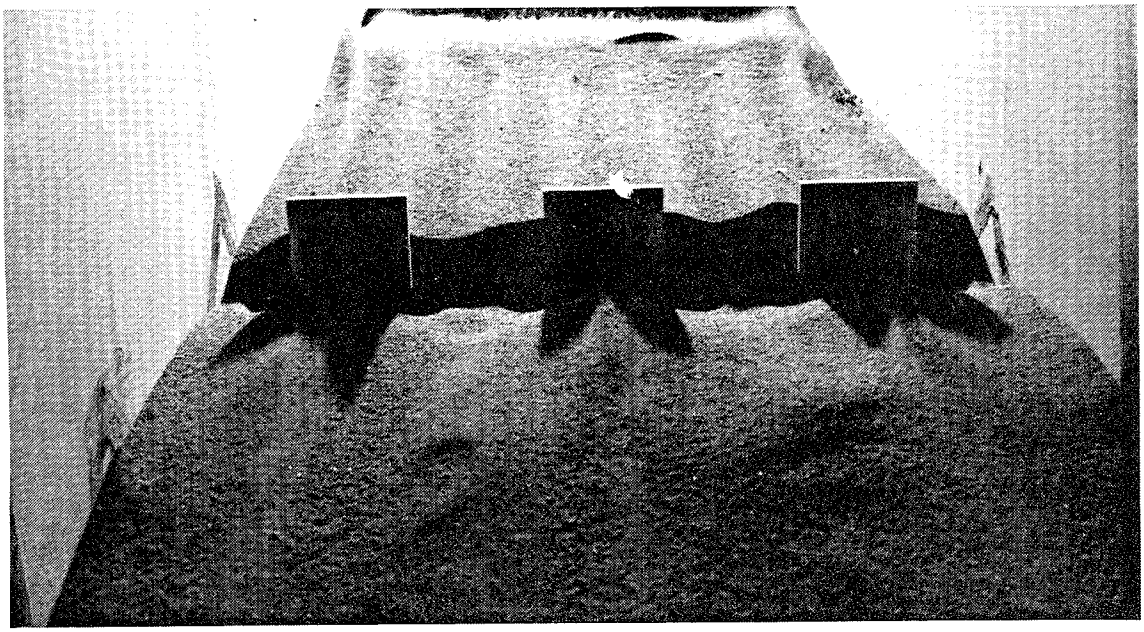

a) Upstream close up view

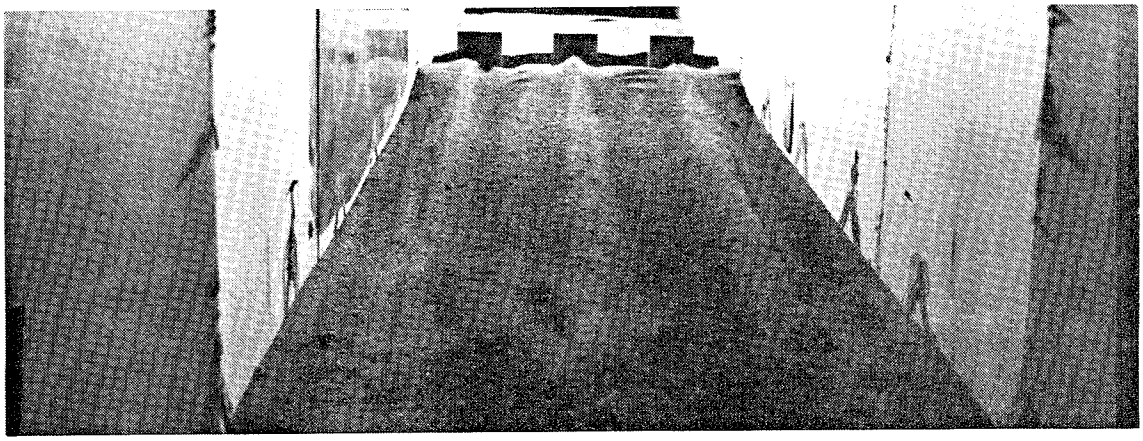

b) Upstream view - back lighted

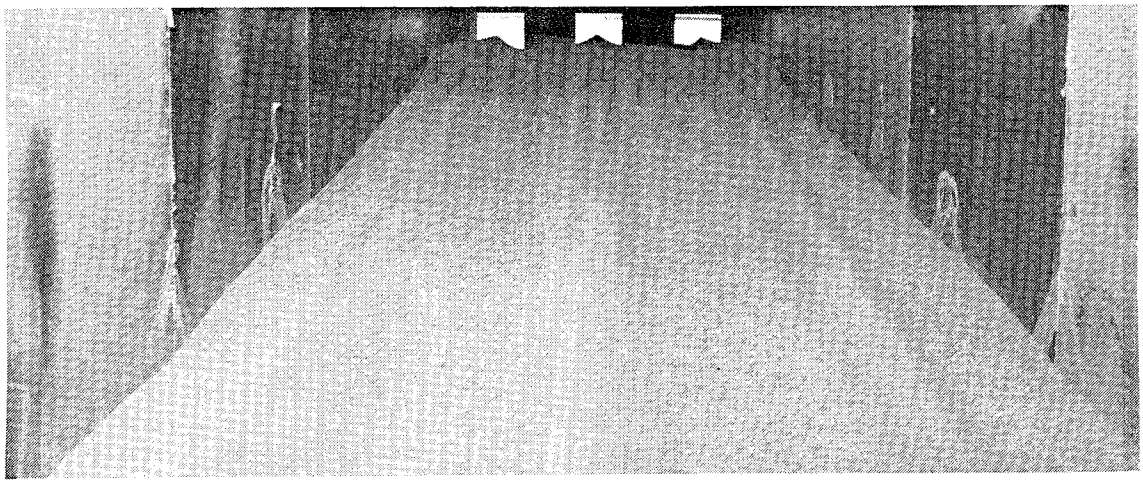

c) Upstream view - front lighted

Figure A-82. Post test photographs of WSMR dust bed with leading edge disturbance - Vortex generator array: RS 76, 234 fps, 1" RS elevation.

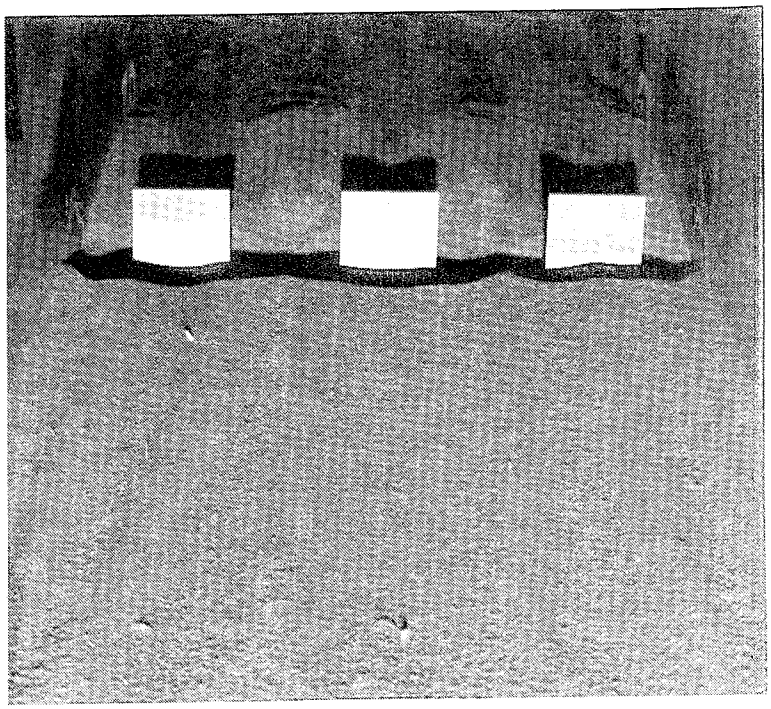

a) Downstream view

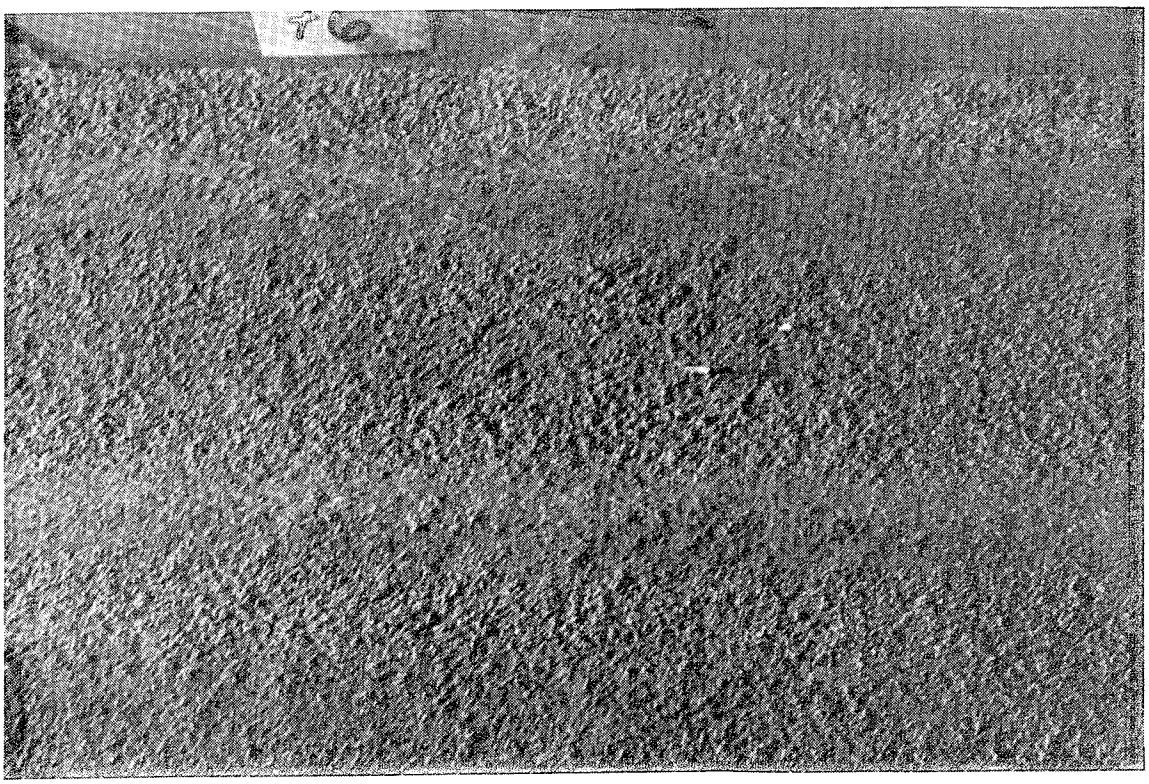

b) Overhead view at 9' location

Figure A-83. Post test photographs of WSMR dust bed with leading edge disturbance - Vortex generator array: RS 76, 234 fps, 1" RS elevation.

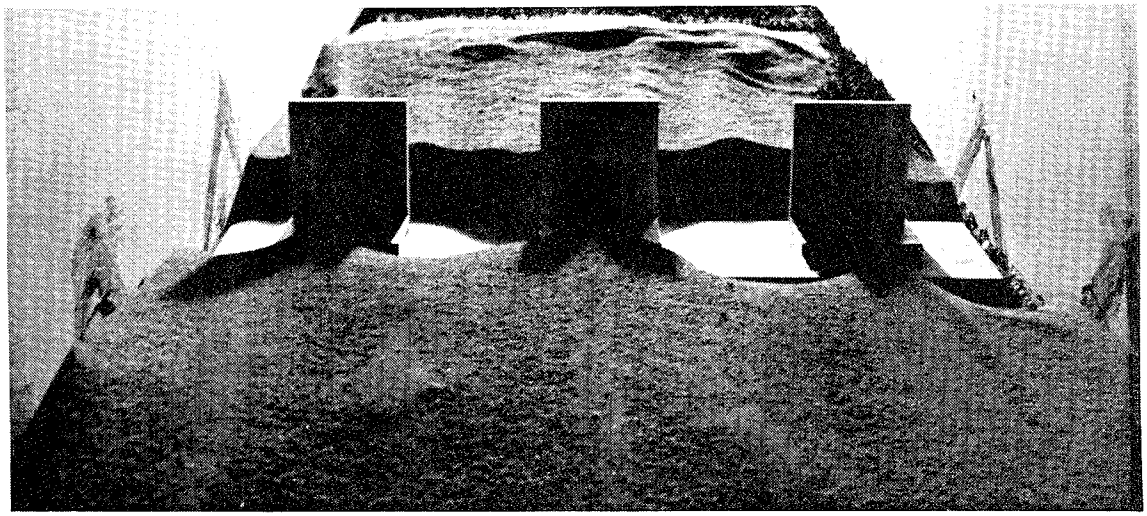

a) Upstream close up view

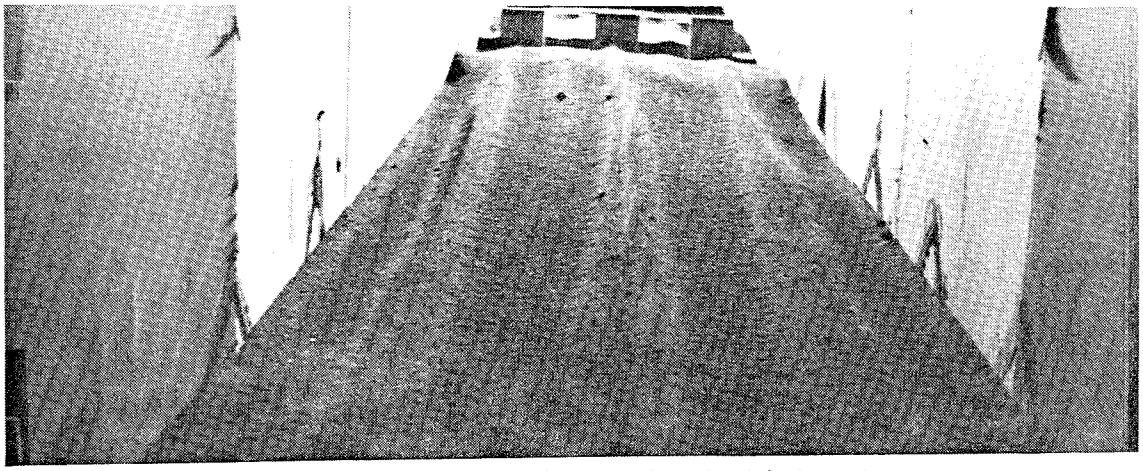

b) Upstream view - back lighted

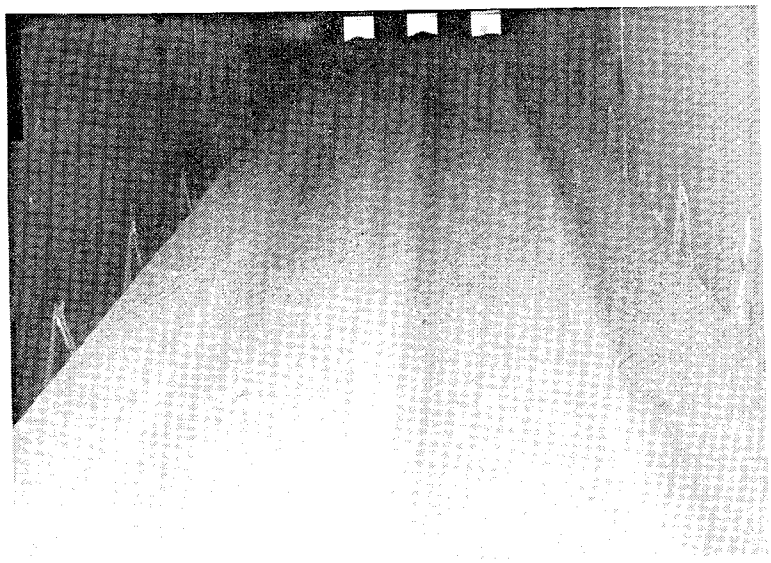

c) Upstream view - front lighted

Figure A-84. Post test photographs of WSMR dust bed with leading edge disturbance - Vortex generator array: RS 77, 364 fps, 1" RS elevation.

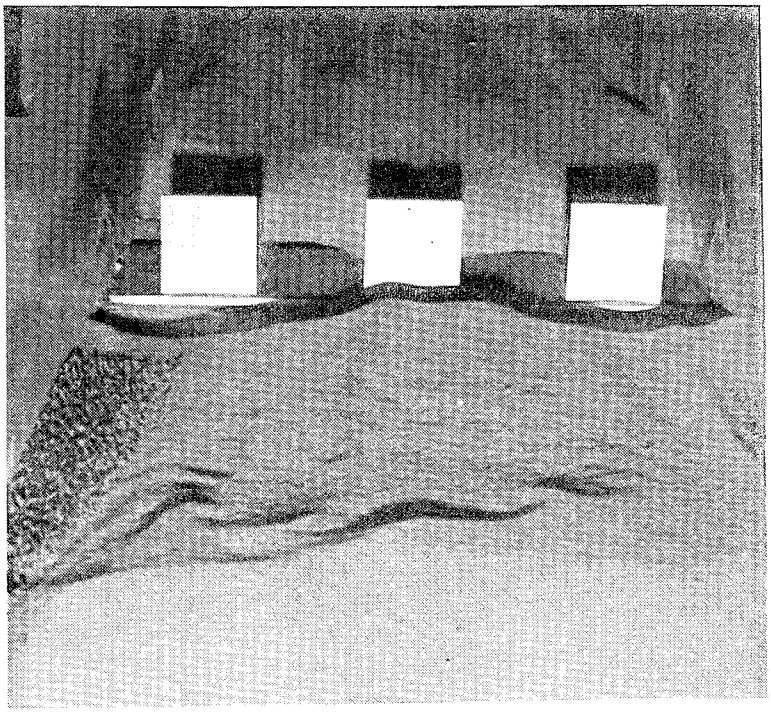

a) Downstream view

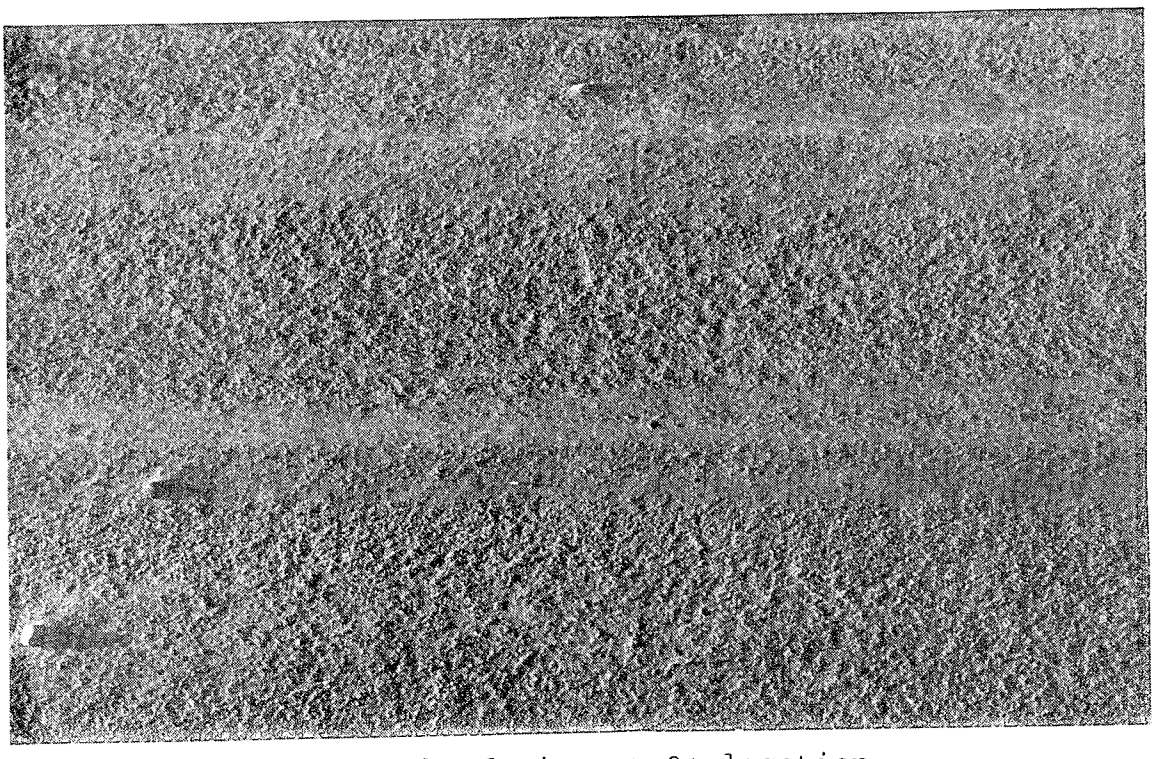

b) Overhead view at 9' location

Figure A-85. Post test photographs of WSMR dust bed with leading edge disturbance - Vortex generator array: RS 77, 364 fps, 1" RS elevation.

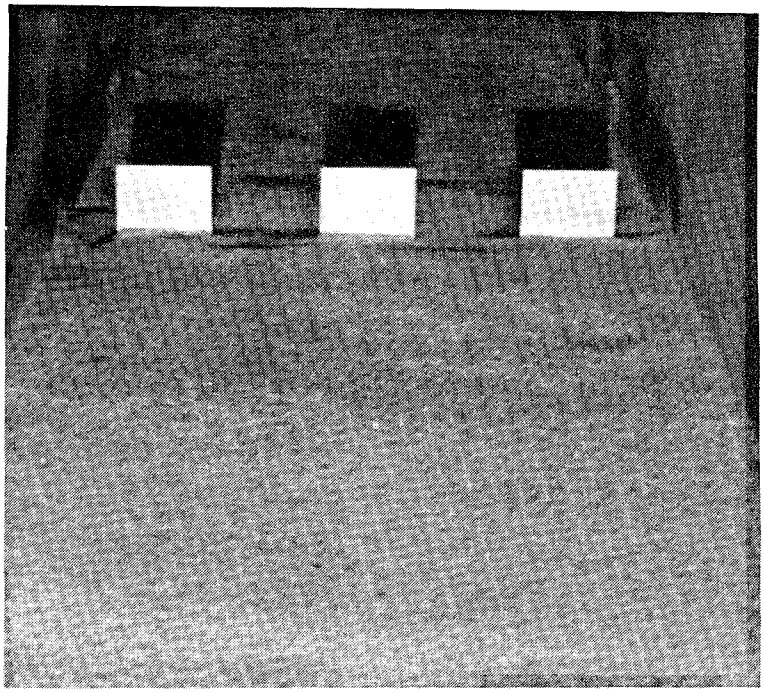

a) Downstream view

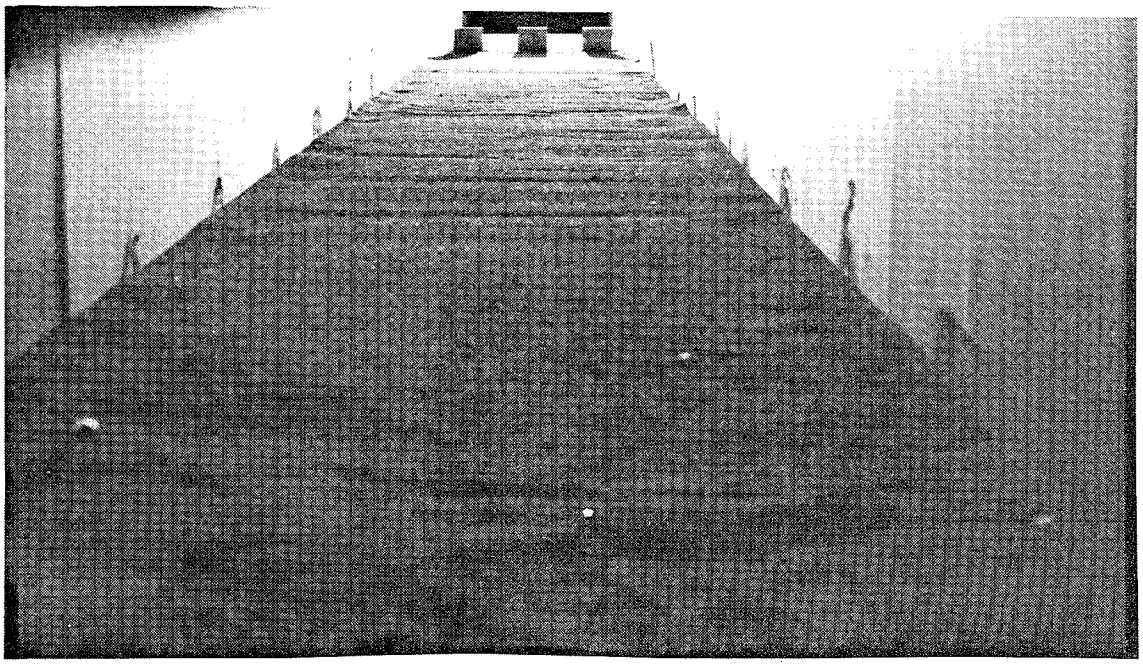

b) Upstream view

Figure A-86. Pre test photographs of WSMR dust bed with leading edge disturbance - Vortex generator array: RS 80, 367 fps, 2" RS elevation.

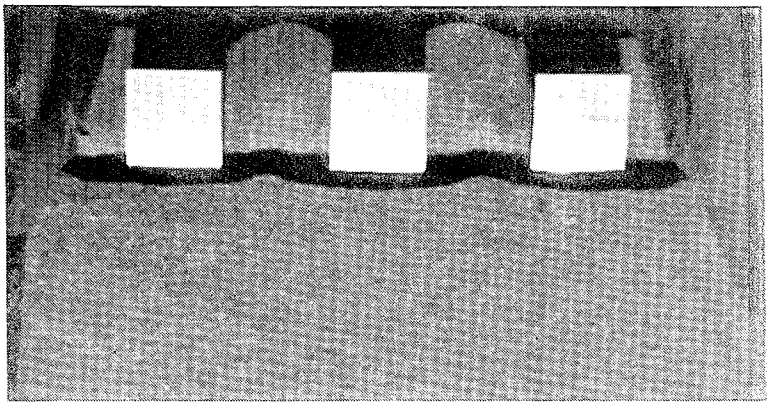

a) Downstream view

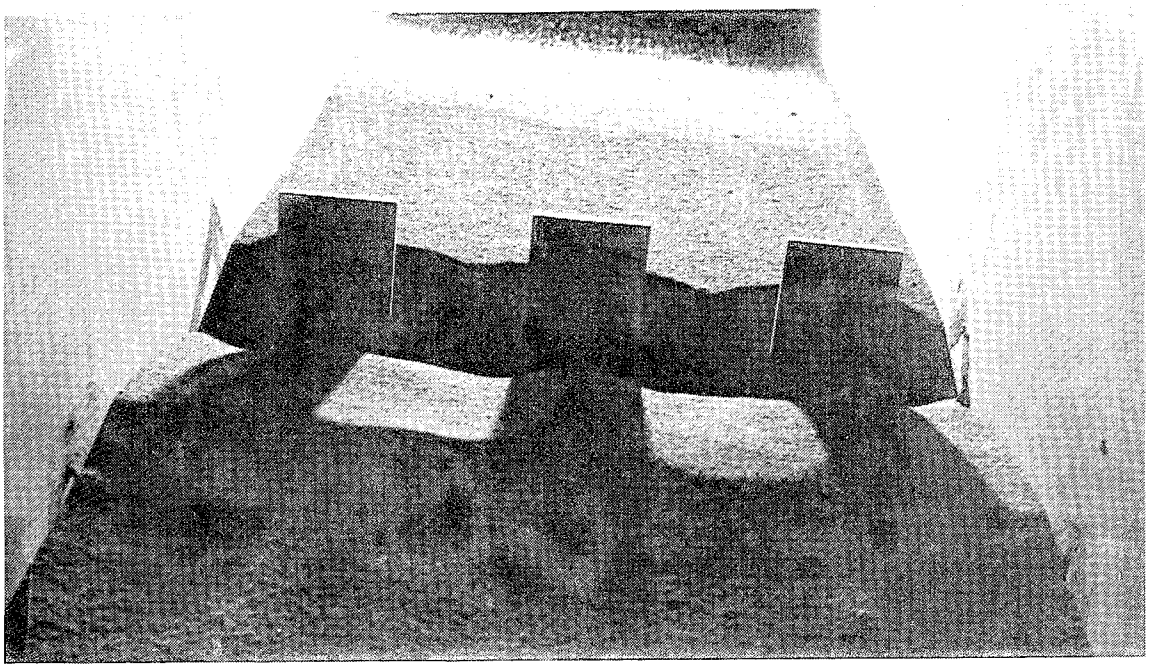

b) Upstream close up view

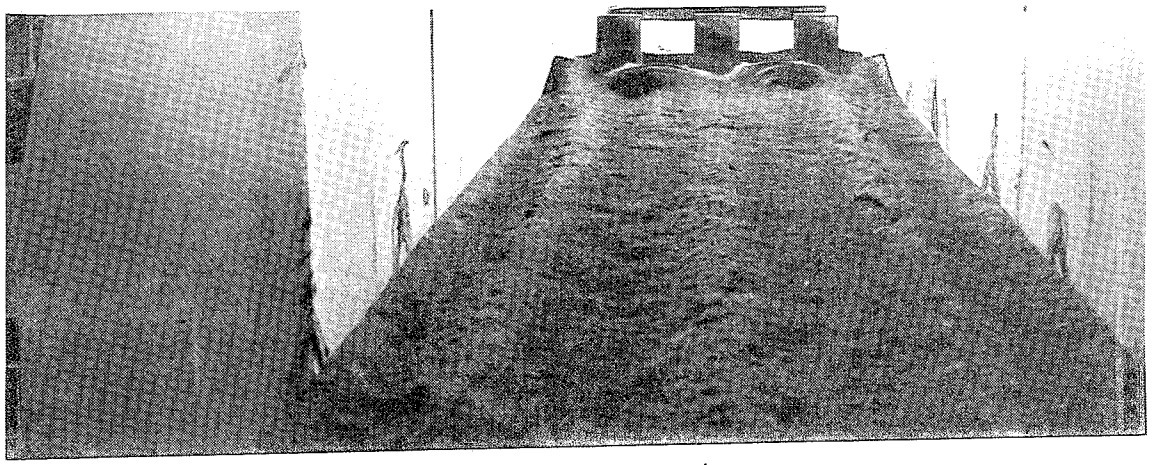

c) Upstream view

Figure A-87. Post test photographs of WSMR dust bed with leading edge disturbance - Vortex generator array: RS 78, 120 fps, 2" RS elevation.

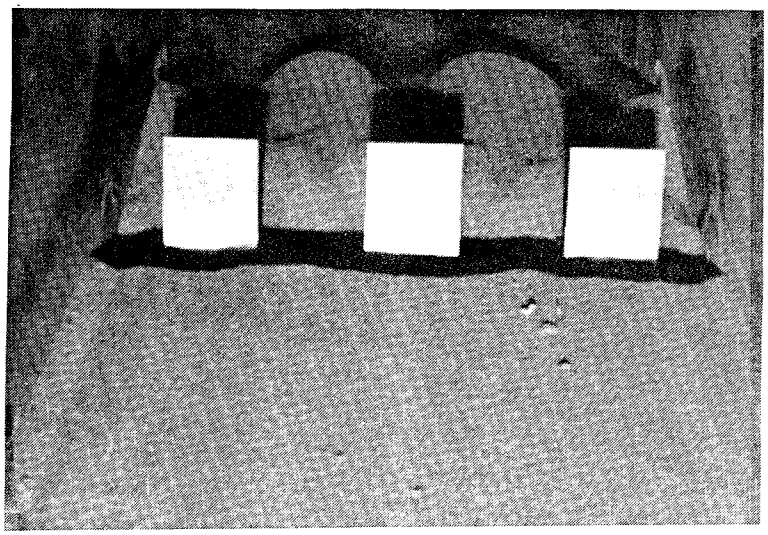

a) Downstream view

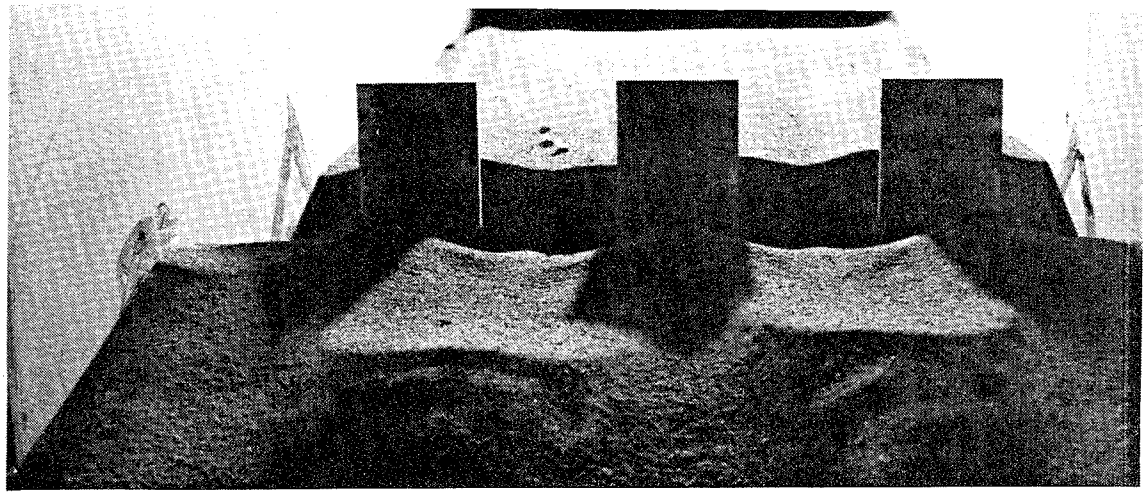

b) Upstream close up view

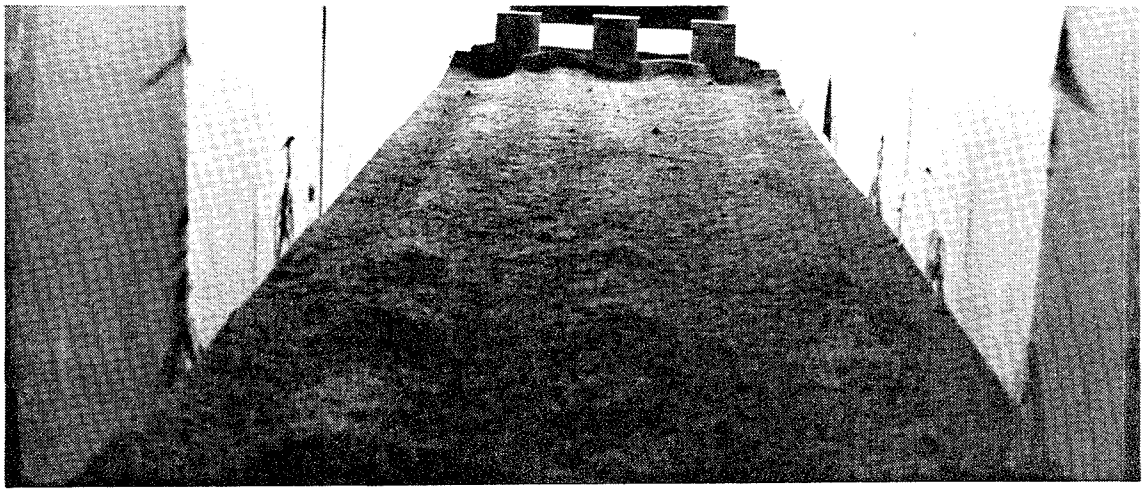

c) Upstream view

Figure A-88. Post test photographs of WSMR dust bed with leading edge disturbance - Vortex generator array: RS 79, 232 fps, 2" RS elevation.

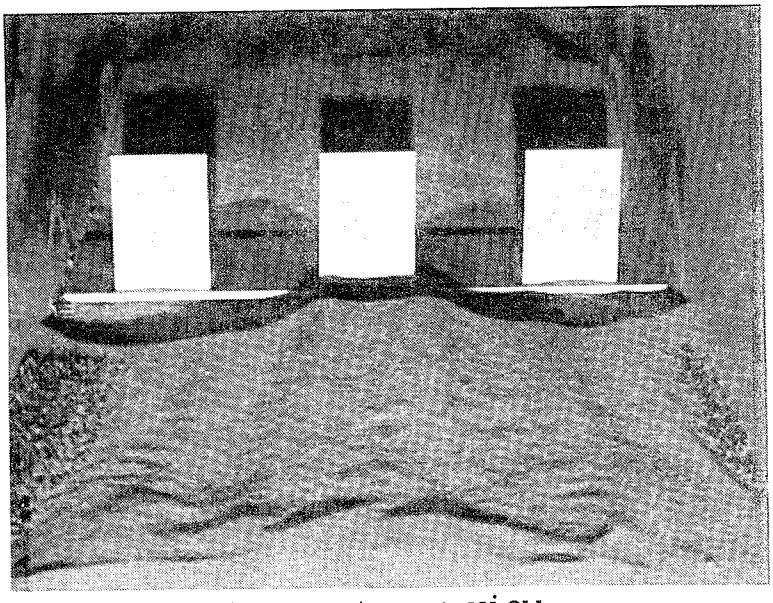

a) Downstream view

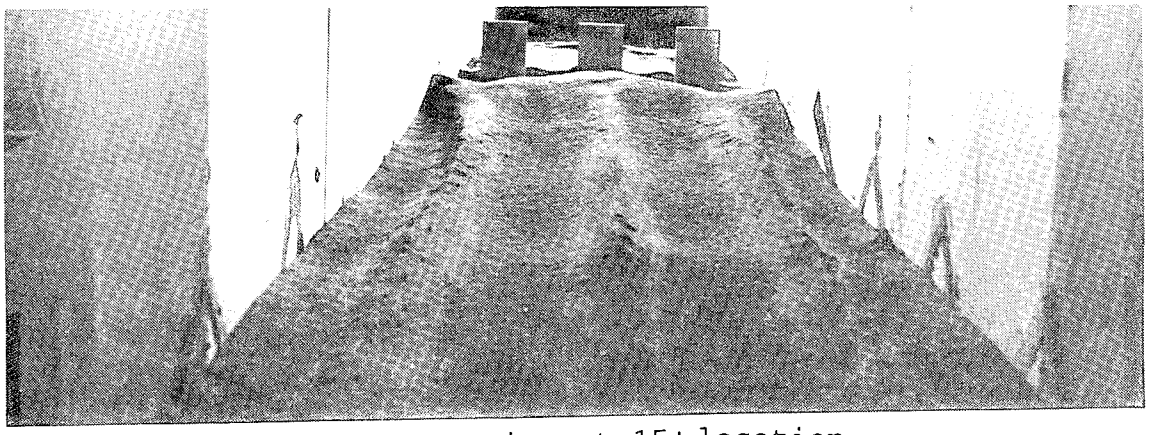

b) Upstream view at 15' location

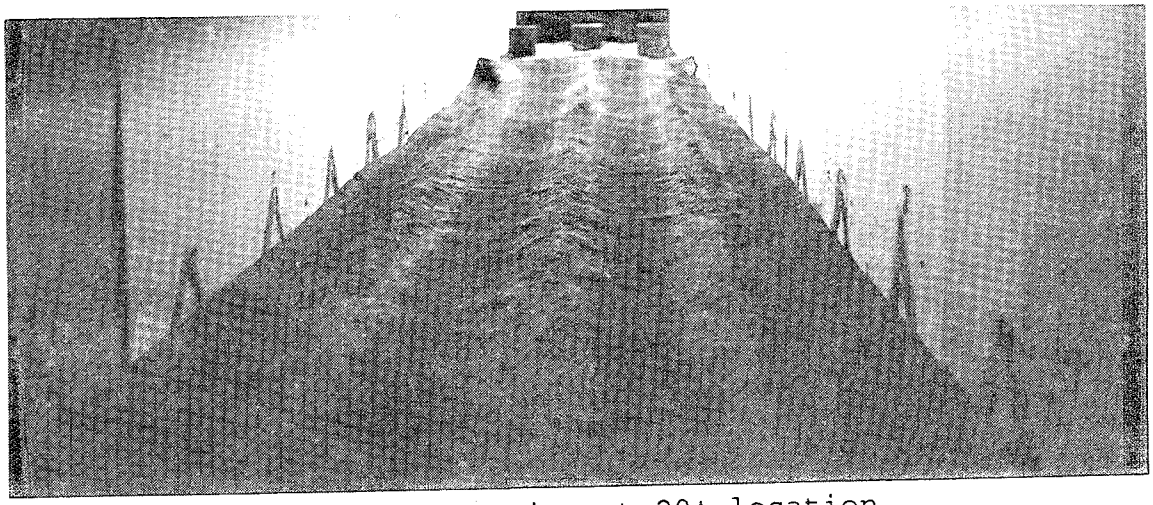

c) Upstream view at 20' location

Figure A-89. Post test photographs of WSMR dust bed with leading edge disturbance - Vortex generator array: RS 80, 367 fps, 2" RS elevation.

DISTRIBUTION LIST

DNA-TR-94-117

DEPARTMENT OF DEFENSE

DEFENSE INTELLIGENCE AGENCY
ATTN: J HEMPSTED

DEFENSE NUCLEAR AGENCY
ATTN: NASF
ATTN: OPNA
ATTN: RAEM
ATTN: RAST W SUMMA
2 CY ATTN: SPWE
ATTN: SPWE LTC JIM HODGE
ATTN: SPWE LTC MARK BYERS
ATTN: SPWE K PETERSEN
2 CY ATTN: SSTL

DEFENSE TECHNICAL INFORMATION CENTER
2 CY ATTN: DTIC/OCP

FIELD COMMAND DEFENSE NUCLEAR AGENCY
ATTN: FCPR

DEPARTMENT OF THE ARMY

U S ARMY ATMOSPHERIC SCIENCES LAB
ATTN: SLCAS-AR-M

U S ARMY NUCLEAR & CHEMICAL AGENCY
ATTN: MONA-NU DR D BASH

U S ARMY TRAINING AND DOCTRINE COMD
ATTN: ATCD-N

U S ARMY CHEMICAL SCHOOL
ATTN: ATZN-CM-CC-003

DEPARTMENT OF THE NAVY

NAVAL RESEARCH LABORATORY
ATTN: CODE 7920

NAVAL SURFACE WARFARE CENTER
ATTN: CODE H-21

OFFICE OF CHIEF NAVAL OPERATIONS
ATTN: NUC AFFAIRS & INT'L NEGOT BR

STRATEGIC SYSTEMS PROGRAM
ATTN: SP0272 R G STANTON

DEPARTMENT OF THE AIR FORCE

AIR FORCE STUDIES AND ANALYSIS
ATTN: AFSAA/SAS

AIR UNIVERSITY LIBRARY
ATTN: AUL-LSE

ASSISTANT CHIEF OF STAFF
ATTN: AFSAA/SAK

HQ ACC/DONB
ATTN: LT COL R EASTERLIN

HQ USAF/XOFS
ATTN: XOFN

OKLAHOMA CITY AIR LOGISTICS CTR
ATTN: OCALC/LPAMB P SHERWIN

412 TW/ LGLXP4
ATTN: P PAUGH

DEPARTMENT OF ENERGY

LAWRENCE LIVERMORE NATIONAL LAB
ATTN: ALLEN KUHL
ATTN: TECH LIBRARY

LOS ALAMOS NATIONAL LABORATORY
ATTN: TECH LIBRARY

SANDIA NATIONAL LABORATORIES
ATTN: TECH LIB 3141

OTHER GOVERNMENT

CENTRAL INTELLIGENCE AGENCY
ATTN: OSWR/NED 5S09 NHB

DEPARTMENT OF DEFENSE CONTRACTORS

AEROSPACE CORP
ATTN: D LYNCH

APPLIED RESEARCH INC
ATTN: J BOSCHMA

CALSPAN CORP
ATTN: M DUNN

GENERAL ELECTRIC CO
ATTN: K KOCH

HORIZONS TECHNOLOGY, INC
ATTN: B LEE
ATTN: E TAGGART

INTERNATIONAL DEVELOPMENT & RESOURCES
ATTN: HERBERT HEAD
ATTN: WILLIAM SCHILLING

JAYCOR
ATTN: CYRUS P KNOWLES

KAMAN SCIENCES CORP
ATTN: D COYNE

KAMAN SCIENCES CORP
ATTN: J HESS

KAMAN SCIENCES CORP
ATTN: D MOFFETT
ATTN: DASIAC

KAMAN SCIENCES CORPORATION
ATTN: DASIAC

LOGICON R & D ASSOCIATES
ATTN: J DRAKE
ATTN: LIBRARY
ATTN: R ROSS

LOGICON R & D ASSOCIATES
ATTN: E FURBEE
ATTN: J WEBSTER
ATTN: R POPE

LOGICON R & D ASSOCIATES
ATTN: G GANONG

MAXWELL LABORATORIES INC
ATTN: S HIKIDA

NORTHROP CORP
ATTN: G CURRY

PACIFIC-SIERRA RESEARCH CORP
ATTN: R LUTOMIRSKI

PACIFIC-SIERRA RESEARCH CORP
ATTN: M ALLERDING

PHYSITRON INC
ATTN: M PRICE

S-CUBED
ATTN: J NORTHROP

SCIENCE APPLICATIONS INTL CORP
ATTN: E SWICK

SCIENCE APPLICATIONS INTL CORP
ATTN: D BACON
ATTN: J COCKAYNE
ATTN: J MCGAHAN
ATTN: P VERSTEEGEN

SCIENCE APPLICATIONS INTL CORP
ATTN: V WATTAWA

SRI INTERNATIONAL
ATTN: E UTHE
ATTN: J PRAUSA
ATTN: M SANAI

TOYON RESEARCH CORP
ATTN: J CUNNINGHAM
ATTN: T W GEYER

TRW INC
2 CY ATTN: R BATT
2 CY ATTN: S PEABODY

W J SCHAFER ASSOCIATES, INC
ATTN: D YOUMANS
ATTN: W BUITENHUYS

W J SCHAFER ASSOCIATES, INC
ATTN: S HOWIE

WILLIAMS INTERNATIONAL CORP
ATTN: D FISHER